SCHOOL OF
CIVIL ENGINEERING

INDIANA
DEPARTMENT OF HIGHWAYS

JOINT HIGHWAY RESEARCH PROJECT

FHWA/IN/JHRP-86/16 — 1

Final Report

DESIGN OF REINFORCED EMBANKMENTS

Dana Norman Humphrey

PURDUE UNIVERSITY

JOINT HIGHWAY RESEARCH PROJECT

FHWA/IN/JHRP-86/16 — 1

Final Report

DESIGN OF REINFORCED EMBANKMENTS

Dana Norman Humphrey

Final Report

DESIGN OF REINFORCED EMBANKMENTS

TO: H. L. Michael, Director
Joint Highway Research Project

DATE: October 14, 1986

PROJECT: C-36-36Q

FROM: R. D. Holtz, Research Engineer
Joint Highway Research Project

FILE: 6-14-17

Attached is the Final Report on the HPR Part II research study entitled "Design of Reinforced Embankments." This report completes all of the tasks of the approved work plan. The author of the report is Mr. Dana N. Humphrey who worked under my supervision.

The study indicates the usefulness of the relatively simple cap-type elastic-plastic work hardening soil behavioral model for the analysis and design of reinforced highway embankments. The primary benefit of the reinforcement is to reduce the shear stresses in the foundation near the toe of the embankment. Reinforcement was also found to be very beneficial for cases in which existing embankments must be widened and their grades raised. The assumptions of common limiting equilibrium design methods for reinforcement were also examined. The report includes a thorough summary of reinforced embankment case histories, as well as procedures to obtain model input parameters from the results of standard soils tests.

Copies of the report will be submitted to the IDOH and FHWA for their review. I look forward to receiving their comments on our research.

Sincerely yours,

Robert D. Holtz

R. D. Holtz, Ph.D., P.E.
Research Engineer

RDH/kr
Attachment
cc: A. G. Altschaeffl
J. M. Bell
M. E. Cantrall
W. F. Chen
W. L. Dolch
R. L. Eskew
J. D. Fricker
D. E. Hancher
R. A. Howden
M. K. Hunter
J. P. Isenbarger
J. F. McLaughlin
K. M. Mellinger
R. D. Miles
P. L. Owens
B. K. Partridge
G. T. Satterly
C. F. Scholer
K. C. Sinha
C. A. Venable
T. D. White
L. E. Wood

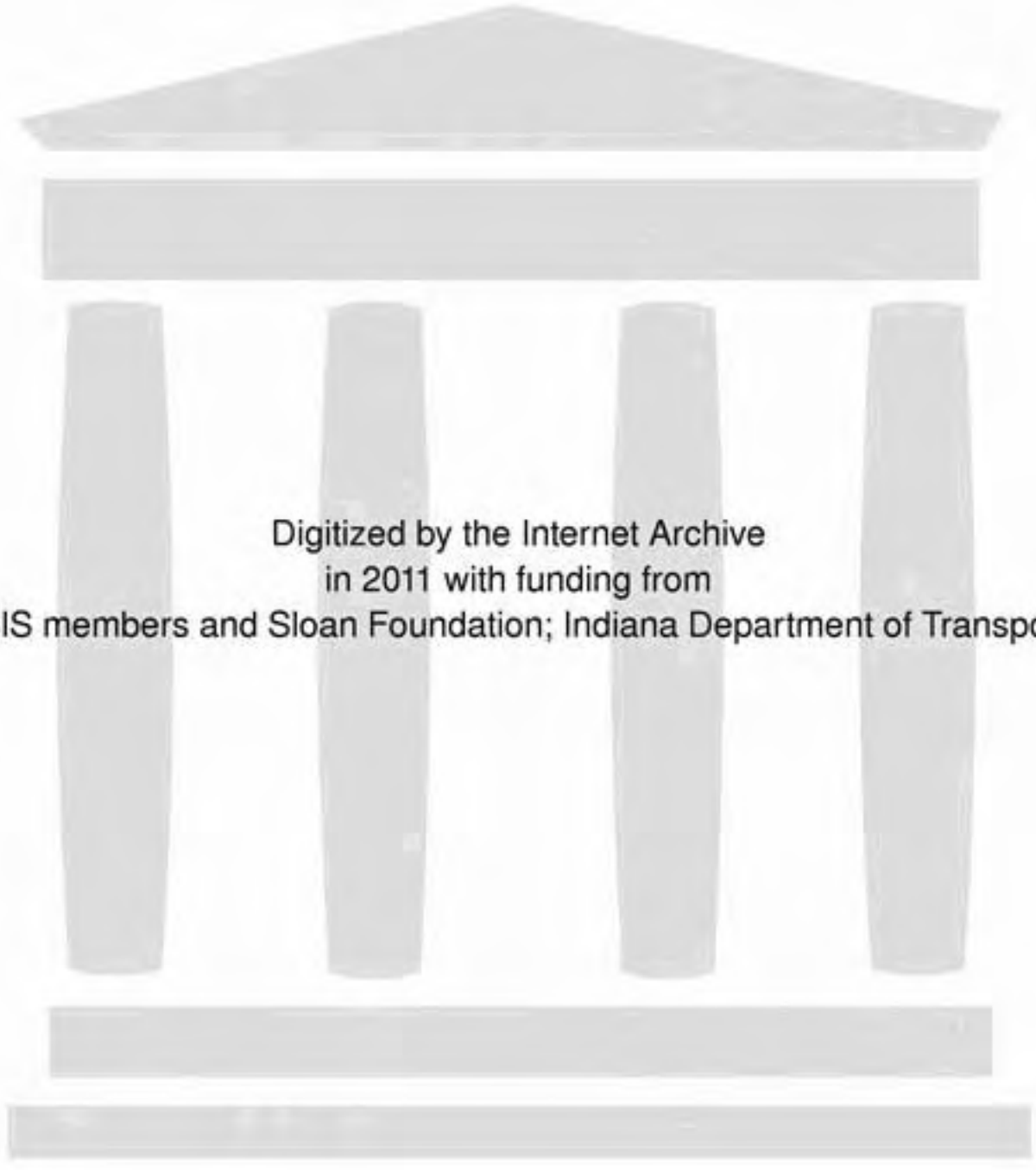

Final Report

DESIGN OF REINFORCED EMBANKMENTS

by

Dana Norman Humphrey
Graduate Instructor in Research

Joint Highway Research Project

Project No.: C-36-36Q

File No.: 6-14-17

An Investigation Conducted by

Joint Highway Research Project
Engineering Experiment Station
Purdue University

in cooperation with the

Indiana Department of Highways
and
U.S. Department of Transportation
Federal Highway Administration

Purdue University
West Lafayette, Indiana
October 14, 1986

ACKNOWLEDGMENTS

The author would like to express his gratitude to his major professor, Robert D. Holtz, for his support, advice, encouragement, and friendship during the preparation of this thesis. He would also like to thank the members of his committee, J.-L. Chameau, W. F. Chen, M. E. Harr, G. A. Leonards and T. R. West, for their useful comments on the final draft of this thesis.

The author thanks fellow graduate students, Carlos Santamarina, Marcus Pacheco and Bill McCarron, for many stimulating discussions which helped to formulate the ideas in this thesis. Helpful discussions with V. Milligan of Golder Associates and R. K. Rowe of the University of Western Ontario are gratefully acknowledged. Special thanks are due to Bill Siciliano, George Crosby, and Somanath Hiremath of the Indiana Department of Highways for their comments on the applied aspects of this thesis.

TECHNICAL REPORT STANDARD TITLE PAGE

1. Report No.	2. Government Accession No.	3. Recipient's Catalog No.
FHWA/IN/JHRP-86/16		

4. Title and Subtitle	5. Report Date
DESIGN OF REINFORCED EMBANKMENTS	October 14, 1986
	6. Performing Organization Code

7. Author(s)	8. Performing Organization Report No.
Dana Norman Humphrey	JHRP-86-16

9. Performing Organization Name and Address	10. Work Unit No.
Joint Highway Research Project Civil Engineering Building Purdue University West Lafayette, IN 47907	11. Contract or Grant No. HPR-1(24) Part II
	13. Type of Report and Period Covered Final Report
12. Sponsoring Agency Name and Address Indiana Department of Highways State Office Building 100 North Senate Avenue Indianapolis, IN 46204	14. Sponsoring Agency Code

15. Supplementary Notes
Prepared in cooperation with the U.S. Department of Transportation, Federal Highway Administration. Study entitled "Design of Reinforced Embankments."

16. Abstract

A study was made of reinforced embankments constructed on undrained soft foundations using the finite element (FE) method with a cap elastic-plastic work hardening soil behavior model. A straightforward procedure was developed to obtain the cap input parameters from standard soil test results. The FE analyses showed that crust strength and foundation compressibility have the greatest influence on the benefit possible with reinforcement. The main effect of the reinforcement is to reduce shear stresses in the foundation near the embankment toe. Reinforcement was found to be very beneficial for widening and raising the grade of existing embankments.

Underlying assumptions of modified limiting equilibrium methods were examined. The assumption of no change in normal stress on the portion of the slip surface passing through the fill due to reinforcement appears to be valid. In addition, a thorough summary of reinforced embankment case histories was presented and evaluated.

17. Key Words	18. Distribution Statement
Embankments, reinforcement, geotextiles, finite element method, weak foundations, design analysis, limiting equilibrium, settlements, embankment widening	No restrictions. This document is available to the public through the National Technical Information Service, Springfield, Virginia 22161

19. Security Classif. (of this report)	20. Security Classif. (of this page)	21. No. of Pages	22. Price
Unclassified	Unclassified	423	

Form DOT F 1700.7

TABLE OF CONTENTS

Page

Page

Page

LIST OF TABLES

Table Page

Table Page

LIST OF FIGURES

Figure Page

Figure Page

Figure Page

Figure Page

Figure Page

Figure Page

Figure Page

Figure Page

Figure Page

ABSTRACT

Humphrey, Dana Norman, Ph.D., Purdue University, December 1986. Design of Reinforced Embankments. Major Professor: R. D. Holtz.

A study was made of reinforced embankments constructed on undrained soft foundations using the finite element (FE) method with a cap elastic-plastic work hardening soil behavior model. A straightforward procedure was developed to obtain the cap input parameters from standard soil test results. The FE analyses showed that crust strength and foundation compressibility have the greatest influence on the benefit possible with reinforcement. The reinforcement's main effect is to reduce shear stresses in the foundation near the embankment toe. Reinforcement is very beneficial for widening and raising the grade of existing embankments.

Underlying assumptions of modified limiting equilibrium methods were examined. The assumption of no change in normal stress on the portion of the slip surface passing through the fill due to reinforcement appears to be valid. In addition, a thorough summary of reinforced embankment case histories was presented and evaluated.

CHAPTER 1

INTRODUCTION

Tensile reinforcement is being used more frequently to increase the end of construction stability of embankments founded on soft soils. It allows embankments to be constructed to greater heights, with steeper side slopes, or without the need for staged construction. In a typical application the reinforcement is placed at the base of the embankment. Geotextiles or geogrids are commonly used as the reinforcing material.

Suitable procedures for designing reinforced embankments are still being developed and all suffer from the limitations that are inherent for any design methods for embankments on soft ground (Tavenas, et al., 1980). Modifications of existing limiting equilibrium techniques are presently the most common procedures but there are several underlying assumptions that have not been confirmed.

Deformations are one of the important factors in reinforced embankment behavior since they control the force which develops in the reinforcement. Finite element

analyses have been used to gain insight into the deformations and resulting embankment behavior. Recent applications include Boutrup and Holtz (1982) and McCarron (1985). The cap model (Chen and Baladi, 1985) has been used to represent behavior of soft foundation soils with reasonable success (McCarron, 1985) but a trial and error procedure was required to obtain the cap parameters.

1.1 OBJECTIVE AND SCOPE

This thesis had several objectives. The first was to develop a straightforward and reliable procedure to determine the cap model parameters from standard soil test results and to investigate the capabilities and limitations of the model to predict undrained soil behavior. This will allow the model to be applied with greater simplicity and more understanding to analysis of embankments constructed on soft ground and other similar problems. The ability of the model to predict drained behavior or the behavior of granular soils was not considered.

The second objective was to identify the range of soil properties and embankment geometries where reinforcement is most beneficial and to gain insight into the factors which contribute to the increase in stability. Special attention was given to widening and raising the grade of existing embankments. This was done with a finite element analysis

technique using the cap soil behavior model. The study was limited to undrained foundation conditions.

The last objective was to examine the validity of some of the assumptions of modified limiting equilibrium analysis methods. In addition, the proper roles of finite element and limiting equilibrium analyses in current design practice were considered.

1.2 THESIS ARRANGEMENT

This thesis is composed of four main parts. The first is Chapter 2 which reviews the available literature on design of reinforced embankments. The review covers both applications of finite element and limiting equilibrium methods. In addition, a thorough summary of reinforced embankment case histories is presented.

The second part is development of a straightforward procedure to determine the cap model parameters from standard soil test results. The main features and governing equations of the model are reviewed in Chapter 3. The procedure is developed in the first few sections of Chapter 4. This is followed by application of the model to laboratory test results on resedimented samples of Boston Blue Clay. Then, the cap parameters for 52 clayey soils are summarized. Finally, the effect of varying the input soil properties on

predicted stress-strain and pore pressure response is examined.

The third part involves the use of a plane strain finite element program with the cap soil model to make a comparative study of reinforced and unreinforced embankment behavior. The analysis procedure is developed in Chapter 5. This is followed by a study of the effect of embankment geometry and foundation soil properties on embankment behavior. The method is applied to widening and raising the grade of existing embankments in Chapter 6.

The last part is Chapter 7 in which limiting equilibrium analysis techniques are examined and some of their underlying assumptions are reassessed in light of results from the finite element studies. Use of finite element and limiting equilibrium analyses for embankment design is also discussed.

CHAPTER 2

REINFORCED EMBANKMENTS A LITERATURE REVIEW

2.1 INTRODUCTION

There is a large volume of literature related to reinforced embankments including three international conferences (International Conference on the Use of Fabrics in Geotechnics, Paris, 1977; Second International Conference on Geotextiles, Las Vegas, 1982; Third International Conference on Geotextiles, Vienna, 1986) and a session at the Eleventh International Conference on Soil Mechanics and Foundation Engineering (San Francisco, 1985). It is also covered in a Federal Highway Administration design manual (Christopher and Holtz, 1984) and in three textbooks (Koerner and Welsh, 1980; Rankilor, 1981; Koerner, 1986).

Literature on reinforced embankment analysis and behavior are reviewed in this chapter and areas that will be addressed in this study are highlighted. In the first section limiting equilibrium analysis of reinforced embankments is examined. This is followed by a review of finite element analyses of reinforced embankments. In the last section a

comprehensive summary of reinforced embankment case histories is presented. Geotextile properties and testing is covered in a separate report (Humphrey, 1985c).

2.2 LIMITING EQUILIBRIUM ANALYSES

Limiting equilibrium analyses are the most common methods used at present to investigate the safety of reinforced embankments against instability. They include both slope stability and bearing capacity analyses. In slope stability methods a slip surface is assumed and the safety factor for a given reinforcing force is calculated. At limiting equilibrium the reinforcement ruptures or reaches a maximum allowable deformation and a slide of the embankment slope and underlying foundation occurs. In bearing capacity methods the embankment is analyzed as an equivalent footing and the presence of the reinforcement is not specifically accounted for. Neither method gives information on deformations prior to failure. Milligan and La Rochelle (1984) recommend that limiting equilibrium methods be used with caution and detailed assessments of geotextile strain should be made when settlements are expected to exceed 10% of the embankment height.

Slope stability methods are discussed in the next section. Special emphasis is given to the underlying assumptions. This is followed by a discussion of bearing capacity

methods. Then, analyses for other failure modes are covered. Finally, design procedures are reviewed.

2.2.1 Slope Stability Methods

Slope stability methods that are applicable to low embankments constructed on weak foundations and with a single layer of reinforcement placed near its base generally make the assumption that the reinforcement provides only a resisting force or moment and does not alter the distribution of normal stress on the assumed slip surface (Bakker, 1977; Bjerin, 1977; Broms, 1977; Maagdenberg, 1977; Haliburton, 1981; Fowler, 1982; Hannon, 1982; Ingold, 1982; Jewell, 1982; Quast, 1983; Christopher and Holtz, 1984; Milligan and La Rochelle, 1984; Rowe, et al., 1984a; Rowe and Soderman, 1985a; Milligan, 1985). It follows that the shear resistance provided by frictional material is also unchanged. This is felt to be conservative since reinforcement is expected to increase the normal stress; however, this has not been confirmed and may even be over conservative if the increase in normal stress is large. Wager (1981) proposed a method which attempts to account for the increase in normal stress and shear resistance on the portion of the slip surface passing through the granular embankment fill. Several other methods that are mainly applicable to embankments on strong foundations with steep side slopes and multiple reinforcing layers do consider the

increase in normal stress (Christie and El Hadi, 1977; Jewell, 1981; Christie, 1982; Murray, 1982; Murray, et. al, 1982; Schneider and Holtz, 1985).

One of the key difficulties in applying these methods is choosing the allowable force in the reinforcement for use in the analysis. An obvious limit is the ultimate tensile strength of the reinforcement but there is evidence based on finite element studies that the strength of the foundation soil and embankment fill are fully mobilized and failure occurs before there are sufficient deformations to develop the reinforcement's tensile strength (Rowe and Soderman, 1985a). This situation may be more severe if the foundation soils reach their peak strength at small strains followed by strain softening. The force in the reinforcement is transmitted to the soil above and below it by shear so the interface strength also limits the allowable force. There is a restriction on the force at working levels since synthetic fabrics experience large creep deformations as their ultimate tensile strength is approached. Shrestha and Bell (1982) feel that the working force should be less than 60% of the ultimate strength for polyester fabrics and 40-50% of the ultimate strength for polypropylene fabrics; however, this is not based on research or field experience.

In the analysis methods a safety factor SF is applied to the soil and reinforcement strengths such that the driving forces D, and the resisting forces provided by the soil R and by the reinforcement dR are related by

$$D = R/SF + dR/SF \qquad (2.1)$$

At failure (SF = 1) the soil strength and allowable reinforcement force are fully mobilized. The reinforcement force required to attain a desired safety factor is found by solving Eq. 2.1 for dR

$$dR = SF(D) - R \qquad (2.2)$$

The reinforcement force under working conditions dR_W is given by

$$dR_W = dR/SF \qquad (2.3)$$

Risseeuw (1977) recommends SF > 1.3 for peaty foundations and SF > 1.5 for clayey foundations. McGown, et al. (1984) proposed that partial safety factors be applied to the dead and live loads and to the fill, reinforcement and soil-reinforcement interface strengths to account for variability of loads and materials, durability of materials, lack of accuracy of the design method, and influence of construction methods.

2.2.1.1 Circular failure mode. In the circular failure mode the reinforcement is assumed to provide an additional resisting moment which is the product of the resisting force in the reinforcement F_R times its moment arm y about the center of the assumed slip circle. The reinforcement force is taken to act either in the direction that the reinforcement was originally placed, generally horizontal, as shown in Fig. 2.1a (Bjerin, 1977; Broms, 1977; Ingold, 1982; Jewell, 1982; Christopher and Holtz, 1984; Milligan and La Rochelle, 1984; Milligan, 1985) or tangent to the slip circle as shown in Fig. 2.1b (Bakker, 1977; Maagdenberg, 1977; Haliburton, 1981; Fowler, 1982; Hannon, 1982; Quast, 1983; Rowe, et al., 1984a). The latter requires that sufficient deformations occur to orient the reinforcement tangent to the slip surface. While this has been observed in some embankment failures (Fowler, 1982) excessive deformations may be required to reach this stage. It is conservative to assume that the resisting force acts in the direction of the original reinforcement (Jewell, 1982) since the corresponding moment arm is smaller. If F_R is taken to act tangent to the circle, y equals the radius r of the slip circle. For horizontal reinforcement and F_R acting in the direction of the reinforcement, y is the elevation difference between the center of the slip circle and the reinforcing layer.

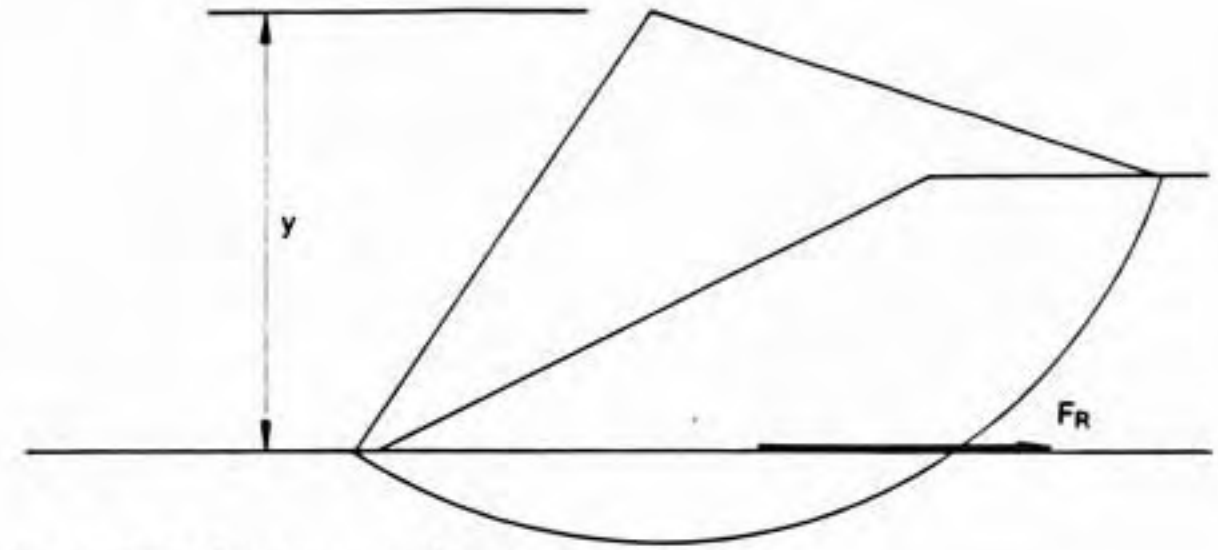

(a.) Reinforcement force horizontal.

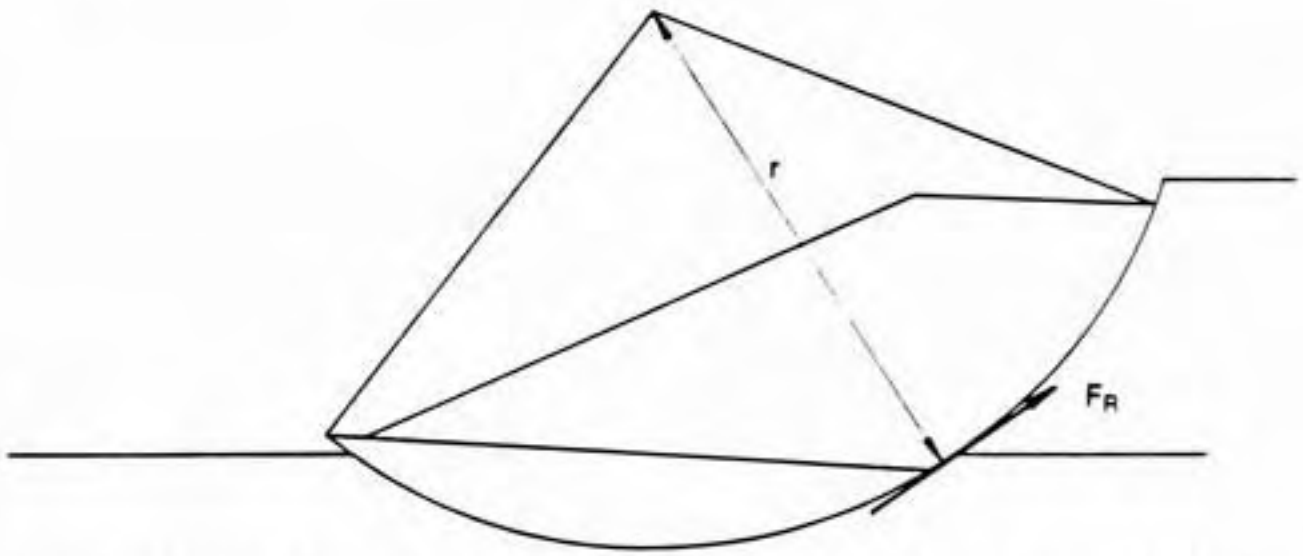

(b.) Sufficient deformations to cause reinforcement to be tangent to slip circle.

Figure 2.1 Orientation of reinforcing force.

The resisting moment provided by the reinforcement is easily incorporated into simplified Bishop's method of slices (Bishop, 1955) which is based on moment equilibrium. This was done by Ingold (1982) for the special case of cohesionless embankment and foundation soils with one or more horizontal reinforcing layers with F_R acting in the direction of the layer

$$SF = [\Sigma W(1-r_u)\tan\phi'/m_\alpha + \Sigma F_R\cos\theta] \; / \; \Sigma W\sin\theta \qquad (2.4)$$

where $m_\alpha = \cos\theta + (\sin\theta\tan\phi')/SF$

W = weight of slice

r_u = pore pressure factor

ϕ' = friction angle on base of slice

θ = inclination of base of slice

An equation for the required F_R for SF = 1.0 was given by Milligan and La Rochelle (1984). It is applicable to the special case of a cohesionless embankment with a height H and side slope β, on a foundation with a crust of thickness t and strength c_t, underlain by soil whose strength increases linearly with depth at a rate of α from an imaginary intercept of zero at the ground surface (Fig. 2.2). The driving force in the embankment was replaced by the active earth pressure. It can be shown analytically that when this assumption is made the center of the critical circle will lie on a vertical line passing through the

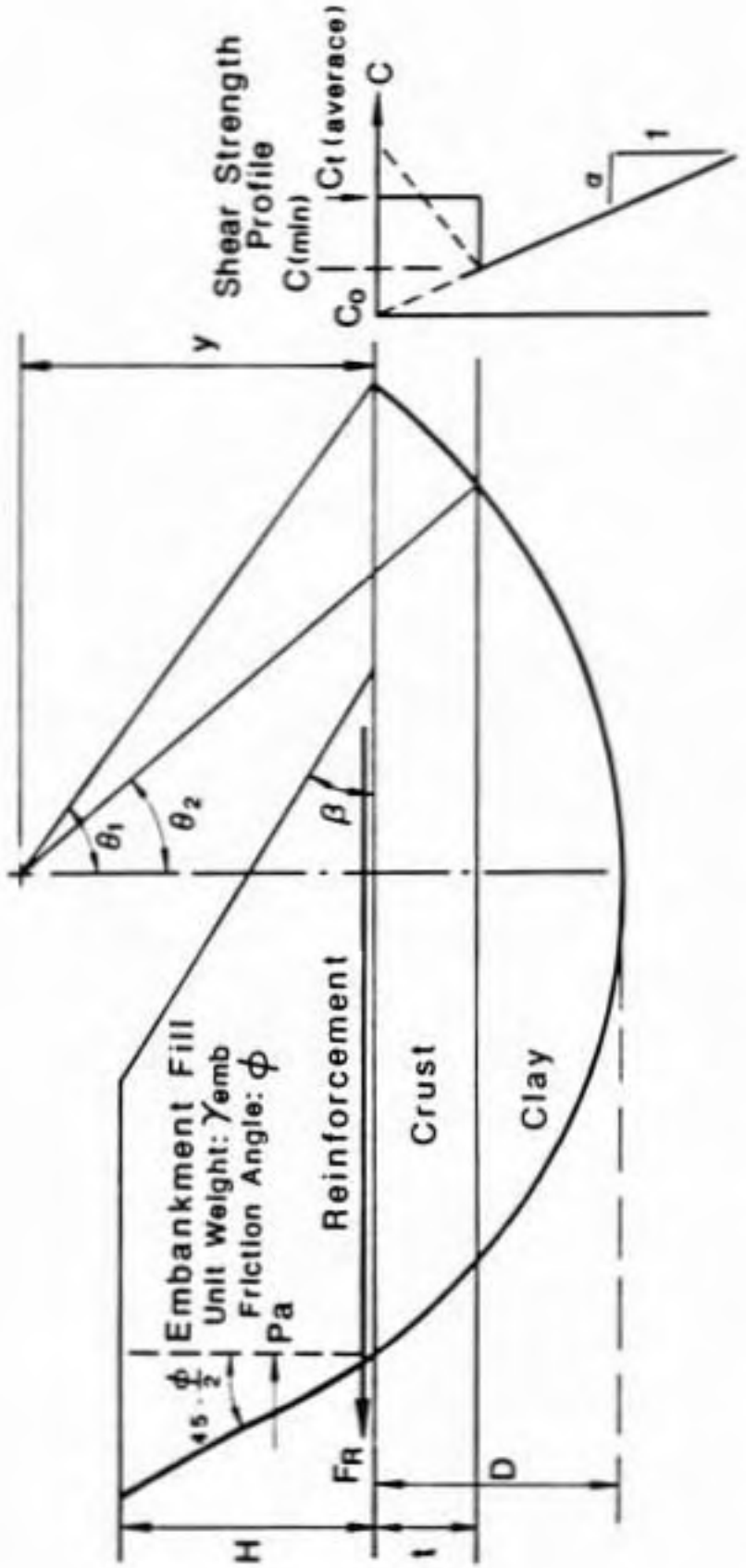

Figure 2.2 Circular failure mode (Hillgan and La Rochelle, 1984).

midpoint of the slope. Their equation in dimensionless form is

$$2F_R Y/(\gamma_{emb} H^2) = 2YZ - \cot^2\beta/12 + K_A(Y-1/3) + Z^2 - 4c_t(Y+Z)^2(\theta_1-\theta_2)/(\gamma_{emb}H) - 4\alpha[(Y+Z)^3\sin\theta_2 - \theta_2 Y(Y+Z)^2]/\gamma_{emb} \quad (2.5)$$

where D = depth of base of slip circle

K_A = active earth pressure coefficient in embankment

γ_{emb} = unit weight of embankment fill

$X = t/H$

$Y = y/H$

$Z = D/H$

$\tan\theta_1 = [2(Z/Y) + (Z/Y)^2]^{1/2}$

$\tan\theta_2 = \{[(Y+Z)/(Y+X)]^2 - 1\}^{1/2}$

Milligan and La Rochelle (1984) recommend that the reinforcement force be taken as horizontal. The usefulness of Eq. 2.5 can be improved by having the strength of the underlying soil layer increase linearly with depth from an imaginary intercept of c_o at the ground surface

$$2F_R Y/(\gamma_{emb} H^2) = 2YZ - \cot^2\beta/12 + K_A(Y-1/3) + Z^2 - 4c_t(Y+Z)^2(\theta_1-\theta_2)/(\gamma_{emb}H) - 4c_o(Y+Z)^2\theta_2/(\gamma_{emb}H) - 4\alpha[(Y+Z)^3\sin\theta_2 - \theta_2 Y(Y+Z)^2]/\gamma_{emb} \quad (2.6)$$

The parameters t, c_t, α, and c_o should be chosen to best model the actual soil strength profile. Caution should be

used when choosing a value for c_t since it is difficult to estimate the strength of the crust.

When the resisting force is taken to act tangent to the slip circle it can be represented as an equivalent cohesion distributed along all or part of the circle (Fowler, 1982; Hannon, 1982). Some authors have replaced the geotextile by a thin cohesive layer at the base of the embankment (Bakker, 1977; Maagdenberg, 1977). For both methods the product of the equivalent cohesion times the length of the slip surface over which it acts equals the reinforcing force. This technique allows existing slope stability analysis computer programs to be used without modification; however, the equivalent cohesion is a function of the length of the slip surface so a different value must be used for each trial circle. Risseeuw (1977) used this method to develop design curves for an embankment with a friction angle of 35° and 1.5h:1v slope. Similar curves are given by Fowler (1982) for an embankment with a friction angle of 30° and 10h:1v slope.

Wager (1981) proposed a method which attempts to account for the increase in normal stress and shear resistance along the portion of the failure surface passing through the embankment. He took the slip surface as vertical through the embankment as shown in Fig. 2.3 and the

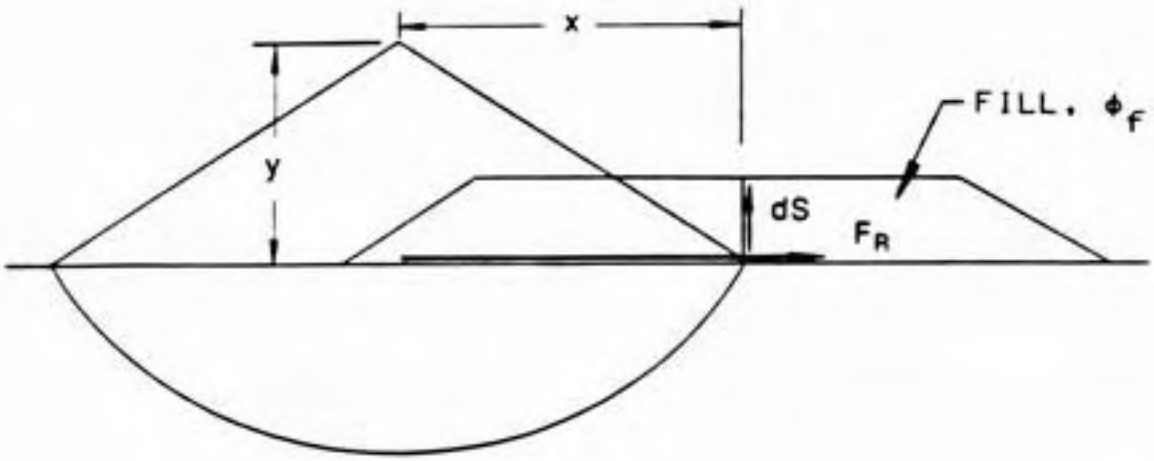

Figure 2.3 Wager's analysis method (Wager, 1981).

increase in shear resistance caused by the reinforcement along this plane was

$$dS = F_R(\tan\phi_f) \tag{2.7}$$

where ϕ_f is the friction angle of the embankment fill. In addition, the reinforcement provides a resisting moment equal to F_R times its moment arm y. The total increase in resisting moment is therefore

$$y(F_R) + x(F_R)(\tan\phi_f) \tag{2.8}$$

where x is the moment arm of dS about the center of the slip circle (Fig. 2.3). The method has been successfully applied to about 30 cases; however, it should be used with caution because the actual increase in stress on the slip surface caused by the reinforcement is unknown.

2.2.1.2 Sliding block failure mode. In the sliding block failure mode a slide is assumed to occur on a horizontal or inclined sliding surface (Fig. 2.4). Active pressure provides the driving force and passive resistance acts at the toe of the sliding block. The reinforcement provides a horizontal resisting force. This failure mode may be more critical for foundations that contain a weak layer or whose strength increases with depth.

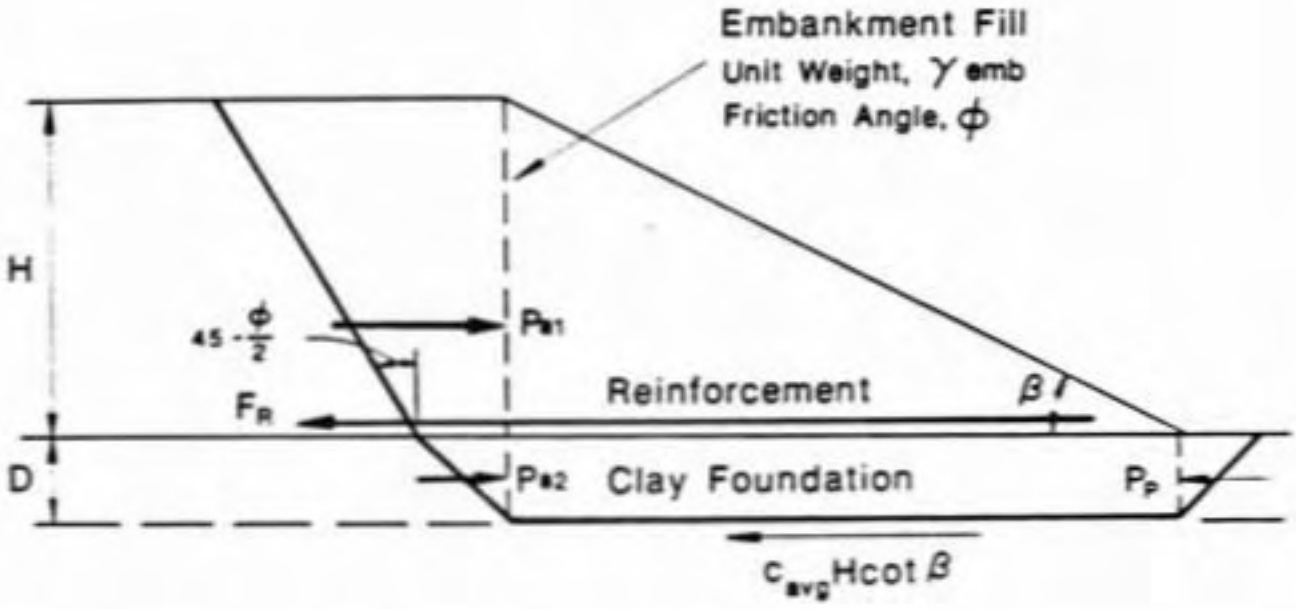

Figure 2.4 Sliding block failure mode (Milligan and La Rochelle, 1984).

Milligan and La Rochelle (1984) present an equation for the F_R required for SF = 1.0 for the case of an embankment on a foundation with a strength of c_{avg}. The base of the sliding block is horizontal and at a depth D (Fig. 2.4). Other variables are as defined previously.

$$F_R/\gamma_{emb}H^2 = K_A/2 + Z - (c_{avg}/\gamma_{emb}H)(4Z + \cot\beta) \quad (2.9)$$

This equation was modified for the case of a strength c on the base of the sliding block and a strength c_t on the active and passive wedges in the foundation

$$F_R/\gamma_{emb}H^2 = K_A/2 + Z - 4c_tZ/\gamma_{emb}H - (c/\gamma_{emb}H)\cot\beta \quad (2.10)$$

Eq. 2.10 is applicable to sliding on a horizontal weak layer.

2.2.1.3 Example problem. The analysis methods presented above are illustrated by an example problem. A 6-ft high granular embankment with a strength of $\phi' = 30^\circ$ and 2h:1v side slope is considered. The foundation consists of a 3-ft thick crust with an undrained strength of 150 psf underlain by a soil whose strength increases linearly with depth at a rate of 25 psf per ft from an imaginary intercept of zero at the ground surface. The critical slip circle was located using STABL4, a slope stability analysis program developed at Purdue University (Siegel, 1975). Without reinforcement the embankment has a safety factor of 1.0.

The reinforcement force required to raise the safety factor to 1.5 was computed for the circular failure mode (critical circle for unreinforced embankment only) with horizontal and tangent reinforcement forces by simplified Bishop's method and Wager's (1981) method with a horizontal reinforcement force. Milligan and La Rochelle's (1984) equations for circular mode and sliding block mode with the base of the block at a depth of 3 ft were also used. The values obtained are summarized in Table 2.1.

Table 2.1
Reinforcement force required to raise safety factor to 1.5 for most critical circle.

Simplified Bishop, horizontal force	2500 lb/ft
Simplified Bishop, tangent force	1600 lb/ft
Wager (1981), circular mode, horizontal force (Eq. 2.8)	1500 lb/ft
Milligan and La Rochelle (1984), circular mode (Eq. 2.5)	2000 lb/ft
Milligan and La Rochelle (1984), sliding block mode (Eq. 2.10)	1800 lb/ft

It is seen that the required force varied greatly for the different analysis methods. For the circular failure mode the orientation of the reinforcing force and including the increase in frictional resistance in the fill makes a significant difference in the required force. The force obtained with Milligan and La Rochelle's (1984) equation for a sliding block failure mode was less than for the circular mode so the latter is more critical for this case.

2.2.2 Bearing Capacity Methods

Bearing capacity methods can be used to assess the stability of embankments constructed on soft ground by treating the embankment as an equivalent footing. The presence of the reinforcement is not considered explicitly in these methods. The failure height H_f from classical bearing capacity theory (Terzaghi and Peck, 1967) for a strip footing is given by

$$H_f = (5.14)c_u/\gamma_{emb} \qquad (2.11)$$

where c_u the undrained shear strength of the foundation soil. This equation assumes that the soft foundation soils are deep relative to the width of the embankment and that its strength is uniform.

2.2.2.1 Strength increasing with depth. The bearing capacity for a foundation whose strength increases with depth was examined by Davis and Booker (1973). The bearing capacity of a footing of width B is

$$Q/B = q = F[(2+\pi)c_o + \alpha B/4] \qquad (2.12)$$

where c_o is the undrained shear strength at the ground surface, α is the rate of increase of the foundation strength with depth, and F is a correction factor depending on the roughness of the footing and the ratio $c_o/\alpha B$. Noting that $q = \gamma_{emb}H_f$ and $\alpha = \gamma'_{fnd}(c_u/\sigma'_{vo})$ where γ'_{fnd} is the

effective unit weight of the foundation soil and c_u/σ'_{vo} is the undrained shear strength ratio, Eq. 2.12 becomes

$$H_f = (\frac{F}{\gamma_{emb}})[(2+\pi)c_o + \gamma'_{fnd}(c_u/\sigma'_{vo})B/4] \quad (2.13)$$

It is felt that a reinforced embankment corresponds to a footing with a rough base since this would account for the shear resistance at the foundation-reinforcement interface.

2.2.2.2 Limited thickness of foundation soil. The effect of a limited thickness of soft foundation soil on the bearing capacity factor was investigated by Mandel and Selencon (1969) using the theory of plasticity. The embankment is assumed to be rigid and the foundation behaves as rigid material up to failure and then is perfectly plastic. The shear strength of the foundation is given by the von Mises failure criteria (Chen and Saleeb, 1982). The problem is analogous to compression of a block between rough rigid parallel platens where the platen width exceeds the material thickness.

The technique was applied by Silvestri (1983) to analysis of unreinforced embankments on soft soils of thickness D_f (Fig. 2.5a). The vertical stress distribution beneath the embankment at failure is given by Eq. 2.14 which was originally developed by Mandel and Selencon (1969). The

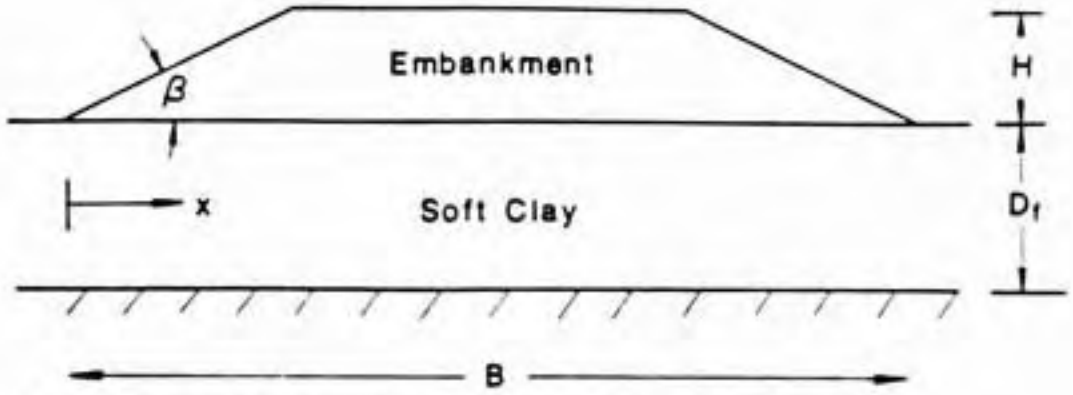

(a.) Unreinforced embankment on soft clay.

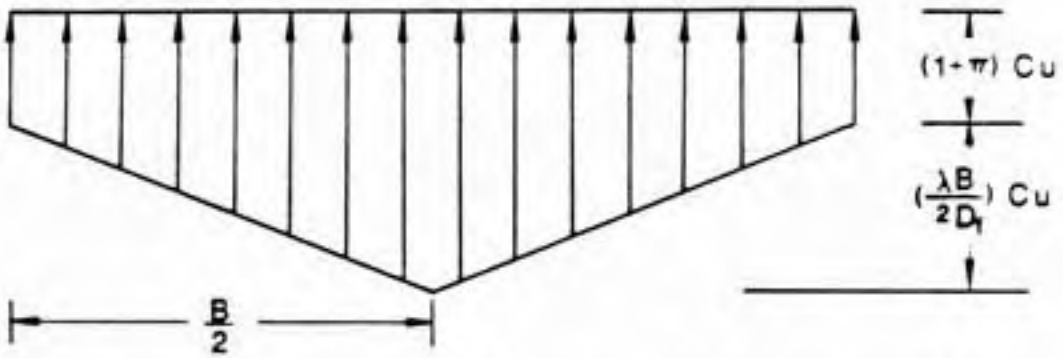

(b.) Available vertical stress (bearing capacity).

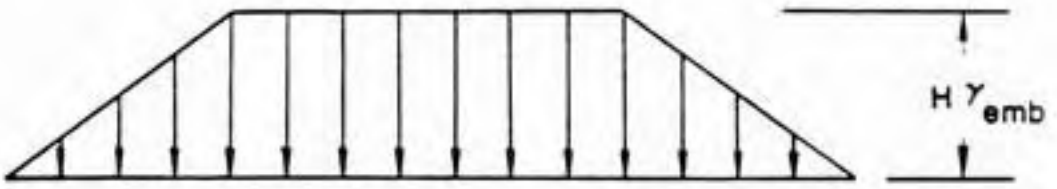

(c.) Applied vertical stress.

Figure 2.5 Bearing capacity analysis of reinforced embankment on foundation of limited depth (Silvestri, 1983).

equation is valid when the width of the embankment B is greater than $4D_f$.

$$\sigma_z = (1 + \pi + \lambda x/D_f)c_u \qquad (2.14)$$

where σ_z = vertical stress

λ = 1 if shear strength at embankment-foundation interface is zero

λ = 2 if shear strength at embankment-foundation interface = c_u

x = horizontal distance from toe of embankment

D_f = thickness of soft foundation

c_u = undrained shear strength of foundation

The λ parameter was introduced to account for partial mobilization of shear strength at the embankment foundation interface. The resulting distribution of available vertical stress is trapezoidal in shape and reaches a maximum value beneath the centerline (Fig. 2.5b). Eq. 2.14 can be rearranged to give the bearing capacity factor at the centerline (i.e., x= B/2)

$$N_c = \gamma_{emb}H/c_u = 1 + \pi + \lambda B_n/2 \qquad (2.15)$$

where B_n is the normalized width defined as

$$B_n = B/D_f \qquad (2.16)$$

Silvestri (1983) assumes that the applied vertical stress is the product of the unit weight times the fill height (Fig. 2.5c). This ignores any stress redistribution which takes place in the fill. The critical point is beneath the crest of the embankment and the safety factor SF is obtained by dividing the available by the applied vertical stress at this point. For an embankment of height H this results in

$$SF = [(1 + \pi)/H + (\lambda \cot B)/D_f](c_u/\gamma_{emb}) \qquad (2.17)$$

Silvestri (1983) used Eq. 2.17 to compute the safety factor for 10 case histories of unreinforced embankment failures. An average c_u was used in cases where the strength varied with depth and vane strengths were corrected according to Bjerrum (1972) or Pilot (1972). Safety factors of nearly one were obtained for all cases when λ was taken to be 2. The safety factor was consistently underpredicted with $\lambda = 1$.

The implication of $\lambda = 2$ is that the embankment applies a force to the top of the foundation soil that is pointed toward the centerline which resists lateral squeezing. For an unreinforced embankment this violates basic considerations of equilibrium. The earth pressure in the embankment applies an outward force so the force applied to the top of the foundation soil must also be outward as shown in Fig.

2.6a. Therefore, the apparent good agreement between predicted and observed safety factors for $\lambda = 2$ must be questioned. The foregoing arguments do not apply to reinforced embankments since the reinforcement can carry a tensile force and can apply an inward force to the foundation soil (Fig. 2.6b). Accordingly, the λ value should be taken as 1 for unreinforced embankments and 2 for reinforced embankments. From Eq. 2.17 it can be seen that the SF is greater when $\lambda = 2$ (reinforced embankment) by $(\cot\beta/D_f)(c_u/\gamma_{emb})$. This implies that reinforcement is more effective for smaller D_f and flatter side slopes; however, the latter is not consistent with reinforced embankment behavior based on finite element studies (Rowe and Soderman, 1985a).

Edgar (1984) used a similar procedure to analyze an embankment constructed on a geogrid mattress. The form of the solution is graphical and was originally developed by Johnson and Mellor (1983; Section 12.5). It was modified to include the passive resistance provided by the foundation soil beneath the toe of the embankment. Edgar (1984) assumed that the mattress is rigid and that the roughness of the base ensures a good contact with the foundation soils allowing the full interface strength to develop (i.e., $\lambda = 2$). The definition of the safety factor is different from that used by Silvestri (1983). Edgar divides the total available vertical force by the total embankment weight.

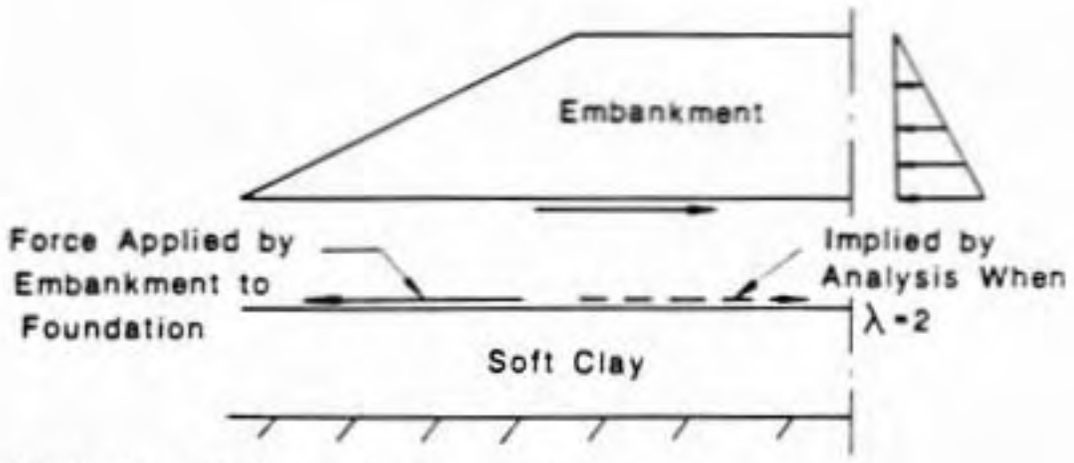

(a.) Unreinforced embankment.

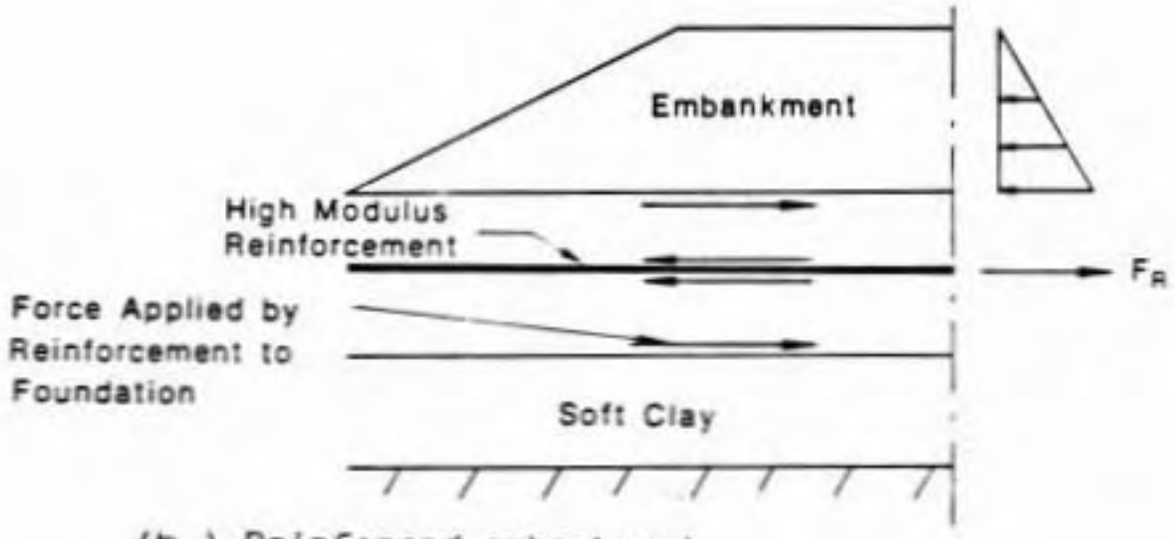

(b.) Reinforced embankment.

Figure 2.6 Force applied to top of clay layer.

Use of this technique for analysis of an embankment on a geogrid mattress was also proposed by Paul (1983).

Edgar's and Silvestri's methods were compared for the case of a 15 m high embankment on a 6 m thick soft foundation described by Edgar (1984). Edgar (1984) calculated a SF of 3.0 while Silvestri (1983) (Eq. 2.17) yields a SF of 2.5. For comparison, the SF when the soft foundation is very thick drops to 0.9 as calculated by classical bearing capacity theory (Eq. 2.11).

2.2.3 Other Failure Modes

The are some other failure modes in addition to slope and bearing capacity failure modes discussed above. The first is a slope failure completely within the embankment. This can be checked with conventional slope stability methods. The next is slipping at the embankment fill-reinforcement interface. This requires a soil-reinforcement friction angle ϕ_{sf} in excess of (Haliburton, 1981; Fowler, 1981)

$$\phi_{sf} = \tan^{-1} [(2(SF)P_a)/(\gamma_{emb} sH^2)] \qquad (2.18)$$

where: P_a = active earth pressure

s = slope parameter (i.e., for 5 on 1 slope s=5)

Lastly, there is lateral splitting-spreading (Halburton, 1981; Fowler, 1981) where the reinforcement must be able to resist the maximum lateral earth pressure exerted by the embankment fill

$$F_R = 0.5\gamma_{emb}H^2K_A \qquad (2.19)$$

An additional restriction is that excessive displacements must be avoided.

2.2.4 Design Procedures

The failure modes discussed above have been incorporated into several design procedures. Procedures proposed by Jewell (1982), Halburton (1981), and FHWA (Christopher and Holtz, 1984) are reviewed below.

2.2.4.1 Jewell's procedure. A procedure was proposed by Jewell (1982) where the distribution of force in the reinforcement required to maintain stability is compared to the distribution of available force. The distribution of required force is computed using limiting equilibrium methods. Several points along the reinforcement are selected. The most critical circle passing through each point is found by trial and error and the reinforcing force required to maintain equilibrium at the desired safety factor is calculated as shown in Fig. 2.7. The effect of a tension crack

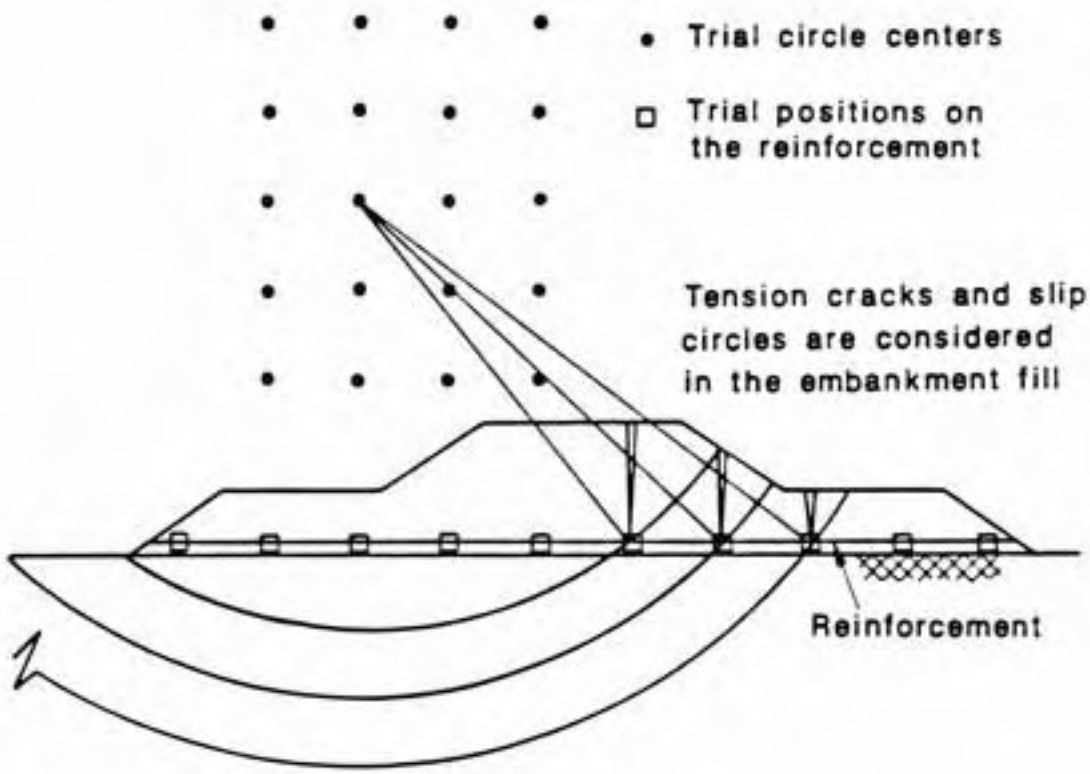

Figure 2.7 Slip circle analysis using Jewell's procedure (Jewell, 1982).

extending through the full depth of fill is checked for each surface.

The available force is calculated by starting at the free end of the reinforcement and working inward. The force is the cumulative sum of the soil-reinforcement shear strength on each side of the reinforcement. An upper limit to the available reinforcement force is set by choosing a maximum allowable tensile strain in the soil and then using the reinforcement stress strain properties to determine the reinforcement force corresponding to this strain. The design is acceptable if the distribution of available reinforcement force exceeds that required at every point (Fig. 2.8).

Internal and foundation stability must also be checked. The former is concerned with sliding at the soil-reinforcement interface and is checked using Eq. 2.18. The latter leads to lateral squeezing of the foundation soils which are restrained only by the foundation soil-reinforcement bond and the shear strength of the soil. This is checked using the bearing capacity procedures discussed above.

The advantages of Jewell's method are that the definition of the safety factor is consistent with accepted practice and there is a clear separation in the analysis of

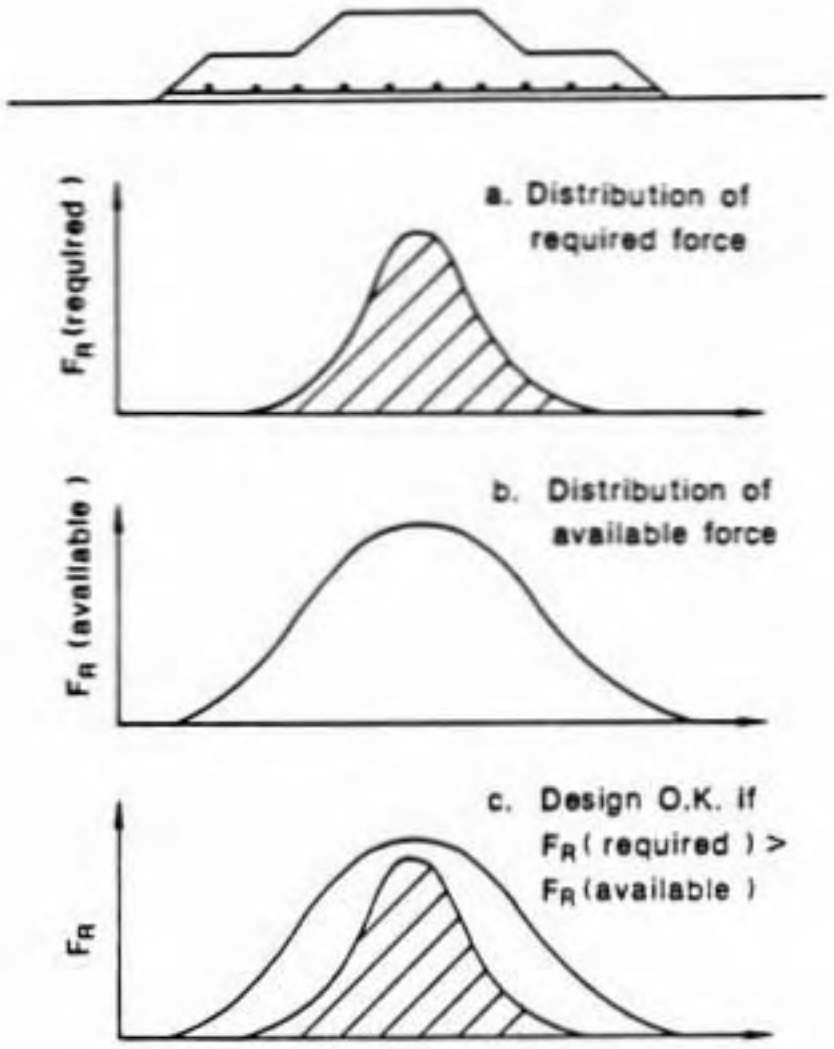

Figure 2.8 Schematic view showing the main design check (Jewell, 1982).

required and available reinforcement forces. This method is recommended by Milligan (1985).

2.2.4.2 Haliburton's procedure. Three failure modes are considered in a procedure proposed by Haliburton (1981) and Fowler (1981), namely: horizontal splitting-spreading, rotational slope-foundation failure and excessive foundation displacement (Fig. 2.9). In the first failure mode the reinforcement must be able to resist the maximum lateral earth pressure as given by Eq. 2.19. Slipping at the fill/reinforcement interface leads to failure by spreading. The minimum required soil-reinforcement friction angle ϕ_{sf} is given by Eq. 2.18. Excessive lateral deformation of the embankment can also constitute failure by spreading. To limit deformations Haliburton (1981) recommends that the average strain in the reinforcement be less than 5%. If the distribution of reinforcement strain is assumed to be linear, varying from zero at the toe to a maximum at the centerline, the maximum allowable centerline strain is 10% and the reinforcement should have a minimum modulus E_F given by

$$E_F = F_R/10\% = 10\ F_R \qquad (2.20)$$

where F_R is computed from Eq. 2.19.

The required reinforcement strength to prevent rotational slope/foundation failure is determined using

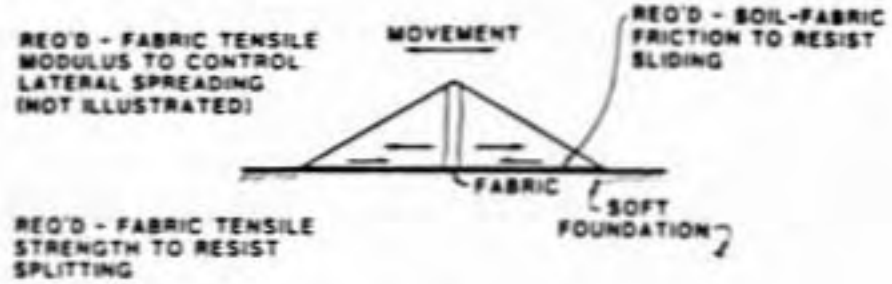

A. POTENTIAL EMBANKMENT FAILURE FROM LATERAL EARTH PRESSURE

B. POTENTIAL EMBANKMENT ROTATIONAL SLOPE/FOUNDATION FAILURE

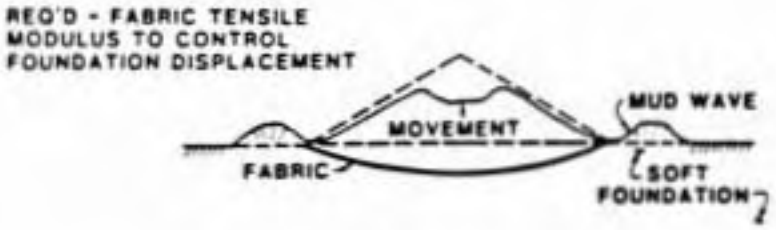

C. POTENTIAL EMBANKMENT FAILURE FROM EXCESSIVE DISPLACEMENT

Figure 2.9 Potential failure modes for fabric-reinforced embankments on soft foundation (Halliburton, 1981).

conventional circular slip surface stability analyses as described above. The most critical circle for the unreinforced slope is located and then the reinforcing force required to obtain the desired safety factor is calculated. It should be noted that others (Broms, 1977; Jewell, 1982) have found that the critical surface for a reinforced and unreinforced slope are generally not the same. It is recommended that the reinforcement force be applied tangent to the slip surface (Fig. 2.1b).

2.2.4.3 FHWA Procedure. The Federal Highway Administration (FHWA) Geotextile Engineering Manual (Christopher and Holtz, 1984) recommends the following five steps for analysis of reinforced embankment stability. (1) Check the overall bearing capacity using conventional methods applicable to strip footings. (2) Check the edge bearing capacity using a modified circular arc stability analysis. (3) Conduct a sliding wedge analysis for lateral spreading. The required reinforcement force is computed using Eq. 2.19 and sliding at the embankment-fabric interface (Eq. 2.18) should be checked. (4) Compute the geotextile modulus to limit deformations due to lateral spreading and incipient circular arc failure. The required modulus is the greater of 10 times the required reinforcement forces computed in steps 2 and 3. (5) Determine the fabric properties in the longitudinal direction required to resist

embankment bending and embankment edge loading during construction. The former is the same as given by Eq. 2.19 and the latter can be computed using a circular arc analysis with the embankment height equal to the maximum lift thickness plus the maximum height of soil piles to be spread. In addition, embankment settlement should be checked using conventional methods and consideration should be given to fabric creep. Christopher and Holtz (1984) should be consulted for further details.

2.2.5 Summary

Limiting equilibrium methods applicable to analysis of reinforced embankments constructed on soft ground were reviewed. The most common method used in current design practice are slope stability methods. These require an estimate of the allowable reinforcing force which is limited by: (1) the reinforcement's ultimate tensile strength; (2) shear resistance between the reinforcement and the surrounding soil; and (3) the deformations which occur prior to failure of the foundation soil. The latter must be obtained from experience or finite element analyses. The methods assume that the normal stress on the failure surface is unchanged so presence of the reinforcement does not affect frictional resistance provided by granular material. For circular failure surfaces there is considerable controversy whether the reinforcing force should be in the original

direction of the reinforcement, generally horizontal, or tangent to the slip circle.

Bearing capacity methods that include the effect of increasing strength with depth and limited thickness of soft foundation soils were reviewed and their applicability to analysis of reinforced embankments was discussed. Sliding within the embankment, slipping on the embankment fill-reinforcement interface, and lateral splitting were also identified as failure modes.

Three procedures for design of reinforced embankments were reviewed. They differ in detail but in general employ similar analysis methods. The main difficulty in applying any of the procedures is estimating the allowable force in the reinforcement as limited by the deformations prior to failure of the foundation soils.

To improve reinforced embankment design procedures this study will examine: (1) the deformation and force in the reinforcement when the foundation soils fail; (2) the change in normal stress on circular failure surfaces caused by the reinforcement; and (3) orientation of the reinforcing force for slope stability analyses with circular failure surfaces. In addition, the stabilizing moment provided by the

reinforcement will be incorporated into a general form of simplified Bishop's slope stability equation.

2.3 FINITE ELEMENT STUDIES OF REINFORCED EMBANKMENT BEHAVIOR

The finite element method (FEM) has been used by several investigators to analyze the behavior of reinforced embankments constructed on soft foundations (Morgat, 1976; Bell, et al., 1977; Ohta, et al., 1980; McGown, et al.,1981; Andrawes, et al., 1980, 1982; Petrik, et al., 1982; Boutrup and Holtz, 1982, 1983; Rowe, 1982, 1984; Rowe, et al., 1982, 1984b; Rowe and Soderman, 1985a, 1985b; McCarron, 1985). Unlike limiting equilibrium methods, FEM gives deformations of the foundation, embankment, and reinforcement prior to failure of the foundation soils and complete collapse. This is important since an embankment may have failed from a functional point of view due to excessive deformations even though collapse has not occurred (Rowe, et al., 1984b). In addition the FEM allows study of variable foundation support characteristics; development of plastic zones in the foundation soils; stress distributions in the embankment and foundation; and the situations where reinforcement can be used to best advantage.

In the following paragraphs, the general considerations of FEM analysis of reinforced embankments are summarized and the methods used to model the embankment and foundation

soils, reinforcement and soil-reinforcement interface are given. This will provide background information for choice of the FE procedures used in this study. Findings of previous FEM analyses of reinforced embankment behavior are then reviewed and areas that require further study are identified.

2.3.1 General Considerations

Embankments are generally constructed in horizontal layers. It is important to model this process for both unreinforced (Clough and Woodward, 1967) and reinforced embankments. Boutrup and Holtz (1982) investigated the effect of single lift versus multi-lift construction for an unreinforced embankment on soft and stiff foundations for both undrained and drained conditions. They found that vertical settlements beneath the centerline and horizontal displacements at the toe were greater for the multi-lift than for the single lift case for all but an undrained stiff foundation. In some cases it may be important to closely model the field construction sequence in the FE analysis. Rowe (1982) computed settlements that were about 10% less when the outside to inside construction sequence used in a field test embankment (Haliburton, et al., 1980) was modeled as compared to construction in horizontal lifts. Furthermore, buoyant unit weight must be used for fill which settles below the water table (Rowe, et al., 1984b).

Large deformations often occur when embankments are constructed on soft ground. These must be accounted for to properly model the forces which develop in the reinforcement (Rowe, et al., 1984b) by periodically updating the nodal coordinates as the embankment load is applied. Strain calculations must be based on the updated embankment geometry using a logarithmic definition of strain. The relation between engineering (Lagrangian) and logarithmic strains is clearly described in Boutrup and Holtz (1982), Section 2.3. A procedure to update nodal coordinates was implemented in the FE program used in this study by McCarron (1985). Deformations also cause a change in pore water pressure as points within the soil change elevation relative to the water table (Rowe, et al., 1984b) and this may be significant if deformations are large.

Embankment construction and the resulting deformations and dissipation of excess pore pressures is a time dependent process. However, most FEM analyses of reinforced embankment behavior reported to date model behavior at a given point in time. Generally two cases are analyzed: end of construction assuming no dissipation of pore pressures and long term assuming drained conditions. This study considers only the former. It is common to use a Poisson's ratio of about 0.5 to model the undrained response of foundation soils for the end of construction case. An alternate

technique is used in this study which imposes the stiffness of water on the compressibility of the soil skeleton (Naylor, 1973; McCarron, 1985). This is discussed in detail in Section 3.5. This technique has also been used by Cheung (1985) and Vaziri (1985) to model the behavior of oil sands.

2.3.2 Behavior Models for Embankment Fill

The embankment is usually constructed of granular fill. The modulus and shear strength of this material depends on the stress level and it cannot support tensile stresses. The approaches used to represent embankment behavior meet these conditions to varying degrees.

The simplest method is to replace the embankment by an equivalent load applied to the ground surface (used by Ohta, et al., 1980). This neglects redistribution of shear and normal stresses at the embankment-foundation contact. It results in overestimation of centerline settlements and may not produce realistic forces in the reinforcement.

Linear elastic models have been used by a few investigators. Boutrup and Holtz (1982, 1983) found that an isotropic linear elastic model resulted in large tensile stresses at the base of the embankment. They concluded that this model is not suitable for representing embankment soil behavior. Similar results were found by Greenway and Bell

(1976). Bell, et al. (1977) avoided tensile stresses by using a linearly elastic orthotropic model with a Poisson's ratio of zero and a high vertical and low horizontal Young's modulus. However, these assumptions reduce the calculated lateral movement of the embankment which is significant to development of tensile forces in the reinforcement (Boutrup and Holtz, 1982).

A nonlinear incrementally elastic hyperbolic model (Duncan and Chang, 1970; Kulhawy and Duncan, 1972) including the effect of a curved Mohr-Coulomb envelope (Wong and Duncan, 1974) was used by McGown, et al. (1981) and Andrawes, et al. (1980, 1982). The modulus and Poisson's ratio are dependent on the stress level. The model only gave adequate predictions prior to the development of local failure.

Recent applications use an elastic-plastic soil model in which the soil behaves elastically until its shear strength as defined by a failure criterion is reached after which it deforms plastically. This model does not allow tensile stresses to develop in cohesionless materials. Boutrup and Holtz (1982, 1983) and McCarron (1985) use a Drucker-Prager (Drucker and Prager, 1952) failure envelope to describe the soil strength. Prior to failure Boutrup and Holtz (1982, 1983) took material behavior to be linear

elastic and McCarron took it to be nonlinear elastic with the bulk and shear moduli dependent on the stress level. The latter procedure was used for this study and is discussed in detail in Chapter 5.

Numerous studies by Rowe (e.g., Rowe, 1982, 1984; Rowe, et al., 1984b) use a nonlinear elastic-plastic stress strain law. The Young's modulus E of the soil is related to the stress level by Janbu's (1963) equation

$$E/P_a = K(\sigma_3'/P_a)^n \qquad (2.21)$$

where σ_3' is the effective minor principal stress, K and n are experimentally determined parameters, and P_a is atmospheric pressure which is used to make the equation dimensionless. The effect of the magnitude of the shear stress on E was not considered. A Mohr-Coulomb failure criterion was adopted. His program has provisions for a non-associated flow rule proposed by Davis (1968). A dilatancy angle of zero was assumed resulting in plastic deformations at constant volume once the failure envelope is reached.

2.3.3 Behavior Models for Foundation Soil

Models for foundation soil behavior have varied from linear elastic for earlier studies to nonlinear elastic-plastic, which more accurately represent soil behavior, for recent studies. Bell, et al. (1977) used a linear elastic

model for a muskeg foundation. Based on work by Hollingshead and Raymond (1972) the foundation was taken to be linearly elastic up to failure as defined by its undrained strength and then it deformed plastically. A Poisson's ratio of 0.25 was used so the results included an unknown amount of drained settlement.

McGown, et al. (1981) and Andrawes, et al. (1980, 1982) used the nonlinear elastic hyperbolic model described in the previous section. Analysis results were compared with model test results. Predicted and observed behavior diverged rapidly after the development of local failure. This was attributed to the inability of the model to account for strain softening.

Boutrup and Holtz (1982, 1983) modeled the foundation soil as a linearly elastic material within the failure surface as defined by the Drucker-Prager criterion and perfectly plastic (shear deformation at constant volume) on that surface. This model does not account for nonlinear elastic behavior or plastic strains which soft soils experience prior to reaching failure.

Rowe (1984) and Rowe, et al. (1984b) modeled the drained nonlinear stress-strain behavior of a peat foundation as series of constrained moduli each valid over a given

range of stress. Rowe (1982) and Rowe and Soderman (1985a) use one modulus valid for all stresses. A constant Poisson's ratio was then used to calculate the drained Young's modulus. A Mohr-Coulomb failure criterion based on drained or undrained strength parameters and the non-associated flow rule proposed by Davis (1968) were used with a dilatancy angle of zero. Pore water pressures for the end of construction case with drained strength parameters were estimated using an empirical pore pressure parameter chosen based on experience. Pore water pressures for the long term case are determined by the static pore pressure due to ground water. Reasonable results have been obtained with this procedure but it does not account for plastic strains which occur prior to reaching the Mohr-Coulomb failure criteria.

Ohta, et al. (1980) used a version of the Cam-clay model (Schofield and Wroth, 1968) modified to include a non-associated flow rule which accounts for anisotropic behavior and rotation of principal stresses; however, few details of the analyses were presented.

McCarron (1985) modeled foundation soil behavior with a non-linear elastic-plastic isotropic work-hardening cap model. It uses a Drucker-Prager ultimate failure surface and an elliptical end cap. The model accounts for

non-linear elastic behavior and plastic deformations prior to reaching the ultimate failure surface. This model was adopted for this study and is discussed in detail in Chapter 3.

2.3.4 Reinforcement Model

The reinforcement is generally modeled as a material capable of sustaining axial tension but with negligible flexural stiffness. This closely represents actual reinforcement behavior. For many types of reinforcement at working stress levels the stress strain behavior is nearly linear so it is reasonable to approximate it as linear elastic (Rowe, 1982, 1984; Boutrup and Holtz, 1982, 1983; McCarron, 1985). If necessary the reinforcement's nonlinear elastic stress-strain curve can be modeled by a series of straight lines each valid for a given range of strain (Bell, et al., 1977; Rowe, et al., 1984b). Andrawes, et al. (1980, 1982) used a polynomial function to represent the nonlinear stress strain curve

$$F_R = A\sigma = a_1\varepsilon + a_2\varepsilon^2 + a_3\varepsilon^3 + \ldots \qquad (2.22)$$

where A = cross sectional area of reinforcement

σ = stress in reinforcement

ε = axial strain in reinforcement

$a_1, a_2, a_3, \ldots$ = constants determined by a least squared fitting technique

A hyperbolic curve fitting procedure (Duncan and Chang, 1970) was used by El-Fermaoui and Nowatzki (1982).

A different approach was used by Ohta, et al. (1980). They replaced the reinforcement by a layer of finite thickness (0.5m to 1.2m in their examples) with a linear elastic Young's modulus and a Poisson's ratio of 0.3. This technique may produce misleading results since the layer would have significant flexural stiffness unlike most geotextile and geogrid reinforcement.

2.3.5 Soil-Reinforcement Interface

Several methods are used to model the behavior at the soil-reinforcement interface. One approach is to assume that no relative movement occurs at the interfaces between the reinforcement and soil above and below it. This method is reasonable provided the shear stresses do not exceed the shear strength at the interface or if the interface shear strength is greater than or equal to the shear strength of the soil. These requirements are satisfied in many instances and this approach was taken by Bell, et al. (1977), Ohta, et al. (1980), Boutrup and Holtz (1982, 1983), and McCarron (1985) and was used for this study.

Rowe (1982, 1984) and Rowe, et al. (1982, 1984b) made provision for slip (tangential displacement between the soil

and reinforcement) at the interfaces above and below the reinforcement. It was assumed that no relative movement occurred until the shear strength as defined by the Mohr-Coulomb failure criteria was exceeded after which slip occurred. However, a soil-geotextile friction angle equal to the fill friction angle was used so no slip was observed.

Andrawes, et al. (1980, 1982) and McGown, et al. (1981) used a special soil-reinforcement interface element. They assumed that interface behavior was purely frictional. It was represented by a pair of springs of zero length, one oriented parallel and the other perpendicular to the interface, connecting the soil node to the adjacent reinforcement node. Contact between the soil and reinforcement was maintained by assigning a very high stiffness to the spring perpendicular to the interface. Relative displacement between the soil and reinforcement is controlled by the stiffness of the spring parallel to the boundary which was represented by a nonlinear elastic hyperbolic model and dependent on the normal stress.

2.3.6 FE Studies of the Influence of Reinforcement

Applications of the FEM and the conclusions drawn from these studies on the influence of reinforcement are summarized in this section.

Morgat (1976) used the FEM to study the behavior of embankments on soft foundations. The effect of a dry surface crust and tensile reinforcement at the base of the embankment were considered. Reinforcement eliminated tensile stresses within the embankment and increased the overall safety factor against instability by as much as 20%.

Bell, et al. (1977) analyzed a 4.5-ft high geotextile reinforced test embankment constructed on a foundation of very soft muskeg. The effects of normal traffic and construction period live loads, and weak and strong geotextiles were considered. Reinforcement was predicted to have very little effect on computed deflections. In contrast, the geotextile had a very large influence on deflections measured in the field.

The effect of reinforcement on undrained and drained deflections of an embankment on a soft clay foundation 5 to 20m thick was studied by Ohta, et al. (1980). Their study considered undrained loading followed by time dependent dissipation of construction pore pressures. Computed settlements and horizontal displacements beneath the toe were reduced by reinforcement but the effects were greatest at the end of undrained loading. However, the reinforcement was represented by a layer with flexural stiffness (as noted in Section 2.3.4) making interpretation of the significance

of the results difficult. Computed consolidation settlements were compared with data from a field trial but agreement was only fair.

Investigators at the University of Strathclyde (Andrawes, et. al., 1980, 1982; McGown, et al., 1981) compared results from FEM analyses with measurements made on model tests of reinforced embankments on an elastic foundation and of footings on a reinforced sand. They considered multiple layers of reinforcement and, in the case of embankments, the effect of inclining the reinforcement upward near the embankment slope so that it would be parallel to lines of maximum extension. FEM predictions of deformations of the model were in good agreement prior to the development of local failure. Principal strains, maximum shear strains, volumetric strains and directions of principal strains were only in fair agreement. Reinforcement reduced horizontal displacements and differential settlement at the embankment base, and shear strains within the embankment.

Rowe has used his FEM program to study two case histories, Pinto Pass (Rowe, 1982; Rowe, et al., 1982) and Bloomington Side Road (Rowe, 1984; Rowe, et al., 1984b), and to develop design charts (Rowe, et al., 1982; Rowe, 1984; Rowe and Soderman, 1985a, 1985b). He found that the geotextile had little effect on vertical settlements but lateral

spreading was significantly reduced and stability was increased. The effect became more important as the extent of local plastic zones increased (i.e. safety factor reduced). Extremely large deformations may be required to develop sufficient tensile forces in reinforcement with low to moderate stiffness. The geotextile at the edge of the embankment was predicted to be unstressed. The effect of fill stiffness was found to be small. He investigated several combinations of foundation strength and modulus and was able to obtain good agreement with observed field performance for some cases. Rowe and Soderman (1985a) found that failure occurred before the ultimate tensile strength of typical reinforcement is reached.

Boutrup and Holtz (1982, 1983) analyzed the test embankment described by Bell, et al. (1977). Undrained and drained response and the effect of live loads were investigated. Reinforcement reduced shear stresses in the foundation and vertical differential settlements of the top of the embankment. The benefit of reinforcement was greater for the undrained case and decreased as the strength of the foundation increased. High modulus geotextile has the largest effect. Multiple layers of reinforcement were investigated and it was found that for maximum benefit the reinforcement should be placed as close as possible to the base of the embankment.

McCarron (1985) used the FEM with the CAP model to analyze drained behavior of an instrumented reinforced embankment constructed on a peat foundation (Rowe, 1984; Rowe, et al., 1984a). Computed centerline settlements were not greatly affected by assumed embankment behavior. Single versus multi-step construction and an embankment with an infinite transverse stiffness were investigated. The reinforcement provides the greatest benefit when located close to the foundation surface. The effect of an initial slack in the reinforcement was examined. Agreement between calculated results and field observations was reasonable. McCarron (1985) also made a parametric study of reinforced embankment behavior but the choice of cap model parameters and details of the analysis procedure makes interpretation of the findings difficult. This is discussed in detail in Chapter 5.

2.3.7 Summary

Finite element procedures for modeling reinforced embankment behavior were described. Incremental construction and large deformations must be accounted for in the analysis. Elastic-plastic models such as the cap model give the most realistic representation of embankment and foundation soil behavior. The reinforcement stress strain behavior can be represented by a piecewise linear approximation but for many cases a linear approximation is adequate.

Allowing no relative movement at the soil-reinforcement interface is reasonable if the shear stress is less than the interface strength or if the interface strength equals the soil strength. Special procedures may be required to allow for slip at the interface if the interface strength is less than the soil strength.

Results from the analyses show that reinforcement reduces shear stresses and lateral deformations in the foundation soils and increases embankment stability. There is little effect on vertical settlements. Reinforcement reduces tensile strains in the embankment. The benefit from reinforcement increases as the strength of the foundation decreases and the reinforcement modulus increases.

The FEM analyses performed for this study address some of the limitations of previous studies. Most of the previous studies did not consider the effect of a dried surface crust or increasing strength and modulus with depth in the foundation soils. This will be examined and special emphasis will be given to the effect of reinforcement on stresses in the embankment and foundation and the reinforcement force when embankment failure occurs. FEM results will be used to check some of the assumptions made in limiting equilibrium analyses. The special problem of widening and raising the grade of existing embankments will also be studied.

2.4 REINFORCED EMBANKMENTS - A REVIEW OF CASE HISTORIES

2.4.1 Introduction

Many case histories of reinforced embankments constructed on soft foundations have been reported in the literature. The reinforcement placed at the base of the embankment is typically one or more layers of geotextile or geogrid. It provides a stabilizing effect and increases the safety factor against slope instability., This review summarizes 40 cases with embankment heights greater than 1 m. It expands on a summary prepared by Milligan (1985) and an earlier review by Boutrup and Holtz (1982). Holtz (1982) lists three criteria for a useful case history. They are a detailed description of (1) a non-conventional approach to the problem; (2) the design assumptions; and (3) verification of the design assumptions. Verification can be either quantitative or qualitative. Unfortunately few of the cases reviewed satisfy these criteria completely.

The case histories are discussed under the following categories based on reinforcement type: nonwoven (low modulus) geotextiles, woven (high modulus) geotextiles, geogrid mattresses, and geotextiles used for embankment widening. Data on foundation conditions, embankment geometry, instrumentation and reinforcement is given in Table 2.2. In 12 cases companion reinforced and unreinforced sections were

CASE NO.	PROJECT NAM	MENT	REINFORCEMENT TENSILE FORCE (kN/m)	STR- AIN (%)	OTHER SPECIAL MEASURES	REFER- ENCES
1	Haul road		>8.8	>50	---	10,17,18,66
2	Quinault		--	0	---	196
3	Mission Island		--	--	---	39
4	Highway embankmen		--	--	B	11
5	Highway embankmen		--	--	---	152
6	Brunswick		--	--	---	62
7	Swan Lake	-28	--	36	---	62
8	Arzal Dam		--	--	D	94,97
9	Bridge approach e	er	--	--	P	77,80
10	Zevenhoven I		--	--	---	202
11	Zevenhoven II		20	15	---	19,202,204
12	Muiderberg Hwy RW		--	<10	SC	204
13	RW12 Motorway		--	--	SC	19
14	RW12 Motorway		44	20	---	60,62
15	Almere		95	5	---	19
16	Cuxhaven, A27 mot		10	--	---	19
17	Embankment I		120-180	3-4.5	D	160
18	Embankment 2		80-180	2-4.5	D	160
19	Pinto Pass		15	4	---	59,60,62,68,167
20	Dumbarton Test em		--	--	D,SC	70,71
21	Dumbarton Main em		--	--	D,LF,SC	70,71
22	Craney Island, Se		--	--	---	61
23	Craney Island, Se		--	--	---	61
24	Craney Island, Se		--	--	---	61
25	Duluth Int. Airpo		--	--	---	64
26	James Bay, NBR-2		--	--	---	118,124,125
27	James Bay, NBR-3		--	--	---	118,124,125
28	Manchester, Hwy I		--	10	---	9,39
29	Bloomington Side		32	1-21	SC	9,168,170,171
30	Embankment		--	0.4	---	13
31	Ebetsu, Hokkaido		--	--	D	151
32	Helsinki harbor		--	--	---	114
33	North area	195	--	--	---	23
34	Musselburgh bypas	2	--	--	D	56
35	Greater Yarmouth	52	--	--	D	207
36	Champlain Clay- E		6.4-9.1	2	---	24
37	Champlain Clay- E		19	3.4	---	24
38	Trunk Hwy 53	35	--	--	W,SC,LF	123
39	Nederhorst-den-Be		--	<10	W	204
40	South area	195	--	--	W	23

LEGEND: See next pag

2.4 REINFORCED EMBANKMENTS - A REVIEW OF CASE HISTORIES

2.4.1 Introduction

Many case histories of reinforced embankments constructed on soft foundations have been reported in the literature. The reinforcement placed at the base of the embankment is typically one or more layers of geotextile or geogrid. It provides a stabilizing effect and increases the safety factor against slope instability., This review summarizes 40 cases with embankment heights greater than 1 m. It expands on a summary prepared by Milligan (1985) and an earlier review by Boutrup and Holtz (1982). Holtz (1982) lists three criteria for a useful case history. They are a detailed description of (1) a non-conventional approach to the problem; (2) the design assumptions; and (3) verification of the design assumptions. Verification can be either quantitative or qualitative. Unfortunately few of the cases reviewed satisfy these criteria completely.

The case histories are discussed under the following categories based on reinforcement type: nonwoven (low modulus) geotextiles, woven (high modulus) geotextiles, geogrid mattresses, and geotextiles used for embankment widening. Data on foundation conditions, embankment geometry, instrumentation and reinforcement is given in Table 2.2. In 12 cases companion reinforced and unreinforced sections were

Table 2.2
Summary of case histories.

CASE NO.	PROJECT NAME	LOCATION	YEAR CONSTRUCTED	FOUNDATION SOIL TYPE	FOUNDATION MAX. EMBTH (m)	FOUNDATION DEPTH TO BF (m)	FOUNDATION r_u	FOUNDATION WATER CONTENT (%)	EMBANKMENT WIDTH AT MID-HT (m)	EMBANKMENT SIDE SLOPE (H:V)	EMBANKMENT HEIGHT (m)	EMBANKMENT BERM(S) (m)	EMBANKMENT H_{ult} (m)	EMBANKMENT $\frac{H_{ult}}{H_{BF}}$	EMBANKMENT S_u/σ_v	EMBANKMENT FILL RATE (m/d)	INSTRUMENTATION REMARKS	REINFORCEMENT TYPE	REINFORCEMENT BRAND	REINFORCEMENT TENSILE FORCE (kN/m)	REINFORCEMENT SPA-CING (m)	OTHER SPECIAL MEASURES	REFERENCES
1	Haul road	Alaska	——	Pt	3.0	——	[1-1]	900	3	3:1	1.4	1.4	2.7	2.7	0.7	0	n.r.	90	Fibretex	18.0	150	——	65,17,18,66
2	Bothell	Washington	——	Org	1.5	0	——	——	——	——	——	——	——	——	——	0	n.r./r	90	2 brands used	——	0	——	196
3	Mission Island	Ontario	——	Pt,S,C,M	0.6	——	——	——	——	——	1.0	1.0 *	——	——	——	1.6	——	80	Mirafi 140	——	——	——	19
4	Highway embankment	Africa	——	Pt	15	0	7	300-400	25	1.5:1	1.0	——	4.5	——	1.7	1	n.r.	90	Stratagrid	——	——	6	11
5	Highway embankment	Mexico	——	Pt,M,Z	17	10.5	1-15	150-500	40	——	3.5	3.5	7.0	7.0	2.4	1.2	n.r./r	90	Typar 3401	——	——	——	132
6	Brunswick	Georgia	——	——	——	——	——	——	12	——	1.5 *	——	——	——	——	5	——	90	Typar 3401	——	——	——	42
7	Swan Lake	Mississippi	——	C	——	——	1	——	14	3:1	2.4 *	——	12.2	——	——	C	n.r./r	90	Stabra T-14 & C-170	——	——	76	42
8	Arzal Dam	France	——	C	30	**	——	——	225	——	15.0	——	——	——	4.1	0	——	10	——	——	——	——	3	96,97
9	Bridge approach emb.	Sweden	——	C	14	——	25-40	——	14	1.2:1	4.5	——	1.9	——	1.1	1.0	n.r./r	0	40 Fabrinsmaider	——	——	0	77,80
10	Oosthaven I	Netherlands	1974	Pt	3	——	——	——	15	3:2	3.0	3.0	——	——	2.0	1	n.	——	——	——	——	——	——	202
11	Oosthaven II	Netherlands	1975	Pt	4	——	——	——	15	3:2	4.5 *	3.5 *	——	——	3.3	5	n.r./r	0	Stabilenka	20	15	——	15,202,204
12	Rijnsburg Max Emb(Old)	Netherlands	——	Pt	2	——	——	——	——	4:1	8.0	9.0	——	——	——	5	n.r.	0	——	——	——	12	204
13	RWS Rotterdam	Netherlands	1976	C,Pt	4	——	——	——	——	——	2.5 *	2.5 *	——	——	——	——	——	0.04	4 brands used	——	——	12	19
14	RWS Rotterdam	Netherlands	——	——	4.0	——	2	——	85	3:1	7.5 *	——	22.5	——	10.0	——	n.r./r	0	Stratex	40	20	——	40,42
15	Klaver	Netherlands	1975	C,Org	4.5	——	40	——	27	1.7:1	4.0 *	2.0 *	9.6	5.3	1.8	1	n.r	0	Stabilenka 150	90	5	——	19
16	Cuxhaven, A31 motorway	W. Germany	1978	S,C	5	-0.5	——	——	——	3:1	5.0	——	——	——	——	5	n.r	——	——	10	——	——	19
17	Embankment A	W. Germany	——	Pt,C	12	0	7-20	70-100	——	4:1	4.5	——	5.1	——	——	1	n.r./r	0	Stabilenka 400	120-200	3-4.5	5	202
18	Embankment B	W. Germany	——	Pt,C	12	0	17-25	90-600	——	4:1	6.0	——	8.0	——	——	1	n.r./r	0	Stabilenka 400	80-200	2-4.5	0	202
19	Pinto Point	Alabama	1979	C,Pt	12	**	2-3	40-120	23	10:1	7.1	——	8.4	——	1.9	5	n.r./r	0	4 brands used	90	0	——	79,80,82,86,202
20	Bombardier Test emb.	California	1970	C,M	12	10.0	5-14	20-100	——	——	5.0	——	9.5	——	——	——	n.r	0.04	4 brands used	——	——	0.32	70,71
21	Bombardier Main emb.	California	1982	C,M	12	10.0[pad=4.0	5-14	30-100	——	——	4.5 *	——	9.0	——	——	——	n.r	0	Mirafi 1000	——	——	0.27,32	70,71
22	Dranco Island, Sec. 1	Virginia	1982	Fg	——	——	5	——	——	——	3.4	1.0 *	12.2	6.5	——	——	——	——	——	——	——	——	61
23	Dranco Island, Sec. 2	Virginia	1982	Fg	——	——	2	——	——	——	3.4	——	10.4	——	——	——	——	——	——	——	——	——	61
24	Dranco Island, Sec. 3	Virginia	1982	Fg	——	——	3	——	——	——	2.4 *	——	10.2	——	——	——	——	——	——	——	——	——	61
25	Duluth Int. Airport	Minnesota	1983	Pt	3	0	14-19	100-600	21	2.0:1-4:1	6.4	——	6.8	——	11.1	1	n.r	0	Proflex 2004	——	——	——	64
26	Jämtö Bas, MOB-2 site	Sweden	——	Pt	3.5	-0.25	10	1400	——	——	1.0 *	1.0 *	1.0	1.0	——	5.0	n.r	0	——	——	——	——	118,119,125
27	Jämtö Bas, MOB-3 site	Sweden	——	Pt	3.5	0	20	350	35	3.0:1-3.0:1	1.5	2.0	1.4	1.0	1.2	5.0	n.r	0.04	——	——	——	——	118,124,125
28	Manchester, New 12	Ontario	——	Pt	4	0	7-10	170-410	22	1.5:1	1.0	——	2.0	——	1.3	0.5	n.r	0.04	4 brands used	——	10	——	5,19
29	Bloomington Side Road	Ontario	——	Pt	7.6	0.0[pad=3.0	4-10	250-1100	19	3:1	3.5	——	5.2	——	2.5	3	n.r./r	0	2 brands used	30	1-2.5	30	5,108,110,111
30	Embankment	Sweden	1974	C	12	——	1-15	——	25	——	5.2	——	2.0	——	1.4	——	r	0	——	——	2.4	——	13
31	Obetsu, Hokkaido	Japan	——	Pt,Z	35	——	——	——	42	——	8.5	3.5 *	——	——	1.2	——	n.r	——	——	——	——	0	152
32	National harbor	Finland	1982	C	40	+1.0[pad=2.5	3-25	30-220	50	——	——	——	——	——	1.2	——	n	0.04,32	3 brands used	——	——	——	119
33	North area	Alberta	——	Pt	5	0	17	420	21	4:1	2.0	——	2.1	——	4.1	C	n	0	Fornassiner R11S	——	——	——	23
34	Musselburgh bypass	England	——	C,M,S	6	(-1.5)-1.0	——	11-25	39	2:1	15.0	——	——	——	9.9	1.0	——	30	Tensar SS2 & SR2	——	——	3	56
35	Greater Yarmouth bypass	England	1983	C,S,Org	22	——	——	——	——	1.75:1	7.5	——	——	——	5.6	——	——	30	Tensar SS1 & SS2	——	——	3	201
36	Champlain Clay Emb. 2	Quebec	1984	C	9.5	-0.3	13-25	60-100	12	1.5:1	6.0 *	5.1 *	7.2	6.1	1.4	1	n.r./r	30	Tensar SR2	6.4-9.1	2	——	24
37	Champlain Clay Emb. 3	Quebec	1984	C	9.5	-0.3	18-25	60-100	15	1.5:1	6.5 *	5.1 *	5.4	6.1	1.6	1	n.r./r	30	Tensar SR2	19	3.4	——	24
38	Trunk Hwy 53	Minnesota	1976	Pt	4.6	——	——	400-500	29	3:1-4:1	2.4	2.4	——	——	4.3	1	n.r	——	Burlington Glass	——	——	0.32,41	123
39	Noderbrotdiden-Berg	Netherlands	——	Pt	4	——	——	——	——	1.4:1	1.5	——	——	——	——	1	——	0	——	——	1.0	0	204
40	South area	Alberta	——	Pt	3	0	10-25	310	18	4:1	2.0	——	2.4	——	4.0	1	n	0	Fornassiner R11S	——	——	0	23

LEGEND: See next page.

Table 2.2
Continued.

LEGEND:

SOIL TYPE
C = clay
Fd = dredged fill
M = silt
Org = organic soil
Pt = peat
S = sand

MAX. THICK.
maximum thickness of soft foundation soil (H_s)

DEPTH TO WT
depth to water table
+ = site submerged under depth of water indicated
- = depth to water table below ground surface
** = site subjected to tidal inundation

s_u / c_u = undrained foundation strength

WIDTH AT MID HT.
width measured at mid-height of embankment (B)

HEIGHT (H)
height of reinforced embankment and comparison unreinforced embankment, if constructed
* = embankment failed at height shown

$\gamma H/c$
bearing capacity factor (N_c)
γ = unit weight of fill; assumed to be 18 kN/m^3

FILL MATERIAL
C = clay
G = gravel
M = silt
R = rockfill
S = sand

INSTRUMENTATION
a = settlement
b = foundation pore pressure
r = reinforcement strain
d = horizontal movement
e = vertical earth pressure

REINFORCEMENT TYPE
GG = geogrid
NW = nonwoven geotextile
SM = steel mesh
W = woven geotextile

TENSILE FORCE & STRAIN
tensile force & strain measured or calculated in reinforcement

OTHER SPECIAL MEASURES
B = stabilizing berms
D = sand or wick drains
LF = light weight fill
P = supported by piles
SC = staged construction
W = embankment widening

constructed. For some cases, particularly those using light weight nonwoven geotextiles, the fabric functioned mainly to separate the fill and foundation soils and the reinforcing effect was small. These cases are included to illustrate the behavior observed for a full range of embankment heights and reinforcement properties. In the last section, relations between the observed height of reinforced embankments at failure and foundation shear strength and between the bearing capacity factor and normalized embankment width are examined and compared to available bearing capacity theories.

2.4.2 Embankments Reinforced with Nonwoven Geotextiles

Case histories from seven embankments reinforced with low modulus, nonwoven geotextiles were reviewed. The first is a low (1.4 m high) haul road embankment on a peat foundation described by Greenway and Bell (1976) and Bell, et al. (1977) [Case 1]*. Reinforced and unreinforced sections were constructed. They reported that the reinforcement reduced heave in front of the advancing fill and reduced intrusion of the fill into the foundation. This resulted in a 28% savings in fill volume. A double fabric thickness did not cause further improvement in embankment behavior. Fabric strains were less than 5% when measured three days after

---

* Refers to case history reference number in Table 2.2.

construction but had increased to greater than 50% when measured three months later. A finite element analysis of this embankment was made by Boutrup and Holtz (1982,1983).

A low fill constructed for a haul road using seven brands of nonwoven geotextile was described by Steward, et al. (1977) [Case 2]. Two sections were constructed with each fabric and there were unreinforced control sections. The foundation shear strength was not given but its CBR was less than 0.1. Settlement occurred rapidly and had magnitudes up to 0.15 m; however, no strain was measured in the fabric.

A 1-m high test fill founded on 0.6 m of peat overlying loose sands and soft clays was described by Cragg (1980) [Case 3]. The section reinforced with a nonwoven geotextile was successfully constructed however an unreinforced section failed. Cragg (1980) estimated that use of reinforcement was 20% cheaper than removal of the soft soils.

A test embankment on a peat foundation was constructed as part of a highway project in Africa (Belloni and Sembenelli, 1977) [Case 4]. Geotextile reinforcement and wide stabilizing berms were employed. They reported that the reinforcement reduced lateral spreading, pore pressure buildup in the foundation, and long term settlement. The

last observation is contrary to the findings of most other investigators.

An embankment on 13-17 m of compressible soils was described by Olivera (1982) [Case 5]. The fill height in Table 2.2 includes a 1 m surcharge. A test section with a nonwoven fabric placed at its base showed less heave at the toe of the embankment and less differential settlement than a similar unreinforced section. Furthermore, intrusion of the fill into the foundation was reduced resulting in a 50% savings in fill volume. However, the geotextile had no effect on time dependent settlement. The fill was placed working outward from the centerline.

Two cases of unsatisfactory embankment performance were reported by Fowler and Haliburton (1980). The first was a 1.5-m high embankment constructed in Brunswick, Georgia [Case 6]. The fabric was unrolled parallel to the axis of the embankment and overlapped 1 m at the joints. The embankment failed due to lateral spreading which apparently pulled the fabric apart at the overlaps. The second was located at Swan Lake, Mississippi [Case 7]. The embankment spread laterally 12 hours after construction was completed. Subsequent investigations showed that 2.5 m of settlement had occurred and that the fabric had stretched 36% but had not ruptured. They concluded that the fabric modulus was

too low. Fabric that was folded over the first lift of fill at the toe of the slope was not tensioned.

2.4.3 Embankments Reinforced with Woven Geotextiles

One of the first uses of a strong, high modulus reinforcement placed at the base of an embankment was reported by Kerisel (1973; see also Jewell, 1982) [Case 8]. The reinforcement was a steel mesh that also protected sand drains in the foundation from a dumped rockfill. Slips occurred in some areas which were then reinforced with two additional layers of mesh.

Woven geotextiles were successfully used to carry the lateral forces imposed by highway embankments supported on piles [Case 9]. The foundation soil was sensitive clay. Holtz (1975) and Holtz and Massarsch (1976) discussed the measurements made at these sites. Reinforcement appeared to reduce horizontal movements.

A series of test embankments reinforced with woven geotextiles were constructed in the Netherlands. Most of the embankments were well instrumented and had companion unreinforced sections. The first was built near Zevenhoven in 1974 (Van Leeuwen and Volman, 1976) [Case 10]. Reinforced and unreinforced embankments were constructed to a height of 3 m directly on the grass covered ground surface. The

reinforced embankment settled more than the unreinforced section but neither showed any signs of instability. It was concluded that the root mat provided significant reinforcement.

A second pair of embankments were constructed at the Zevenhoven site the following year (Volman, et al., 1977; Van Leeuwen and Volman, 1976) [Case 11]. Based on experience from the first trial, the root mat was removed prior to fill placement. Reinforced and unreinforced embankments failed at heights of 4.5 m and 3.5 m, respectively. Again settlement was greater for the reinforced embankment. Geotextile strains varied from 10-15% beneath the centerline to only a few percent under the toe. Brakel, et al. (1982) calculated that the reinforcement increased the safety factor by only 5-10% compared to a 29% increase observed in the field trial.

A pair of 8-m high test embankments were built using staged construction near Mulderberg, Netherlands (Volman, et al., 1977) [Case 12]. More settlement was observed in the unreinforced section. Fabric strains were less than 10% and may even have been less than 2%. These low values were attributed to the flat side slopes.

Several test sections incorporating six different woven and nonwoven fabrics and an unreinforced control section were constructed near Harmelen, Netherlands in 1976 (Brakel, et al., 1982) [Case 13]. It was planned to raise the embankment to 2.5 m in one step, however, this resulted in loss of stability. No significant difference was observed between reinforced and unreinforced sections. Fowler (1982) gives a more detailed discussion of one of these embankments [Case 14] reinforced with a woven fabric which failed at a height of 2.5 m. The fabric strain was 20% measured at a point not located on the failure surface. The torn fabric was observed to be tangent to the slip surface in an excavation made after the failure.

A well documented case history located near Almere, Netherlands was described by Brakel, et al. (1982) [Case 15]. Companion embankments, one reinforced using a high strength woven fabric (tensile strength of about 200 kN/m) and the other unreinforced, failed at heights of 4.8 m and 3.8 m, respectively. The heights include a 2-m deep ditch excavated at the embankment toe. An excavation into the failed embankment showed that the reinforcement had torn.

Brakel, et al. (1982) gives a brief description of a test embankment located near Cuxhaven, West Germany

[Case 16]. The small force in the geotextile was attributed to low construction pore pressures and flat side slopes.

A woven geotextile was used to reinforce two embankments founded on soft organic soils (Quast, 1983) [Cases 17 and 18]. Wick drains were employed to speed consolidation of the foundation. The rate of load take-up in the fabric increased with the applied load. Fabric strains generally increased with time and a maximum value of 4.5% occurred at the embankment centerline. Horizontal displacements were small and no heave was observed at the embankment toe.

One of the first well documented cases in the United States of an embankment reinforced with a woven geotextile was the Pinto Pass test section (Haliburton, et al., 1978; Fowler and Haliburton, 1980; Fowler, 1981; Fowler, 1982) [Case 19]. Four brands of woven fabric were used: Nicolon 66475, Nicolon 66186, Polyfilter X and Advance Type 1. A typical cross section and construction sequence is shown in Fig. 2.10. The leading edge of the fill was maintained in a "U-shape" with the mouth of the U pointing outward and fill placement proceeded from the outside edges working inward. The outside edges were kept higher than the center. This was believed to keep the fabric in tension, making better use of the fabric's tensile strength and resulting in greater reinforcement. The final embankment height was

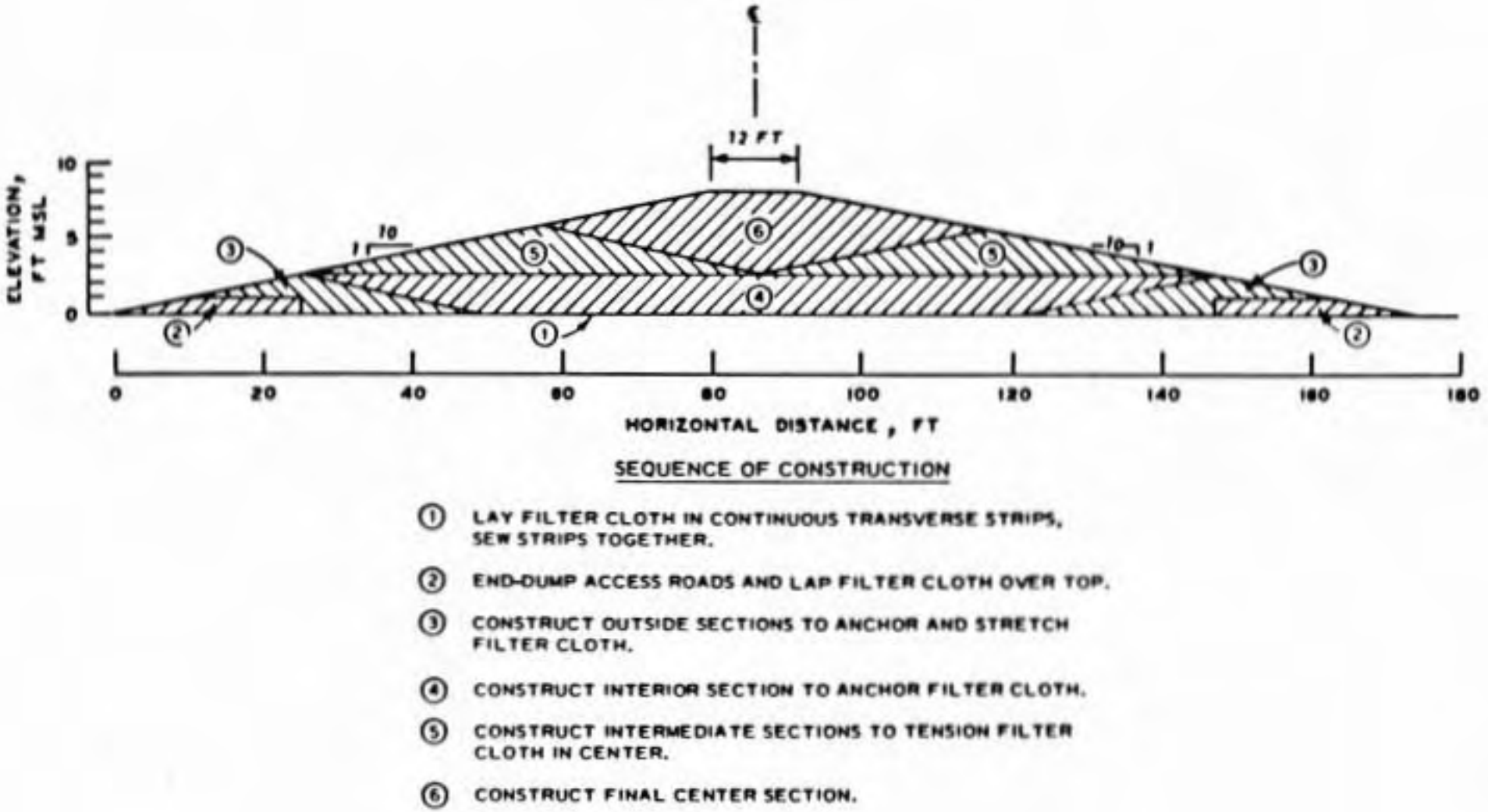

Figure 2.10 Cross section and construction sequence for Pinto Pass [Case 19] (Fowler, 1981).

about 2.1 m. Fabric folded over the first lift of fill at the embankment toe was observed to be untensioned. The reinforcement maintained stability even though the safety factor based on classical bearing capacity theory (Terzaghi and Peck, 1967) was 0.4 to 0.6. Rowe (1982) presented a finite element analysis of the embankment.

Reinforcement was used in conjunction with wick drains, light weight fill and staged construction to build a test fill and an approach embankment on San Francisco Bay mud for the Dumbarton Bridge (Hannon, 1982; Hannon and Walsh, 1982) [Cases 20 and 21, respectively]. They were designed to have an after settlement height of 3.7 m. Both woven and nonwoven fabrics were used in the test fill but a woven fabric was chosen for the main embankment. A sample of fabric excavated from the test fill one year after construction showed no loss of strength. It was estimated that the fabric increased the safety factor for slope stability by 10%. The failure of one portion of a retaining dike was attributed to an excessive fill placement rate. It was speculated that the geotextile failed at a sewn longitudinal seam.

Test embankments were constructed on very soft dredged fill at the Craney Island Disposal Area (Fowler, 1985). Two reinforced sections, one on an area with a dried crust

[Case 22] and the other with no crust [Case 23], were constructed to the design height of 3.4 m but a third section on very soft fill with no crust [Case 24] failed at a height of 2.4 m. Previous attempts to construct unreinforced embankments had been unsuccessful.

Woven fabric was used to reinforce an embankment constructed on peat for a new taxiway at the Duluth International Airport (Gale and Henderson, 1984) [Case 25]. Fig. 2.11 shows a typical cross section. The fabric was pretensioned prior to fill placement to eliminate wrinkles. It was pulled taut by hand and then weighted down with pieces of rock. The rocks were removed as the first lift of fill was placed (S. Gale, 1986, personal communication). A 1.8 m surcharge was added to reduce the time required for consolidation and is included in the fill height in Table 2.2. Performance was satisfactory even though excess pore pressures were high and about 1 m of settlement occurred.

Test fills founded on fibrous peat were built at two sites in northern Ontario (Lupien, et al., 1983) [Cases 26 and 27]. Additional soil properties are given in Lefebvre, et al. (1984) and Lupien, et al. (1981). The fill material was a wet till composed of silty sand with some gravel. High foundation pore pressures were transmitted to the fill causing loss of strength at unreinforced sections of the

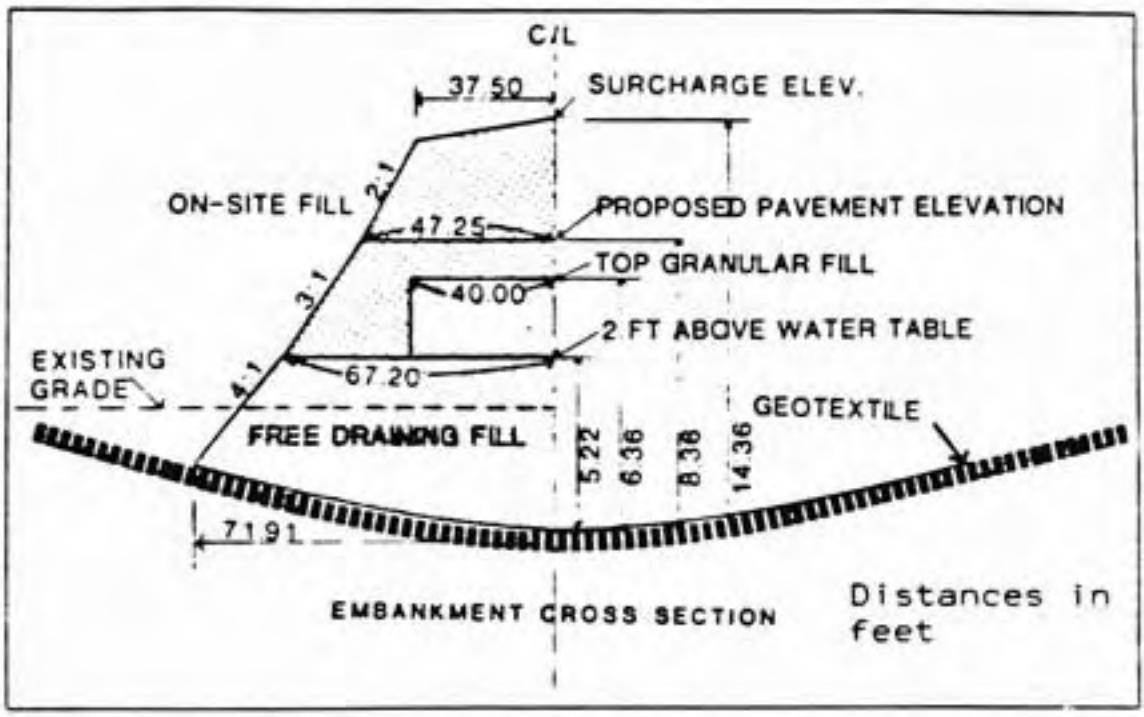

Figure 2.11 Cross section of taxiway, showing geotextile in place, Duluth International Airport [Case 25].

NBR-3 site. These sections were excavated and reinforced with geotextile placed at the mid-height of the embankment. Significant lateral displacement and heave were observed at the NBR-2 site for both the reinforced and unreinforced sections. It was assumed that the geotextile failed since strains of 40-65% were inferred which were well in excess of the fabric's elongation at break of about 20%. The NBR-3 site had a stronger foundation and similar problems were not observed.

A low embankment on peat located near Manchester, Ontario was reinforced with two brands of woven and two brands of nonwoven geotextile (Barsvary, et al., 1982; Cragg, 1980) [Case 28]. All the fabrics performed well and effectively separated the foundation soil from the fill. The reinforcing effect may have been small. Fabric strains peaked a few days after construction and then decreased with time. Geotextile samples taken one year after construction had lost 25 to 36% of their strength.

A highway embankment for Bloomington Side Road was built using staged construction with two brands of woven fabric (Barsvary, et al., 1982; Rowe, 1984; Rowe, et al., 1984a, 1984b) [Case 29]. The fabric was placed on a gravel working pad that was up to 1 m thick. The embankment was well instrumented as shown in Fig. 2.12. The reinforcement

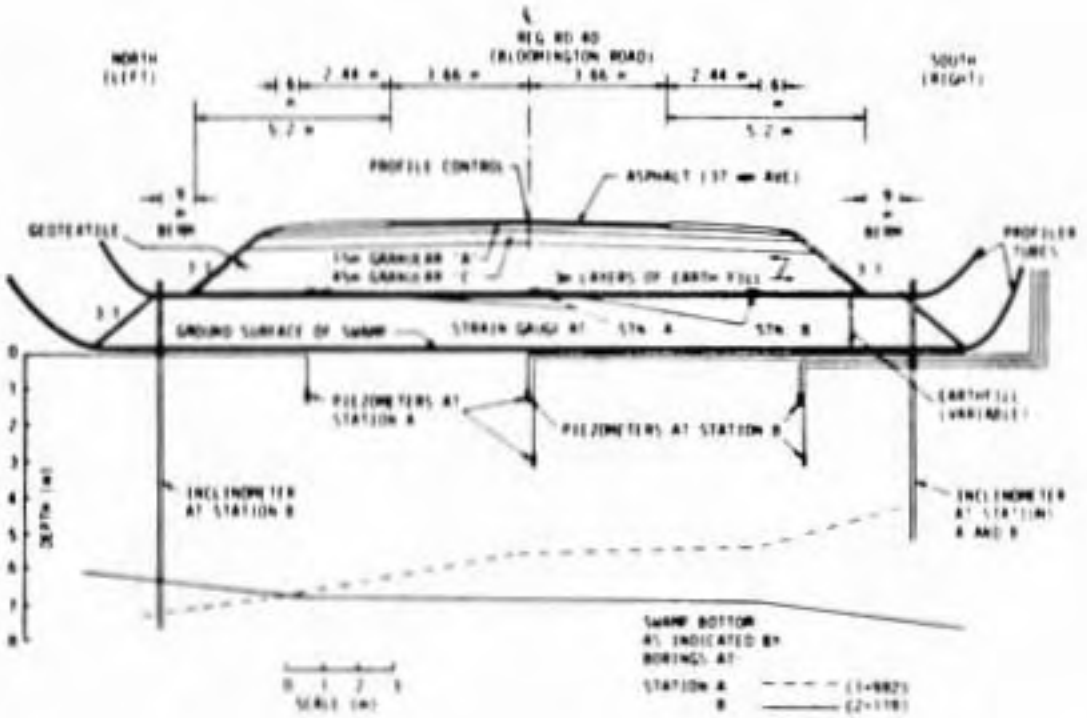

Figure 2.12 Cross section of Bloomington Side Road embankment (Case 29) (Rowe, et al., 1984a).

appeared to have little effect since: (1) large settlements and lateral deformations were observed; and (2) mud waves and tension cracks developed at the edge of the fill. The foundation had gained little strength 60 days after the end of the first stage of construction and geotextile strains decreased with time. The geotextile at the edge of the embankment appeared to be unstressed so anchoring the fabric by folding it back over the first lift of fill was unnecessary for this case.

A short description of a 1.2 m high embankment reinforced with two layers of woven fabric was given by Bjerin (1977) [Case 30]. The embankment successfully carried 700 ton vehicle loads.

Ohta, et al. (1980) reported a field trial conducted in Japan [Case 31]. An embankment with no reinforcement or foundation treatment failed at a height of 3.5 m. A similar embankment with reinforcement and sand drains in the foundation was completed to a height of 8.5 m. The sand drains probably accounted for the majority of the increase in height.

Several reinforced test sections built in Helsinki, Finland were briefly described by Lahtinen (1983) [Case 32]. Total and differential settlements were less for sections

reinforced with woven fabrics and geogrids than for a similar section with a low modulus nonwoven fabric. The observation of lower total settlement is contrary to the findings of many other investigators.

Geotextile reinforcement was used to construct an embankment on peat in northeast Alberta (Burwash, 1980) [Case 33]. It was designed to have a final height of 2 m and an extra 1 m of fill was added to account for expected settlement. Construction was scheduled for winter to minimize disturbance to the root mat. Geotextiles were used to reinforce the shoulders for widening of a nearby existing embankment [Case 40] as discussed in Section 2.4.5.

2.4.4 Embankments Reinforced with Geogrid Mattress

A recent innovation is to construct a geogrid mattress by forming cells with vertical strips of geogrid and then filling the cells with granular soil. This results in a composite material that has flexural stiffness. Edgar (1984) reported that a 1-m thick mattress was used to reinforce a 15-m high embankment founded on 6 m of soft alluvial soil [Case 34]. Wick drains were installed in the foundation to speed consolidation.

A mattress consisting of a layer of granular fill encapsulated with geogrid was described by Williams (1984)

[Case 35]. Ditches lined with geogrid and filled with granular soil were constructed beneath the toe of the embankment to provide additional resistance against lateral spreading. Wick drains were also used. Williams (1984) states that the embankment was still under construction but that initial performance was encouraging.

Three instrumented test embankments were constructed to failure at a test site near St. Alban, Quebec (Busbridge, et al., 1985). The foundation has a 1.5-m thick weathered clay crust underlain by soft sensitive marine clay with a minimum strength of about 10 kPa. One embankment was reinforced with two horizontal layers of geogrid [Case 36], the second was reinforced with a geocell mattress consisting of cells of geogrid filled with sand [Case 37] and the third was an unreinforced control section. The embankments failed at the heights shown in Table 2.2. The authors point out the importance of crust strength on observed failure heights. The horizontal reinforcement was calculated to increase the failure height by 34 percent while the geocell allowed a 17.5 percent increase. They concluded that horizontal reinforcement was more effective than the geocell mattress for the conditions at the side. Reinforcement had little effect on pore pressures or lateral strains in the foundation.

2.4.5 Geotextiles used for Embankment Widening

Geotextiles have been employed in three cases to reinforce the shoulders for widening of existing embankments. The first case was reported by Lukanen and Teig (1976) [Case 38]. An existing 2.4-m high embankment with a 7.3 m crest width which had been placed directly on a peat foundation was widened to 14.3 m. A total of nine test sections using different combinations of lightweight fill, reinforcement and conventional staged construction were built. There was a "full width fabric" section where fabric was placed across the full embankment width (Fig. 2.13) and a "ditch fabric" section where reinforcement was placed only under the widened portion of the embankment (Fig. 2.14). In all sections light weight fill (wood chips) was used to fill a ditch at the toe of the existing embankment. Strains beneath the pavement of the widened roadway were measured beginning after construction was substantially complete. Strains at the outside edge of the pavement were less than for other sections for both fabric reinforced sections but were greater between the centerline and pavement edge for the full width fabric section. Very little longitudinal cracking was observed in the ditch fabric section compared with numerous cracks which developed with time for the full width fabric and conventional staged construction sections. This may indicate that the fabric modified time dependent deformations.

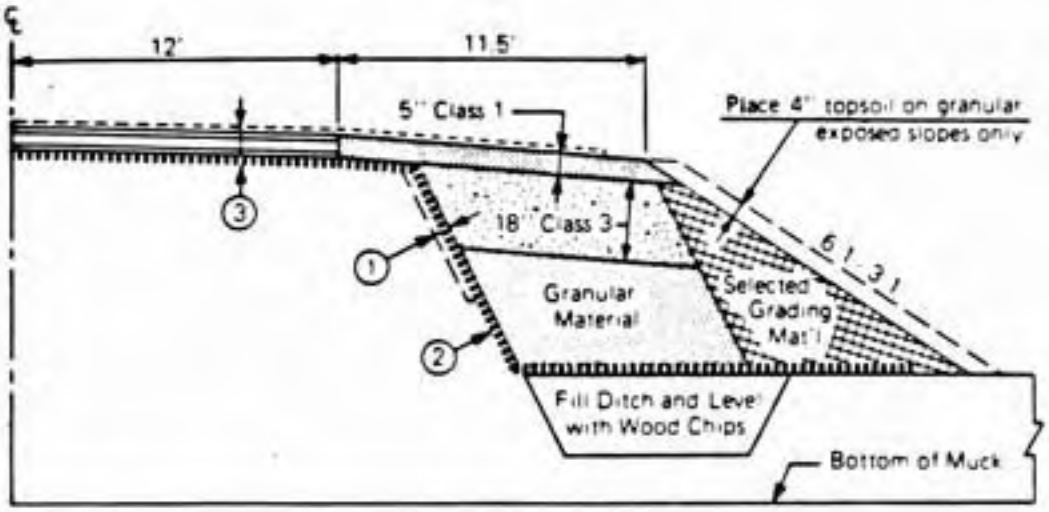

① Remove the upper 4" of soil from the inp. inslope to 2.5' below shoulder.

② Center 60' rolls of fabric on ℄ and place over inp. road and ground rt. and lt. Place 1" of bituminous on traffic lane and proceed with embankment.

③

1-1/2"	2341 Bit. Wearing Course (Future)
	Tack Coat (Future)
1-1/2"	2341 Bit. Wearing Course
	Tack Coat
2-1/2"	2331 Bit. Leveling Course
	Tack Coat
1"	2331 Bit. Leveling Course
	Fabric ②
	Tack Coat

Figure 2.13 Roadway widening - fabric (full width) section (Lukanen and Teig, 1976).

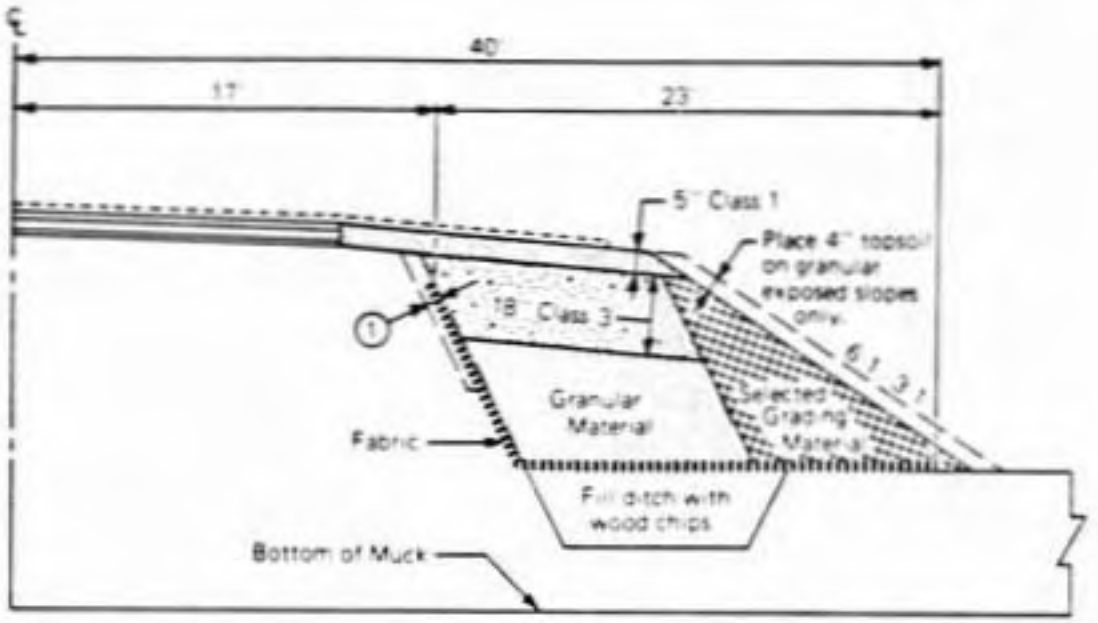

(1) Remove the upper 4" of soil from the inp. inslope to 2.5' below shoulder.

Figure 2.14 Roadway widening - fabric (ditch) section (Lukanen and Teig, 1976).

An application of geotextiles to roadway widening in the Netherlands was described by Volman, et al. (1977) [Case 39]. Fabric was placed across the width of the existing embankment and beneath the widened section. It was then folded back over the outside of the new fill. Fabric strains measured 6 months after construction were less than 10%.

An existing 1-m high embankment was widened and raised to an after settlement height of 2 m (Burwash, 1980) [Case 40]. To account for expected settlement 1 m of additional fill was added. Geotextile was placed beneath the widened shoulders. Construction was scheduled for winter to minimize disturbance to the root mat. Another embankment was constructed in a previously undeveloped area [Case 33].

2.4.6 Summary of Case Histories

The cases had several common characteristics. Foundation materials were usually soft organic soils of limited thickness underlain by a stronger layer (Table 2.2). Reinforcement probably has the greatest effect when the undrained foundation strength is less than about 15 kPa or 300 psf (Milligan, 1985). The lower bound strength for most of the cases in Table 2.2 is below this value. Many investigators pointed out the importance of root mat and dried crust strength on embankment stability (Van Leeuwen and

Volman, 1976; Burwash, 1980; Rowe, 1984; Busbridge, et al., 1985).

The embankments were typically constructed of granular soils ranging from sand to rockfill. Finer grained soils such as clay and glacial till were used in four cases [Cases 5, 7, 28 and 33]. Embankment heights up to 15 m were reported and side slopes ranged from 1h:1v to 10h:1v (Table 2.2). Special construction techniques and high strength reinforcement were generally required for the higher embankments. Geotextile reinforcement also provided a separating effect, thereby reducing intrusion of fill into the foundation soils. Several of the embankments were instrumented as shown in Table 2.2.

Fill placement techniques varied. For Case 19, fill was placed starting at the outside edge and then working inward. This is recommended to fully mobilize fabric tension when the foundation soils are very soft (CBR<0.5) and a mud wave forms at the edges of the advancing fill (Fowler and Hallburton, 1980; Christopher and Holtz, 1984). For stronger foundations (CBR>1) fill placement that proceeds from the center and progresses outward has been successful (Christopher and Holtz, 1984). Even though the foundation soils were soft, the later procedure was used for Case 5 and may have contributed to the large observed settlements. For

Case 25, the fabric was pretensioned prior to fill placement to eliminate wrinkles. It was pulled taut by hand and then weighted down with pieces of rock. The rocks were removed as the first lift of fill was placed (S. Gale, 1986, personal communication). In some cases a working pad of granular soil was spread on the ground surface before the reinforcement was placed. The effectiveness of the reinforcement may be reduced if the working pad is thick (Boutrup and Holtz, 1982; Rowe, et al., 1984b).

Reinforcement types included nonwoven and woven geotextiles, geogrids and steel mesh (Table 2.2). There is no clear indication that one type performs better; however, recent cases use strong high-modulus reinforcement, especially when the foundation soils are very soft. Cases 34 and 37 used a geocell mattress consisting of cells formed with vertical strips of geogrid backfilled with granular soil.

Geotextile strains were generally less than 20% but were 36% for Case 7 and greater than 50% for Case 1 (Table 2.2). For Case 2, zero strain was measured in the fabric even though 0.15 m of settlement occurred. Geotextile strains have been observed to both increase [Cases 1, 17, and 18] and to decrease [Cases 28 and 29] with time after the end of construction. This might be because there are

two opposing factors: (1) consolidation of the foundation which tends to cause movement of the base of the embankment toward the centerline and strains to decrease, and (2) lateral creep of the foundation which has the opposite effect (R. K. Rowe, 1984, personal communication). Observed behavior depends on which factor dominates. In contrast, Bell, et al. (1977) feel that time dependent settlement may increase fabric strain. In Cases 7, 19, and 29 the reinforcement was folded back over the fill at the embankment toe; however, it was observed to remain untensioned.

The strength of geotextile samples excavated some time after construction from embankments reported herein [Cases 20, 21, and 28] and from other applications (Christopher, 1983; Hoffman and Turgeon, 1983) were found to be 0-50% less than their original strength. It is not possible to correlate strength loss with in situ conditions.

Reinforcement has been shown theoretically to reduce differential settlement and lateral spreading of the embankment (Boutrup and Holtz, 1982, 1983; Rowe, 1982) and these effects were reported for Cases 4 and 5. Reinforcement may also reduce total settlement at the end of construction. In Cases 10 and 11 settlement of the reinforced embankment was greater than the companion unreinforced section.

Reinforcement generally has little or no effect on time dependent settlement but it was reportedly reduced for Cases 4 and 32. Based on finite element analyses (Rowe, et al., 1984b), lateral strains in the foundation soils are expected to be less for reinforced embankments, however, this was not observed for Cases 36 and 37. Reinforcement had no effect on foundation pore pressures for Cases 36 and 37.

To maintain an acceptable safety factor it was often necessary to combine reinforcement with other techniques including staged construction, light weight fill or berms as summarized in Table 2.2. Vertical wick drains or sand drains were sometimes installed to increase the rate of consolidation and strength gain of the foundation (Table 2.2). In a few cases a surcharge load was applied to reduce the time required for consolidation. The vertical load was carried by piles for Case 9. Reinforcement was used for widening and raising the grade of existing embankments in three cases [Cases 38, 39, and 40].

Three causes were reported for the reinforced embankments which failed: (1) the reinforcement modulus was too low, allowing excessive deformations to occur [Case 7]; (2) tensile failure of the reinforcement leading to slope failure or excessive deformations [Cases 13, 15, 26, 36, and

37]; and (3) geotextiles pulling apart at a joint or sewn seam causing excessive deformations [Cases 6 and 21].

2.4.7 Effect of Reinforcement on Stability

Reinforcement increases the stability of embankments constructed on soft ground; however the amount of improvement is subject to debate. There are four cases in Table 2.2 where both a reinforced and an unreinforced embankment were constructed to failure and other special measures such as staged construction or sand drains were not used [Cases 11, 15, 36, and 37]. For Case 22 only the unreinforced embankment was constructed to failure. In Cases 11, 15, 22, and 36 the reinforced embankments were constructed 0.9-2 m higher than the companion unreinforced embankments. This corresponds to a 18%-110% increase in height. For Case 37 the reinforced embankment failed at a lower height than the unreinforced embankment but Busbridge, et al. (1985) noted the importance of variations in crust strength on the failure heights. Reinforcement appeared to have no effect on stability for Case 13. Possible explanations for this are open for discussion.

The calculated increase in safety factor for slope stability ranged from 5 to 34% for Cases 14, 24, 36, and 37. Finite element analyses also indicate that reinforcement is effective for low strength soils. Boutrup and Holtz (1982,

1983) calculated that reinforcing an embankment on soft soil with an undrained strength of 7.5 kPa caused up to a 13% reduction in the shear stress in the foundation. Analyses by McCarron (1985) showed that reinforcement increased the embankment height at failure by 15% for a foundation with a crust strength of 6.5 kPa but that there was only a 7% increase for a crust strength of 12.5 kPa.

In the next few sections the relations between the foundation shear strength and the embankment height, and between the bearing capacity factor and normalized embankment width are examined and compared to available bearing capacity theories. The embankment widening cases [Cases 38, 39, and 40] are not included in the comparisons.

2.4.7.1 Relation between embankment height and foundation strength. Embankment height is plotted against average foundation strength for stable and failed embankments in Fig. 2.15. A more detailed assessment of the foundation strength is desirable but is not possible with the data available for most cases. Also shown in Fig. 2.15 is the height at failure calculated using classical bearing capacity theory for a strip footing on clay (Eq. 2.11) using a unit weight of fill γ_{emb} = 18 kN/m^3 (plotted as 'line a'). It closely approximates the observed height at failure for three unreinforced embankments. The stable unreinforced

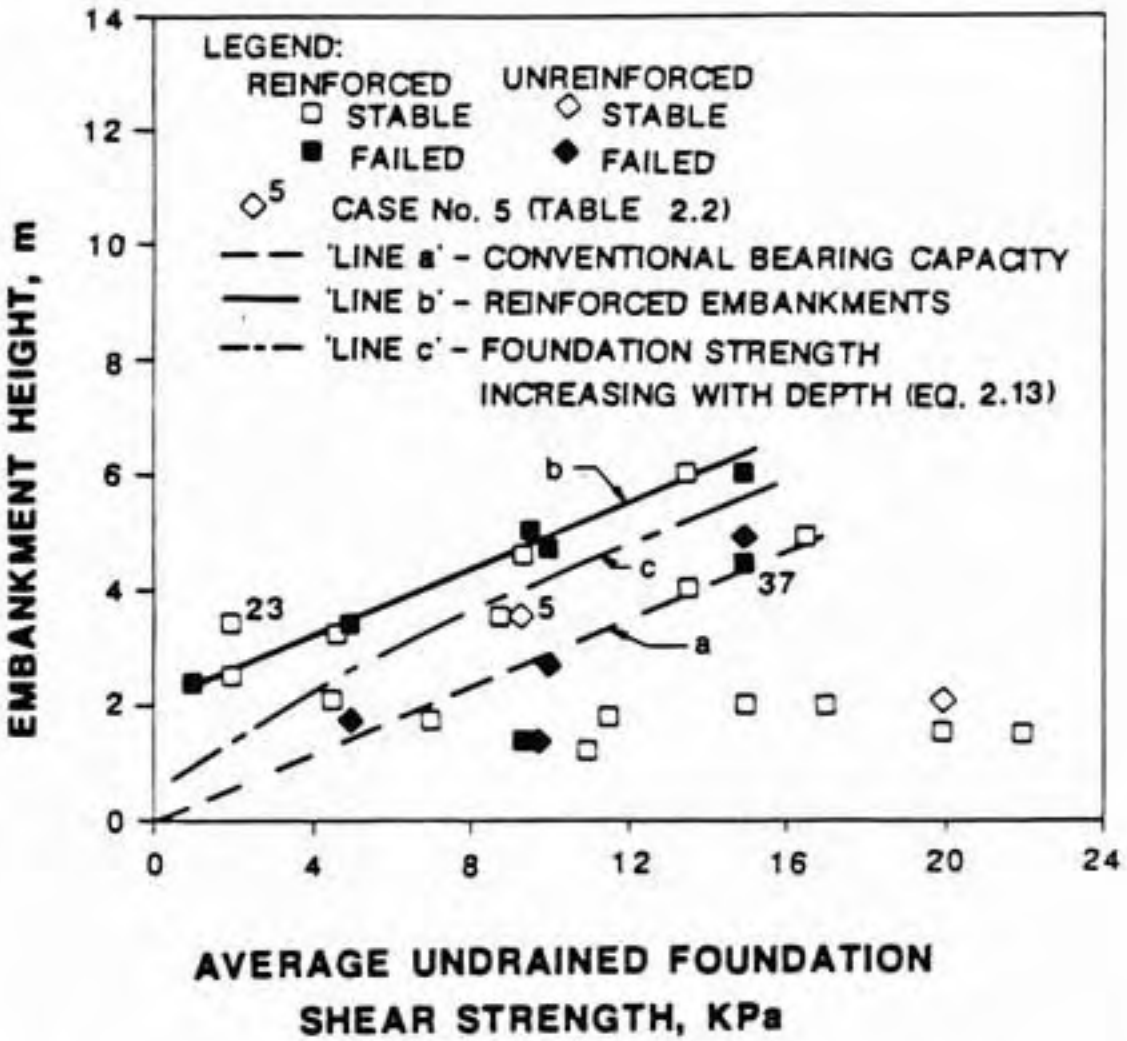

Figure 2.15 Reinforced and unreinforced embankment height vs. undrained shear strength of the foundation for the cases in Table 2.2.

embankments plot below 'line a' except for Case 5. This case did not exhibit a slope failure but settlement of the fill into the foundation was excessive and much of the soft peat foundation soils were displaced indicating that the bearing capacity was surely exceeded.

Five reinforced embankments which failed fall on a straight line shown as 'line b' on Fig. 2.15. One failed reinforced embankment (Case 37) plots below this line. Stable reinforced embankments plot on or below this line except for Case 23. Although line b is based on a limited number of data points, it appears to indicate that reinforced embankments can under some circumstances be constructed up to 2 m higher than predicted by conventional bearing capacity theory. This suggests that the increase in height is independent of c_u but the percent increase in height is greater for smaller c_u. The reason for the increase may be that the reinforcement enhances the beneficial effect that the following factors have on bearing capacity: (1) limited thickness of the soft foundation soils, (2) increase in strength with depth of the soft foundation soils, (3) strength of the dried surface crust, (4) flat side slopes, and (5) dissipation of excess pore water pressures during construction and the resulting increase in strength of the foundation soils (e.g. Leroueil, et al., 1978). It seems logical that high

modulus reinforcement would have a greater benefit but there is insufficient data to confirm this.

2.4.7.2 Effect of increasing strength with depth. The possible increase in bearing capacity due to increasing foundation strength with depth was investigated using Eq. 2.13. This equation is shown on Fig. 2.15 as 'line c' for γ_{emb} = 18 kN/m^3, γ'_{fnd} = 7 kN/m^3 (for water table at ground surface), c_u/σ'_{vo} = 0.22 (Mesri, 1975), B = 10 m and F from Davis and Booker (1973) for a footing with a rough base which accounts for the shearing resistance at the foundation-reinforcement interface. For the assumed parameters, an increase in strength with depth accounts for about 25% (for c_u = 15 kPa) to 160% (for c_u = 2 kPa) of the difference between the observed height at failure and that calculated with classical bearing capacity theory.

2.4.7.3 Relation between bearing capacity factor and normalized embankment width. The relation between the bearing capacity factor N_c as given by Eq. 2.23 and the normalized embankment width (Eq. 2.16) is shown in Fig. 2.16. The embankment was represented by a uniform applied stress of γH_f and width B measured at the mid-height of the embankment. The resulting vertical force is the same as applied by the embankment.

$$N_c = \gamma H_f / c_u \qquad (2.23)$$

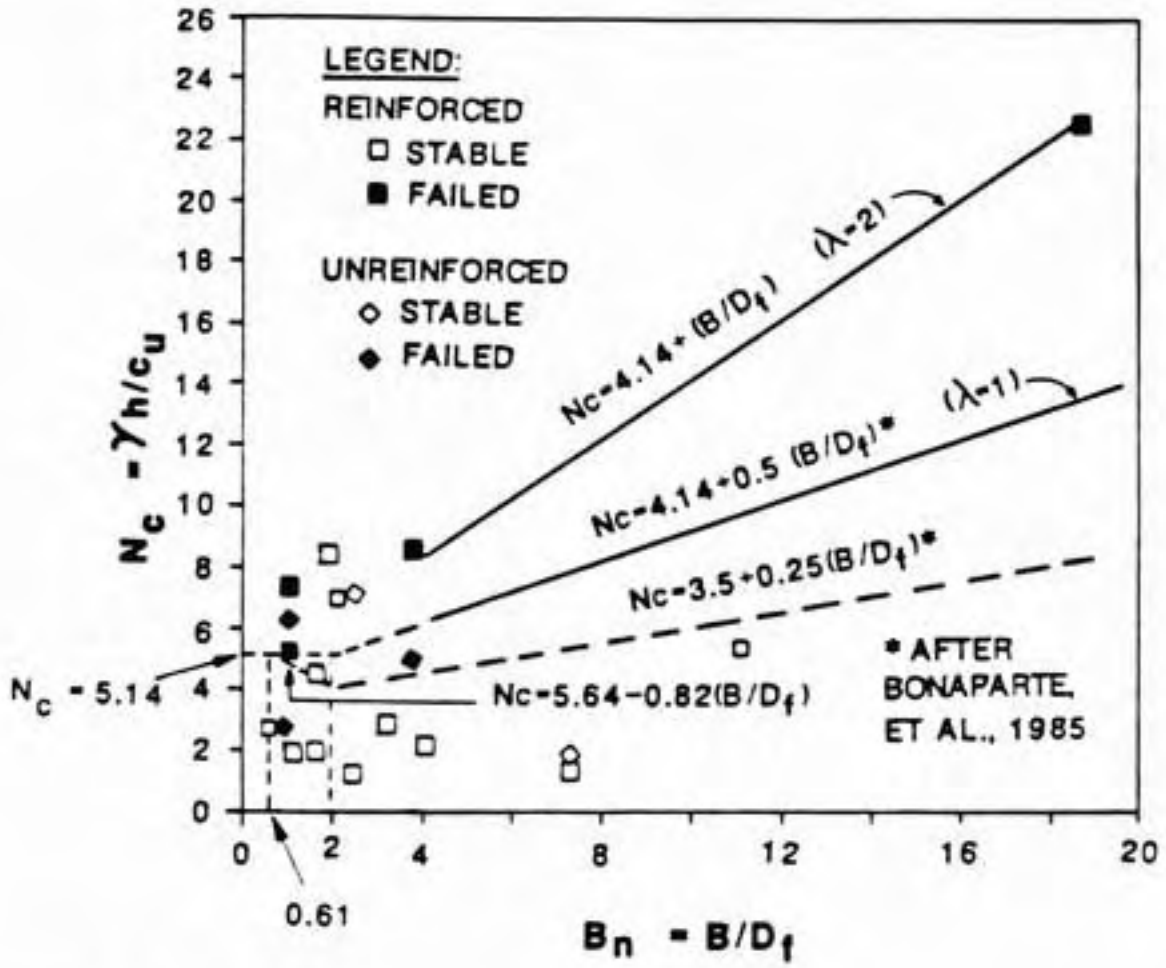

Figure 2.16 Relation between bearing capacity factor and normalized embankment width.

Only four cases of failed reinforced embankments [Cases 17, 18, 36, and 37] have sufficient data to be plotted.

Note that the data from Cases 26 and 27 involving fibrous peat foundations are not included in Figs. 2.15 and 2.16. The reported foundation shear strengths are felt to be unreliable since they were measured with a field vane which can give erroneous results when used in such soils (Landva, 1980).

2.4.7.4 Effect of limited thickness of soft soils. The effect of a limited thickness of soft foundation soils on the calculated bearing capacity factor was investigated using Eq. 2.15 for the bearing capacity factor at the embankment centerline. Eq. 2.15 is plotted on Fig. 2.16 for λ=1 and λ=2. The line with λ=2 agrees well with two failed reinforced embankments with $B_n > 4$ and accounts for the shearing resistance developed at the foundation-geotextile interface. The line with λ=1 neglects the shearing resistance at the interface and plots below the observed failures. A relation proposed by Giroud, et al. (1973) is also shown but it greatly underestimates the observed N_c. It is cautioned that these observations are based on only two cases and the reliability of the shear strength data is not known.

There are two cases with B_n of 1.3 and 1.6 and three other cases where the actual B_n is unknown but is likely to be less than 2 [Cases 7, 20 and 24]. They had N_c ranging from 5.4 to 43.2. It is likely that N_c based on average foundation strength is not a reliable index of reinforced embankment stability for thick foundations.

2.4.8 Conclusions

The data from the 40 cases summarized above can be used as a guide for preliminary designs and as a basis of comparison for new analysis techniques. They are summarized in a concise format to allow easy identification of cases most pertinent to a particular problem.

The cases had several common characteristics. Foundation materials were typically soft organic soils with a shear strength of less than 15 kPa underlain by a stronger layer. In many cases it was necessary to combine reinforcement with other special measures such as wick or sand drains, staged construction or berms to maintain an acceptable safety factor. Reinforced embankments were observed to fail by excessive elongation of low modulus reinforcement, tensile failure of the reinforcement, and pulling apart of joints or sewn seams between strips of reinforcement. Reinforcement was used for widening and raising the grade of existing embankments in 3 cases.

In addition the following general conclusions are drawn.

1. The height of a reinforced embankments at failure was observed to be up to 2 m greater than predicted by conventional bearing capacity theory. The explanation for this is open for discussion but may be that reinforcement enhances the beneficial effect that the following factors have on stability: limited thickness or increase in strength with depth of the soft foundation soils, the dried surface crust, flat embankment side slopes, or dissipation of pore water pressures during construction. It was shown that the bearing capacity of footings on soil with increasing strength with depth can partially account for the difference.

2. The bearing capacity factor for foundations of limited depth with full shearing resistance at the foundation-geotextile interface agreed well with the values observed at failure for two reinforced embankments. This relation merits further study.

3. In four cases reinforced embankments were constructed 0.9-2 m higher than companion unreinforced embankments which failed. However, in one case reinforcement appeared to have an insignificant effect on stability and in another the reinforced embankment failed at a lower height.

CHAPTER 3

CAP SOIL BEHAVIOR MODEL

3.1 INTRODUCTION

The cap soil behavior model is a nonlinear elastic-plastic isotropic work-hardening plasticity model. It was developed from the classical incremental theory of work-hardening plasticity for materials which have time and temperature independent properties. In general, cap models describe the yielding behavior of soil with an ultimate yield surface that is fitted with a movable end cap. Both the ultimate yield and cap surfaces are symmetric about the hydrostatic axis. The movement of the cap is controlled by the hardening and softening behavior of the soil which is expressed as a hardening law. For some versions of the cap model the ultimate failure surface is also allowed to move as controlled by a hardening law. Strains are elastic for stress changes that fall within the region bounded by the ultimate yield and cap surfaces but are elastic-plastic for stress changes on the surfaces.

The first such model for use in soil mechanics was proposed by Drucker, et al. (1957). It consisted of a cone shaped extended von Mises or Drucker-Prager ultimate yield surface (Drucker and Prager, 1952) fitted with a spherical end cap. Both the cone and cap expand as the soil strain hardens. The current soil density was used in the hardening law to control the position of successive yielding surfaces.

The concept of isotropic hardening plasticity was developed into the Cam-clay model (Schofield and Wroth, 1968) for triaxial behavior of normally and lightly overconsolidated clay. This was extended to a general three dimensional stress state by Roscoe and Burland (1968). The model uses the concept of a critical state line on which failure of initially isotropically consolidated samples will occur regardless of the stress path (Atkinson and Bransby, 1978).

A generalized cap model was proposed by DiMaggio and Sandler (1971) and developed further by Sandler, et al. (1976). The yield function consists of a fixed ultimate yield surface fitted with a movable elliptical strain-hardening cap. Movement of the cap was controlled by the plastic volumetric strain. The cap controls plastic dilation once the failure stress is reached. The cap model has advantages over the Cam-clay models of being expressed in terms of the three-dimensional state of stress and

formulated using consistent mechanical principles. The form of the model used in this study was developed by several investigators at Purdue University (Mizuno and Chen, 1982; Saleeb and Chen, 1982; Chen and McCarron, 1983; Chen, 1984; McCarron, 1985; Chen and Baladi, 1985). A good introduction to the model is also given by Desai and Siriwardane (1984).

The sign convention used to develop the cap soil behavior model is that compressive stresses and strains are negative. This is opposite to the normal soil mechanics convention but is used to be consistent with engineering mechanics. The implication is that stresses for almost all problems encountered in soil mechanics will be negative.

The model is formulated in terms of effective stresses using the first invariant of the stress tensor I_1' and the second invariant of the stress deviator tensor J_2, where

$$I_1' = \sigma_1' + \sigma_2' + \sigma_3' \tag{3.1}$$

$$J_2^{1/2} = \{\frac{1}{6}[(\sigma_1-\sigma_2)^2 + (\sigma_2-\sigma_3)^2 + (\sigma_3-\sigma_1)^2]\}^{1/2} \tag{3.2}$$

where σ_1' = major effective principal stress

σ_2' = intermediate effective principal stress

σ_3' = minor effective principal stress

The underlying assumption is that soil behavior is independent of the orientation of the principal axes.

3.2 DESCRIPTION OF CAP MODEL

The main features of the cap soil behavior model are a cone shaped ultimate failure surface and an elliptical shaped cap. They are shown in I_1'-$J_2^{1/2}$ space in Fig. 3.1. For convenience the $-I_1'$ axis is plotted to the right. The ultimate failure surface is of the Drucker-Prager type (Drucker and Prager, 1952) and is a straight line in I_1'-$J_2^{1/2}$ space with a slope α and an intercept with the $J_2^{1/2}$ axis of κ (Fig. 3.1). The equation for the ultimate failure surface is

$$f_1 = \alpha I_1' + J_2^{1/2} - \kappa = 0 \qquad (3.3)$$

The elliptical cap intersects the I_1' axis at x and the ultimate failure surface at coordinates (ℓ, (x-ℓ)/R) as shown in Fig. 3.1. The aspect ratio R is defined as the ratio of the major and minor radii. The cap's shape is described by the equation of an ellipse

$$f_2 = (I_1' - \ell)^2 + R^2 J_2 - (x - \ell)^2 = 0 \qquad (3.4)$$

The position of the cap is coupled to the plastic volumetric strain ε_v^p by the hardening rule

$$\varepsilon_v^p = W[\exp(Dx) - 1] \qquad (3.5)$$

where W is the limiting value of ε_v^p at very high stress and D is a curve fitting parameter with units of $(\text{stress})^{-1}$.

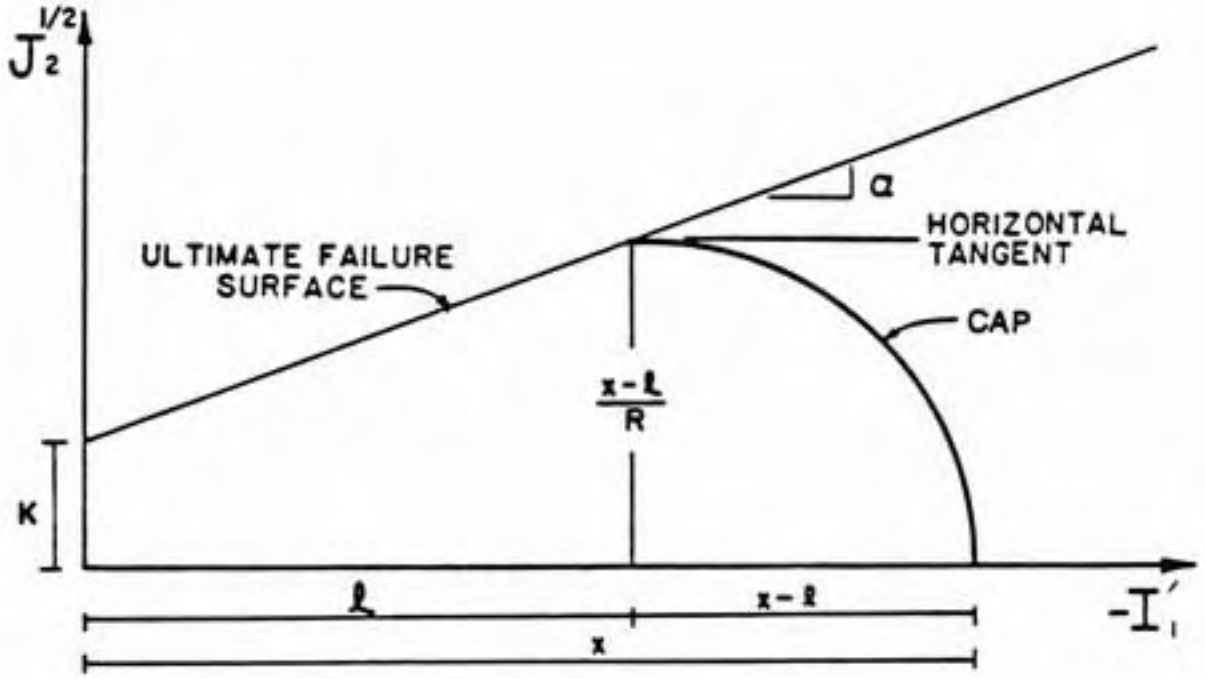

Figure 3.1 Cap model in $I_1' - \sqrt{J_2}$ space.

Elastic strains are governed by the bulk K and shear G moduli. Elastic volumetric strain ε_v^e is produced by changes in I_1'

$$\varepsilon_v^e = I_1'/(3K) \tag{3.6}$$

The elastic shear strain is given by

$$\varepsilon_{ij} = s_{ij}/(2G) \tag{3.7}$$

where ε_{ij} = deviatoric strain tensor

s_{ij} = deviatoric stress tensor

$= \sigma_{ij} - \delta_{ij}(I_1/3)$

δ_{ij} = Kronecker delta tensor = $\begin{bmatrix} 1 & 0 & 0 \\ 0 & 1 & 0 \\ 0 & 0 & 1 \end{bmatrix}$ (3.8)

Stress changes in the region bounded by the ultimate failure surface and the cap produce only elastic strains. Loading on the ultimate failure surface or cap results in both elastic and plastic strains.

A normal (associated) flow rule is used to compute plastic strains for loading on both the ultimate failure and cap surfaces. This means that an increment of plastic strain is normal to the surface. This assumption is mathematically convenient and leads to reasonable predictions of soil behavior. An increment of loading on the cap causes it to expand and results in negative plastic volumetric strain (contraction) and plastic shear strain (Fig. 3.2a). Loading

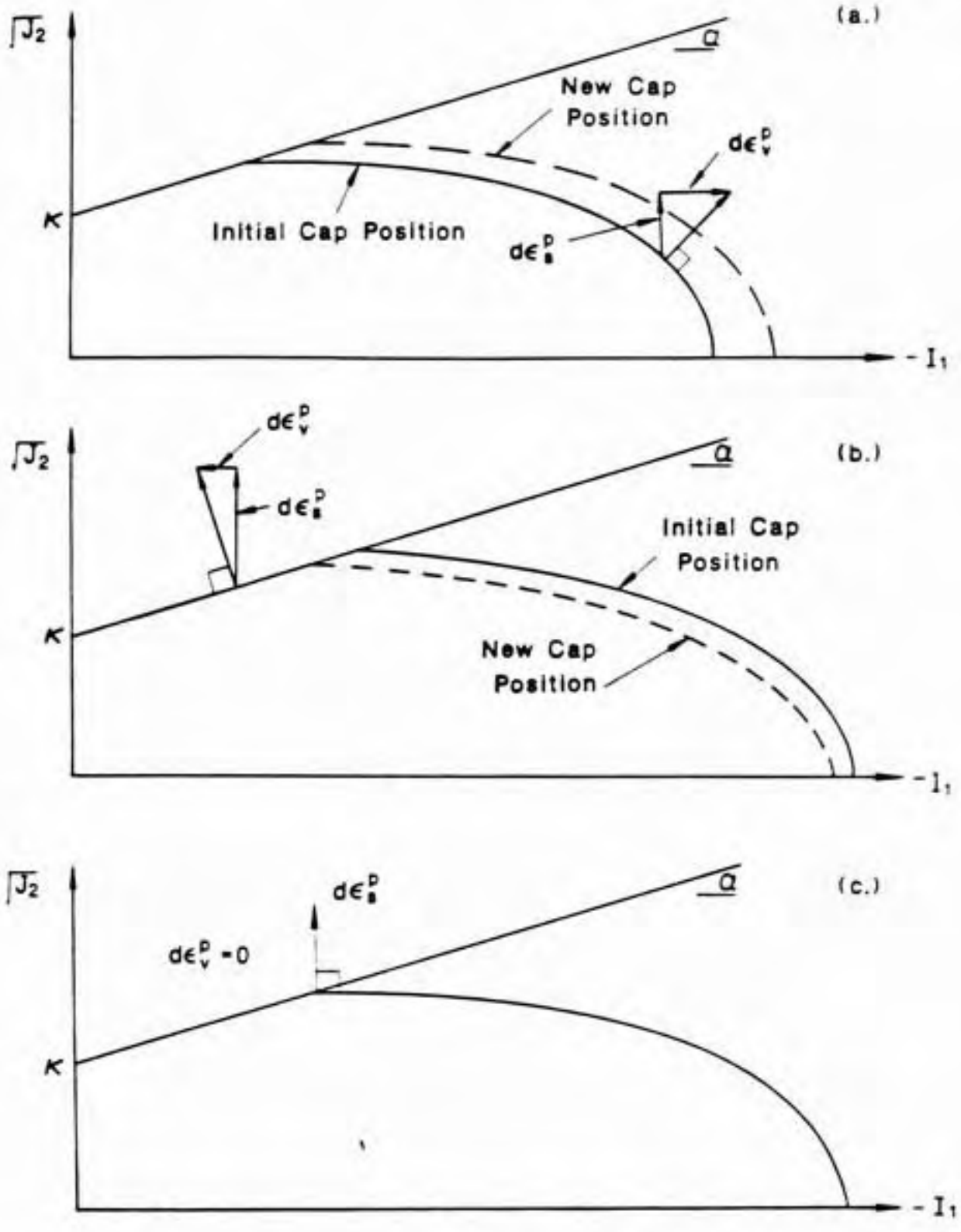

Figure 3.2 Response due to an increment of loading (a) loading on cap, (b) loading on ultimate failure surface, and (c) loading at corner.

on the ultimate failure surface produces positive plastic volumetric strain (dilation) and plastic shear strain. The dilation causes the cap to contract (as shown in Fig. 3.2b) since the position of the cap is determined by the plastic volumetric strain (Eq. 3.5). For a stress state at the intersection between the cap and the ultimate failure surface, the increment of plastic strain is taken to be normal to the cap. This allows plastic shear to occur at constant volumetric strain (Fig. 3.2c) as observed for real soils at large strain.

3.3 CONSTITUTIVE EQUATION FOR GENERAL FORM OF CAP MODEL

The constitutive equations for the general form of the cap model are presented in this section. They are specialized to the form used in this study in the next section. The equations were originally presented by Chen and McCarron (1983) and McCarron (1985). A detailed derivation is given in Humphrey (1985a). The derivation is based on the principles of engineering mechanics (Yamada, 1969). Vector and tensor quantities such as the components of stress and strain are expressed using indicial notation (Chapter 1, Chen and Saleeb, 1982).

A general form of the yield surface F is assumed to be a function of the current state of stress σ_{ij}, a hardening parameter X which is a function of the plastic strain ϵ^p_{ij},

and a material constant K which is a function of the effective plastic strain e^p

$$F = F(\sigma_{ij}, X(\varepsilon^p_{ij}), K(e^p)) \tag{3.9}$$

The effective plastic strain is given by

$$e^p = h\int(d\varepsilon^p_{ij}d\varepsilon^p_{ij})^{1/2} \tag{3.10}$$

where h is a proportionality constant. The increment of plastic strain is obtained by the flow rule

$$d\varepsilon^p_{ij} = d\lambda\frac{\partial\psi}{\partial\sigma_{ij}} \tag{3.11}$$

where ψ is the plastic potential function and $d\lambda$ is a positive scalar proportionality factor. For an associated flow rule $\psi = F$. The total strain increment $d\varepsilon_{ij}$ may be separated into an elastic $d\varepsilon^e_{ij}$ and a plastic $d\varepsilon^p_{ij}$ part

$$d\varepsilon_{ij} = d\varepsilon^e_{ij} + d\varepsilon^p_{ij} \tag{3.12}$$

The elastic stress-strain matrix relates an increment of elastic strain to the stress increment

$$d\sigma_{ij} = C^e_{ijkl}[d\varepsilon^e_{kl}] \tag{3.13}$$

where

$$C^e_{ijkl} = \lambda\delta_{ij}\delta_{kl} + \mu(\delta_{ik}\delta_{jl} + \delta_{il}\delta_{jk}) \tag{3.14}$$

and where λ and μ are Lame's constants and δ_{ij} is the Kronecker delta (Eq. 3.8). Lame's constants are related to the bulk and shear moduli by $\lambda = K - (2/3)G$ and $\mu = G$.

The elastic-plastic stiffness matrix is derived using the consistency condition. This requires that a state of stress that starts on the yield surface remains on the yield surface after an increment of loading. This condition is stated as

$$dF = 0 = \frac{\partial F}{\partial \sigma_{ij}} d\sigma_{ij} + \frac{\partial F}{\partial \varepsilon^p_{ij}} d\varepsilon^p_{ij} + \frac{\partial F}{\partial e^p} de^p \qquad (3.15)$$

Substituting Eqs. 3.9 through 3.13 into Eq. 3.15 leads to the following equation for $d\lambda$

$$d\lambda = \frac{1}{H} \frac{\partial F}{\partial \sigma_{ij}} C^e_{ijkl} d\varepsilon_{kl} \qquad (3.16)$$

where

$$H = \frac{\partial F}{\partial \sigma_{ij}} C^e_{ijkl} \frac{\partial \psi}{\partial \sigma_{kl}} - \frac{\partial F}{\partial \varepsilon^p_{ij}} \frac{\partial \psi}{\partial \sigma_{ij}} - \frac{\partial F}{\partial e^p} h \left[\frac{\partial \psi}{\partial \sigma_{ij}} \frac{\partial \psi}{\partial \sigma_{ij}} \right]^{1/2} \qquad (3.17)$$

Substituting Eq. 3.16 into Eq. 3.11 and using Eq. 3.12 leads after simplification to the elastic-plastic constitutive equations

$$d\sigma_{ij} = C^e_{ijkl} - \frac{H^*_{ij} H_{kl}}{H} d\varepsilon_{kl} = C^{ep}_{ijkl} d\varepsilon_{kl} \qquad (3.18)$$

where

$$H_{kk} = A(3\lambda+2\mu) + 2B\mu s_{kk} + 2C\mu t_{kk} \quad \text{no summation} \tag{3.19}$$

$$H^*_{ii} = L(3\lambda+2\mu) + 2M\mu s_{ii} + 2N\mu t_{ii} \quad \text{no summation} \tag{3.20}$$

$$H_{kl} = 2B\mu s_{kl} + 2C\mu t_{kl} \qquad k \neq l \tag{3.21}$$

$$H^*_{ij} = 2M\mu s_{ij} + 2N\mu t_{ij} \qquad i \neq j \tag{3.22}$$

and $$A = \frac{\partial F}{\partial I_1} \qquad B = \frac{\partial F}{\partial J_2} \qquad C = \frac{\partial F}{\partial J_3} \tag{3.23}$$

$$L = \frac{\partial \psi}{\partial I_1} \qquad M = \frac{\partial \psi}{\partial J_2} \qquad N = \frac{\partial \psi}{\partial J_3} \tag{3.24}$$

$$t_{ij} = \frac{\partial J_3}{\partial \sigma_{ij}} = s_{ia}s_{aj} - (2/3)J_3\delta_{ij} \tag{3.25}$$

J_3 = third invariant of stress deviator tensor

$$= (1/3)s_{ij}s_{jk}s_{ki} \tag{3.26}$$

Finally, Eq. 3.17 is expanded yielding

$$H = 3AL(3\lambda+2\mu) + 2B\mu(2MJ_2+3NJ_3) + 2C\mu(3MJ_3 + Ns_{ia}s_{aj}s_{ib}s_{bj} - \tfrac{4}{3}NJ_2^2) - 3L\frac{\partial F}{\partial X}\frac{\partial X}{\partial \varepsilon_v^p} - \frac{\partial F}{\partial K}\frac{\partial K}{\partial e^p}\, h(3L^2+2M^2J_2+6MNJ_3+N^2(s_{ia}s_{aj}s_{ib}s_{bj}-\tfrac{4}{3}J_2^2))^{1/2} \tag{3.27}$$

The above equations are general and the exact form of the yield surface and the hardening function have not been

specified. In the next section these equations are reduced to the form of the cap model used in this study.

3.4 ELASTIC-PLASTIC CONSTITUTIVE EQUATION FOR LOADING ON CAP

The general elastic-plastic constitutive relations developed in the previous section were specialized to the cap shape (Eq. 3.4) and hardening rule (Eq. 3.5) used in this study for loading on the cap (Fig. 3.2a). This study uses an associated flow rule so $\psi = F = f_2$ (Eq. 3.4). A detailed derivation of the equations is given in Humphrey (1985a). The equations were originally presented by Chen and McCarron (1983) and McCarron (1985).

Beginning with Eqs. 3.4, 3.23, and 3.24 along with the associated flow rule the following are found

$$A = L = 2(I_1 - \ell) \quad ; \quad B = M = R^2 \quad ; \quad C = N = 0 \qquad (3.28)$$

The following partial derivatives are obtained from Eq. 3.4

$$\frac{\partial f_2}{\partial x} = -2(x - \ell) \qquad (3.29)$$

$$\frac{\partial f_2}{\partial \kappa} = 0 \qquad (3.30)$$

The hardening rule (Eq. 3.5) is used to find

$$\frac{\partial \chi}{\partial \varepsilon_v^p} = 1/[D(\varepsilon_v^p + W)] \tag{3.31}$$

Substituting Eqs. 3.28 through 3.31 into Eqs. 3.19, 3.21, and 3.27 yields

$$H_{ii} = 2(I_1-\ell)(3\lambda+2\mu) + 2R^2\mu s_{ii} \quad \text{no summation} \tag{3.32}$$

$$H_{ij} = 2R^2\mu s_{ij} \qquad i \neq j \tag{3.33}$$

$$H = 12(I_1-\ell)^2(3\lambda+2\mu) + 4R^2\mu J_2 + \frac{12(\chi-\ell)(I_1-\ell)}{D(\varepsilon_v^p+W)} \tag{3.34}$$

The general form of the elastic-plastic constitutive equation (Eq. 3.18) is simplified for an associated flow rule to

$$d\sigma_{ij} = C^e_{ijkl} - \frac{H_{ij}H_{kl}}{H}\, d\varepsilon_{kl} \tag{3.35}$$

This equation is expanded for the special case of plane-strain conditions resulting in the elastic-plastic constitutive equation used in this study (McCarron, 1985)

$$\begin{Bmatrix} d\sigma_x \\ d\sigma_y \\ d\tau_{xy} \\ d\sigma_z \end{Bmatrix} = \begin{bmatrix} \lambda+2\mu - \frac{H_{xx}H_{xx}}{H} & \lambda - \frac{H_{xx}H_{yy}}{H} & - \frac{H_{xx}H_{xy}}{H} \\ \lambda - \frac{H_{yy}H_{xx}}{H} & \lambda+2\mu - \frac{H_{yy}H_{yy}}{H} & - \frac{H_{yy}H_{xy}}{H} \\ - \frac{H_{zz}H_{xx}}{H} & - \frac{H_{xy}H_{yy}}{H} & \mu - \frac{H_{xy}H_{xy}}{H} \\ \lambda - \frac{H_{yy}H_{xx}}{H} & \lambda - \frac{H_{zz}H_{yy}}{H} & - \frac{H_{zz}H_{xy}}{H} \end{bmatrix} \begin{Bmatrix} d\varepsilon_x \\ d\varepsilon_y \\ d\gamma_{xy} \end{Bmatrix} \tag{3.36}$$

where H_{xx}, H_{yy} and H_{zz} are given by Eq. 3.32, H_{xy} is given by Eq. 3.33, and H is given by Eq. 3.34.

Equations for loading on the Drucker-Prager ultimate failure surface are derived in a similar manner and are given in Chen and McCarron (1983).

3.5 UNDRAINED CONDITIONS

For undrained loading the condition of no volume change is obtained by adding the apparent stiffness of the pore fluid/solid particle system D_f to the stiffness of the soil skeleton D_s (Naylor, et al., 1981; McCarron, 1985). The total stiffness D_t is given by

$$D_t = D_s + D_f \tag{3.37}$$

D_s has the form $[K_{ij}]$ where K_{ij} are the components of the stiffness matrix. Since fluids cannot resist shear distortions, D_f has the form

$$D_f = \begin{bmatrix} K_f & K_f & K_f & 0 & 0 & 0 \\ & K_f & K_f & 0 & 0 & 0 \\ & & K_f & 0 & 0 & 0 \\ & \text{SYM} & & 0 & 0 & 0 \\ & & & & 0 & 0 \\ & & & & & 0 \end{bmatrix} \tag{3.38}$$

where K_f is the apparent bulk modulus of the pore fluid/solid particle system. For a given displacement field, the resistance provided by the solids is

$$\{\sigma'\} = D_s \{\varepsilon\} \tag{3.39}$$

where the transpose of σ' is

$$\{\sigma'\}^T = (\sigma'_x \ \sigma'_y \ \sigma'_z \ \tau_{xy} \ \tau_{yz} \ \tau_{zx}) \tag{3.40}$$

and the transpose of ε is

$$\{\varepsilon\}^T = (\varepsilon_x \ \varepsilon_y \ \varepsilon_z \ \gamma_{xy} \ \gamma_{yz} \ \gamma_{zx}) \tag{3.41}$$

The pore pressure developed is

$$u = K_f \varepsilon_v \tag{3.42}$$

where ε_v is the total volumetric strain given by

$$\varepsilon_v = \varepsilon_x + \varepsilon_y + \varepsilon_z \tag{3.43}$$

The total stress $\{\sigma\}$ is then

$$\{\sigma\} = \{\sigma'\} + u\{1\} \tag{3.44}$$

where

$$\{1\}^T = (1 \ 1 \ 1 \ 0 \ 0 \ 0) \tag{3.45}$$

The apparent bulk modulus K_f of the pore fluid/solid particle system for saturated undrained conditions is (Naylor, et al., 1981)

$$\frac{1}{K_f} = \frac{n}{K_w} + \frac{1-n}{K_s} \tag{3.46}$$

where K_w = bulk modulus of water

K_s = bulk modulus of solid particles

n = porosity

Since $K_s \geq 30K_w$ (Lambe and Whitman, 1969), the second term in Eq. 3.46 can be neglected with only a few percent error, therefore

$$K_f \geq K_w/n \tag{3.47}$$

The bulk modulus of water is 2.1×10^6 kPa (43×10^6 psf; 300,000 psi). It is convenient to express K_f in terms of the bulk modulus of the soil skeleton K using a pore pressure response factor B which is defined as

$$B = K_f/K \tag{3.48}$$

For partially saturated conditions K_f is related to the Henkel pore pressure parameter (Naylor, et al., 1981)

$$K_f = \frac{KB_h}{1-B_h} \tag{3.49}$$

where

$$\Delta u = B_h(\Delta I_1/3) + A_h(3J_2)^{1/2} \tag{3.50}$$

A_h and B_h are the Henkel pore pressure parameters (Henkel, 1960; Henkel and Wade, 1966). B_h is zero for dry soil and

approaches 1 for saturated soils. Comparison of Eqs. 3.48 and 3.49 shows that

$$B = \frac{B_h}{1-B_h} \tag{3.51}$$

It may therefore be possible to use B to simulate partially drained conditions.

3.6 SUMMARY

The equations for the cap soil behavior model and the elastic-plastic constitutive equation for loading on the cap were presented in this section. The method used to model undrained behavior was given.

CHAPTER 4

PROCEDURE FOR DETERMINING THE CAP PARAMETERS

4.1 INTRODUCTION

One of the main obstacles to using the cap soil behavior model has been the lack of an easy and reliable way to determine the model parameters from conventional test results (Chen and Baladi, 1985). In this chapter a procedure is developed which overcomes this problem. Input soil properties are obtained from conventional tests and the required computations can be done using a hand calculator. The form of the cap model used in this study was developed and implemented in a computer program by McCarron (1985) and McCarron and Chen (1986a, 1986b). The features and equations for the cap model are given in Chapter 3. It is recalled that compressive stresses and strains are negative.

The chapter is organized as follows. First, the procedure is derived and the steps to find the cap parameters are outlined. The procedure is illustrated with example problems. Next, cap parameters are computed for Boston Blue Clay using results from triaxial tests with hydrostatic and

nonhydrostatic consolidation and using plane strain tests with nonhydrostatic consolidation. Sample behavior predicted by the cap model is compared to observed behavior. Then, the cap parameters are derived for a wide range of clayey soils and their correlation with basic soil properties is examined. Parameters for tests with hydrostatic and nonhydrostatic consolidation are compared. Finally, the results of a parametric study are given which examines the effect of input soil properties on calculated response.

4.2 DEVELOPMENT OF PROCEDURE FOR DETERMINING CAP PARAMETERS

There are 16 parameters used to describe soil behavior in the current version of the cap model. They are conveniently grouped into parameters for the ultimate failure surface, elastic behavior, strain hardening, cap, initial stresses, and pore pressure response and are summarized in Table 4.1. New procedures were developed to determine the bulk modulus, hardening parameters, cap aspect ratio, and initial cap position which eliminate the need for a trial and error solution. Procedures to determine the remaining parameters were given by McCarron (1985). The parameters can be determined from commonly available soil properties such as results from consolidation tests and consolidated-undrained triaxial tests on normally consolidated samples. The procedures are given in the following sections.

Table 4.1
Summary of cap parameters.

Ultimate failure surface	
α	slope in I_1'-$J_2^{1/2}$ space
κ	intercept with $J_2^{1/2}$ axis
T_c	tension cut-off
Elastic behavior	
K_1	bulk modulus parameter
K_2	bulk modulus parameter
A_p	atmospheric pressure
G_1	shear modulus parameter
G_2	shear modulus parameter
Strain hardening	
D	hardening parameter
W	hardening parameter
Cap	
R	cap aspect ratio
x_o	initial position of cap
Initial stresses	
A_2	surcharge
γ	average unit weight of soil
$\hat{K}_o$	initial coefficient of lateral earth pressure
Pore pressure response	
B	factor for bulk modulus of fluid/solids

4.2.1 Ultimate Failure Surface

The Drucker-Prager criterion is used to describe the ultimate failure surface. Its circular cross section is an approximation of the Mohr-Coulomb criterion which has a hexagonal shape in stress space (Chen and Saleeb, 1982). For triaxial compression ($\sigma_2 = \sigma_3$) the criteria can be matched on the compressive meridian (Fig. 4.1) and the two sets of material constants (α, κ and c', ϕ') are related by

$$\alpha = \frac{2\sin\phi'}{\sqrt{3}(3-\sin\phi')} \tag{4.1}$$

$$\kappa = \frac{6c'\cos\phi'}{\sqrt{3}(3-\sin\phi')} \tag{4.2}$$

For triaxial extension ($\sigma_1 = \sigma_2$) the criteria are related by

$$\alpha = \frac{2\sin\phi'}{\sqrt{3}(3+\sin\phi')} \tag{4.3}$$

$$\kappa = \frac{6c'\cos\phi'}{\sqrt{3}(3+\sin\phi')} \tag{4.4}$$

For plane strain conditions and a flow rule that is normal to the Drucker-Prager surface the constants are related by (Drucker and Prager, 1952; Chen and Saleeb, 1982)

$$\alpha = \frac{\tan\phi'}{(9 + 12\tan\phi')^{1/2}} \tag{4.5}$$

$$\kappa = \frac{3c'}{(9 + 12\tan\phi')^{1/2}} \tag{4.6}$$

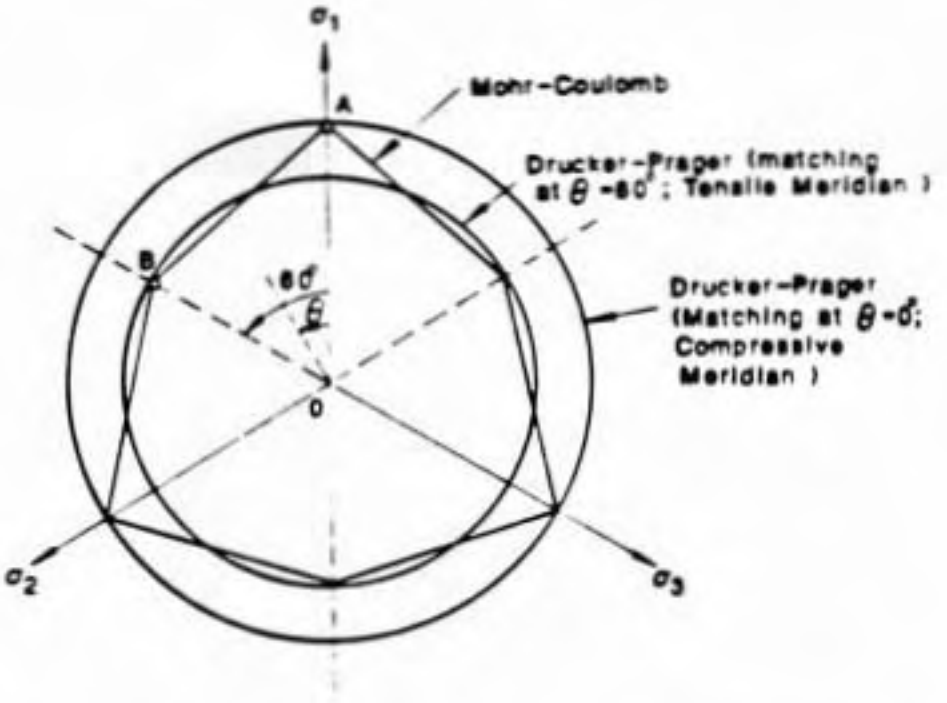

Figure 4.1 Drucker-Prager and Mohr-Coulomb failure criterion matched on compression and extension meridians (after Chen and Saleeb, 1982).

For other conditions the match between Mohr-Coulomb and Drucker-Prager depends on the intermediate principal stress at failure. The following ratio is defined

$$\eta = (\sigma_3 - \sigma_2)_f \; / \; (\sigma_3 - \sigma_1)_f \qquad (4.7)$$

The values of α and κ are given by

$$\alpha = \frac{1}{3}\sin\phi' \; / \; [\sin(\theta + \pi/3) - \frac{1}{\sqrt{3}}\cos(\theta + \pi/3)\,\sin\phi'] \qquad (4.8)$$

$$\kappa = c\,\cos\phi' \; / \; [\sin(\theta + \pi/3) - \frac{1}{\sqrt{3}}\cos(\theta + \pi/3)\,\sin\phi'] \qquad (4.9)$$

where

$$\cos 3\theta = \frac{1}{2}\,\frac{2\eta^3 - 3\eta^2 - 3\eta + 2}{(\eta^2 - \eta + 1)^{3/2}} \qquad (4.10)$$

For triaxial compression ($\eta = 0$) Eqs. 4.8 and 4.9 reduce to Eqs. 4.1 and 4.2, respectively; for triaxial extension ($\eta = 1$) Eqs. 4.8 and 4.9 reduce to Eqs. 4.3 and 4.4. Choice of the η parameter is discussed in Chapter 5. When plane strain test results are available it is recommended that for each specimen $(J_2^{1/2})_{max}$ and the corresponding I_1' be calculated with Eqs. 3.1 and 3.2 using measured effective stresses at failure. The parameters α and κ are then determined from the best fit line through these points.

The tension cut-off T_c specifies a limiting value of tensile stress for soils with non-zero cohesion. Since most

soils cannot support significant tensile stress T_c can be taken as slightly greater than zero.

4.2.2 Elastic Behavior

Elastic behavior is governed by the bulk K and shear G moduli. The model assumes K is related to a power of I_1'

$$K = K_1 A_p \left[I_1'/(3A_p)\right]^{K_2} \tag{4.11}$$

where A_p is atmospheric pressure and is used to obtain a dimensionless term raised to the power K_2. The bulk modulus parameters, K_1 and K_2, are determined from the unloading/reloading portion a hydrostatic consolidation test. This curve is assumed to be linear on an ε_v-ln(p') plot where p' is the mean effective stress

$$p' = I_1'/3 \tag{4.12}$$

Furthermore, curves for unloading from different maximum values of p' are assumed to be parallel, all having a slope of b

$$b = \frac{\varepsilon_{v2} - \varepsilon_{v1}}{\ln(p_2') - \ln(p_1')} \tag{4.13}$$

A similar approach is used in the modified Cam-clay soil model (Wroth and Houlsby, 1985). In the limit as point 1 approaches point 2 Eq. 4.13 becomes

$$b = d\varepsilon_v/d(\ln p') = (d\varepsilon_v)p'/dp' \qquad (4.14)$$

rearranging and using the definition of K

$$K = dp'/d\varepsilon_v = p'/b \qquad (4.15)$$

For linear unloading/reloading curves $K_2 = 1$ and using Eqs. 4.11, 4.12, and 4.15

$$K_1 = 1/b \qquad (4.16)$$

A_p should be chosen with units consistent with I_1'. Values of A_p for different unit systems are given in Table 4.2.

Table 4.2
Values of atmospheric pressure
in different unit systems.

2116.3536 psf
14.6969 psi
101.325 kPa (kN/m^2)
1.03323 kg/cm^2

In many cases only results of one-dimensional consolidation tests are available. For this test, the average slope of the unloading/reloading curve on a void ratio-$\log(\sigma_v')$ plot is the recompression index C_r. If the unloading/reloading curves from hydrostatic and one-dimensional consolidation tests are assumed to be parallel, b and C_r are related by

$$b = \frac{C_r}{2.303(1+e_o)} \qquad (4.17)$$

where e_o is the initial void ratio. Wroth and Houlsby (1985) note that the curves are not parallel since the coefficient of lateral earth pressure K_o is not constant during unloading/reloading and that Eq. 4.17 will underestimate b; however, the approximation is adequate for most purposes (Atkinson and Bransby, 1978). Assuming the curves are parallel, the b-parameter is also equal to $1/m_{sw}$ where m_{sw} is the swelling modulus number determined from a one-dimensional consolidation test (Janbu, 1985).

The shear modulus is known to increase with I_1' and with overconsolidation ratio (OCR) (Wroth and Houlsby, 1985); however, test data on the relationship is limited. In this work it is assumed that G is either constant or proportional to the bulk modulus. The latter allows G to increase with I_1' but the effect of OCR is not considered. The following relation is used

$$G = G_2 + G_1 K \qquad (4.18)$$

G is a constant = G_2 when $G_1 = 0$. For $G_2 = 0$, G is a multiple of K which implies that Poisson's ratio ν' is constant.

The shear modulus can be evaluated directly using the stress strain curve from simple shear test results since by definition (Chen and Saleeb, 1982)

$$G = \frac{\tau}{2\varepsilon_{12}} \tag{4.19}$$

where τ is the shear stress and ε_{12} is the shear strain. Alternately, Young's modulus E can be evaluated from the slope of an unloading/reloading cycle of a triaxial test and then G is given by (Chen and Saleeb, 1982)

$$G = \frac{3KE}{9K-E} \tag{4.20}$$

If test data is unavailable, a reasonable value of Poisson's ratio for effective stress ν' can be assumed (Wroth and Houlsby, 1985) and G is computed from

$$G = \frac{3K(1-2\nu')}{2(1+\nu')} \tag{4.21}$$

When G is computed using Eq. 4.21, G_2 is taken as zero and

$$G_1 = \frac{3(1-2\nu')}{2(1+\nu')} \tag{4.22}$$

Taking G as a function of K can lead to generation of energy on some loading/unloading paths (Houlsby, 1985), however, this will not occur for monotonic loading as considered herein. Alternately, if G is approximately constant, G_1 is taken as 0 and $G_2 = G$.

4.2.3 Hardening Parameters

The hardening parameters, D and W, are used in Eq. 3.5 which relates movement of the cap to plastic volumetric strain. They are determined from the results of hydrostatic consolidation tests. It is assumed that the unloading/reloading curves are linear and parallel on an ε_v-ln(p') plot as discussed above. Two versions of the procedure are presented. The first is applicable if the virgin loading curve is approximately linear on an ε_v-ln(p') plot over the range of stress of interest and the second if it is nonlinear.

4.2.3.1 Linear virgin loading curve. Loading on the virgin loading curve causes both elastic and plastic volumetric strains. Three points on the virgin loading curve shown on Fig. 4.2 have the following x-values and corresponding total, elastic, and plastic volumetric strains where x is the value of I_1' for stress states on the hydrostatic axis.

$$(x_o, \varepsilon_{vo}) \; ; \; (x_m, \varepsilon_{vm}) \; ; \; (x_f, \varepsilon_{vf}) \qquad (4.23a)$$

$$(x_o, \varepsilon^e_{vo}) \; ; \; (x_m, \varepsilon^e_{vm}) \; ; \; (x_f, \varepsilon^e_{vf}) \qquad (4.23b)$$

$$(x_o, \varepsilon^p_{vo}) \; ; \; (x_m, \varepsilon^p_{vm}) \; ; \; (x_f, \varepsilon^p_{vf}) \qquad (4.23c)$$

The x and ε^p_v are related by Eq. 3.5.

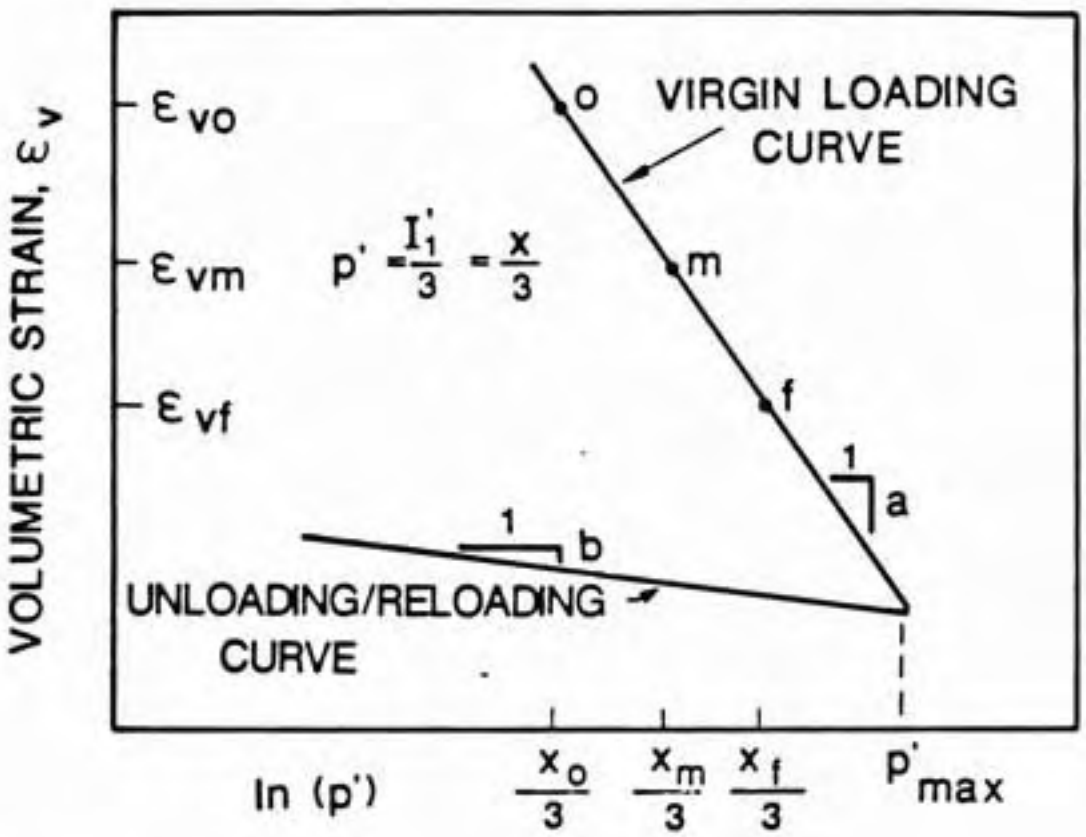

Figure 4.2 Volumetric strain vs. ln(p').

$$\varepsilon^{p}_{vo} = W[\exp(Dx_o) - 1] \tag{4.24a}$$

$$\varepsilon^{p}_{vm} = W[\exp(Dx_m) - 1] \tag{4.24b}$$

$$\varepsilon^{p}_{vf} = W[\exp(Dx_f) - 1] \tag{4.24c}$$

Subtracting Eq. 4.24a from Eqs. 4.24b and 4.24c gives the change in plastic volumetric strain.

$$\Delta\varepsilon^{p}_{vo\to m} = W[\exp(Dx_m) - \exp(Dx_o)] \tag{4.25a}$$

$$\Delta\varepsilon^{p}_{vo\to f} = W[\exp(Dx_f) - \exp(Dx_o)] \tag{4.25b}$$

Dividing Eq. 4.25a by Eq. 4.25b eliminates W and rearrangement gives

$$\frac{\Delta\varepsilon^{p}_{vo\to m}}{\Delta\varepsilon^{p}_{vo\to f}} = \frac{\exp(Dx_m) - \exp(Dx_o)}{\exp(Dx_f) - \exp(Dx_o)} \tag{4.26}$$

Assuming the virgin loading curve is linear with a slope of a on an ε_v-ln(p') plot, as shown on Fig. 4.2, the change in total volumetric strain is given by

$$\Delta\varepsilon_{vo\to m} = -a \ln(x_m/x_o) \tag{4.27a}$$

$$\Delta\varepsilon_{vo\to f} = -a \ln(x_f/x_o) \tag{4.27b}$$

The change in elastic volumetric strain is

$$\Delta\varepsilon^{e}_{vo\to m} = -b \ln(x_m/x_o) \tag{4.28a}$$

$$\Delta\varepsilon^{e}_{vo\to f} = -b \ln(x_f/x_o) \tag{4.28b}$$

Subtracting Eqs. 4.28 from Eqs. 4.27 gives the change in plastic volumetric strain.

$$\Delta\varepsilon^{p}_{vo\rightarrow m} = -(a-b)\ \ln(x_m/x_o) \tag{4.29a}$$

$$\Delta\varepsilon^{p}_{vo\rightarrow f} = -(a-b)\ \ln(x_f/x_o) \tag{4.29b}$$

Substituting these equations into Eq. 4.26, (a-b) is eliminated giving

$$\frac{\ln(x_m/x_o)}{\ln(x_f/x_o)} = \frac{\exp(Dx_m) - \exp(Dx_o)}{\exp(Dx_f) - \exp(Dx_o)} \tag{4.30}$$

Assuming $x_m = (x_o+x_f)/2$ and solving for Dx_o

$$Dx_o = 2\ \ln[(1-P)/P]\ /\ (x_f/x_o-1) \tag{4.31a}$$

$$P = \frac{\ln[(1+x_f/x_o)/2]}{\ln[x_f/x_o]} \tag{4.31b}$$

This shows that for the assumption for x_m given above the curve fitting parameter D is a function only of the initial stress level x_o and the ratio of final to initial stress x_f/x_o. Values of Dx_o for selected x_f/x_o are given in Table 4.3 and the solution is shown in graphical form in Fig. 4.3a. Small increments are shown on Table 4.3 for x_f/x_o slightly greater than 1 and the solution to Eq. 4.31 is shown at an expanded scale in Fig. 4.3b since x_f/x_o for most undrained problems fall in this range. D is then found

Table 4.3
Values of Dx_o and $W/(a-b)$
for selected values of x_f/x_o.

x_f/x_o	Dx_o	$W/(a-b)$
0.10	-2.3286	3.3139
0.20	-1.9144	3.0113
0.30	-1.6712	2.8825
0.40	-1.5014	2.8134
0.50	-1.3727	2.7727
0.60	-1.2702	2.7478
0.70	-1.1858	2.7327
0.80	-1.1146	2.7239
0.90	-1.0534	2.7195
1.00	-1.0000	2.7183
1.02	-0.9901	2.7183
1.04	-0.9805	2.7185
1.06	-0.9711	2.7187
1.08	-0.9619	2.7190
1.10	-0.9529	2.7193
1.12	-0.9442	2.7197
1.14	-0.9356	2.7202
1.16	-0.9272	2.7208
1.18	-0.9190	2.7214
1.20	-0.9110	2.7220
1.25	-0.8917	2.7239
1.30	-0.8733	2.7261
1.40	-0.8392	2.7311
1.50	-0.8082	2.7369
1.60	-0.7798	2.7433
1.70	-0.7537	2.7502
1.80	-0.7295	2.7574
1.90	-0.7072	2.7650
2.00	-0.6864	2.7727
2.50	-0.6006	2.8134
3.00	-0.5362	2.8550
4.00	-0.4451	2.9359
5.00	-0.3829	3.0113
6.00	-0.3374	3.0810
7.00	-0.3024	3.1455
8.00	-0.2746	3.2055
9.00	-0.2518	3.2614

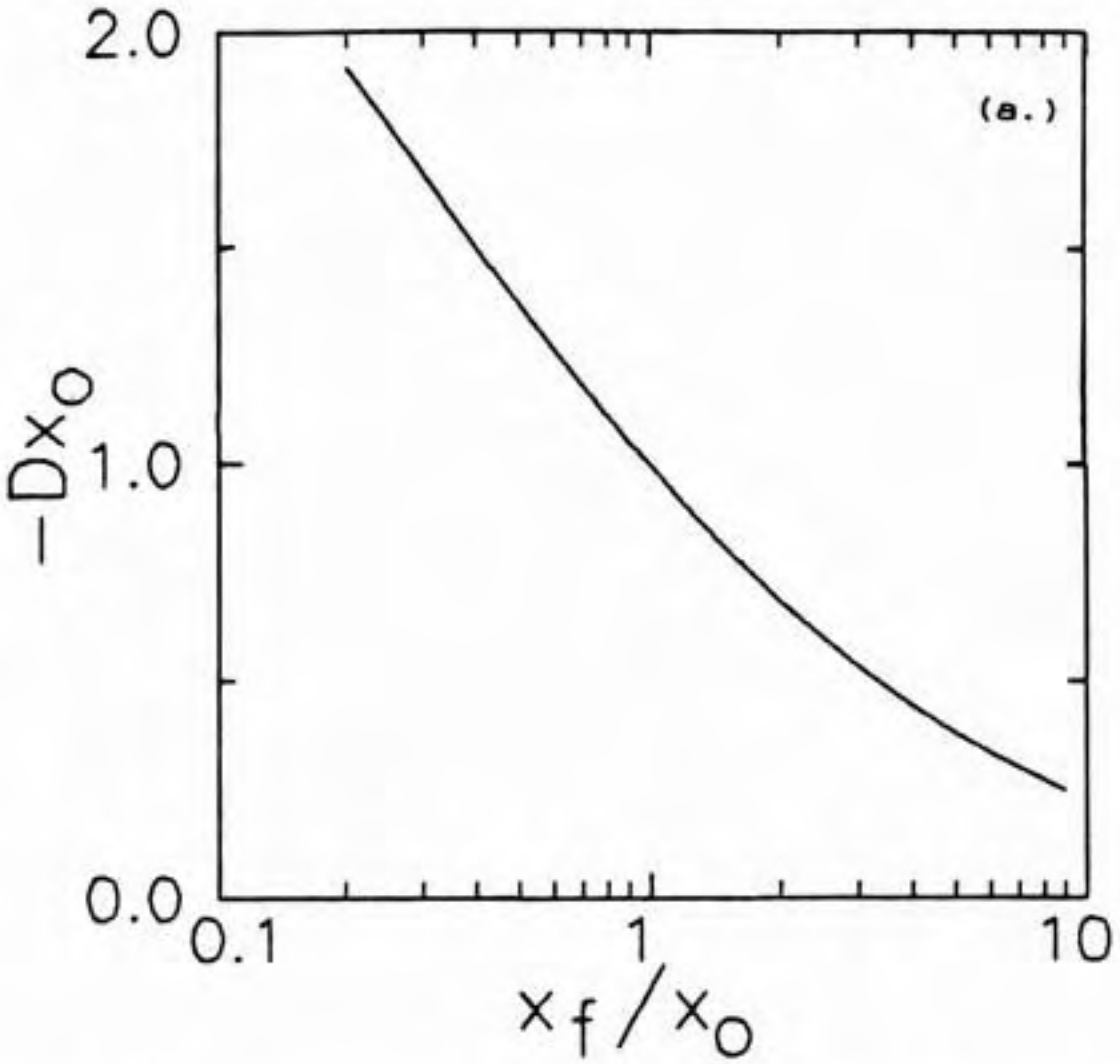

Figure 4.3 Dimensionless hardening parameter Dx_o vs. x_f/x_o.

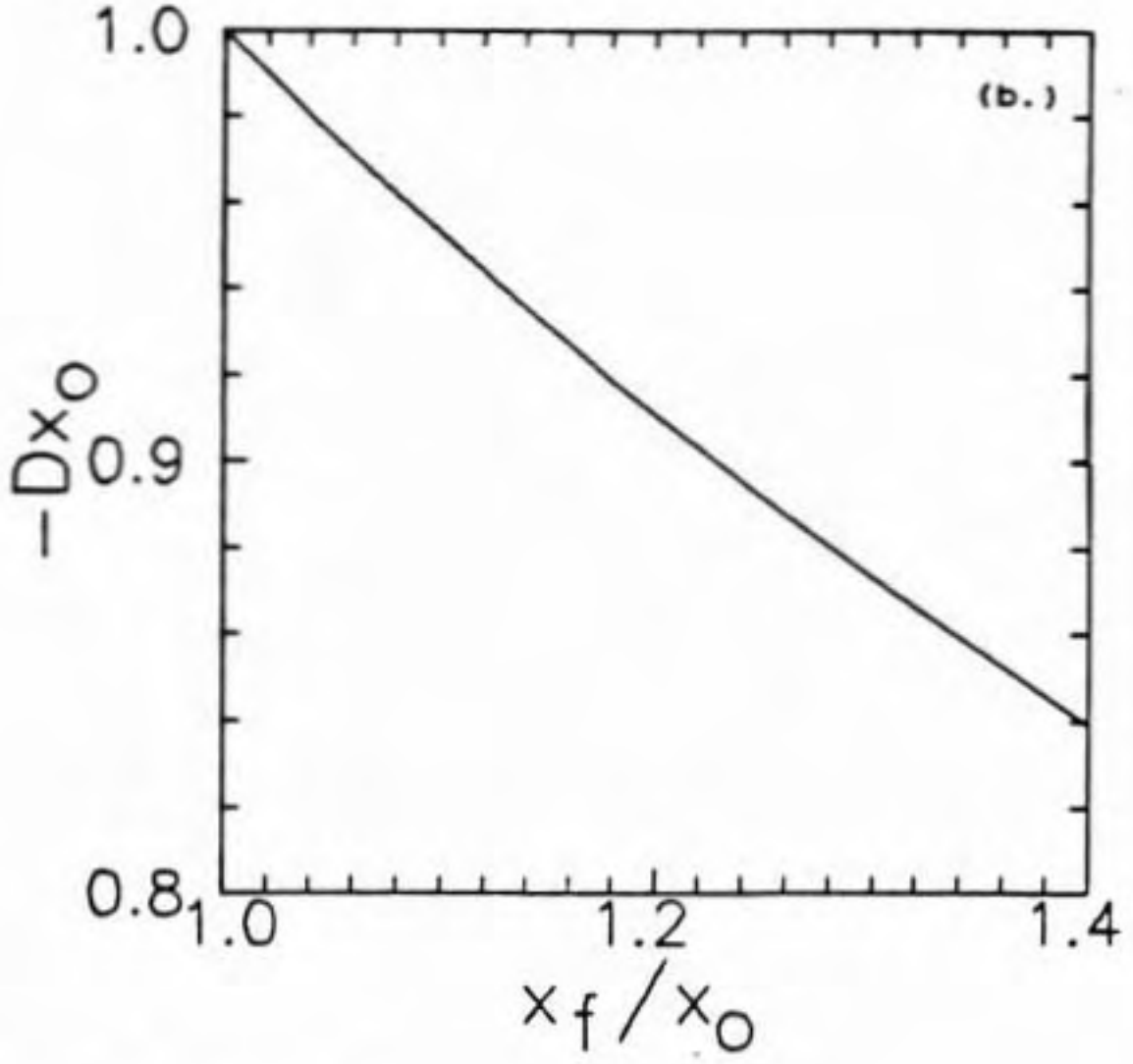

Figure 4.3. continued.

after x_o is calculated. Methods to calculate x_f/x_o and x_o are given in the next section.

The W parameter is determined by combining Eqs. 4.25b and 4.29b.

$$W[\exp(Dx_f) - \exp(Dx_o)] = -(a-b)\ \ln(x_f/x_o) \qquad (4.32)$$

Converting to dimensionless form and rearranging gives

$$\frac{W}{(a-b)} = \frac{-\ln(x_f/x_o)}{\exp[(Dx_o)(x_f/x_o)] - \exp[Dx_o]} \qquad (4.33)$$

Since Dx_o is a function only of x_f/x_o, the value of $W/(a-b)$ is also a function only of x_f/x_o. The solution to Eq. 4.33 is shown on Figs. 4.4a and 4.4b. $W/(a-b)$ is given for selected values of x_f/x_o in Table 4.3. W is then calculated using (a-b).

In most cases hydrostatic consolidation test results are unavailable. However, the virgin consolidation curves on ε_v-ln(p') plots from hydrostatic and one-dimensional consolidation tests are parallel since K_o is constant for virgin loading (Wroth and Houlsby, 1985) and a can be computed from

$$a = \frac{C_c}{2.303(1+e_o)} \qquad (4.34)$$

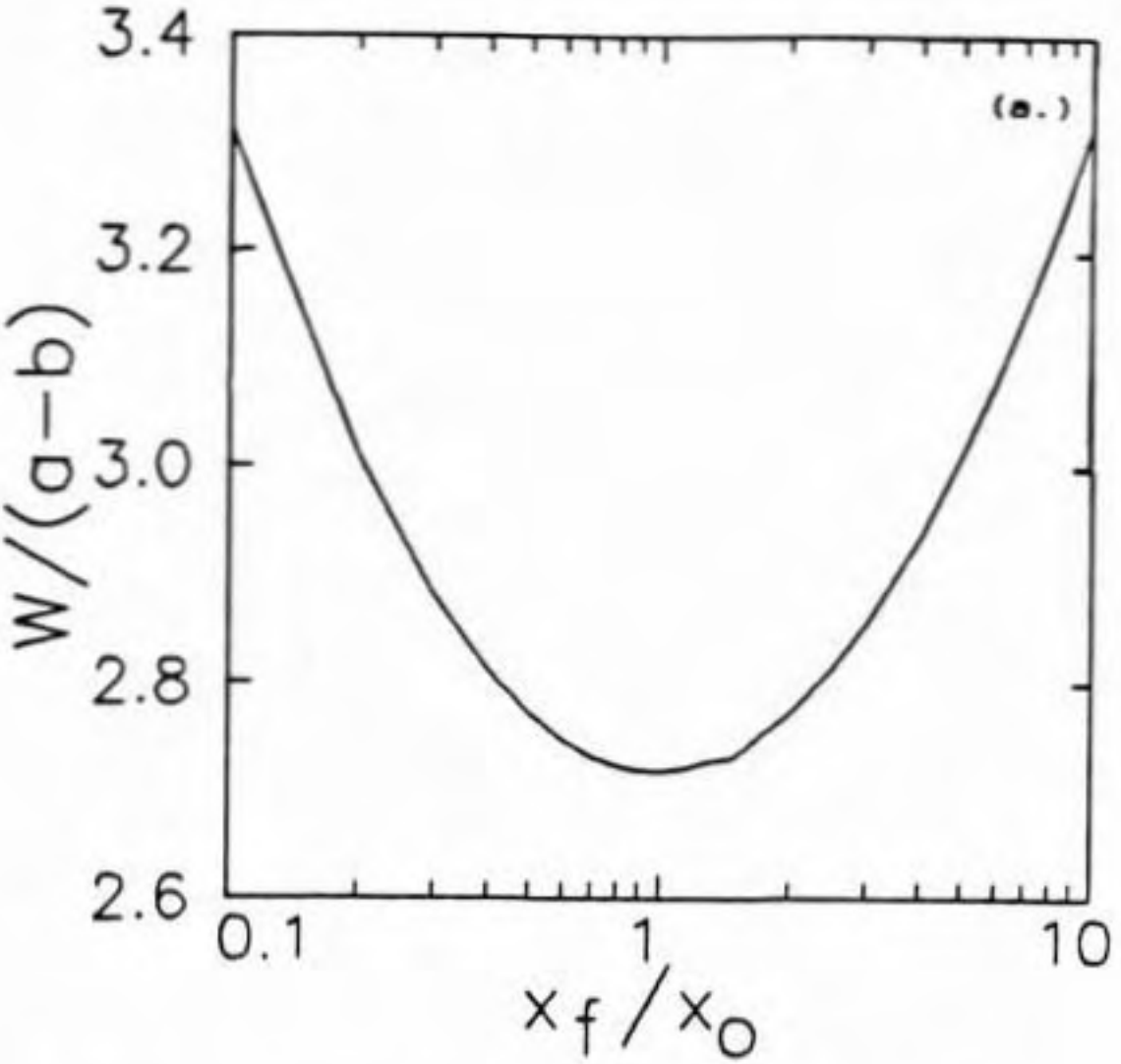

Figure 4.4 Hardening parameter W/(a-b) vs. x_f/x_o.

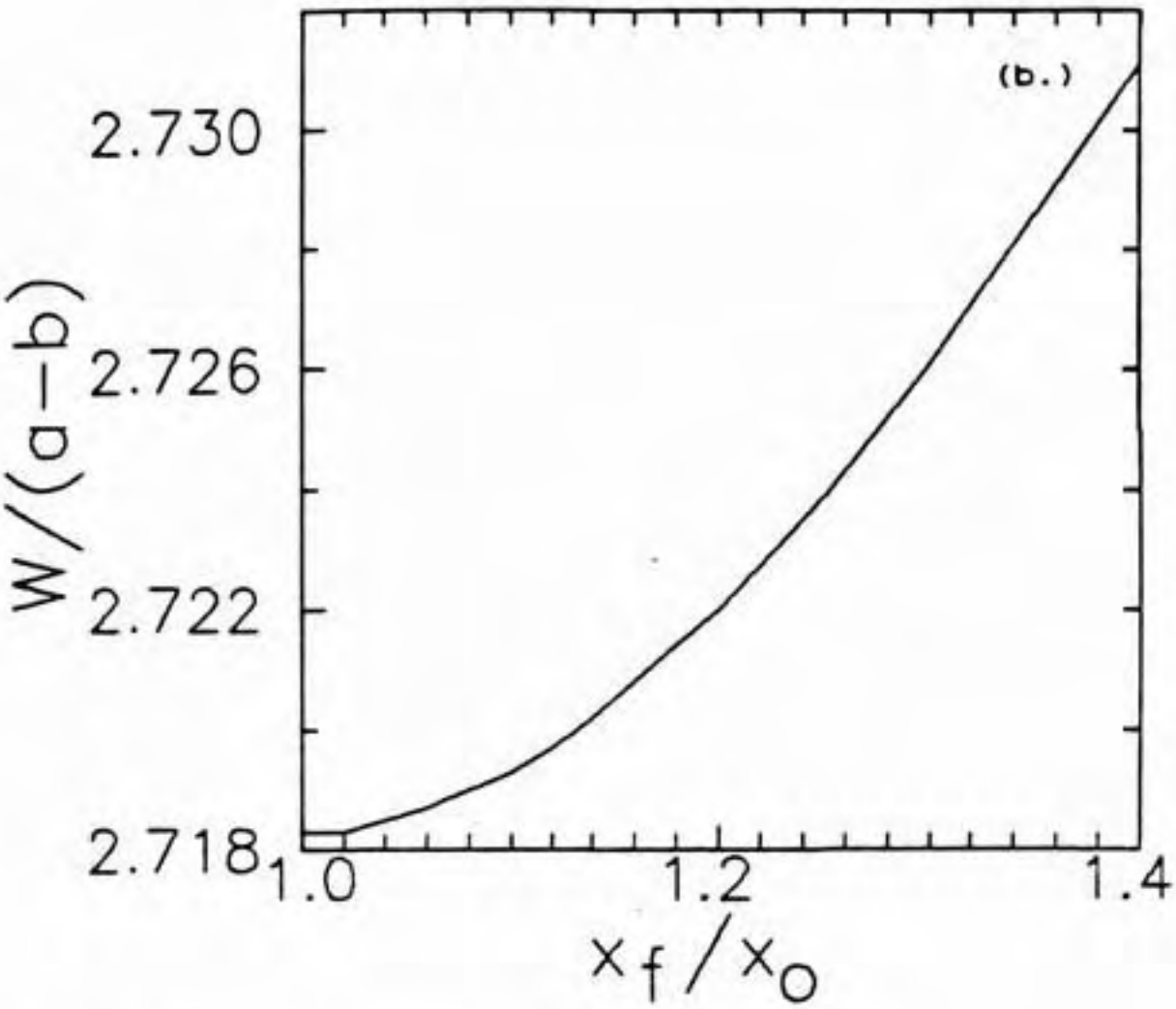

Figure 4.4, continued.

where C_c is the coefficient of consolidation from a one-dimensional consolidation test. The a-parameter is also equal to $1/m_o$ where m_o is the modulus number determined from one-dimensional consolidation tests (Janbu, 1985). The value of b is computed using Eq. 4.17.

4.2.3.2 Nonlinear virgin loading curve. For undrained loading the movement of the cap from its initial to its failure position is small and x_f/x_o is slightly greater than 1. A close approximation to the a-value over the range of stress from x_o to x_f is obtained from the slope of the virgin consolidation curve at x_o. Similarly C_c is approximated by the slope at σ'_{vo}. The hardening parameters are then determined using the procedure given above for linear virgin loading curves.

A general procedure is now given for drained conditions where x_f/x_o is often much greater than 1 and the virgin loading curve is nonlinear. Three points on the virgin loading curve in an ε_v-ln(p') or ε_v-p' plot spanning the range of stress involved in the problem are chosen giving three pairs of x and total volumetric strain (Eq. 4.23a) as shown in Fig. 4.2. The change in total volumetric strain is

$$\Delta\varepsilon_{vo\to m} = \varepsilon_{vm} - \varepsilon_{vo} \qquad (4.35a)$$

$$\Delta\varepsilon_{vo\to f} = \varepsilon_{vf} - \varepsilon_{vo} \qquad (4.35b)$$

Next, the change in elastic volumetric strain is computed using Eqs. 4.28a and 4.28b. The change in plastic volumetric strain is obtained directly from test results using Eqs. 4.36 rather than from Eq. 4.29 which assumes that the virgin loading curve is linear.

$$\Delta\varepsilon^{p}_{vo\rightarrow m} = \Delta\varepsilon_{vo\rightarrow m} - \Delta\varepsilon^{e}_{vo\rightarrow m} \tag{4.36a}$$

$$\Delta\varepsilon^{p}_{vo\rightarrow f} = \Delta\varepsilon_{vo\rightarrow f} - \Delta\varepsilon^{e}_{vo\rightarrow f} \tag{4.36b}$$

These results are then substituted in Eq. 4.26 and D is found by trial and error. Finally, W is calculated using Eq. 4.25a or 4.25b. The fit of the predicted curve (Eq. 3.5) to the observed data should be checked for several values of x. A similar procedure was given by Desai and Siriwardane (1984) and Humphrey (1985a).

4.2.4 Cap Parameters

4.2.4.1 Aspect ratio. The aspect ratio R is determined from shear tests on normally consolidated soil where the loading path causes the cap to expand. It is assumed that R remains constant as the state of stress moves from the initial to the failure condition and that R is independent of x_o.

The initial state of stress (I'_{1o}, $J^{1/2}_{2o}$) for normally consolidated soil is on the cap and the failure state

of stress (I'_{1f}, $J_{2f}^{1/2}$) is at the intersection of the cap and ultimate failure surface as shown on Fig. 4.5. The movement of the cap is exaggerated for clarity. The initial state of stress is calculated from the vertical consolidation stress σ'_{vo} and the normally consolidated coefficient of lateral earth pressure K_o which is given by

$$K_o = \sigma'_{ho}/\sigma'_{vo} \tag{4.37}$$

where σ'_{ho} is the horizontal effective stress. Eqs. 3.1 and 3.2 are used to calculate I'_{1o} and $J_{2o}^{1/2}$ for $\sigma'_1 = \sigma'_{vo}$ and $\sigma'_2 = \sigma'_3 = \sigma'_{ho}$.

$$I'_{1o} = \sigma'_{vo}(1+2K_o) \tag{4.38}$$

$$J_{2o}^{1/2} = \frac{1}{\sqrt{3}}\sigma'_{vo}(1-K_o) \tag{4.39}$$

At failure Eq. 3.3 is used to relate I'_{1f} and $J_{2f}^{1/2}$

$$I'_{1f} = (\kappa - J_{2f}^{1/2})/\alpha \tag{4.40}$$

The ratio $J_{2f}^{1/2}/\sigma'_{vo}$ is introduced as a normalized measure of the shear stress at failure. The ratio is negative since compressive stresses and hence σ'_{vo} are negative. For undrained triaxial compression or extension, Eq. 3.2 is used to show that

$$J_{2f}^{1/2}/\sigma'_{vo} = -\frac{2}{\sqrt{3}}(s_u/\sigma'_{vo}) \tag{4.41}$$

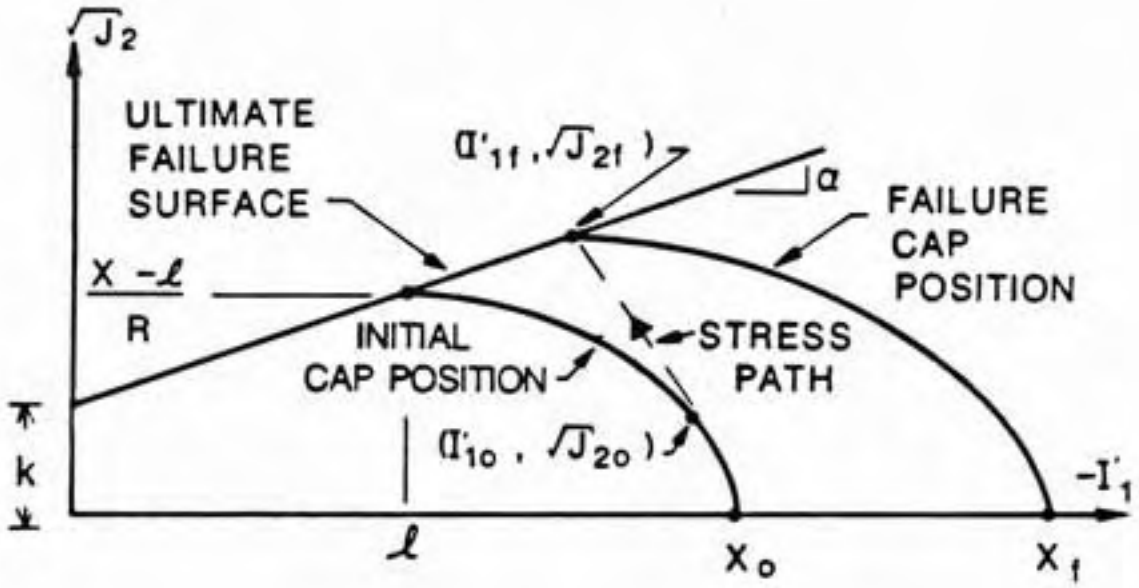

Figure 4.5 Cap model response for undrained shear.

where s_u/σ'_{vo} is the undrained shear strength ratio of normally consolidated samples. For undrained plane strain conditions the relation depends on η (Eq. 4.7)

$$J_{2f}^{1/2}/\sigma'_{vo} = -\frac{2}{\sqrt{3}}(s_u/\sigma'_{vo})\ (\eta^2-\eta+1)^{1/2} \qquad (4.42)$$

Choice of the η parameter is discussed in Chapter 5. When results from plane strain or true triaxial tests are available, $J_{2f}^{1/2}$ should be calculated using Eq. 3.2 and the measured principal stresses at failure.

The plastic volumetric strain caused by the cap moving from the initial to the failure position is given by Eq. 4.25b which is rearranged giving

$$x_f/x_o = \frac{1}{Dx_o}\ln[\exp(Dx_o) + \frac{1}{W}\Delta\varepsilon^p_{vo\to f}] \qquad (4.43)$$

For a linear unloading/reloading curve on an ε_v-ln(p') plot Eq. 4.28b gives

$$\Delta\varepsilon^e_{vo\to f} = -b\ \ln(I'_{1f}/I'_{1o}) \qquad (4.44)$$

For undrained conditions $\Delta\varepsilon^p_{vo\to f} = -\Delta\varepsilon^e_{vo\to f}$ so combining Eqs. 4.43 and 4.44

$$x_f/x_o = \frac{1}{Dx_o}\ln[\exp(Dx_o) - \frac{1}{W/b}\ln(I'_{1f}/I'_{1o})] \qquad (4.45)$$

Substituting Eqs. 4.38 and 4.40 gives

$$x_f/x_o = \frac{1}{Dx_o} \ln\{\exp(Dx_o) - \frac{1}{W/b}\ln[\frac{\kappa/\sigma'_{vo} - J_{2f}^{1/2}/\sigma'_{vo}}{\alpha(1+2K_o)}]\} \quad (4.46)$$

This equation should be used to calculate x_f/x_o when the virgin loading curve is nonlinear.

If both the virgin loading and unloading/reloading curves are linear, using Eq. 4.29b

$$x_f/x_o = \exp[-\Delta\varepsilon^p_{vo\to f}/(a-b)] \quad (4.47)$$

which for undrained conditions and substituting Eq. 4.44 becomes

$$x_f/x_o = \exp[\frac{-b}{a-b}\ln(I'_{1f}/I'_{1o})] \quad (4.48)$$

Note that $(a-b)/b \equiv (C_c-C_r)/C_r$. Substituting Eqs. 4.38 and 4.40

$$x_f/x_o = \exp\{\frac{-b}{a-b}\ln[\frac{\kappa/\sigma'_{vo} - J_{2f}^{1/2}/\sigma'_{vo}}{\alpha(1+2K_o)}]\} \quad (4.49)$$

This equation is used for undrained conditions if both the virgin loading and unloading/reloading curves are linear.

The equations for the cap (Eq. 3.4) and ultimate failure surface (Eq. 3.3) are used to relate the initial x_o and failure x_f positions of the cap to the aspect ratio R

$$x_o = \frac{-R\kappa+1'_{1o} - R[\,J_{2o}(a^2R^2-1)+(a1'_{1o})^2+\kappa^2-2a\kappa1'_{1o}\,]^{1/2}}{1 - aR} \quad (4.50)$$

$$x_f = [\kappa - J_{2f}^{1/2}(1+aR)]/a \quad (4.51)$$

Dividing Eq. 4.51 by Eq. 4.50

$$x_f/x_o = \frac{[\kappa(1-aR) - J_{2f}^{1/2}(1+a^2R^2)]/a}{-R\kappa+1'_{1o} - R[\,J_{2o}(a^2R^2-1)+(a1'_{1o})^2+\kappa^2-2a\kappa1'_{1o}\,]^{1/2}} \quad (4.52)$$

This expression is rewritten by substituting Eqs. 4.38, 4.39, and 4.40.

$$x_f/x_o = \frac{[(\kappa/\sigma'_{vo})(1-aR) - (J_{2f}^{1/2}/\sigma'_{vo})(1-a^2R^2)]/a}{-R(\kappa/\sigma'_{vo}) + (1+2K_o) - R(H)^{1/2}} \quad (4.53)$$

where

$$H = (1-K_o)^2(a^2R^2-1)/3 + a^2(1+2K_o)^2 + (\kappa/\sigma'_{vo})^2 - 2a(\kappa/\sigma'_{vo})(1+2K_o) \quad (4.54)$$

The dimensionless ratios κ/σ'_{vo} and $J_{2f}^{1/2}/\sigma'_{vo}$ were introduced. It is recalled that $J_{2f}^{1/2}/\sigma'_{vo}$ is related to s_u/σ'_{vo} (Eqs. 4.41 and 4.42). Both ratios are negative since compressive stresses are negative. For soils with zero cohesion, $\kappa = 0$, and Eqs. 4.53 and 4.54 become

$$x_f/x_o = \frac{-(J_{2f}^{1/2}/\sigma'_{vo})(1-a^2R^2)/a}{1+ 2K_o - R[\tfrac{1}{3}(1-K_o)^2(a^2R^2-1) + a^2(1+2K_o)^2]^{1/2}} \quad (4.55)$$

For initial hydrostatic conditions ($K_o = 1$) Eq. 4.55 is solved directly for R

$$R = -3(x_f/x_o)/(J_{2f}^{1/2}/\sigma'_{vo}) - \frac{1}{\alpha} \qquad (4.56)$$

R is found using Eqs. 4.53 through 4.56 using the value of x_f/x_o from Eq. 4.46 (non-linear virgin loading curve) or Eq. 4.49 (linear virgin loading curve). Eqs. 4.53 through 4.55 cannot be solved explicitly for R so a trial and error solution is necessary.

Examination of the equations relating R to x_f/x_o (Eqs. 4.53 through 4.56) and x_f/x_o to compressibility for linear virgin loading and unloading/reloading curves (Eq. 4.49) shows that R is a function of α, κ/σ'_{vo}, $J_{2f}^{1/2}/\sigma'_{vo}$, K_o, and the ratio (a-b)/b. There are three limitations on allowable combinations of these parameters. The first is that $J_{2o}^{1/2}$ be less than $J_{2f}^{1/2}$. This is satisfied provided

$$(1-K_o)/\sqrt{3} < -J_{2f}^{1/2}/\sigma'_{vo} \qquad (4.57)$$

The second is that the aspect ratio R must be greater than 0. For undrained conditions this requires that $I'_{1o} > I'_{1f}$. This restriction is met provided

$$|J_{2f}^{1/2}/\sigma'_{vo}| < |\kappa/\sigma'_{vo} - \alpha(1+2K_o)| \qquad (4.58)$$

The third restriction is on the value of x_f/x_o. For a given set of κ/σ'_{vo}, $J_{2f}^{1/2}/\sigma'_{vo}$ and K_o, a plot of x_f/x_o versus R calculated using Eq. 4.52 shows that a maximum value of x_f/x_o occurs at R_{max} (Fig. 4.6). The value of x_f/x_o obtained from Eq. 4.46 or 4.49 must be less than $(x_f/x_o)_{max}$. This restriction is violated only when $J_{2o}^{1/2}$ approaches $J_{2f}^{1/2}$ and (a-b)/b is small. R_{max} is the value which satisfies the first derivative of Eq. 4.53 with respect to R

$$\frac{\partial(\text{Eq. 4.53})}{\partial R} = \frac{u'v-uv'}{v^2} = 0 \qquad (4.59)$$

where

$$u = [(\kappa/\sigma'_{vo})(1-aR) - (J_{2f}^{1/2}/\sigma'_{vo})(1-a^2R^2)]/a \qquad (4.60)$$

$$v = -R(\kappa/\sigma'_{vo}) + (1+2K_o) - RH^{1/2} \qquad (4.61)$$

$$u' = 2aR(J_{2f}^{1/2}/\sigma'_{vo}) - \kappa/\sigma'_{vo} \qquad (4.62)$$

$$v' = -\kappa/\sigma'_{vo} - [aR(1-K_o)]^2/(3H^{1/2}) - H^{1/2} \qquad (4.63)$$

Eq. 4.59 is solved by trial and error for R_{max}. A simple program on a programmable calculator or computer facilitates the computations (Humphrey and Holtz, 1986a). The value of $(x_f/x_o)_{max}$ is then found by substituting R_{max} in Eq. 4.52. R_{max} and $(x_f/x_o)_{max}$ equal infinity when both $\kappa = 0$ and $K_o = 1$.

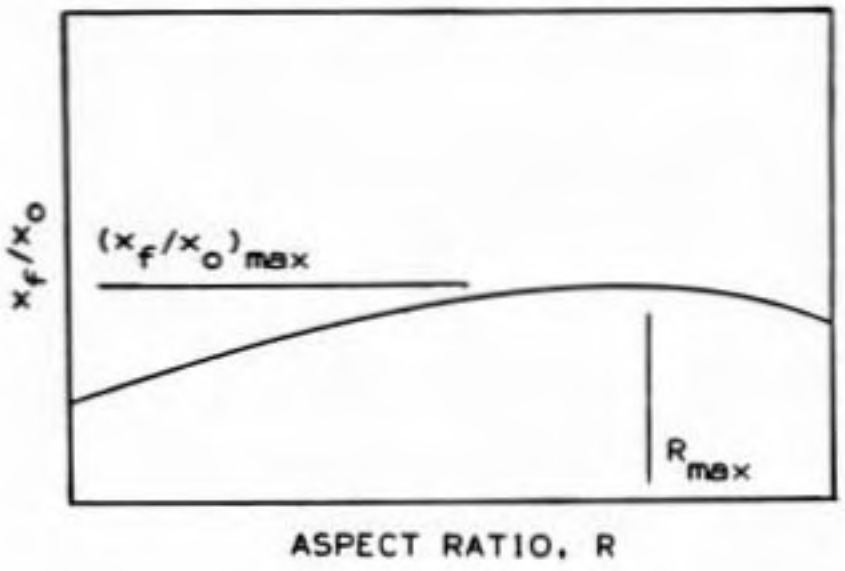

Figure 4.6 x_f/x_o vs. aspect ratio calculated using Eq. 4.53.

The relation between the input parameters and R was examined. R is plotted against $J_{2f}^{1/2}/\sigma'_{vo}$ for $\kappa = 0$ and selected values of α, K_o, and $(a-b)/b$ in Figs. 4.7 through 4.15. α-values of 0.1090, 0.1893, and 0.2730 were used which correspond to ϕ' of 15^o, 25^o, and 35^o for triaxial compression. For α and K_o fixed, R is seen to decrease as $J_{2f}^{1/2}/\sigma'_{vo}$ or $(a-b)/b$ increase. The effect of K_o on R is shown in Fig. 4.16 for $\alpha = 0.1893$, $\kappa = 0$, and $(a-b)/b = 5$. In general, R for initial hydrostatic ($K_o = 1$) and non-hydrostatic conditions are different. For given α, $J_{2f}^{1/2}/\sigma'_{vo}$, and $(a-b)/b$, the effect of $\kappa/\sigma'_{vo} > 0$ is to increase R as shown in Fig. 4.17.

4.2.4.2 Initial cap position for normally consolidated soil. The initial cap position x_o depends on σ'_{vo}, K_o, α, κ/σ'_{vo}, and R. It is calculated using Eq. 4.50 modified by substituting Eqs. 4.38 and 4.39; rearrangement gives

$$x_o = [\sigma'_{vo}/(1-\alpha R)]\ \{-R(\kappa/\sigma'_{vo}) + (1+2K_o) - RH^{1/2}\} \qquad (4.64)$$

where H is given by Eq. 4.54. For $\kappa = 0$ Eq. 4.64 reduces to

$$x_o = [\sigma'_{vo}/(1-\alpha R)]$$
$$\{(1+2K_o) - R[(1-K_o)^2(\alpha^2R^2-1)/3 + \alpha^2(1+2K_o)^2]^{1/2}\} \qquad (4.65)$$

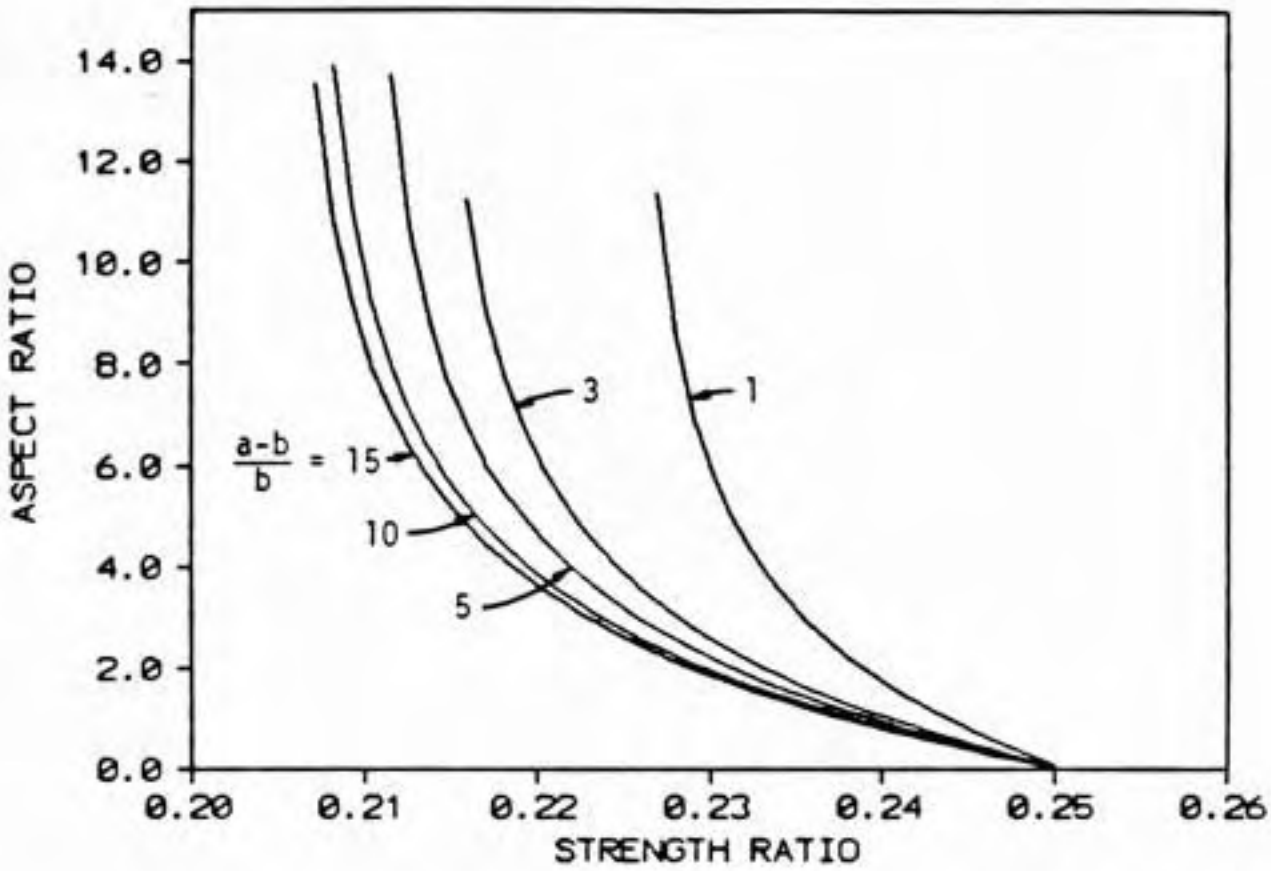

Figure 4.7 Aspect ratio vs. strength ratio ($J_{2f}^{1/2}/\sigma'_{vo}$) for $\alpha = 0.1090$, $\kappa = 0$, and $K_o = 0.65$.

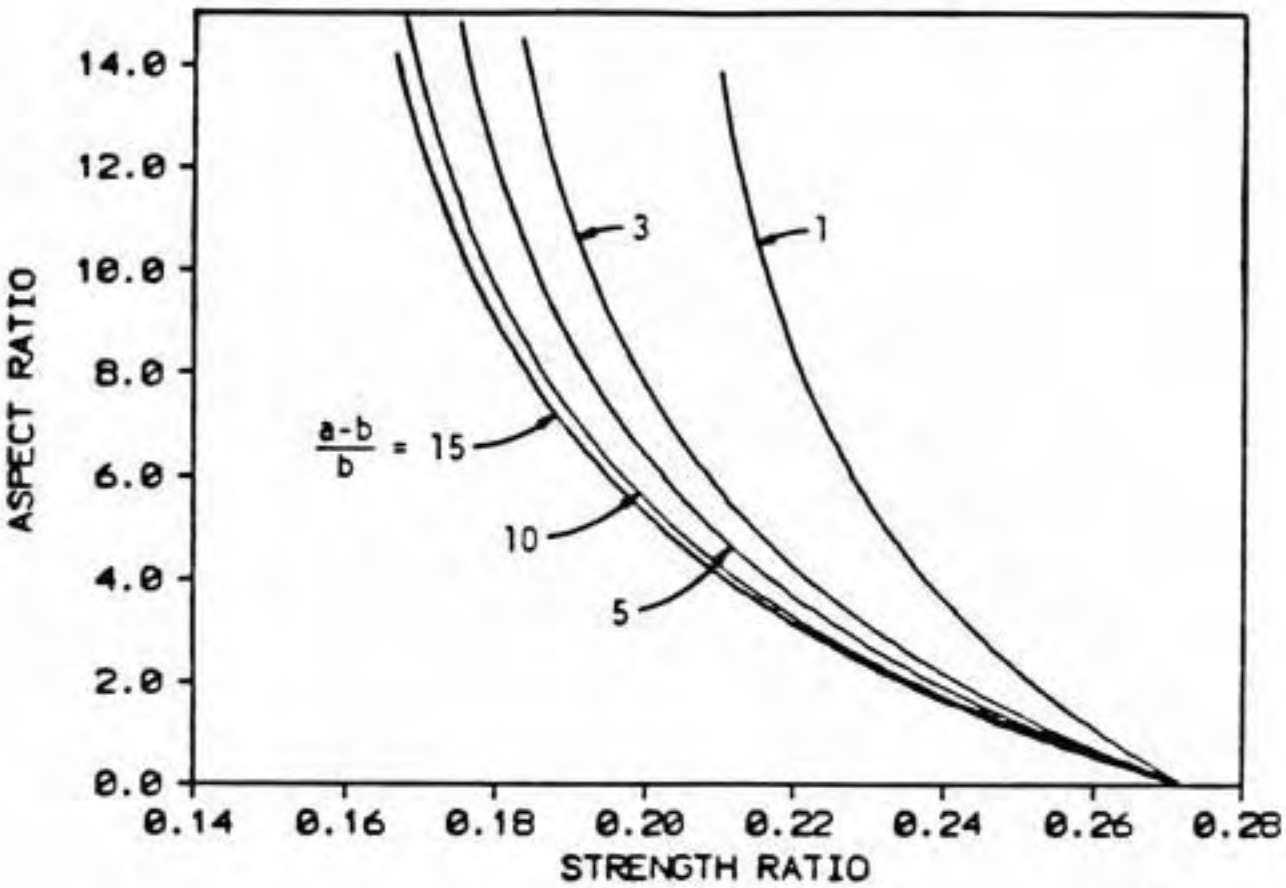

Figure 4.8 Aspect ratio vs. strength ratio ($J_{2f}^{1/2}/\sigma'_{vo}$) for $\alpha = 0.1090$, $\kappa = 0$, and $K_o = 0.75$.

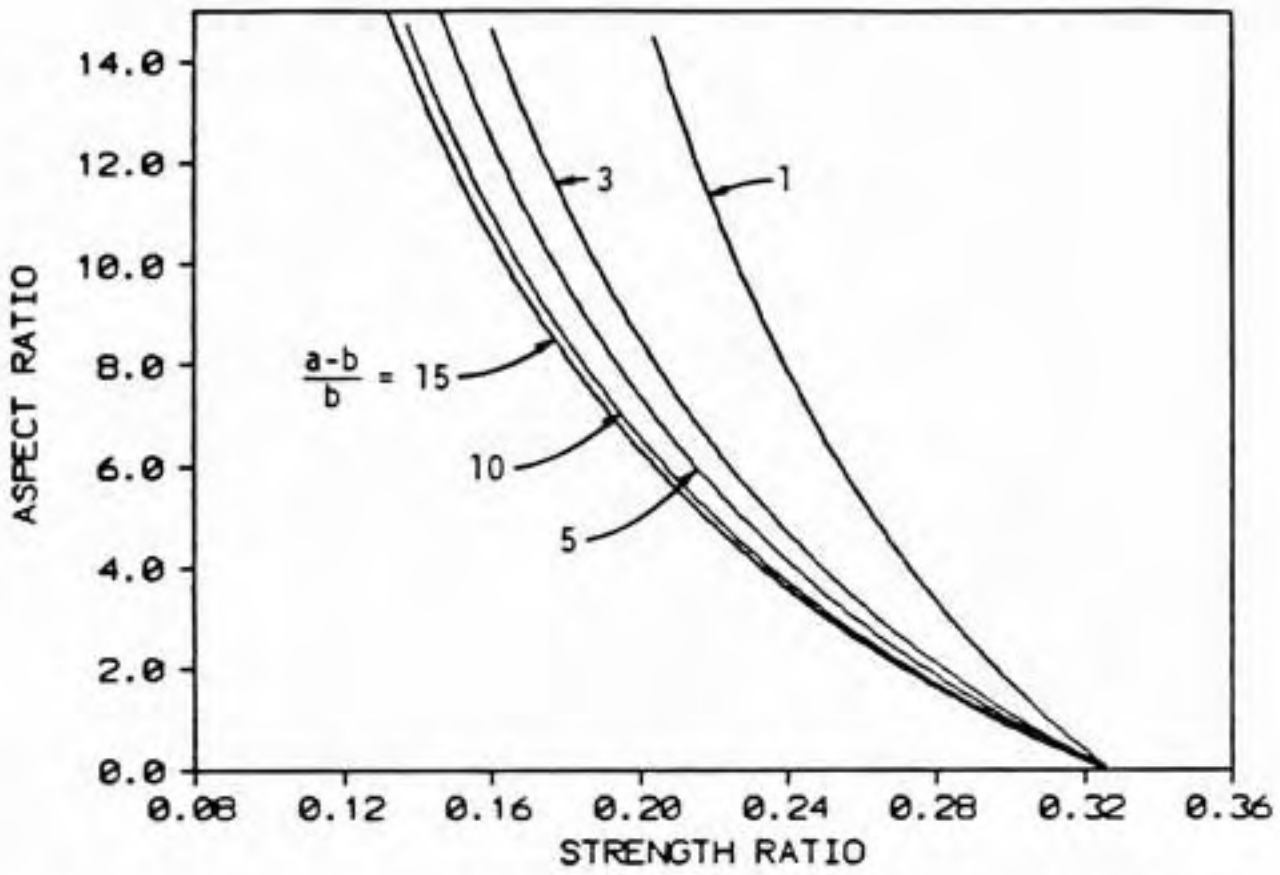

Figure 4.9 Aspect ratio vs. strength ratio ($J_{2f}^{1/2}/\sigma'_{vo}$) for $\alpha = 0.1090$, $\kappa = 0$, and $K_o = 1.00$.

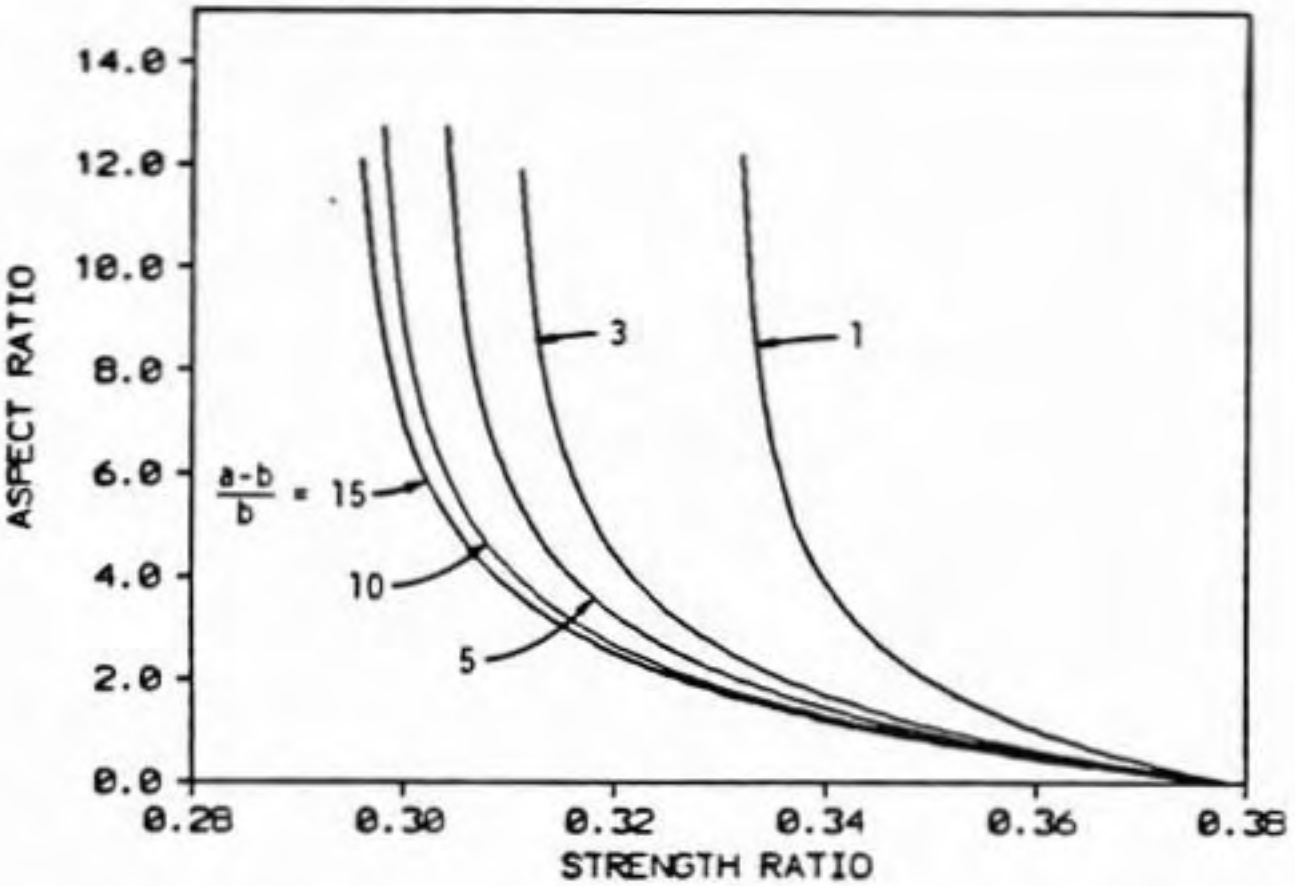

Figure 4.10 Aspect ratio vs. strength ratio ($J_{2f}^{1/2}/\sigma'_{vo}$) for $a = 0.1893$, $\kappa = 0$, and $K_o = 0.50$.

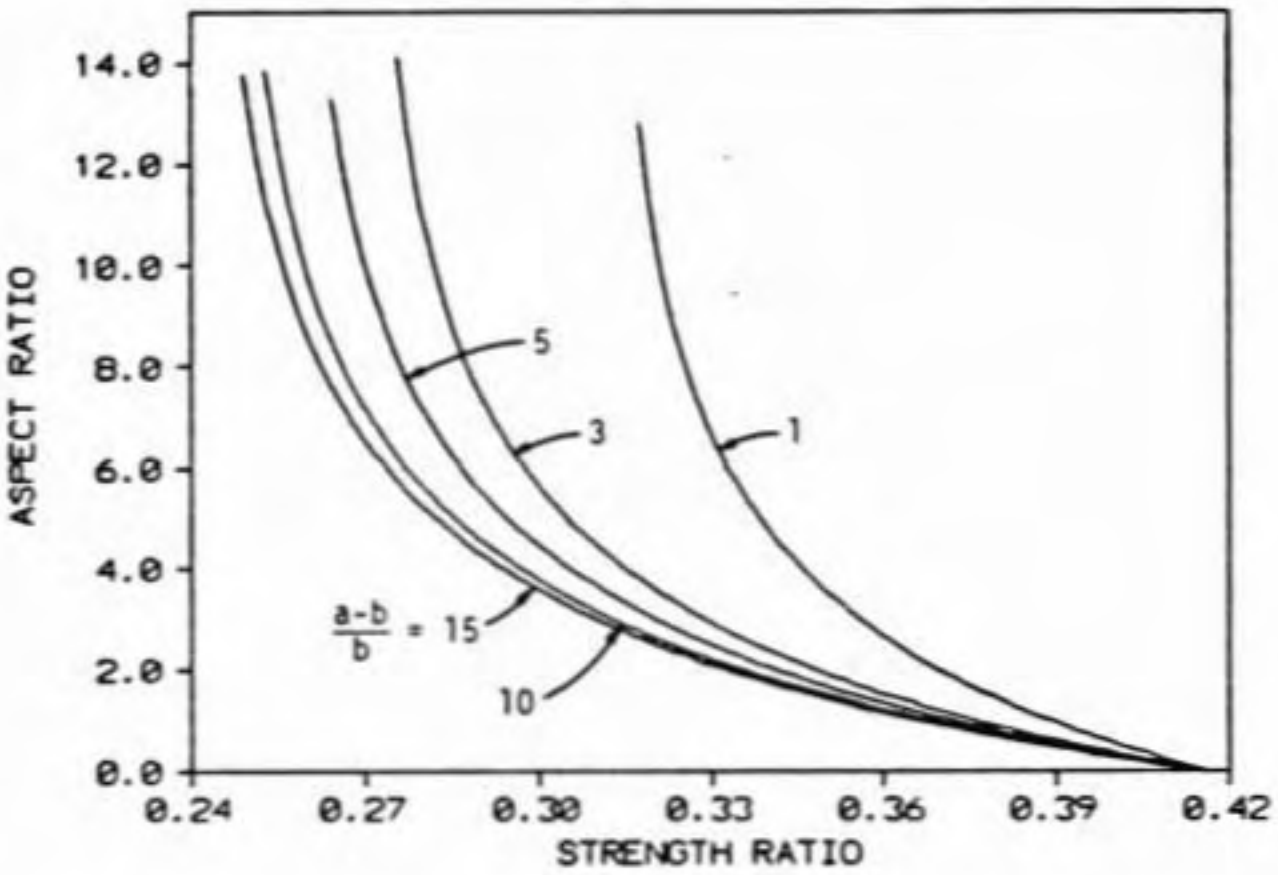

Figure 4.11 Aspect ratio vs. strength ratio ($J_{2f}^{1/2}/\sigma'_{vo}$) for $a = 0.1893$, $\kappa = 0$, and $K_o = 0.60$.

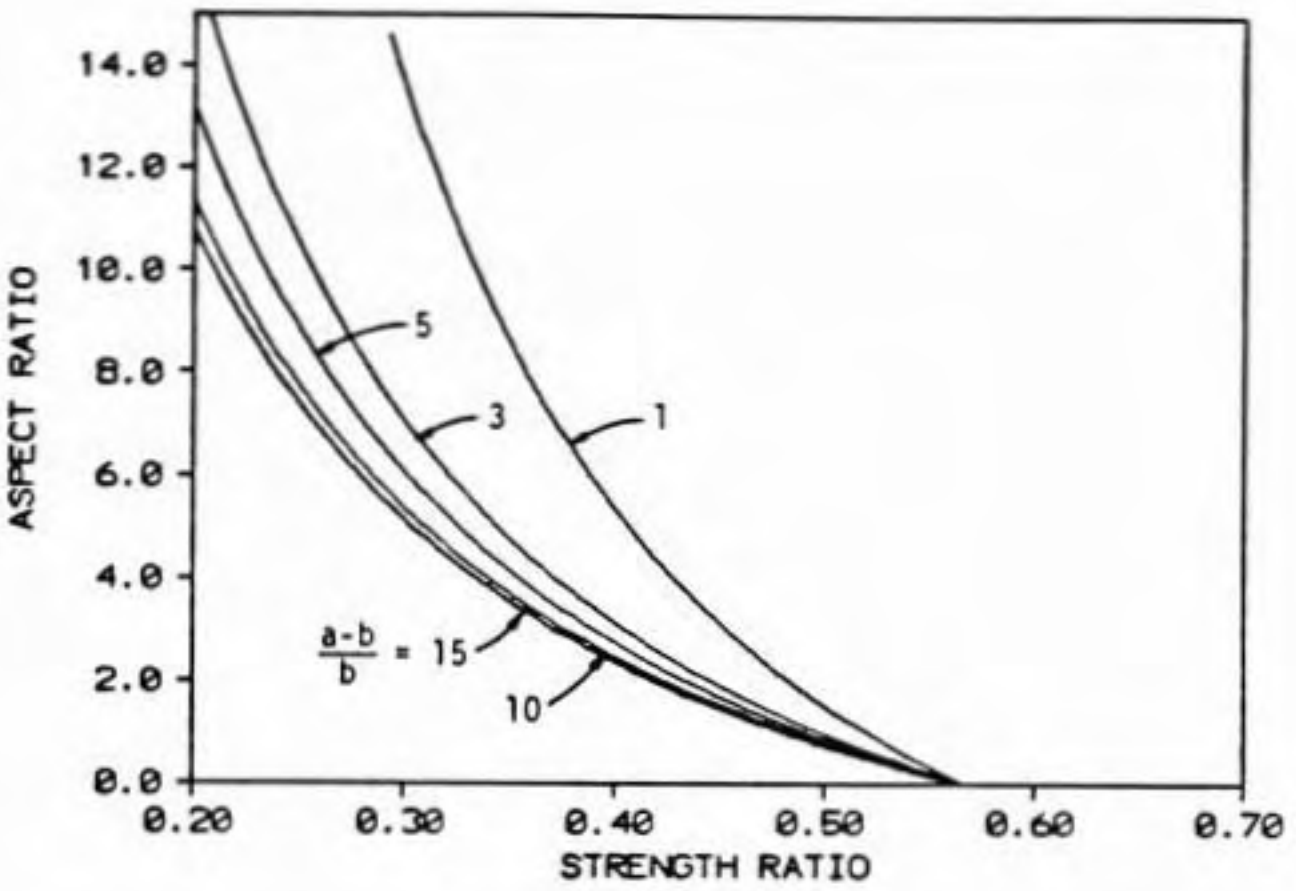

Figure 4.12 Aspect ratio vs. strength ratio ($J_{2f}^{1/2}/\sigma'_{vo}$) for $\alpha = 0.1893$, $\kappa = 0$, and $K_o = 1.00$.

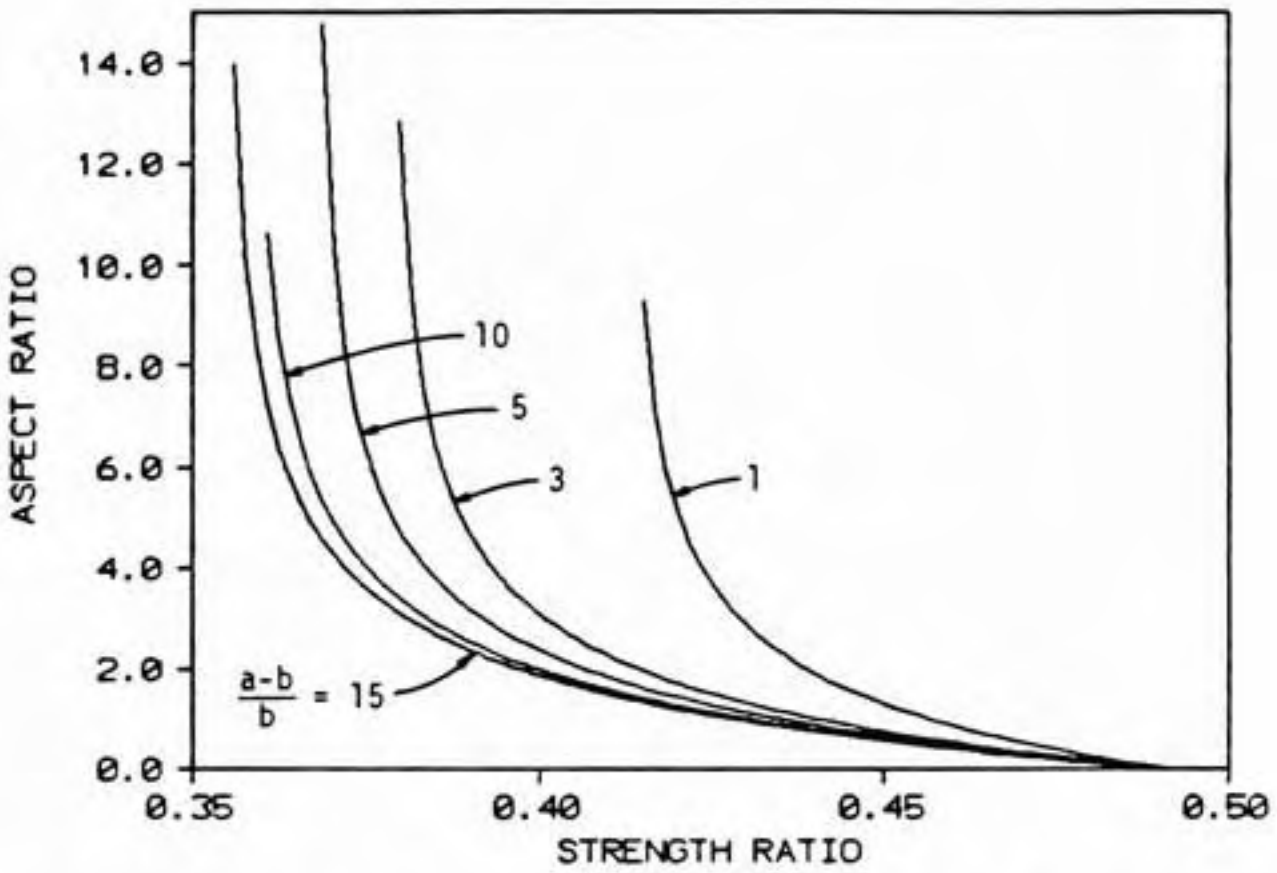

Figure 4.13 Aspect ratio vs. strength ratio ($J_{2f}^{1/2}/\sigma'_{vo}$) for $\alpha = 0.2730$, $\kappa = 0$, and $K_o = 0.40$.

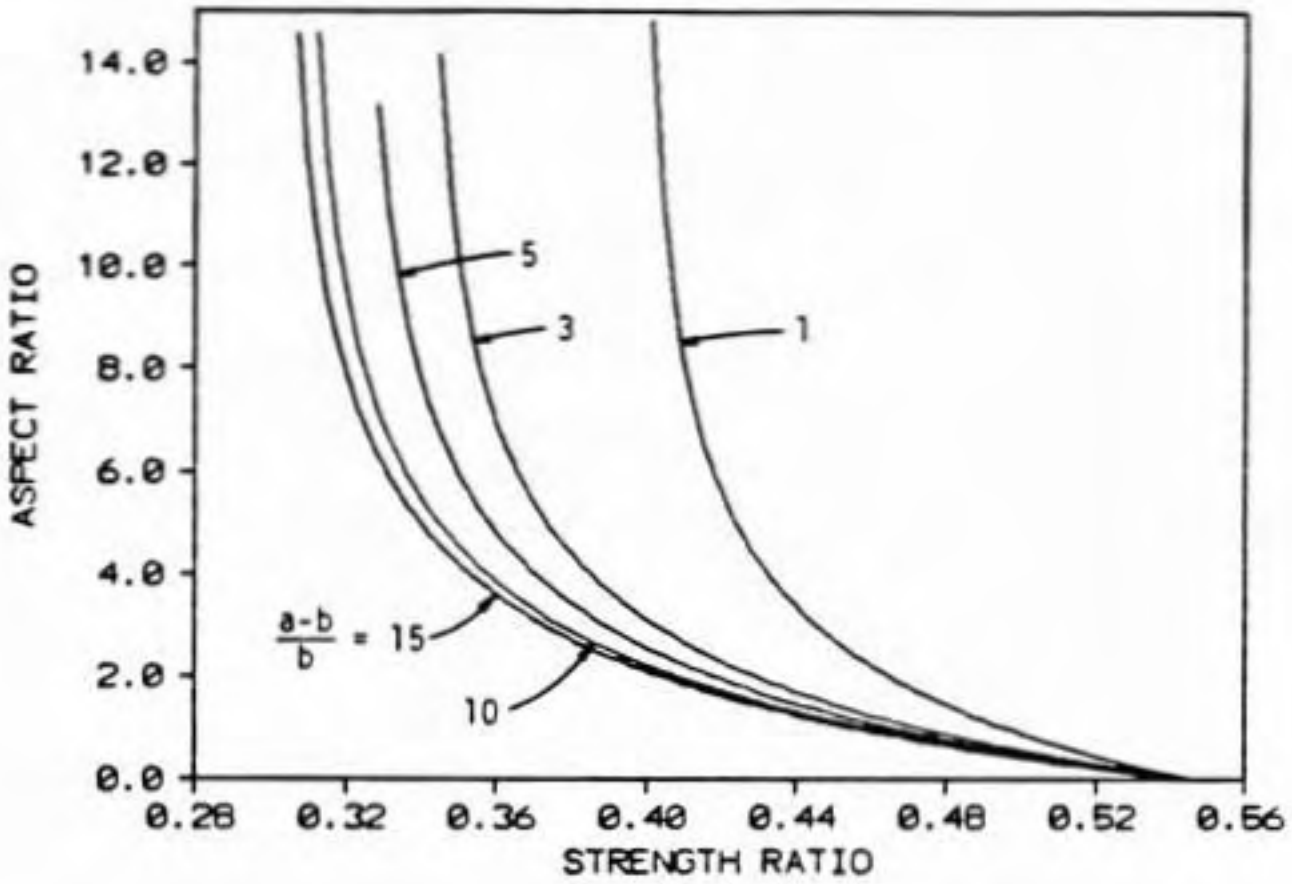

Figure 4.14 Aspect ratio vs. strength ratio ($J_{2f}^{1/2}/\sigma'_{vo}$) for $a = 0.2730$, $\kappa = 0$, and $K_o = 0.50$.

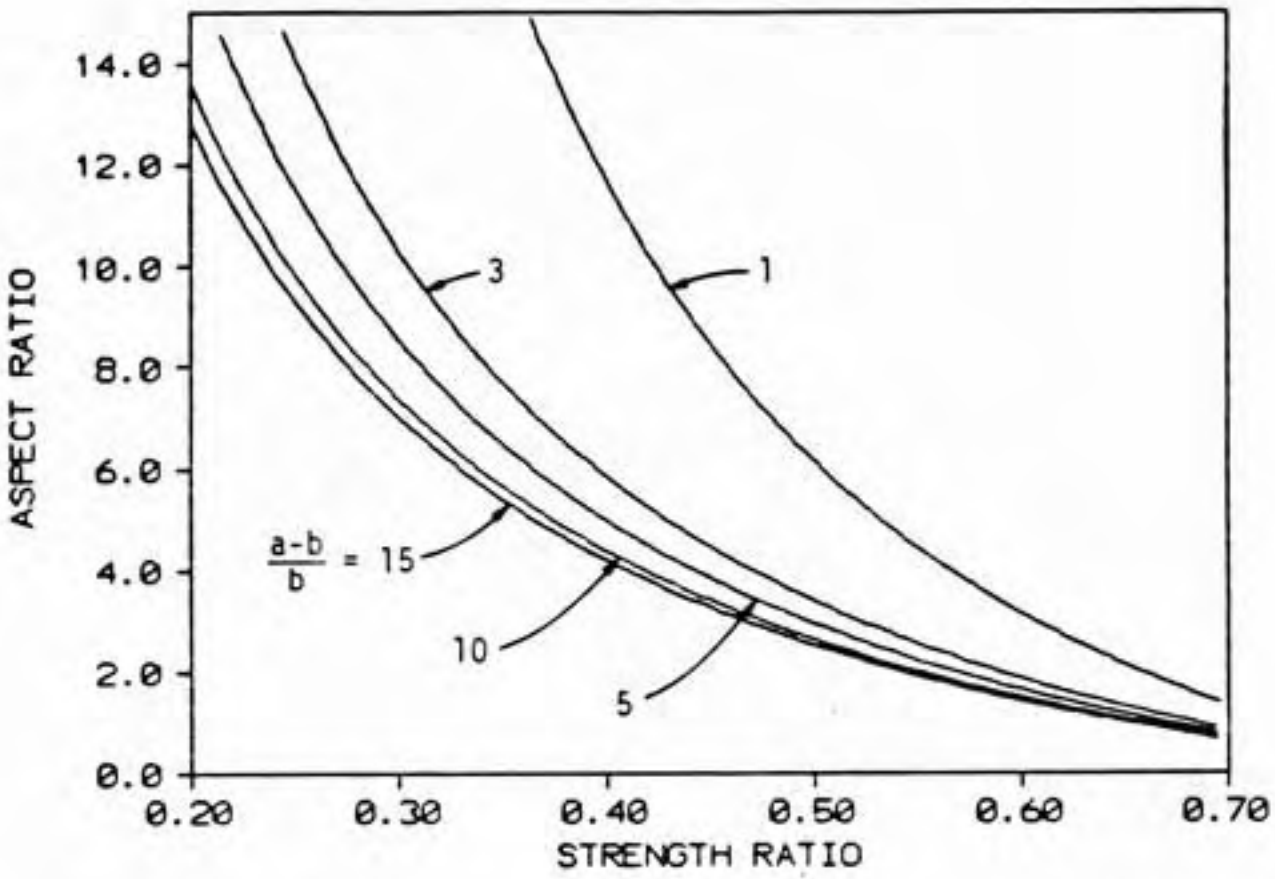

Figure 4.15 Aspect ratio vs. strength ratio ($J_{2f}^{1/2}/\sigma'_{vo}$) for $\alpha = 0.2730$, $\kappa = 0$, and $K_o = 1.00$.

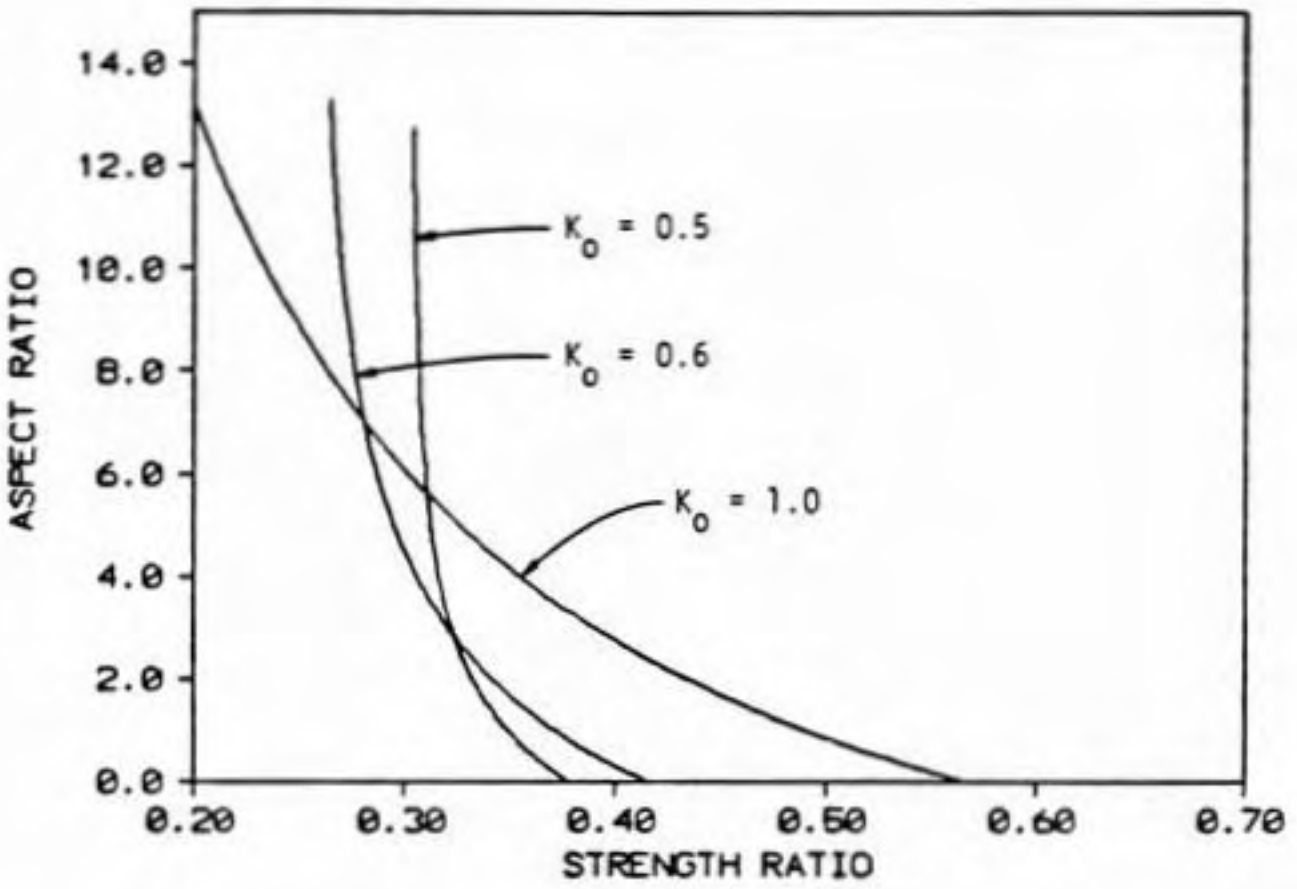

Figure 4.16 Effect of K_o on the aspect ratio for $a = 0.1893$, $\kappa = 0$, and $(a-b)/b = 5$.

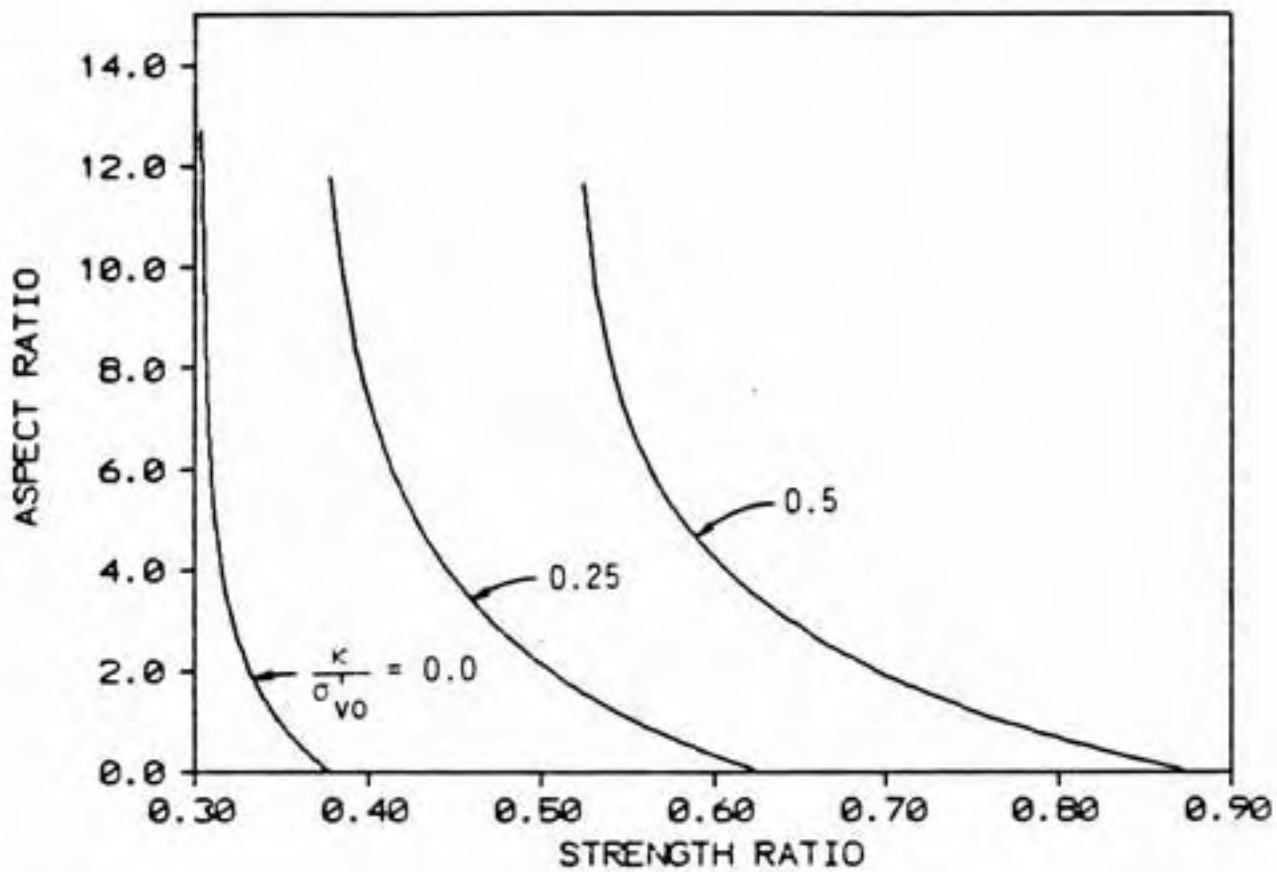

Figure 4.17 Effect of $\kappa/\sigma'_{vo} > 0$ on the aspect ratio for $\alpha = 0.1893$, $(a-b)/b = 5$, and $K_o = 0.5$.

For the further restriction of hydrostatic conditions (K_o = 1) Eq. 4.65 becomes

$$x_o = 3\sigma'_{vo} \tag{4.66}$$

4.2.4.3 Initial cap position for overconsolidated soil. The ratio s_u/σ'_{vc} is generally less for overconsolidated (OC) than for normally consolidated (NC) soil where σ'_{vc} is the maximum past vertical consolidation stress. Note that the commonly used ratio s_u/σ'_{vo} is higher for OC soil (Ladd, et al., 1977). The cap model represents this behavior by contraction of the cap due to the dilation that occurs for loading on the ultimate failure surface. No dilation or contraction is allowed for loading within the region bounded by the cap and ultimate failure surface.

The stress path for overconsolidated soils whose stress path intersects the ultimate failure surface prior to reaching the cap is shown in Fig. 4.18. The path rises vertically until reaching the ultimate failure surface, then follows the surface causing positive plastic volumetric strain (dilation) and contraction of the cap (Fig. 3.2b). This is intended to account for the reduction in strength that OC soils experience when they dilate. The stress path continues to follow the ultimate failure surface until intersecting the corner of the cap at $J_{2f}^{1/2}$. McCarron (1985) found that the model underestimated contraction of the cap

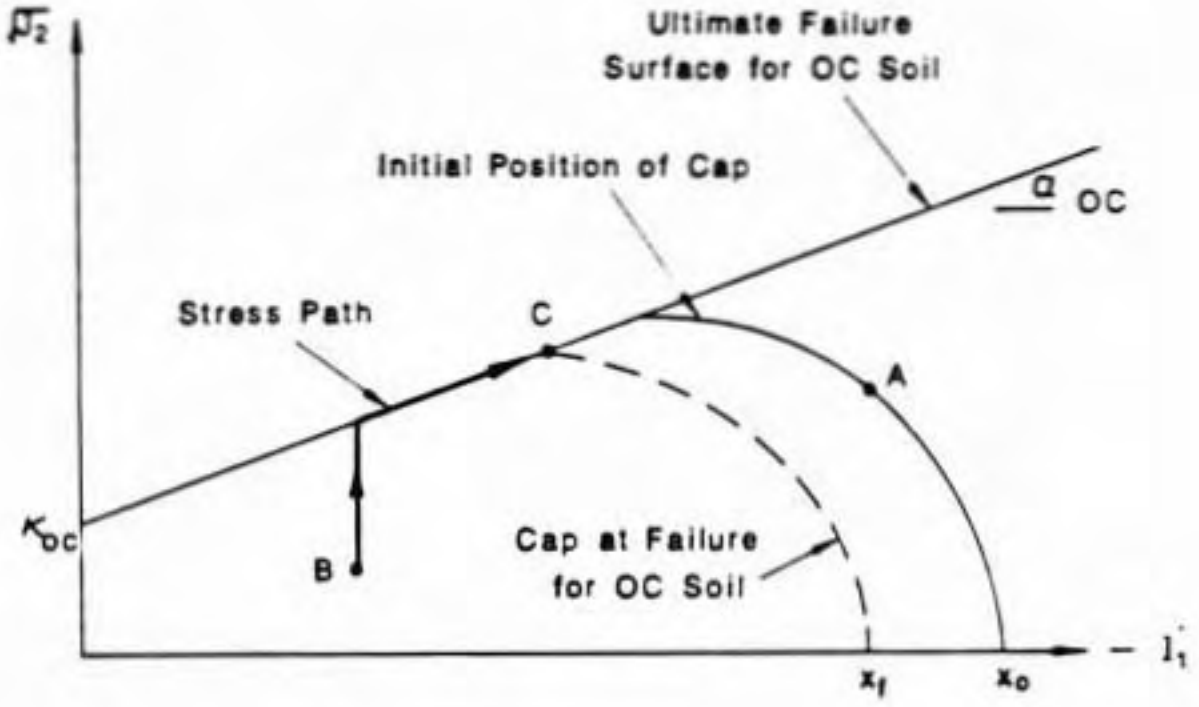

State of stress:
- A - Normally consolidated
- B - After unloading (overconsolidated)
- C - Overconsolidated at failure

Figure 4.18 Effective stress path predicted by cap model for overconsolidated soil.

due to plastic dilation for the portion of the stress path on the ultimate failure surface. Consequently the undrained shear strength for OC soil is overestimated. This is felt to be due to plastic dilation which overconsolidated soils undergo for loading in the region bounded by the ultimate failure surface and the cap, and possibly because the assumption of a normal flow rule for the ultimate failure surface is not valid.

To obtain a correct prediction of the undrained shear strength McCarron (1985) proposed that the cap be fixed at the position passing through the correct $(I'_{1f}, J_{2f}^{1/2})$. For this condition x_o is given by

$$x_o = \kappa/\alpha - J_{2f}^{1/2}(R + 1/\alpha) \qquad (4.67)$$

The cap is not allowed to contract due to the dilation which occurs for the portion of the stress path on the ultimate failure surface. The consequence of this procedure is that pore pressure predictions are unreliable.

The ultimate yield surface for overconsolidated soil generally lies above the normally consolidated ultimate yield surface. Where possible α and κ should be determined for the overconsolidated state.

4.2.4.4 Reversal of principal stresses. Reversal of principal stresses occurs when the minor principal stress is increased to failure or the major principal stress is decreased to failure. This occurs for K_o consolidated samples sheared on axial extension and lateral compression stress paths. The state of stress begins on the cap, however, the shear stress is initially reduced and the stress state moves into the elastic region. The cap model predicts a stress path having the shape shown in Fig. 4.19. For convenience states of stress where $\sigma_v' < \sigma_h'$ are plotted below the I_1' axis. The path moves vertically downward until it reaches the cap and only elastic strains occur. Then the path follows the cap and the cap expands causing plastic strains. Failure occurs when the state of stress reaches the ultimate failure surface. This stress path differs significantly from the behavior of many soils (Fig. 4.19) and often $J_{2f}^{1/2}$ is less than $J_{2o}^{1/2}$. It is not possible to calibrate the model for this situation since Eq. 4.57 is not satisfied. However, when $J_{2o}^{1/2}$ is less than $J_{2f}^{1/2}$ the model can be calibrated to yield the correct $J_{2f}^{1/2}$, although predicted pore pressures will likely be in error.

The inability of the model to represent this behavior is because stress changes within the region bounded by the cap and ultimate failure surfaces cause only elastic strains

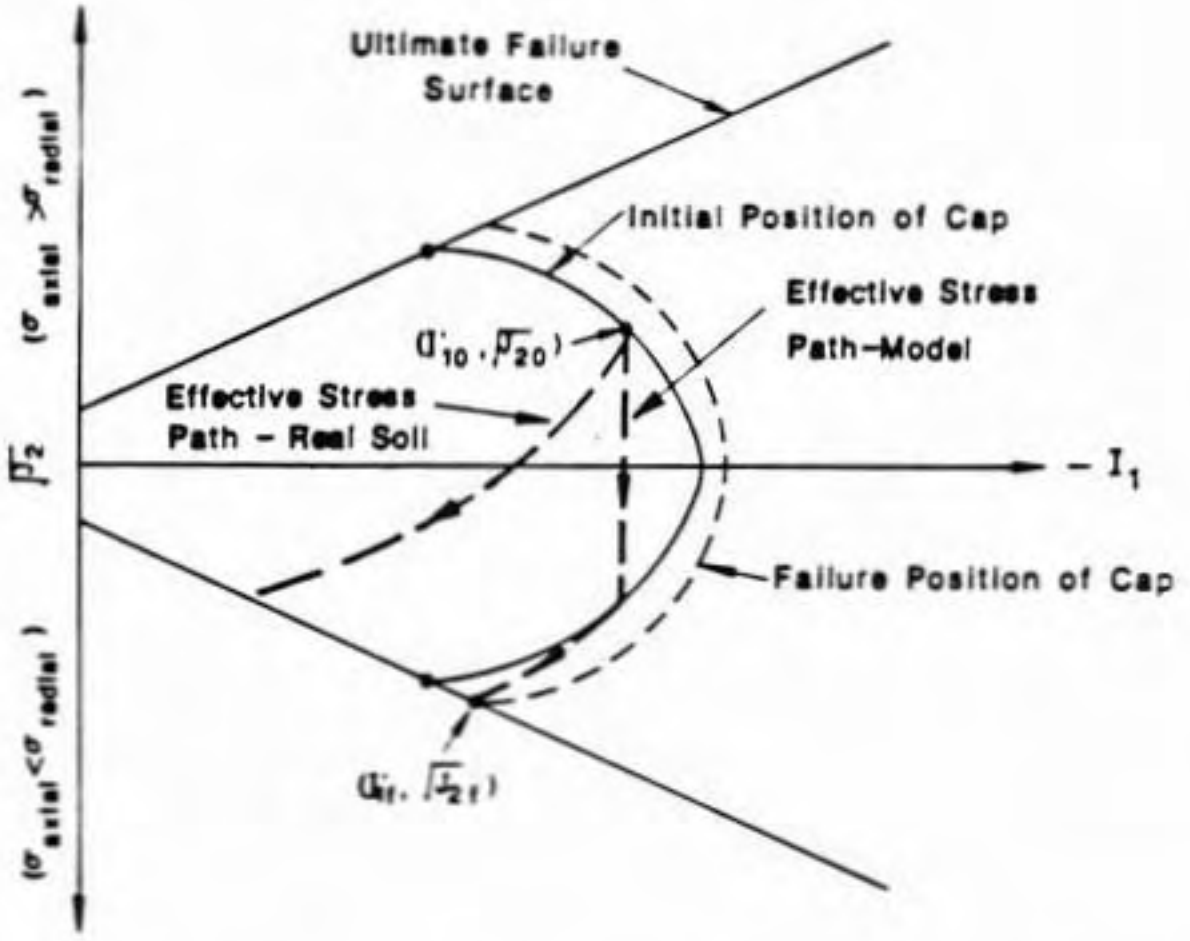

Figure 4.19 Effective stress path predicted by cap model for samples that undergo reversal of principal stresses.

and the cap and ultimate failure surfaces are symmetric about the I_1' axis. This is not the case for real soils.

4.2.5 Initial Stresses

The initial state of effective stress is calculated using the following equations

$$\sigma'_{vo} = A_2 + z\gamma \tag{4.68}$$

$$\sigma'_{ho} = \hat{K}_o \sigma'_{vo} \tag{4.69}$$

where A_2 = surcharge load

γ = average unit weight of soil

z = depth below ground surface

$\hat{K}_o$ = initial coefficient of lateral earth pressure

The ground surface is assumed to be horizontal. The average unit weight γ is a weighted average of the unit weights of soil above the depth z such that

$$\gamma = \frac{\sum_{i=1}^{i=n} z_i \gamma_i}{z} \tag{4.70}$$

where z_i = thickness of i^{th} soil layer

γ_i = unit weight of i^{th} soil layer- total unit weight above water table; buoyant unit weight below water table

n = number of soil layers

For normally consolidated soils $\hat{K}_o$ is the same as the K_o used to calculate the hardening parameters and aspect ratio. For overconsolidated soils $\hat{K}_o$ is generally greater than the normally consolidated K_o.

4.2.6 Pore Pressure Response Factor

The pore pressure response factor β was defined in Section 3.5. The actual value of β has a small effect on computed soil behavior provided the stiffness of the pore fluid/soil particle system K_f is much greater than the stiffness of the soil skeleton K. Naylor (1973) recommends β = 10 for undrained saturated conditions. β is zero for completely drained conditions. The model calculates pore pressures with Eq. 3.42.

4.3 PROCEDURE TO FIND CAP PARAMETERS

The procedure to find the input parameters for the cap model for undrained conditions is given below. The soil properties required to calibrate the model are shown in Table 4.4. Most of them are obtained from consolidation tests and laboratory or in situ strength tests. In some

cases it may be necessary to estimate a few of these properties. The values of K_o and s_u/σ'_{vo} should correspond to normally consolidated conditions since the shape of the cap is determined by normally consolidated soil behavior. Furthermore, K_o should be chosen to match the test or in situ conditions that will be modeled.

Table 4.4
Soil properties required to
calibrate cap model.

ϕ'
c'
s_u/σ'_{vo}
C_c
C_r
ν'
e_o
γ_t for soil above water table
γ_{sub} for soil below water table
K_o

The procedure assumes that the virgin loading and unloading/reloading curves can be approximated as straight lines on an ε_v-ln(p') or e-log(σ'_v) plot over the range of stress involved in the problem. For nonlinear virgin loading curves it is generally sufficient to approximate C_c as the tangent at σ'_{vo}.

The steps in the procedure are outlined below. As a general rule the cap parameters should be matched to the soil properties for the field or test conditions that will be analyzed. For example, if the parameters will be used to analyze the soft soil beneath an embankment then they should be determined for plane strain conditions with the in situ K_o even if the soil strength properties were obtained from hydrostatically consolidated triaxial tests. Application of the procedure is illustrated with two examples. A simple computer program to calculate Dx_o, $W/(a-b)$, x_f/x_o, $(x_f/x_o)_{max}$, and R_{max} is given in Humphrey and Holtz (1986a). Equations used in the procedure are summarized in Table 4.5 for easy reference.

4.3.1 Steps to Find Cap Parameters

1. Initial vertical stress. Calculate the initial vertical effective stress σ'_{vo} using total unit weight above the water table and buoyant unit weight below the water table. The ground surface is assumed to be horizontal.

2. α and κ. The Drucker-Prager parameters (α and κ) are matched to the Mohr-Coulomb parameters (ϕ' and c') for the conditions that will be modeled. Use Eqs. 4.1 and 4.2 if triaxial compression tests will be modeled or Eqs. 4.3 and 4.4 for triaxial extension texts. For plane strain

Table 4.5
Summary of equations for cap parameters.

A. Ultimate failure surface

1. Triaxial compression

$$\alpha = \frac{2\sin\phi'}{\sqrt{3}(3-\sin\phi')} \tag{4.1}$$

$$\kappa = \frac{6c'\cos\phi'}{\sqrt{3}(3-\sin\phi')} \tag{4.2}$$

2. Triaxial extension

$$\alpha = \frac{2\sin\phi'}{\sqrt{3}(3+\sin\phi')} \tag{4.3}$$

$$\kappa = \frac{6c'\cos\phi'}{\sqrt{3}(3+\sin\phi')} \tag{4.4}$$

3. Other conditions

$$\alpha = \frac{1}{3}\sin\phi' \;/\; [\sin(\theta + \pi/3) - \frac{1}{\sqrt{3}}\cos(\theta + \pi/3)\,\sin\phi'] \tag{4.8}$$

$$\kappa = c\,\cos\phi' \;/\; [\sin(\theta + \pi/3) - \frac{1}{\sqrt{3}}\cos(\theta + \pi/3)\,\sin\phi'] \tag{4.9}$$

where

$$\cos 3\theta = \frac{1}{2}\,\frac{2\eta^3 - 3\eta^2 - 3\eta + 2}{(\eta^2 - \eta + 1)^{3/2}} \tag{4.10}$$

B. Elastic behavior

$$K_1 = 1/b \;\; ; \;\; K_2 = 1 \tag{4.16}$$

$$b = \frac{C_r}{2.303(1+e_o)} \tag{4.17}$$

$$G_1 = \frac{3(1-2\nu')}{2(1+\nu')} \;\; ; \;\; G_2 = 0 \tag{4.22}$$

Table 4.5
Continued.

C. Hardening parameters (virgin loading curve linear on ε_v-ln(p') plot)

1. Equation for Dx_o

$$Dx_o = 2\ \ln[(1-P)/P]\ /\ (x_f/x_o - 1) \qquad (4.31a)$$

$$P = \frac{\ln[(1+x_f/x_o)/2]}{\ln[x_f/x_o]} \qquad (4.31b)$$

2. Equation for W/(a-b)

$$\frac{W}{(a-b)} = \frac{-\ln(x_f/x_o)}{\exp[(Dx_o)(x_f/x_o)] - \exp[Dx_o]} \qquad (4.33)$$

$$a = \frac{C_c}{2.303(1+e_o)} \qquad (4.34)$$

D. Aspect ratio

1. Equations for $J_{2f}^{1/2}/\sigma'_{vo}$

$$J_{2f}^{1/2}/\sigma'_{vo} = -\frac{2}{\sqrt{3}}(s_u/\sigma'_{vo}) \qquad (4.41)$$

$$J_{2f}^{1/2}/\sigma'_{vo} = -\frac{2}{\sqrt{3}}(s_u/\sigma'_{vo})\ (n^2-n+1)^{1/2} \qquad (4.42)$$

2. Equation for x_f/x_o (virgin loading curve linear on ε_v-ln(p') plot)

$$x_f/x_o = \exp\{\frac{-b}{a-b}\ln[\frac{\kappa/\sigma'_{vo} - J_{2f}^{1/2}/\sigma'_{vo}}{a(1+2K_o)}]\} \qquad (4.49)$$

Table 4.5
Continued.

D. Aspect ratio (continued)

3. Equations for R

a. General equation

$$x_f/x_o = \frac{[(\kappa/\sigma'_{vo})(1-aR) - (J_{2f}^{1/2}/\sigma'_{vo})(1-a^2R^2)]/a}{-R(\kappa/\sigma'_{vo}) + (1+2K_o) - R(H)^{1/2}} \quad (4.53)$$

where

$$H = (1-K_o)^2(a^2R^2-1)/3 + a^2(1+2K_o)^2 + (\kappa/\sigma'_{vo})^2 - 2a(\kappa/\sigma'_{vo})(1+2K_o) \quad (4.54)$$

b. Special case, $\kappa = 0$

$$x_f/x_o = \frac{-(J_{2f}^{1/2}/\sigma'_{vo})(1-a^2R^2)/a}{1+ 2K_o - R[\frac{1}{3}(1-K_o)^2(a^2R^2-1) + a^2(1+2K_o)^2]^{1/2}} \quad (4.55)$$

c. Special case, $\kappa = 0$ and $K_o = 1$

$$R = -3(x_f/x_o)/(J_{2f}^{1/2}/\sigma'_{vo}) - \frac{1}{a} \quad (4.56)$$

3. Restrictions on input parameters

$$(1-K_o)/\sqrt{3} < -J_{2f}^{1/2}/\sigma'_{vo} \quad (4.57)$$

$$|J_{2f}^{1/2}/\sigma'_{vo}| < |\kappa/\sigma'_{vo} - a(1+2K_o)| \quad (4.58)$$

See also Eqs. 4.59 through 4.63

Table 4.5
Continued.

E. Initial position of cap

1. Normally consolidated soil
   a. General equation

$$x_o = [\sigma'_{vo}/(1-aR)]\ \{-R(\kappa/\sigma'_{vo}) + (1+2K_o) - RH^{1/2}\} \quad (4.64)$$

   b. Special case, $\kappa = 0$

$$x_o = [\sigma'_{vo}/(1-aR)] \times \{(1+2K_o) - R[(1-K_o)^2(a^2R^2-1)/3 + a^2(1+2K_o)^2]^{1/2}\} \quad (4.65)$$

   c. Special case, $\kappa = 0$ and $K_o = 1$

$$x_o = 3\sigma'_{vo} \quad (4.66)$$

2. Overconsolidated soil

$$x_o = \kappa/a - J_{2f}^{1/2}(R + 1/a) \quad (4.67)$$

F. Initial stress - average unit weight

$$\gamma = \frac{\sum_{i=1}^{i=n} z_i\gamma_i}{z} \quad (4.70)$$

conditions a value of η (Eq. 4.7) is estimated (see Chapter 5) and Eqs. 4.8 and 4.9 are used. Alternately, if plane strain test results are available, α and κ should be obtained from the slope and intercept of the best fit straight line on an plot of $J_{2f}^{1/2}$ versus I'_{1f}.

The value of the tension cut-off T_c for soils with non-zero cohesion is estimated to be a small positive value. Soils with zero cohesion cannot develop tension so the value of T_c is not important and it can be taken as 1.0.

3. $J_{2f}^{1/2}/\sigma'_{vo}$ ratio. The match between s_u/σ'_{vo} and $J_{2f}^{1/2}/\sigma'_{vo}$ also depends on the condition to be modeled. If triaxial compression or extension tests will be modeled use Eq. 4.41. To model plane strain conditions use Eq. 4.42 with the estimated η or, if plane strain test results are available, the ratio should be obtained from measured stresses using Eq. 3.2.

4. a and b. These parameters are the slopes on an ε_v-ln(p') plot of the virgin loading and unloading/reloading curves from hydrostatic consolidation tests. If only C_c and C_r are available from one-dimensional consolidation tests, Eqs. 4.34 and 4.17 are used to find a and b. The a-value for nonlinear virgin loading curves is approximated as the tangent at the estimated x_o. The estimated x_o is compared

to the value calculated in step 9 and, if necessary, a new a-value should be computed.

5. Compatibility of strength parameters with initial state of stress. Check the compatibility using Eqs. 4.57 and 4.58 with the K_o for the conditions that will be modeled. If they are incompatible revise the input parameters.

6. Modulus parameters. K_1 is found using Eq. 4.16 and $K_2 = 1$. Values of A_p are given in Table 4.2 and it should be chosen to have units consistent with the stress units. Calculate G_1 using Eq. 4.22 and take $G_2 = 0$ or, if G is approximately constant, set $G_1 = 0$ and $G_2 = G$.

7. x_f/x_o ratio. Use Eq. 4.49 to calculate x_f/x_o. Calculate R_{max} using Eq. 4.59 and the corresponding $(x_f/x_o)_{max}$ from Eq. 4.53 or 4.55. Check that $x_f/x_o \leq (x_f/x_o)_{max}$; if not, revise the input parameters. When both $\kappa = 0$ and $K_o = 1$, R_{max} and $(x_f/x_o)_{max}$ are infinite.

8. Aspect ratio, R. Use Eq. 4.53, 4.55, or 4.56 with the value of K_o for the problem that will be modeled. Eqs. 4.53 and 4.55 require trial and error solution for R. Figs. 4.7 through 4.15 are helpful in estimating an initial guess for R. Check that R is less than R_{max}; if not, revise the input parameters.

9. Initial position of cap, x_o. For normally consolidated soil use Eq. 4.64, 4.65, or 4.66 to calculate x_o. If necessary, compare this value to the x_o estimated in step 4. For overconsolidated soil use Eq. 4.67.

10. Hardening parameters, D and W. First use Figs. 4.3 and 4.4, Table 4.3, or Eqs. 4.31 and 4.33 with the x_f/x_o from step 7, to find Dx_o and $W/(a-b)$; then use x_o and $(a-b)$ to find D and W.

11. Pore pressure response. Set $B = 10$ for undrained conditions.

12. Initial stresses. Calculate the average unit weight γ using Eq. 4.70 and set A_2 equal to the surcharge applied to the ground surface, if any. Use the given or estimated initial $\hat{K}_o$ which for normally consolidated soils equals the normally consolidated K_o. For overconsolidated soils $\hat{K}_o$ is generally greater than the normally consolidated value.

4.3.2 Example 1 - Hydrostatic Initial Conditions

This example illustrates the procedure to obtain the cap parameters for hydrostatic initial conditions to model the behavior of consolidated isotropic undrained triaxial compression (CIUC) samples. Input soil properties were

obtained from CIUC and one-dimensional consolidation tests and are summarized in Table 4.6. K_o = 1 since hydrostatic conditions will be modeled.

Table 4.6
Soil properties for Example 1.

$\phi' = 25^o$
$c' = 0$
$s_u/\sigma'_{vo} = 0.30$
$C_c = 0.3$
$C_r = 0.1$
$\nu' = 0.25$
$e_o = 0.9$
$\gamma_t = 16.0$ kN/m^3
$\gamma_{sub} = 8.5$ kN/m^3
$K_o = 1.0$ (hydrostatic)

The initial vertical stress σ'_{vo} will represent a soil layer at a depth of 5 m with the water table at a depth of 1 m. The steps in the procedure are given below.

1. The initial vertical effective stress σ'_{vo} is $-((1m)(16.0\ kN/m^3) + (4\ m)(8.5\ kN/m^3)) = -50$ kPa. Recall that the negative sign is because compressive stresses are negative.

2. The α and κ parameters are calculated to be 0.189 and 0.0 using Eqs. 4.1 and 4.2 which are valid for triaxial compression. T_c is irrelevant for soils with zero cohesion and is taken to be 1.0 kPa.

3. $J_{2f}^{1/2}/\sigma'_{vo} = -0.346$ using Eq. 4.41 which is applicable for triaxial conditions.

4. The a and b parameters are found from one-dimensional consolidation tests results using Eqs. 4.34 and 4.17. Values of a = 0.069 and b = 0.023 are calculated.

5. The compatibility of the strength parameters with initial state of stress are checked using Eqs. 4.57 and 4.58. These criteria are satisfied since $(1-K_o)/\sqrt{3} = 0 < -J_{2f}^{1/2}/\sigma'_{vo}$ (Eq. 4.57) and $|J_{2f}^{1/2}/\sigma'_{vo}| = |-0.346| < |-0.567|$ (Eq. 4.58).

6. The parameters for the bulk modulus are $K_1 = 43.7$ (using Eq. 4.16), $K_2 = 1.0$, and $A_p = 101.3$ kPa (Table 4.2). Poisson's ratio is given so the shear modulus parameters are: $G_1 = 0.6$ (from Eq. 4.22) and $G_2 = 0$.

7. The ratio x_f/x_o is found using Eq. 4.49 which results in $x_f/x_o = 1.28$. R_{max} and $(x_f/x_o)_{max}$ are infinite for hydrostatic initial conditions with $\kappa = 0$.

8. For hydrostatic conditions R is calculated to be 5.81 using Eq. 4.56.

9. The initial position of the cap is $3\sigma'_{vo}$ (Eq. 4.66) for hydrostatic initial conditions which gives x_o = -150 kPa.

10. The hardening parameters are found from Figs. 4.3b and 4.4b; for x_f/x_o = 1.28, Dx_o = -0.881 and W/(a-b) = 2.73. Using x_o, a, and b computed above D = $-0.881/(3\sigma'_{vo})$ = $-0.294/\sigma'_{vo}$ = 0.0020 $(kPa)^{-1}$ and W = 0.13.

11. The pore pressure response factor B is 10 for undrained conditions.

12. For hydrostatic conditions $\hat{K}_o$ = 1.0 and, since there is no surcharge, A_2 = 0.0. The average unit weight γ is calculated to be 10 kN/m^3 using Eq. 4.70.

The parameters calculated above are summarized in Table 4.7.

4.3.3 Example 2 - Nonhydrostatic Initial Conditions

This example illustrates the procedure to obtain the cap parameters for nonhydrostatic initial conditions to model the behavior of K_o consolidated undrained triaxial

Table 4.7
Summary of cap parameters for example problems.

Parameter	Example 1	Example 2
α	0.189	0.189
κ	0.0	0.0
T_c	1.0 kPa	1.0 kPa
K_1	43.7	43.7
K_2	1.0	1.0
A_p	101.3 kPa	101.3 kPa
G_1	0.6	0.6
G_2	0.0	0.0
R	5.8	2.3
x_o	-150 kPa	-121 kPa
D	0.0020 $(kPa)^{-1}$	0.0079 $(kPa)^{-1}$
W	0.13	0.12
β	10.0	10.0
A_2	0.0	0.0
γ	10 kN/m^3	10 kN/m^3
$\hat{K}o$	1.0	0.58

compression (CK_oUC) tests. The same soil properties are used as in Example 1 (Table 4.6) except that K_o is estimated to be 0.58. The same soil and water table depths are used. It is assumed that the strength properties obtained from CIUC tests are valid for nonhydrostatic conditions.

1. through 4. Same as Example 1.

5. The strength parameters and the initial state of stress are compatible since $0.33 < -J_{2f}^{1/2}/\sigma'_{vo}$ (Eq. 4.57) and $|J_{2f}^{1/2}/\sigma'_{vo}| = |-0.346| < |-0.408|$ (Eq. 4.58).

6. Same as Example 1.

7. Eq. 4.49 results in $x_f/x_o = 1.086$. R_{max} is found using Eq. 4.59 but for this case R_{max} is so large ($>5x10^5$) that it is difficult to calculate. The corresponding $(x_f/x_o)_{max}$ is greater than 1.4 (Eq. 4.55). The actual x_f/x_o is less than this value.

8. R is found by trial and error solution of Eq. 4.55 using the value of x_f/x_o computed using Eq. 4.49. An initial guess for R can be estimated using Fig. 4.10 which was computed with $\alpha = 0.1893$, $\kappa = 0$, and $K_o = 0.5$ and Fig. 4.11 which was computed with $\alpha = 0.1893$, $\kappa = 0$, and $K_o = 0.6$. Using $(a-b)/b = 2.0$ and $J_{2f}^{1/2}/\sigma'_{vo} = -0.346$, R is

estimated to be 2.0 for K_o = 0.5 (Fig. 4.10) and 2.6 for K_o = 0.6 (Fig. 4.11). A value of 2.5 was chosen for the first guess. After a few trials it is found that R = 2.3 satisfies Eq. 4.55. This value is less than R_{max}.

9. The initial position of the cap is computed to be $x_o = 2.42\sigma'_{vo}$ = -121 kPa using Eq. 4.65.

10. Using Figs. 4.3b and 4.4b with x_f/x_o = 1.086, it is found that Dx_o = -0.959 and W/(a-b) = 2.719; therefore, D = $-0.396/\sigma'_{vo}$ = 0.0079 $(kPa)^{-1}$ and W = 0.12.

11. and 12. Same as Example 1.

The parameters calculated above are summarized in Table 4.7.

4.4 CAP PARAMETERS FOR BOSTON BLUE CLAY

The procedure described in the previous section was used to calculate the cap parameters for resedimented samples of normally consolidated Boston Blue Clay. The samples had an average liquid limit of 41 and an average plasticity index of 21. Parameters were determined using input soil properties from consolidated isotropic (hydrostatic) undrained compression (CIUC), consolidated isotropic (hydrostatic) undrained extension (CIUE), K_o consolidated

undrained compression (CK_oUC), and $1/K_o$ consolidated undrained extension ($C(1/K_o)UE$) triaxial tests as well as K_o consolidated undrained plane strain active (CK_oUPSA) tests. The $1/K_o$ tests were consolidated with the confining stress greater than the axial stress. K_o consolidated undrained extension and $1/K_o$ consolidated undrained compression triaxial tests which undergo reversal of principal stresses during loading are also considered. In addition, the parameters were calculated for CK_oUPSA tests on overconsolidated samples. The triaxial tests had an average initial water content of 30% and the average for the plane strain tests was 36%. The test results were obtained from Ladd and Varallyay (1965) and Ladd, et al. (1971).

The cap model is implemented in a computer program called CAP developed by McCarron and Chen (1986a). This program was used with the calculated parameters to verify that the test sample's stress-strain, pore pressure, and effective stress path behavior were predicted correctly.

4.4.1 Triaxial Tests

A comprehensive set of triaxial tests on normally consolidated samples of resedimented Boston Blue Clay were performed by Ladd and Varallyay (1965). The virgin loading and unloading/reloading one-dimensional consolidation curves were approximately linear on a semi-log plot with average

e_o = 0.892, C_c = 0.34, and C_r = 0.051. An a = 0.078 and b = 0.012 were calculated using Eqs. 4.34 and 4.17. The bulk modulus parameter K_1 was calculated to be 85.5 (Eq. 4.16) and K_2 = 1.0. Stresses were expressed in units of kg/cm^2 so A_p was chosen to be 1.033 kg/cm^2 (Table 4.2). Reliable data to determine the shear modulus was unavailable so ν' = 0.25 was assumed and G_1 was calculated to be 0.60 (Eq. 4.22) and G_2 = 0.0. The hardening parameter W was calculated to be approximately 0.18 for all tests. The value of κ was taken to be 0. The axial consolidation stress σ'_{vo} was input by setting the surcharge A_2 equal to σ'_{vo} and taking γ = 0.0. In addition, the following parameters where chosen in accordance with the recommendations given in the previous section: T_c = 1.0 kg/cm^2, and β = 10.0. All these parameters are summarized in Table 4.8.

The values of α, R, x_o, D, and K_o were different for each test and are summarized in Table 4.9 along with the soil properties ϕ' and s_u/σ'_{vo} and the sample consolidation conditions. The ratio s_u/σ'_{vo} was defined as s_u divided by the vertical (axial) consolidation stress (σ'_{vo}) even when σ'_{vo} was the minor principal stress. For a given test type, values of ϕ' and s_u/σ'_{vo} were independent of confining pressure and average values were used. An exception was the C(1/K_o)UE tests which exhibited different values of ϕ' and s_u/σ'_{vo} for each confining pressure so the actual

Table 4.8
Summary of cap parameters for Boston Blue Clay.

Parameter	Triaxial tests	Plane strain tests
α	See Table 4.9	0.190
κ	0.0	0.0
T_c	1.0 kg/cm^2	1.0 kg/cm^2
K_1	85.5	220.0
K_2	1.0	1.0
A_p	1.033 kg/cm^2	1.033 kg/cm^2
G_1	0.6	0.6
G_2	0.0	0.0
R	See Table 4.9	0.21
S	1	1
x_o	See Table 4.9	-7.71 kg/cm^2
D	See Table 4.9	0.129 (kg/cm^2)$^{-1}$
W	0.180	0.141
β	10.0	10.0
A_1	See Table 4.9	-3.87 kg/cm^2
γ	0.0	0.0
K_o	See Table 4.9	0.48

Table 4.9
Soil properties, consolidation conditions and cap parameters for triaxial tests.

Test no.	Soil properties		Consolidation conditions			Cap parameters		
	ϕ'	s_u/σ'_{vo}	$-\sigma'_{vo}$	K_o	α	x_o	D	R
	(^{o})	---	(kg/cm^2)	---	---	---	(kg/cm^2)$^{-1}$	---
CIUC-1	29.5	0.285	6.00	1.00	0.227	-18.0	0.052	6.0
CIUC-2	29.5	0.285	4.00	1.00	0.227	-12.0	0.078	6.0
CIUC-3	29.5	0.285	8.00	1.00	0.227	-24.0	0.039	6.0
CIUE-1	39	0.23	4.00	1.00	0.202	-12.0	0.077	8.1
CIUE-3	39	0.23	6.00	1.00	0.202	-18.0	0.052	8.1
CK_oUC-1	26	0.33	4.10	0.53	0.198	-8.74	0.114	0.61
CK_oUC-2	26	0.33	6.10	0.53	0.198	-13.0	0.077	0.61
$C\frac{1}{K_o}UE$-1	30	0.65	2.02	1.98	0.164	-10.5	0.095	0.94
$C\frac{1}{K_o}UE$-3	27	0.55	3.20	1.88	0.152	-17.0	0.058	2.1
$C\frac{1}{K_o}URC$	35	0.55	2.09	1.92	0.270	-10.9	0.086	14.6

values were used. Eq. 4.1 was used to calculate α for compression tests and Eq. 4.3 was used for extension tests. Note that R for K_o and $1/K_o$ consolidation is significantly less than for hydrostatic consolidation.

The CAP program was used to calculate sample behavior with the parameters given in Tables 4.8 and 4.9. The calculated and observed normalized principal stress difference $(\sigma_1-\sigma_3)/\sigma'_{vo}$ vs. axial strain, normalized pore pressure $\Delta u/\sigma'_{vo}$ vs. axial strain and effective stress path in I'_1-$J_2^{1/2}$ space are compared for selected tests in Figs. 4.20 through 4.29. In general, there is very good agreement although the calculated initial slope of the $(\sigma_1-\sigma_3)/\sigma'_{vo}$ vs. axial strain curve was slightly less than the observed slope. Also, $\Delta u/\sigma'_{vo}$ is slightly less than observed values especially at small strains. In K_o and $1/K_o$ consolidated tests, the initial portion of the calculated effective stress path was to the left of the observed path. For a given test type, comparison of samples with different initial stresses shows that the model parameters are independent of consolidation pressure. The model does not predict post peak behavior for normally consolidated strain softening soil as shown for tests CK_oUC-1 and CK_oUC-2 in Figs. 4.26 and 4.27. Calculated and observed values of s_u/σ'_{vo} and the $\Delta u/\sigma'_{vo}$ at the corresponding strain are compared in Table 4.10. There is excellent agreement. This is expected

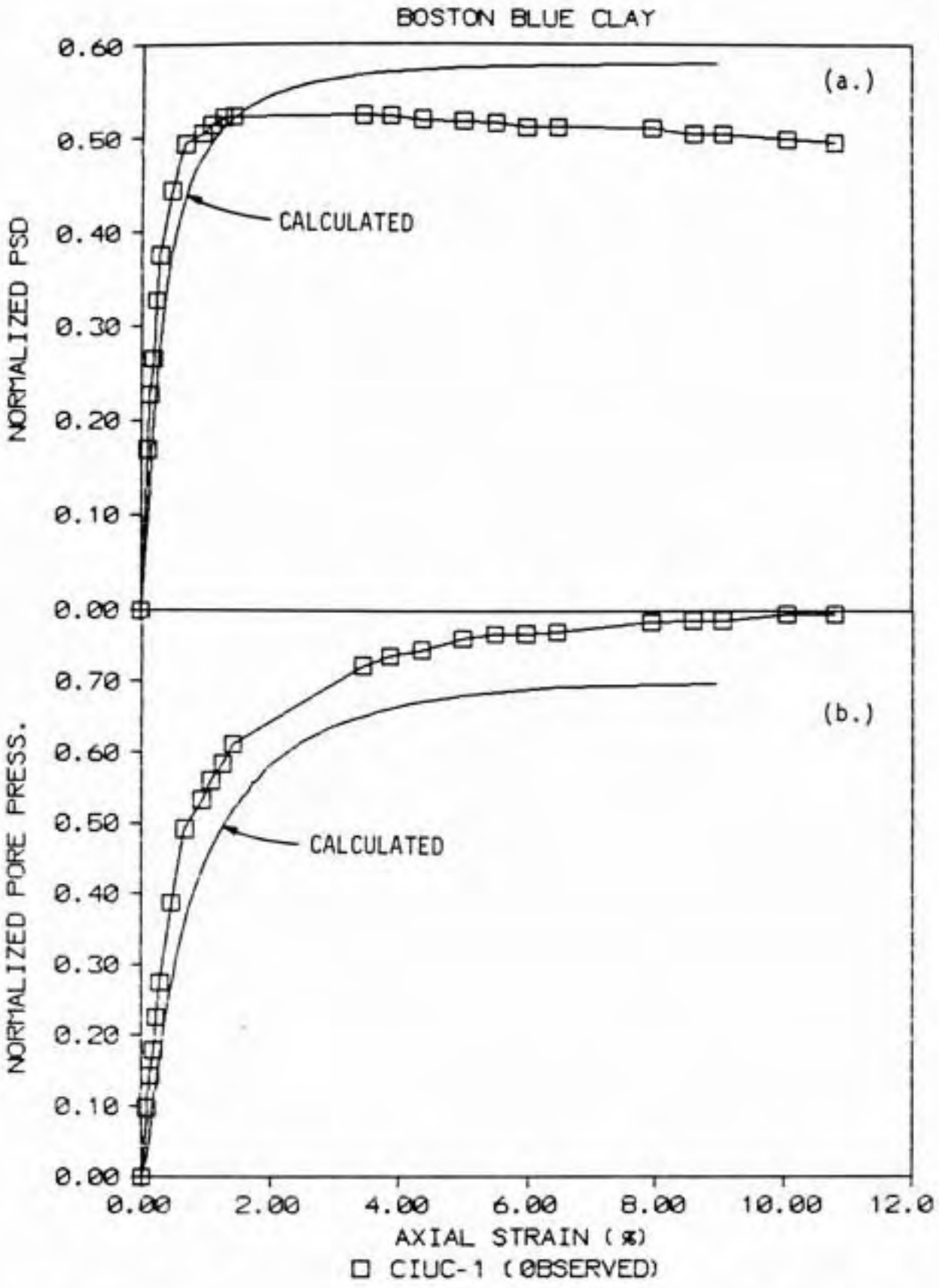

Figure 4.20 Calculated and observed (a) stress-strain and (b) pore pressure response for triaxial test CIUC-1 on Boston Blue Clay.

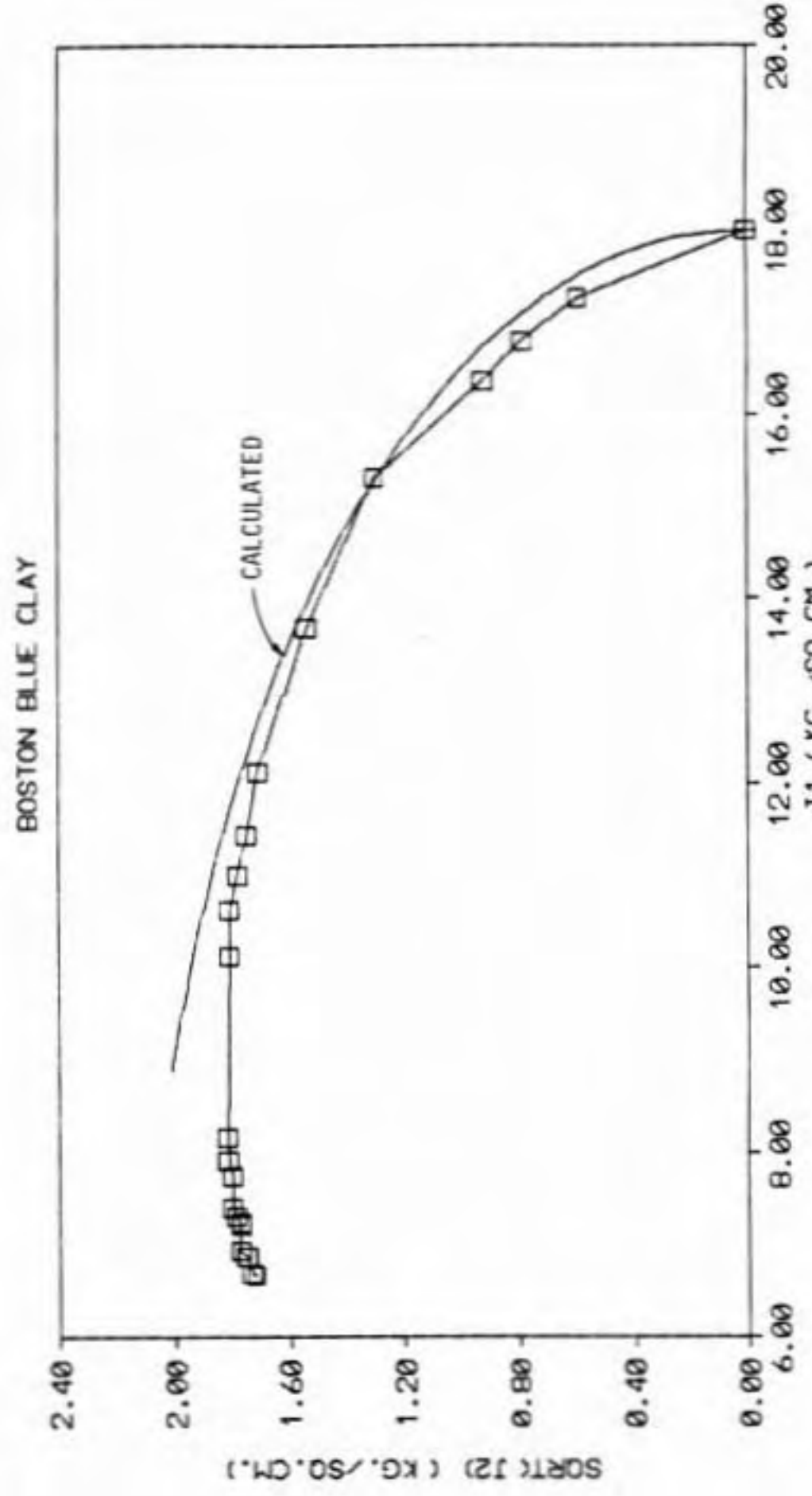

Figure 4.21 Calculated and observed effective stress path for triaxial test CIUC-1 on Boston Blue Clay.

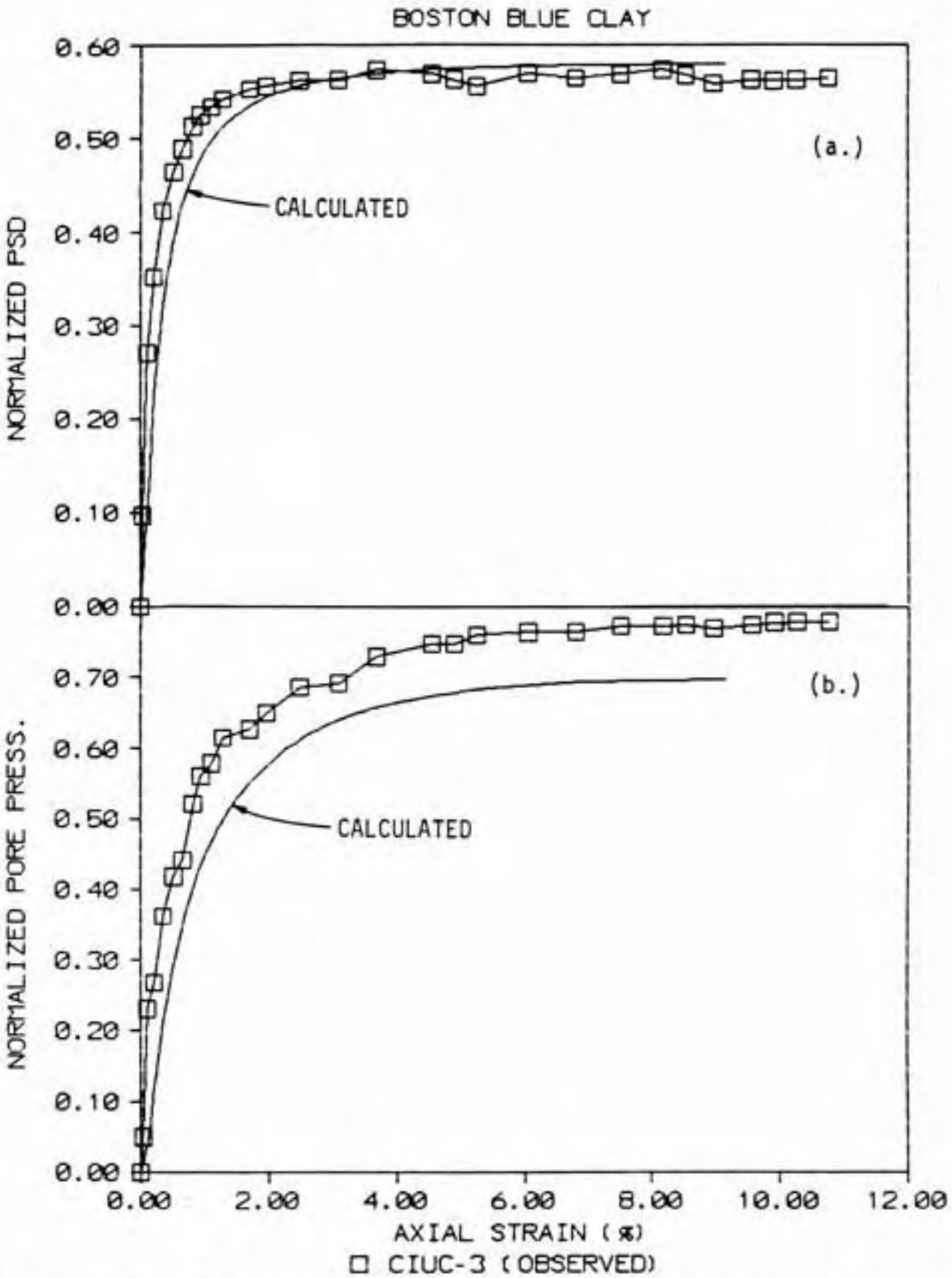

Figure 4.22 Calculated and observed (a) stress-strain and (b) pore pressure response for triaxial test CIUC-3 on Boston Blue Clay.

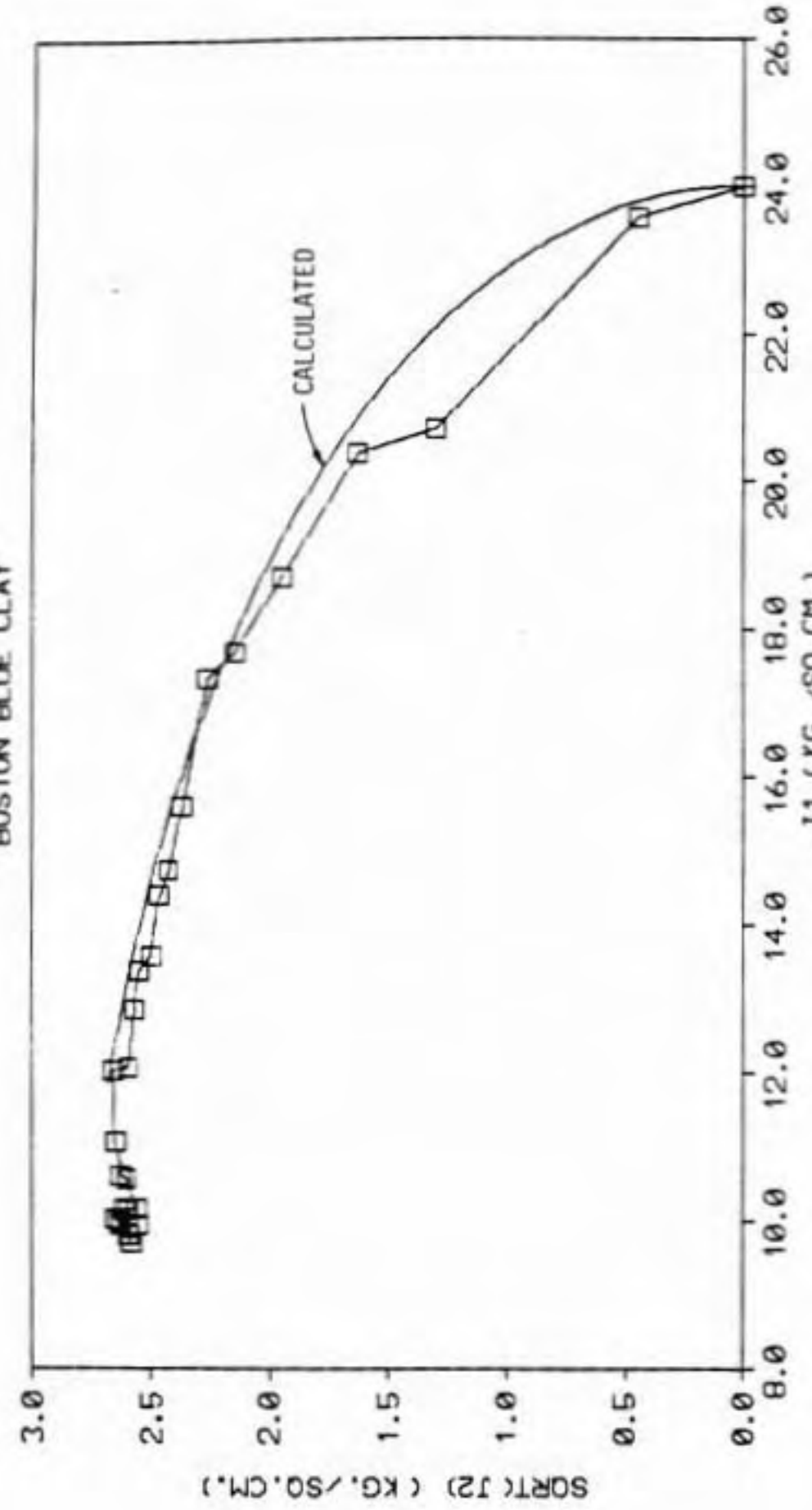

Figure 4.23 Calculated and observed effective stress path for triaxial test CIUC-3 on Boston Blue Clay.

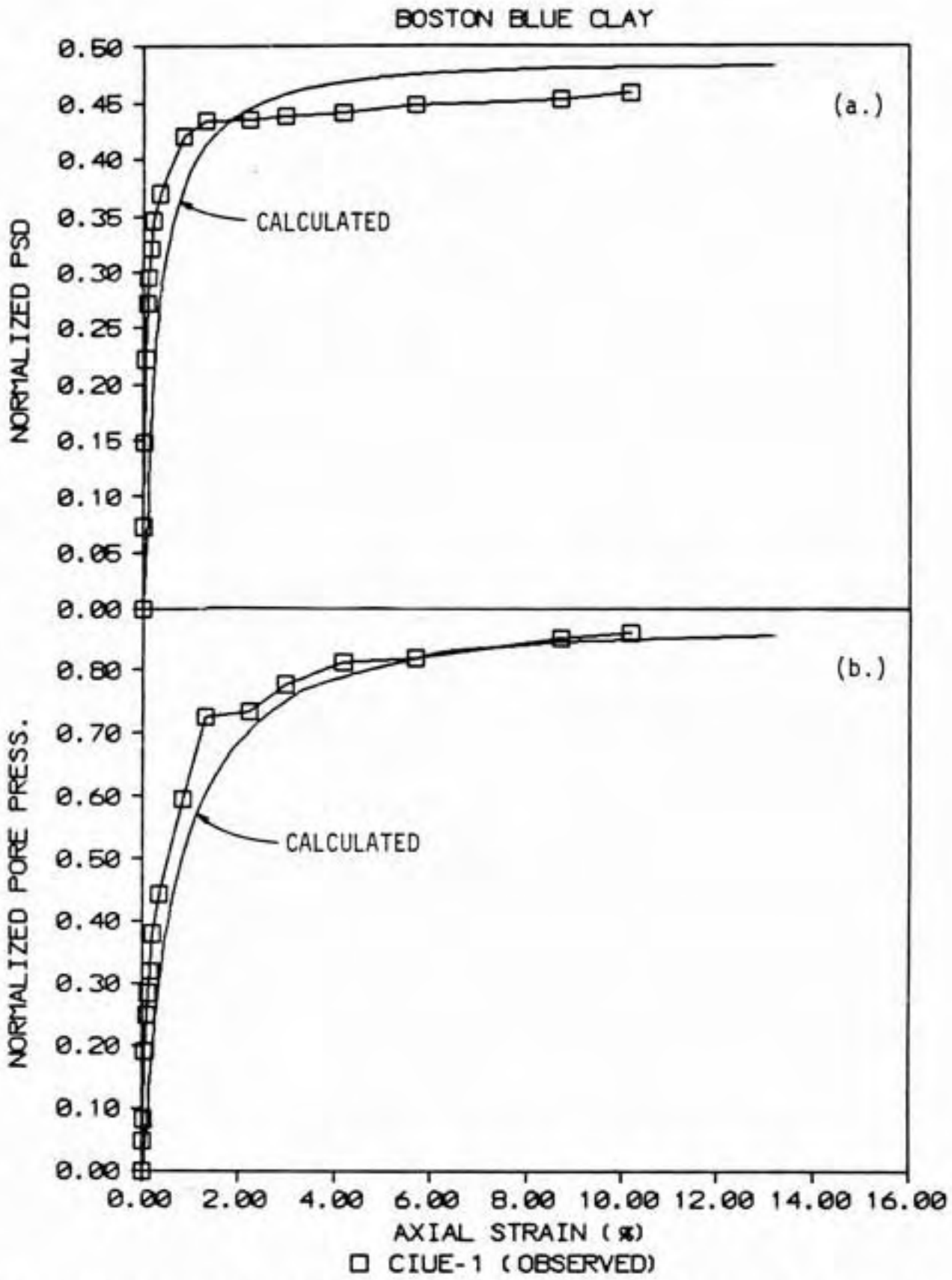

Figure 4.24 Calculated and observed (a) stress-strain and (b) pore pressure response for triaxial test CIUE-1 on Boston Blue Clay.

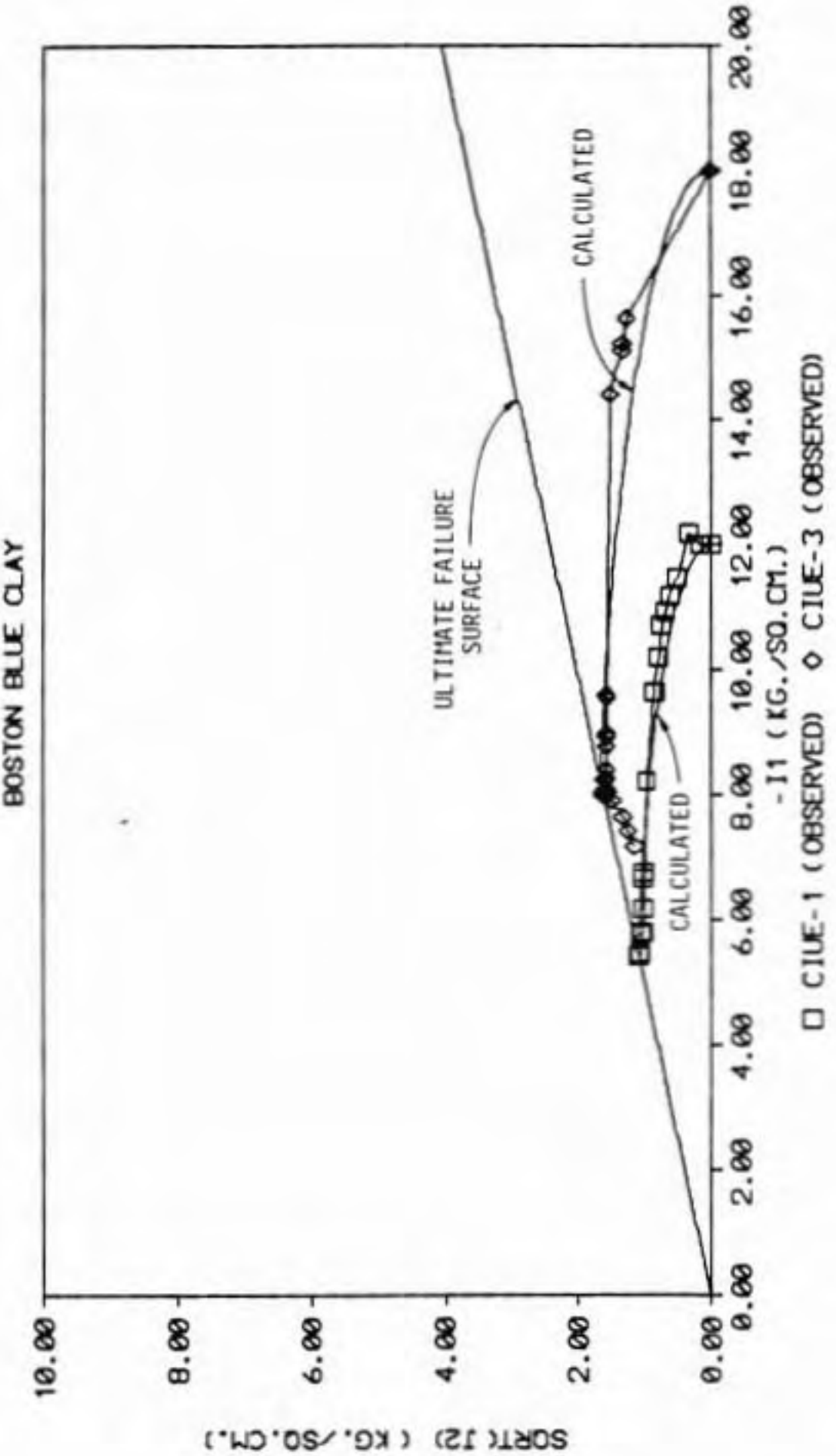

Figure 4.25 Calculated and observed effective stress path for triaxial test CIUE-1 on Boston Blue Clay.

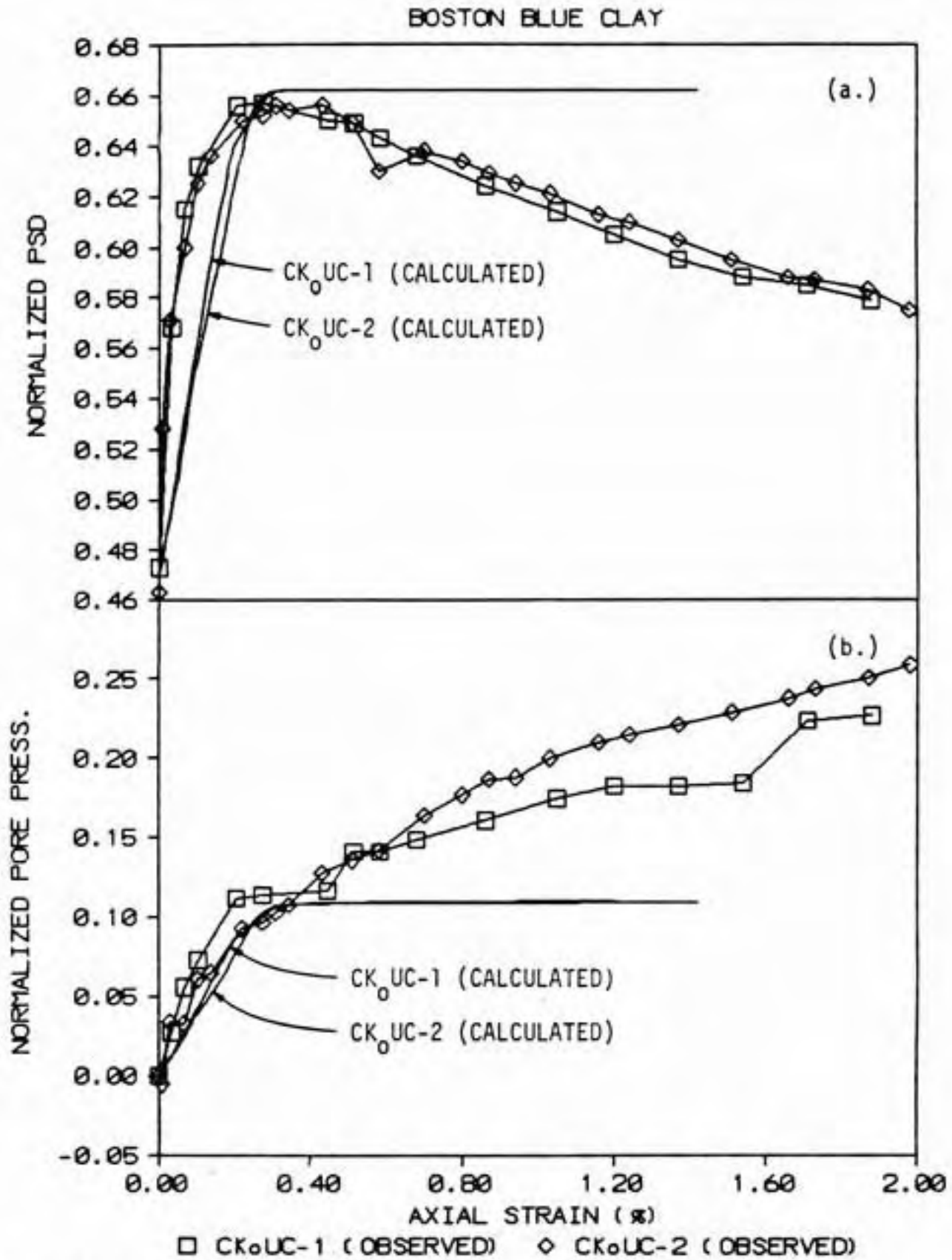

Figure 4.26 Calculated and observed (a) stress-strain and (b) pore pressure response for triaxial test CK_oUC-1 on Boston Blue Clay.

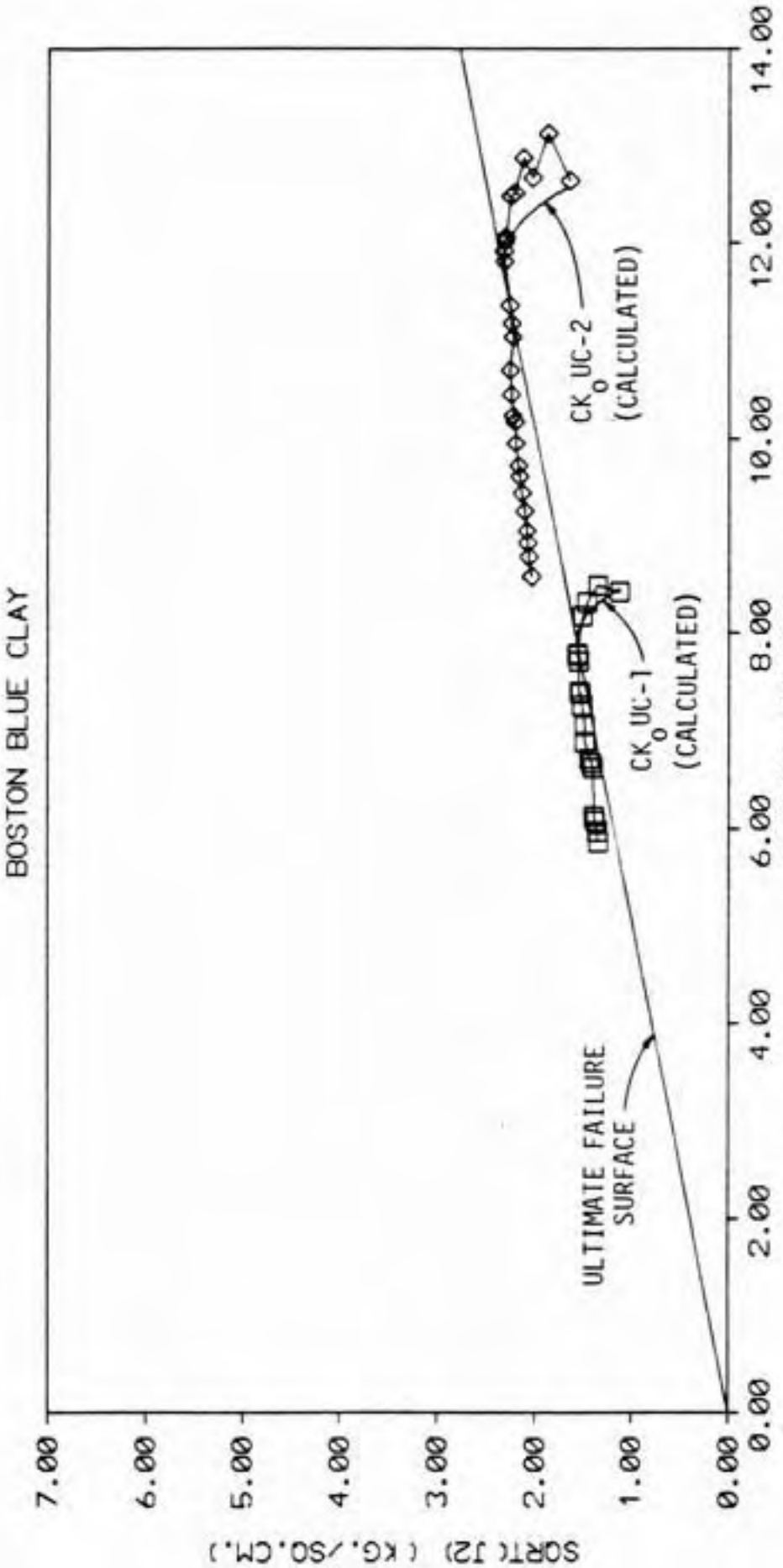

Figure 4.27 Calculated and observed effective stress path for triaxial test CK_oUC-1 on Boston Blue Clay.

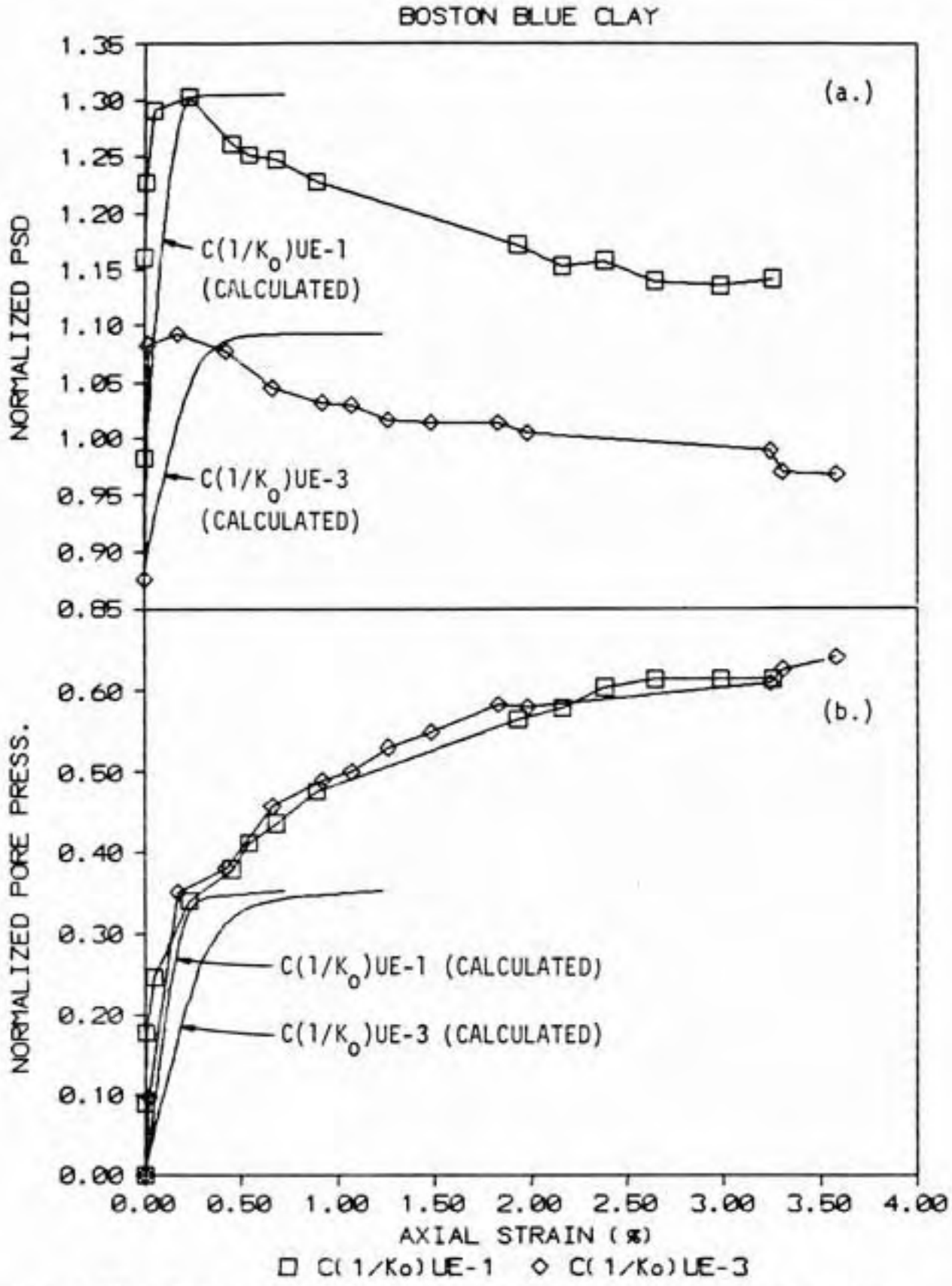

Figure 4.28 Calculated and observed (a) stress-strain and (b) pore pressure response for triaxial tests C(1/K_o)UE-1 and C(1/K_o)UE-3 on Boston Blue Clay.

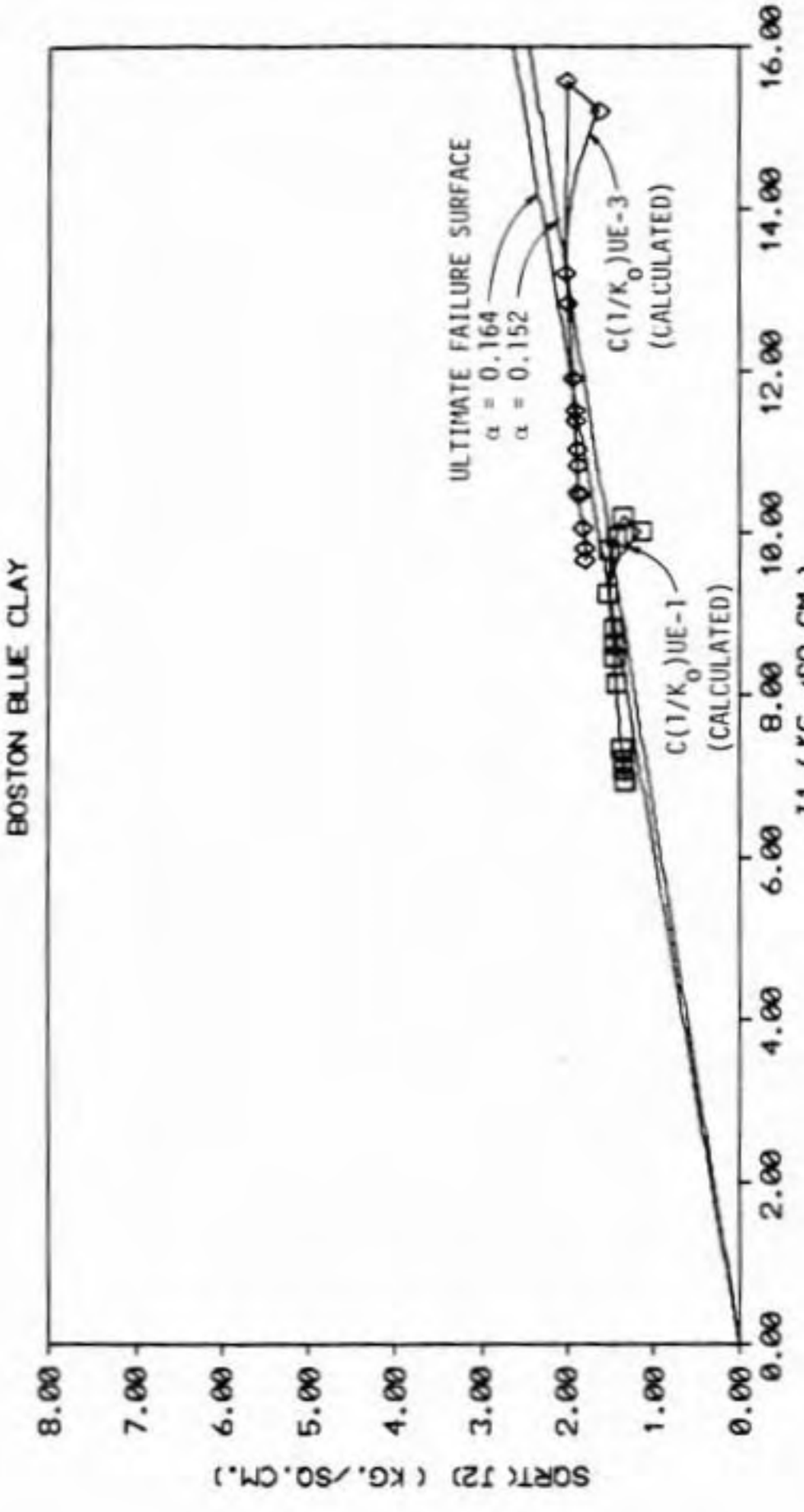

Figure 4.29 Calculated and observed effective stress path for triaxial tests C(1/K$_o$)UE-1 and C(1/K$_o$)UE-3 on Boston Blue Clay.

Table 4.10
Calculated and observed s_u/σ'_{vo} and $\Delta\mu/\sigma'_{vo}$
for triaxial tests on normally consolidated Boston Blue Clay.

Test no.	---- s_u/σ'_{vo} ----		---- $\Delta\mu/\sigma'_{vo}$ ----	
	observed	calculated	observed	calculated
CIUC-1	0.263	0.290	0.722	0.697
CIUC-2	0.308	0.292	0.662	0.698
CIUC-3	0.287	0.292	0.730	0.698
CIUC-AVG.	0.286	0.291	0.705	0.698
CIUE-1	0.230	0.241	0.862	0.858
CIUE-3	0.235	0.241	0.868	0.863
CIUE-AVG.	0.232	0.241	0.865	0.860
CK_oUC-1	0.329	0.331	0.114	0.112
CK_oUC-2	0.328	0.331	0.103	0.110
CK_oUC-AVG.	0.329	0.331	0.109	0.111
$C\frac{1}{K_o}UE$-1	0.651	0.652	0.341	0.353
$C\frac{1}{K_o}UE$-3	0.547	0.547	0.352	0.353
$C\frac{1}{K_o}UE$-AVG.	0.599	0.600	0.347	0.353

for s_u/σ'_{vo} since this is one of the soil properties used to calibrate the model. In general, the good agreement shown in Figs. 4.20 through 4.29 and Table 4.10 indicates the underlying assumptions of the cap model, such as normality, and the procedure used to determine the model parameters are reasonable.

4.4.2 Plane Strain Tests

Plane strain active tests where the major principal stress was increased to failure were performed by Ladd, et al. (1971). The resedimented samples of Boston Blue Clay had nearly linear virgin loading and unloading/reloading one-dimensional consolidation curves on a semi-log plot with average C_c = 0.27 and C_r = 0.022. The average e_o was 1.06. Eqs. 4.34 and 4.17 were used to calculate a = 0.056 and b = 0.0046. The three reliable tests on normally consolidated samples are numbers CK_oUPSA-4, 6, and 10. The average σ'_{vo} was -3.88 kg/cm^2, K_o was 0.48, ϕ' was 29°, and c' was 0.0. The ϕ' value was substituted in Eq. 4.5 which relates α and ϕ' for plane strain conditions and a flow rule that is normal to the Drucker-Prager surface (Drucker and Prager, 1952; Chen and Saleeb, 1982, p. 486) resulting in α = 0.156; however, the latter condition is not met since at failure the increment of plastic strain is normal to the cap (Fig. 3.2c). The α-value obtained from a plot of $J_{2f}^{1/2}$ vs. I'_{1f} was 0.190. This value is considered to be more

realistic and was used in the analysis. The $J_{2f}^{1/2}/\sigma'_{vo}$ were computed using Eq. 3.2. The values for the three tests were -0.375, -0.365, and -0.357 with an average of -0.365. For comparison with the triaxial tests, the average s_u/σ'_{vo} was -0.34. A Poisson's ratio ν' of 0.25 was assumed. The computed cap parameters are summarized in Table 4.8.

Calculated and observed sample behavior are compared in Figs. 4.30 and 4.31. To account for the intermediate principal stress, the stress strain behavior is given as $J_{2f}^{1/2}$ rather than $(\sigma_1-\sigma_3)/\sigma'_{vo}$ versus axial strain. The $J_{2f}^{1/2}/\sigma'_{vo}$ is correctly predicted and the stress-strain behavior up to failure is well modeled. The agreement of calculated pore pressures with tests CK_oUPSA-6 and 8 is good. Test CK_oUPSA-4 had a measured pore pressure response of only 72% at the start of shearing and was probably not fully saturated which caused the lower observed pore pressures.

In practice it probably will be necessary to calibrate the model for plane strain conditions using results from CIUC triaxial tests. To examine the accuracy of predictions for this case the strength parameters from the CIUC tests (α = 0.227 and $J_{2f}^{1/2}/\sigma'_{vo}$ = -0.329) were used to calibrate the model for plane strain conditions (K_o = 0.48). This results in R = 4.9, x_o = -11.6 kg/cm^2 and D = 0.085

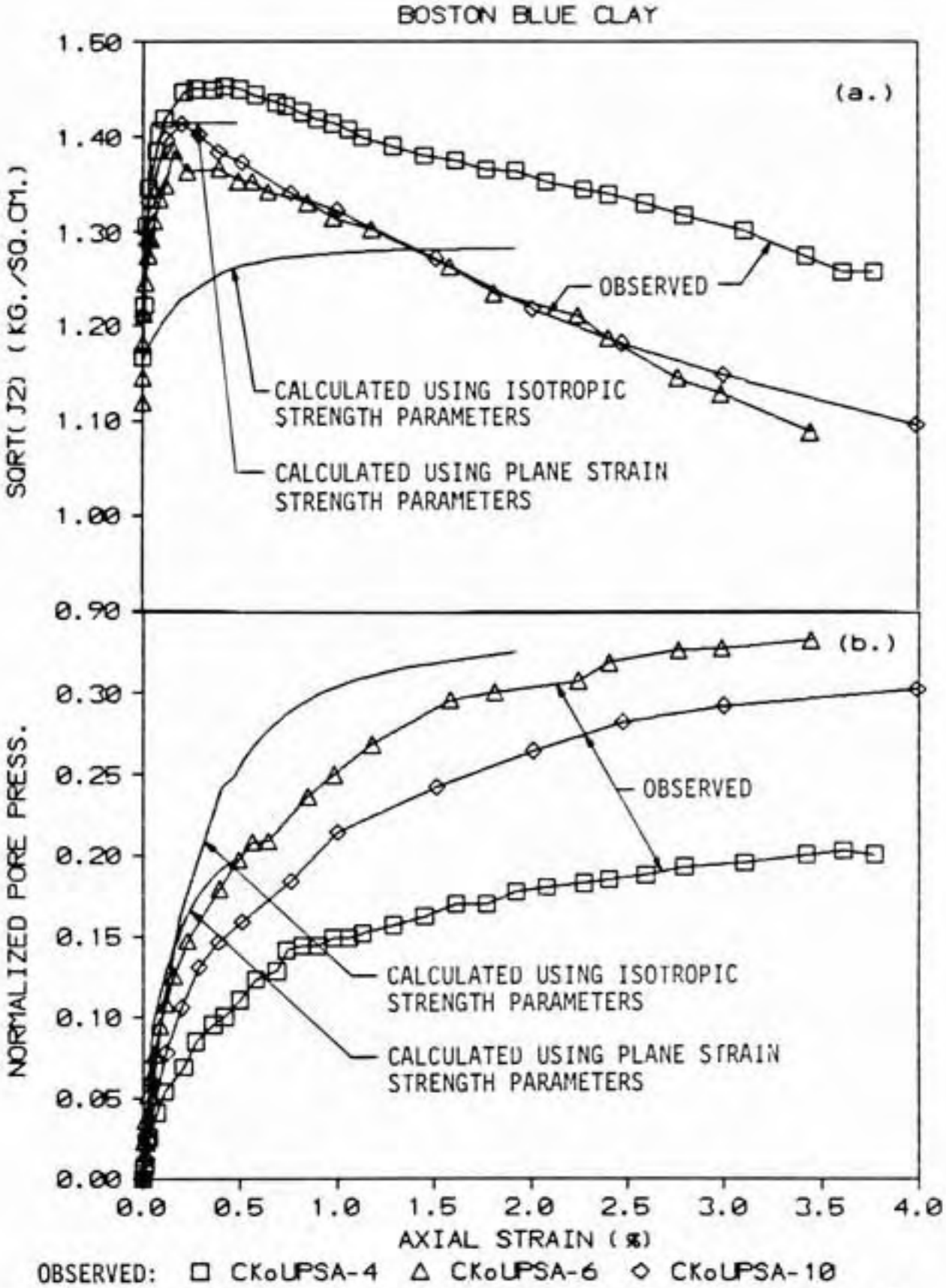

Figure 4.30 Calculated and observed (a) stress-strain and (b) pore pressure response for plane strain tests on normally consolidated Boston Blue Clay.

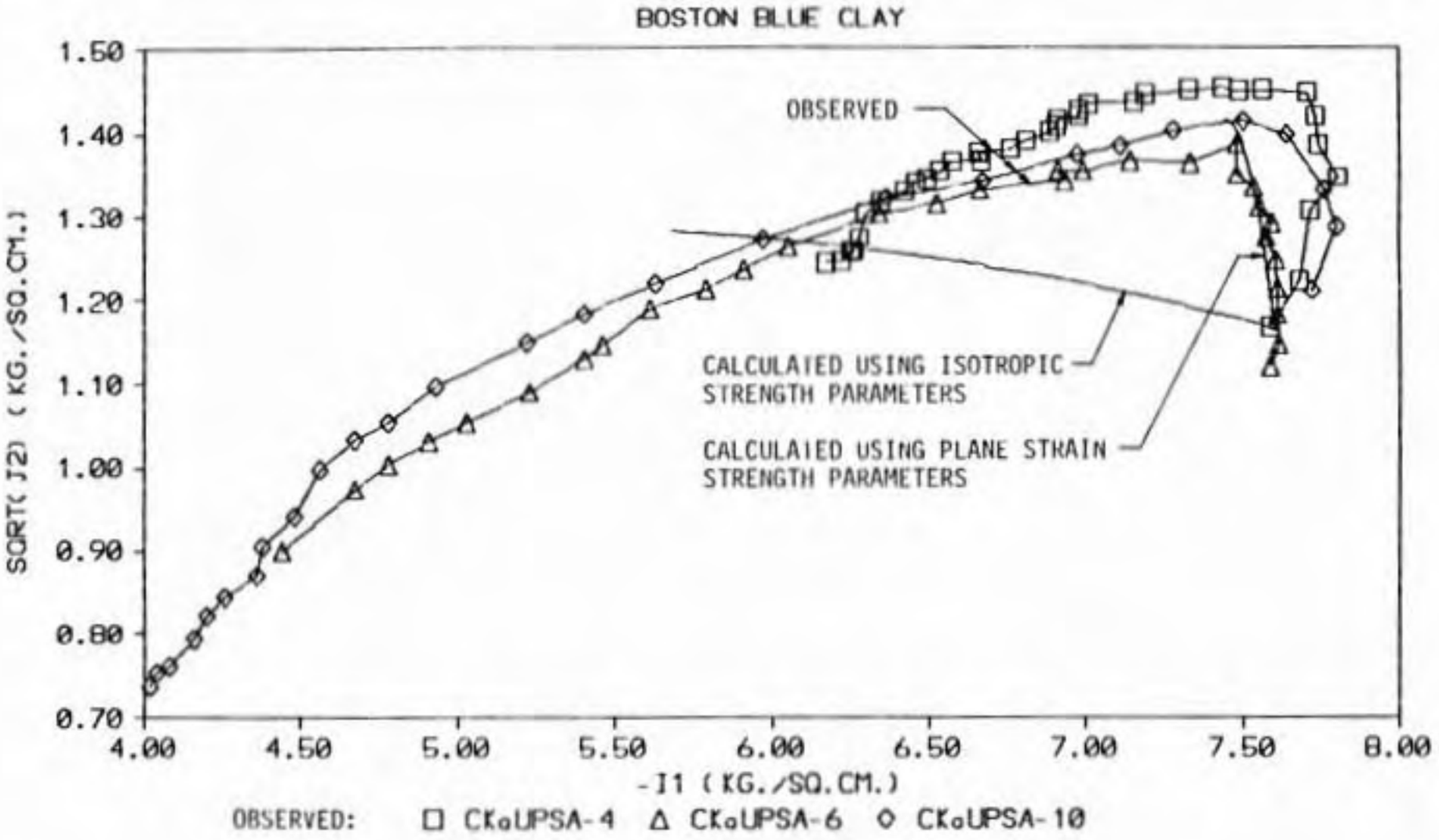

Figure 4.31 Calculated and observed effective stress paths for plane strain tests on normally consolidated Boston Blue Clay.

$(kg/cm^2)^{-1}$; other parameters are the same as shown in Table 4.8. The observed stress-strain behavior and effective stress path are poorly predicted as shown in Figs. 4.30a and 4.31. There is better agreement for pore pressures (Fig. 4.30b). This illustrates that for Boston Blue Clay it is necessary to calibrate the model using tests that approximate the initial state of stress.

4.4.3 Triaxial Tests with Reversal of Principal Stresses

Reversal of principal stresses occurred in three $C(1/K_o)URC$ triaxial tests on Boston Blue Clay (Ladd and Varallyay, 1965). The 'R' stands for reversal. The tests had average σ'_{vo} = -2.09 kg/cm^2 and K_o = 1.92. The average $J_{2o}^{1/2}$ was 1.11 kg/cm^2 and $J_{2f}^{1/2}$ was 1.34 kg/cm^2 so the failure state of stress was outside the initial position of the cap and the model can be calibrated using the procedure for normally consolidated clay. The resulting cap parameters are shown in Tables 4.8 and 4.9. Observed and calculated behavior is compared in Figs. 4.32 and 4.33. The predicted s_u/σ'_{vo} was -0.59 versus an observed value of -0.55. The agreement between observed and calculated stress-strain curves (Fig. 4.32) was good except near failure where the test samples showed greater strain. Pore pressure response and effective stress paths were poorly modeled.

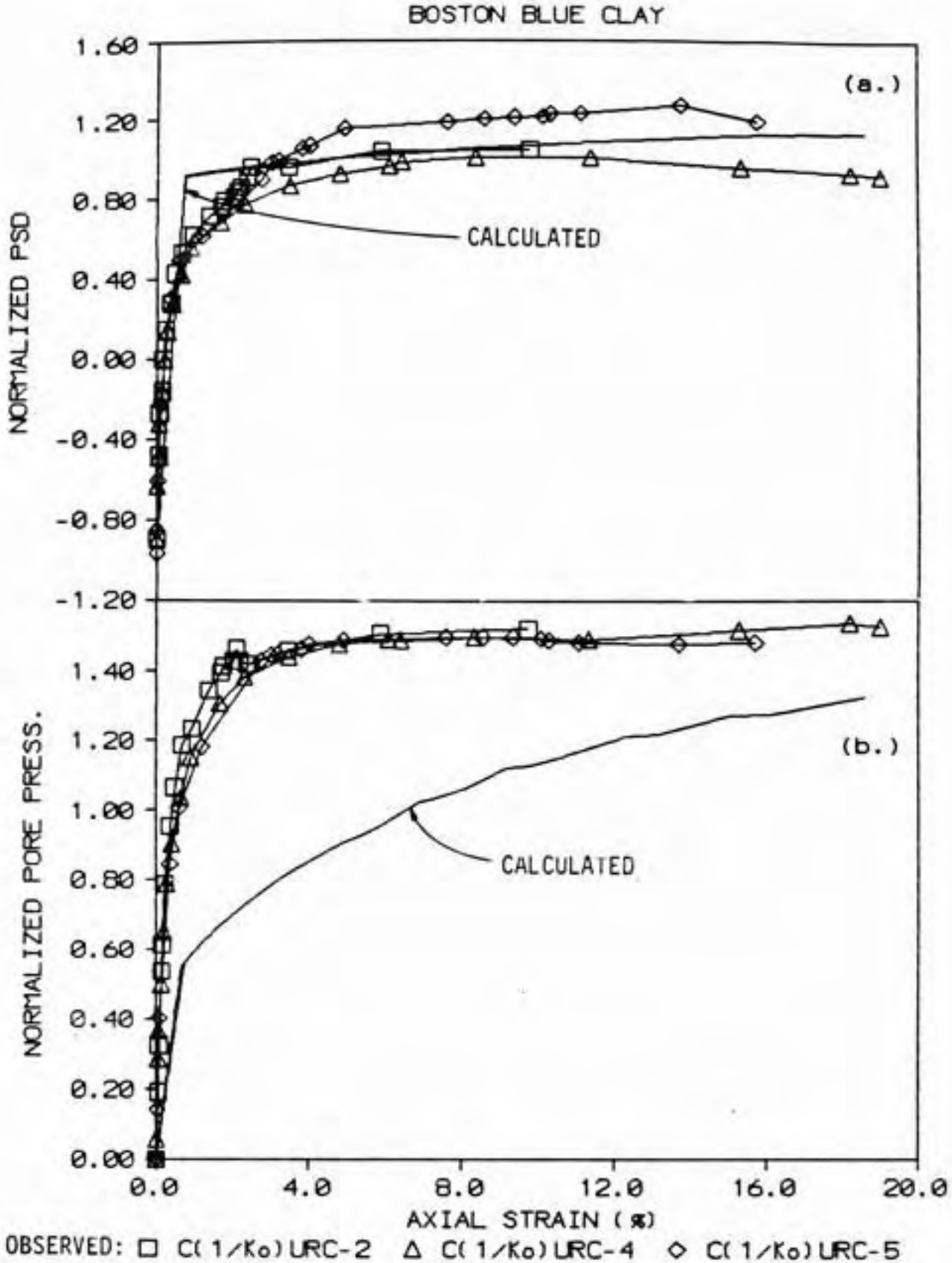

Figure 4.32 Calculated and observed (a) stress-strain and (b) pore pressure response for triaxial tests with reversal of principal stresses on Boston Blue Clay.

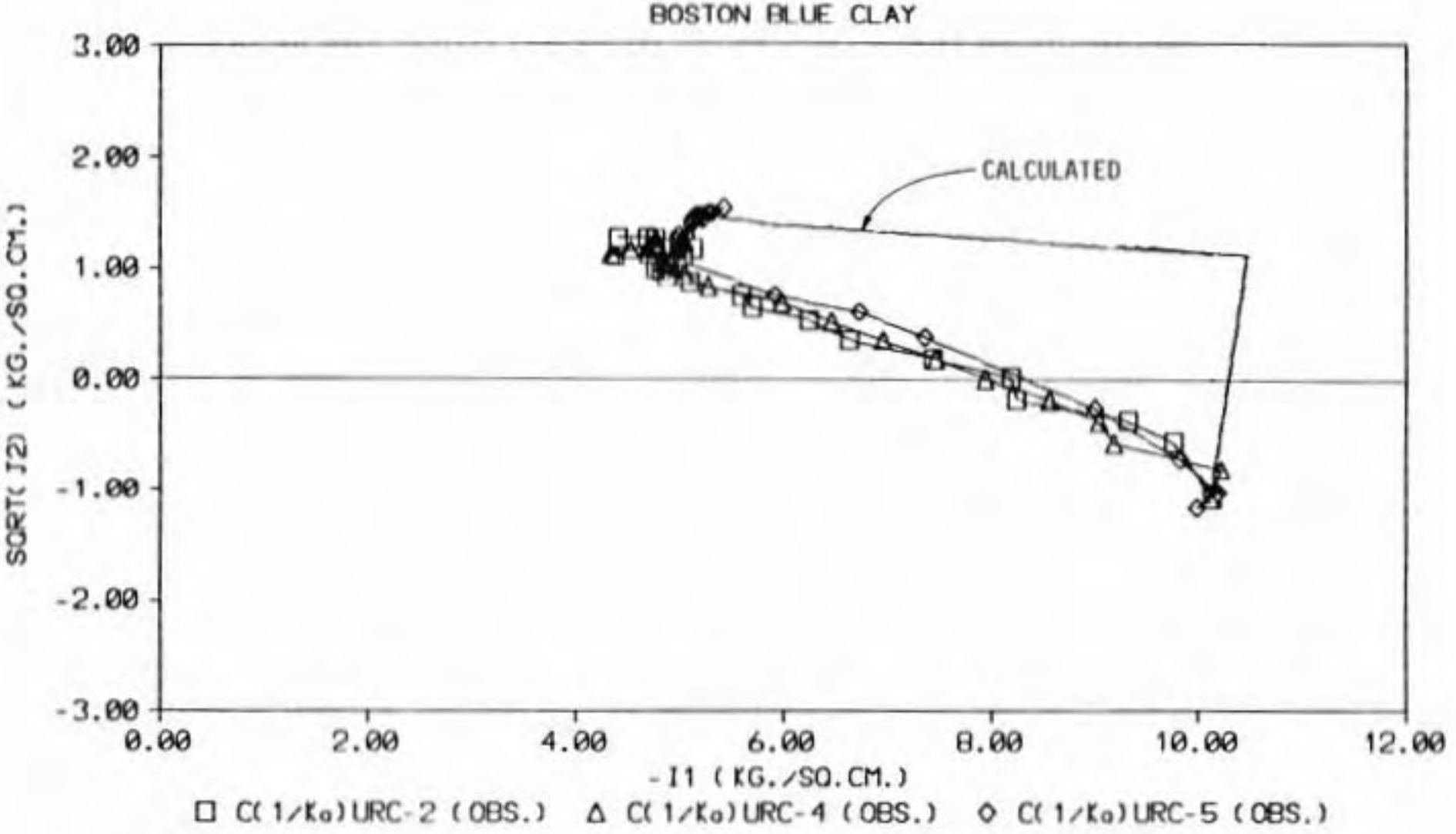

Figure 4.33 Calculated and observed effective stress paths for triaxial tests with reversal of principal stresses on Boston Blue Clay.

Ladd and Varallyay (1965) also report results for C(1/K_o)URE triaxial tests. However, $J_{2o}^{1/2}$ is greater than $J_{2f}^{1/2}$ so it is not possible to calibrate the model for this condition.

4.4.4 Plane Strain Tests on Overconsolidated Samples

Results from three CK_oUPSA tests with OCR ranging from 2.01 to 4.10 were reported by Ladd, et al. (1971). The test results are summarized in Table 4.11.

Table 4.11
Summary of results from CK_oUPSA tests
(Ladd, et al., 1971).

Property	Test no. PSA-5	PSA-7	PSA-8
σ'_{vc} (kg/cm^2)	2.89	5.99	3.94
OCR	3.96	4.10	2.01
I_{1f}/σ'_{vc}	1.921	1.921	1.921
$J_{2f}^{1/2}/\sigma'_{vc}$	-0.365	-0.365	-0.365
$(I_{1f}/\sigma'_{vc})^{OC}$	1.101	0.995	1.289
$(J_{2f}^{1/2}/\sigma'_{vc})^{OC}$	-0.244	-0.252	-0.307
$\hat{K}_o$	0.844	0.853	0.650

In addition the samples had the following average properties: e_o = 1.055, C_r = 0.0216 and normally consolidated K_o = 0.48. A b-value of 0.00456 was computed using Eq. 4.17.

The best fit line through the 3 pairs of $(I_{1f}/\sigma'_{vc})^{OC}$ and $(J_{2f}^{1/2}/\sigma'_{vc})^{OC}$ gives $\alpha = 0.12$ and $\kappa/\sigma'_{vc} = -0.15$. The initial position of the cap x_o was calculated using Eq. 4.67 and D was calculated from Eq. 4.31. The values for each test are summarized in Table 4.12. Other cap parameters are as given in Table 4.8.

Table 4.12
Cap parameters for overconsolidated CK_oPSA tests on Boston Blue Clay.

Test No.	x_o (kg/cm^2)	D ---
PSA-5	-2.38	0.457
PSA-7	-5.34	0.204
PSA-8	-5.36	0.203

The stress-strain curve, pore pressure response, and effective stress path were determined using the CAP computer program and the parameters in Tables 4.8 and 4.12. The position of the cap was fixed at x_o. The calculated and observed behavior for sample CK_oUPSA-7 are compared in Figs. 4.34 and 4.35. Similar results were obtained for tests CK_oUPSA-5 and 8. It is recalled that for OC soils the model is calibrated to yield the correct $J_{2f}^{1/2}$ but that pore pressure predictions will be in error. Examination of Fig. 4.34 shows that this is the case. There is reasonable agreement between calculated and observed stress-strain behavior for low strains because the stress strain

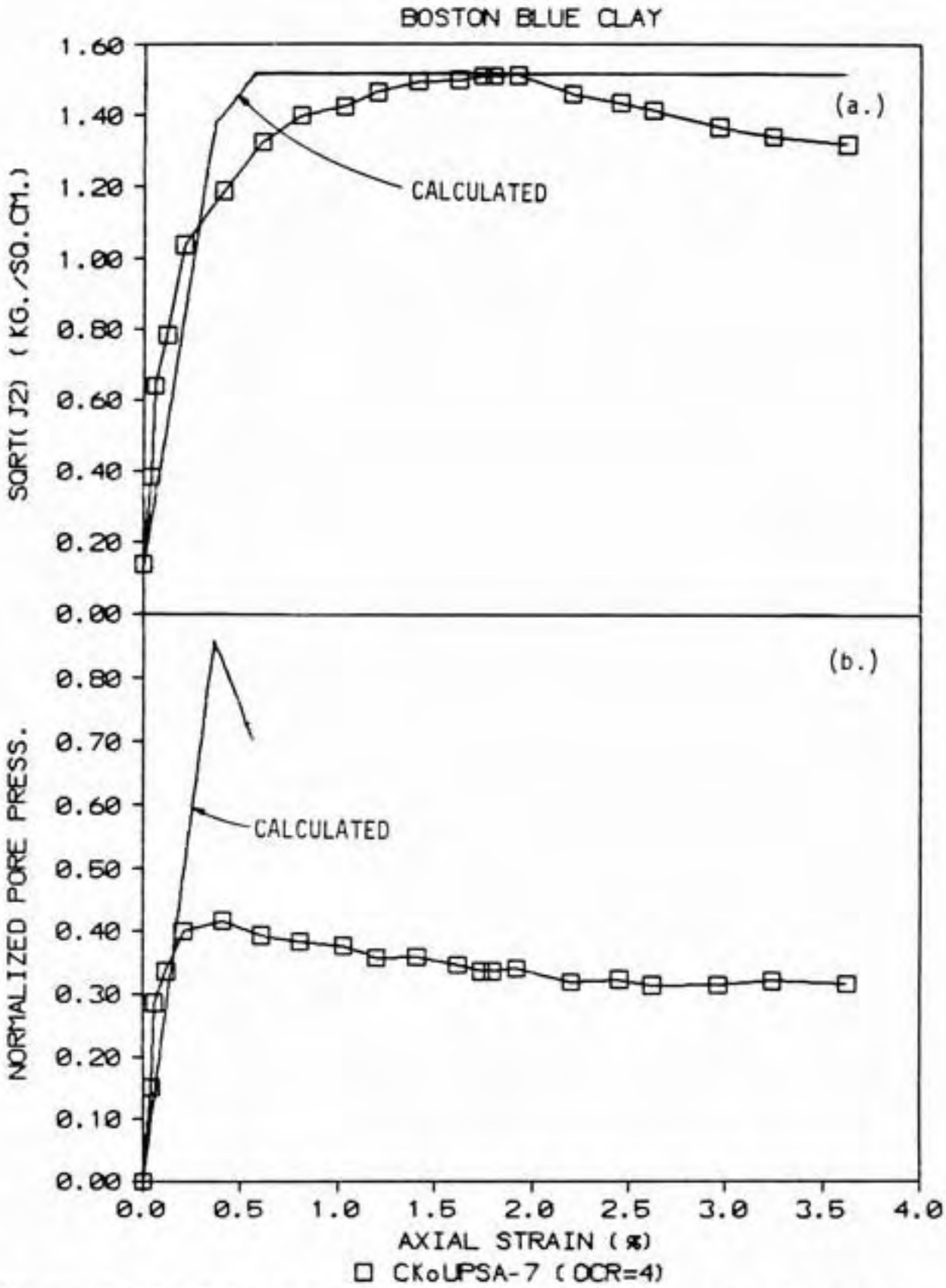

Figure 4.34 Calculated and observed (a) stress-strain and (b) pore pressure response for plane strain tests on overconsolidated Boston Blue Clay.

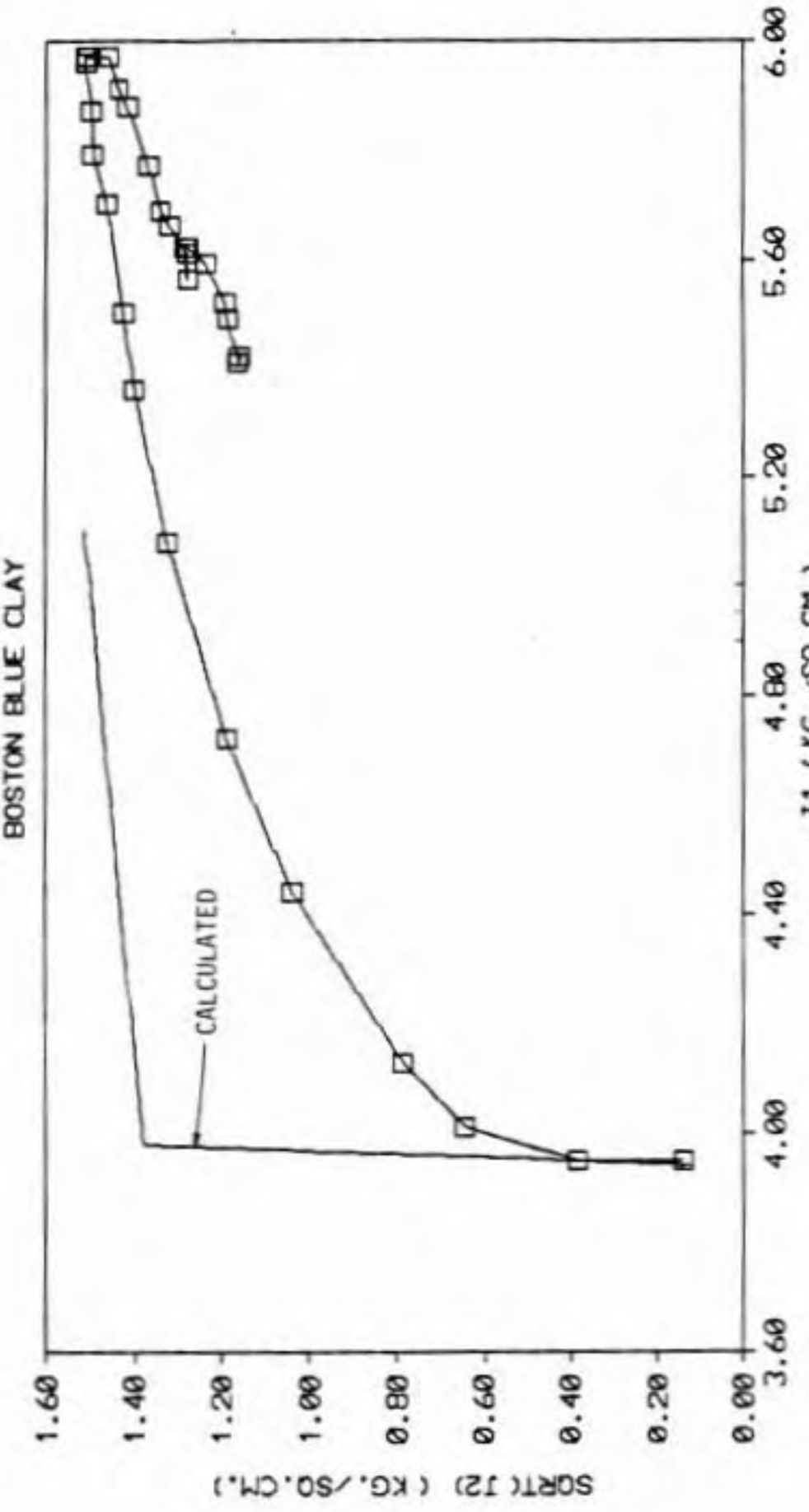

Figure 4.35 Calculated and observed effective stress path for plane strain test on overconsolidated Boston Blue Clay.

characteristics in this area are dominated by elastic behavior. Observed strains were greater than calculated near failure.

Pore pressure response was in good agreement only for the first 0.1 to 0.2% strain. After that the calculated pore pressures were much greater than the observed values. Agreement between observed and predicted effective stress paths was very poor. The reason may be that the model does not allow for plastic volumetric dilation within the region bounded by the cap and ultimate failure surface. These results suggest that this procedure gives reasonable predictions of stress-strain behavior and shear strength at failure but that predicted pore pressures and effective stress paths are greatly in error.

4.5 SOIL PROPERTIES AND CAP PARAMETERS FOR CLAYEY SOILS

Test data was gathered for clayey soils to examine typical ranges of input soil properties and calculated cap parameters. The survey includes both undisturbed and laboratory prepared samples. A summary of soil data prepared by Mayne (1980) and Mayne and Swanson (1980) was the primary source of information. It was supplemented with other data obtained from the literature. Statistical correlations between basic index properties, input soil properties and cap parameters were examined and regression analyses were

made if appropriate. Cap parameters calculated for tests with initial hydrostatic and nonhydrostatic conditions were compared. The data is useful for choosing parameters for preliminary designs.

4.5.1 Volume Change Properties

Soil index and consolidation properties for 88 soils are summarized in Table 4.13. Their Atterberg limits are shown in Fig. 4.36. Most of the consolidation properties were obtained from one-dimensional consolidation tests. The values of $a(1+e_o)$ and $b(1+e_o)$ were calculated from C_c and C_r using Eqs. 4.34 and 4.17 although for a few data sets $b(1+e_o)$ was obtained directly from test results. The initial void ratio e_o was not readily available so a and b were not calculated. The quantities $a(1+e_o)$, $b(1+e_o)$, $(a-b)(1+e_o)$ (which is used to compute W), and $(a-b)/b$ (which is used in Eq. 4.49 to compute x_f/x_o) are shown in Table 4.13.

Correlation of the consolidation properties with liquid limit was examined. Fair to poor correlation was found for C_c, C_r, and $(a-b)(1+e_o)$. A linear regression analysis was performed and the results are summarized in Table 4.14 and shown in Figs. 4.37 through 4.39. Note that there is a large scatter of observed data about the best fit lines and

Table 4.13
Volume change properties.

NUMBER	SOIL	LL	PI	Cc	Cr	a(1+eo)	b(1+eo)	(a-b)• (1+eo)	(a-b)/b	REFERENCE
1.0	WEALD (REMOLDED)	43	25	0.214	0.081	0.0929	0.0352	0.0578	1.642	Henkel (1960)
2.0	SPESTONE KAOLIN	72	31	0.573	0.170	0.2488	0.0738	0.1750	2.371	Amerasinghe and Parry (1975)
2.1	SPESTONE KAOLIN	72	31	0.580	0.165	0.2518	0.0716	0.1802	2.515	Amerasinghe and Parry (1975)
3.0	SAN FRANCISCO BAY MUD	88	45	0.665	0.221	0.2888	0.0960	0.1928	2.009	Mitchell (1976)
4.0	LONDON CLAY (REMOLDED)	78	52	0.371	0.143	0.1611	0.0621	0.0990	1.594	Henkel (1960)
5.0	KEUPER MARL	32	14	0.272	0.058	0.1181	0.0252	0.0929	3.690	Brown, et al. (1975)
6.0	PORTLAND MARINE CLAY	44	20	0.550	NA	0.2388	NA	NA	NA	Ladd and Edgers (1972)
7.0	ILLITE	57	31	0.431	0.138	0.1871	0.0599	0.1272	2.123	France and Sangrey (1977)
8.0	RESEDIMENTED BOSTON BLUE	41	21	0.338	0.051	0.1468	0.0221	0.1246	5.627	Ladd and Edgers (1972)
9.0	BANGKOK	65	41	0.511	0.092	0.2219	0.0399	0.1819	4.554	Ladd and Foott (1974)
10.0	OSLO	39	18	0.175	0.035	0.0760	0.0152	0.0608	4.000	Simons (1960b)
11.0	BRADWELL	95	65	0.714	0.152	0.3100	0.0660	0.2440	3.697	Skempton (1961)
13.0	SHELLHAVEN	110	80	0.937	0.051	0.4069	0.0221	0.3847	17.373	Skempton and Henkel (1953)
15.0	NEWFIELD	28	10	0.210	0.018	0.0912	0.0078	0.0834	10.667	Sangrey, Henkel and Esrig (1969)
16.0	VIENNA (REMOLDED)	47	25	0.299	0.055	0.1298	0.0239	0.1059	4.436	Hvorslev (1960)
17.0	VIRGINIA COASTAL	54	27	0.444	0.055	0.1928	0.0239	0.1689	7.073	Swanson and Brown (1977)
18.0	SPESTONE KAOLIN	72	32	0.693	0.069	0.3009	0.0300	0.2710	9.043	Parry and Nadarajah (1973)
19.0	JAPANESE	64	37	0.403	0.078	0.1750	0.0339	0.1411	4.167	Shibata and Karube (1969)
20.0	LITTLE BELT (REMOLDED)	127	91	0.889	0.442	0.3860	0.1919	0.1941	1.011	Hvorslev (1960)
21.0	ATCHAFALAYA	95	75	1.040	0.104	0.4516	0.0452	0.4064	9.000	Ladd and Edgers (1972)
23.0	MILAZZO	61	33	0.431	0.111	0.1871	0.0482	0.1389	2.883	Croce, et al. (1969)
24.0	CALCIUM ILLITE	85	48	0.758	0.274	0.3291	0.1190	0.2102	1.766	Olson (1962)
26.0	DRAMMEN	33	15	0.265	0.055	0.1151	0.0239	0.0912	3.818	Simons (1960a)
27.0	BACKSWAMP	70	40	0.583	0.163	0.2531	0.0708	0.1824	2.577	Whitman (1960)
28.0	KARS LEDA	45	21	1.121	0.021	0.4868	0.0091	0.4776	52.381	Raymond (1972)
29.0	PORTSMOUTH	35	15	1.040	0.104	0.4516	0.0452	0.4064	9.000	Simon, Christian and Ladd (1974)
31.0	PLASITC HOLOCENE	65	38	0.640	0.087	0.2779	0.0378	0.2401	6.356	Koutsoftas and Fischer (1976)

Table 4.13
Continued.

NUMBER	SOIL	LL	PI	Cc	Cr	a(1+eo)	b(1+eo)	(a-b)·(1+eo)	(a-b)/b	REFERENCE
32.0	GHANA	42	29	0.182	0.058	0.0790	0.0252	0.0538	2.138	deGraft-Johnson, et al. (1969)
33.0	HALLOYSITE	62	26	0.304	0.053	0.1320	0.0230	0.1090	4.736	Taylor and Bacchus (1969)
35.0	SEATTLE	52	26	0.260	0.081	0.1129	0.0352	0.0777	2.210	Sheriff, Wu and Bostrum (1972)
37.0	SODIUM ILLITE	79	44	0.362	0.200	0.1572	0.0868	0.0703	0.810	Olson and Hardin (1963)
38.0	GRUNDITE	55	29	0.359	0.177	0.1559	0.0769	0.0790	1.028	Perloff and Osterberg (1963)
39.0	TERRA ROXA	43	22	0.216	0.046	0.0938	0.0200	0.0738	3.696	da Cruz (1963)
40.0	AMUAY	71	42	0.488	NA	0.2119	NA	NA	NA	Lambe (1963)
41.0	SCOTT	34	12	0.138	0.037	0.0599	0.0161	0.0439	2.730	Ladanyi, et al. (1965)
43.0	TOLEDO	42	23	0.288	0.067	0.1251	0.0291	0.0960	3.299	Wu, Chang and Ali (1978)
44.0	KAWASAKI	65	31	0.668	0.058	0.2901	0.0252	0.2649	10.517	Ladd and Lambe (1963)
47.0	CONCORD BLUE	32	10	0.163	0.039	0.0708	0.0169	0.0538	3.179	Egan (1977)
48.0	AGNEW	54	24	0.159	0.048	0.0690	0.0208	0.0482	2.312	Egan (1977)
49.0	LAGUNILLAS	61	37	0.771	0.127	0.3348	0.0551	0.2796	5.071	Ladd and Lambe (1963)
51.0	LISKEARD	56	33	1.073	0.035	0.4659	0.0152	0.4507	29.657	Raymond (1973)
56.0	LILLA EDET	61	32	0.860	0.140	0.3734	0.0608	0.3126	5.143	Bjerrum and Simons (1960)
60.0	HOKKAIDO SILT A	52	21	0.299	0.058	0.1298	0.0252	0.1046	4.155	Mitachi and Kitago (1976)
60.1	HOKKAIDO SILT A	52	21	0.290	0.060	0.1259	0.0261	0.0999	3.833	Mitachi and Kitago (1976)
61.0	HOKKAIDO SILT B	51	21	0.193	0.030	0.0838	0.0130	0.0708	5.433	Mitachi and Kitago (1976)
61.1	HOKKAIDO SILT B	51	21	0.193	0.030	0.0838	0.0130	0.0708	5.433	Mitachi and Kitago (1976)
62.0	HOKKAIDO CLAY	72	32	0.412	0.058	0.1789	0.0252	0.1537	6.103	Mitachi and Kitago (1976)
62.1	HOKKAIDO CLAY	72	32	0.410	0.060	0.1780	0.0261	0.1520	5.833	Mitachi and Kitago (1976)
65.0	KANPUR CLAY	38	18	0.284	0.060	0.1233	0.0261	0.0973	3.733	Yudhbir and Varadarajah (1974)
66.0	RANN OF KUTCH	91	49	0.610	0.264	0.2649	0.1146	0.1502	1.311	Yudhbir and Varadarajah (1974)
70.0	OHIO SILT	24	4	0.133	0.040	0.0578	0.0174	0.0404	2.325	Montgomery (1978)
72.0	LANSISALMI	78	46	1.059	0.401	0.4598	0.1741	0.2857	1.641	Korhonen (1977)
73.0	SAULT STE MARIE	55	32	0.165	0.050	0.0716	0.0217	0.0499	2.300	Wu, Douglas and Goughnour (1962)
74.0	BATH KAOLINITE	48	15	0.189	0.045	0.0821	0.0195	0.0625	3.200	Broms and Ratnam (1963)

Table 4.13
Continued.

NUMBER	SOIL	LL	PI	Cc	Cr	a(1+eo)	b(1+eo)	(a-b)•(1+eo)	(a-b)/b	REFERENCE
81.0	LONG ISLAND COASTAL	64	34	0.222	0.068	0.0964	0.0295	0.0669	2.265	Swanson and Brown (1977)
82.0	HACKENSACK VARVED	65	35	0.481	0.068	0.2089	0.0295	0.1793	6.074	Saxena, Hedberg and Ladd (1978)
85.0	EAST ATCHAFALAYA	79	53	0.479	NA	0.2080	NA	NA	NA	Donaghe and Townsend (1978)
86.0	BUCKSHOT CLAY	57	36	0.402	NA	0.1746	NA	NA	NA	Donaghe and Townsend (1978)
89.0	KODIAK ISLAND	30	14	0.124	0.056	0.0538	0.0243	0.0295	1.214	Sparrow, Swanson and Brown (1978)
90.0	WINNIPEG CLAY	94	60	0.996	0.240	0.4325	0.1042	0.3283	3.150	Crawford (1964)
92.0	WEALD CLAY	46	24	0.193	NA	0.0838	NA	NA	NA	Henkel and Sowa (1964)
92.1	WEALD CLAY	46	24	0.195	NA	0.0847	NA	NA	NA	Henkel and Sowa (1964)
96.0	DRAMMEN CLAY	57	27	0.526	0.043	0.2284	0.0187	0.2097	11.233	Andersen, et al. (1980)
98.0	CONNECTICUT VARVED	65	39	0.569	0.101	0.2471	0.0439	0.2032	4.634	Ladd (1975); Ladd and Edgers (1972)
100.0	PORTSMOUTH	35	15	0.711	0.035	0.3087	0.0152	0.2935	19.314	Ladd (1972); Ladd and Edgers (1972)
101.0	HELSINKI SILT	27	8	0.300	NA	0.0400	0.0150	0.0250	1.667	Saarelainen (1981)
102.0	HELSINKI LEAN CLAY	41	18	0.600	NA	0.1910	0.0330	0.1580	4.788	Saarelainen (1981)
103.0	HELSINKI FAT CLAY	53	28	0.900	NA	0.3370	0.0480	0.2890	6.021	Saarelainen (1981)
104.0	HELSINKI VERY FAT CLAY	72	43	1.300	NA	0.5360	0.0730	0.4630	6.342	Saarelainen (1981)
105.0	HELSINKI ORGANIC CLAY	128	87	1.500	NA	0.5730	0.0900	0.4830	5.367	Saarelainen (1981)
116.0	UNDISTURBED CLAY (CL)	46	24	0.290	0.045	0.1259	0.0195	0.1064	5.444	Coumoulos (1979)
117.0	COMPACTED CLAY (CL)	32	15	0.215	0.022	0.0934	0.0096	0.0838	8.773	Coumoulos (1979)
118.0	UNDISTURBED SOFT CLAY (CL)	28	8	0.240	0.034	0.1042	0.0148	0.0894	6.059	Coumoulos (1979)
119.0	UNDISTURBED HARD CLAY (CL)	28	14	0.102	0.027	0.0443	0.0117	0.0326	2.778	Coumoulos (1979)
120.0	UNDISTURBED SOFT CLAY (CH)	56	32	0.340	0.050	0.1476	0.0217	0.1259	5.800	Coumoulos (1979)
121.0	UNDISTURBED HARD CLAY (CH)	53	22	0.198	0.080	0.0860	0.0347	0.0512	1.475	Coumoulos (1979)
122.0	COMPACTED CLAY (CL)	37	19	0.177	0.033	0.0769	0.0143	0.0625	4.364	Coumoulos (1979)
123.0	SOFT CLAY (CL)	41	17	0.340	0.025	0.1476	0.0109	0.1368	12.600	Kaufman and Sherman (1964)
124.0	FIRM CLAY (CL)	50	27	0.440	0.043	0.1911	0.0187	0.1724	9.233	Kaufman and Sherman (1964)
125.0	SANDY SILT (ML)	31	6	0.160	0.012	0.0695	0.0052	0.0643	12.333	Kaufman and Sherman (1964)
126.0	SOFT CLAY (CH)	81	56	0.840	0.170	0.3647	0.0738	0.2909	3.941	Kaufman and Sherman (1964)

Table 4.13
Continued.

NUMBER	SOIL	LL	PI	Cc	Cr	a(1+eo)	b(1+eo)	(a-b)• (1+eo)	(a-b)/b	REFERENCE
127.0	CLAY WITH SILT STRATA (CH)	71	43	0.520	0.092	0.2258	0.0399	0.1858	4.652	Kaufman and Sherman (1964)
128.0	OVERCONSOLIDATED CLAY TILL	27	13	0.110	0.021	0.0478	0.0091	0.0386	4.238	MacDonald and Sauer (1970)
129.0	OVERCONSOLIDATED CLAY TILL	24	12	0.080	0.011	0.0347	0.0048	0.0300	6.273	MacDonald and Sauer (1970)
130.0	OVERCONSOLIDATED CLAY TILL	34	14	0.190	0.026	0.0825	0.0113	0.0712	6.308	Soderman and Kim (1970)
131.0	ORGANIC SILT (OH)	81	37	0.760	0.140	0.3300	0.0608	0.2692	4.429	Lowe, et al. (1964)
132.0	ORGANIC SILT (OH)	59	23	0.330	0.050	0.1433	0.0217	0.1216	5.600	Lowe, et al. (1964)
133.0	MAINE ORGANIC CLAY	65	34	0.682	NA	0.2961	NA	NA	NA	Ladd and Edgers (1972)

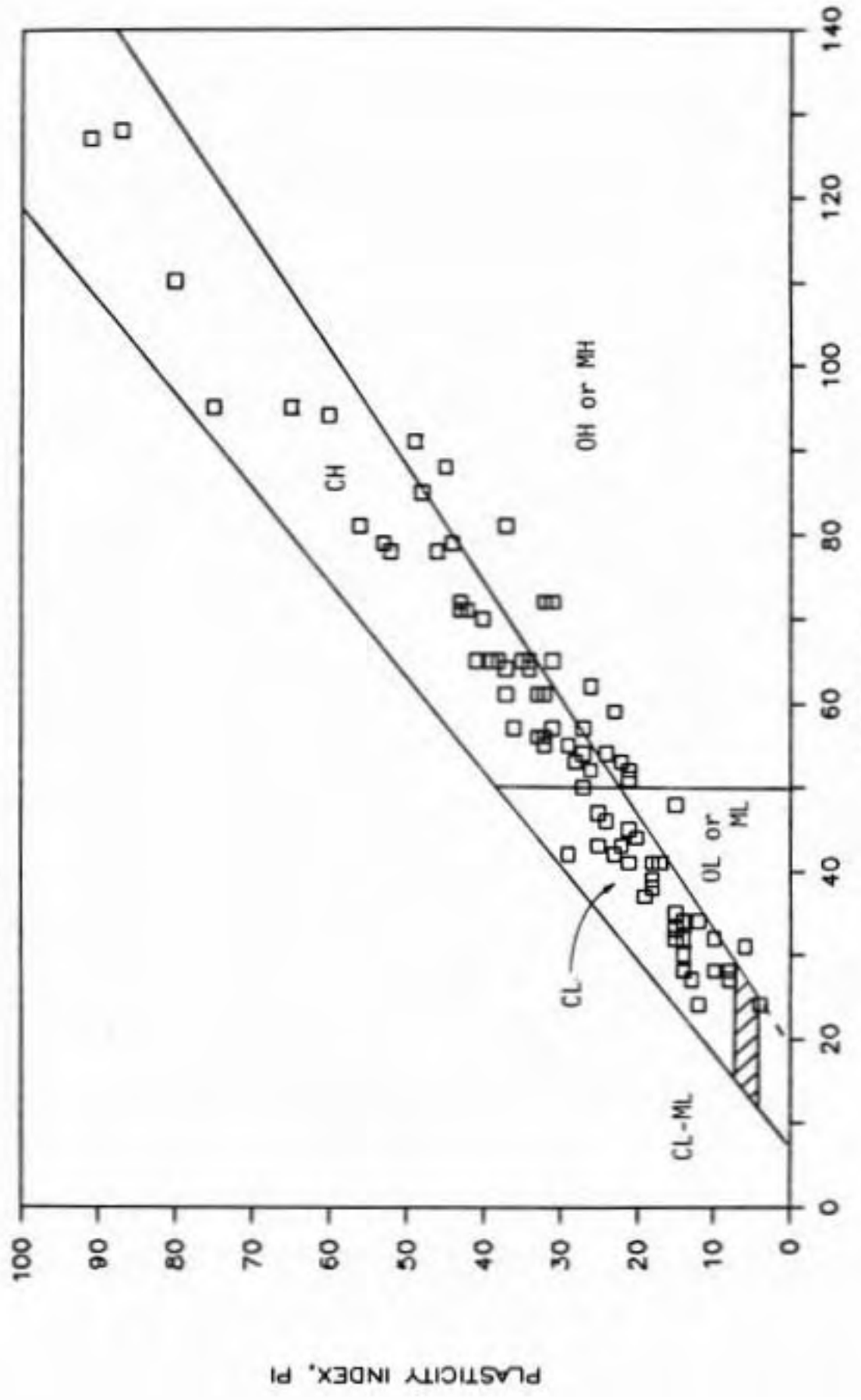

Figure 4.36 Atterberg limits of clayey soils used in correlations for compressibility properties.

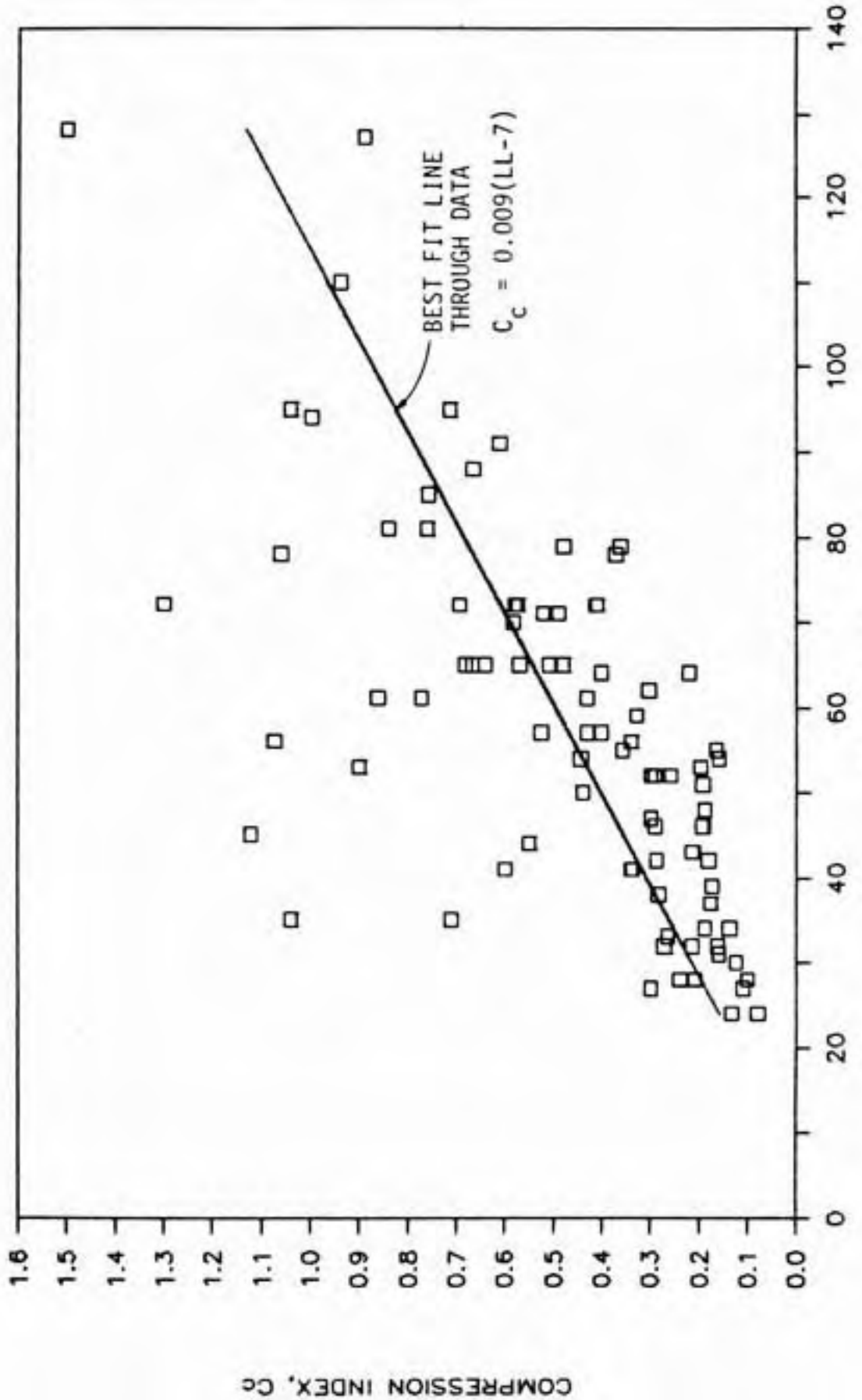

Figure 4.37 Compression Index C_c vs. liquid limit.

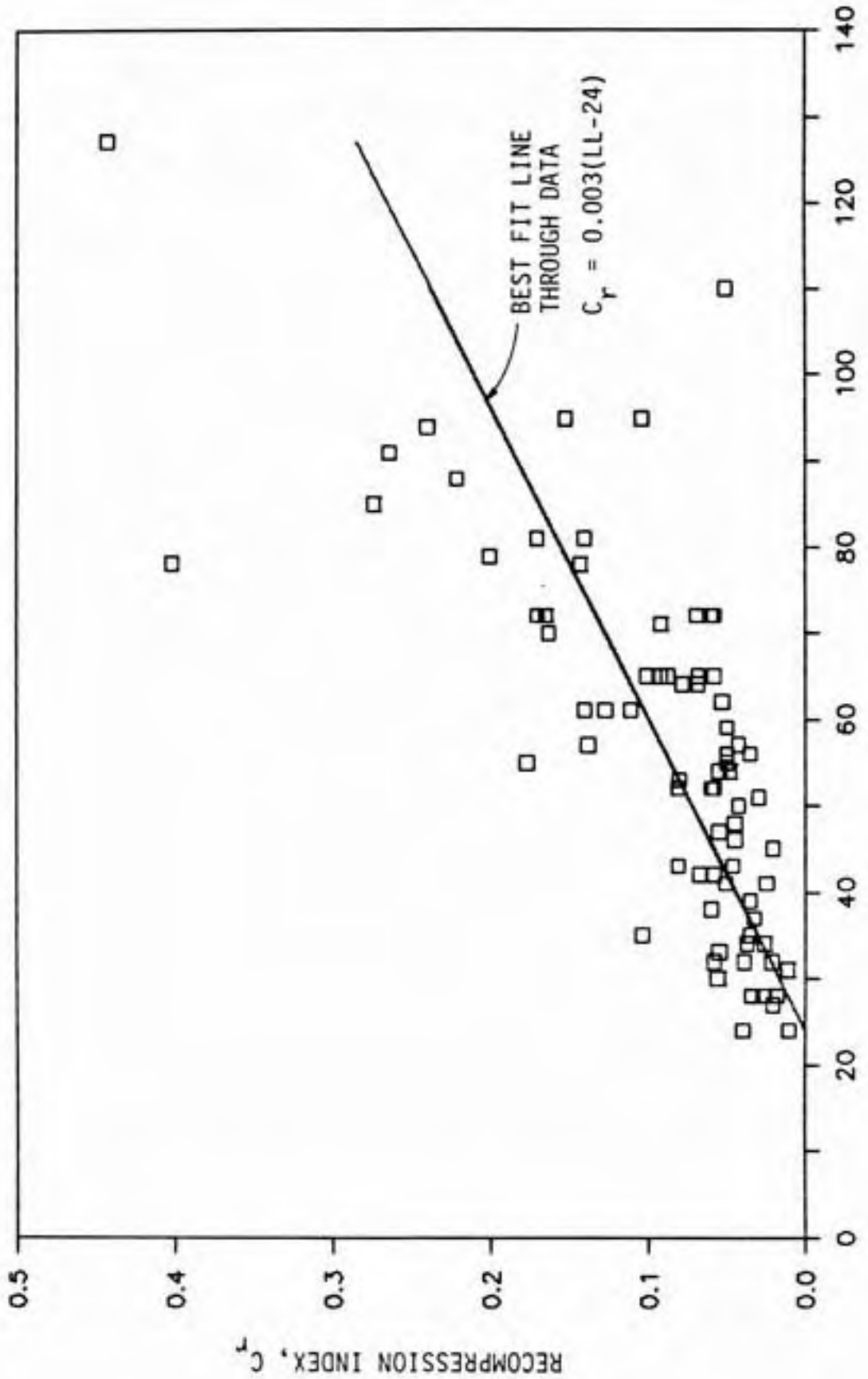

Figure 4.38 Recompression index C_r vs. liquid limit.

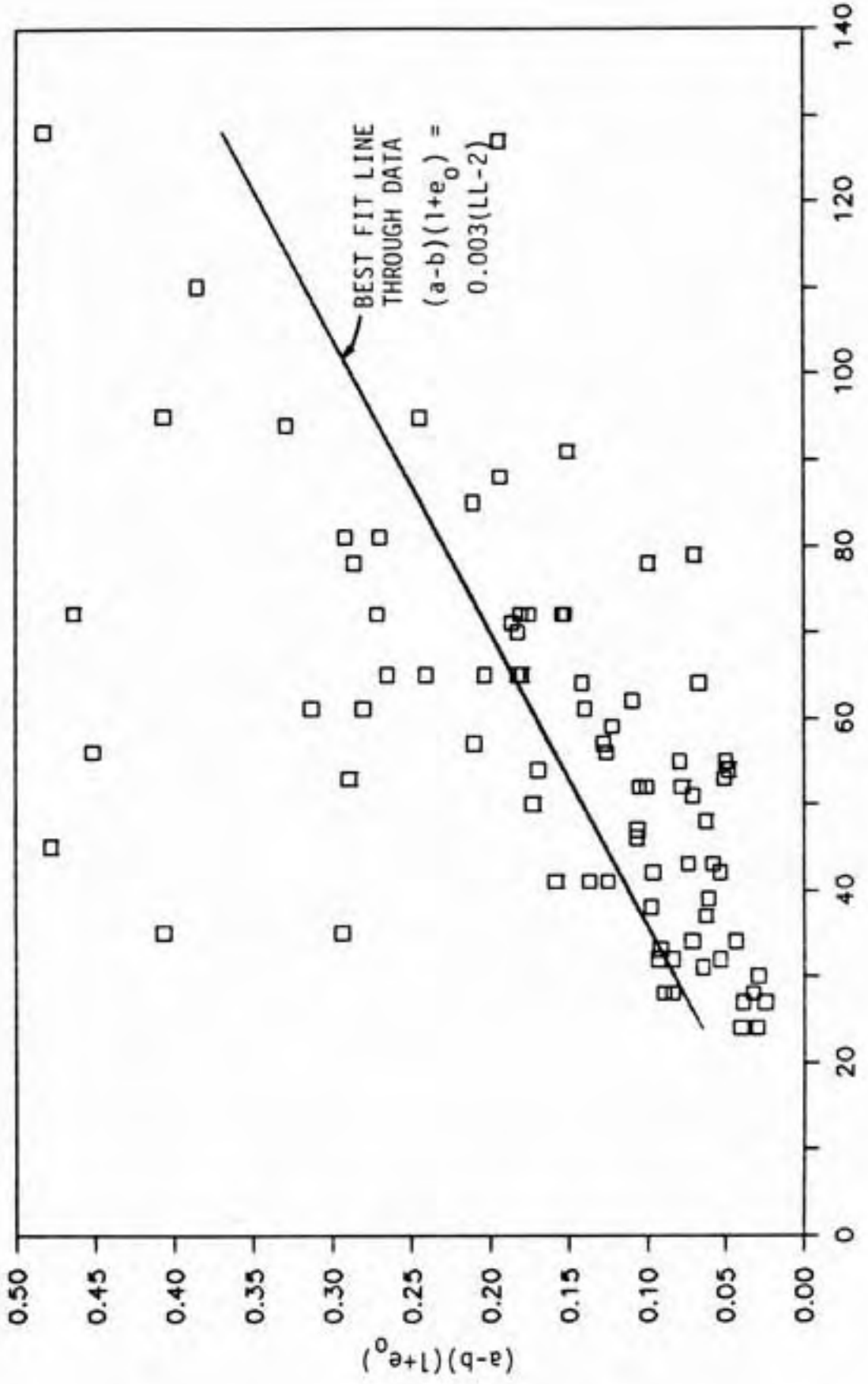

Figure 4.39 (a-b)(1+e$_o$) vs. liquid limit.

that the locations of the lines are influenced by the extreme values.

Table 4.14
Regression analysis for volume change properties.

Property	No. of samples	Regression equation	r^2
C_c	88	0.009(LL - 7)	0.446
C_r	76	0.003(LL - 24)	0.522
(a-b) $\times(1+e_o)$	81	0.003(LL - 2)	0.318

The regression equation for C_c is similar to that reported by other authors. Mayne (1980) obtained the following relation using a subset of the data in Table 4.13.

$$C_c = 0.009(LL - 13) \qquad (4.71)$$

Terzaghi and Peck (1967) recommend the following equation for undisturbed clays of low to medium sensitivity

$$C_c = 0.009(LL - 10) \qquad (4.72)$$

Other empirical equations for C_c were summarized by Azzouz, et al. (1976) (see also Holtz and Kovacs, 1981, p. 341).

The ratio (a-b)/b did not correlate well with liquid limit as shown in Fig. 4.40. It ranged from 0.81 to 52.38 with an average of about 6. The frequency distribution of

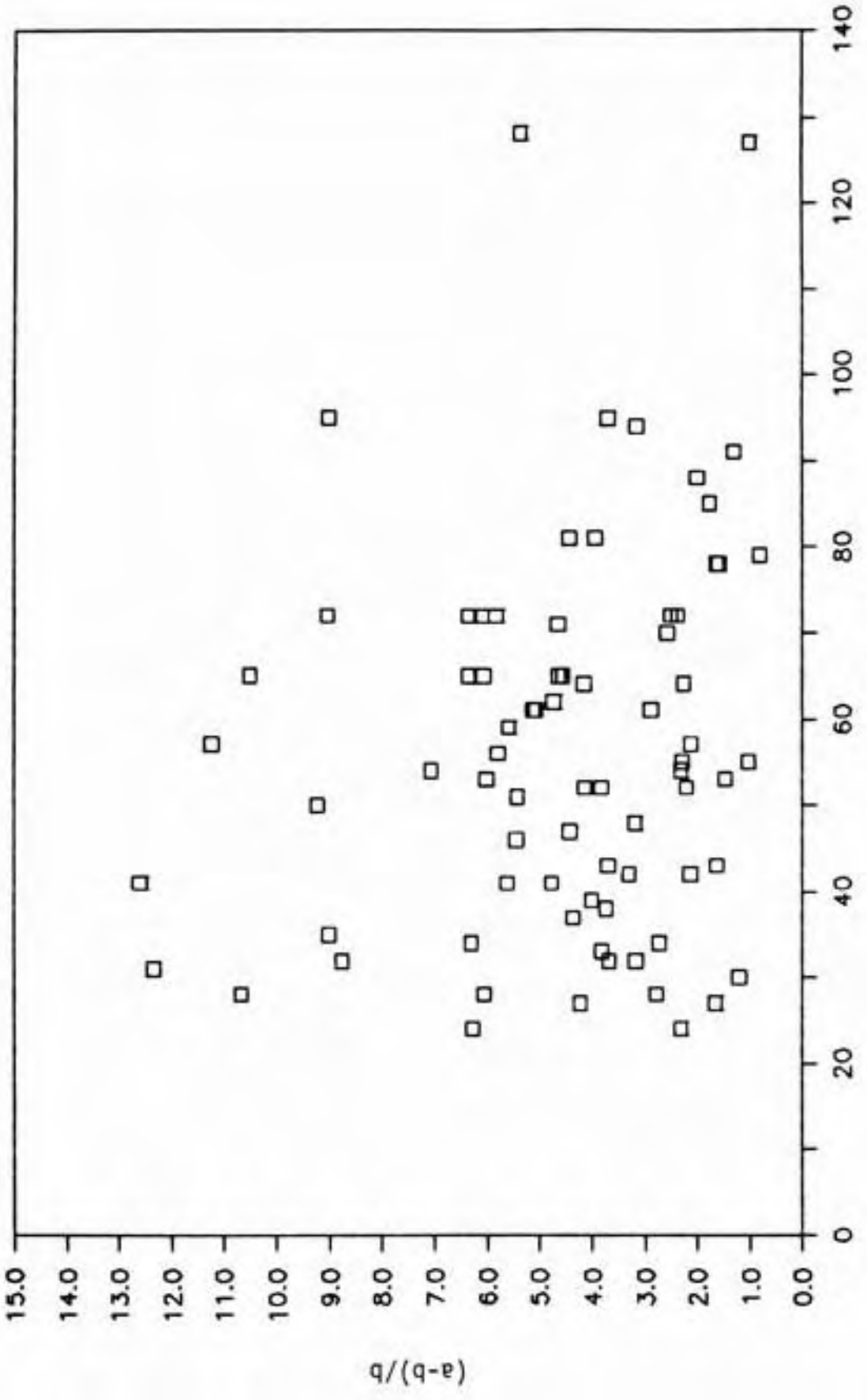

Figure 4.40 (a-b)/b vs. liquid limit.

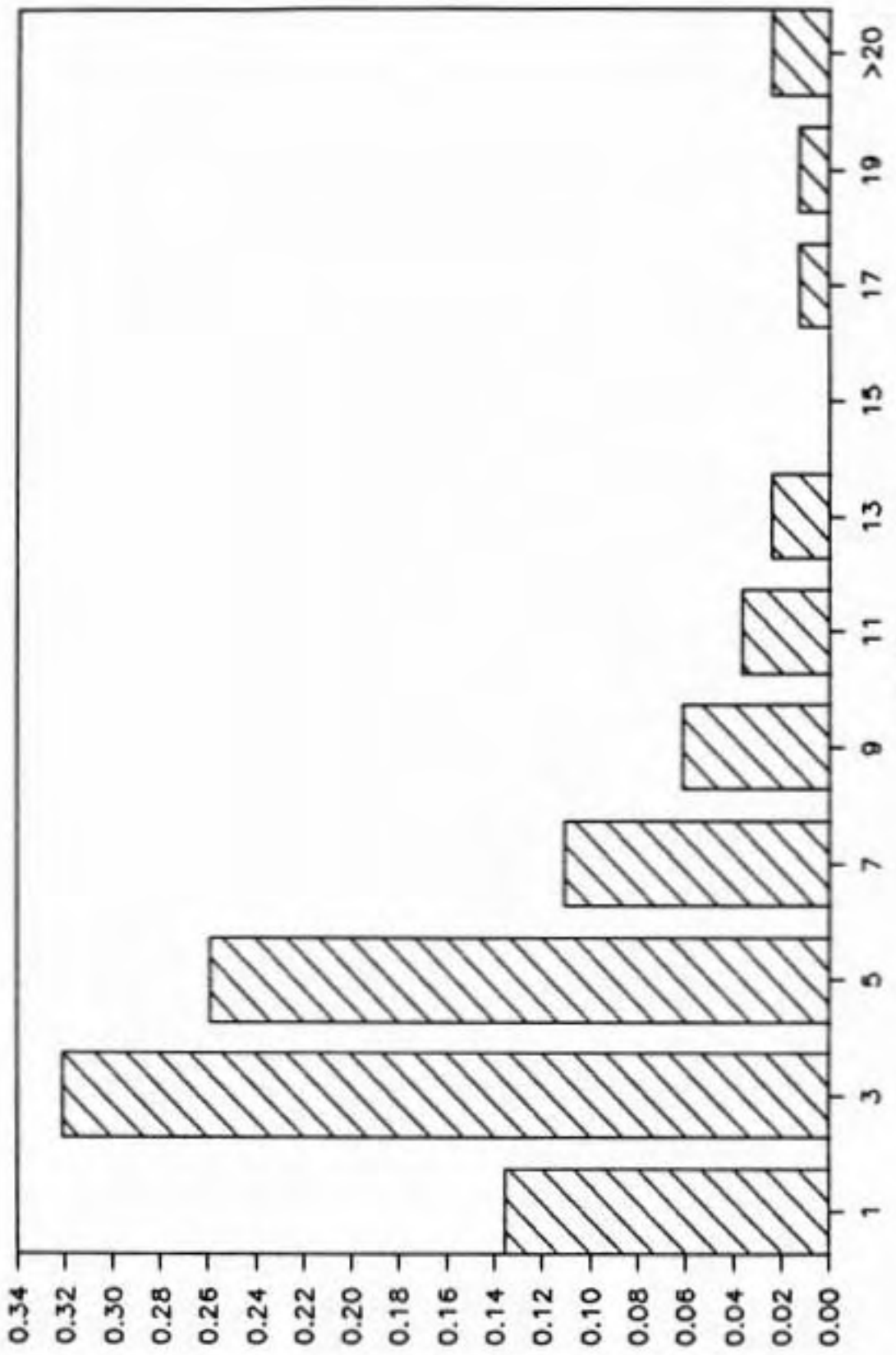

Figure 4.41 Frequency distribution of (a-b)/b.

the ratio from 81 samples is shown in Fig. 4.41. The poor correlation emphasizes the importance of obtaining a and b from consolidation tests. C_c and C_r chosen based on correlations is unlikely to result in reasonable values of (a-b)/b.

4.5.2 Aspect Ratio

4.5.2.1 CIU triaxial tests. The aspect ratio R, Dx_o, and W/(a-b) were computed from consolidation and CIU triaxial test data for 52 soils. The data and calculated parameters are summarized in Table 4.15. The α value was computed using Eq. 4.1 and κ was assumed to be 0.0. The ratio x_f/x_o was calculated using Eq. 4.49. Eqs. 4.31, 4.33, and 4.56 were used to compute Dx_o, W/(a-b), and R, respectively. $J_{2f}^{1/2}/\sigma'_{vo}$ used in Eq. 4.56 was found with Eq. 4.41.

The computed aspect ratios ranged from 0.57 to 12.80 and their frequency distribution is shown on Fig. 4.42. There was no significant correlation of R with Atterberg limits (Fig. 4.43). Statistical analyses were made of the correlation between R and the input soil properties. R was found to decrease as s_u/σ'_{vo} increased as shown in Fig. 4.44. This is reasonable when compared to the results on Figs. 4.7 through 4.16. The equation of the best fit straight line through the data is

Table 4.15
Cap parameters for hydrostatically consolidated triaxial tests.

NUMBER	SOIL	LL	PI	ϕ'	Cc	Cr	SR	α	(a-b)/b	xf/xo	D(xo)	W/(a-b)	R	REFERENCE
1.0	WEALD (REMOLDED)	43	25	22.0	0.214	0.081	0.279	0.165	1.642	1.298	-0.8741	2.7260	6.02	Henkel (1960)
2.0	SPESTONE KAOLIN	72	31	23.5	0.573	0.170	0.313	0.177	2.371	1.176	-0.9205	2.7213	4.11	Amerasinghe and Parry (1975)
3.0	SAN FRANCISCO BAY MUD	88	45	35.2	0.665	0.221	0.432	0.275	2.009	1.284	-0.8792	2.7253	4.08	Mitchell (1976)
4.0	LONDON CLAY (REMOLDED)	78	52	18.4	0.371	0.143	0.250	0.136	1.594	1.241	-0.8950	2.7236	5.53	Henkel (1960)
5.0	KEUPER MARL	32	14	25.9	0.272	0.058	0.256	0.197	3.690	1.206	-0.9085	2.7223	7.16	Brown, et al. (1975)
7.0	ILLITE	57	31	24.6	0.431	0.138	0.341	0.186	2.123	1.179	-0.9196	2.7213	3.60	France and Sangrey (1977)
8.0	RESED. BOSTON BLUE CL.	41	21	29.5	0.338	0.051	0.285	0.227	5.627	1.138	-0.9365	2.7202	5.96	Ladd and Edgers (1972)
10.0	OSLO	39	18	27.0	0.175	0.035	0.380	0.206	4.000	1.089	-0.9570	2.7191	2.59	Simons (1960b)
11.0	BRADWELL	95	65	20.0	0.714	0.152	0.300	0.149	3.697	1.071	-0.9641	2.7188	2.54	Skempton (1961)
13.0	SHELLHAVEN	110	80	23.0	0.937	0.051	0.205	0.173	17.373	1.046	-0.9688	2.7186	7.48	Skempton and Henkel (1953)
14.0	CALCIUM MONTMORILL.	203	169	12.5	0.979	0.440	0.221	0.090	1.225	1.045	-0.9688	2.7186	1.15	Mesri and Olson (1970)
15.0	NEWFIELD	28	10	30.5	0.210	0.018	0.475	0.235	10.667	1.024	-0.9568	2.7197	1.35	Sangrey, Henkel and Esrig (1969)
17.0	VIRGINIA COASTAL	54	27	28.5	0.444	0.055	0.409	0.218	7.073	1.047	-0.9688	2.7186	2.07	Swanson and Brown (1977)
18.0	SPESTONE KAOLIN	72	32	22.6	0.693	0.069	0.210	0.170	9.043	1.085	-0.9585	2.7190	7.53	Parry and Nadarajah (1973)
19.0	JAPANESE	64	37	33.7	0.403	0.078	0.400	0.262	4.167	1.136	-0.9372	2.7201	3.56	Shibata and Karube (1969)
21.0	ATCHAFALAYA	95	75	23.5	1.040	0.104	0.250	0.177	9.000	1.070	-0.9642	2.7188	5.47	Ladd and Edgers (1972)
23.0	MILAZZO	61	33	23.0	0.431	0.111	0.333	0.173	2.883	1.109	-0.9485	2.7195	2.87	Croce, et al. (1969)
24.0	CALCIUM ILLITE	85	48	24.2	0.758	0.274	0.250	0.183	1.766	1.438	-0.8271	2.7332	9.47	Olson (1962)
26.0	DRAMMEN	33	15	28.0	0.265	0.055	0.310	0.214	3.818	1.166	-0.9249	2.7209	5.10	Simons (1960a)
27.0	BACKSWAMP	70	40	22.2	0.583	0.163	0.280	0.166	2.577	1.184	-0.9175	2.7215	4.97	Whitman (1960)
28.0	KARS LEDA	45	21	28.3	1.121	0.021	0.265	0.217	52.381	1.014	-0.9396	2.7224	5.33	Raymond (1972)
31.0	PLASITC HOLOCENE	65	38	32.9	0.640	0.087	0.335	0.255	6.356	1.113	-0.9468	2.7196	4.72	Koutsoftas and Fischer (1976)
32.0	GHANA	42	29	20.8	0.182	0.058	0.380	0.155	2.138	1.028	-0.9611	2.7193	0.58	deGraft-Johnson, et al. (1969)
33.0	HALLOYSITE	62	26	34.3	0.304	0.053	0.418	0.267	4.736	1.113	-0.9470	2.7196	3.17	Taylor and Bacchus (1969)
34.0	SIMPLE CLAY	NA	NA	23.1	0.207	0.083	0.290	0.174	1.494	1.345	-0.8577	2.7282	6.29	Ladd (1964)
35.0	SEATTLE	52	26	28.8	0.260	0.081	0.372	0.221	2.210	1.217	-0.9044	2.7226	3.97	Sheriff, Wu and Bostrum (1972)
37.0	SODIUM ILLITE	79	44	20.7	0.362	0.200	0.340	0.154	0.810	1.225	-0.9013	2.7229	2.87	Olson and Hardin (1963)
38.0	GRUNDITE	55	29	32.3	0.359	0.177	0.356	0.250	1.028	1.796	-0.7304	2.7572	9.11	Perloff and Osterberg (1963)

Table 4.15
Continued.

NUMBER	SOIL	LL	PI	ϕ'	Cc	Cr	SR	a	(a-b)/b	xf/xo	D(xo)	W/(a-b)	R	REFERENCE
39.0	TERRA ROXA	43	22	29.2	0.216	0.046	0.313	0.224	3.696	1.183	-0.9178	2.7215	5.36	da Cruz (1963)
41.0	SCOTT	34	12	33.4	0.138	0.037	0.231	0.259	2.730	1.481	-0.8140	2.7357	12.80	Ladanyi, et al. (1965)
43.0	TOLEDO	42	23	20.0	0.288	0.067	0.200	0.149	3.299	1.221	-0.9029	2.7228	9.13	Wu, Chang and Ali (1978)
44.0	KAWASAKI	65	31	35.9	0.668	0.058	0.370	0.281	10.517	1.067	-0.9653	2.7188	3.92	Ladd and Lambe (1963)
47.0	CONCORD BLUE	32	10	24.8	0.163	0.039	0.355	0.188	3.179	1.105	-0.9504	2.7194	2.76	Egan (1977)
49.0	LAGUNILLAS	61	37	26.5	0.771	0.127	0.305	0.202	5.071	1.113	-0.9471	2.7196	4.52	Ladd and Lambe (1963)
50.0	DRAMMEN	NA	NA	30.7	0.599	0.127	0.285	0.237	3.717	1.230	-0.8992	2.7231	6.99	Van Eekelen and Potts (1978)
51.0	LISKEARD	56	33	26.1	1.073	0.035	0.298	0.198	29.657	1.019	-0.9486	2.7209	3.84	Raymond (1973)
56.0	LILLA EDET	61	32	24.3	0.860	0.140	0.290	0.184	5.143	1.102	-0.9519	2.7193	4.42	Bjerrum and Simons (1960)
60.0	HOKKAIDO SILT A	52	21	37.2	0.299	0.058	0.420	0.291	4.155	1.152	-0.9303	2.7206	3.70	Mitachi and Kitago (1976)
61.0	HOKKAIDO SILT B	51	21	35.1	0.193	0.030	0.362	0.274	5.433	1.132	-0.9388	2.7200	4.47	Mitachi and Kitago (1976)
62.0	HOKKAIDO CLAY	72	32	36.1	0.412	0.058	0.410	0.282	6.103	1.100	-0.9526	2.7193	3.43	Mitachi and Kitago (1976)
65.0	KANPUR CLAY	38	18	29.0	0.284	0.060	0.295	0.223	3.733	1.198	-0.9119	2.7220	6.05	Yudhbir and Varadarajah (1974)
66.0	RANN OF KUTCH	91	49	26.0	0.610	0.264	0.326	0.198	1.311	1.414	-0.8346	2.7319	6.21	Yudhbir and Varadarajah (1974)
72.0	LANSISALMI	78	46	19.5	1.059	0.401	0.215	0.145	1.641	1.405	-0.8376	2.7314	10.06	Korhonen (1977)
73.0	SAULT STE MARIE	55	32	28.9	0.165	0.050	0.327	0.222	2.300	1.279	-0.8808	2.7251	5.65	Wu, Douglas and Goughnour (1962)
74.0	BATH KAOLINITE	48	15	24.5	0.189	0.045	0.425	0.185	3.200	1.040	-0.9679	2.7187	0.96	Brons and Ratnam (1963)
76.0	BANGALORE MONTMORILL.	580	495	12.5	2.260	1.350	0.211	0.090	0.674	1.160	-0.9270	2.7208	3.15	Sridharan, et al. (1971)
81.0	LONG ISLAND COASTAL	64	34	22.8	0.222	0.068	0.271	0.171	2.265	1.245	-0.8936	2.7237	6.10	Swanson and Brown (1977)
82.0	HACKENSACK VARVED	65	35	19.0	0.481	0.068	0.158	0.141	6.074	1.148	-0.9322	2.7204	11.76	Saxena, Hedberg and Ladd (1978)
89.0	KODIAK ISLAND	30	14	42.2	0.124	0.056	0.510	0.333	1.214	1.546	-0.7948	2.7398	4.87	Sparrow, Swanson and Brown (1978)
90.0	WINNIPEG CLAY	94	60	12.8	0.996	0.240	0.211	0.092	3.150	1.041	-0.9682	2.7187	1.95	Crawford (1964)
97.0	REMOLDED BOSTON BLUE	33	15	27.5	0.338	0.051	0.300	0.210	5.627	1.112	-0.9474	2.7196	4.87	Ladd (1965)
100.0	PORTSMOUTH	35	15	21.1	0.711	0.035	0.253	0.157	19.314	1.025	-0.9585	2.7196	4.18	Ladd (1972); Ladd and Edgers (1972)

Note: SR = s_u/σ'_{vo} for normally consolidated condition

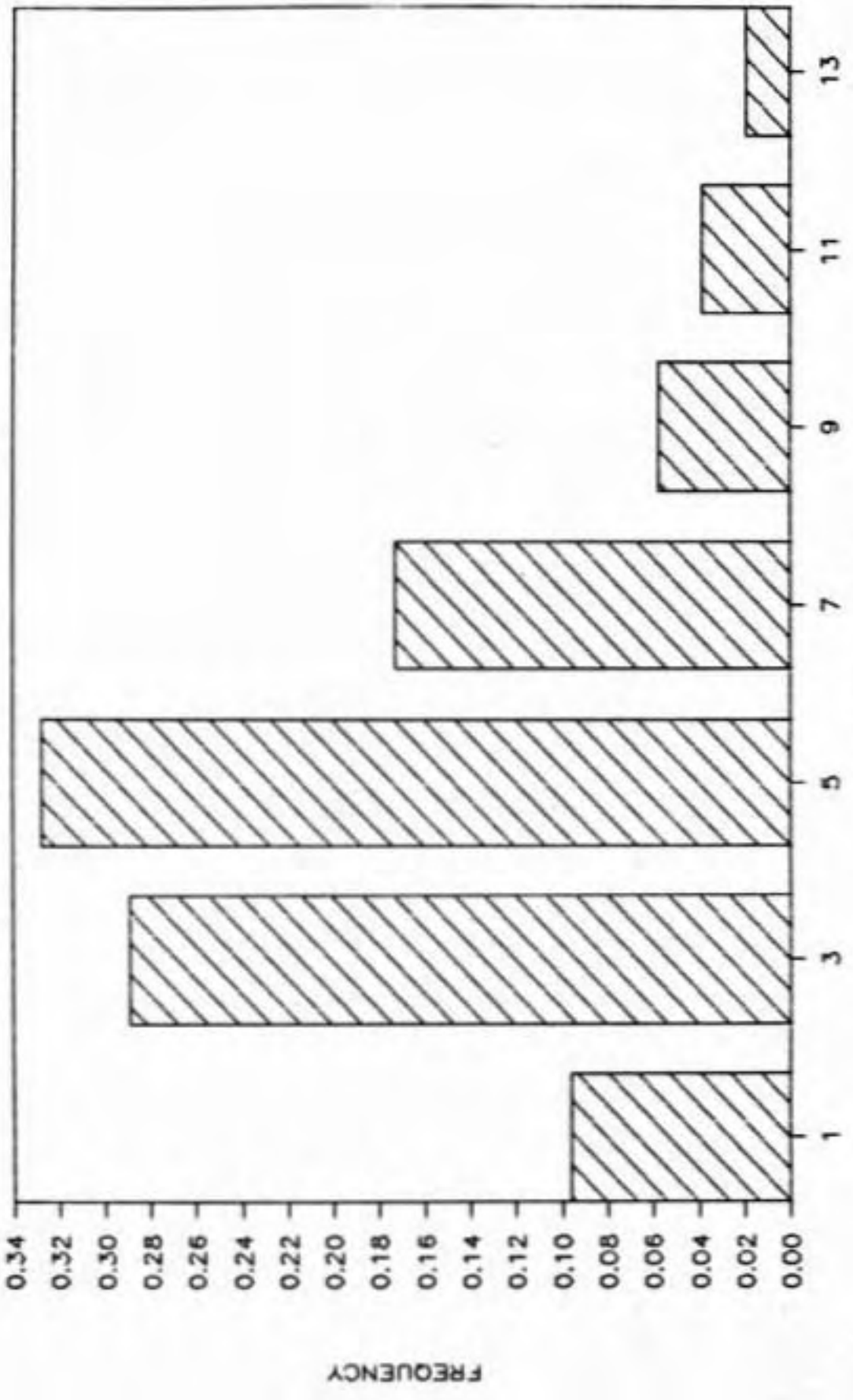

Figure 4.42 Frequency distribution of the aspect ratio R.

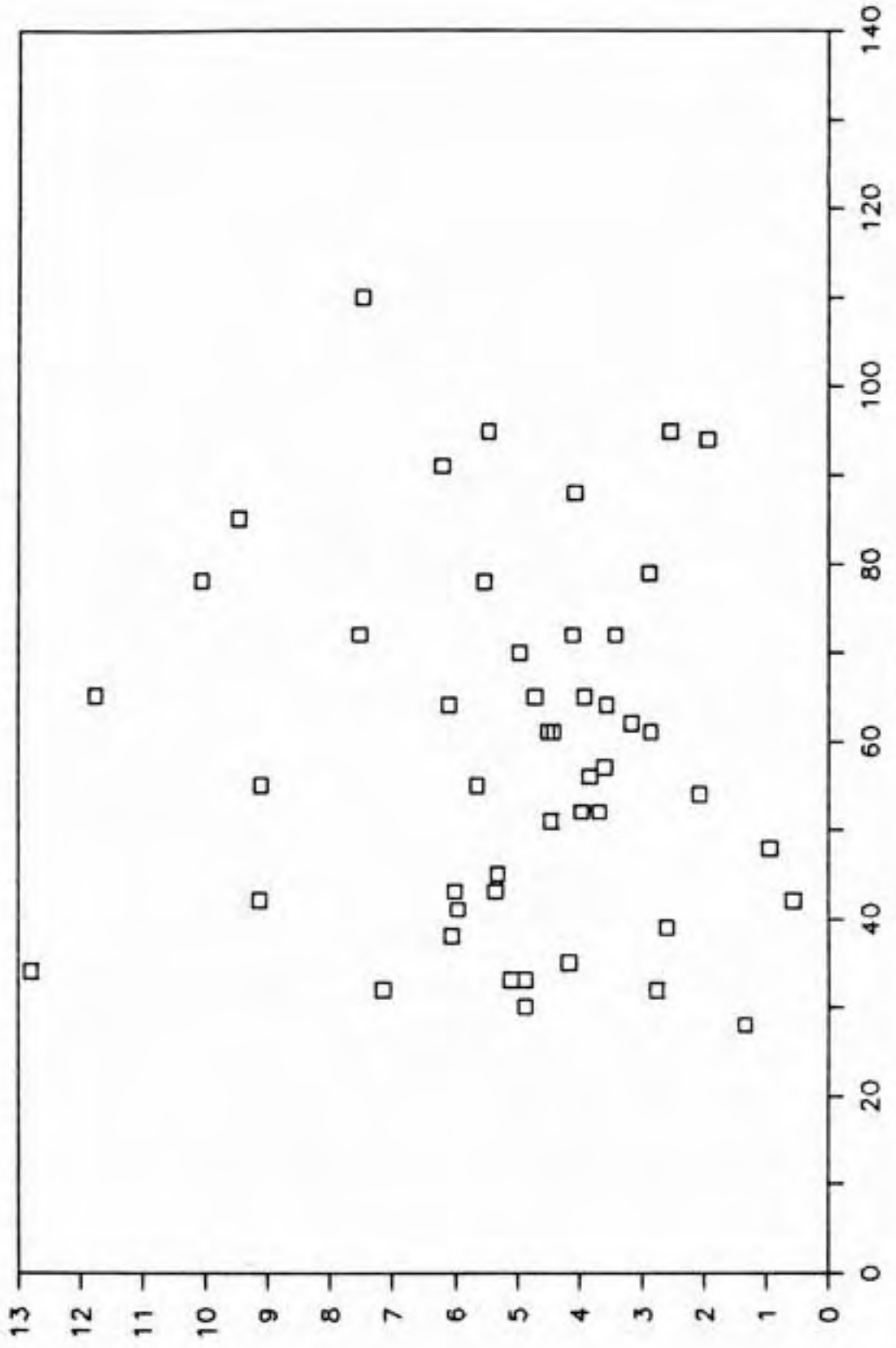

Figure 4.43 Aspect ratio R vs. liquid limit.

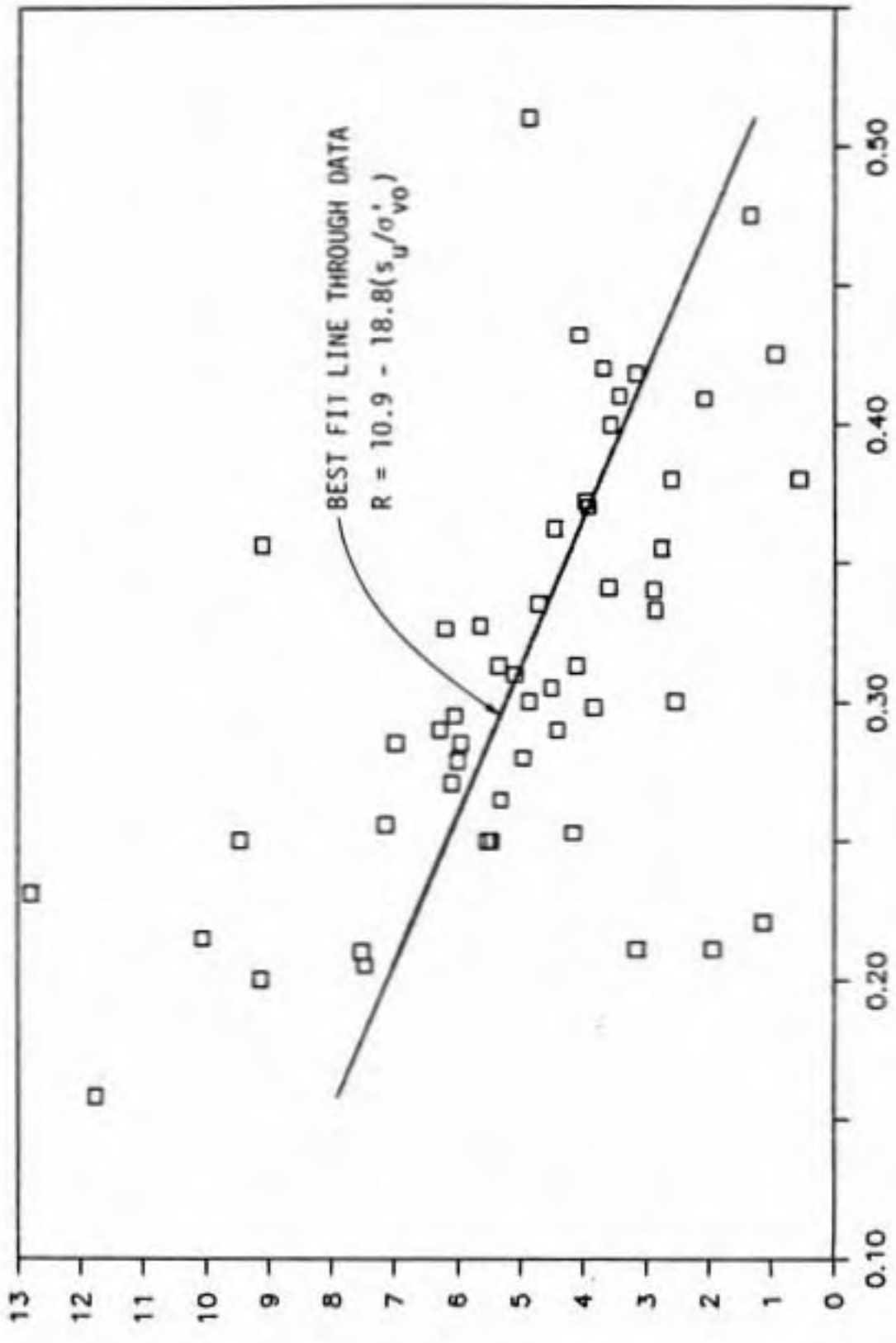

Figure 4.44 Aspect ratio R vs. s_u/σ'_{vo}.

$$R = 10.9 - 18.8(s_u/\sigma'_{vo}) \qquad (4.73)$$

The r^2 was 0.306 which indicates only poor correlation. There was no significant correlation of R with ϕ' or (a-b)/b.

4.5.2.2 Shear tests with nonhydrostatic initial consolidation. Input data and computed cap parameters for shear tests with nonhydrostatic initial consolidation are shown in Table 4.16. Most of the tests are CK_oU or CAU triaxial tests although there is one CK_oUPSA test. For 10 soils results from CIU triaxial tests are shown for comparison. The values of α, x_f/x_o, Dx_o, W/(a-b), and R for the CK_oU and CAU triaxial tests were computed using Eqs. 4.1, 4.49, 4.31, 4.33, and 4.55, respectively. $J_{2f}^{1/2}/\sigma'_{vo}$ was found using Eq. 4.41. For the CK_oUPSA test, α and $J_{2f}^{1/2}/\sigma'_{vo}$ were computed directly from the measured effective stresses at failure.

The ϕ', s_u/σ'_{vo}, and R from nonhydrostatic and hydrostatic consolidated tests are compared in Table 4.17. For 8 soils the ϕ' from nonhydrostatic tests was greater than from hydrostatic tests but the reverse was true for one soil and they were equal for another. The ratio s_u/σ'_{vo} for nonhydrostatic consolidation is both higher and lower than the corresponding hydrostatic value. It is difficult to

Table 4.16
Cap parameters for nonhydrostatically consolidated shear tests.

NUMBER	SOIL	LL	PI	φ'	Cc	Cr	SR	TEST TYPE	Kc	e	(a-b)/b	xf/xo	D(xo)	W/(a-b)	R	REFERENCE
8.0	RESED. BOSTON BLUE	41	21	29.5	0.338	0.051	0.285	CIU	1.00	0.227	5.627	1.138	-0.9365	2.7202	5.96	Ladd and Edgers (1972)
8.1	RESED. BOSTON BLUE	41	21	26.5	0.338	0.051	0.330	CKoU	0.51	0.202	5.627	1.012	-0.9940	2.7183	0.62	Ladd and Edgers (1972)
8.2	RESED. BOSTON BLUE	41	21	29.0	0.338	0.051	0.365*	CKoPSA	0.52	0.194	5.627	1.014	-0.9928	2.7183	0.81	Ladd and Edgers (1972)
21.0	ATCHAFALAYA	95	75	23.5	1.040	0.104	0.250	CIU	1.00	0.177	9.000	1.070	-0.9664	2.7188	5.47	Ladd and Edgers (1972)
21.1	ATCHAFALAYA	95	75	21.0	1.040	0.104	0.240	CKoU	0.71	0.157	9.000	1.035	-0.9827	2.7184	3.41	Ladd and Edgers (1972)
25.0	MEXICO VOLCANIC	426	286	47.0	7.145	2.577	0.430	CKoU	0.36	0.372	1.773	1.154	-0.9296	2.7206	2.56	Lo (1962)
48.0	AGNEW	54	24	25.0	0.159	0.048	0.308	CKoU	0.58	0.189	2.313	1.062	-0.9700	2.7187	1.70	Egan (1977)
60.0	HOKKAIDO SILT A	52	21	37.2	0.299	0.058	0.420	CIU	1.00	0.291	4.155	1.152	-0.9304	2.7206	3.70	Mitachi and Kitago (1976)
60.1	HOKKAIDO SILT A	52	21	35.1	0.290	0.060	0.400	CKoU	0.45	0.274	3.833	1.032	-0.9845	2.7184	0.84	Mitachi and Kitago (1976)
61.0	HOKKAIDO SILT B	51	21	35.1	0.193	0.030	0.362	CIU	1.00	0.274	5.433	1.132	-0.9388	2.7200	4.47	Mitachi and Kitago (1976)
61.1	HOKKAIDO SILT B	51	21	34.9	0.193	0.030	0.361	CKoU	0.45	0.272	5.433	1.040	-0.9803	2.7185	1.75	Mitachi and Kitago (1976)
62.0	HOKKAIDO CLAY	72	32	36.1	0.412	0.058	0.410	CIU	1.00	0.282	6.103	1.100	-0.9530	2.7193	3.43	Mitachi and Kitago (1976)
62.1	HOKKAIDO CLAY	72	32	34.0	0.410	0.060	0.360	CKoU	0.47	0.265	5.833	1.037	-0.9820	2.7184	1.64	Mitachi and Kitago (1976)
92.0	WEALD CLAY	46	24	25.9	0.193	NA	0.323	CIU	1.00	0.197	1.642	1.323	-0.8653	2.7271	5.56	Henkel and Sowa (1964)
92.1	WEALD CLAY	46	24	25.0	0.195	NA	0.256	CKoU	0.59	0.189	1.642	1.225	-0.9010	2.7230	19.53	Henkel and Sowa (1964)
96.0	DRAMMEN CLAY	57	27	30.7	0.526	0.043	0.280	CKoU	0.50	0.237	11.233	1.035	-0.9831	2.7184	5.68	Andersen, et al. (1980)
97.0	REMOLDED BOSTON BLUE	33	15	27.5	0.338	0.051	0.300	CIU	1.00	0.210	5.627	1.112	-0.9476	2.7196	4.87	Ladd (1965)
97.1	REMOLDED BOSTON BLUE	33	15	26.5	0.338	0.051	0.330	CKoU	0.54	0.202	5.627	1.017	-0.9915	2.7183	0.85	Ladd (1965)
98.1	CONNECTICUT VARVED	65	39	20.3	0.569	0.101	0.234	CKoU	0.68	0.151	4.634	1.062	-0.9704	2.7187	3.85	Ladd (1975)
100.0	PORTSMOUTH	35	15	21.1	0.711	0.035	0.253	CIU	1.00	0.157	19.314	1.025	-0.9876	2.7184	4.18	Ladd (1972)
100.1	PORTSMOUTH	35	15	24.2	0.711	0.035	0.245	CAU	0.63	0.183	19.314	1.020	-0.9907	2.7183	4.19	Ladd and Edgers (1972)
106.0	MIDDLETON FIBROUS PT.	NA	NA	57.4	6.650	0.250	0.740	CAU	0.47	0.451	25.600	1.001	-0.9995	2.7183	0.06	Dhowian and Edil (1981)
111.0	REMOLDED WEALD CLAY	46	24	26.0	NA	NA	0.320	CIU	1.00	0.198	1.642	1.334	-0.8615	2.7277	5.77	Skempton and Sowa (1963)
111.1	REMOLDED WEALD CLAY	46	24	26.0	NA	NA	0.270	CKoU	0.61	0.198	1.642	1.231	-0.8988	2.7232	8.10	Skempton and Sowa (1963)

Notes: 1. SR = s_u/σ'_{vo} for normally consolidated condition.

2. * For CKoPSA test SR = $J_{2f}^{1/2}/\sigma'_{vo}$ and e determined directly from measured effective stresses at failure.

3. (a-b)/b for soils 92.0, 92.1, 111.0, and 111.1 assumed to be the same as for soil 1.0, Table 4.13.

Table 4.17
Comparison of tests with hydrostatic and nonhydrostatic consolidation.

No.	Soil	Anisotropic Test type	K_o	ϕ' I	ϕ' A	s_u/σ'_{vo} I	s_u/σ'_{vo} A	R I	R A	R (1)
8.1	Resedimented Boston Blue	CK_oU	0.51	29.5	26.5	0.285	0.330	5.96	0.62	5.11
8.2	Resedimented Boston Blue	(2)	0.52	29.5	29.0	0.285	0.365	5.96	0.81	4.87
21.1	Atchafalaya	CK_oU	0.71	23.5	21.0	0.250	0.240	5.47	3.41	3.91
25.0	Mexico Volcanic	CK_oU	0.36	----	47.0	-----	0.430	----	2.56	----
48.0	Agnew	CK_oU	0.58	----	25.0	-----	0.308	----	1.70	----
60.1	Hokkaido silt A	CK_oU	0.45	37.2	35.1	0.420	0.400	3.70	0.84	0.85
61.1	Hokkaido silt B	CK_oU	0.45	35.1	34.9	0.362	0.361	4.47	1.75	1.76
62.1	Hokkaido clay	CK_oU	0.47	36.1	34.0	0.410	0.360	3.43	1.64	0.88
92.1	Weald clay	CK_oU	0.59	25.9	25.0	0.323	0.256	5.56	19.53	1.78
96.0	Drammen clay	CK_oU	0.50	----	30.7	-----	0.280	----	5.68	----
97.1	Remolded Boston Blue	CK_oU	0.54	27.5	26.5	0.300	0.330	4.87	0.85	2.49
98.1	Connecticut varved	CK_oU	0.68	----	20.3	-----	0.234	----	3.85	----
100.1	Portsmouth	$CA\bar{U}$	0.63	21.1	24.2	0.253	0.245	4.18	4.19	2.17
106.0	Middleton fibrous peat	CAU	0.47	----	57.4	-----	0.740	----	0.06	----
111.1	Remolded weald clay	CK_oU	0.61	26.0	26.0	0.320	0.270	5.77	8.10	2.19

Notes: (1) R computed for anisotropic conditions using strength parameters from CIU tests.
(2) CK_oUPSA
(3) I = isotropic
A = anistropic

generalize on the relationship between strength parameters from hydrostatic and nonhydrostatic tests.

For several soils, R for nonhydrostatic consolidation was significantly different than for hydrostatic consolidation. The same was true for R computed from hydrostatic strength parameters but with the nonhydrostatic K_o. As shown previously for Boston Blue clay, use of R based on hydrostatic strengths gave poor predictions for samples with nonhydrostatic consolidation. This emphasizes the importance, for at least some soils, of using strength parameters obtained from tests with nonhydrostatic consolidation.

4.6 PARAMETRIC STUDY OF INPUT PARAMETERS

A parametric study was made of the effect of varying the input soil properties on calculated stress-strain curves, pore pressure response, and effective stress paths. The results show which parameters have the greatest effect on computed behavior and are useful for guidance if it is necessary to adjust the input soil properties to obtain a better fit between calculated and observed behavior. Sample response calculated using the parameters shown in Tables 4.8 and 4.9 for test CIUC-1 was used as the basis for comparison. The soil properties ν', a, b, ϕ', and s_u/σ'_{vo} were varied individually and the effect on calculated response was observed. The influence of β was also investigated.

4.6.1 Poisson's Ratio

The effect of Poisson's ratios ν' of 0.15, 0.25, and 0.35 was investigated. These correspond to G_1 = 0.913, 0.60, and 0.333 (Eq. 4.22). Lower ν' result in steeper stress-strain and pore pressure response curves but have no effect on the values at failure as shown in Fig. 4.45. The closest match between observed and calculated curves is for ν' = 0.15. The influence on the effective stress path was too small to plot.

4.6.2 Slope of Unloading/Reloading Curve

The influence of the slope of the unloading/reloading curve b ± 25% was examined. A higher b results in a lower bulk modulus (Eq. 4.16). The calculated cap parameters are shown in Table 4.18; other parameters are unchanged and are given in Tables 4.8 and 4.9.

Table 4.18
Cap parameters for b ± 25%.

±b	b	K_1	W	R
-25%	0.0088	113.9	0.187	5.60
0%	0.0117	85.5	0.180	6.00
+25%	0.0146	68.5	0.171	6.39

A higher b results in a flatter stress-strain response but has no effect on the $(\sigma_1-\sigma_3)/\sigma'_{vo}$ at failure (Fig. 4.46a).

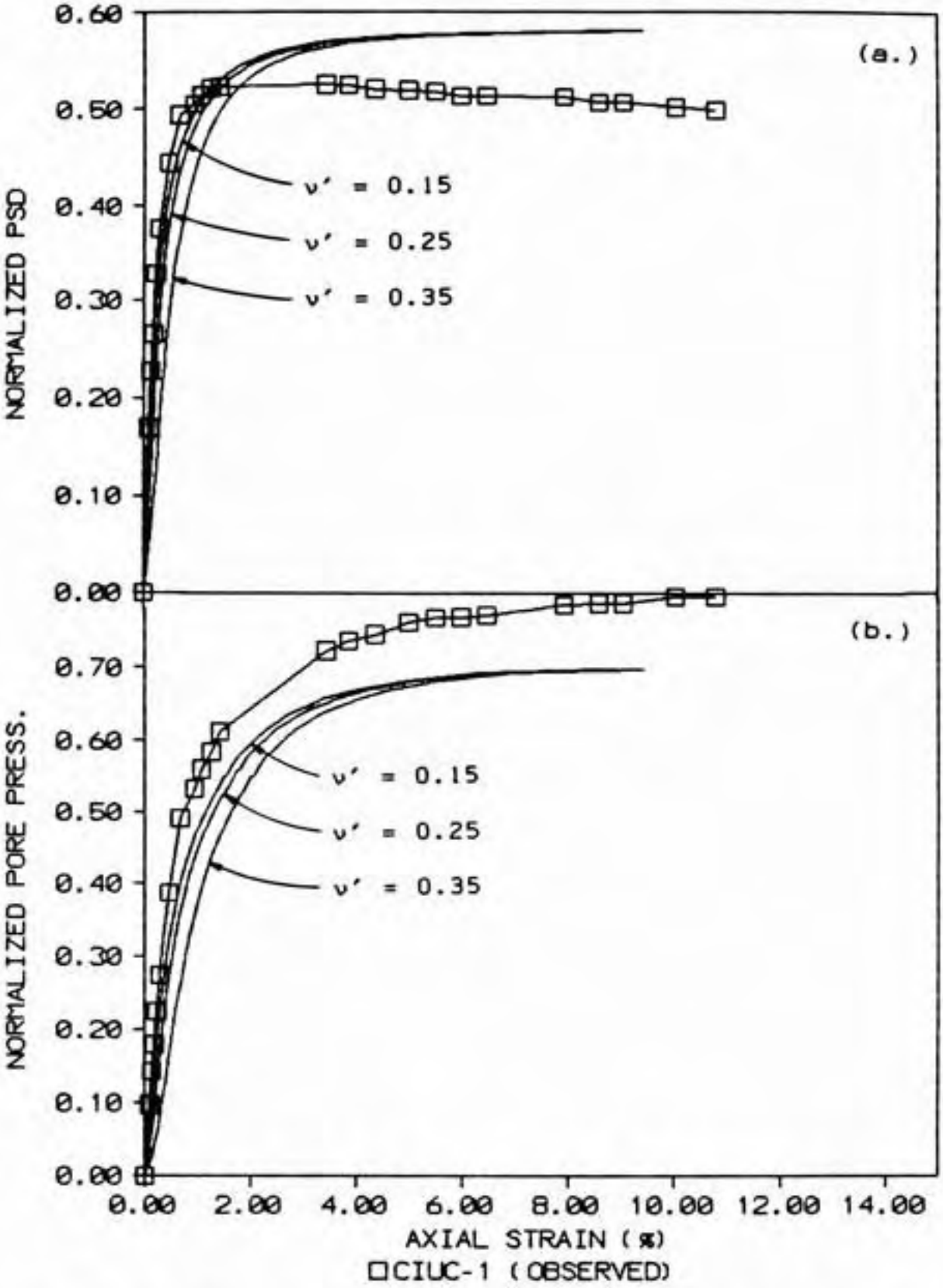

Figure 4.45 Effect of Poisson's ratio on calculated (a) stress-strain and (b) pore pressure response.

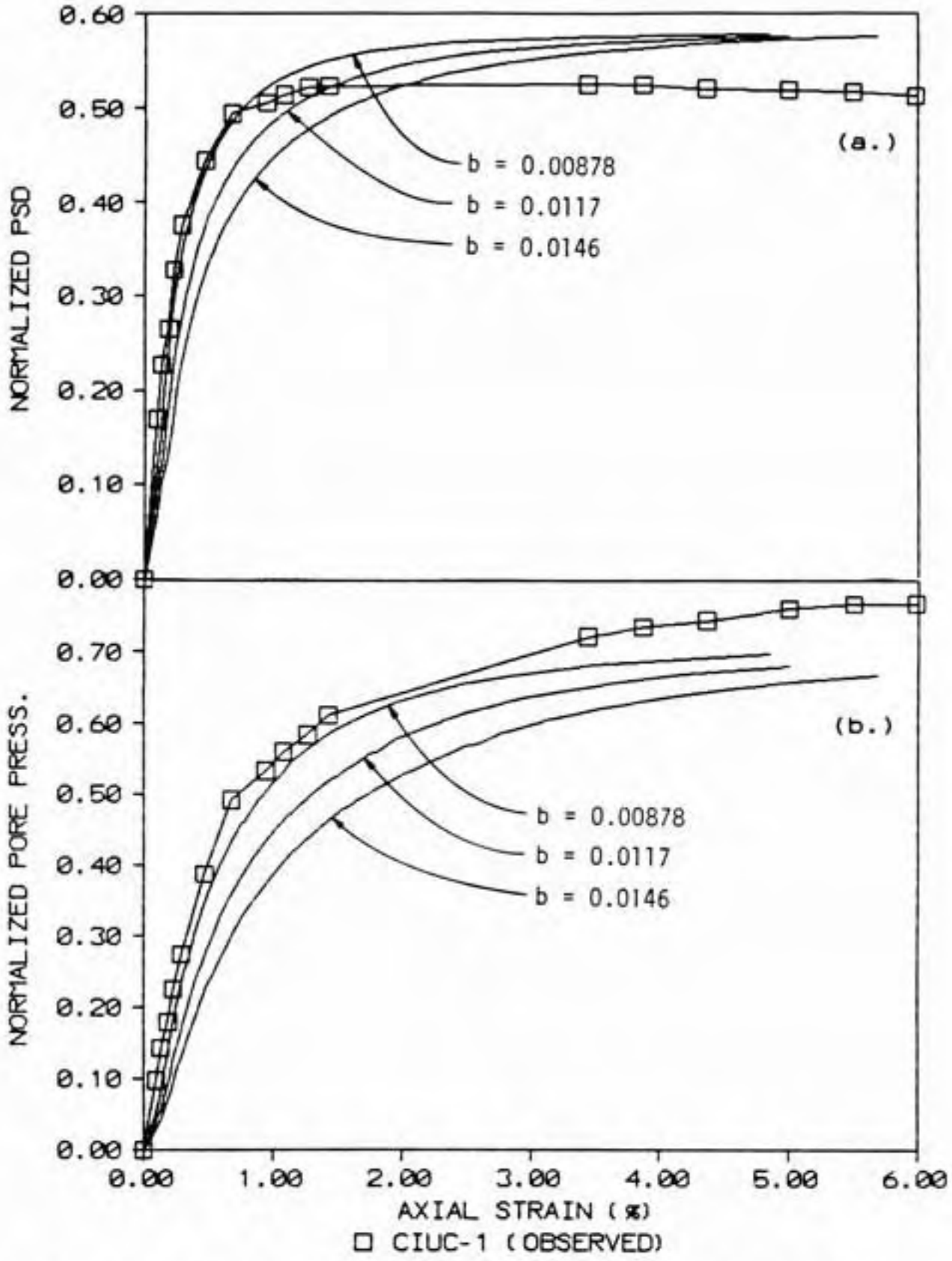

Figure 4.46 Effect of b-value on calculated (a) stress-strain and (b) pore pressure response.

Increasing b lowers the pore pressure as shown in Fig. 4.46b but they are about the same when compared at equal $(\sigma_1-\sigma_3)/\sigma'_{vo}$. It also shifts the effective stress path slightly to the left (Fig. 4.47).

4.6.3 Slope of Virgin Compression Curve

The effect of the slope of the virgin compression curve a ± 25% was investigated. The parameters shown in Table 4.19 were calculated; other parameters are the same as in Tables 4.8 and 4.9.

Table 4.19
Cap parameters for a ± 25%.

±a	a	W	R
-25%	0.0582	0.126	6.55
0%	0.0776	0.180	6.00
+25%	0.0970	0.232	5.67

Fig. 4.48 show that there is little effect on the stress-strain or pore pressure response. For both curves an increase in the a-value (steeper slope of virgin consolidation curve) results in slightly steeper slopes. The maximum $(\sigma_1-\sigma_3)/\sigma'_{vo}$ was increased slightly by a lower a-value but the pore pressure at large strain was slightly reduced. The influence on the effective stress path was too small to plot.

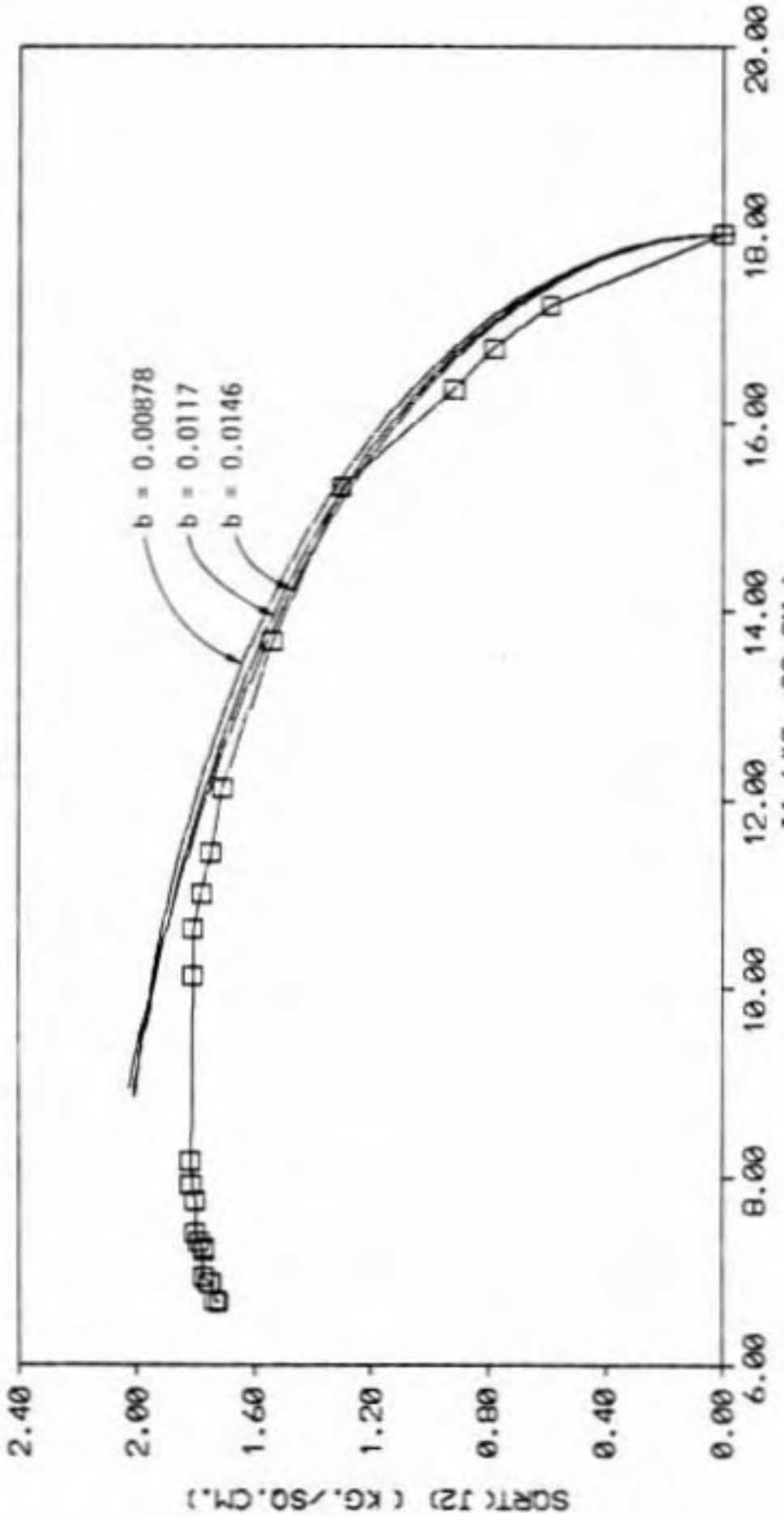

Figure 4.47 Effect of b-value on calculated effective stress path.

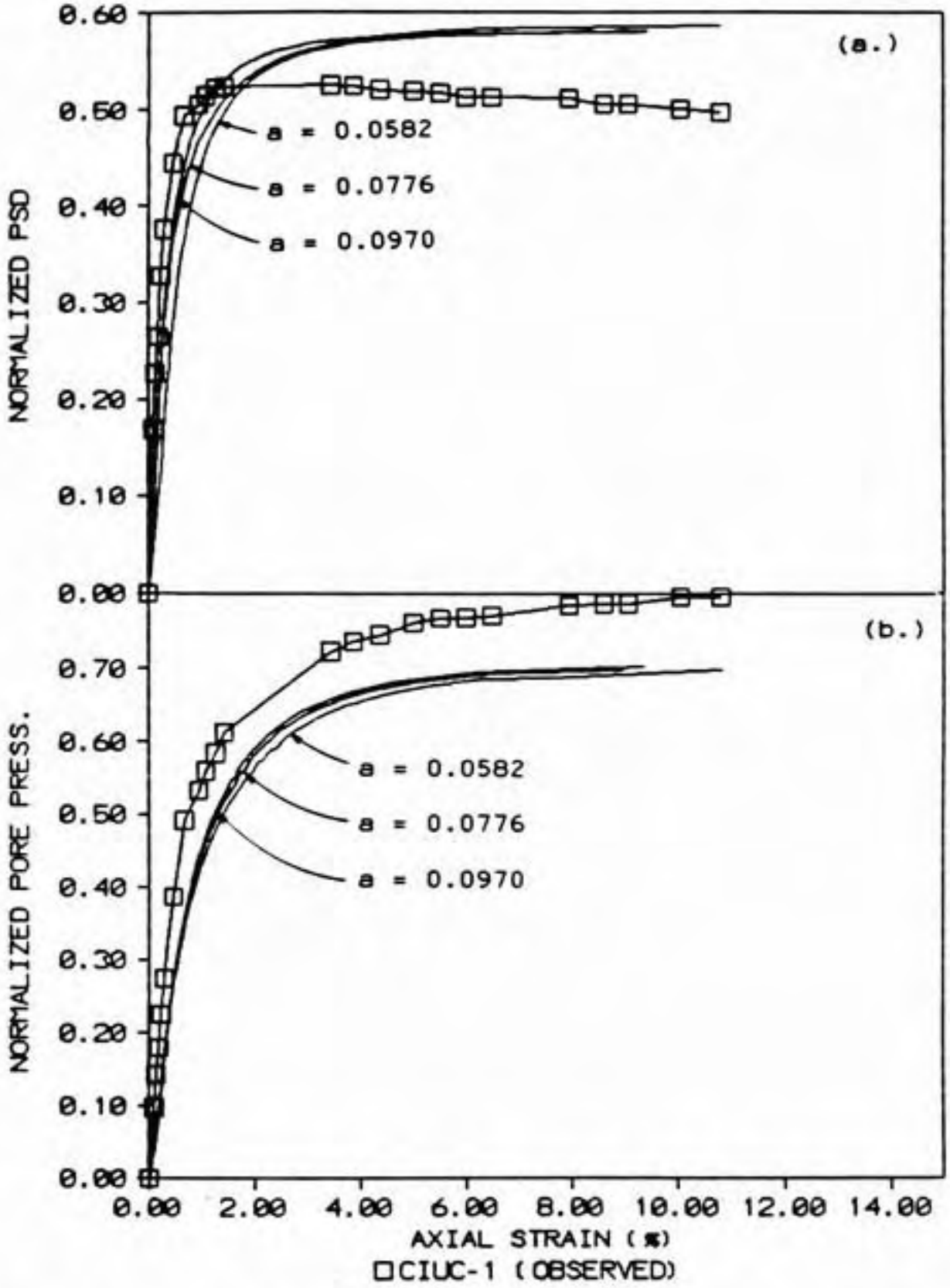

Figure 4.48 Effect of a-value on calculated (a) stress-strain and (b) pore pressure response.

4.6.4 Effective Stress Friction Angle

The influence of varying the effective stress friction angle ϕ' was examined. The parameters corresponding to $\tan\phi' \pm 10\%$ are shown in Table 4.20; other parameters are given in Tables 4.8 and 4.9.

Table 4.20
Cap parameters for $\tan\phi' \pm 10\%$.

$\tan\phi'$	ϕ'	α	R
-10%	27.0	0.206	5.34
0%	29.5	0.227	6.00
+10%	31.9	0.247	6.48

Raising the friction angle results in a slightly flatter stress strain curve (Fig. 4.49a), causes higher pore pressures at failure (Fig. 4.49b), and shifts the effective stress path to the left (Fig. 4.50). This is because higher ϕ' yields a larger R which increases the shear and volumetric components of plastic strain. There is no effect on $(\sigma_1-\sigma_3)/\sigma'_{vo}$ at failure (Fig. 4.49a) since s_u/σ'_{vo} was unchanged.

4.6.5 Undrained Shear Strength Ratio

Varying $s_u/\sigma'_{vo} \pm 10\%$ results in the cap parameters shown in Table 4.21; other parameters are as shown in Tables 4.8 and 4.9.

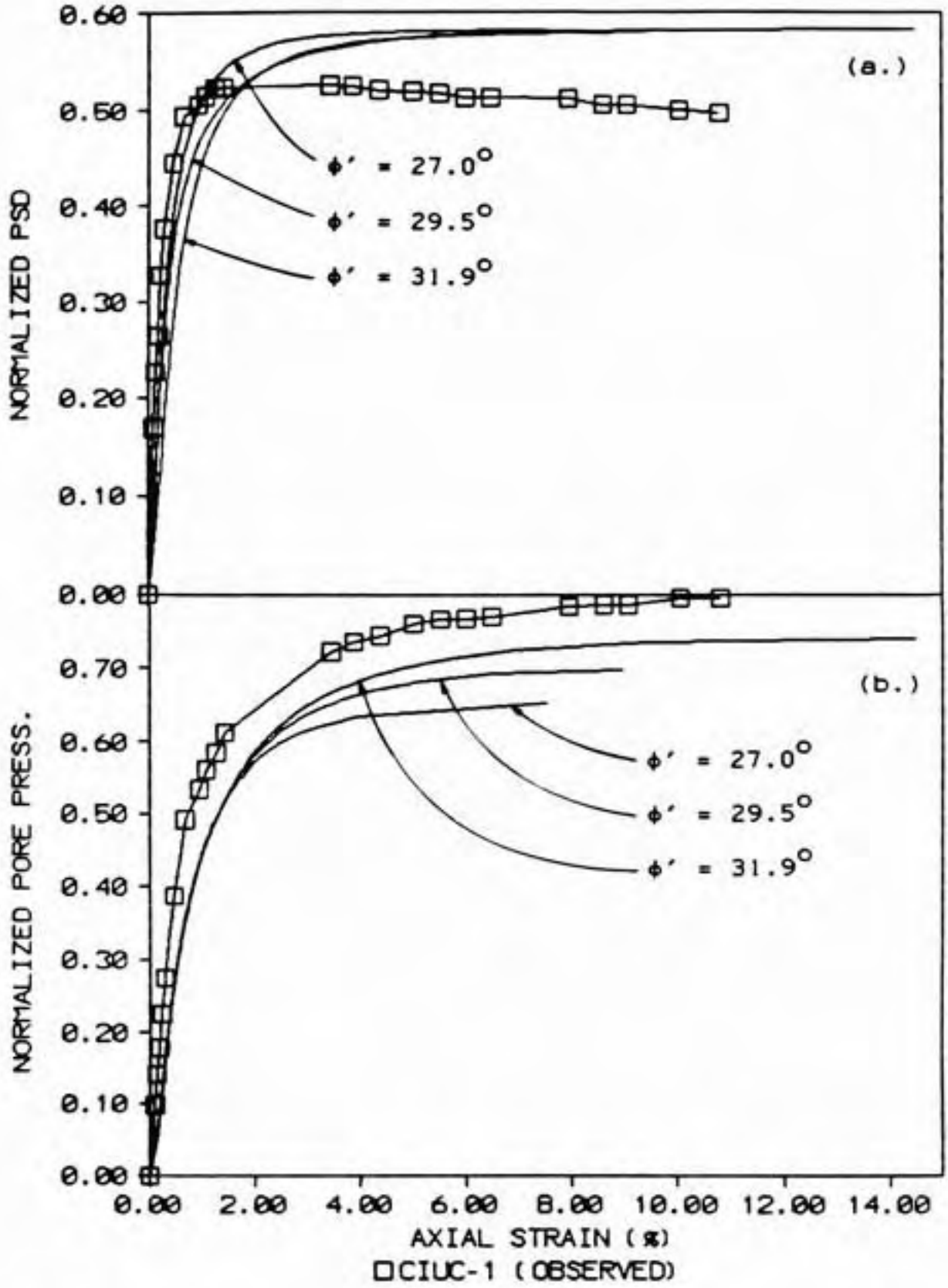

Figure 4.49 Effect of ϕ' on calculated (a) stress-strain and (b) pore pressure response.

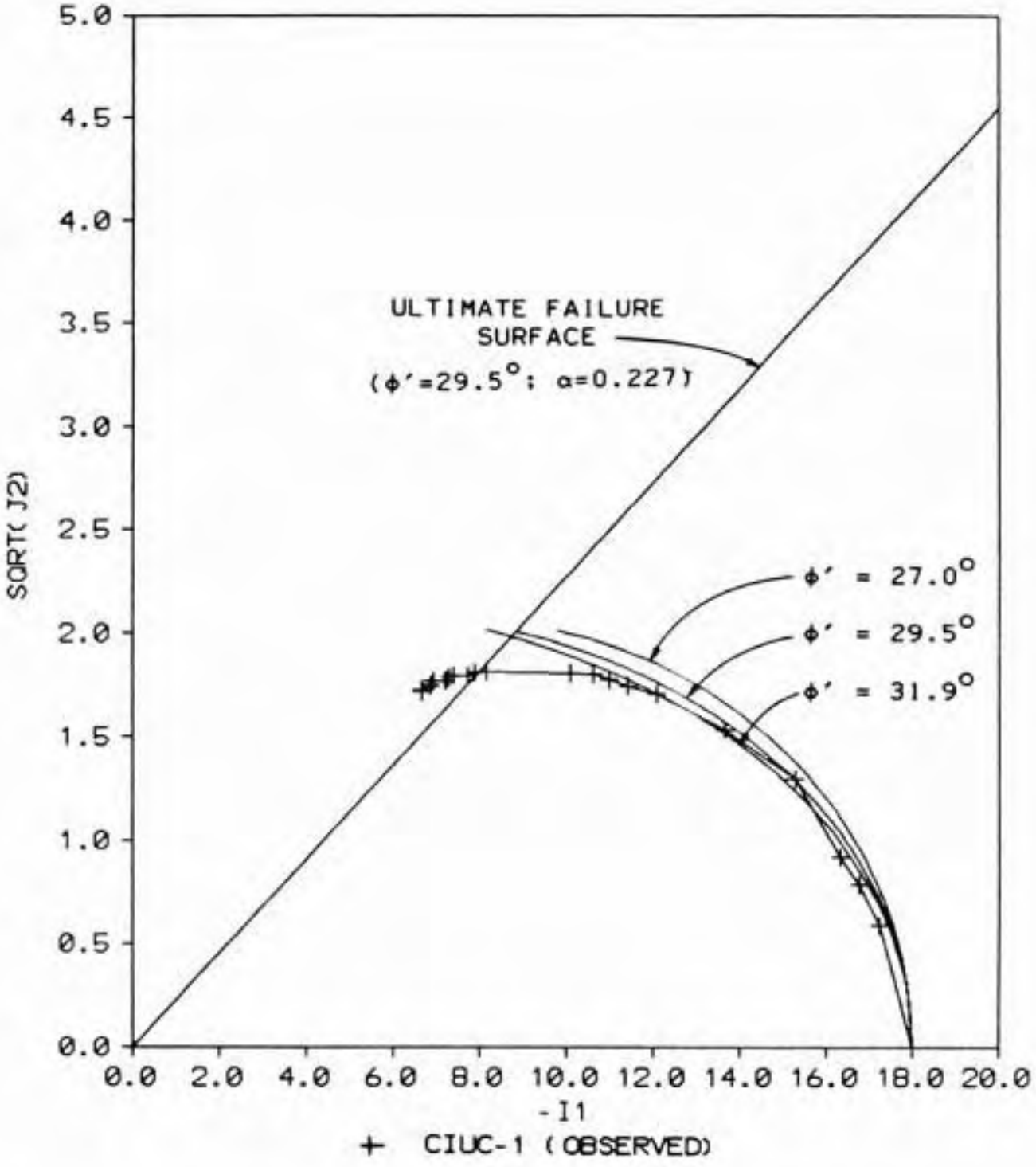

Figure 4.50 Effect of φ' on calculated effective stress path.

Table 4.21
Cap parameters for s_u/σ'_{vo} ± 10%.

$\pm s_u/\sigma'_{vo}$	s_u/σ'_{vo}	R
-10%	0.257	7.35
0%	0.285	6.00
+10%	0.314	4.89

Higher s_u/σ'_{vo} result in smaller R and steeper stress-strain curves with higher $(\sigma_1-\sigma_3)/\sigma'_{vo}$ at failure as shown in Fig. 4.51a. A value of s_u/σ'_{vo} = 0.257 provides the best match to the observed value at failure for test CIUC-1 which was 0.263 (Table 4.10) although the average for all CIUC tests was 0.286. The pore pressure response is slightly steeper for higher s_u/σ'_{vo} but the pore pressure at large strains is somewhat lower (Fig. 4.51b). Increasing s_u/σ'_{vo} shifts the effective stress path significantly to the right (Fig. 4.52).

4.6.6 Pore Pressure Response Factor

The influence of the pore pressure response factor B on the calculated response was examined. The B-value calculated for this soil using Eqs. 3.47 and 3.48 is about 100 but Naylor, et al. (1983) recommends B = 10 to minimize numerical problems. The calculated response for B = 1, 5, 10, and 100 is shown in Figs. 4.53 and 4.54. Lower B result in lower pore pressures, higher $(\sigma_1-\sigma_3)/\sigma'_{vo}$ at failure,

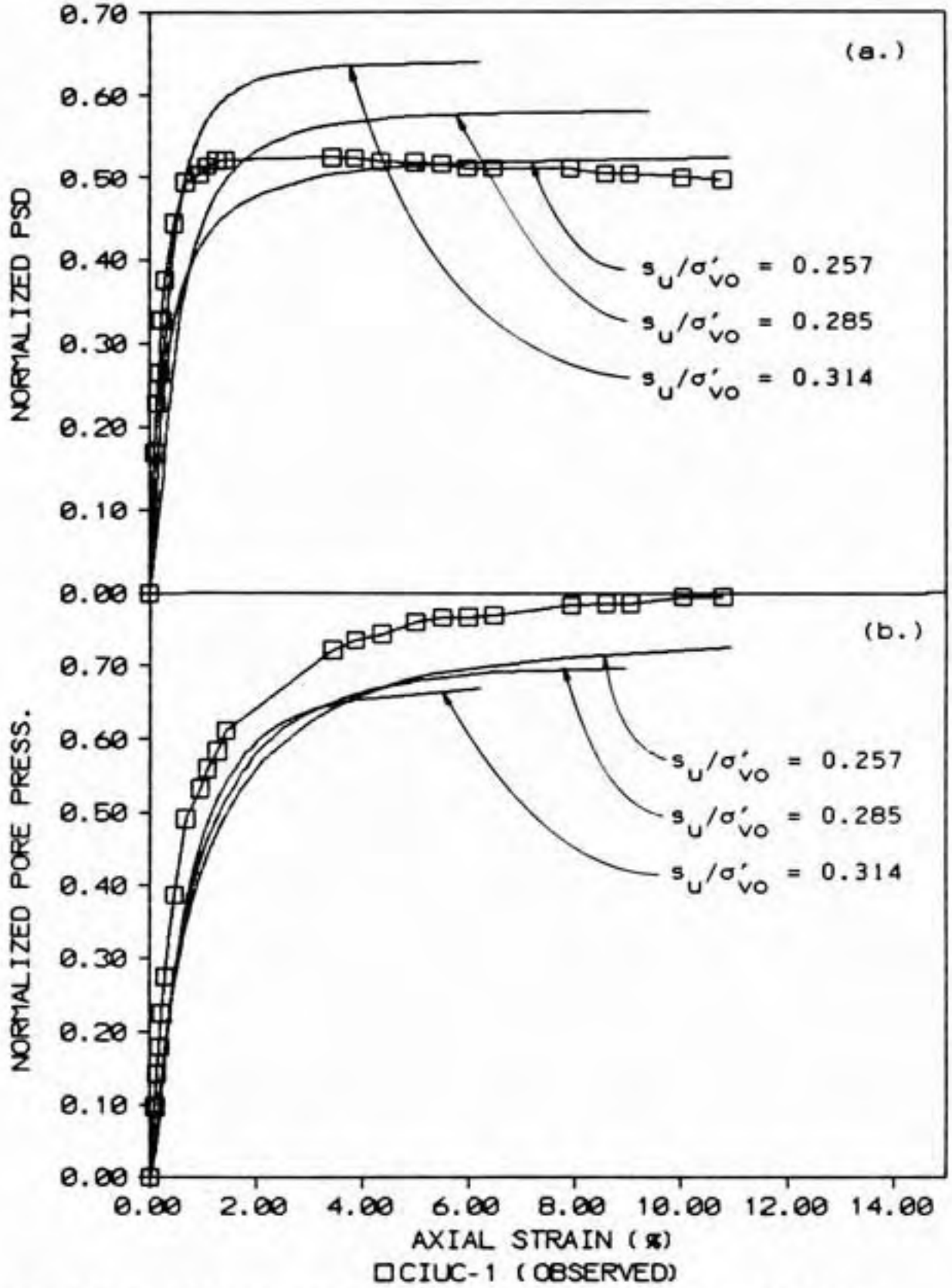

Figure 4.51 Effect of s_u/σ'_{vo} on calculated (a) stress-strain and (b) pore pressure response.

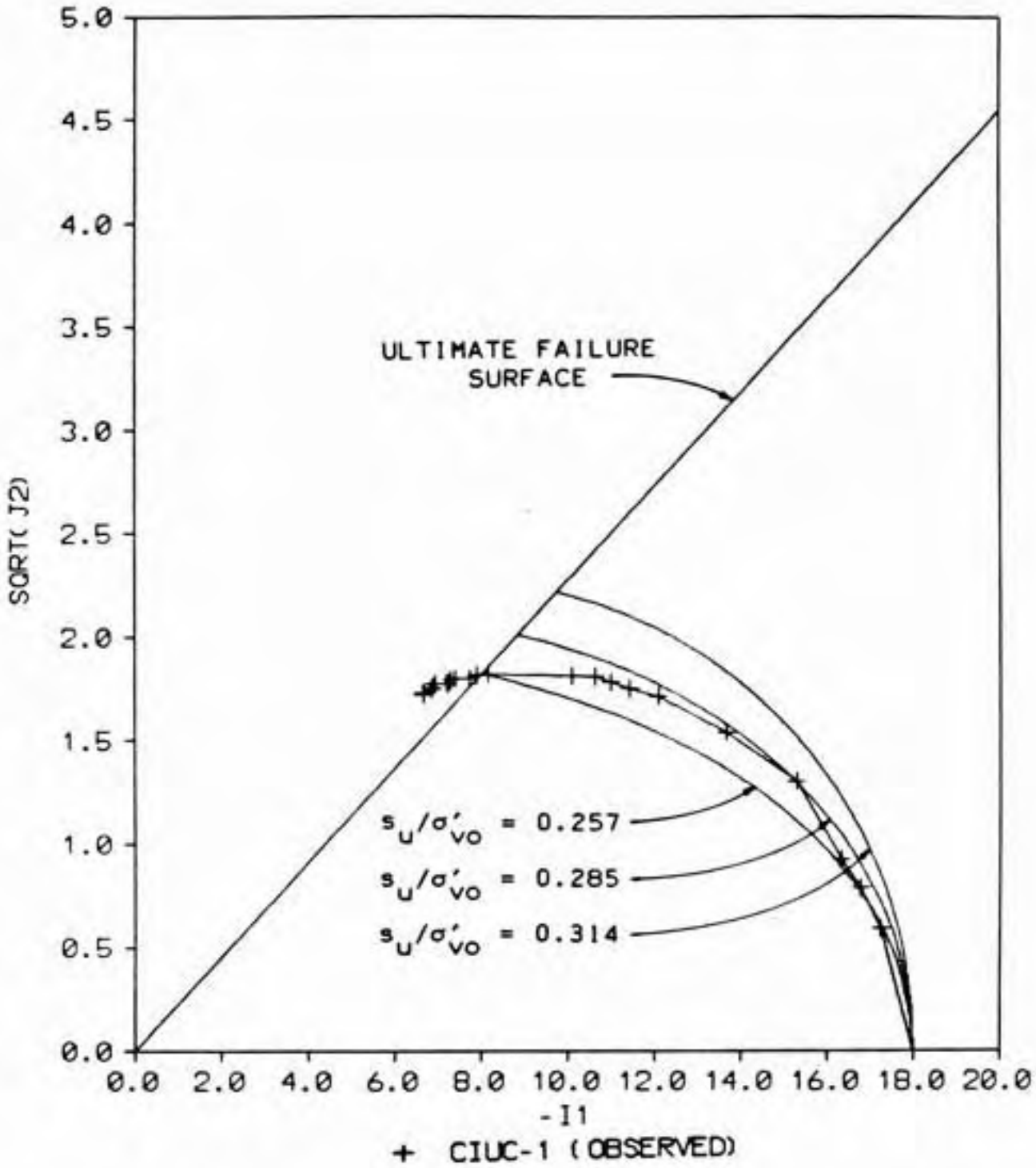

Figure 4.52 Effect of s_u/σ'_{vo} on calculated effective stress path.

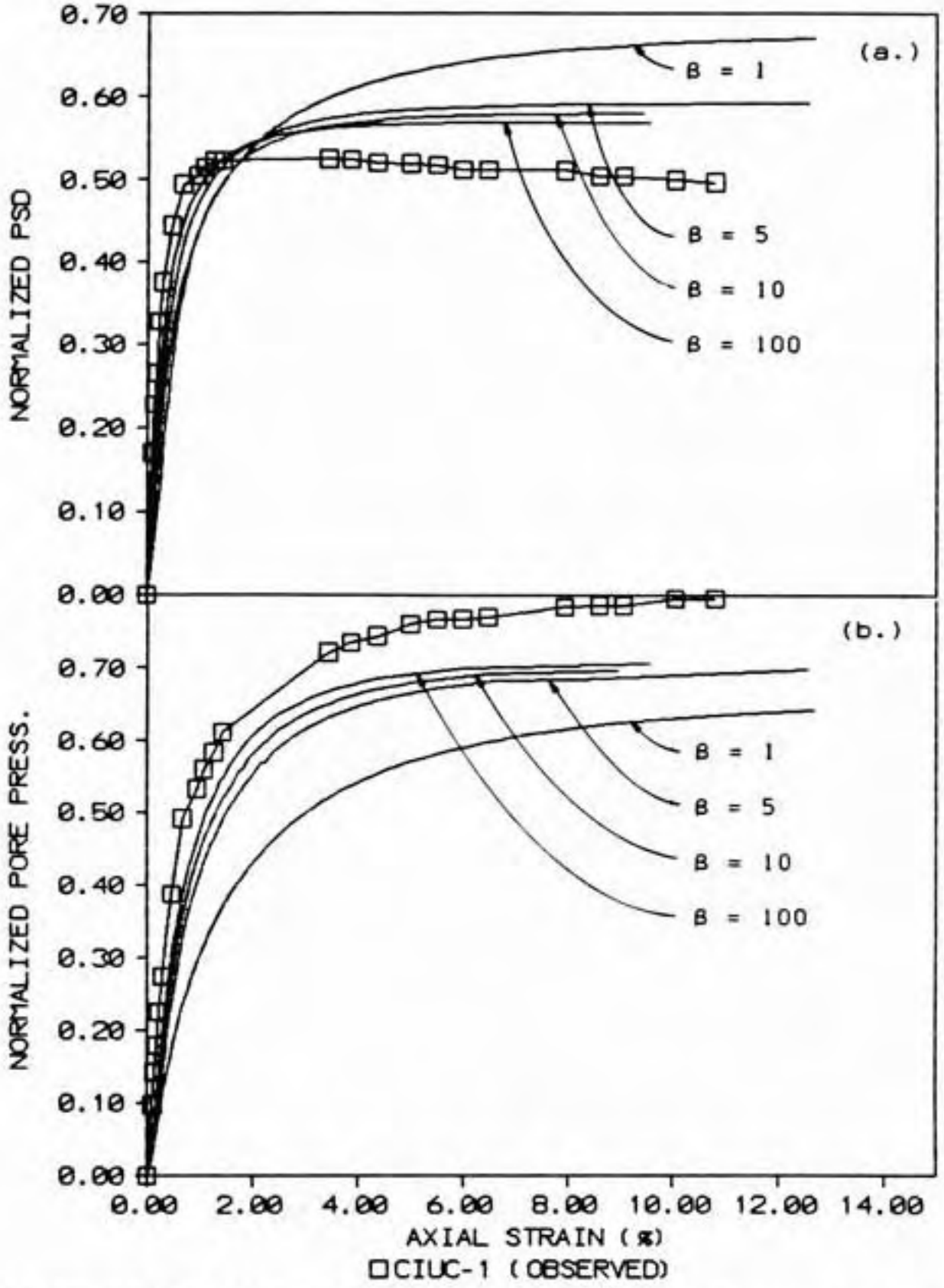

Figure 4.53 Effect of B on calculated (a) stress-strain and (b) pore pressure response.

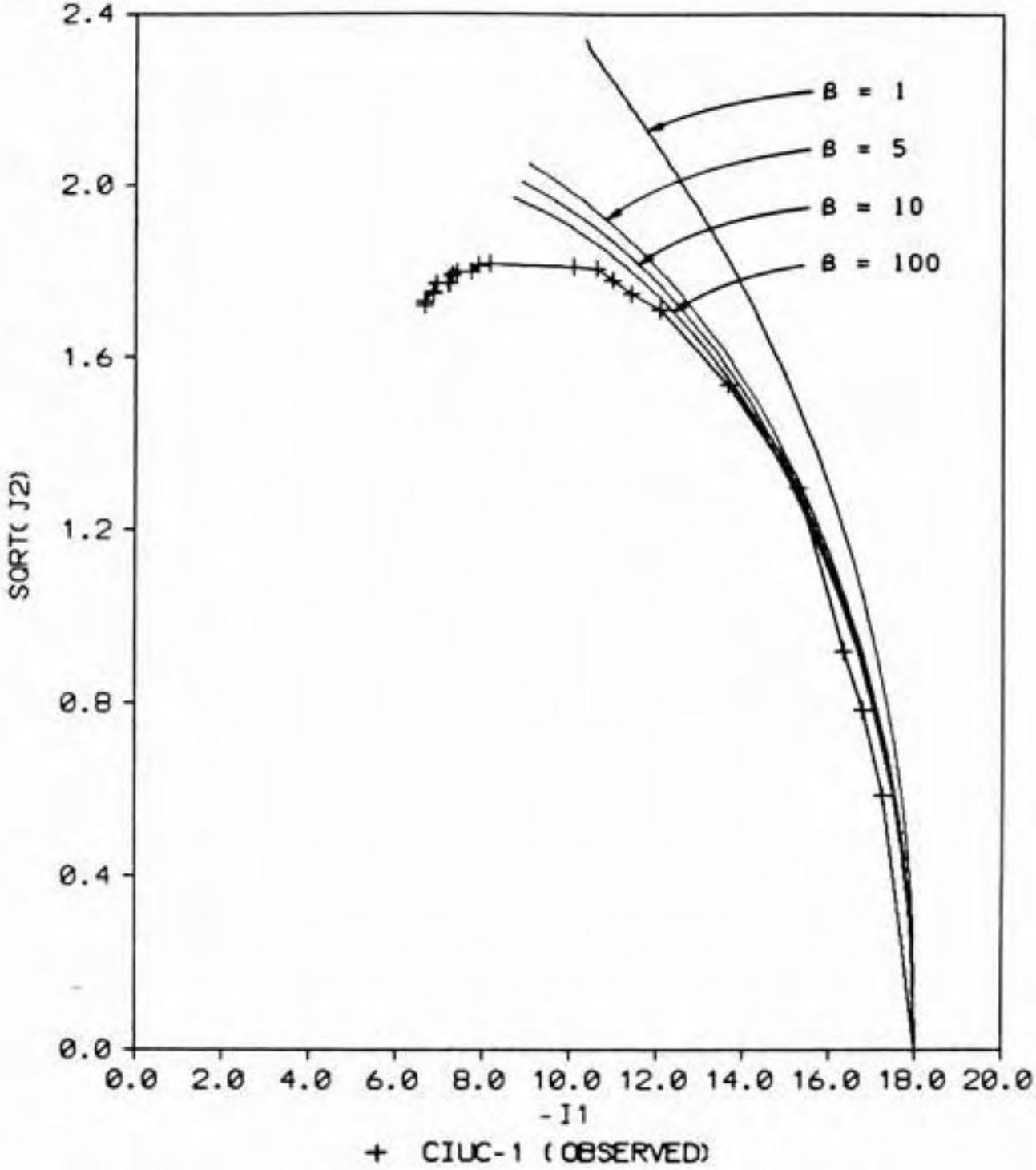

Figure 4.54 Effect of B on calculated effective stress path.

and shifts the effective stress path to the right; however, there is little difference between β = 10 and 100. No numerical problems were encountered with β = 100 but if necessary β = 10 can be used with only a small error.

4.6.7 Summary

The value of s_u/σ'_{vo} had the largest effect on the $(\sigma_1-\sigma_3)/\sigma'_{vo}$ at failure and the effective stress path. Pore pressure at large strain was most influenced by ϕ'. The initial slopes of the $(\sigma_1-\sigma_3)/\sigma'_{vo}$ and $\Delta u/\sigma'_{vo}$ versus axial strain curves were most affected by ν' and b. The effect of a was small. The influence of increasing each of the input soil properties while holding the other properties constant is summarized in Table 4.22.

Table 4.22
Summary of effect of increasing input soil properties.

Input soil property increased	Effect on $(\sigma_1-\sigma_3)/\sigma'_{vo}$ slope	$(\sigma_1-\sigma_3)/\sigma'_{vo}$ at large strain	Effect on $\Delta u/\sigma'_{vo}$ slope	$\Delta u/\sigma'_{vo}$ at large strain	shifts effective stress path
ν'	flatter	none	flatter	none	v. small
b	flatter	none	flatter	lower	right
a	steeper	lower	steeper	higher	v. small
ϕ'	flatter	none	none	higher	left
s_u/σ'_{vo}	steeper	higher	steeper	lower	right
β	steeper	lower	steeper	higher	left

This table can be used for guidance when adjusting the input soil properties to obtain a better fit between observed and calculated behavior. For test CIUC-1 a lower b, higher s_u/σ'_{vo}, and lower ν' would result in a much better fit to the observed data.

4.7 SUMMARY

The main findings of this chapter are summarized below.

1. A straight forward procedure to determine the cap parameters for normally consolidated soils was developed. The main input soil properties are the compressibilities in virgin loading and unloading/reloading, the effective Mohr-Coulomb shear strength parameters (ϕ' and c'), and the undrained shear strength ratio s_u/σ'_{vo}. Solutions are given in graphical form and equations suitable for hand calculation. Worked examples illustrate the procedure. In addition, a procedure was presented for overconsolidated soils to determine the initial position of the cap the yields the correct undrained shear strength.

2. The procedure was used to determine the cap parameters for Boston Blue Clay using results from hydrostatic and K_o consolidated triaxial and plane strain tests. These parameters were then used in a computer program called CAP to calculate stress-strain curves, pore pressure response,

and effective stress paths. Comparisons were made to observed test results. In general there was excellent agreement except for a large discrepancy for pore pressures and effective stress paths in tests that underwent reversal of principal stress during shearing and tests on overconsolidated samples. The discrepancy is at least partially because this implementation of the cap model does not allow plastic volumetric strain for stress changes within the region bounded by the cap and ultimate failure surfaces.

3. The model incorrectly predicts pore pressures for overconsolidated soils and for soils that experience reversal of principal stresses. It does not represent strain softening or pore pressure increase after the peak strength is reached.

4. Cap parameters were calculated using CIU triaxial test results for 52 clayey soils. The summary can be used for guidance when selecting parameters for preliminary designs. The aspect ratio R ranged from 0.58 to 19.5 with an average of about 5. It tended to decrease with increasing s_u/σ'_{vc}. Compressibility and ϕ' had a much smaller influence. Fair to poor correlation of C_c, C_r, and $(a-b)(1+e_o)$ with liquid limit was found. The ratio $(a-b)/b$ does not correlate with liquid limit and should be determined directly from consolidation test results.

5. The equations developed indicate that R is independent of the initial consolidation pressure but varies with K_o. R was found to be independent of σ'_{vo} for a series of triaxial tests on Boston Blue Clay.

6. Cap parameters were calculated for 15 nonhydrostatically consolidated triaxial and plane strain tests. For 10 soils they were compared to parameters based on specimens with hydrostatic consolidation. The nonhydrostatically consolidated R were both higher and lower than the corresponding hydrostatic values. For Boston Blue Clay the difference was nearly an order of magnitude. There was little improvement when the parameters were calculated using hydrostatically consolidated shear strength parameters with the nonhydrostatic K_o.

7. Cap parameters calculated with CIU strength data and the normally consolidated K_o were used to model CK_oUPSA tests on Boston Blue Clay. There was poor agreement with observed test behavior. This suggests that proper predictions for cases with initial nonhydrostatic consolidation may require cap parameters calculated using strength data from nonhydrostatically consolidated tests.

8. A parametric study was made of the effect of the input soil properties on calculated CIU triaxial sample

behavior. The results can be used for guidance if it is necessary to adjust the input parameters to obtain better agreement between predicted and observed behavior. s_u/σ'_{vo} was found to have the largest influence on predicted behavior.

CHAPTER 5

FINITE ELEMENT STUDY OF REINFORCED EMBANKMENT BEHAVIOR

5.1 INTRODUCTION

A comparative study between reinforced and unreinforced embankment behavior was made using a finite element analysis technique with a cap type soil behavior model. An embankment composed of granular fill was reinforced by a single layer of reinforcement placed at its base. A typical embankment construction sequence was simulated. The foundation soils were soft and no drainage was allowed during construction. The purpose of the study was to investigate the effect of reinforcement on deformations and stresses and to identify which aspects of embankment geometry and foundation properties had the greatest effect on behavior. A study of reinforcement applied to embankment widening is the subject of Chapter 6.

The chapter is organized as follows. First, the finite element analysis procedure is discussed. Then the cases analyzed by McCarron (1985) in an earlier study are summarized and reassessed in light of the improved techniques to

determine the input parameters for the cap model presented in Chapter 4. Next the embankment geometries and foundation properties used in the present study are presented followed by results of the finite element analysis. Then the results are compared to finite element analyses of reinforced embankments available in the literature. Finally, the findings of this study are summarized. The results are compared to limiting equilibrium methods in Chapter 7.

5.2 FINITE ELEMENT ANALYSIS PROCEDURE

The finite element program used in this study is based on a general purpose FE program named NFAP which was originally developed by Chang (1980). The cap model described in Chapter 3 was implemented by McCarron (1985) and McCarron and Chen (1986a, 1986b). Segments of the program that are unnecessary for analysis of plane strain problems were eliminated by Humphrey (1985b). This reduced version is named PS-NFAP. The solution algorithm is outlined in McCarron (1985) and McCarron and Chen (1986a) and input preparation is described in Humphrey and Holtz (1986a). A mesh generator was developed and documented by McCarron and Chen (1985). Its operation is also documented in Humphrey and Holtz (1986a).

The program performs an incremental load-displacement analysis. After each increment of load is applied the

displacement field is modified using an iterative procedure until an equilibrium configuration is reached. Convergence was based on the difference between two successive displacement norms.

$$\frac{\|U_n^{i+1}\| - \|U_n^{i}\|}{\|U_n^{i}\|} \leq \text{Tolerance} \qquad (5.1)$$

where

$$\text{Norm } U = \|U\| = (\{U\}^T\{U\})^{1/2} \qquad (5.2)$$

and {U} is the matrix of nodal displacements, T indicates transpose, n is load increment number, and i is iteration number. McCarron (1985) found that a tolerance of 1% produced an acceptable solution but notes that this is only an indirect method of minimizing residual or unbalanced forces which exist after a load increment is applied. The problem was analyzed with an updated Lagrangian formulation in which the equilibrium equations were written in terms of the most recent equilibrium configuration. Geometric (large displacement) and material nonlinearities can be represented (McCarron, 1985).

5.2.1 Modeling Foundation Soils

The foundation soils were modeled with two dimensional 4 to 8 node isoparametric plane strain elements using second order Gauss integration. Soil behavior was represented with

the strain hardening cap model described in Chapter 3. Cap parameters for the foundation soils were chosen using the procedure given in Chapter 4.

5.2.2 Modeling Embankment Fill

The embankment fill was also modeled with two dimensional 4 to 8 node plane strain isoparametric elements using second order Gauss integration. Stress-strain behavior was taken to be elastic-plastic with an ultimate failure surface of the Drucker-Prager type. For soils that become normally consolidated this ignores plastic strains which occur prior to the stress state reaching the ultimate failure surface. Use of the cap model would require knowledge of the preconsolidation pressure in the compacted fill which is generally unknown. Finite element studies by Rowe (1982) found that fill stiffness had only a secondary effect on reinforced embankment behavior so it is felt that this procedure is adequate.

5.2.3 Modeling Reinforcement

The reinforcement was modeled with 2 or 3 node one-dimensional truss elements which supported only axial tensile load. Geometric and material nonlinearity were represented. No slip was allowed to occur at the fill-reinforcement or reinforcement-foundation soil interfaces. This

assumption is adequate provided: (1) the shear stresses developed at the interface are less than the interface strength; or (2) the soil-reinforcement interface shear strength equals or exceeds the soil-soil shear strength. The latter case was assumed for this study. It implies that slip will occur in the adjacent soil when its shear strength is exceeded rather than at the interface. This restricts interface movement.

5.2.4 Incremental Construction

Construction of the embankment was simulated using an incremental loading technique (McCarron, 1985). The embankment was divided into horizontal layers each represented by a row of elements with zero initial stress. During each increment the gravity stresses in the next layer were increased from zero to their full value in one or more subincrements. Additional layers are applied until failure occurs.

There is a trade-off between layer thickness and the number of subincrements. Thicker layers require more subincrements to achieve a stable solution (Naylor, et al., 1981), so there is little savings in solution time by using excessively thick layers. Thicker layers also result in a stiffer embankment response. It is not necessary to represent each construction lift (typically 6 to 10 inches thick)

by a layer of elements. Provided the thickness of the layers is chosen so that 4 to 5 layers are applied prior to embankment failure, computed behavior is approximately the same as obtained with thinner layers. This recommendation should be reexamined for layers that are many times thicker than the construction lift.

5.2.5 Effect of Submergence

Large settlements are often experienced by embankments constructed on soft ground. A ground water table at or near the ground surface is often associated with such foundation conditions. Thus, a significant portion of the fill may settle below the water table. PS-NFAP accounts for buoyancy forces by using the buoyant unit weight to evaluate the gravity load for integration points that settle below the ground water surface (McCarron, 1985). Submergence was assumed to have no effect on the fill's effective strength parameters.

5.2.6 Matching the Mohr-Coulomb and Drucker-Prager Criterion

The Drucker-Prager parameters (α and κ) can be evaluated directly from plane strain tests consolidated to initial conditions corresponding to in situ stresses. However, for most problems α and κ must be evaluated from Mohr-Coulomb parameters (ϕ' and c') obtained from triaxial tests.

The circular cross-section of the Drucker-Prager criterion are matched to the hexagonal shaped Mohr-Coulomb criterion for selected stress systems using the equations in Section 4.2.1.

Conditions in the fill satisfy the assumptions used to develop the plane strain matching equations (Eqs. 4.5 and 4.6) namely: (1) stresses correspond to plane strain conditions, and (2) increments of plastic strain are normal to the Drucker-Prager surface. Analyses with PS-NFAP confirmed that the intermediate principal effective stress at failure did correspond to plane strain conditions. Hence, Eqs. 4.5. and 4.6 were used for the fill material.

Conditions in the foundation soils at failure do not satisfy the assumptions of Eqs. 4.5 and 4.6. Even though the overall mode of deformation is plane strain, analyses with PS-NFAP showed that the stresses at failure did not correspond to plane strain conditions. Furthermore, it is recalled that the stress state at failure is at the intersection between the cap and ultimate failure surfaces and the plastic strain increments are normal to the cap not the Drucker-Prager surface (Fig. 3.2c).

An alternate procedure was developed for the foundation soils. A value of η (Eq. 4.7) was assumed and α and κ were

computed using Eqs. 4.8 and 4.9. These were used as input to PS-NFAP and the average calculated η at failure were compared to the assumed value. If necessary a revised η was assumed and the process repeated. For normally consolidated and lightly overconsolidated soils, the comparison was made at the point where the state of stress reached the intersection of the cap and Drucker-Prager surfaces. For more heavily overconsolidated soils the stress path intersects the Drucker-Prager surface before reaching the cap. This intersection is the transition from small elastic strains to much larger elastic plus plastic strains. It was felt to be most important to model this point correctly so the calculated and assumed η were compared there. For all soils the resulting α and κ are between the triaxial compression and triaxial extension values. Matching $J_{2f}^{1/2}/\sigma'_{vo}$ and s_u/σ'_{vo} also is a function of η. They were matched using Eq. 4.42.

5.2.7 Definition of Failure

Failure or collapse load was defined as the point at which some of the nodal displacements for an increment of load became so large that the solution was unable to converge or the point at which the system of equations became nonpositive definite (McCarron, 1985) which means the strain energy is less than zero (Cook, 1974). This point can only be determined approximately due to the size of the loading

increments and numerical details of the solution technique. Direct comparisons between calculated collapse heights for different cases should therefore be made with caution. It is better to examine the load-deformation behavior prior to failure when comparing different cases.

As a measure of the benefit provided by reinforcement the relative increase in surcharge made possible by the reinforcement is defined. Consider the horizontal displacement at the embankment toe versus surcharge curves for a pair of companion reinforced and unreinforced embankments as shown on Fig. 5.1. Each has a corresponding horizontal displacement at the toe at failure (D_r, D_u). The percent increase in surcharge applied at the centerline (or equivalently the embankment height) is compared at the smaller of the two displacements at failure. For the example shown on Fig. 5.1 the reinforced embankment failed at a smaller displacement. At this displacement, the surcharge of the unreinforced embankment L_u is 0.86 ksf and the increase in surcharge made possible by the reinforcement ΔL is 0.19 ksf. The surcharge for the reinforced embankment is $\Delta L/L_u$ = 22% greater than the unreinforced embankment, i.e., the relative increase is 22%.

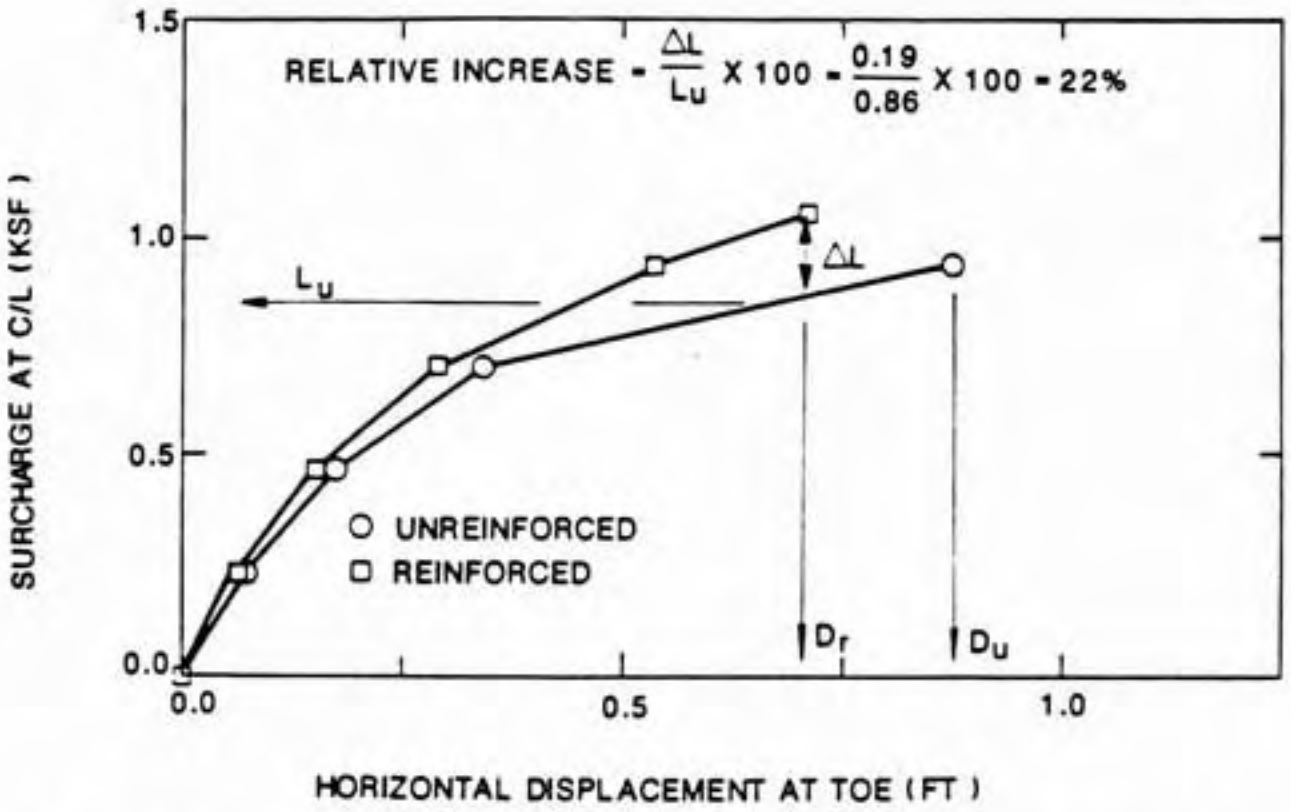

Figure 5.1 Definition of relative increase in surcharge made possible by reinforcement.

5.2.8 Limitations of Cap Model

The cap model has some limitations which impact upon the problems analyzed in this study. One is that pore pressure changes due to reversal of principal stresses in initially normally consolidated soils are not modeled as discussed in Section 4.2.4.4. Because of this limitation, it was necessary to assume that the undrained shear strength ratio s_u/σ'_{vo} was the same regardless of stress path, and low values of s_u/σ'_{vo} typically observed for extension loading could not be modeled. Reversal of principal stresses occurs near the toe of the embankment. In this area the computed shear strengths are overestimated, pore pressures underestimated, and deformations underestimated (Almeida, et al., 1986). It is felt that this would underestimate the deformations and force in the reinforcement and the relative increase in surcharge made possible by the reinforcement. However, the height at failure may be overestimated for both reinforced and unreinforced embankments.

The model does not predict the reduction in undrained strength or increase in pore water pressure that occurs after the peak strength is reached in strain softening soil. Again this would overestimate the shear strength and underestimate the pore pressures and deformations. The reinforcing force at a given surcharge and relative increase in

surcharge due to reinforcement would be underestimated, but the height at failure would be overestimated.

Another limitation is the ability to model behavior of overconsolidated soils as discussed in Section 4.2.4.3. Eq. 4.67 was used to establish the initial position of the cap. This leads to correct prediction of undrained strength at failure and fair agreement between predicted and observed strains (Section 4.4.4). However, pore pressures are not predicted correctly and plastic strains which many overconsolidated soils experience for stress changes in the elastic region bounded by the cap and ultimate failure surfaces are not accounted for. Also, strain softening after failure can not be modeled. It is speculated that this would lead to underestimation of deformations and force in the reinforcement but overestimation of the failure height.

5.3 CASES ANALYZED

The behavior of reinforced and unreinforced embankments was compared to evaluate the influence of reinforcement. The effect of embankment geometry and soil properties on reinforced embankment behavior was examined. The study, initiated by McCarron (1985), was continued in the present work.

5.3.1 Cases Analyzed by McCarron

McCarron (1985) analyzed embankments with base widths of 90, 120, and 180 ft and 2h:1v side slopes. Fill material was granular with properties similar to those used by Rowe, et al. (1984b). The effective friction angle was $\phi' = 32^{\circ}$ which corresponds to $\alpha = 0.17$ for plane strain conditions (Eq. 4.5). A small cohesion intercept of $\kappa = 0.01$ ksf was used. The following equation was used for the bulk modulus

$$K = K_{max}[1 - K_1 \exp(K_2 I_1')] \qquad (5.3)$$

The fitting parameters were based on nonlinear stress strain parameters given by Rowe, et al. (1984b): $K_{max} = 600$ ksf, $K_1 = 0.95$, and $K_2 = 0.02$. Eq. 5.3 is different than the equation used in the present study and is less convenient to fit to commonly available soil parameters. Poisson's ratio was $\nu' = 0.35$ and Eqs. 4.18 and 4.22 were used to relate the shear and bulk moduli. A layer thickness of 7.5 ft was used for incremental construction which was about the same as the calculated failure heights. Consequently, incremental construction was not modeled realistically by McCarron (1985).

Three sets of foundation properties were considered. The first, designated type I, was intended to have properties representative of Indiana Glacial clay with saturated unit weight $\gamma_{sat} = 115$ pcf, $C_r = 0.01$-0.07, $C_c = 0.08$-0.37, $\phi' = 28^{\circ}$, and $s_u/\sigma'_{vo} = 0.34$-0.36 (Wu, 1958; IDOH, 1985a,

1985b; D'Appolonia, 1964a, 1964b). Poisson's ratio was assumed to be 0.3. The Drucker-Prager and Mohr-Coulomb criterion were matched for triaxial compression (Eq. 4.1) which overestimated α. The aspect ratio R was calculated with an approximate procedure and the resulting value was too high. Unfortunately the hardening parameters D and W were fit at stresses much greater than occurring in the cases analyzed. They actually correspond to C_c = 0.06 which is much less than the average of typical values given above. This resulted in underestimation of plastic strains. The foundation had a 7.5-ft thick dried crust with s_u = 0.25 ksf. K_o was assumed to be 1.0 in the crust and 0.47 in the normally consolidated soils underlying the crust. The cap parameters are summarized in Table 5.1.

The second set of soil properties, designated type II, was intended to represent a very soft clay with C_c = 1.5 and C_r = 0.2. Other soil properties were the same as for type I. The cap parameters, calculated using an approximate procedure, are summarized in Table 5.1. Again the hardening parameters D and W were fit at stresses much greater than occurring in the cases analyzed and actually correspond to C_c = 0.8. Also, the parameters for the bulk modulus (Eq. 5.3) were fit at stress levels that were too high and actually correspond to C_r = 0.08. The effect of both was to underestimate strains. A 7.5-ft thick dried crust with

Table 5.1
Cap parameters for foundation soils
used by McCarron (1985).

Parameter	Foundation Type I	Foundation Type II	Foundation Type III
K_{max}*	5000 ksf	5000 ksf	5000 ksf
K_1*	0.999	0.999	0.999
K_2*	0.007	0.004	0.004
G_1	0.46	0.46	0.46
G_2	0.0	0.0	0.0
R	2.0	2.0	2.0
W	0.29	1.0	1.0
D	0.012 ft^2/k	0.1 ft^2/k	0.1 ft^2/k
α	0.2	0.2	0.2
κ	0.01 ksf	0.01 ksf	0.01 ksf
γ_{sat}	115 pcf	115 pcf	102 pcf
s_u (crust)	0.25 ksf	0.25 ksf	0.13 ksf

* Used in Eq. 5.3

s_u = 0.25 ksf was assumed. The third set of parameters, designated type III, had the same properties and cap parameters as type II except that γ_{sat} = 102 pcf and the undrained shear strength of the crust was 0.13 ksf.

A single layer of reinforcement with a modulus of 60 k/ft (5000 lb/in.; 880 kN/m) located at the interface between the embankment and foundation was considered. This corresponds to a strong woven fabric or geogrid.

Only general conclusions can be drawn from McCarron's work for the following reasons: (1) C_c for all three foundations and C_r for types II and III were underestimated; (2) the Drucker-Prager and Mohr-Coulomb criterion were matched for triaxial compression, this overestimated the α-value; (3) the approximate procedure used to determine R yielded values that were too large; and (4) the layers used in the incremental construction were too thick. Nonetheless McCarron's work suggests that reinforcement was more effective for the more compressible foundation and weaker crust, and the influence of embankment width was small. McCarron (1985) also investigated the bearing capacity of the three foundation types by applying a uniform surface load of width B. There was reasonable agreement between failure loads calculated by the program and predicted by conventional bearing capacity theory.

5.3.2 Cases Analyzed in this Study

The influence of several factors on reinforced embankment behavior were studied. In addition, some of the cases examined by McCarron (1985) were reanalyzed because of the problems noted above. The influence of reinforcement was assessed by comparing behavior of reinforced and unreinforced embankments. A total of 15 combinations of embankment geometry and soil properties were considered. The effect of crust strength, pockets of weak soil in the crust, foundation compressibility, foundation thickness, embankment width, and embankment side slopes were studied.

Several embankment geometries and foundation depths were considered. An embankment with a 180-ft base width and 2h:1v side slopes on a 30-ft thick foundation was chosen as the standard embankment and was used as the basis for comparison with other cases. Analyses were made for embankments with 120 and 180-ft base widths and 2h:1v and 3h:1v side slopes. Foundation depths of 15, 30, and 60 ft were considered. The finite element meshes for each depth are shown in Figs. 5.2, 5.3, and 5.4. Similar meshes were used for the 120-ft base width and 3h:1v side slope embankments. For all analyses the water table was at the ground surface.

The fill material was granular with properties similar to those used by McCarron (1985). The Mohr-Coulomb friction

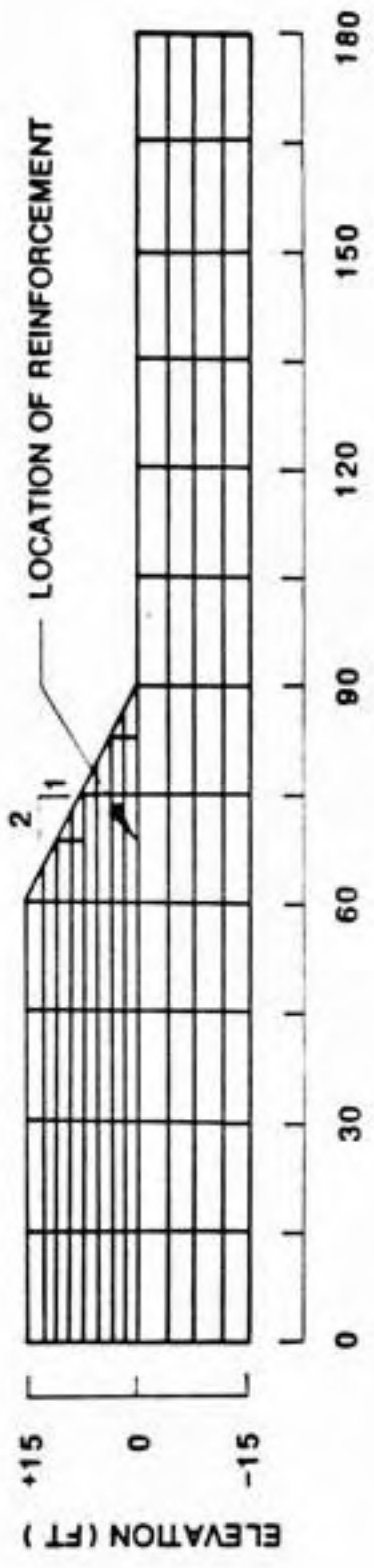

Figure 5.2 Finite element mesh for 15-ft thick foundation.

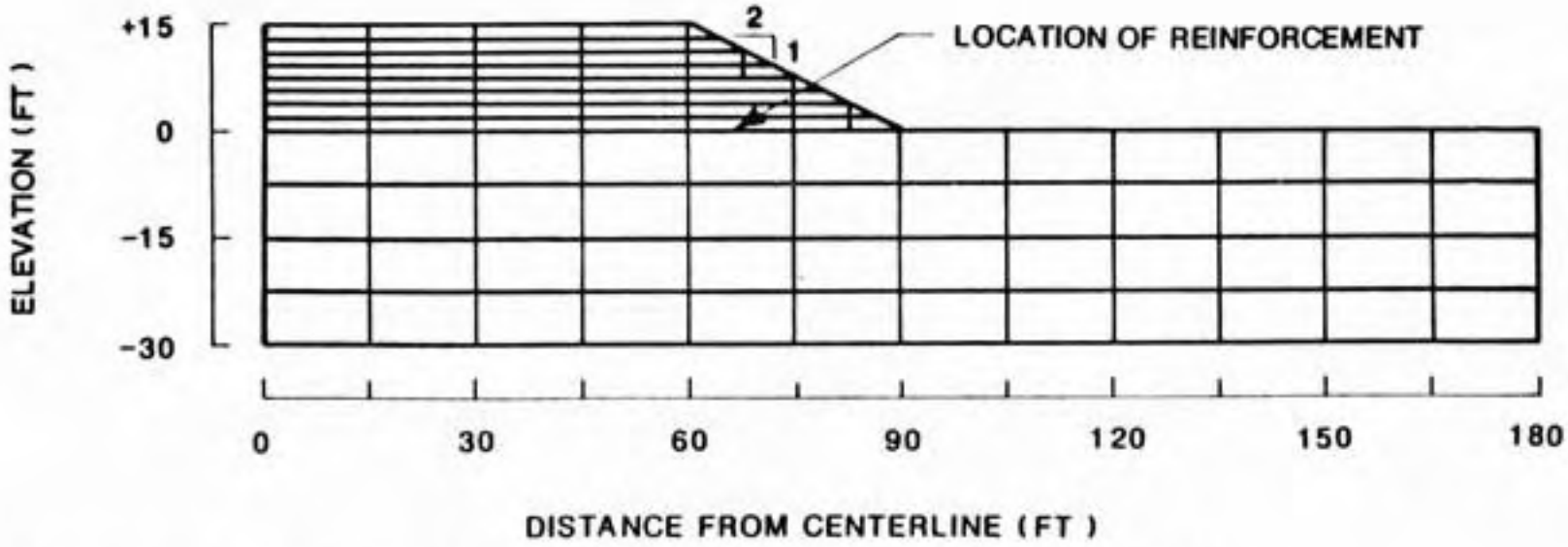

Figure 5.3 Finite element mesh for 30-ft thick foundation.

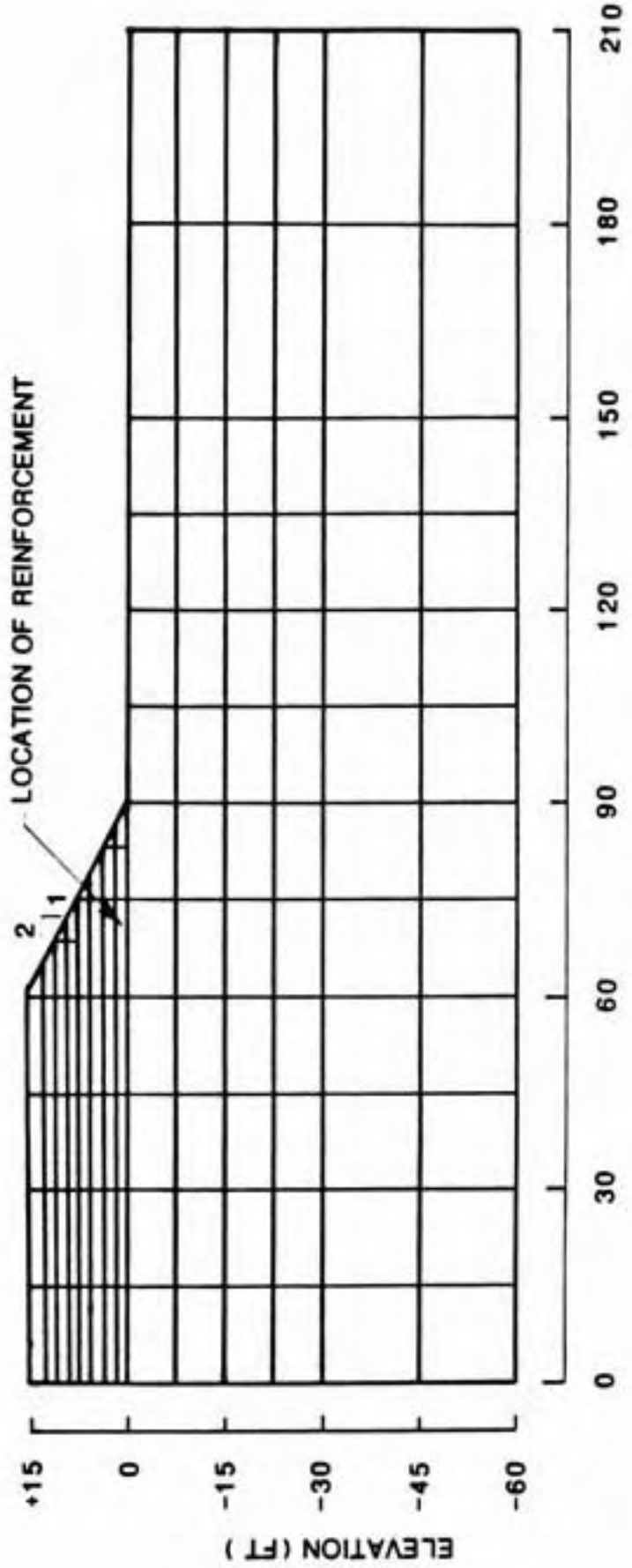

Figure 5.4 Finite element mesh for 60-ft thick foundation.

angle was 32° so α was 0.17 for plane strain conditions (Eq. 4.5). A small cohesion intercept of κ = 0.0001 ksf was used because analyses with κ = 0 experienced numerical difficulties under some circumstances. The bulk modulus fitting parameters were chosen by trial and error to match nonlinear stress strain parameters given by Rowe, et al. (1984b). K_1 = 190 and K_2 = 0.65 provided a reasonable fit. A_p = 2.116 ksf was used. The equation for the bulk modulus (Eq. 4.11) allows K to approach zero for small values of I_1'. This caused numerical difficulties during incremental embankment construction since the elements have zero initial stress and hence zero modulus. To avoid this difficulty a minimum modulus of 20 ksf, corresponding to an overburden pressure of a few ft of fill, was specified. Poisson's ratio was taken to be 0.35 resulting in G_1 = 0.33 and G_2 = 0.0 (Eq. 4.22). The unit weight of the fill was 125 pcf. The model parameters are summarized in Table 5.2.

A layer thickness of 1.875 ft was used to simulate embankment construction. This resulted in 2 to 6 layers being placed prior to embankment failure. Thinner layers were not possible with a reasonable size finite element mesh. A limited study with 7.5, 3.75, and 1.875-ft thick layers showed that thinner layers caused slightly greater horizontal displacements at the embankment toe, maximum force in the reinforcement, and extent of the plastic zone

Table 5.2
Model parameters for fill material.

α	=	0.17
κ	=	0.0001 ksf
K_1	=	190
K_2	=	0.65
K_{min}	=	20 ksf
A_p	=	2.116 ksf
G_1	=	0.33
G_2	=	0.0
γ	=	125 psf

in the foundation but a slightly lower height at failure. This is because thicker layers result in a stiffer embankment response. Similar results were found by Boutrup and Holtz (1982).

The input soil properties for the normally consolidated foundation soils are similar to those used by McCarron (1985) for Indiana Glacial clay. They are summarized in Table 5.3. The cap parameters were determined using the procedure given in Chapter 4 and are summarized in Table 5.4. A minimum bulk modulus of 1 ksf was assumed. The s_u/σ'_{vo} value of 0.32 is greater than the average value typically observed for embankment failures (Milligan and La Rochelle, 1984), however, a smaller value cannot be modeled due to the limitations discussed in Section 5.2.8. This value is near the minimum that satisfies the condition that $J_{2o}^{1/2}$ be less than $J_{2f}^{1/2}$ (Eq. 4.57). The η-value was found using the procedure given in Section 5.2.6. For the normally consolidated soils the average value of η at failure was 0.2. For this η, the calculated s_u/σ'_{vo} were within ± 2% of the value used to calibrate the model but the $J_{2f}^{1/2}/\sigma'_{vo}$ was overpredicted by 1-4%. β was chosen to be 10 (Naylor, 1973).

The effect of crust strength was examined for three cases: (1) 7.5-ft thick crust with s_u = 0.25 ksf, (2) 7.5-ft

Table 5.3
Normally consolidated soil properties used to calibrate the cap model.

ϕ'	$= 28^{\circ}$
c'	$= 0.0$
s_u/σ'_{vo}	$= 0.32$
C_c	$= 0.25$
C_r	$= 0.04$
e_o	$= 0.7$
ν'	$= 0.3$
γ_{sat}	$= 115$ pcf

Table 5.4
Cap parameters for normally consolidated soil.

α	=	0.183
κ	=	0.0001 ksf
K_1	=	98.0
K_2	=	1.0
K_{min}	=	1.0 ksf
A_p	=	2.116 ksf
G_1	=	0.46
G_2	=	0.0
Dx_o	=	-0.996
W	=	0.146
R	=	0.75
γ_{sat}	=	115 pcf
K_o	=	0.47
β	=	10

thick crust with s_u = 0.125 ksf, and (3) no crust (i.e., normally consolidated). The strength and modulus profiles for each case are shown in Fig. 5.5. K_o was taken to be 1.0 for the strong crust and 0.6 for the weak crust. The η that gives the correct match between the Mohr-Coulomb and Drucker-Prager criterion (Section 5.2.5) was 0.45 for s_u = 0.25 ksf and 0.30 for s_u = 0.125 ksf. The cap parameters for the strong and weak crusts are summarized in Table 5.5. Parameters for the no crust case are given in Table 5.4. The influence of a pocket of weak, normally consolidated soil in an otherwise strong crust was investigated. Two locations were considered: one at the toe of the embankment and the other beneath the embankment slope as shown on Fig. 5.6.

The behavior of an embankment on a compressible foundation was also investigated. The input soil properties were the same as in Table 5.3 except that C_c = 0.70 and C_r = 0.15. The ratio between C_c and C_r is near the median observed for 76 clayey soils (Table 4.13). Cap parameters for the normally consolidated layers and the strong and weak crusts are shown in Table 5.6. It was desired to investigate only the effect of compressibility so the same s_u/σ'_{vo} was used even though for a real soil it would probably be higher for a more compressible (and hence more plastic) soil.

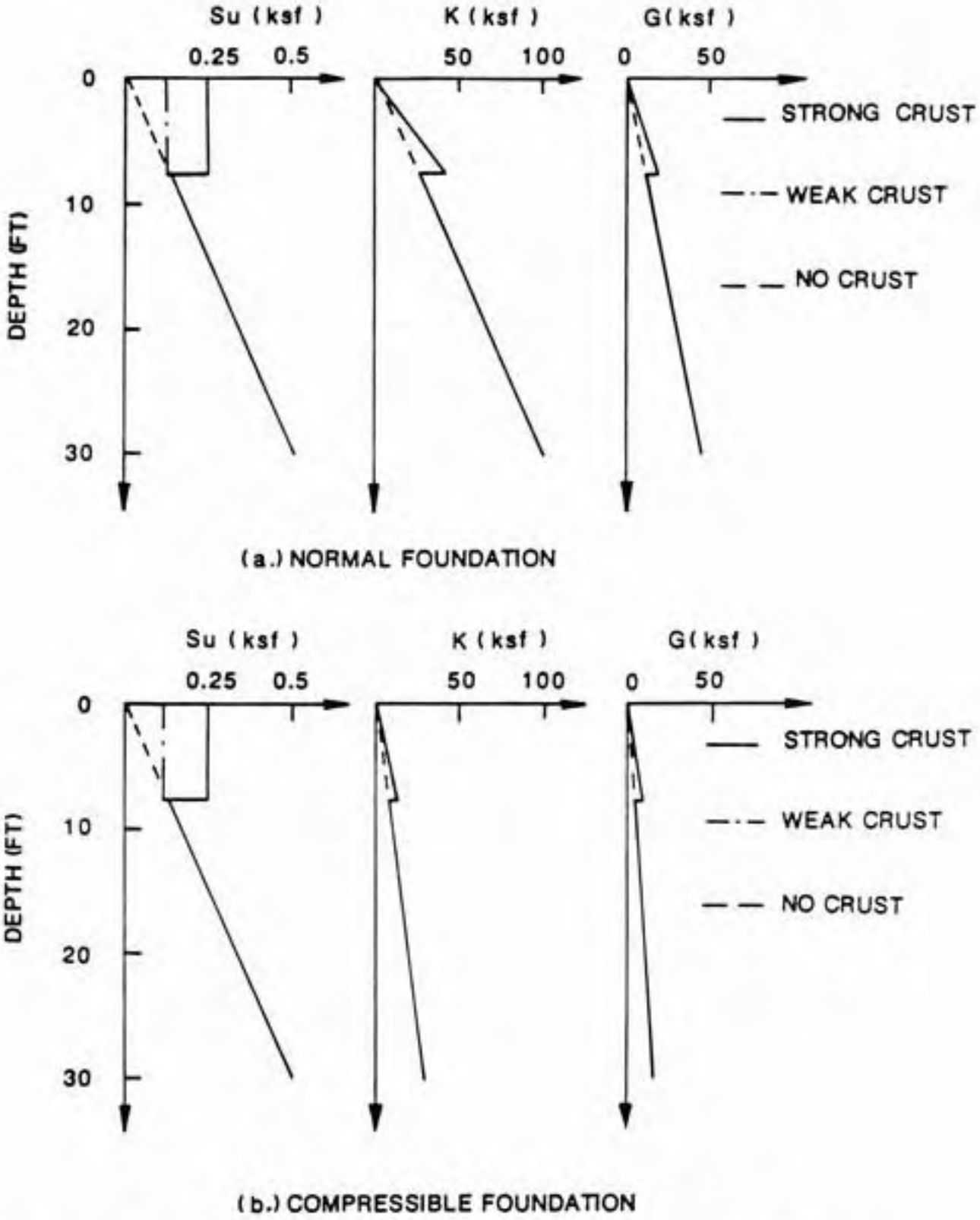

Figure 5.5 Profile of undrained shear strength, bulk modulus, and shear modulus for normal and compressible foundations.

Table 5.5
Cap parameters for overconsolidated layers.

Parameter	Strong crust	Weak crust
α	0.16	0.17
κ	0.0001 ksf	0.0001 ksf
K_1	98.0	98.0
K_2	1.0	1.0
K_{min}	1.0 ksf	1.0 ksf
A_p	2.116 ksf	2.116 ksf
G_1	0.46	0.46
G_2	0.0	0.0
Dx_o	-0.996	-0.996
x_o	-1.75	-0.83
W	0.146	0.146
R	0.75	0.75
γ_{sat}	115 pcf	115 pcf
K_o	1.0	0.6
B	10	10

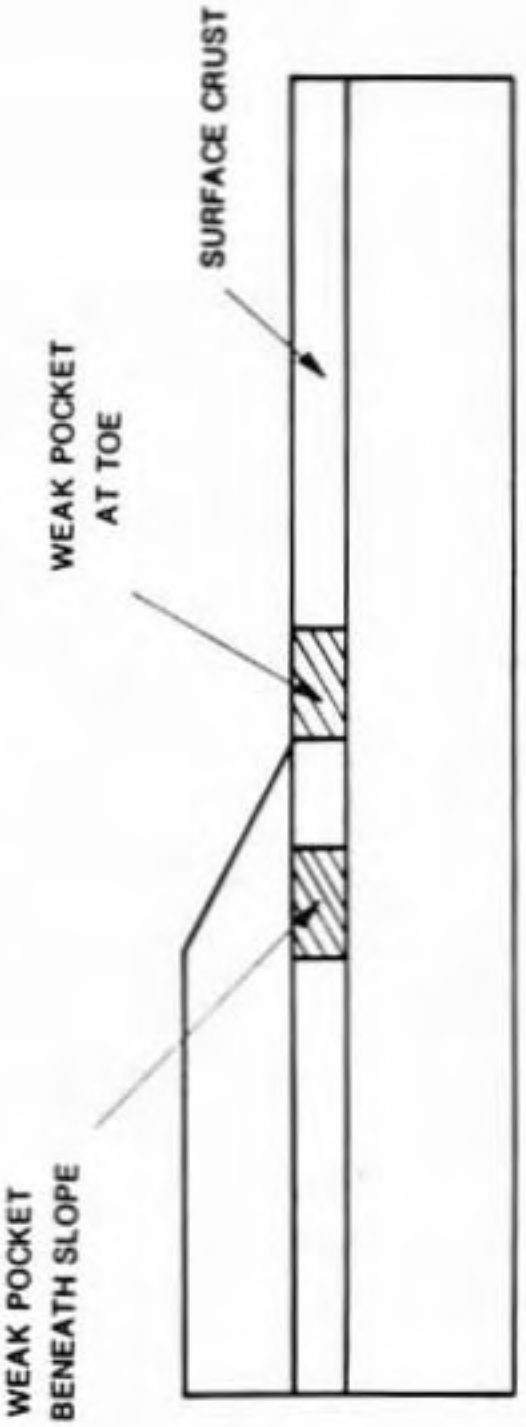

Figure 5.6 Location of weak pockets.

Table 5.6
Cap parameters for compressible foundation.

Parameter	Normally consolidated	Strong crust	Weak crust
α	0.18	0.16	0.17
κ	0.0001 ksf	0.0001 ksf	0.0001 ksf
K_1	26.1	26.1	26.1
K_2	1.0	1.0	1.0
K_{min}	1.0 ksf	1.0 ksf	1.0 ksf
A_p	2.116 ksf	2.116 ksf	2.116 ksf
G_1	0.46	0.46	0.46
G_2	0.0	0.0	0.0
Dx_o	-0.994	-0.994	-0.994
x_o	Eq. 4.76	-1.77	-0.84
W	0.382	0.382	0.382
R	0.82	0.82	0.82
γ_{sat}	115 pcf	115 pcf	115 pcf
K_o	0.47	1.0	0.6
β	10	10	10

A single layer of reinforcement with a modulus of 60 k/ft (5000 lb/in.; 880 kN/m) extending across the full width of the embankment base was used. The modulus is the same as used by McCarron (1985) and corresponds to a high modulus woven geotextile or geogrid. For example, Tensar SR2 geogrid has an average modulus of about 40 k/ft (3300 lb/in.; 580 kN/m) and a breaking strength of 5 k/ft (420 lb/in.; 73 kN/m) (McGown, et al., 1984). The effect of varying the reinforcement modulus on embankment behavior was not investigated.

A total of 15 combinations of embankment geometry, foundation depth and foundation soil properties were analyzed. They are summarized in Table 5.7.

5.4 RESULTS OF ANALYSIS

Results of a comparative study of reinforced and unreinforced embankment behavior are given in this section. First, the behavior of reinforced and unreinforced embankments with 180-ft base widths and 2h:1v side slopes on a 30-ft thick foundation with a 7.5-ft thick weak crust (s_u = 0.125 ksf) and the development of the reinforcement forces are examined in detail. Then the effect of crust strength, foundation compressibility, foundation thickness, base width and side slope on embankment behavior is presented. Finally, the effect of reinforcement for all the cases

Table 5.7
Summary of cases analyzed.

	Strong Crust	Weak Crust	No Crust
I. 180′ wide embankment			
A. 2h:1v side slope			
1. Normal foundation compressibility			
a. 15′ foundation depth	X	X	X
b. 30′ foundation depth	X	X	X
c. 60′ foundation depth	X		
2. Compressible foundation			
a. 30′ foundation depth	X	X	X
3. Weak pocket at toe			
a. 30′ foundation depth	X		
4. Weak pocket beneath slope			
a. 30′ foundation depth	X		
B. 3h:1v side slope			
1. Normal foundation compressibility			
a. 30′ foundation depth	X		X
II. 120′ wide embankment			
A. 2h:1v side slope			
1. Normal foundation compressibility			
a. 30′ foundation depth	X		

studied is summarized. Unless noted otherwise, the embankments discussed in this section have a 180-ft base width and 2h:1v side slopes and the foundations are 30 ft thick with a 7.5-ft thick weak crust and normal compressibility (i.e., C_c = 0.25 and C_r = 0.04).

5.4.1 Comparison of Reinforced and Unreinforced Embankment Behavior

A detailed examination is presented of the behavior of reinforced and unreinforced embankments with a 180-ft base width and 2h:1v side slopes on a 30-ft thick foundation with a 7.5-ft thick weak crust (s_u = 0.125 ksf). Horizontal displacement at the embankment toe and maximum settlement at the base of the embankment versus the surcharge applied at the centerline are shown in Fig. 5.7. The height at failure was 8.4 ft (surcharge = 1.05 ksf) for the reinforced embankment compared to 7.5 ft (surcharge = 0.94 ksf) for the unreinforced embankment. For both embankments the rate of displacement increased as the applied surcharge increased. The relative increase in surcharge (defined in Section 5.2.7) made possible by the reinforcement was 22%. The maximum reinforcement force versus surcharge is also shown in Fig 5.7. The force was 1.34 k/ft (110 lb/in.; 20 kN/m) at failure.

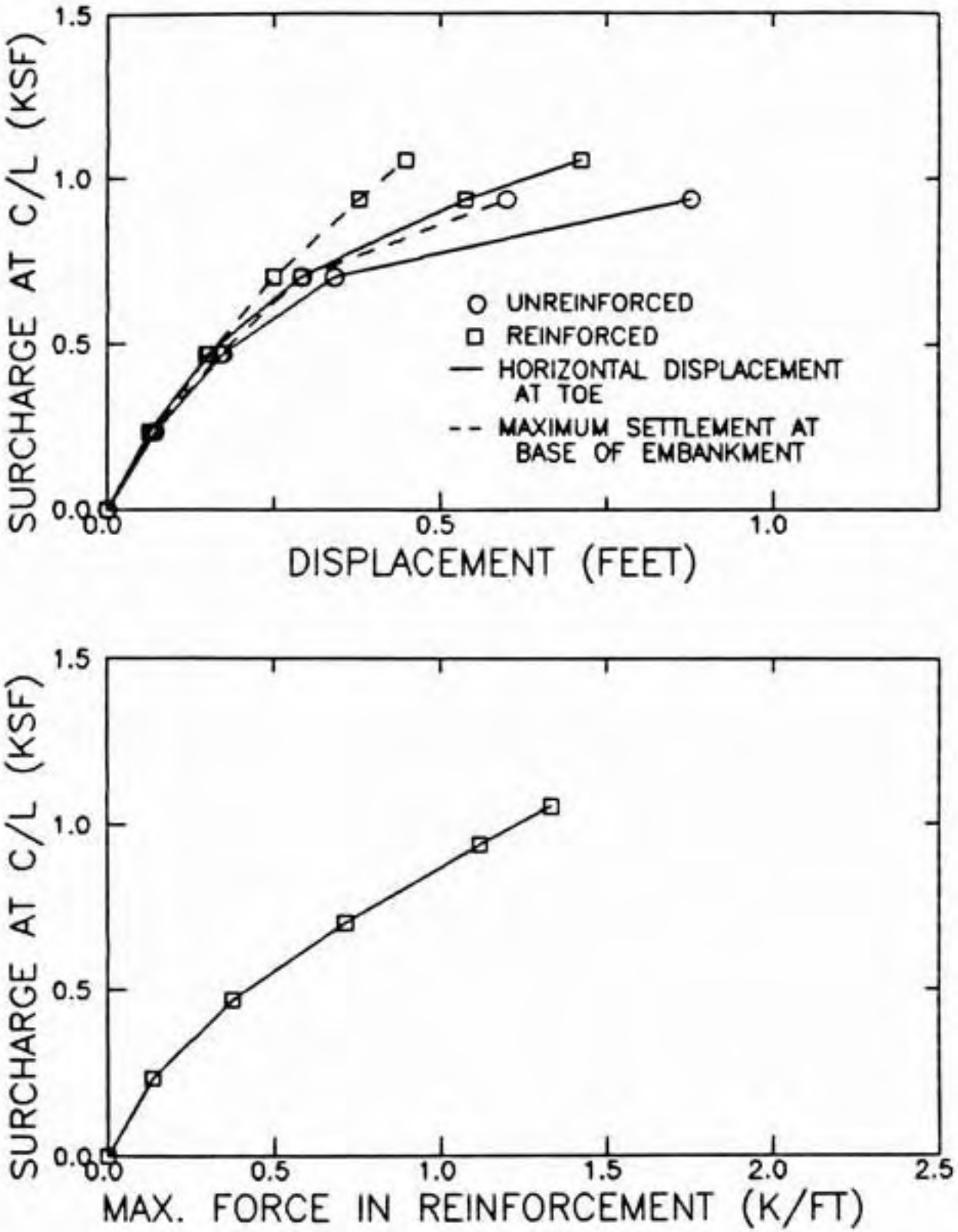

Figure 5.7 Comparison of behavior for reinforced and unreinforced embankments, 30-ft thick foundation, weak crust.

Reinforcement locally alters the magnitude of the displacements but does not alter the overall pattern of displacements. Horizontal displacement at the embankment toe and maximum settlement at the base of the embankment were reduced (Fig. 5.7). Horizontal displacements along several vertical sections in the foundation for an embankment height of 7.5 ft are shown in Fig. 5.8. The largest displacements occur in the upper 10 ft at the sections beneath the slope (75 ft from centerline) and at the toe (90 ft from centerline). Reinforcement clearly reduces deformations in this region but has a much smaller effect at other sections and at greater depths. Settlement at the ground surface for an embankment height of 7.5 ft is shown in Fig. 5.9. The maximum settlement occurred beneath the embankment shoulder. The location of the maximum settlement is felt to depend primarily on the embankment width, foundation depth, and foundation compressibility. The reinforcement reduces settlement beneath the slope and heave at the toe. There is almost no effect beneath the central portion of the embankment or more than 30 ft beyond the toe. Displacement vectors for reinforced and unreinforced embankments at failure are compared in Fig. 5.10. Reinforcement does not alter the overall displacement pattern. It is seen that the largest movements occur near the toe. These findings are in general agreement with the results of previous studies (e.g., Ohta, et al., 1980; Andrawes, et al., 1980, 1982; McGown, et al.,

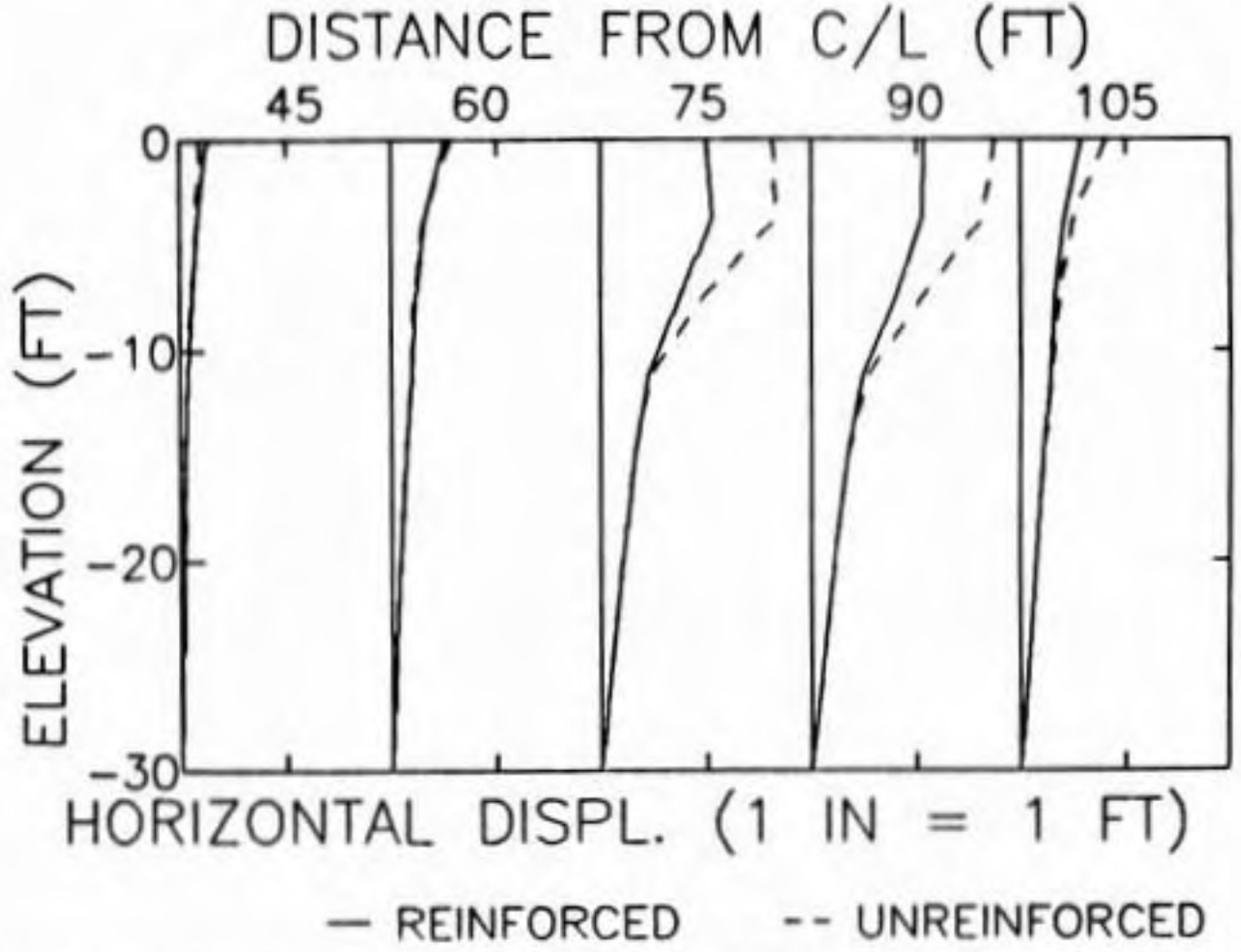

Figure 5.8 Comparison of horizontal displacement profiles for reinforced and unreinforced embankment, 30-ft thick foundation, weak crust.

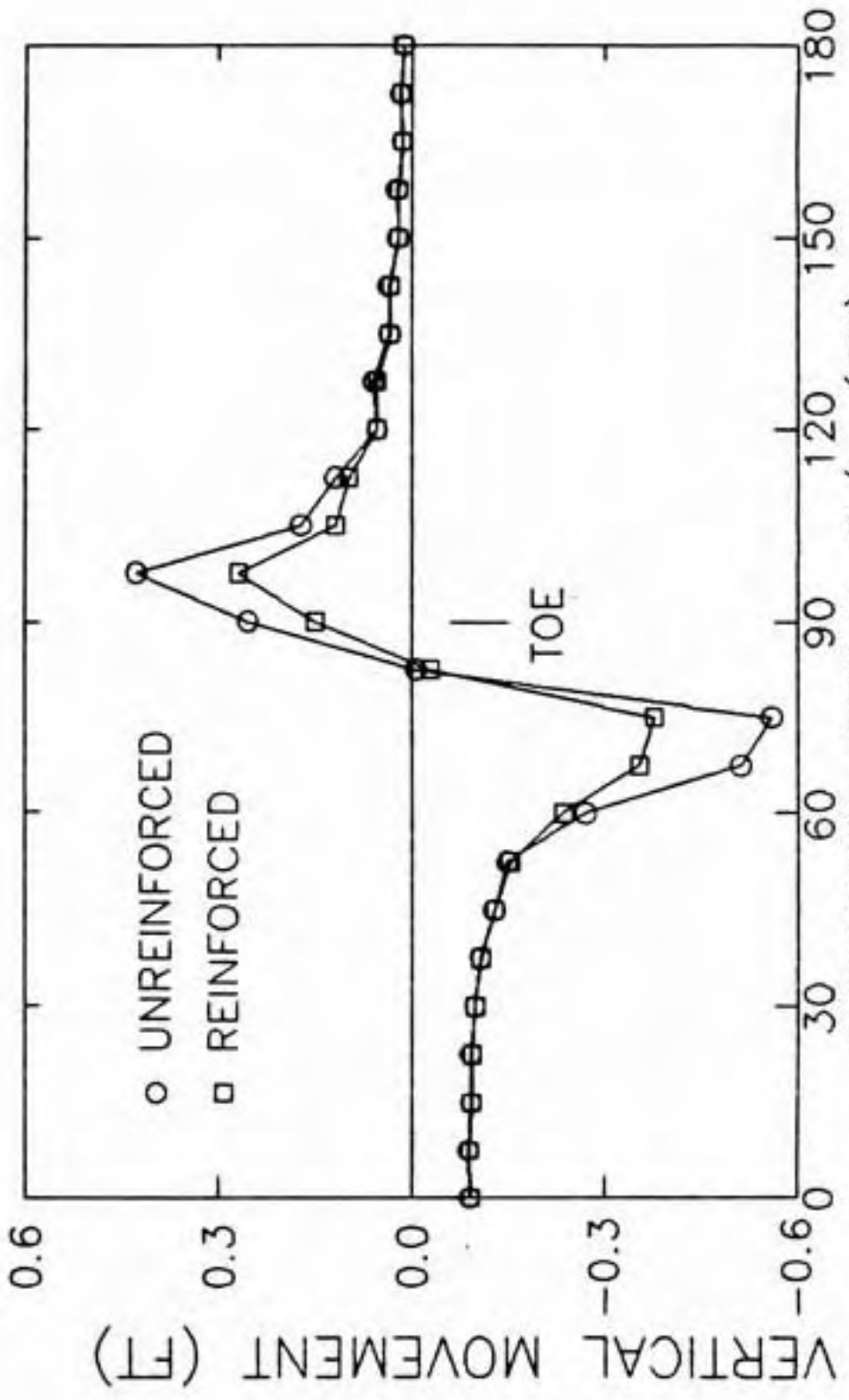

Figure 5.9 Comparison of settlement profile at base of embankment for reinforced and unreinforced embankment, 30-ft thick foundation, weak crust.

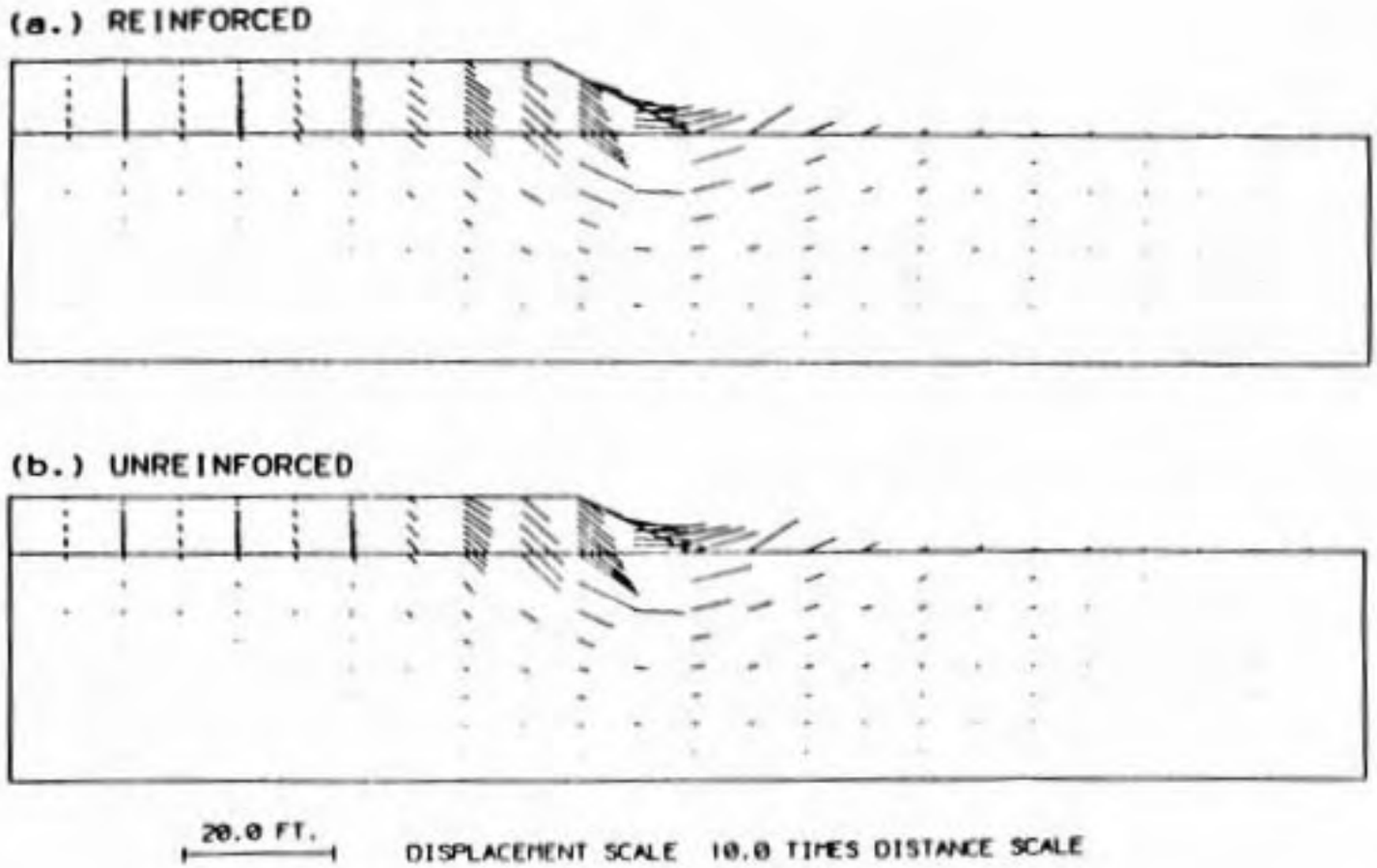

Figure 5.10 Displacement vectors for reinforced and unreinforced embankments, 30-ft thick foundation, weak crust.

1981; Rowe, 1982; Boutrup and Holtz, 1982, 1983; McCarron, 1985).

The effect of reinforcement on stresses in the foundation was examined. There are 4 possible states of stress within the framework of the cap model as discussed in Chapter 3: elastic, failure, cap, and corner. The corner state of stress is perfectly plastic. As the extent of soil at the corner state increases with the applied load and becomes unbounded, i.e. approaches the ground surface, failure occurs. The state of stress for reinforced and unreinforced embankments at heights of 3.75 and 7.5 ft and for the reinforced embankment at a height of 8.4 ft are compared in Fig. 5.11. Initially the crust is elastic and the normally consolidated soils are on the cap. For the 3.75-ft height there is very little difference except that for the reinforced case the failure zone in the crust is shifted slightly toward the centerline and the extent of the cap zone in the normally consolidated soil beyond the toe is slightly reduced. There is a large elastic zone in the normally consolidated soil beyond the toe. It is due to reduction in shear stress caused by increase in horizontal stress from the embankment load while the vertical stress remains nearly constant. This causes the state of stress to move from the cap into the elastic state. Part of the overconsolidated layer beneath the embankment has become normally

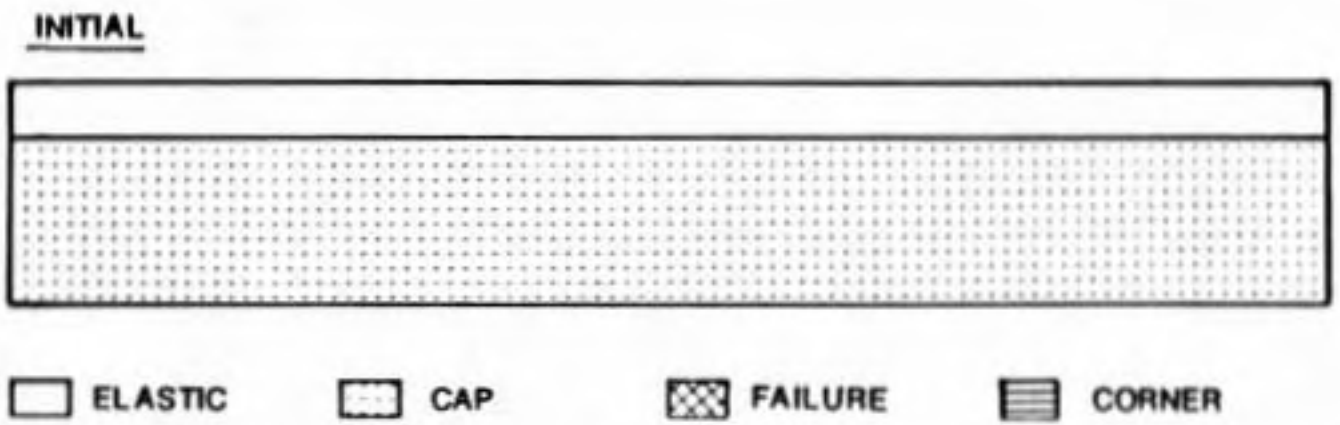

Figure 5.11 State of stress in foundation, reinforced and unreinforced embankments, 30-ft thick foundation, weak crust.

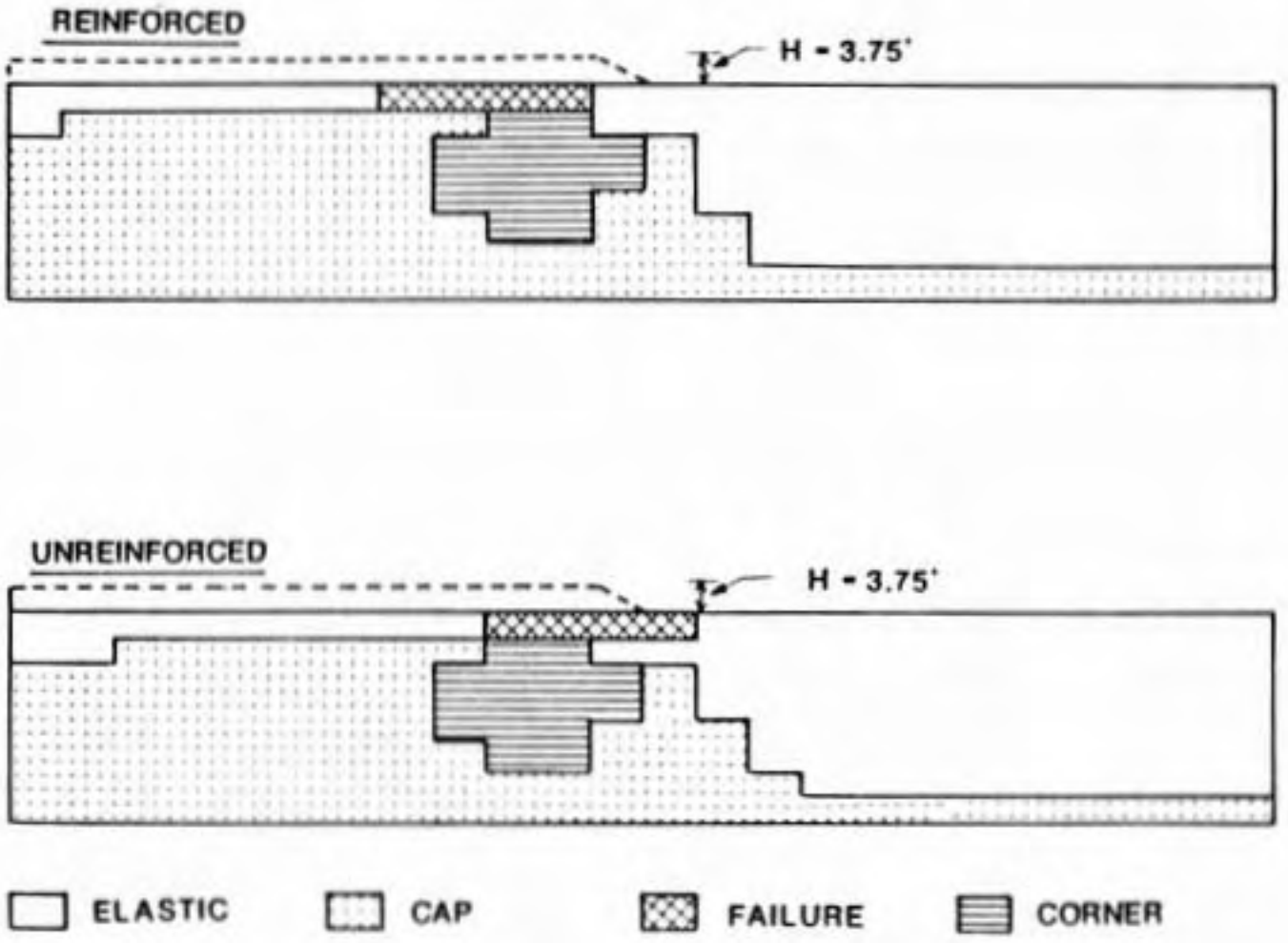

Figure 5.11, continued.

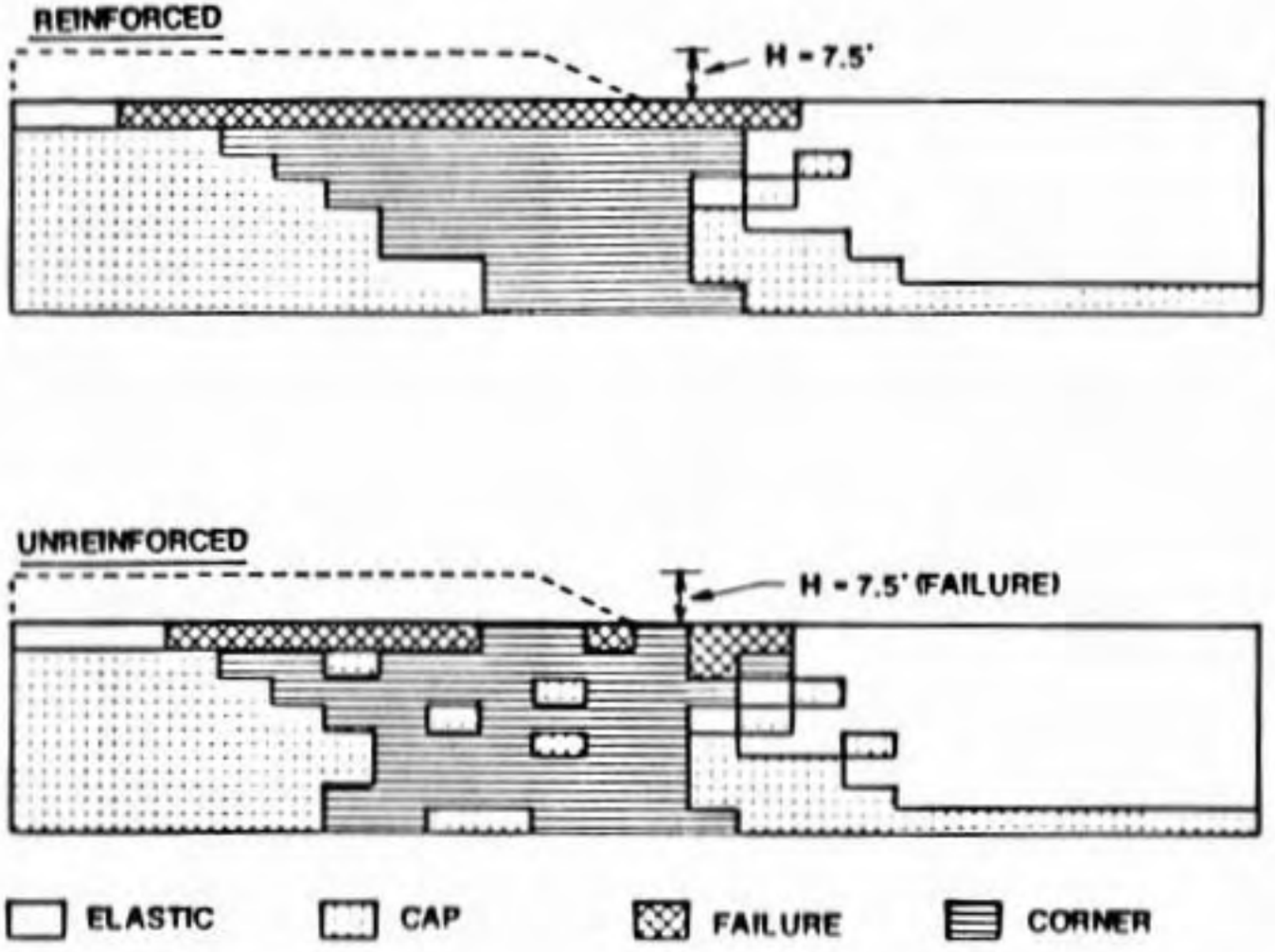

Figure 5.11. continued.

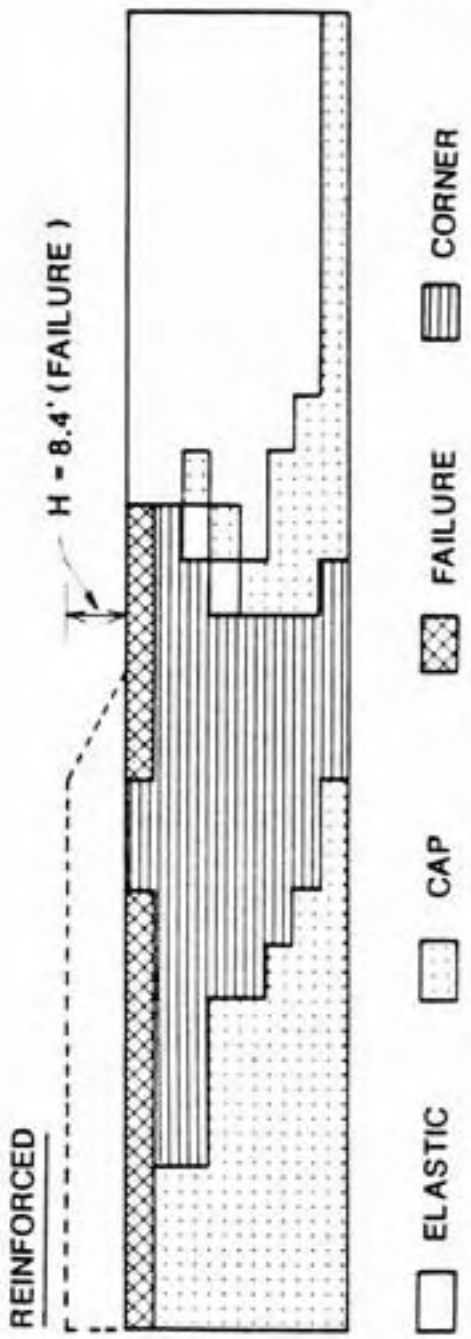

Figure 5.11. continued.

consolidated (i.e. cap or corner). At a height of 7.5 ft the extent of the corner zone has increased and more of the overconsolidated layer has become normally consolidated. The main effect of the reinforcement was to reduce the extent of corner loading. For the unreinforced embankment, the corner zone has reached the ground surface indicating uncontained plasticity and imminent failure. Also note that a few elements moved from the corner to the cap state indicating that some redistribution of load occurred or that the solution introduces some numerical inaccuracies as failure is approached. The FE solution for the unreinforced embankment did not converge at the next load step at a height of 8.4 ft. Comparing the reinforced embankment at heights of 7.5 and 8.4 ft (failure) it is seen that the extent of corner loading has increased and is approaching uncontained plasticity. None of the foundation soil was in tension for either reinforced or unreinforced embankments.

The change in $J_2^{1/2}$ in the foundation caused by reinforcement for an embankment height of 7.5 ft is shown in Fig. 5.12. $J_2^{1/2}$ was reduced beneath and beyond the toe with the greatest effect in the upper 3.75 ft of the overconsolidated layer. This increases the safety factor against instability. $J_2^{1/2}$ was increased slightly in the overconsolidated layer beneath the central portion of the embankment and at distances greater than 45 ft from the toe

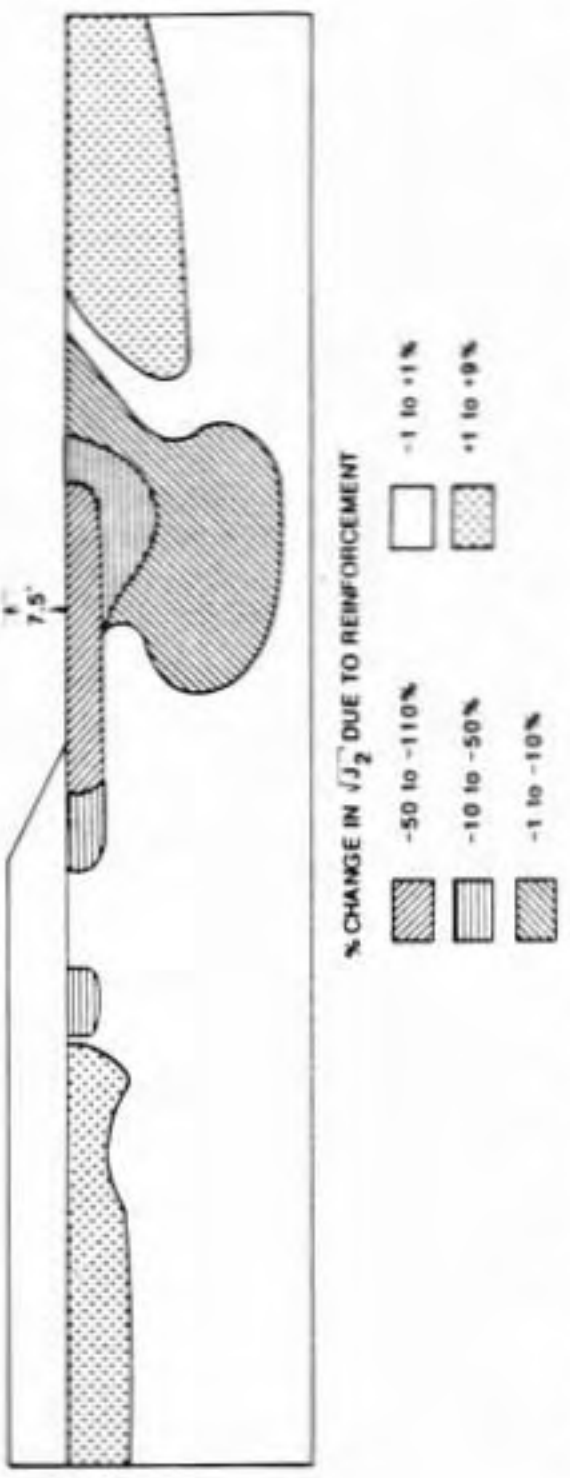

Figure 5.12 Change in $\sqrt{J_2}$ in foundation due to reinforcement, 30-ft thick foundation, weak crust, at an embankment height of 7.5 ft.

but this has a negligible effect on stability. As was discussed in Sections 4.2.4.3 and 5.2.8 the cap model only approximately represents the behavior of the overconsolidated crust so it is felt that the computed stress changes in the crust are approximate.

The state of stress in the fill is shown in Fig. 5.13. For both reinforced and unreinforced embankments much of the fill is at failure. At a height of 7.5 ft, the elastic zone near the centerline is larger for the unreinforced than for the reinforced embankment but the elastic zone near the shoulder is smaller for the unreinforced case. The change in $J_2^{1/2}$ in the fill for an embankment height of 7.5 ft is shown in Fig. 5.14. The general pattern shows reduction in the outer portion of the embankment but increase in the central portion. The former would tend to increase stability. There are a few seemingly erratic changes in $J_2^{1/2}$ that may be due to slight inaccuracies in the stresses computed by PS-NFAP as failure is approached.

5.4.2 Forces Developed in Reinforcement

The distribution of force in the reinforcement as the centerline surcharge increases is shown in Fig. 5.15 for an embankment with a 180-ft base width and 2h:1v side slope on a 30-ft thick foundation with a 7.5-ft thick weak crust (s_u = 0.125 ksf). It is seen that the force is low near the

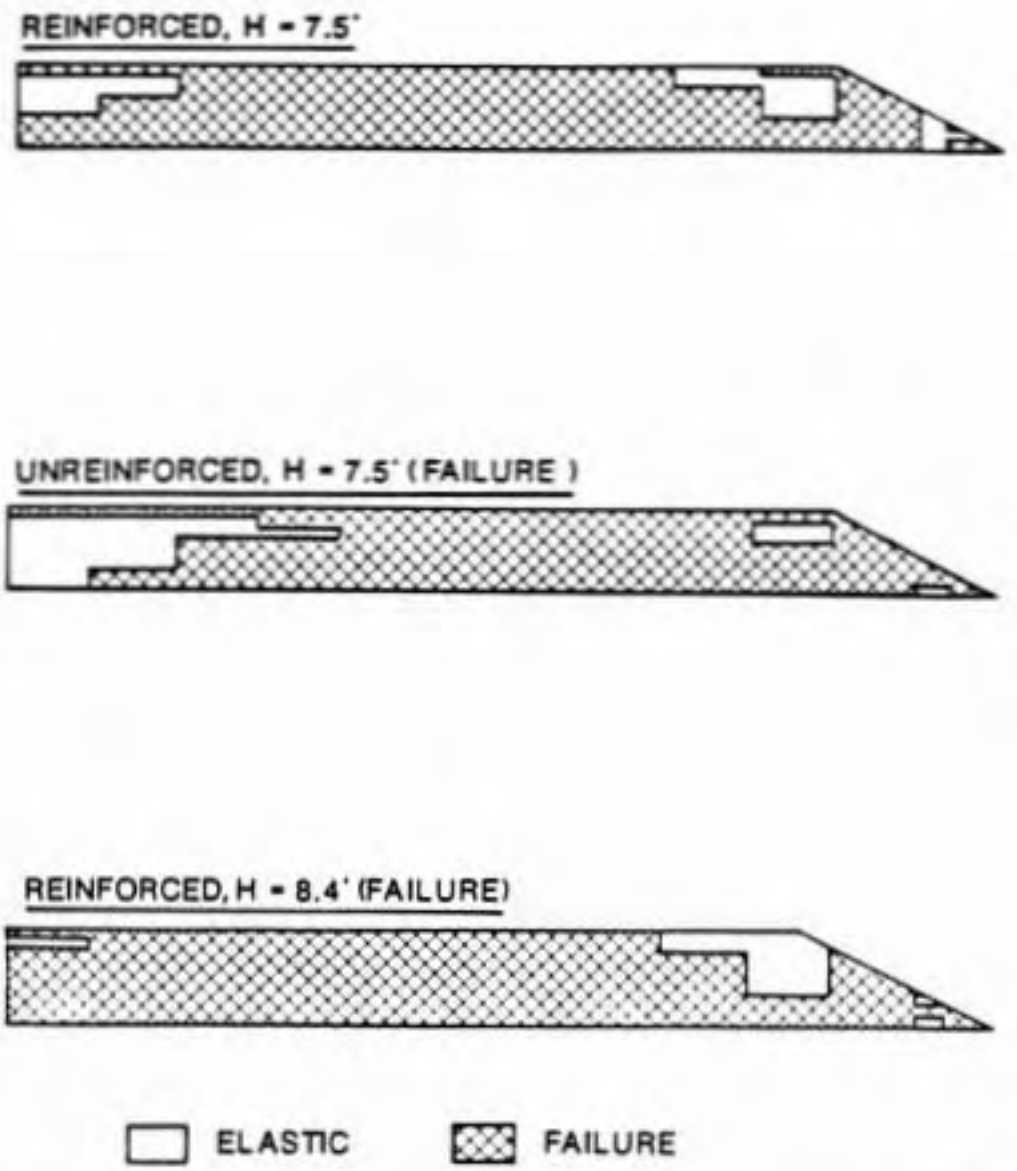

Figure 5.13 State of stress in fill, reinforced and unreinforced embankments, 30-ft thick foundation, weak crust.

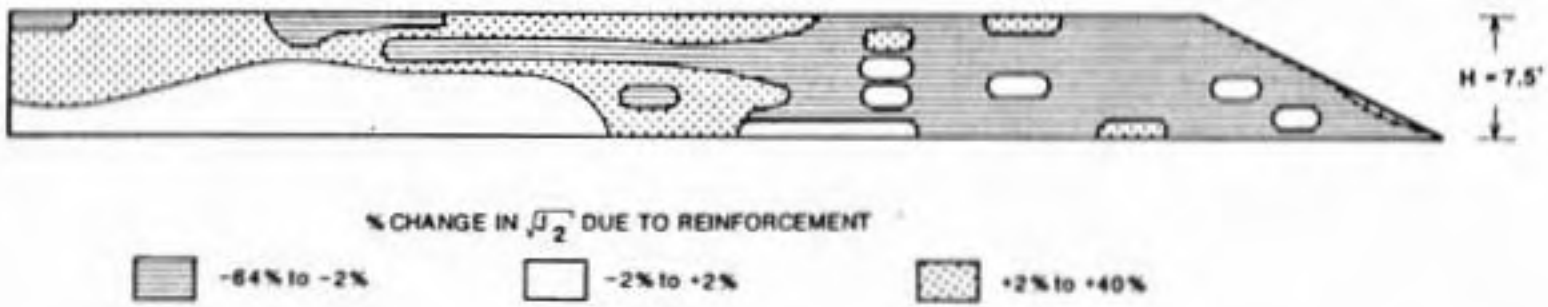

Figure 5.14 Change in $\sqrt{J_2}$ in fill due to reinforcement, 30-ft thick foundation, weak crust, at an embankment height of 7.5 ft.

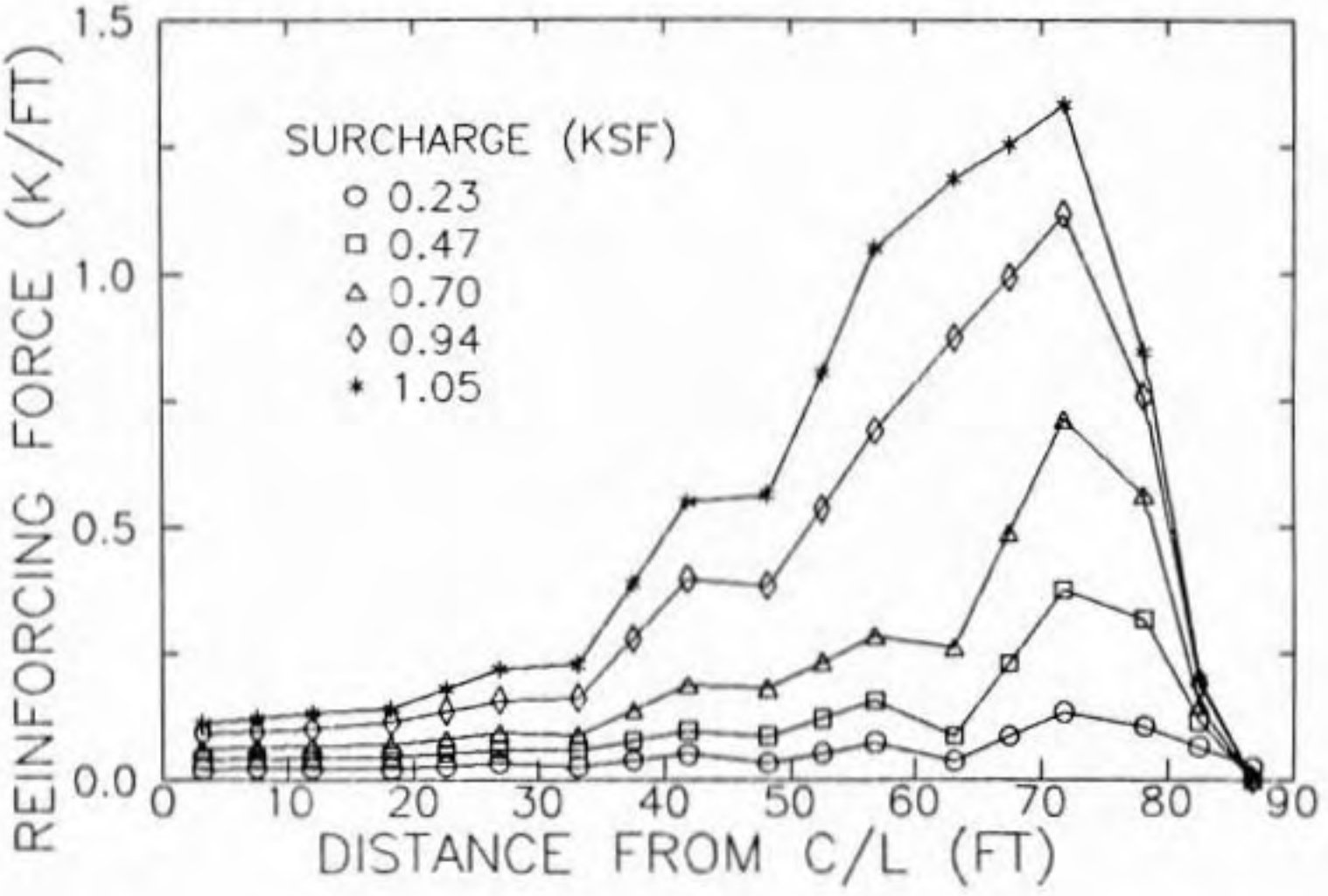

Figure 5.15 Distribution of force in reinforcement vs. surcharge, 30-ft thick foundation, weak crust.

centerline and increases to a maximum near the embankment shoulder. It then decreases to zero a few ft inside of the toe which is consistent with field observations (Fowler, 1981; Fowler and Haliburton, 1980; Rowe, et al., 1984a) and FE results reported by others (Rowe, 1982; Rowe, et al., 1984b). The location of the maximum force did not change as the surcharge increased although for some other cases it tended to move slightly toward the centerline. The maximum reinforcing force versus surcharge is shown in Fig. 5.7. It shows that the rate of load takeup in the reinforcement increases as the surcharge increases. The force at failure was 1.34 k/ft (110 lb/in.; 20 kN/m) which is much less than the typical breaking strength of strong geotextiles or geogrids. This indicates that the strength of the embankment fill and foundation soils are fully mobilized and failure occurs before there are sufficient deformations to develop the full tensile capacity of the reinforcement.

The largest force gradient in the reinforcement at a height of 8.4 ft occurred about 80 ft from the centerline and was 0.15 k/ft/ft. This must be transferred by shear stress to the soil above and below the reinforcement. The available shear resistance between the reinforcement and fill equals the vertical stress times $\tan(\phi_{f-r})$ where ϕ_{f-r} is the fill-reinforcement friction angle. Assuming ϕ_{f-r} equals the friction angle of the fill and taking the

vertical stress to be the height of fill times its unit weight the available shear resistance is 0.4 ksf. In addition, if the available resistance between the reinforcement and foundation soil is taken to be s_u = 0.125 ksf, the total available shear resistance is about 0.5 ksf. This is much greater than the gradient so slip between the reinforcement and surrounding soil did not occur. Similar results were obtained by Boutrup and Holtz (1982).

5.4.3 Effect of Crust Strength

Displacements for reinforced and unreinforced embankments on foundations with strong, weak, and no crust are compared in Fig. 5.16 for the 30-ft foundation thickness and in Fig. 5.17 for the 15-ft foundation thickness. Crust strength is seen to have a large effect on surcharge at failure. The relative increases in surcharge made possible by reinforcement are compared in Table 5.8. Reinforcement is much more effective for the weak and no crust cases.

Table 5.8
Relative increase in surcharge made possible by reinforcement for strong, weak, and no crusts.

Crust strength	-- Foundation thickness -- 15	30	60
Strong	5%	7%	9%
Weak	15%	22%	---
None	60%	70%	---

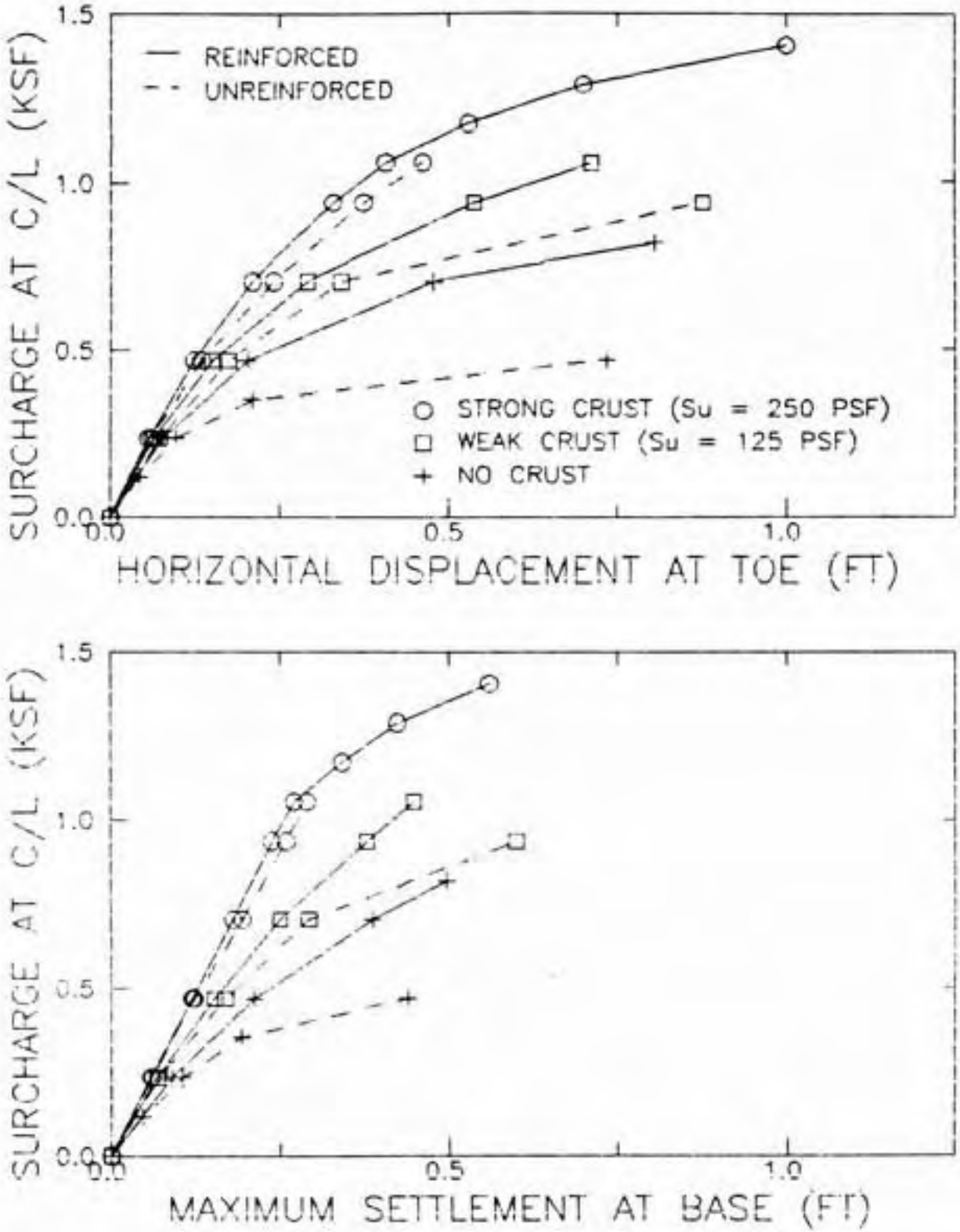

Figure 5.16 Effect of crust strength on horizontal displacement at toe and maximum settlement. 30-ft thick foundation.

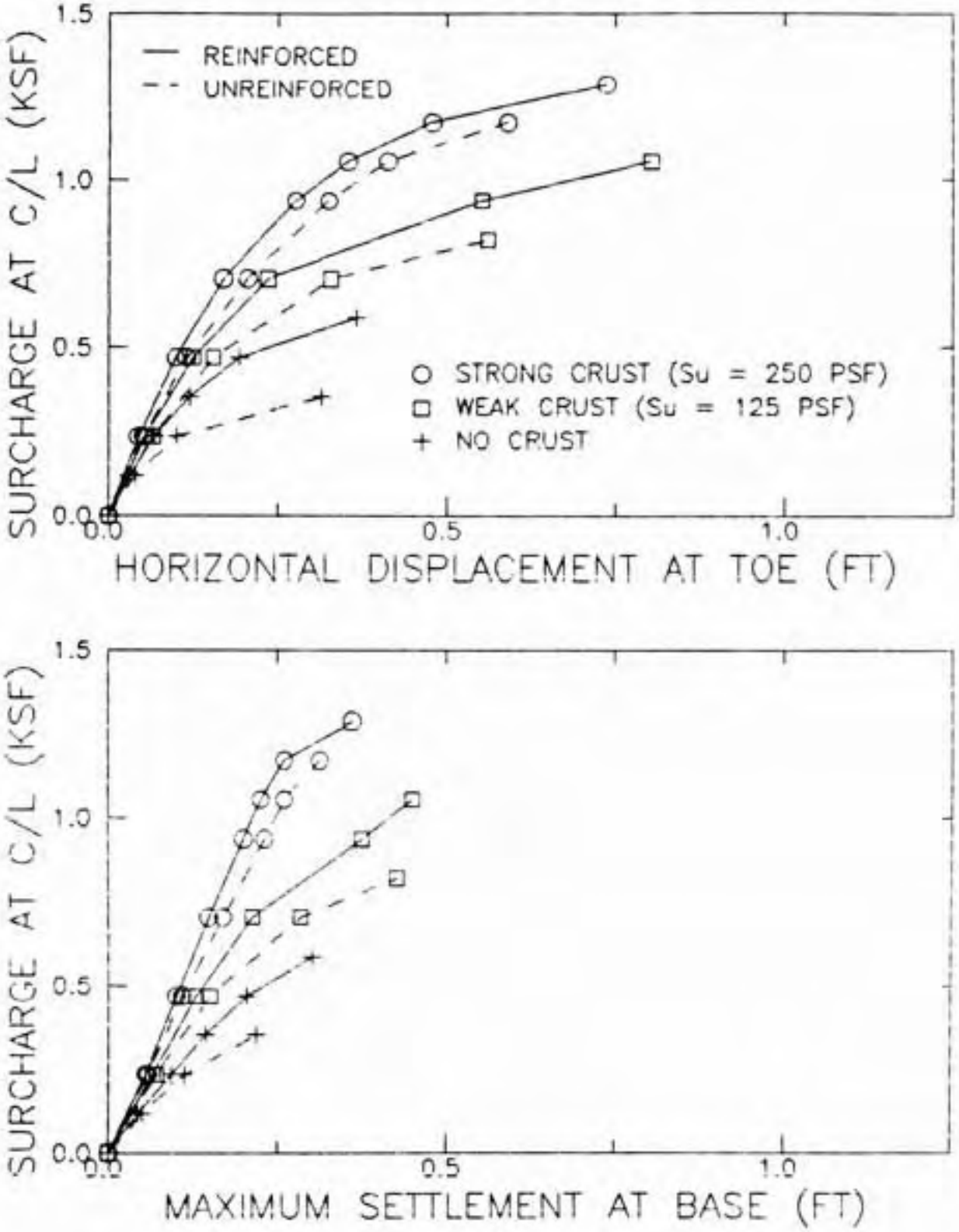

Figure 5.17 Effect of crust strength on horizontal displacement at toe and maximum settlement, 15-ft thick foundation.

Horizontal displacements in the foundation at failure along several vertical sections for the strong and weak crust cases with reinforced embankments are compared in Fig. 5.18. Displacements are greater for the strong crust case since it failed at a greater height but note that the zone of larger displacements extend deeper for this case. For both cases the zone of largest displacements is in the upper 10 ft. It follows that the properties of this zone should have the largest influence on embankment behavior.

The maximum reinforcement force versus centerline surcharge are compared in Fig. 5.19 for 30 and 15-ft foundation depths. For a given surcharge the force increases as crust strength decreases. The values at failure did not show a consistent trend but were between 0.96 and 1.67 k/ft (80 to 140 lb/in.; 14 to 24 kN/m) for all cases.

The influence of a pocket of weak, normally consolidated soil in an otherwise strong crust was investigated. The two cases shown on Fig. 5.6 were analyzed. One had a weak pocket at the toe and the other had a weak pocket beneath the slope. Horizontal displacement at the toe and maximum reinforcement force are compared to the strong crust case with no weak pocket in Fig. 5.20. The weak pocket in either location increased the horizontal displacement and reduced the height at failure but the difference between the

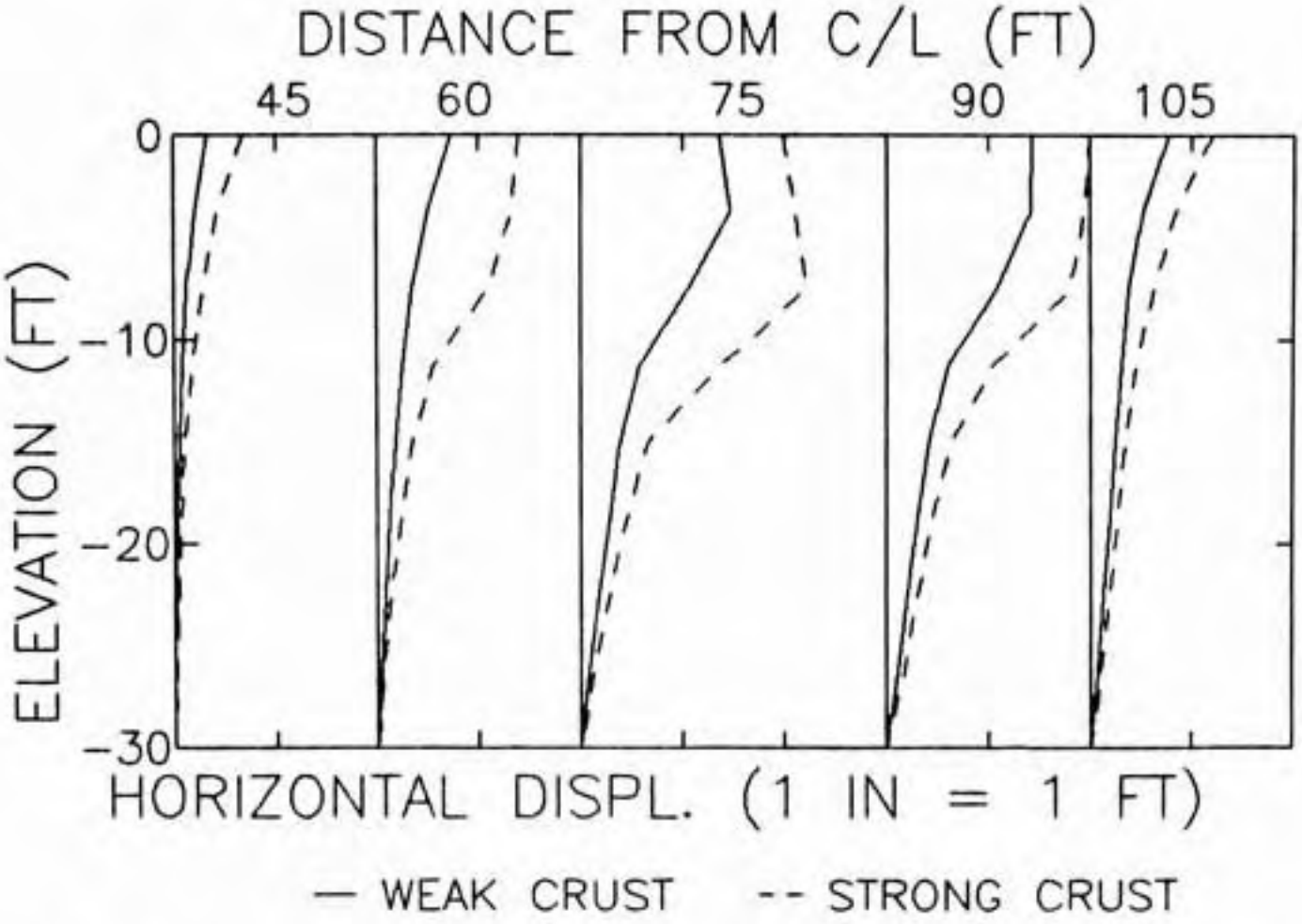

Figure 5.18 Effect of crust strength on horizontal displacement profiles, 30-ft thick foundation.

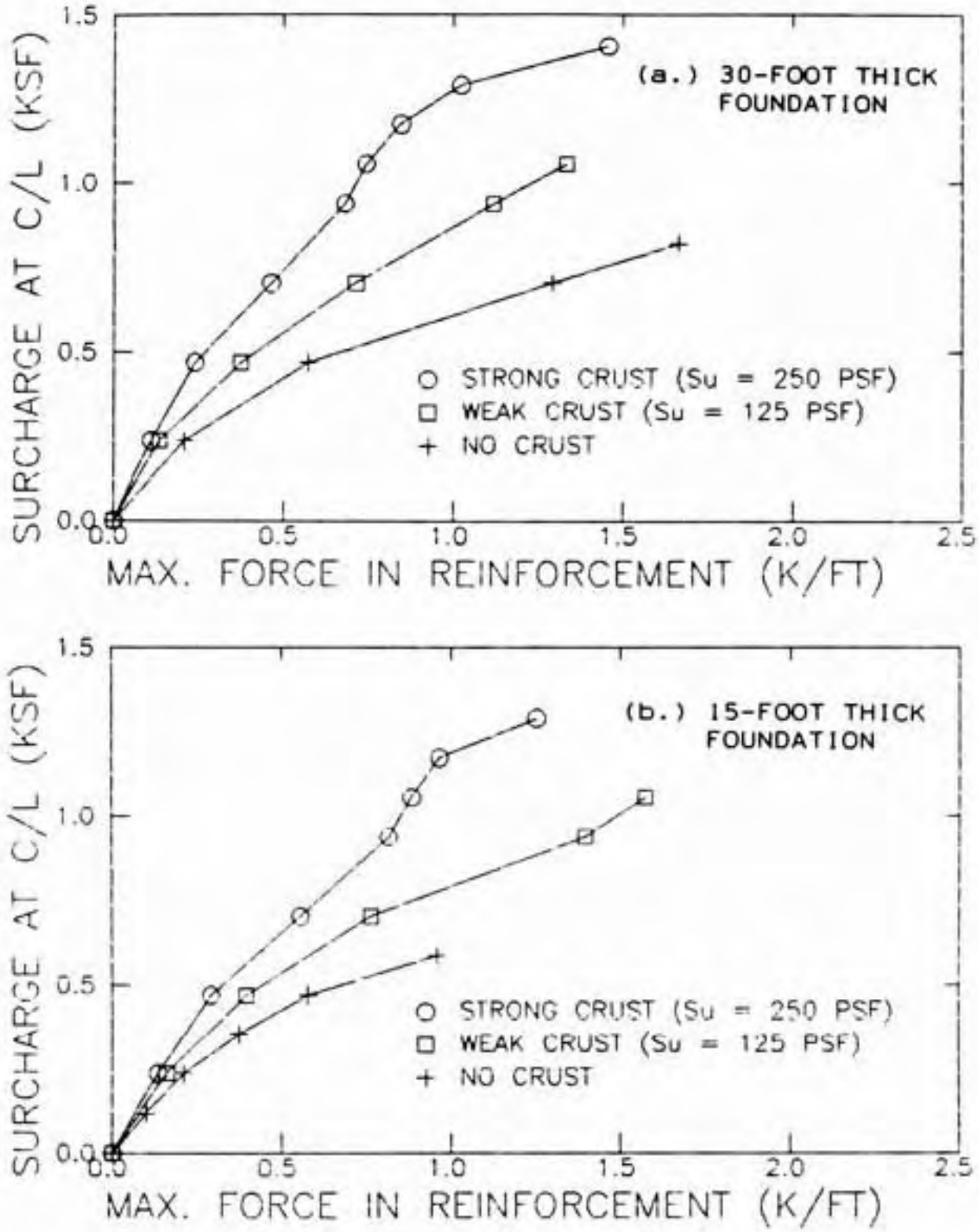

Figure 5.19 Effect of crust strength on maximum force in reinforcement, 30-ft and 15-ft thick foundations.

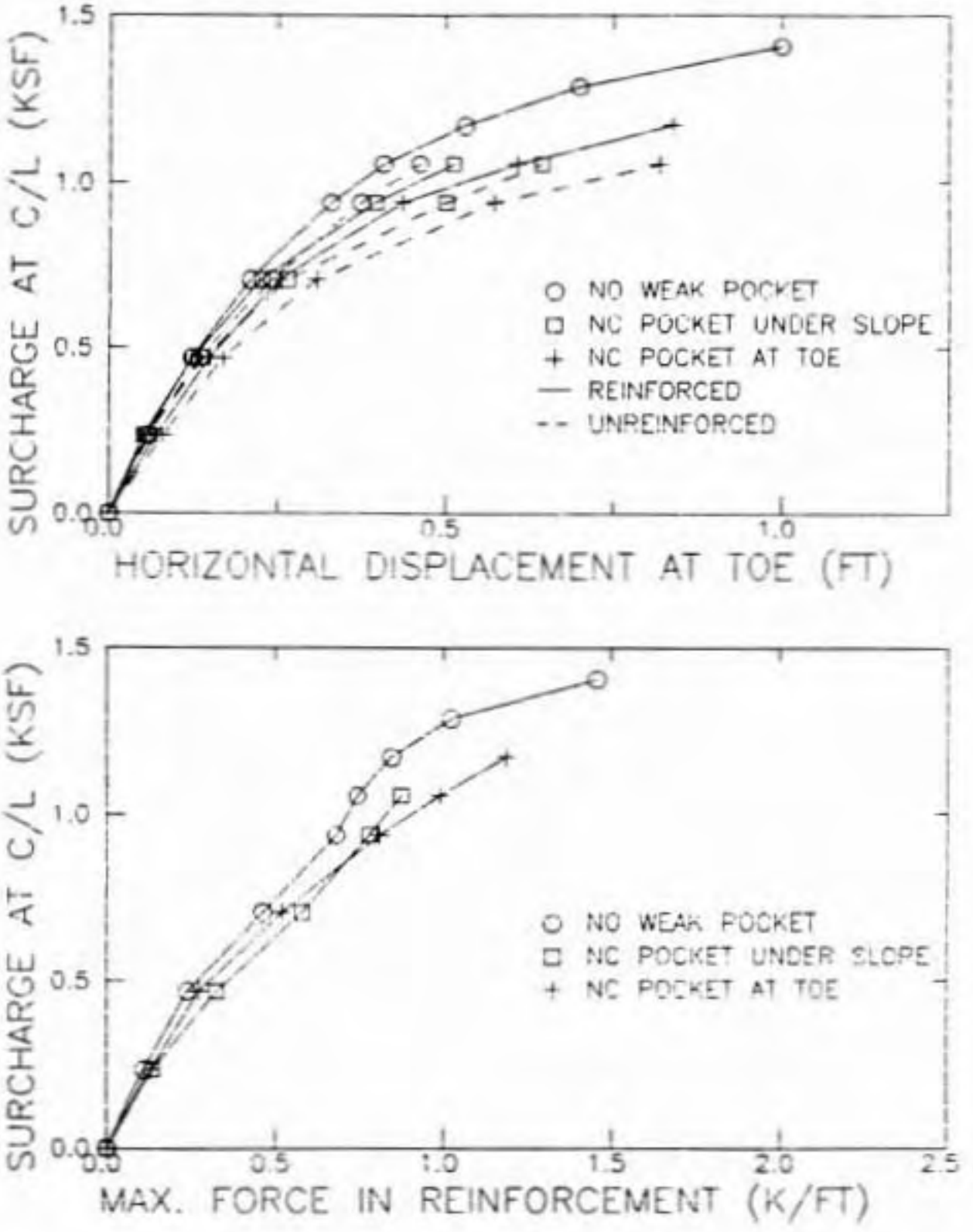

Figure 5.20 Effect of soft pocket on displacements at toe and maximum force in reinforcement for reinforced embankment, 30-ft thick foundation.

no weak pocket case was modest. Reinforcement is seen to have only a small effect. The relative increase in surcharge made possible by reinforcement was 10% for the weak pocket at the toe and 12% for the weak pocket beneath the slope. This is compared to 7% for the strong crust with no weak pocket. The maximum reinforcing force for a given surcharge were increased only slightly by the presence of the weak pocket. It is concluded that weak, normally consolidated pockets in an otherwise strong crust adversely affects overall stability but the effect is modest and the benefit provided by the reinforcement is small.

5.4.4 Effect of Foundation Compressibility

The effect of a compressible foundation was investigated using the cap parameters in Table 5.6. Displacements for 180-ft wide reinforced and unreinforced embankments with 2h:1v side slopes on a 30-ft deep foundation with strong, weak, and no crust are compared in Fig. 5.21. The reinforcement had a beneficial effect. The relative increases in surcharge made possible by reinforcement were 22%, 29%, and 50% for the strong, weak, and no crust cases, respectively. The maximum force in the reinforcement versus surcharge is shown in Fig. 5.22. For a given surcharge the force increased as the crust strength decreased as was observed for the foundation with normal compressibility.

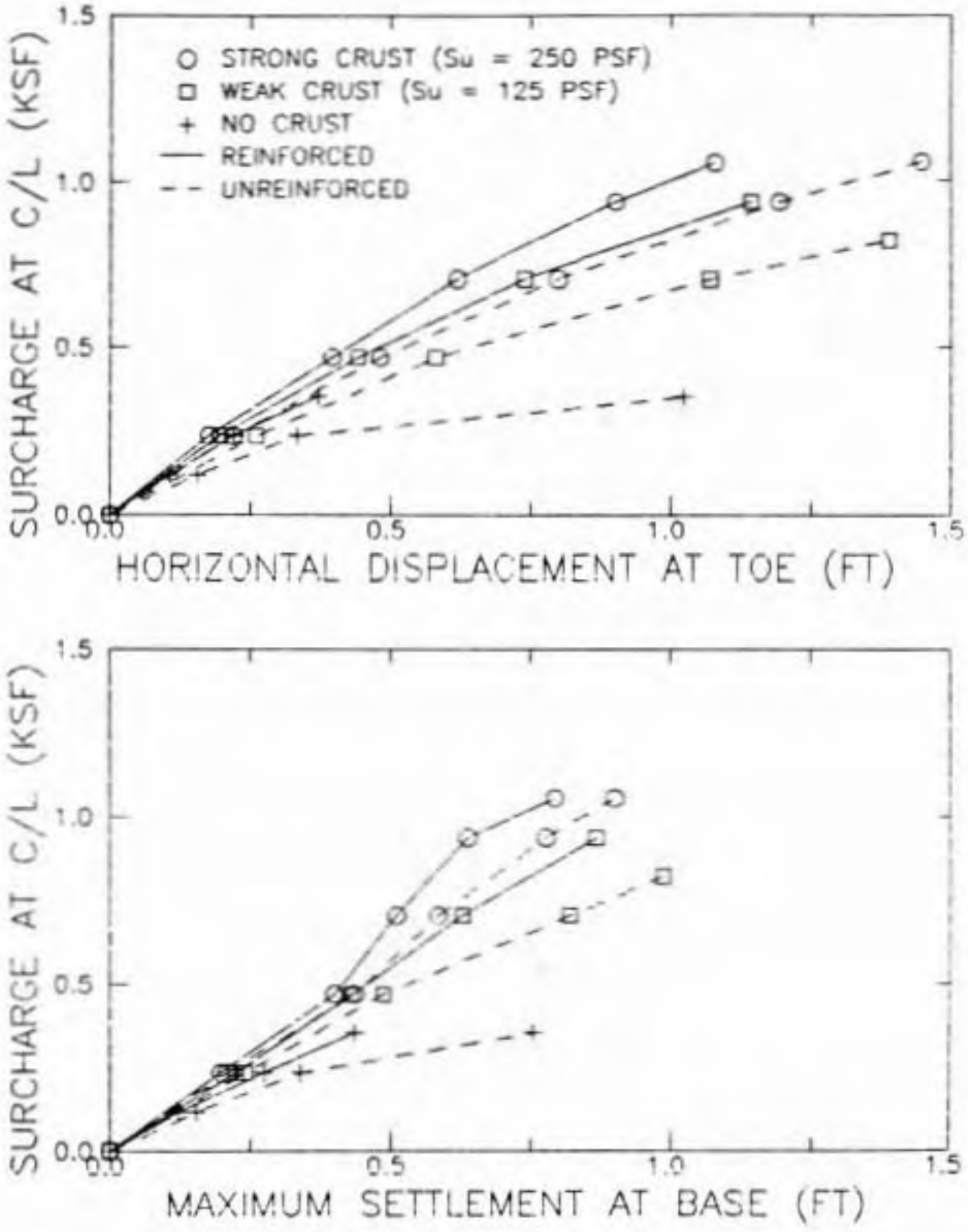

Figure 5.21 Horizontal displacement at toe and maximum settlement for reinforced and unreinforced embankment on compressible foundation, 30-ft thick foundation.

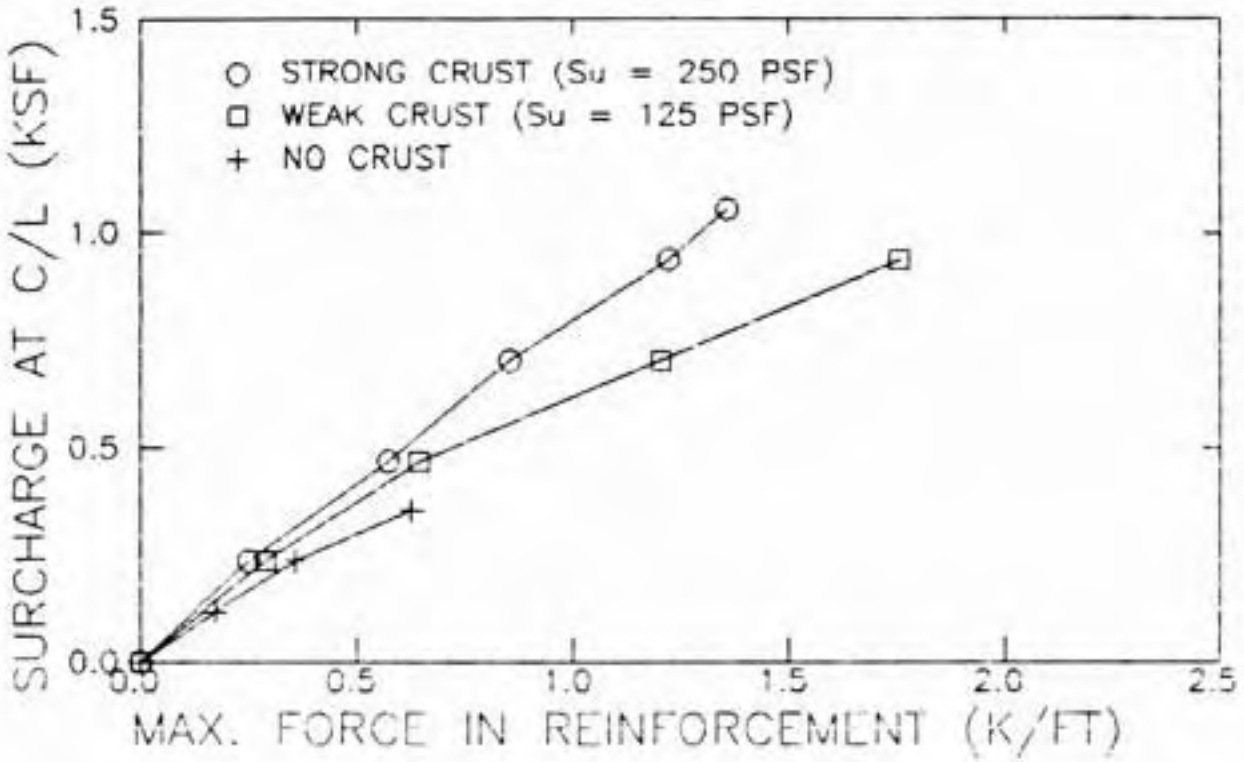

Figure 5.22 Maximum force in reinforcement vs. surcharge for embankment on compressible foundation. 30-ft thick foundation.

Displacements and reinforcement forces for reinforced embankments on normal and compressible foundations with weak crusts are compared in Fig. 5.23. For a given surcharge the compressible foundation showed greater displacements and higher reinforcing forces. The relative increase in surcharge made possible by reinforcement for normal and compressible foundations are summarized in Table 5.9. The reinforcement is seen to be more beneficial for the compressible foundation and strong crust, about the same for the weak crust, and less beneficial for no crust.

Table 5.9
Relative increase in surcharge made possible by reinforcement for normal and compressible foundations.

Crust Strength	-- Compressibility -- Normal	Compressible
Strong	7%	22%
Weak	22%	29%
None	70%	50%

Displacement vectors at failure for the reinforced, compressible foundation, weak crust case are shown in Fig. 5.24. Comparison with Fig. 5.10 for the normal foundation shows that the large deformations in the foundation extend to a greater depth for the compressible foundation.

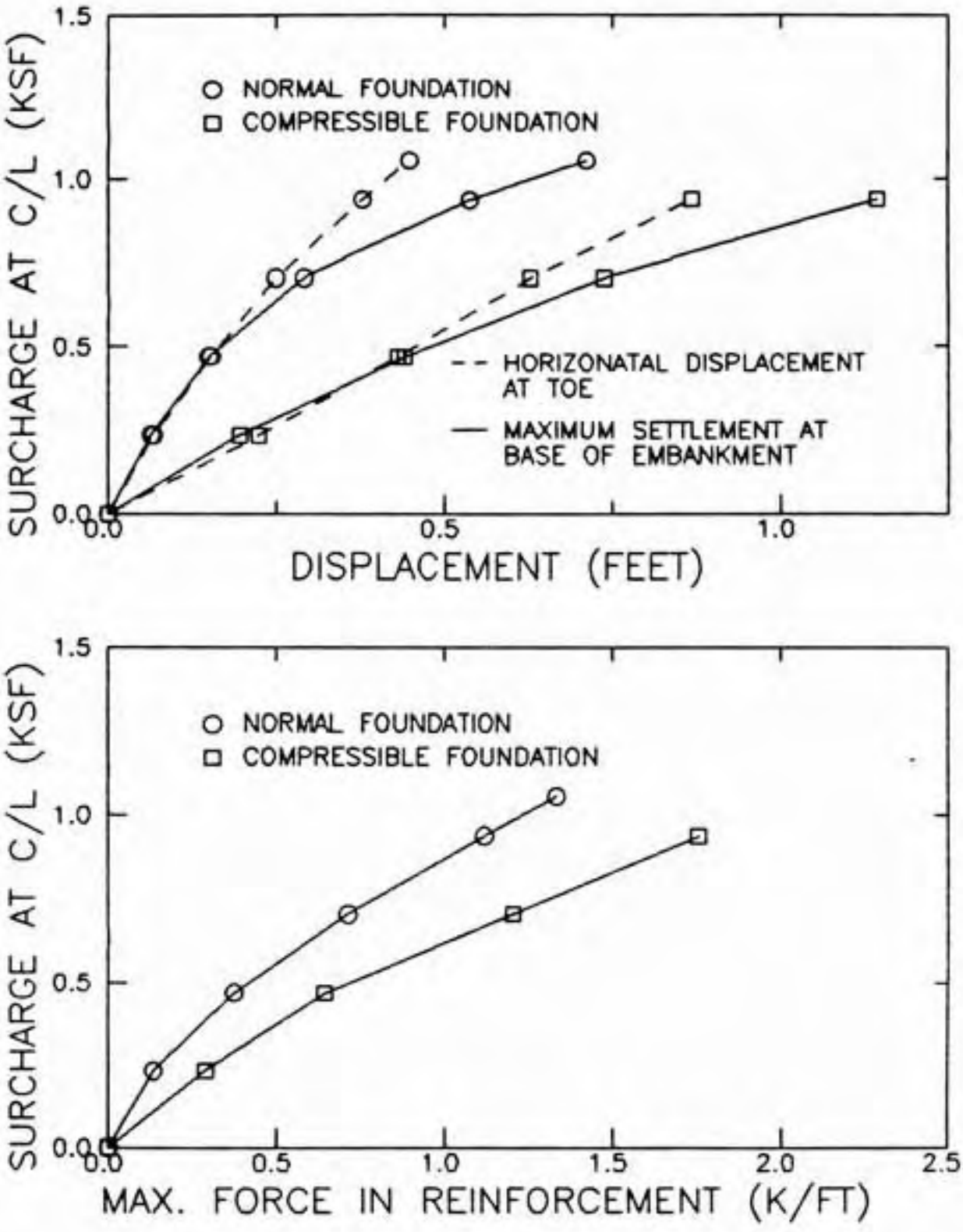

Figure 5.23 Comparison of displacements and maximum force in reinforcement for embankment on normal and compressible foundations, 30-ft thick foundation, weak crust.

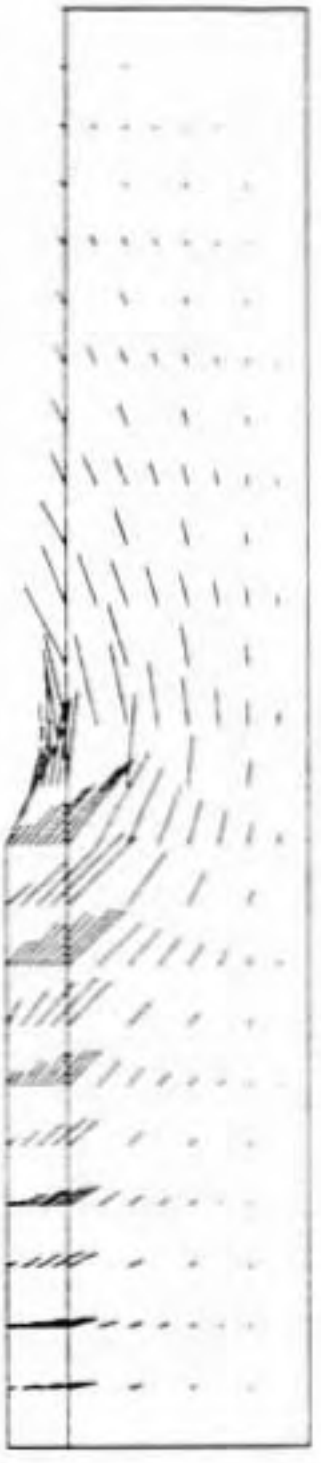

Figure 5.24 Displacement vectors for reinforced embankment on compressible foundation, 30-ft thick foundation, weak crust.

5.4.5 Effect of Foundation Thickness

The effect of foundation thickness was studied. Displacements for 15, 30, and 60-ft thick foundations with a strong crust are compared in Fig. 5.25 and on 15 and 30-ft thick foundations with a weak crust in Fig. 5.26. Horizontal displacements at the toe and maximum settlement at the base are larger for deeper foundations at low surcharges but approach similar values near failure. Displacement vectors at failure for the strong crust cases are compared in Fig. 5.27. The pattern of movement near the toe is similar for all three depths but for the thicker foundations larger movements occur beneath the central portion of the embankment and at greater distances from the toe. Horizontal displacements in the foundation along several vertical sections for thicknesses of 15 and 30 ft and a weak crust are compared in Fig. 5.28. For both thicknesses the largest movements occur in the upper 10 ft.

The maximum force in the reinforcement versus surcharge at the centerline are compared in Fig. 5.29. For a given surcharge slightly higher forces develop for thinner foundations.

The relative increase in surcharge made possible by reinforcement for the three thicknesses are shown in Table

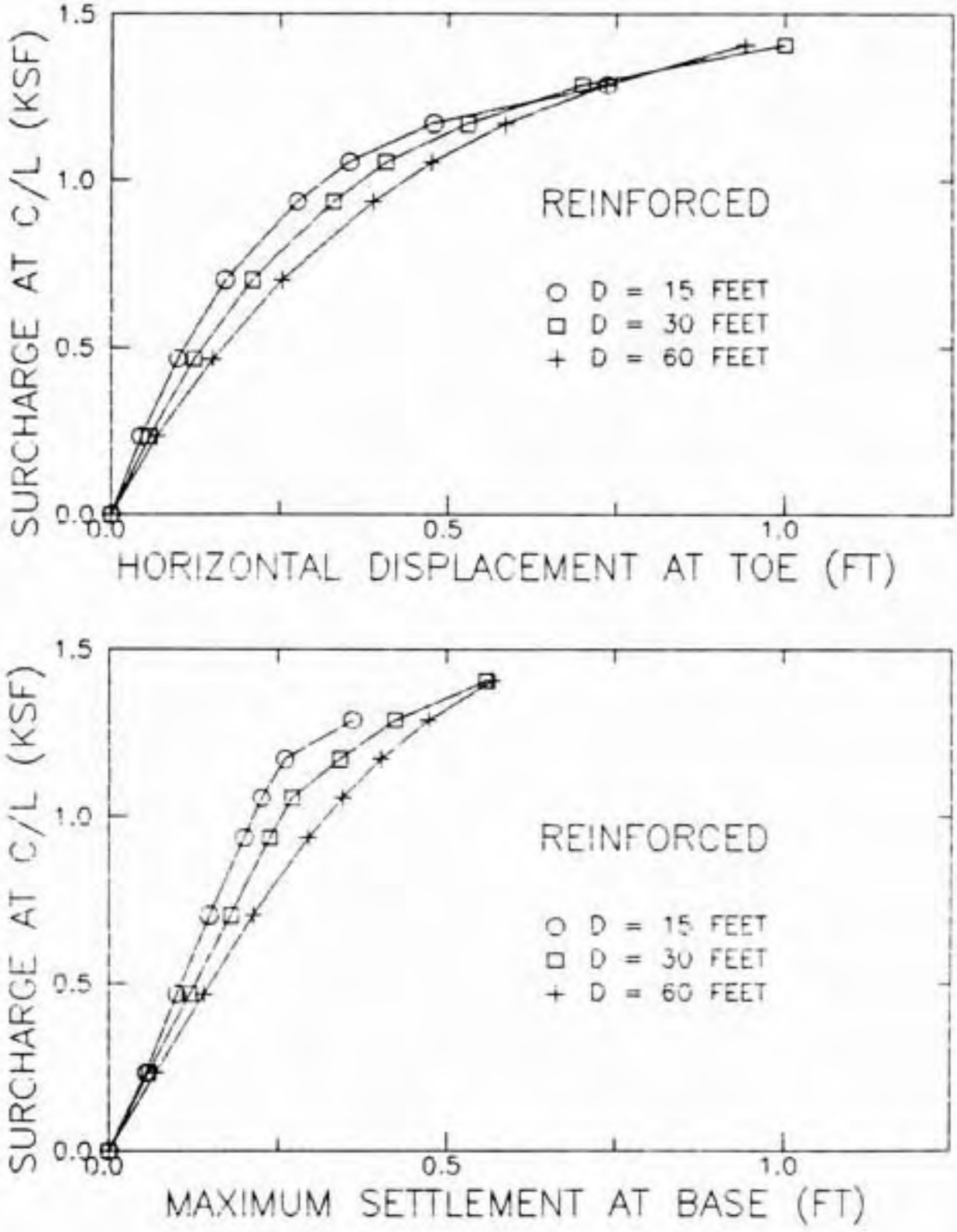

Figure 5.25 Effect of foundation thickness on horizontal displacement at toe and maximum settlement at base of embankment for reinforced embankment on strong crust.

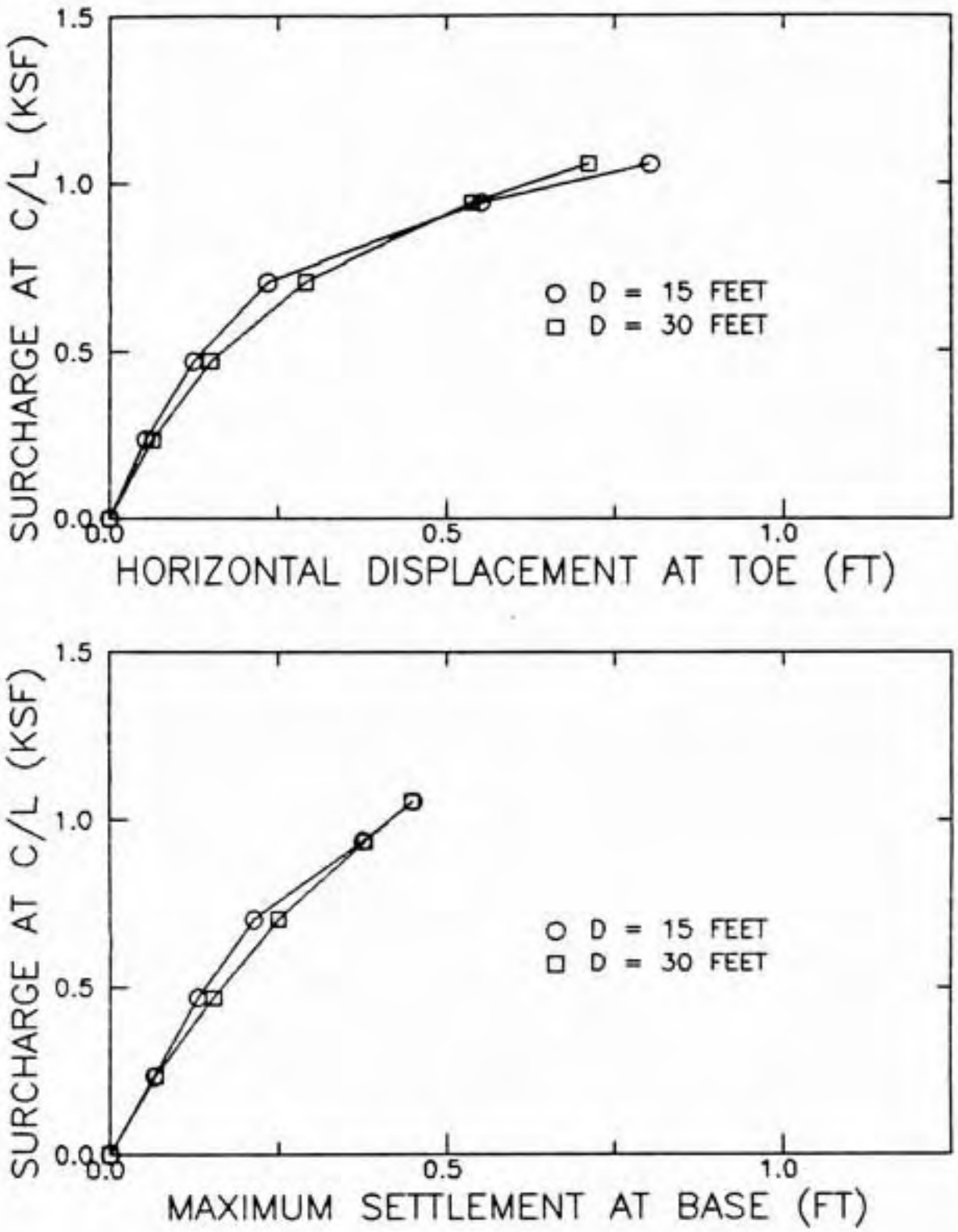

Figure 5.26 Effect of foundation thickness on horizontal displacement at toe and maximum settlement for reinforced embankment on weak crust.

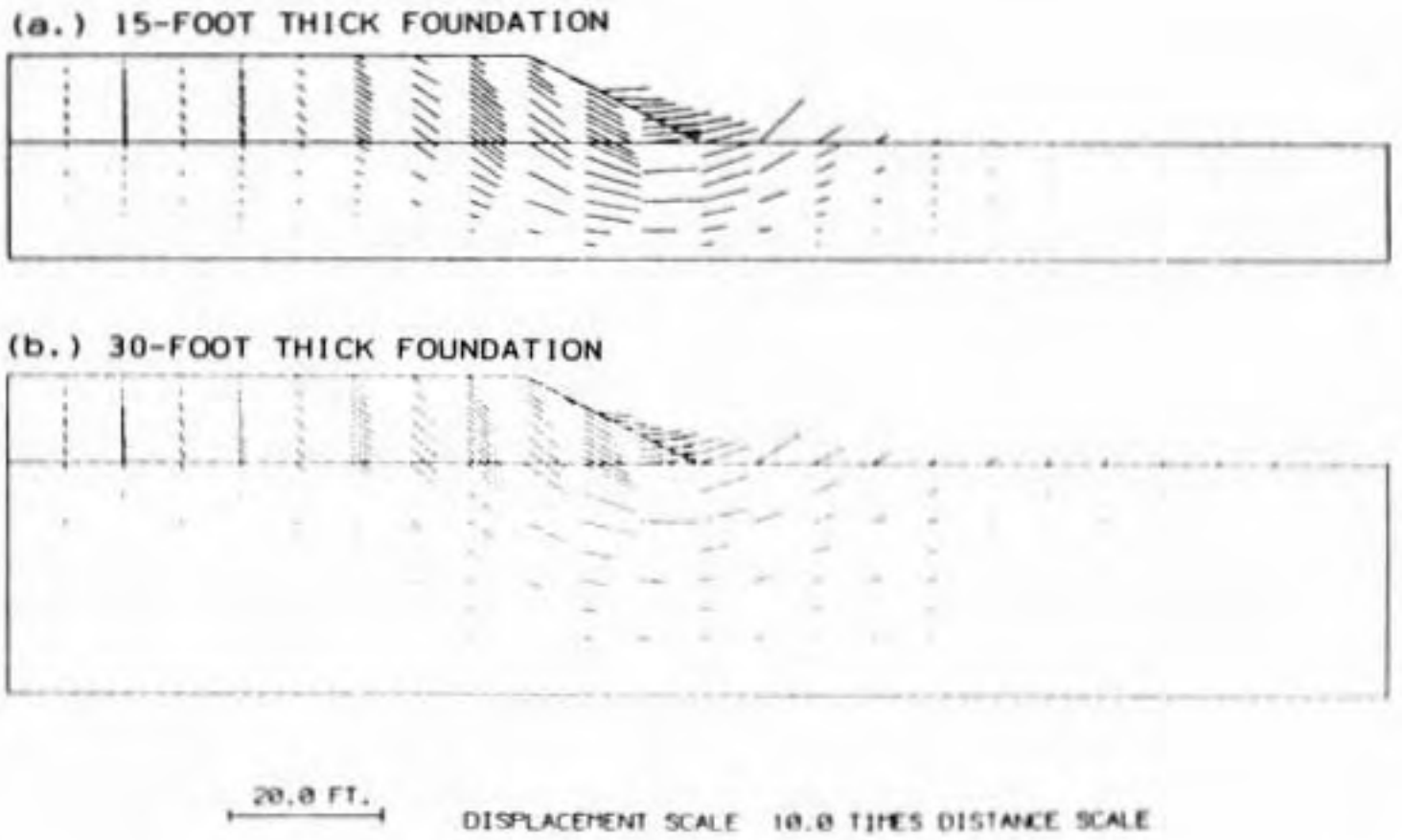

Figure 5.27 Effect of foundation thickness on displacement vectors for reinforced embankment on strong crust.

(c.) 60-FOOT THICK FOUNDATION

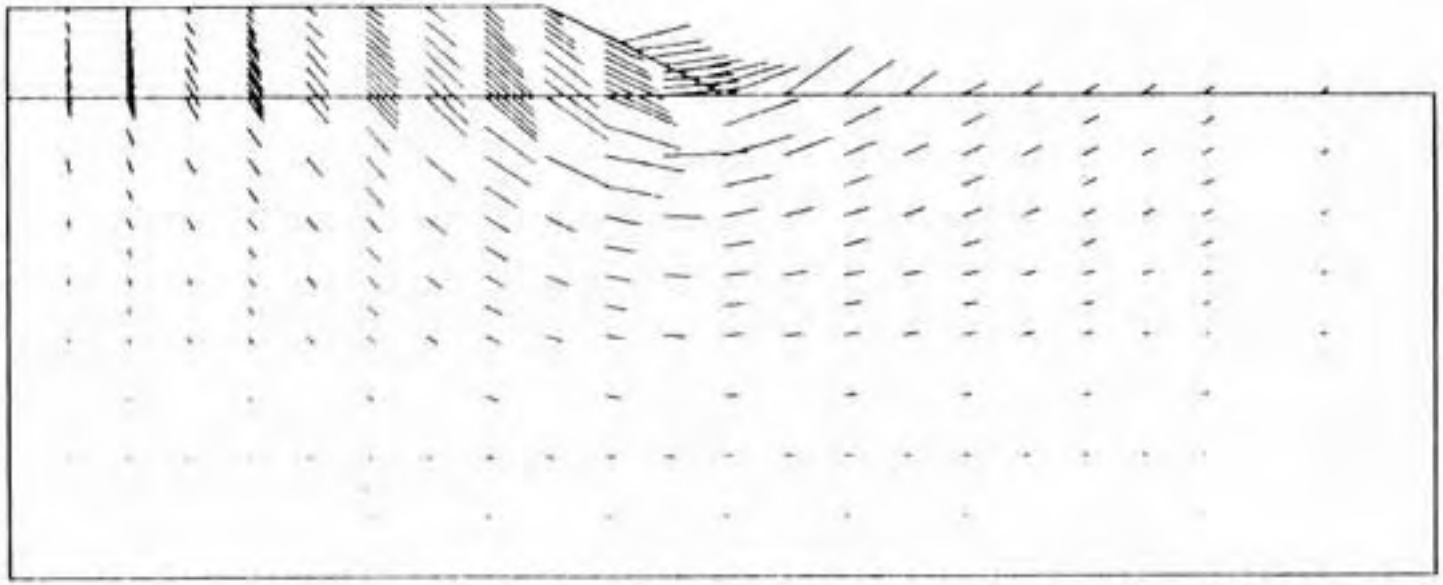

20.0 FT. DISPLACEMENT SCALE 10.0 TIMES DISTANCE SCALE

Figure 5.27. continued.

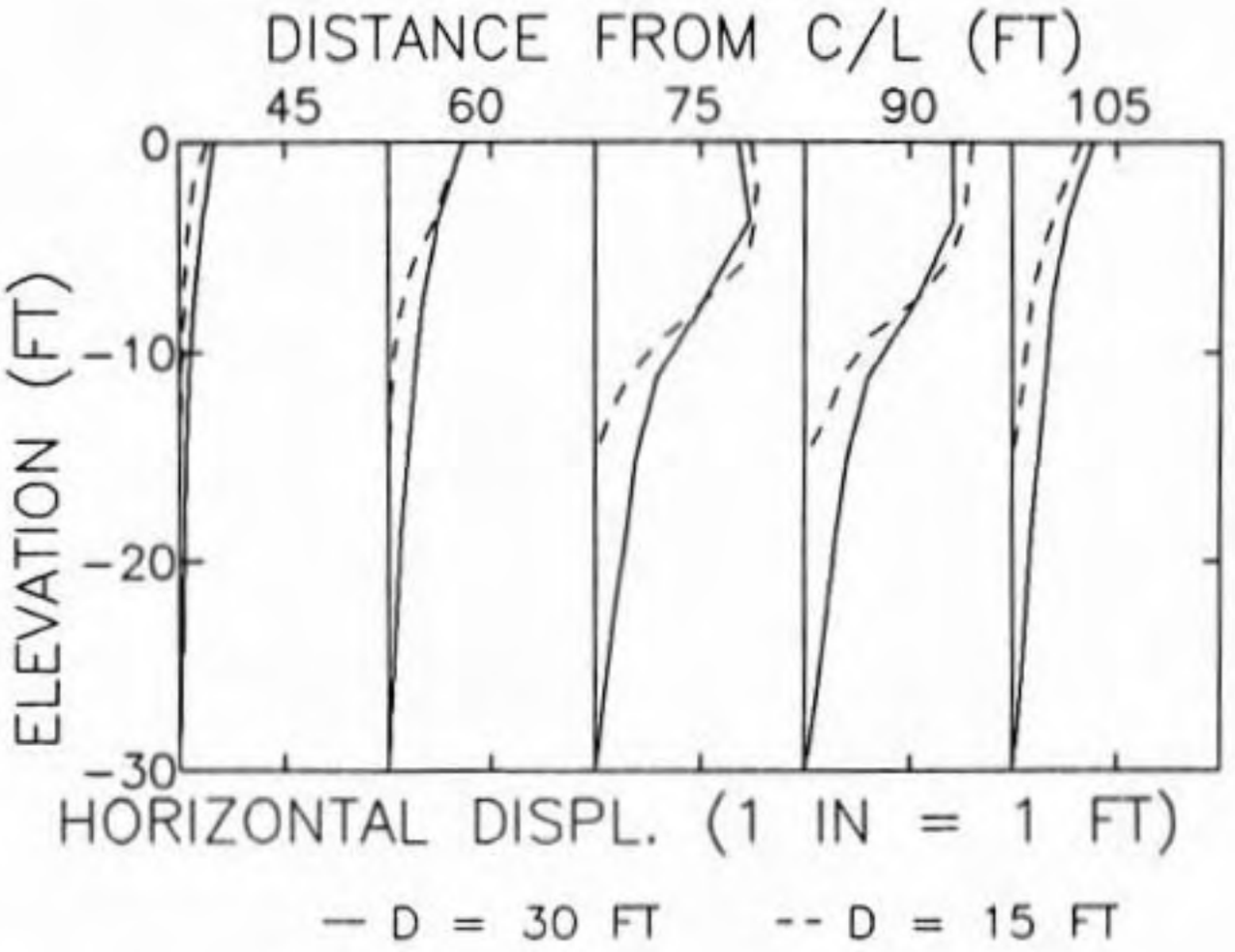

Figure 5.28 Effect of foundation thickness on horizontal displacement profiles for reinforced embankment on weak crust.

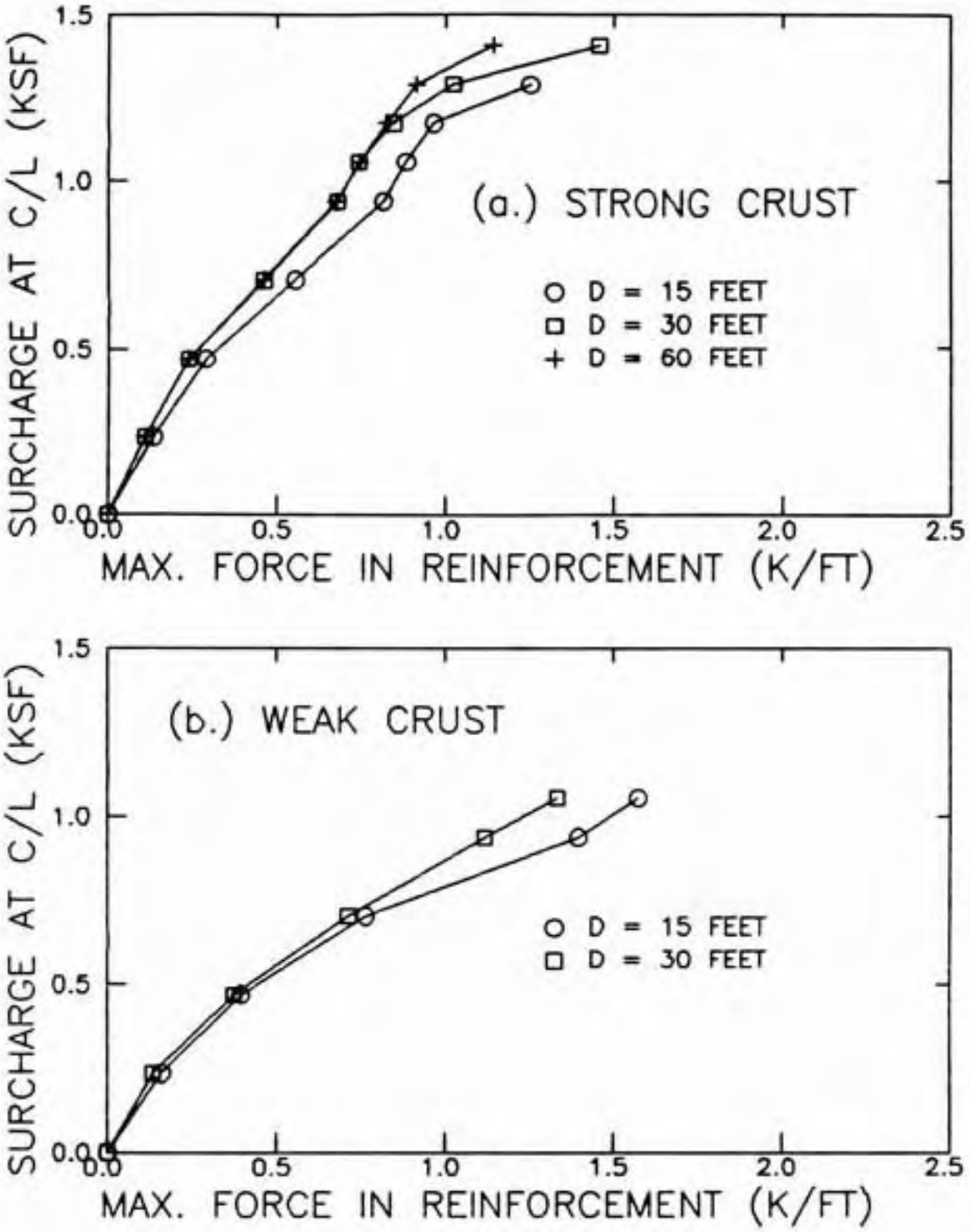

Figure 5.29 Effect of foundation thickness on maximum force in reinforcement, strong and weak crusts.

5.10. It is seen that the beneficial effect of reinforcement increases slightly as the thickness increases.

Table 5.10
Relative increase in surcharge made possible by reinforcement for foundation thicknesses of 15, 30, and 60 ft.

Foundation thickness	Crust strength		
	Strong	Weak	None
15	5%	15%	60%
30	7%	22%	70%
60	9%	---	---

In summary, the effect of foundation depth on reinforced and unreinforced embankment behavior is small.

5.4.6 Effect of Embankment Width

The effect of embankment width was examined for base widths of 120 and 180 ft for the 2h:1v side slope, 30-ft deep foundation, strong crust case only. For the reinforced embankment there was almost no effect on displacements or the maximum force in the reinforcement as shown in Fig. 5.30. Similarly, there was almost no effect on displacements for unreinforced embankments. The relative increase in surcharge made possible by reinforcement for the 120-ft width was 6% compared to 7% for the 180-ft width. Therefore, base width has little effect on behavior for widths between 120 and 180 ft.

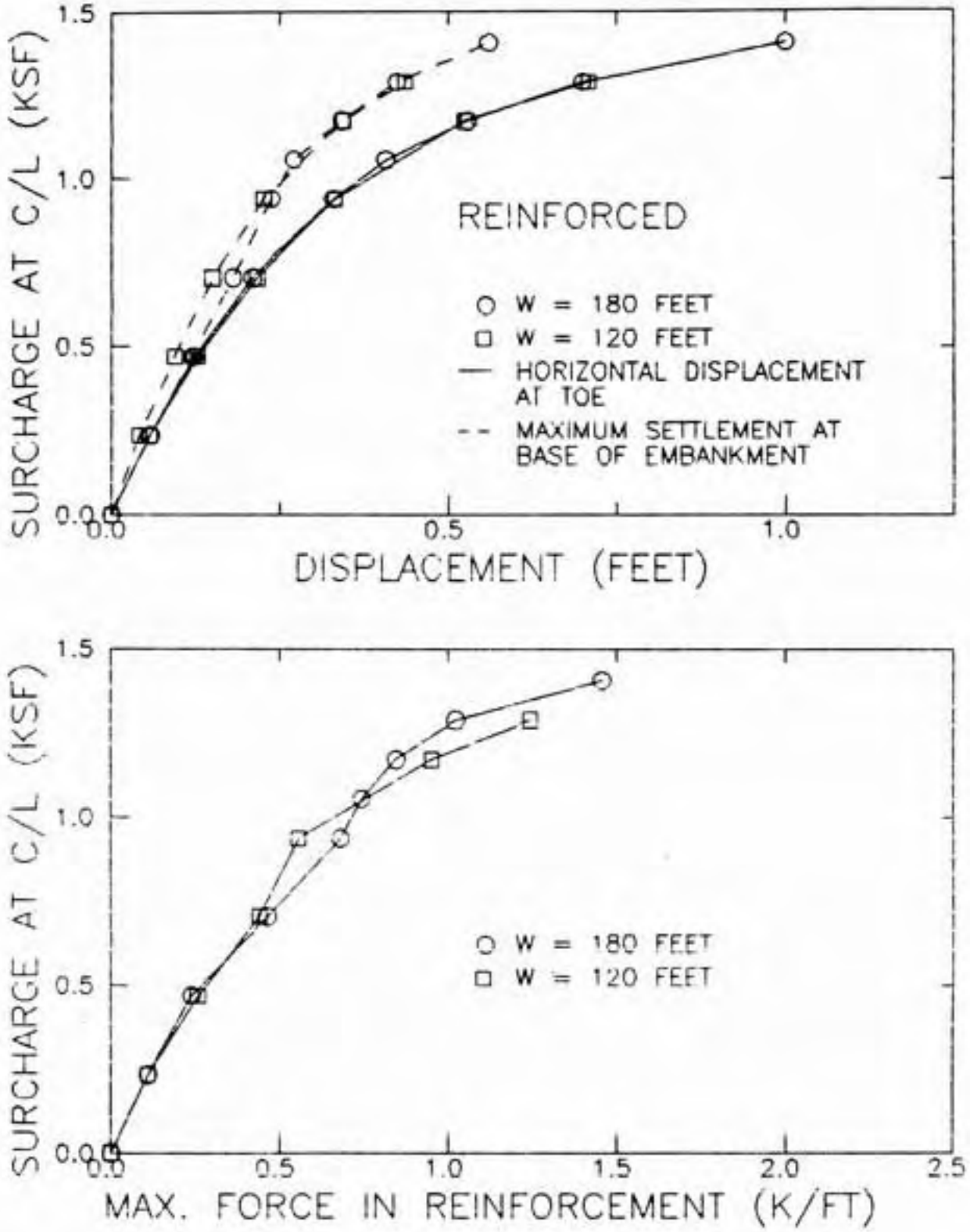

Figure 5.30 Effect of embankment width on displacements and maximum force in reinforcement for reinforced embankment, 30-ft thick foundation, strong crust.

5.4.7 Effect of Embankment Side Slope

Behavior of 180-ft base width embankments with side slopes of 2h:1v and 3h:1v were compared for the 30-ft deep foundation with strong and no crusts. Displacements of the reinforced embankments and maximum force in the reinforcement are compared in Fig. 5.31 for the strong crust case and in Fig. 5.32 for the no crust case. Displacements and the maximum force are greater for the steeper slope. The difference increases as the surcharge increases. The relative increase in surcharge made possible by reinforcement were 7% for both side slopes for the strong crust case. For the no crust case it was 70% for the 2h:1v slope and 53% for the 3h:1v slope. Hence, reinforcement is more beneficial for steeper embankment side slopes at least for the no crust case.

5.4.8 Summary

The height at failure, reinforcement force at failure, and relative increase in surcharge made possible by reinforcement for the 15 cases analyzed are summarized in Table 5.11. Failure heights ranged from 2.8 ft for no crust to 11.3 ft for a strong crust. The relative increase in surcharge made possible by reinforcement ranged from 5 to 70%. Crust strength was found to be the most important factor governing embankment behavior. The height at failure of

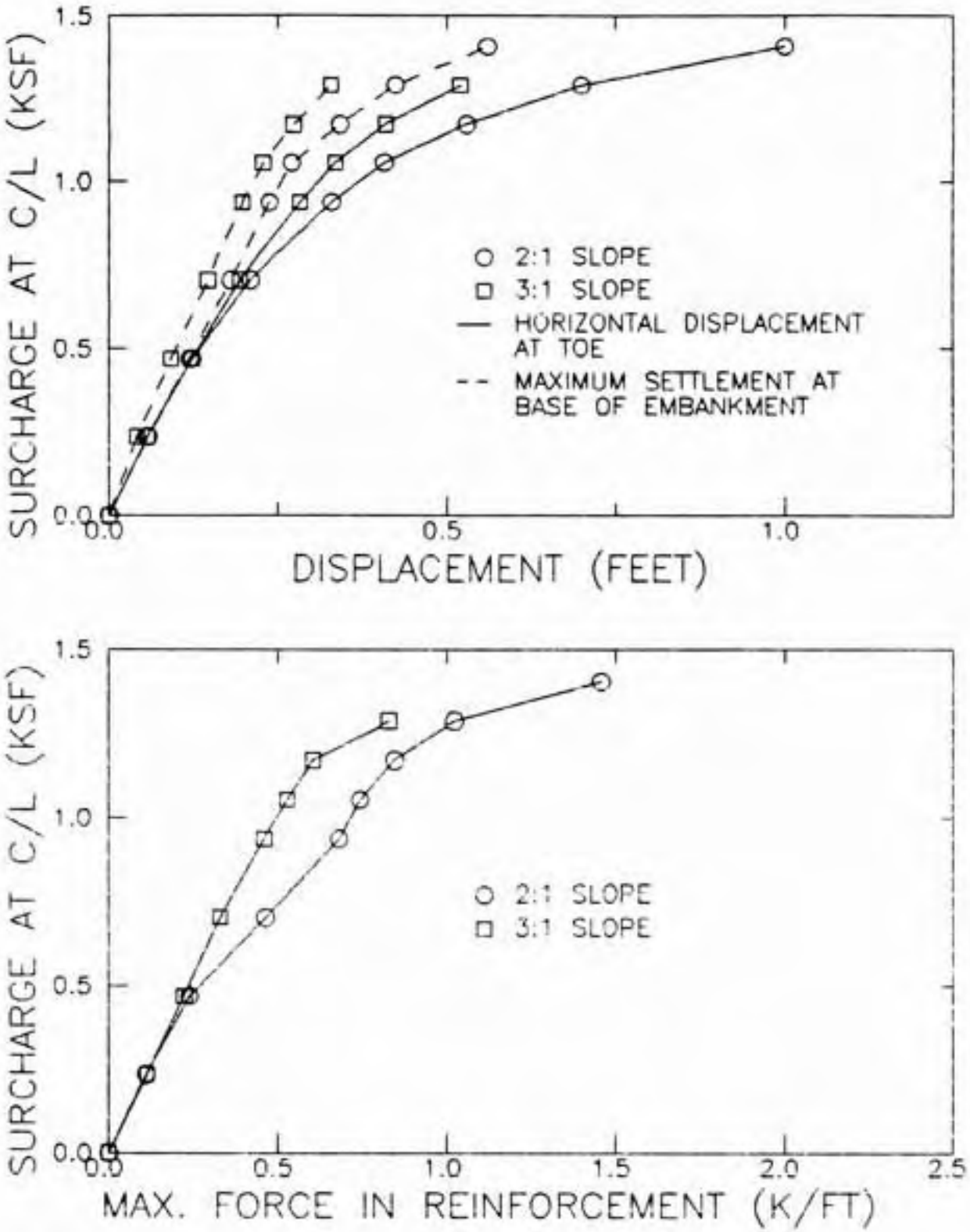

Figure 5.31 Effect of side slope on displacements and maximum force in reinforcement for reinforced embankment, 30-ft thick foundation, strong crust.

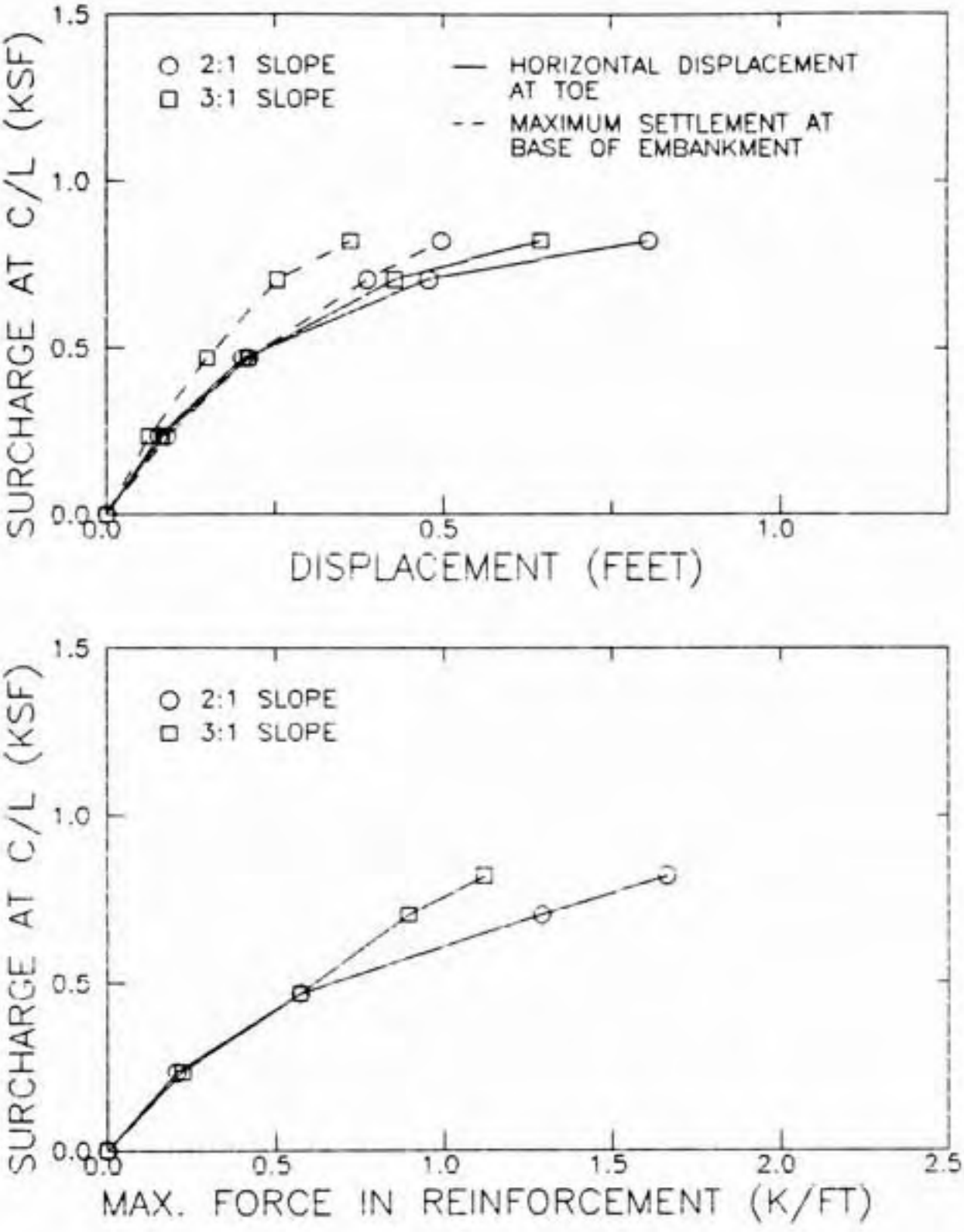

Figure 5.32 Effect of side slope on displacements and maximum force in reinforcement for reinforced embankment, 30-ft thick foundation, no crust.

Table 5.11
Summary of results of analysis.

Base Width (ft)	Side Slope (h:v)	Fnd Depth (ft)	Crust Strength ---	Special Case ----	-Ht. at Failure- Unreinf. (ft)	Reinf. (ft)	Reinf. Force at Failure (k/ft)	Relative Increase in Surcharge
180	2:1	15	Strong		9.4	10.3	1.3	5%
180	2:1	15	Weak		6.6	8.4	1.6	15%
180	2:1	15	None		2.8	4.7	1.0	60%
180	2:1	30	Strong		8.4	11.3	1.5	7%
180	2:1	30	Weak		7.5	8.4	1.3	22%
180	2:1	30	None		3.8	6.6	1.7	70%
180	2:1	60	Strong		11.3	11.3	1.1	9%
180	2:1	30	Strong	(1)	8.4	8.4	1.4	22%
180	2:1	30	Weak	(1)	6.6	7.5	1.8	29%
180	2:1	30	None	(1)	2.8	2.8	0.6	50%
180	2:1	30	Strong	(2)	8.4	9.4	1.2	10%
180	2:1	30	Strong	(3)	8.4	8.4	0.9	12%
180	3:1	30	Strong		9.4	10.3	0.8	7%
180	3:1	30	None		3.8	6.6	1.1	53%
120	2:1	30	Strong		7.5	10.3	1.2	6%

Special Cases:
(1) Compressible foundation
(2) Weak pocket at toe
(3) Weak pocket beneath slope

both reinforced and unreinforced embankments decreased with crust strength. The beneficial effect of reinforcement increased significantly as the crust strength decreased. A pocket of normally consolidated soil in an otherwise strong crust had only a small effect. Deformations were greater for a compressible foundation and reinforcement was effective for the strong, weak, and no crust cases. The effect of foundation depth was small but reinforcement was slightly more beneficial for deeper foundations. Embankment base widths of 120 and 180 ft had an insignificant influence on behavior. Reinforcement was slightly more effective for steeper side slopes.

The maximum reinforcement force at failure ranged from 0.6 k/ft to 1.8 k/ft (50 lb/in. to 150 lb/in.; 9 kN/m to 26 kN/m) (Table 5.11). This is less than the ultimate strength of typical woven geotextiles and geogrids. It indicates that the strength of the embankment fill and foundation soils are fully mobilized and failure occurs before there are sufficient deformations to develop the reinforcement's tensile strength.

There was no discernible relation between the maximum reinforcement force at failure and foundation properties or embankment geometry. This may be due in part to details of the analysis technique which affected the height at which

the FE solution failed to converge as discussed in Section 5.2.7. Comparing the maximum reinforcing force at equal surcharge, the force increased as crust strength decreased and was higher for the compressible foundation and steeper side slope. It also was slightly higher for shallower foundations but base width had an insignificant effect.

5.5 COMPARISON WITH BEHAVIOR PREDICTED BY OTHERS

The results of the present study were compared to other finite element studies reported in the literature. The purpose was to identify similarities and differences between this work and previous studies. Comparisons were made with analyses by Rowe (1982), a design method proposed by Rowe and Soderman (1985a), analyses by Boutrup and Holtz (1982) and analyses with the cap model by McCarron (1985).

5.5.1 Comparison with Rowe (1982)

Rowe (1982) made an FE analysis to study the effect of foundation properties and fabric modulus using the same geometry as the Pinto Pass test embankment (Fowler, 1981, 1982; Fowler and Haliburton, 1980; Haliburton, et al., 1978). The embankment was 7.9 ft high with a 172-ft wide base and 10h:1v side slopes founded on very soft, highly plastic clays and loose clayey fine sands and silts which extend to depths of 32 to 39 ft. A single layer of

reinforcement was placed at the base of the embankment. In the analysis the soil was assumed to be elastic-plastic with a Mohr-Coulomb failure criterion. Rowe compared calculated responses for the two profiles in Table 5.12. The profile numbers are the same as used by Rowe. Profile 2 has a lower modulus and the soft soils extend to greater depths than in profile 4. Conditions are undrained except as noted for profile 4 in Table 5.12. To facilitate comparisons with this study the equivalent elastic moduli are also shown. They were calculated for $\nu' = 0.3$ using (Wroth and Houlsby, 1985; Chen and Saleeb, 1982)

$$E = E_u \, [2(1+\nu')/3] \tag{5.4}$$

$$K = E \, / \, [3(1-2\nu')] \tag{5.5}$$

$$G = E \, / \, [2(1+\nu')] \tag{5.6}$$

Comparison of the undrained shear strengths in Table 5.12 with those for the no crust case in Fig. 5.5 shows that the values for profile 2 and 4 are slightly less than those used in this study with the difference increasing with depth. The moduli used in this study for the no crust, compressible foundation case are smaller than Rowe's values for shallow depths but lie between the values for profiles 2 and 4 at greater depths. Thus, the properties of the foundation soils used by Rowe and in the present study are similar.

Table 5.12
Soil Profiles for Pinto Pass test embankment.

Depth	Profile 2				Profile 4				
	s_u	E_u	K	G	s_u	ϕ	E_u	K	G
(ft)	(ksf)					($^\circ$)	(ksf)		
0.0- 2.0	0.05	2.5	1.8	0.8	0.05	0	7.3	5.3	2.4
2.0- 4.9	0.05	3.8	2.7	1.3	0.05	0	7.3	5.3	2.4
4.9- 7.9	0.10	5.0	3.6	1.7	0.07	0	10.4	7.5	3.5
7.9-11.8	0.10	6.3	4.5	2.1	0.10	0	14.6	10.6	4.9
11.8-18.0	0.15	8.1	5.9	2.7	0.01	35	*	95.7	44.2
18.0-24.9	0.28	10.4	7.5	3.5	0.01	35	*	121.8	56.2
24.9-32.0	0.35	12.5	9.1	4.2	0.35	0	146.2	105.6	48.7

* Layer is drained; actual drained K and G corresponding to $\nu' = 0.3$ are given

Note: $\phi = 0$ for profile 2

Rowe reported results for several fabric moduli but only results for a modulus of 85.7 k/ft (7100 lb/in.; 1250 kN/m), which is somewhat higher than the value used in the present study, are reviewed here. The largest settlements were calculated at the centerline and horizontal displacements were greater 50 ft from the centerline than at the toe (86 ft from centerline). The reduction in displacements due to the reinforcement at an embankment height of 7.9 ft are summarized in Table 5.13. The benefit from using reinforcement was greater for profile 2 which was deeper and had a lower modulus. Reinforcement had a larger effect on horizontal displacements than on settlements. The maximum force in the reinforcement was 1.8 k/ft (150 lb/in.; 26 kN/m) for profile 2 and 0.8 k/ft (67 lb/in.; 12 kN/m) for profile 4. Reinforcement reduced the extent of the plastic region in the foundation and the effect was greater for profile 2 than for profile 4.

Table 5.13
Summary of reductions in displacements due to reinforcement with modulus of 85.7 k/ft.

	Profile 2	Profile 4
Settlement		
at centerline	8%	3%
50 ft from centerline	2%	1%
Horizontal movement		
50 ft from centerline	40%	35%
at toe	20%	15%

Direct comparison of the results from Rowe (1982) and the present study are not possible because of the much flatter side slopes analyzed by Rowe but there is general agreement. His results show that reinforcement was more beneficial for the more compressible foundation and that reinforcement had a greater effect on horizontal displacements than vertical settlement. Rowe (1982) and the present study both found that reinforcement reduced the extent of the plastic zone in the foundation. The magnitude of the force in the reinforcement is similar to the no crust, compressible foundation case from the present study.

5.5.2 Comparison with Rowe and Soderman (1985a)

Rowe and Soderman (1985a) made an extensive finite element study to develop an approximate procedure to estimate the allowable reinforcement strain at embankment collapse. They termed this the "allowable compatible strain", ε_a. It is defined as the maximum horizontal strain at the base of an unreinforced embankment just prior to collapse. They found that ε_a was related to a dimensionless parameter Ω as shown in Fig. 5.33. Ω is defined as

$$\Omega = (\gamma_f H_c / s_u)(s_u / E_u)(D/B)_e^2 \qquad (5.7)$$

where γ_f = unit weight of embankment fill

H_c = height of unreinforced embankment at collapse

s_u = undrained shear strength of foundation soil

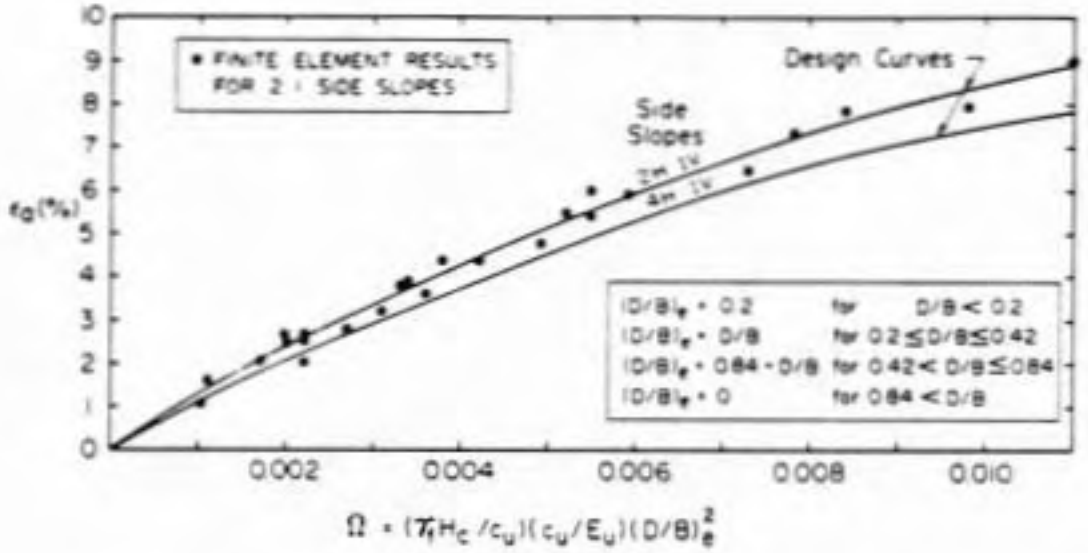

Figure 5.33 Allowable compatible strain ε_a vs. dimension less Ω (Rowe and Soderman, 1985a).

E_u = undrained Young's modulus of the foundation soil

and $(D/B)_e$ is the effective ratio of the depth of the foundation soil to the crest width. A consistent relationship between ε_a and Ω was obtained when the ratio was taken as

$$(D/B)_e = 0.2, \qquad D/B < 0.2 \qquad (5.8a)$$

$$(D/B)_e = D/B, \qquad 0.2 \leq D/B \leq 0.42 \qquad (5.8b)$$

$$(D/B)_e = 0.84 - D/B, \qquad 0.42 < D/B \leq 0.84 \qquad (5.8c)$$

$$(D/B)_e = 0, \qquad 0.84 < D/B \qquad (5.8d)$$

where D = depth of the soft foundation soil

B = embankment crest width

Eq. 5.8a applies to embankments that are wide relative to their foundation depth and only the outer portion of the embankment is involved in the failure. For the range governed by Eq. 5.8b increasing D/B increases ε_a. The largest $(D/B)_e$ is 0.42. It is obtained for D/B = 0.42 (Eq. 5.8b or 5.8c). For D/B greater than 0.42 (Eq. 5.8c) the horizontal component of displacement at the base of the embankment decreases, hence, ε_a decreases. Finally, for large D/B in excess of 0.84 (Eq. 5.7d) reinforcement has no effect because deep seated bearing capacity failure controls.

Comparison of their results with the present study requires proper choice of a representative s_u and E_u. In the present study, the properties of the upper 7.5 ft of foundation soil (i.e., the crust) had the dominant influence on embankment behavior. Therefore, s_u and E_u were taken to be the average values in this zone. E_u was related to the drained elastic moduli using Eqs. 5.4, 5.5, and 5.6. D/B was less than 0.2 for most cases so $(D/B)_e$ = 0.2 (Eq. 5.8a). For the few cases with D/B greater than 0.2, it is felt that $(D/B)_e$ is still 0.2 because the increasing strength and modulus with depth reduced the effective D. The procedure developed by Rowe and Soderman (1985a) was used with $(D/B)_e$ = 0.2 for all cases to obtain ε_a. The allowable force was calculated for a reinforcement modulus of 60 k/ft (5000 lb/in.; 880 kN/m) and is compared to the force at failure obtained with PS-NFAP in Table 5.14. Except for the compressible foundation, the force in the reinforcement by Rowe and Soderman was within -53% to +60% of the value at failure calculated with PS-NFAP with an average difference of -6%. Some of the scatter may be due to numerical factors of the PS-NFAP solution which influence the height at failure as discussed in Section 5.2.7. Rowe and Soderman's procedure overestimated the force for the compressible foundation cases but the moduli were smaller that the range included in their study. Also shown in Table 5.14 are ε_a determined using Rowe and Soderman's definition from unreinforced

Table 5.14
Comparison of forces in reinforcement calculated with Rowe and Soderman (1985a) and PS-NFAP.

Base Width	Side Slope	Fnd Depth	Crust Strength	Rowe and Soderman Ω	Rowe and Soderman ϵ_a	Rowe and Soderman F_R	PS-NFAP F_R	% DIFF.	PS-NFAP ϵ_a
(ft)	(h:v)	(ft)	---	---	(%)	(k/ft)	(k/ft)	(%)	(%)
180	2:1	15	Strong	0.0018	2.2	1.3	1.3	0	2.5
180	2:1	15	Weak	0.0017	2.2	1.3	1.6	-19	3.7
180	2:1	15	None	0.0008	1.1	0.7	1.0	-30	2.2
180	2:1	30	Strong	0.0016	2.0	1.2	1.5	-20	1.7
180	2:1	30	Weak	0.0019	2.3	1.4	1.3	+8	4.1
180	2:1	30	None	0.0011	1.4	0.8	1.7	-53	5.2
180	2:1	60	Strong	0.0022	2.5	1.5	1.1	+36	2.1
180	2:1	30	Strong(1)	0.0062	6.1	3.7	1.4	+230	4.9
180	2:1	30	Weak (1)	0.0063	6.1	3.7	1.8	+105	6.5
180	2:1	30	None (1)	0.0030	3.3	2.0	0.6	+233	4.9
180	3:1	30	Strong	0.0018	2.1	1.3	0.8	+60	1.3
180	3:1	30	None	0.0011	1.2	0.7	1.1	-36	6.6
120	2:1	30	Strong	0.0014	1.8	1.1	1.2	-8	1.3

Special case:
(1) Compressible foundation

embankments analyzed with PS-NFAP. These values are much higher than those reported by Rowe and Soderman and would have overestimated the force in the reinforcement at failure.

5.5.3 Comparison with Boutrup and Holtz (1982)

Boutrup and Holtz (1982, 1983) used the FEM to analyze a 4.5-ft high test embankment described by Bell, et al. (1977). It had 1h:1v side slopes and a 22-ft base width on a 9-ft deep foundation. The foundation soils were modeled as a von Mises elasto-plastic material (Chen and Saleeb, 1982). Two cases of undrained loading were considered: a stiff foundation with E_u = 30 ksf and s_u = 0.15 ksf, and a soft foundation with E_u = 3 ksf and s_u = 0.15 ksf. The foundation soil was undrained so ν = 0.48 was used. The properties of the stiff foundation are similar to the weak crust, normal compressibility case (s_u in crust = 0.125 ksf and average equivalent E_u in crust = 20 ksf) of the present study and the soft foundation are similar to the weak crust, compressible foundation case (s_u = 0.125 ksf and average equivalent E_u in crust = 5 ksf). Reinforcement moduli of 6, 10, and 20 k/ft were analyzed.

They found that there was no plastic yield in the foundation at an embankment height of 4.5 ft for either set of foundation properties. Therefore, foundation response was

elastic in contrast to the present study where significant yielding occurred.

One effect of reinforcement was to alter the maximum shear stress in the foundation. For the stiff foundation and reinforcement modulus = 20 k/ft (1700 lb/in.; 290 kN/m) it was reduced by a maximum of 12% near the toe with smaller reductions elsewhere. This pattern is consistent with the results of the present study (Fig. 5.12). For the soft foundation the maximum shear stress was reduced in most of the foundation with the maximum reduction beneath the centerline. However, immediately beneath the toe the maximum shear stress was increased. Greater changes occurred with the higher modulus reinforcement.

Reinforcement reduced settlement beneath the embankment and heave beyond the toe as was found for the present study (Fig. 5.9). Horizontal displacements were also reduced. Again, the higher modulus reinforcement provided greater benefit.

5.5.4 Comparison with McCarron (1985)

McCarron (1985) performed FE analyses with the cap model using the computer program NFAP with the input parameters and embankment geometries discussed in Section 5.3.1. The validity of the results is limited primarily because

improved methods to determine the cap input parameters (Chapter 4) were not available. Nonetheless, it is of interest to compare his results to the present study. He found that the relative increase in surcharge made possible by reinforcement was 3-5% for foundation type I (Section 5.3.1), 7% for foundation type II, and 9-11% for foundation type III. This indicates that reinforcement was more beneficial for the weaker, more compressible foundation. Comparison with Table 5.11 shows that the relative increases are less than obtained in the present study. The maximum force in the reinforcement at failure were 0.76, 0.54, and 0.56 k/ft for foundation types I, II, and III, respectively. These are lower than the values in Table 5.11. McCarron found that the maximum force occurred near the embankment shoulder and that the reinforcement near the toe was unstressed as was found for the present study. Both studies showed that reinforcement reduced the extent of the plastic zone in the foundation. In summary, the present study indicates that reinforcement is more beneficial than found by McCarron. This is attributed to the reasons given in Section 5.3.1.

5.6 SUMMARY

A comparative finite element study of reinforced and unreinforced embankment behavior was made using an incremental procedure which simulated embankment construction.

Foundation behavior was represented with a strain hardening cap model. A procedure was developed to match the Mohr-Coulomb and Drucker-Prager failure criteria.

The results showed that the properties of the crust had the primary influence on embankment behavior and the potential benefit possible with reinforcement. A pocket of weak, normally consolidated soil in an otherwise strong crust had only a limited influence on embankment behavior and the benefit from using reinforcement was modest. The effect of foundation depth and embankment width was small. Reinforcement was slightly more beneficial for steeper side slopes and was very effective for compressible foundation soils.

Reinforcement increases the height at failure and reduces displacements in the foundation. The largest reduction occurs in the upper 10 ft of the foundation near the toe. It is logical that the properties of the soil in this zone (i.e. the crust) have the primary influence on embankment behavior. Reinforcement significantly reduces shear stresses in the foundation at the toe. The forces developed in the reinforcement were much less than its tensile strength. This indicates that the strength of the embankment fill and foundation soils are fully mobilized and failure occurs before there are sufficient deformations to develop the reinforcement's ultimate tensile strength.

Shear stresses at the soil-reinforcement interface were less than the interface strength so slip along this plane did not occur. The reinforcement beneath the embankment toe was unstressed.

The results of the present study are in general agreement with results reported by others. An design procedure developed by Rowe and Soderman (1985a) gave reasonable estimates of the reinforcing force at failure provided the input parameters were chosen properly.

CHAPTER 6

EMBANKMENT WIDENING

6.1 INTRODUCTION

Reinforcement has been used successfully in three field applications for widening and raising the grade of existing embankments constructed on soft ground (Lukanen and Teig, 1976; Volman, et al., 1977; Burwash, 1980) as discussed in Section 2.4.5. It is believed that the reinforcement had a significant stabilizing effect but there was insufficient data to confirm this. Furthermore, no analytic studies have been made of the problem.

In a typical application, the foundation soils are fully consolidated under the weight of the existing embankment so the foundation's undrained shear strength is increased over and above that of the natural soil. The reinforcement is usually placed over the crest and slope of the existing embankment and on the natural ground surface beneath the widened section as shown on Fig. 6.1. Additional fill for the widened and raised section is then

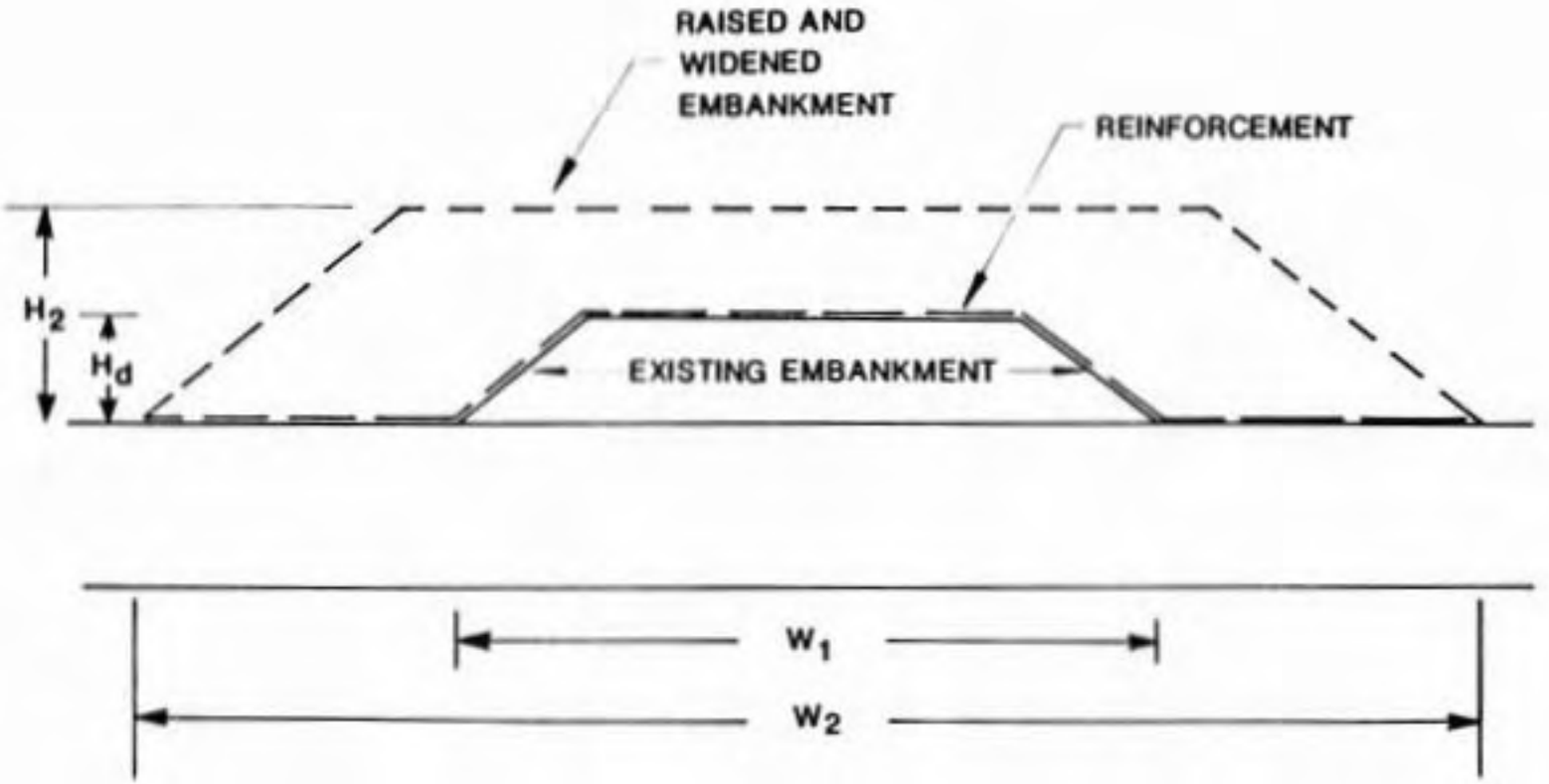

Figure 6.1 Geometry for embankment widening.

placed rapidly. Consequently, little dissipation of excess pore pressure occurs in the foundation during construction.

In this chapter FEM procedures developed to analyze embankment widening are described. Then results of a comparative study of reinforced and unreinforced embankment behavior are given including the effect of reinforcement on displacements, embankment height at failure, and state of stress in the foundation and embankment fill. Next the forces developed in the reinforcement are examined. Then the influence of existing embankment height, strength of the surface crust, and width of the widened section on behavior is presented. Finally, the results of the analysis are summarized.

6.2 ANALYSIS PROCEDURE

The effect of reinforcement on widened embankment behavior was studied using PS-NFAP with the cap soil behavior model. The analysis procedures were the same as described in Chapter 5 except for the modifications discussed in this section.

The initial state of stress and shear strength in the foundation was obtained by simulating construction of the existing embankment under drained conditions with a pore pressure response factor in the foundation of $\beta = 0.0$. This

accounted for the consolidation and increase in strength of the foundation soils under the existing embankment. The resulting $J_{2f}^{1/2}/\sigma'_{vo}$, where σ'_{vo} is the vertical stress due to the overburden and existing embankment computed by PS-NFAP, was within 2 to 5% of the value used to calibrate the cap model which was 0.339 for the strong crust case. The volumetric strains at this stage were stored and the foundation soils were switched to undrained conditions by using β = 10.0. Then, the widened and raised section was constructed. Further tendency for volumetric strain caused generation of excess pore pressure.

At the end of drained loading the state of stress beneath the existing embankment is on the cap and beyond the toe it is elastic, as shown for a typical case in Fig. 6.2a. The stress state in the embankment is elastic except for a small zone in the failure state at its shoulder. Placing the first layer of the widened section increases the horizontal stress beneath the existing embankment with little change in the vertical stress thereby reducing the shear stress and causing the state of stress to move from the cap into the elastic region, as shown in Fig. 6.2b. The stress state beneath the widened section remains on the cap except for small areas that reach the failure or corner states. The area beyond the toe of the widened section remains in the elastic state.

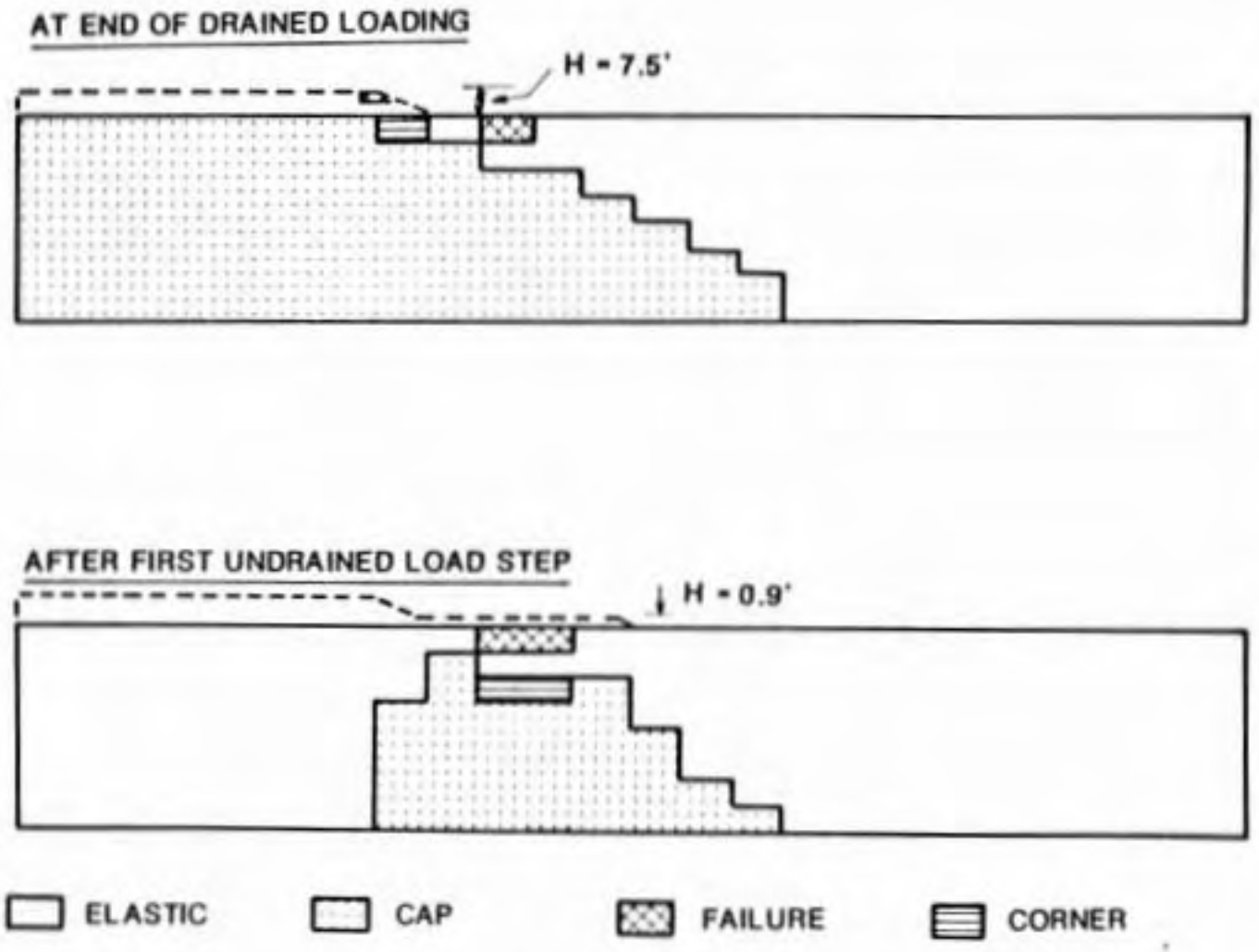

Figure 6.2 State at end of drained loading and after first undrained load step, 3.75-ft high existing embankment, 30-ft widened section, weak crust.

PS-NFAP normally bases the stiffness matrix on the stress state at the end of the previous load step. For placement of the first layer of the widened section, this would result in the elastic-plastic stiffness being used for soil beneath the existing embankment even though the deformations are elastic. This prevents the solution from converging. To avoid this problem the elastic stiffness matrix was used to calculate deformations caused by placing the first layer of the widened section. The strains for soil beneath the widened section that are not in the elastic state are slightly underestimated but the effect is small. Subsequent load steps were based on the elastic-plastic stiffness matrix.

Special procedures were developed to model the reinforcement. The reinforcement is placed on top of the existing embankment and it is assumed that no forces develop until fill is placed on top of it. To model this the reinforcement was present in the FE mesh at the beginning of the analysis but its stiffness was zero. The reinforcement was activated when the first layer of fill was placed on it and the strain at each integration point was stored. Additional strain due to subsequent load steps was used to evaluate the stiffness which was then added to the global stiffness matrix. Horizontal portions of the reinforcing layer on the original ground surface beneath the widened section and over

the crest of the existing embankment were activated just prior to placing the first layer of fill on it. The portion of the layer on the slope of the existing embankment was activated after the first layer was placed over it. The option of activating reinforcing layers at specific times could be used to analyze construction of embankments with multiple reinforcing layers, but this is beyond the scope of the present study.

6.3 CASES ANALYZED

The cases analyzed had the basic geometry shown in Fig. 6.1. The existing embankment was 120 ft wide at its base (W_1) with 2h:1v side slopes. The foundation was 30 ft thick. Existing embankment heights (H_d) of 3.75 and 7.5 ft were examined. The widened section also had 2h:1v side slopes and fill widths [$(W_2 - W_1)/2$] of 15, 30, and 45 ft were added to each side of the embankment. Horizontal, 1.875-ft thick layers of fill were added until the FE solution failed to converge. The embankment FE mesh for the 30-ft widened section is shown in Fig. 6.3. The reinforcement was located as shown in Fig. 6.1 and had a modulus of 60 k/ft, the same as was used in Chapter 5.

The embankment fill was granular and had the same cap parameters as given Table 5.2 except that κ = 0.05 ksf was used to avoid numerical difficulties experienced when

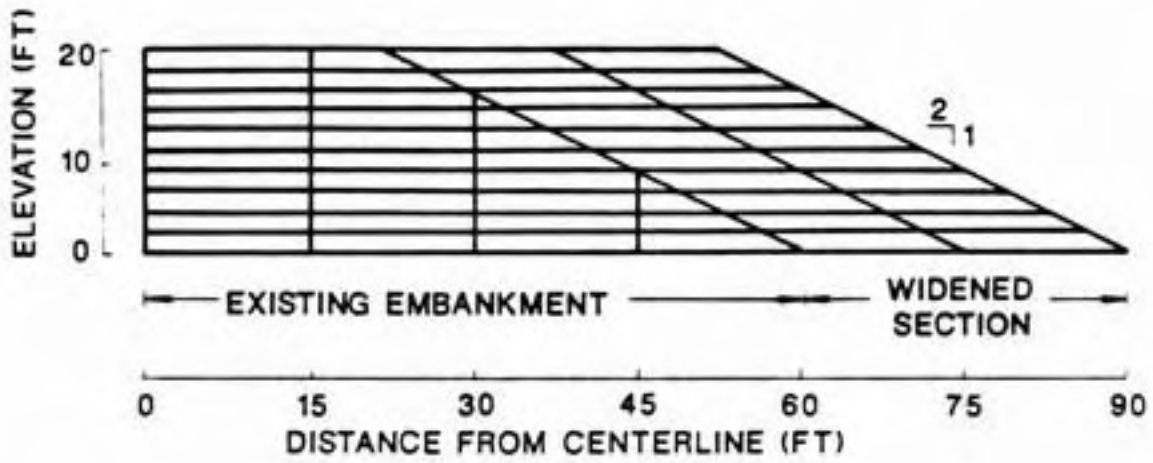

Figure 6.3 Finite element mesh for embankment widening.

κ = 0.001 ksf. This had an insignificant effect on embankment behavior. The normally consolidated foundation soils had the same cap parameters as given in Table 5.4. Strong and weak crusts were analyzed with the parameters given in Table 5.5.

6.4 BEHAVIOR OF REINFORCED EMBANKMENTS

6.4.1 Comparison of Reinforced and Unreinforced Embankment Behavior

The horizontal displacement at the toe and maximum settlement at the base of reinforced and unreinforced embankments are compared in Fig. 6.4 for a 30-ft widened section, existing embankment heights of 3.75 and 7.5 ft, and a foundation with a weak crust. The reinforcement is seen to increase the height at failure and reduce deformations. The relative increase in surcharge made possible by reinforcement (defined in Section 5.2.7) was 12% for the 3.75-ft high existing embankment and 40% for the 7.5-ft high existing embankment. The height at failure and relative increase in surcharge for all cases is summarized in Table 6.1. Failure heights for all cases ranged from 10.2 to 17.2 ft for reinforced embankments and 7.6 to 12.6 ft for unreinforced embankments. The relative increase in surcharge made possible by reinforcement ranged from 10% to 40%.

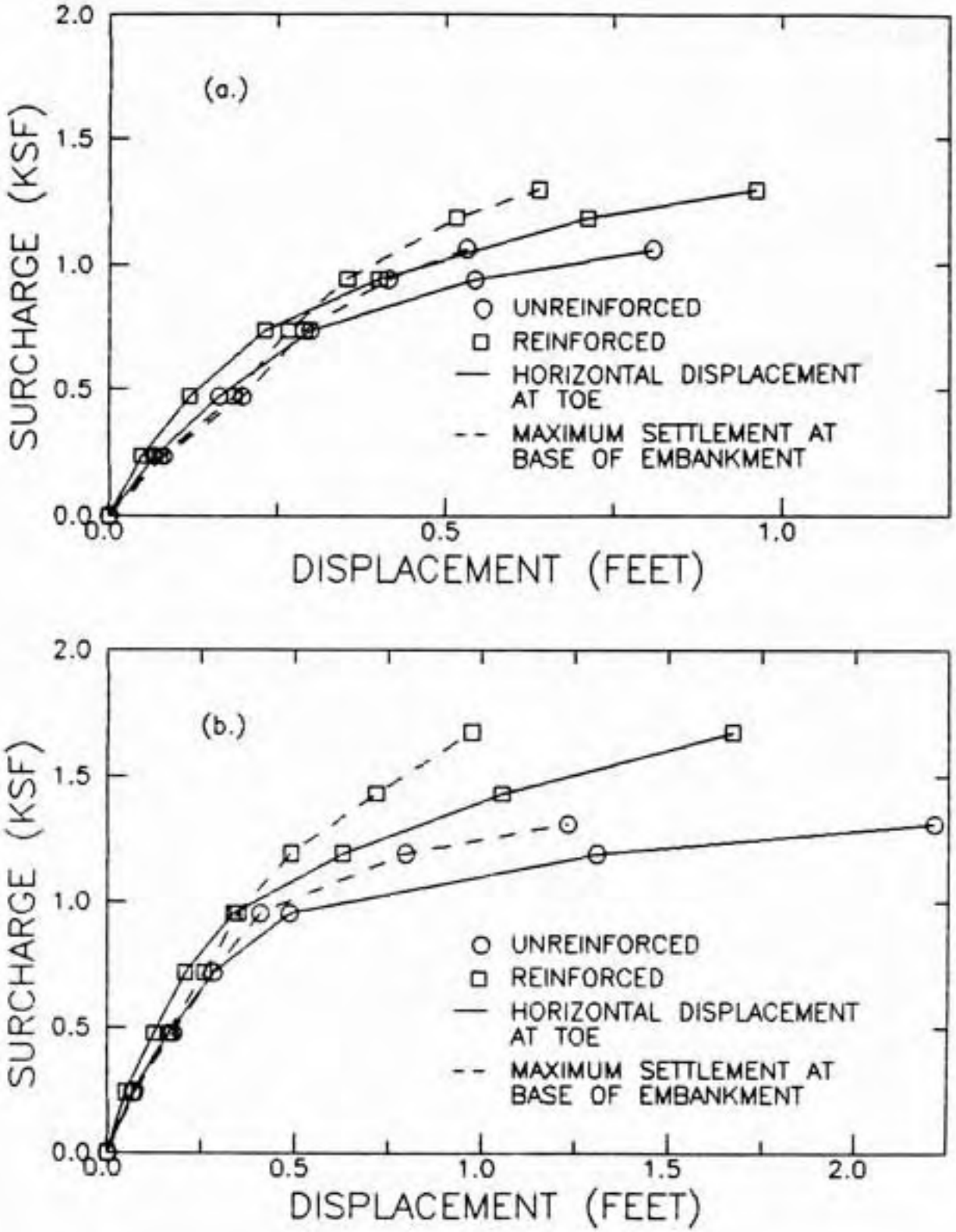

Figure 6.4 Horizontal displacement at toe and maximum settlement at base for reinforced and unreinforced embankments. 30-ft widened section, weak crust; (a) 3.75-ft high existing embankment, (b) 7.5-ft high existing embankment.

Table 6.1
Summary of results of embankment widening analysis.

Existing embankment height (ft)	Width of widened section (ft)	Crust strength ----	-Ht. at failure- Unreinf. (ft)	Reinf. (ft)	Reinf. force at failure (k/ft)	Relative increase in surcharge (%)
7.5	15	Weak	12.6	17.2	2.4	17
7.5	30	Weak	10.2	13.4	3.9	40
7.5	45	Weak	9.0	10.2	2.3	25
7.5	30	Strong	12.6	13.2	2.1	10
3.75	30	Weak	8.8	10.2	2.3	12
3.75	30	Strong	7.6	12.8	1.8	13

Displacement vectors at failure due to placing the widened section for the 7.5-ft high existing embankment case with reinforcement are shown in Fig. 6.5. The largest movements occur in the upper 15 ft of the foundation beneath the widened section. Movements beneath the existing embankment are small.

Reinforcement alters the state of stress in the foundation. For the case of a 3.75-ft high existing embankment with a 30-ft widened section on a foundation with a weak crust the unreinforced embankment failed at a height of 8.8 ft. The state of stress at this height for reinforced and unreinforced embankments are compared in Fig. 6.6. Reinforcement reduces the extent of the failure, corner, and cap states beyond the toe. The state of stress in the foundation for the reinforced embankment at failure is shown in Fig. 6.7. Comparison of Figs. 6.2b, 6.6a, and 6.7 shows that the extent of the corner state increases as the applied load increases. Similar behavior was observed for the 7.5-ft high existing embankment as shown in Figs. 6.8 and 6.9. The isolated elements in the cap and failure states within the zone in the corner state are due to load redistribution and numerical inaccuracies as discussed in Chapter 5.

In the embankment reinforcement reduced the extent of soil in the tension state in the upper portion of the fill

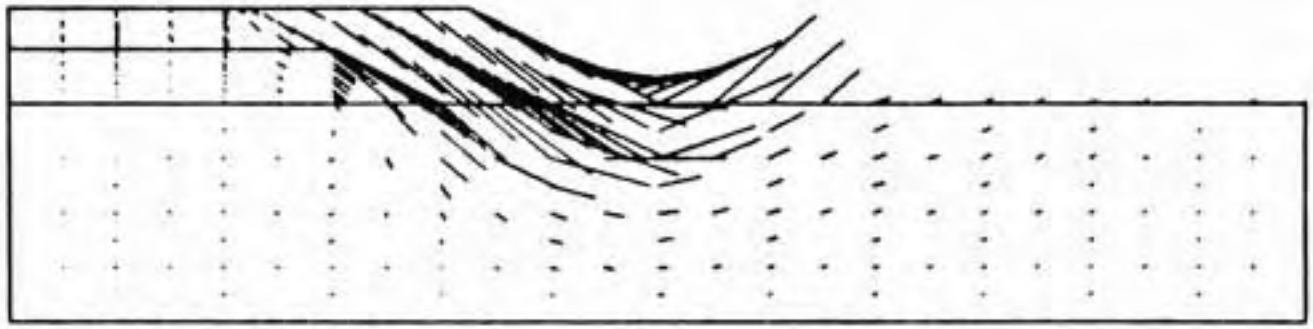

HORIZONTAL SCALE: 1 IN. = 30.0 FT.
VERTICAL SCALE: 1 IN. = 30.0 FT.
DISPLACEMENT SCALE 10.0 TIMES DISTANCE SCALE

Figure 6.5 Displacement vectors for due to placing widened section, 7.5-ft high existing embankment, 30-ft widened section, weak crust.

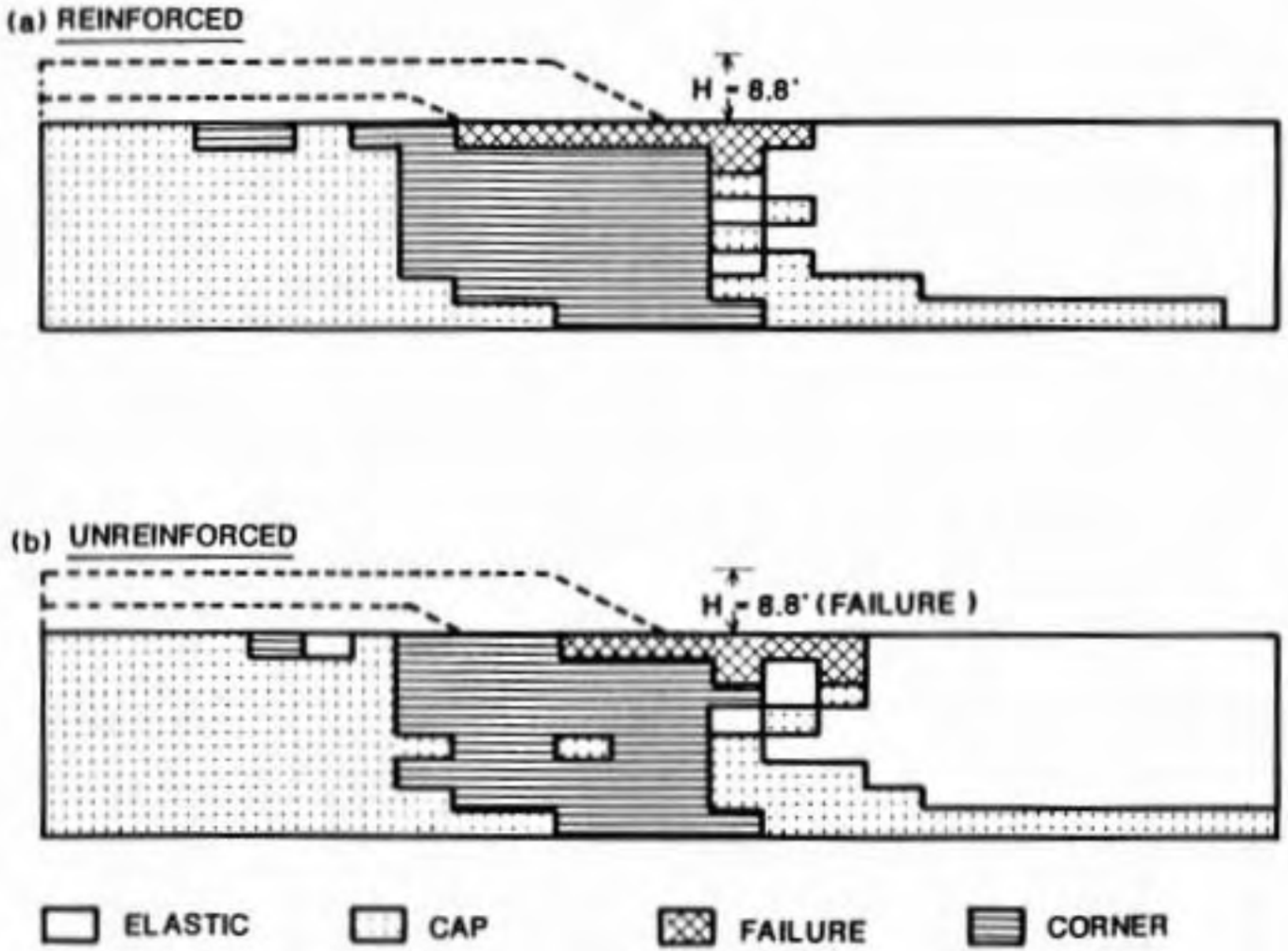

Figure 6.6 State in foundation for reinforced and unreinforced embankments at height of 8.8 ft, 3.75-ft high existing embankment, 30-ft widened section, weak crust.

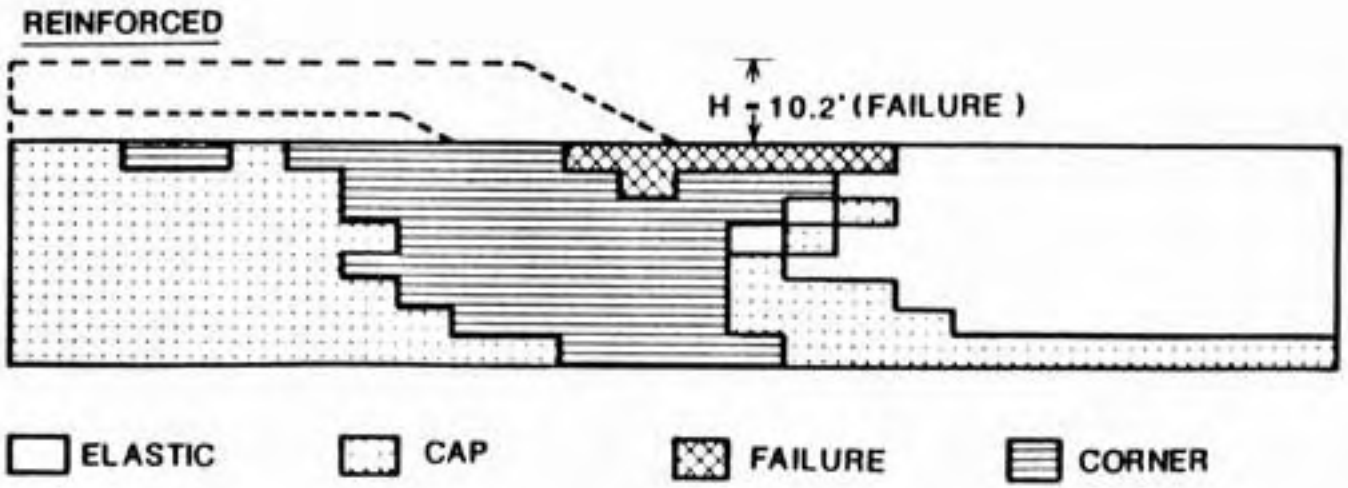

Figure 6.7 State in foundation for reinforced embankment at height of 10.2 ft (failure), 3.75-ft high existing embankment, 30-ft widened section, weak crust.

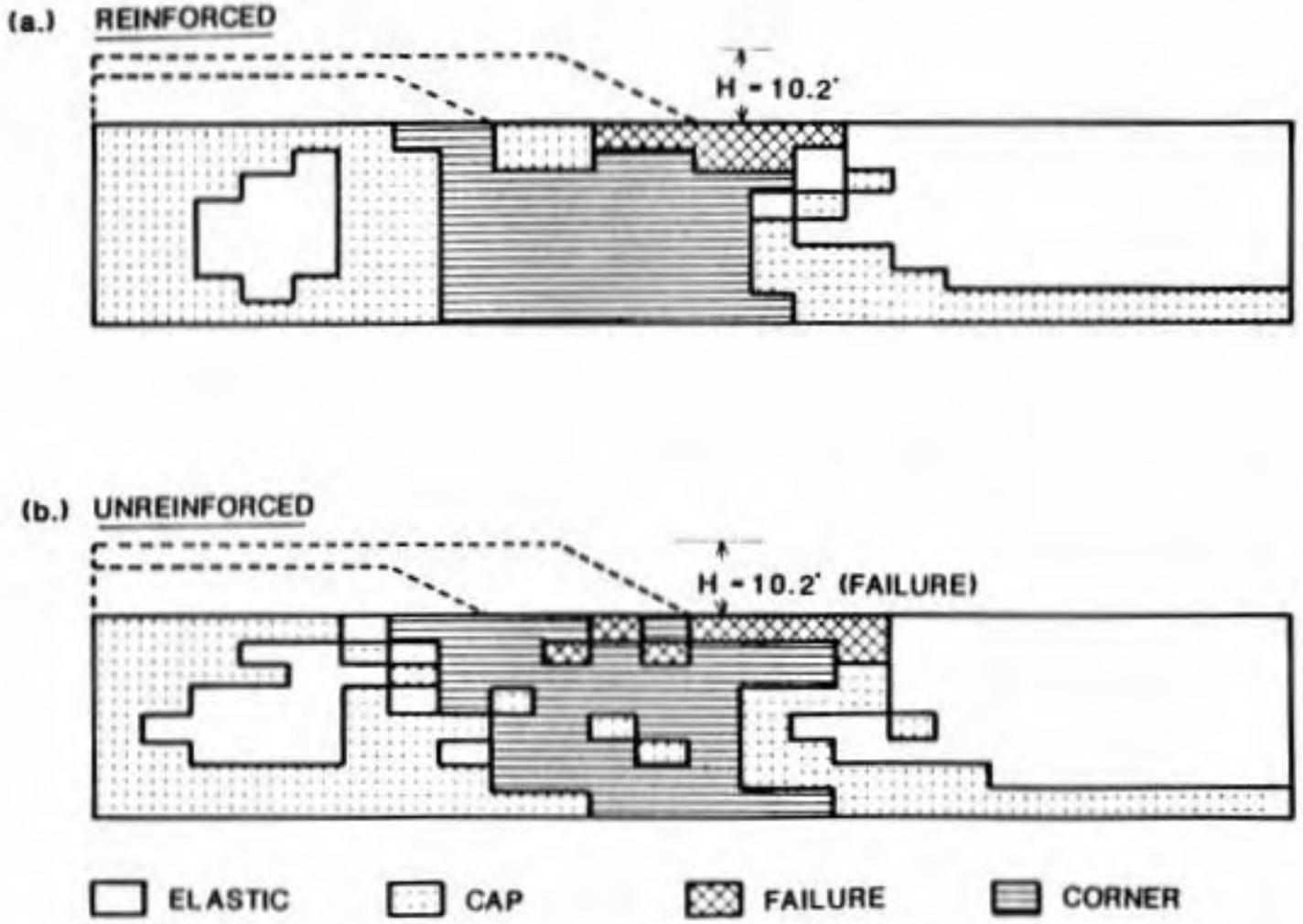

Figure 6.8 State in foundation for reinforced and unreinforced embankments at height of 10.2 ft, 7.5-ft high existing embankment, 30-ft widened section, weak crust.

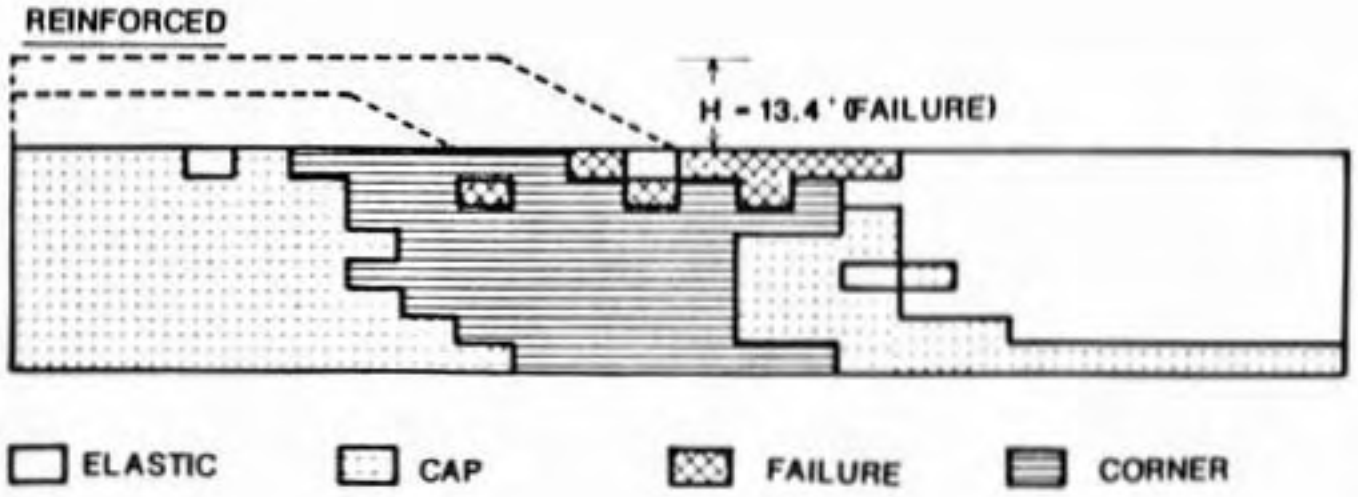

Figure 6.9 State in foundation for reinforced embankment at height of 13.4 ft (failure), 7.5-ft high existing embankment, 30-ft widened section, weak crust.

as seen by comparing Figs. 6.10a and 6.10b for the 3.75-ft high existing embankment and Figs. 6.11a and 6.11b for the 7.5-ft high existing embankment. This increases the available shear resistance in the fill thereby increasing stability. At failure most of the outer portion of the reinforced and unreinforced embankments are at the failure state as shown in Figs. 6.10b and 6.10c and Figs. 6.11b and 6.11c indicating the the shear strength is fully mobilized in the region. The central portion of the embankment is in the elastic state in contrast to the results of Chapter 5 which showed that the central portion of the embankment was in the failure state.

6.4.2 Forces in Reinforcement

The maximum force in the reinforcement versus applied surcharge are shown in Fig. 6.12 for a 30-ft widened section, 3.75 and 7.5-ft high existing embankments, and a foundation with a weak crust. The force increases with the applied load and the increase is quite rapid as failure is approached. The force at failure was 2.3 k/ft for the 3.75-ft high existing embankment and 3.9 k/ft for the 7.5-ft high existing embankment. The latter value is approaching the tensile capacity of a typical strong reinforcement. The maximum force at failure for all cases ranged from 1.8 to 3.9 k/ft and is summarized in Table 6.1.

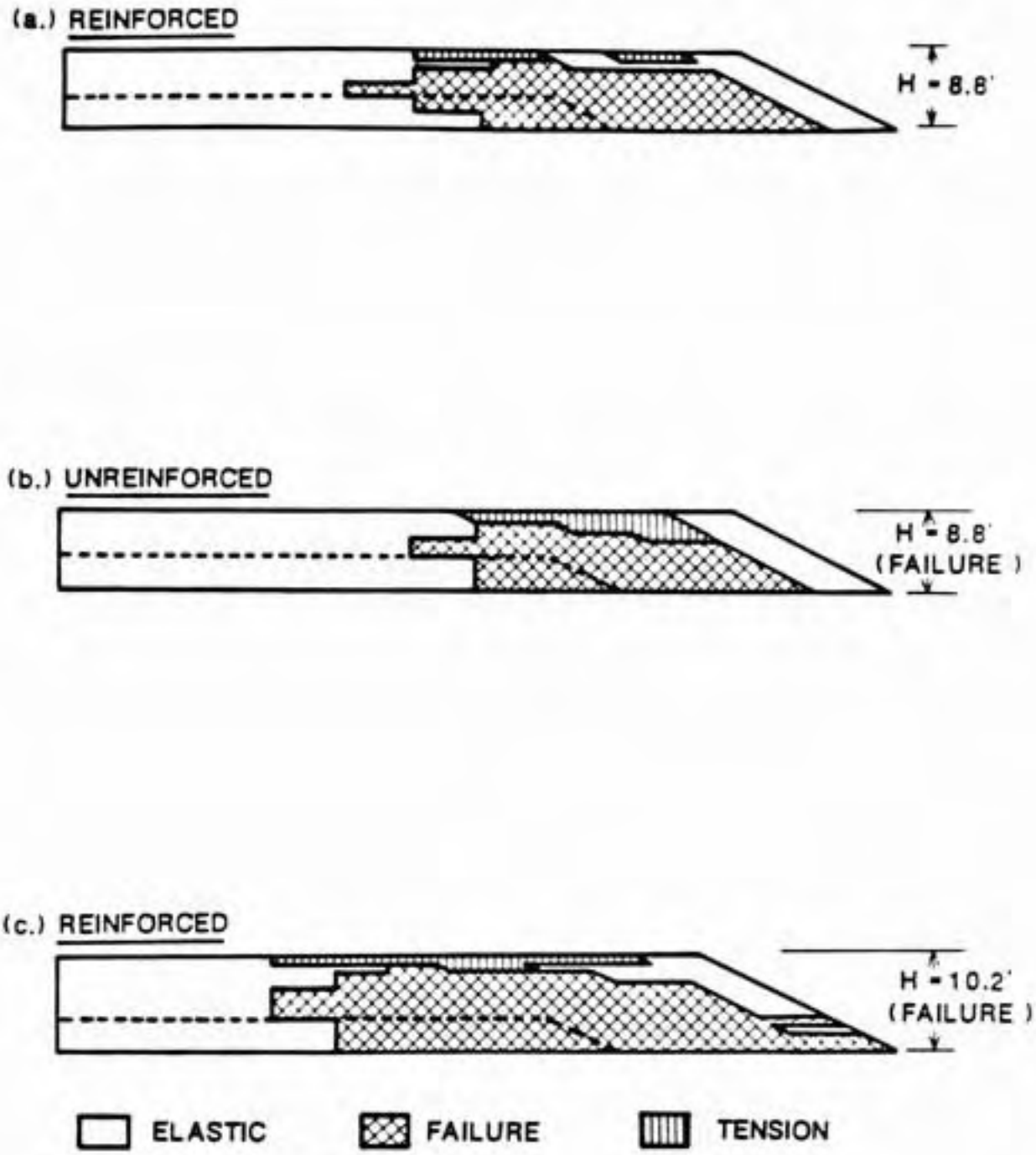

Figure 6.10 State in embankment for reinforced and unreinforced embankments, 3.75-ft high existing embankment, 30-ft widened section, weak crust.

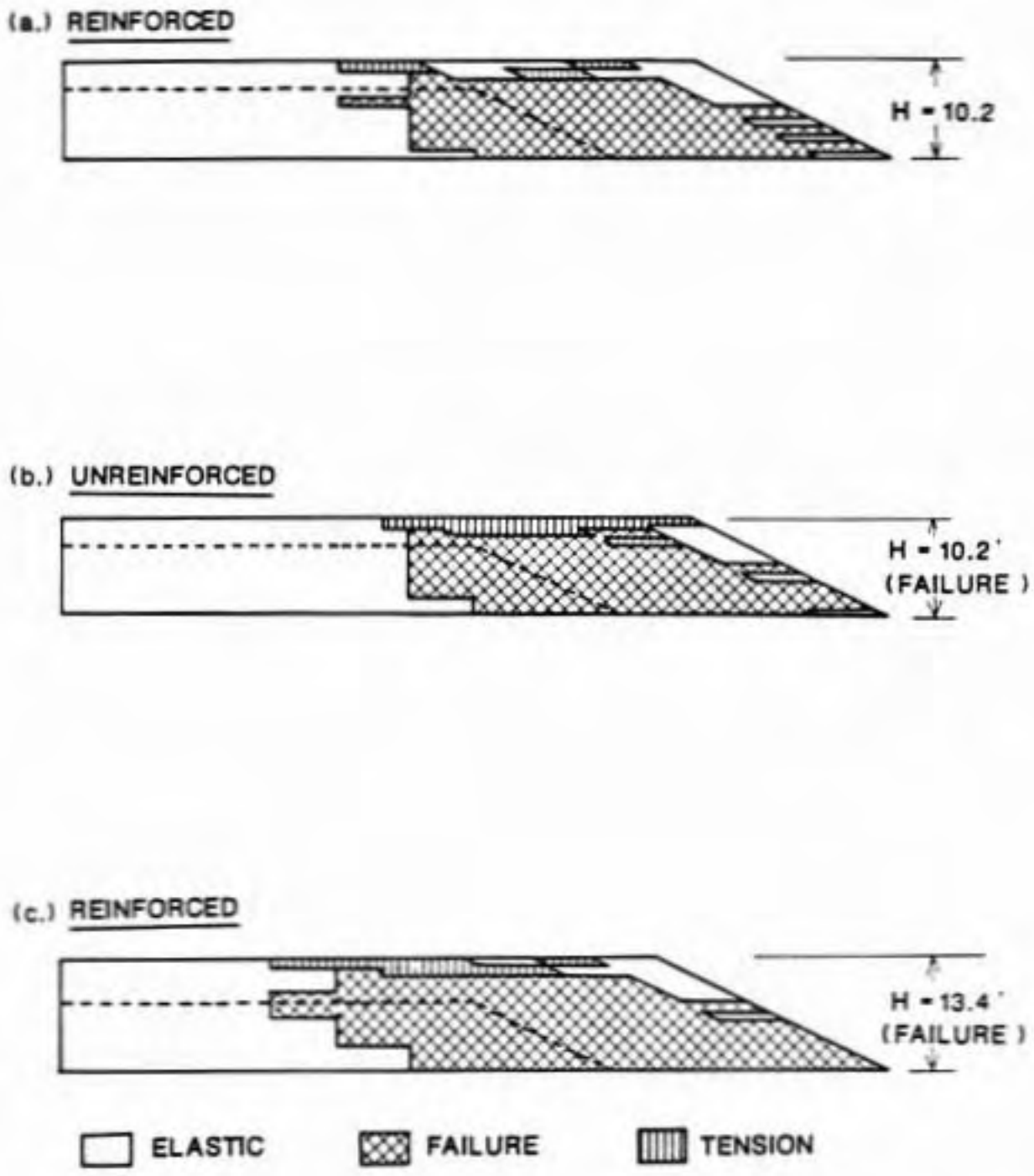

Figure 6.11 State in embankment for reinforced and unreinforced embankments, 7.5-ft high existing embankment, 30-ft widened section, weak crust.

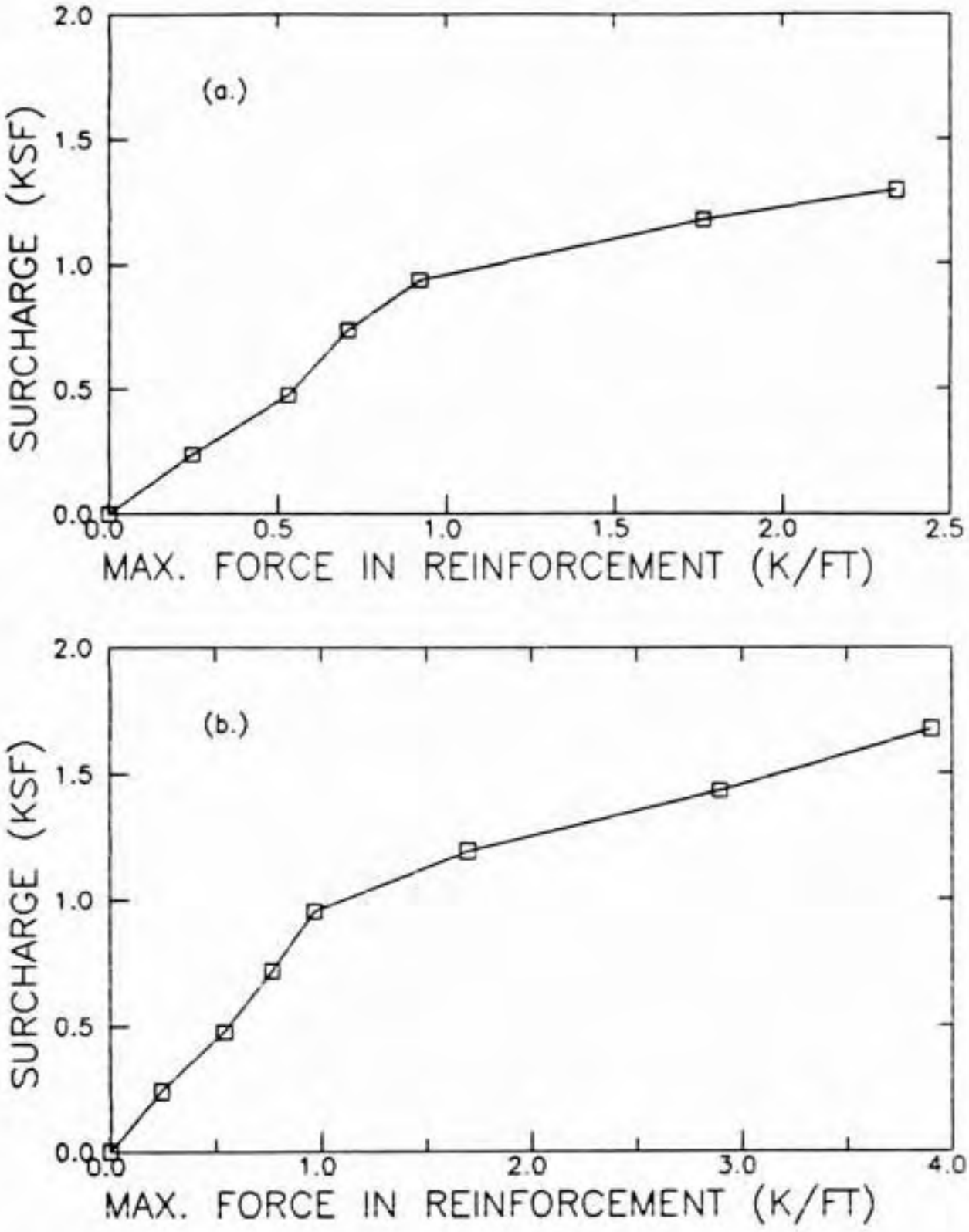

Figure 6.12 Maximum reinforcement force vs. surcharge, 30-ft widened section, weak crust; (a) 3.75-ft high existing embankment and (b) 7.5-ft high existing embankment.

The distribution of the reinforcing forces for the two existing embankment heights at several surcharges is shown in Figs. 6.13 and 6.14. The location of the maximum force moves from the mid-point of the widened section to near the toe of the existing embankment as the surcharge increases. The force near the center of the embankment and near the toe are small. The former suggests that it may not be necessary to place the reinforcement across the full width of the existing embankment crest. Significant reinforcing forces develop near the shoulder and on the slope of the existing embankment. The fluctuations in the force 40 to 60 ft from the centerline correspond to the reinforcement on the embankment slope. They may be due to small inaccuracies introduced into the analysis by using long, thin elements to represent the embankment fill. The sharp change in reinforcing force 33 ft from the centerline (Fig. 6.13) corresponds to the transition from the central portion of the existing embankment where deformations are small to the outer portion where deformations are larger (Fig. 6.5).

The maximum gradient of the reinforcing force occurs near the toe of the existing embankment. It was 0.22 k/ft/ft for the 3.75-ft high embankment and 0.25 k/ft/ft for the 7.5-ft high embankment. This must be transferred by shear stress to the soil above and below the reinforcement. Assuming that the interface strength is the same as the soil

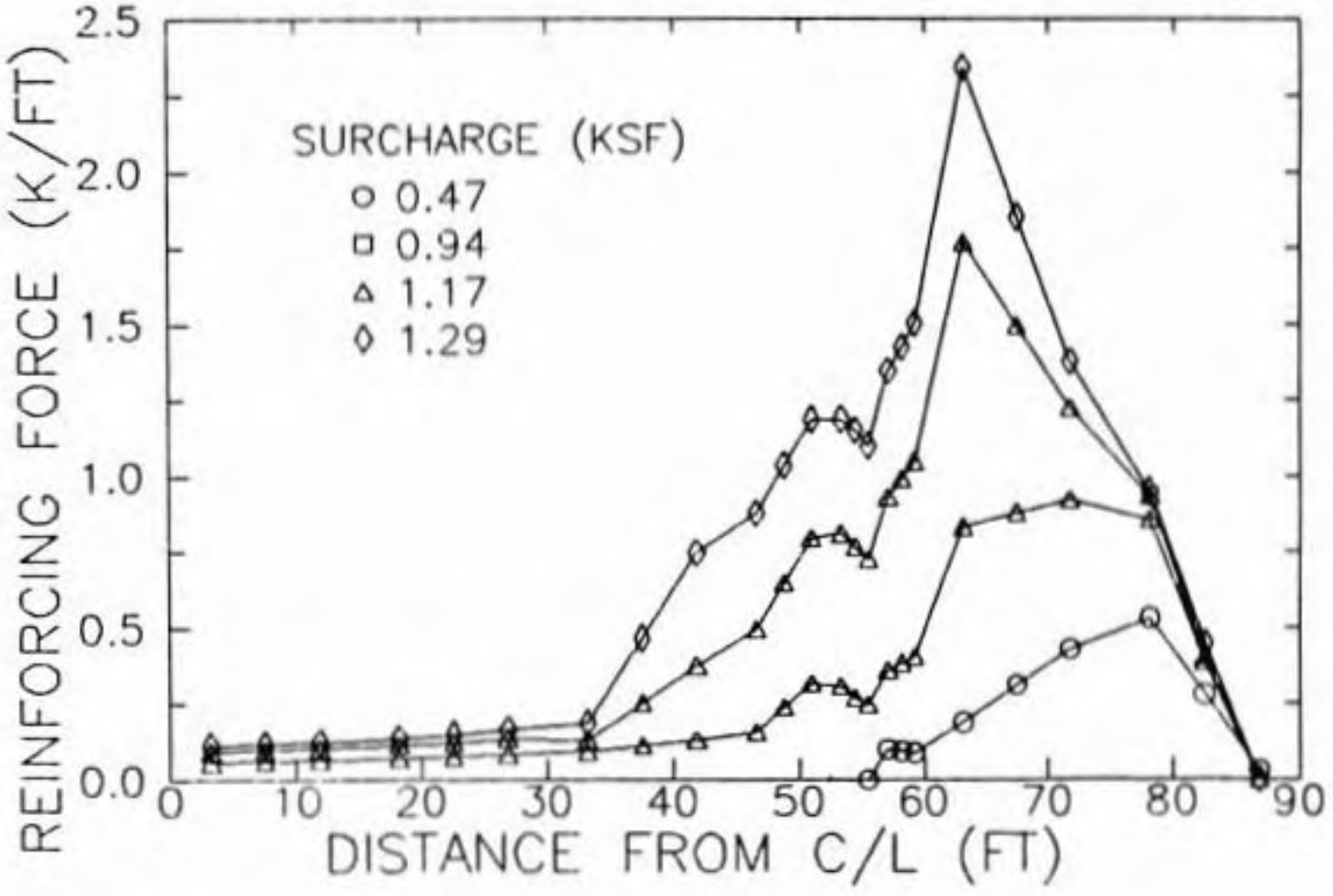

Figure 6.13 Distribution of force in reinforcement vs. surcharge, 3.75-ft high existing embankment, 30-ft widened section, weak crust, reinforced.

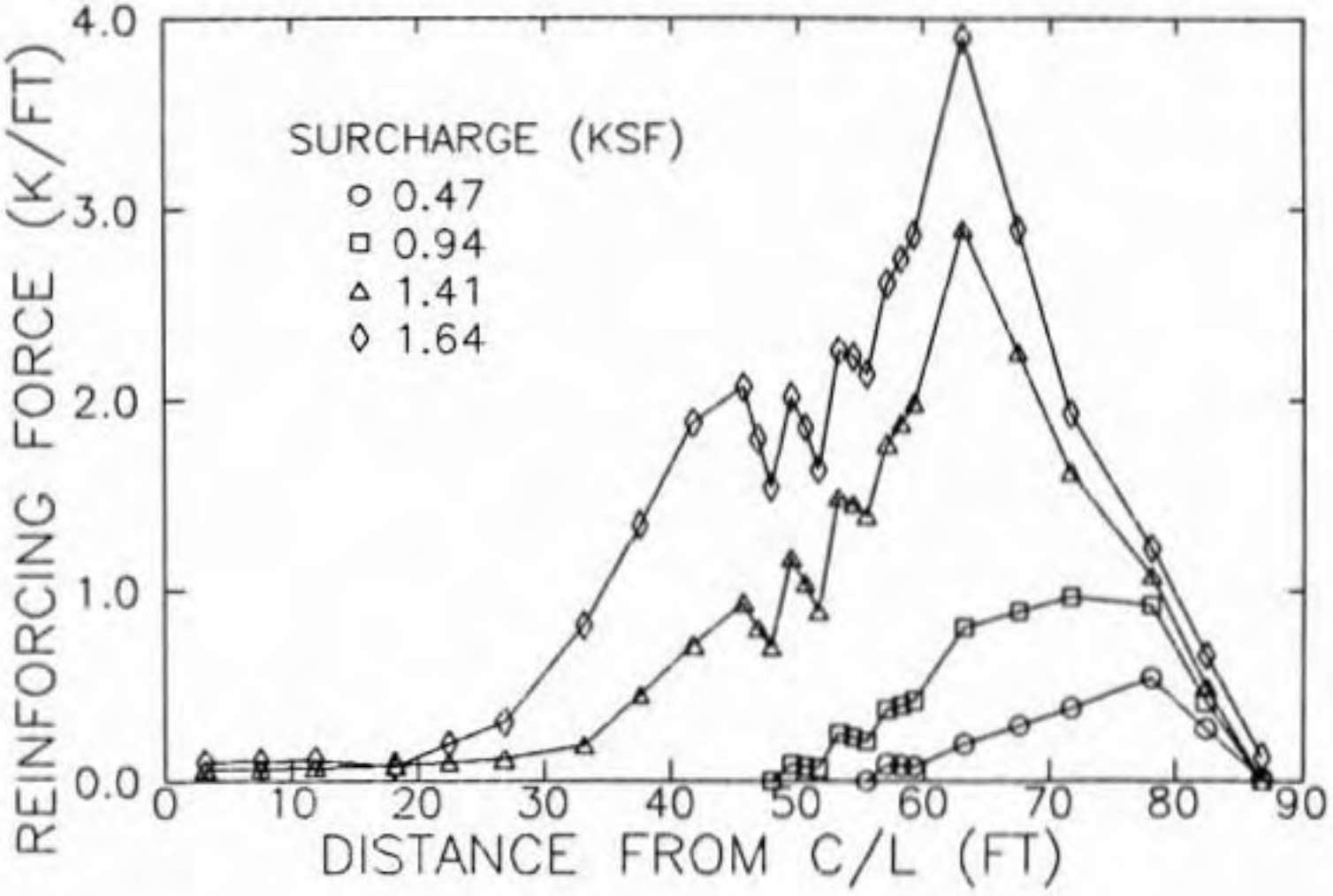

Figure 6.14 Distribution of force in reinforcement vs. surcharge, 7.5-ft high existing embankment, 30-ft widened section, weak crust, reinforced.

strength (see Section 5.4.2), the available resistances for the two cases are 0.8 ksf and 1.0 ksf, respectively. These are much greater than the required resistance so slip between the reinforcement and surrounding soil did not occur.

6.4.3 Effect of Existing Embankment Height

The effect of existing embankment height was examined. Horizontal displacement at the toe vs. surcharge for reinforced embankments with 3.75 and 7.5-ft high existing embankments as well as a normal section constructed with horizontal lifts under undrained conditions (i.e., existing embankment height of zero) are compared in Fig. 6.15 for the weak crust case and in Fig. 6.16 for the strong crust case. For a given surcharge the displacement decreases as the existing embankment height increases. The relative increase in surcharge made possible by reinforcement did not show a consistent trend as shown in Table 6.2.

Table 6.2
Effect of existing embankment height on relative increase in surcharge made possible by reinforcement.

Existing embankment height	- Crust strength - Weak	Strong
Normal section	22%	7%
Widened section, H_d = 3.75′	12%	13%
Widened section, H_d = 7.5′	40%	10%

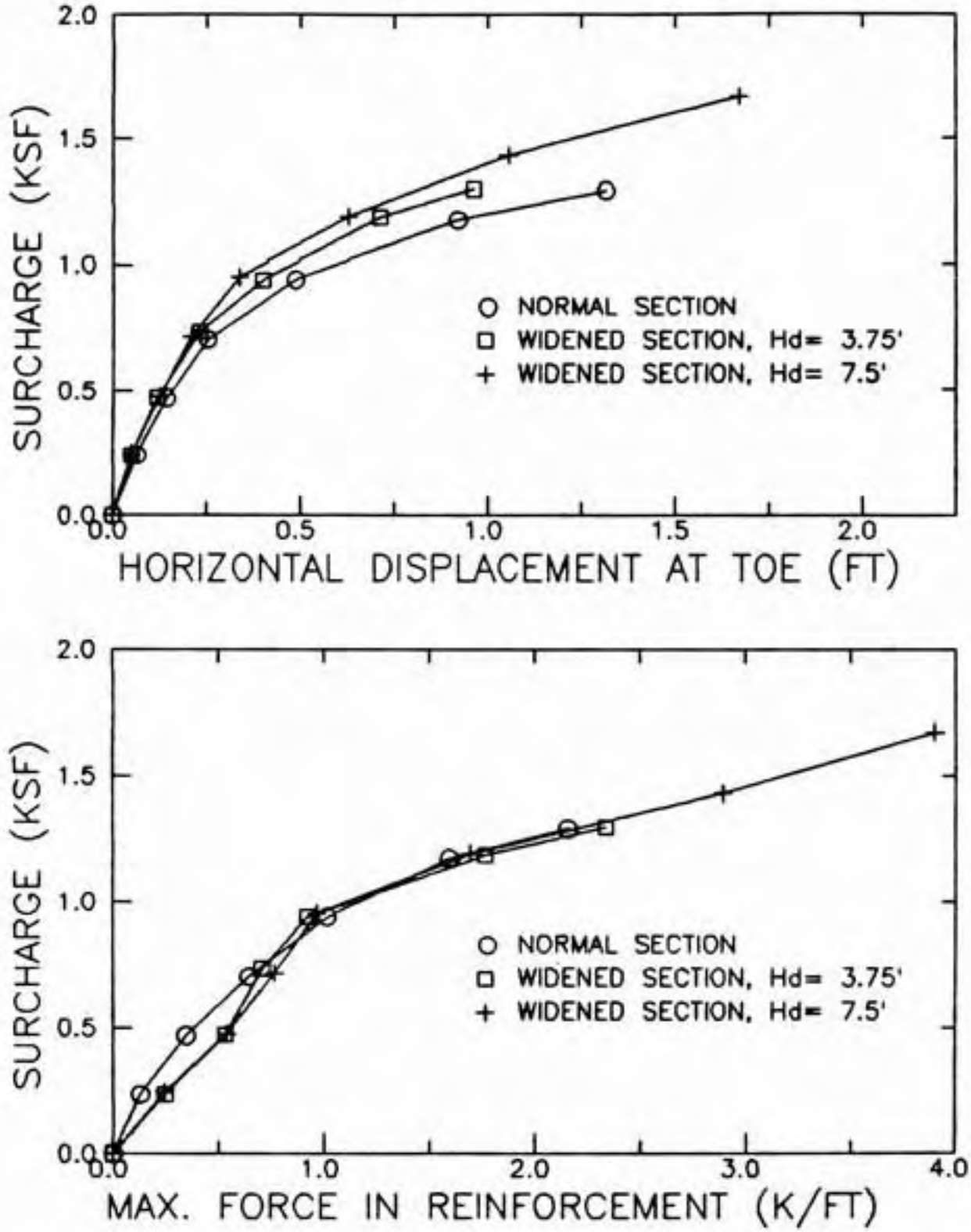

Figure 6.15 Effect of existing embankment height on displacement at toe and maximum force in reinforcement, 30-ft widened section, weak crust, reinforced.

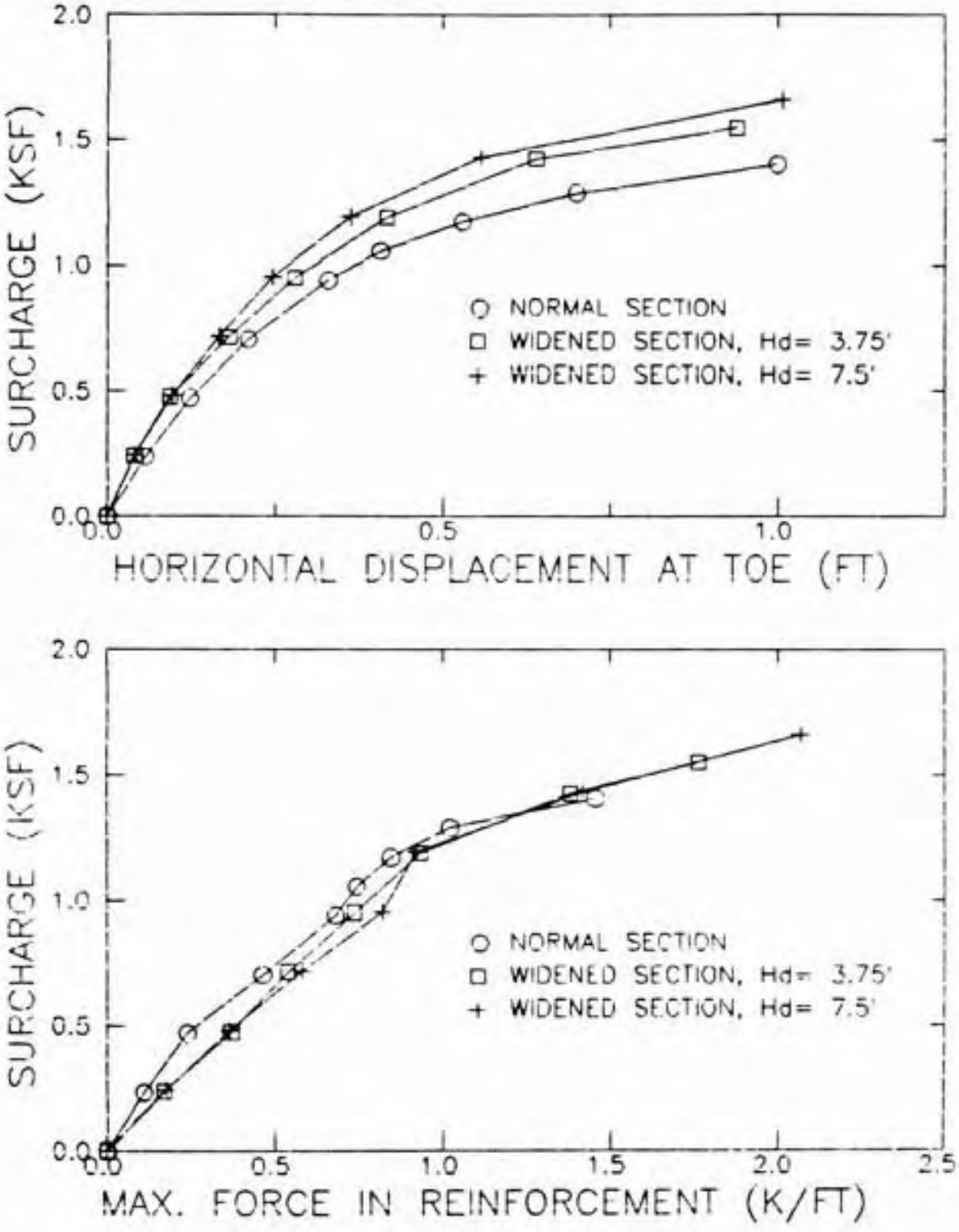

Figure 6.16 Effect of existing embankment height on displacement at toe and maximum force in reinforcement, 30-ft widened section, strong crust, reinforced.

The maximum force in the reinforcement versus surcharge is also shown in Figs. 6.15 and 6.16. The curves are nearly independent of the height of the existing embankment.

6.4.4 Effect of Width of Widened Section

The effect of width of the widened section on horizontal displacements at the toe is shown in Fig. 6.17 for a 7.5-ft high existing embankment and a foundation with a weak crust. A normal section is also shown for comparison. Displacements increase as the width of the widened section increases and approach that of the normal section for the +45-ft width. The relative increase in surcharge made possible by reinforcement is summarized in Table 6.3. It is seen that the increase is quite high for the +30′ section. The increase is about the same for the normal and +45′ sections suggesting that the influence of the existing embankment is small for wide widened sections.

Table 6.3
Effect of width of widened section on relative increase in surcharge made possible by reinforcement, 7.5-ft high existing embankment, weak crust.

Width of widened section	Relative increase in surcharge
Normal section	22%
+15′	17%
+30′	40%
+45′	25%

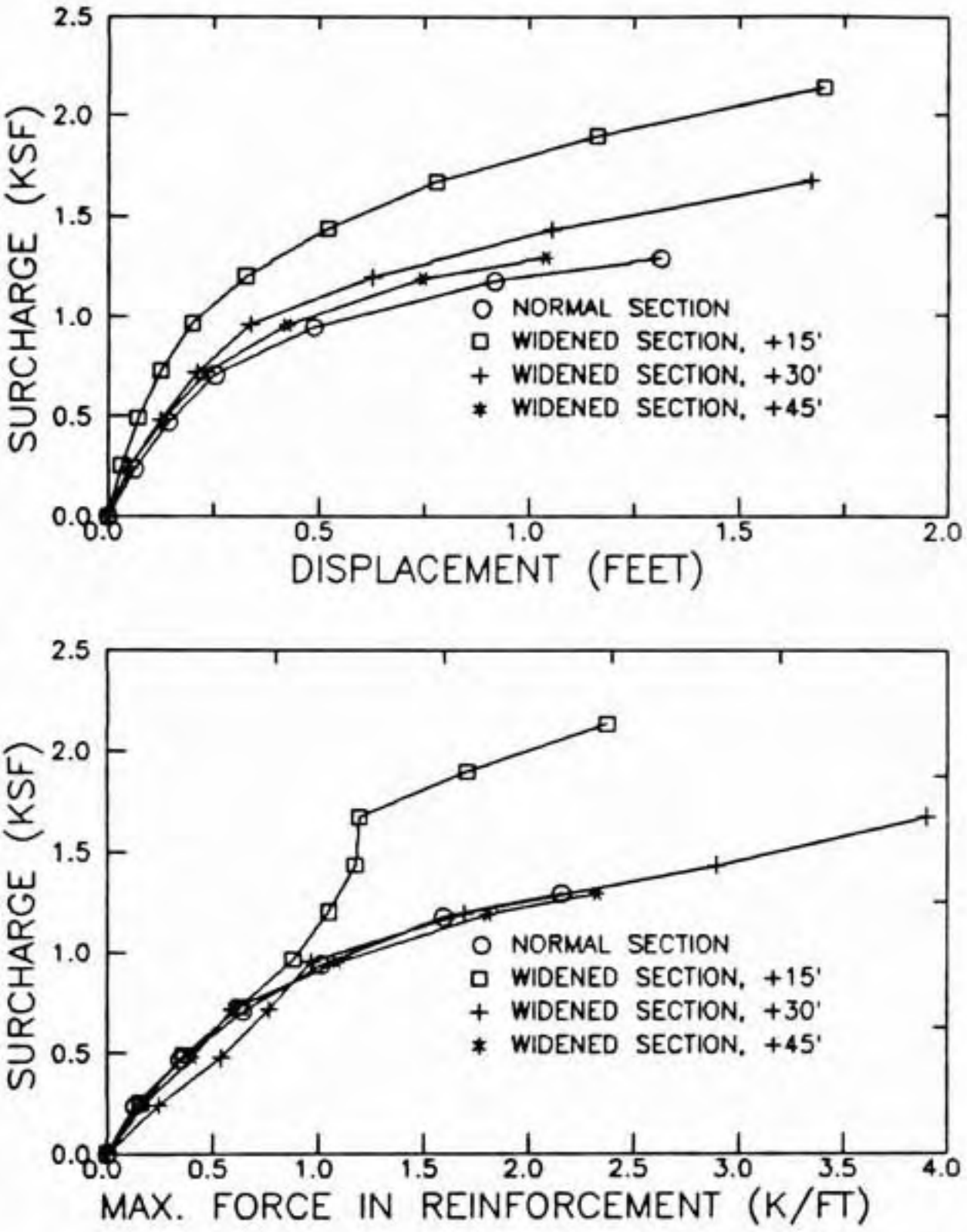

Figure 6.17 Effect of width of widened section on displacement at toe and maximum force in reinforcement, 7.5-ft high existing embankment, weak crust, reinforced.

The maximum force in the reinforcement versus the surcharge is also shown in Fig. 6.17. The curves for the normal, +30-ft, and +45-ft sections are very similar but it is quite different for the +15-ft section. The reason for this is seen by examining the distribution of reinforcing force at failure (surcharge = 1.99 ksf) as shown in Fig. 6.18. The maximum reinforcing force occurs near the shoulder rather than the toe of the existing embankment as occurred for the +30-ft and +45-ft cases. This suggests that the critical slip surface passes near the shoulder of the existing embankment and the reinforcement on the original ground surface beneath the widened section does not directly contribute to stability. Considering a circular failure surface, the moment arm of a reinforcing force near the shoulder would be less than a force near the toe and may account for the relative increase in surcharge made possible by reinforcement being less for the +15' than the +30' or +45' cases.

6.4.5 Effect of Crust Strength

The effect of crust strength on horizontal displacement at the toe and maximum settlement at the base for reinforced embankments with 30-ft widened sections and 7.5-ft high existing embankments is shown in Fig. 6.19. The displacements are greater for the weak than for the strong crust. Similar results were obtained for the 3.75-ft high existing

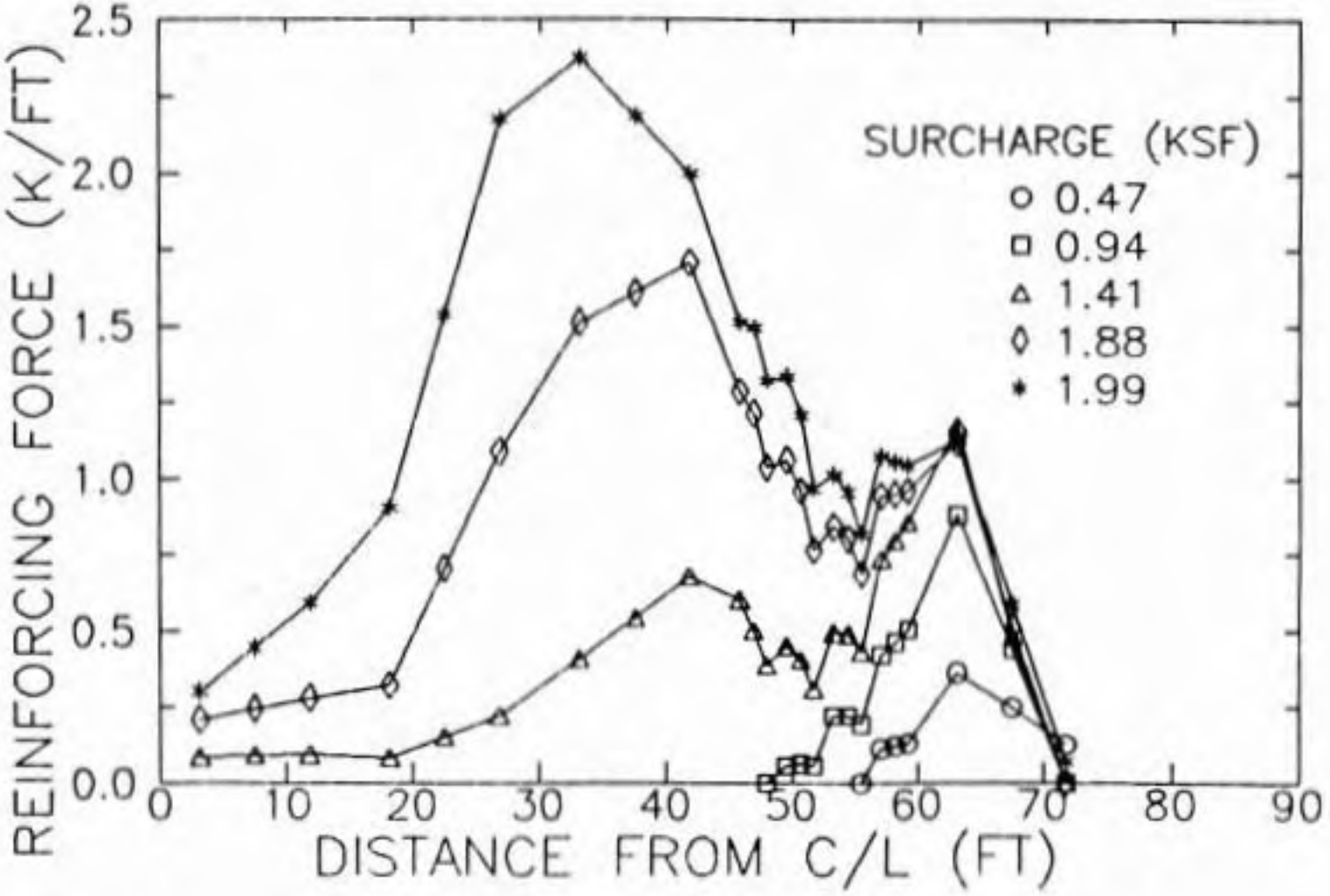

Figure 6.18 Distribution of force in reinforcement vs. surcharge. 7.5-ft high existing embankment. 15-ft widened section. weak crust.

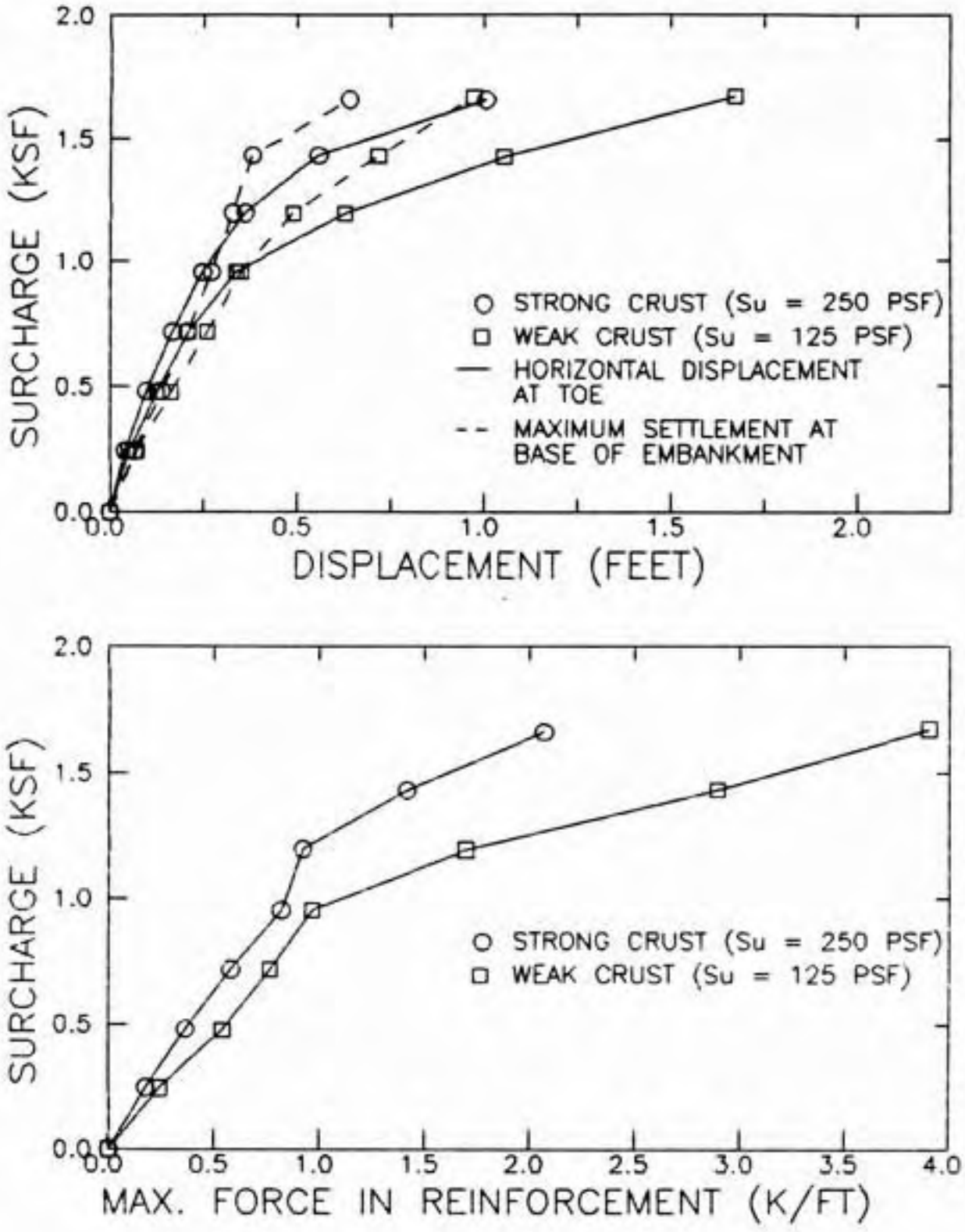

Figure 6.19 Effect of crust strength on displacement at toe and maximum force in reinforcement, 7.5-ft high existing embankment, 30-ft widened section, weak crust, reinforced.

embankment. The relative increase in surcharge made possible by reinforcement is summarized in Table 6.4. It shows that reinforcement is more effective for the weak crust for the 7.5-ft high case but are about the same for the 3.75-ft high case.

Table 6.4
Effect of crust strength on relative increase in surcharge made possible by reinforcement, 30 ft widened section.

Existing embankment height	-- Crust strength -- Weak	Strong
7.5'	40%	10%
3.75'	12%	13%

The maximum force in the reinforcement versus surcharge is also shown in Fig. 6.19. For a given surcharge the force is higher for the weak than the strong crust.

6.5 SUMMARY

The behavior of existing embankments on soft foundations that are widened and have their grade raised was studied using PS-NFAP with the cap soil behavior model. Reinforcement had a significant beneficial effect especially for some combinations of existing embankment height, width of the widened section, and crust strength. In one case the relative increase in surcharge made possible by reinforcement was as high as 40%. The behavior of embankments with a

45-ft widened section approached that of a normal section constructed with horizontal lifts under undrained conditions. The benefit was less for a narrow, 15-ft widened section than for 30 and 45-ft widened sections. It was suggested that the critical failure surface for the narrow section passed near the shoulder of the existing embankment so the moment arm of the reinforcing force was small. The effect of the reinforcement is to reduce the extent of the plastic (corner) zone in the foundation and to reduce the tensile zone in the embankment fill. Forces in the reinforcement were small near the embankment centerline so there may be little benefit to reinforcing the central portion of the existing embankment crest.

CHAPTER 7

LIMITING EQUILIBRIUM METHODS

7.1 INTRODUCTION

Limiting equilibrium methods which are modified to account for the stabilizing effect of reinforcement are the most common techniques currently used to design reinforced embankments. The methods generally assume that the reinforcement provides only a resisting force or moment but does not alter the normal stress on the assumed failure surface and hence the shear resistance provided by frictional materials is unchanged. All methods require an estimate of the allowable force in the reinforcement.

This chapter is organized as follows. In the next section simplified Bishop's (1955) method of slices is modified to include the stabilizing moment provided by the reinforcing force. This is followed by a discussion of the factors which limit the allowable force in the reinforcement. Then, simplified Bishop's method is applied to the cases analyzed with the finite element (FE) method in Chapter 5 and assumptions regarding the direction of the reinforcing force and

stresses on the failure surface are examined. In addition, equations for slip circle and sliding block failure modes proposed by Milligan and La Rochelle (1984) and classical bearing capacity are discussed. Finally, the role of FE and limiting equilibrium analysis methods in reinforced embankment design are considered.

7.2 SIMPLIFIED BISHOP'S METHOD WITH REINFORCING FORCE

The stabilizing effect of tensile reinforcement was incorporated into the simplified Bishop (1955) method of slope stability analysis. It was assumed that the reinforcement provides only a resisting moment and does not alter the normal stress on the slip surface. The method uses a circular slip surface that is divided into a number of slices. A slip surface and the forces acting on a typical slice are shown in Fig. 7.1. The allowable reinforcing force F_R acting at the intersection of the slip surface and the reinforcement is also shown. F_R has units of force/unit width. It provides a resisting moment equal to F_R times its moment arm y about the center of the circle. If there are multiple reinforcing layers, the total resisting moment is the sum of the resisting moments provided by each layer. This additional resisting moment is included as the right most term in the denominator of Eq. 7.1. The term is divided by the safety factor as is the resistance provided by the soil.

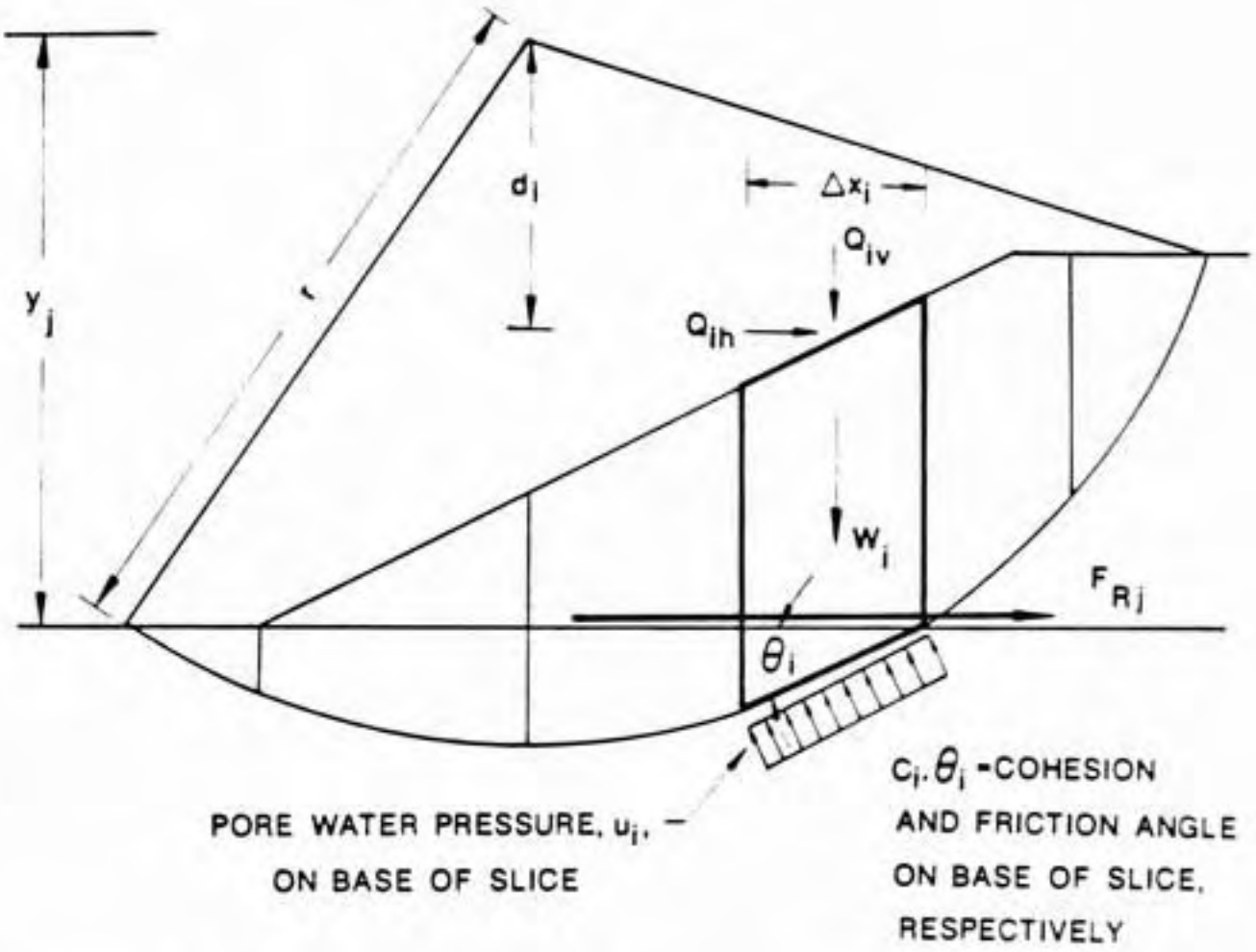

Figure 7.1 Simplified Bishop's method of slices including horizontal reinforcing force showing forces acting on i^{th} slice.

$$SF = \frac{\sum_{i=1}^{n} \frac{c_i \Delta x_i + [W_i + Q_{iv} - u_i \Delta x_i] \tan\phi_i}{\cos\theta_i + (\sin\theta_i \tan\phi_i)/SF}}{\sum_{i=1}^{n} (W_i + Q_{iv}) \sin\theta_i - [\sum_{i=1}^{n} Q_{ih} d_i]/r - (\sum_{j=1}^{m} F_{Rj} y_j)/(rSF)} \quad (7.1)$$

where W_i = weight of the i^{th} slice

Q_{iv} = vertical surface load applied to the i^{th} slice

Q_{ih} = horizontal surface load applied to the i^{th} slice

d_i = moment arm of Q_{ih}

u_i = pore water pressure acting on base of i^{th} slice

Δx_i = width of i^{th} slice

θ_i = inclination of base of i^{th} slice

c_i = cohesion on base of i^{th} slice

ϕ_i = friction angle on base of i^{th} slice

r = radius of assumed trial circle

n = number of slices

F_{Rj} = force in j^{th} reinforcing layer

y_j = moment arm for j^{th} reinforcing layer

m = number of reinforcing layers

SF = safety factor

The safety factor which satisfies Eq. 7.1 is found by trial and error. A simplified version of this equation (Eq. 2.4)was presented by Ingold (1982).

Eq. 7.1 was implemented in a slope stability analysis program (STABL5) developed at Purdue University (Siegel, 1975; Lovell, et al., 1984; Carpenter, 1985). The modified program (Humphrey and Holtz, 1986b) is capable of analyzing multiple layers of reinforcement with the distribution of available force in each layer specified. The program locates the critical circle by a random searching technique.

In some instances it is more convenient to calculate the force required to achieve a desired safety factor. For the special case of a single reinforcing layer Eq. 7.1 may be solved directly for F_R in terms of the desired SF

$$F_R = (SFr/y)\left[\sum_{i=1}^{n}(W_i+Q_{iv})\sin\theta_i - [\sum_{i=1}^{n}Q_{ih}d_i]/r - \sum_{i=1}^{n}\frac{c_i\Delta x_i + [W_i+Q_{iv}-u_i\Delta x_i]\tan\phi_i}{\cos\theta_i + (\sin\theta_i\tan\phi_i)/SF}\right] \qquad (7.2)$$

As discussed in Chapter 2 the reinforcing force is taken to act either: (1) in the direction that the reinforcement was originally placed, so for horizontal reinforcement the moment arm y is the difference in elevation between the reinforcing layer and the center of the assumed slip circle (Fig. 2.1a); or (2) tangent to the slip circle in which case y is the radius r of the slip circle (Fig. 2.1b). The assumption that is most appropriate is discussed later in this chapter.

7.3 ALLOWABLE FORCE IN REINFORCEMENT

The allowable force F_R in the reinforcement must be estimated to use limiting equilibrium analysis methods. F_R is limited by three factors. The first is the ultimate tensile strength of the reinforcement. In addition, since geotextiles experience large creep deformations as the applied stress approaches the ultimate strength there is a restriction on the working force ($=F_R/SF$). There is no criterion to chose the allowable working force based on research or field experience but Sherestha and Bell (1982) feel that it should be less than 60% of the ultimate strength for polyester fabrics and 40-50% of the ultimate strength for polypropylene fabrics.

The second factor is that the reinforcing force is developed through shear between the reinforcement and the surrounding soil. Considering the reinforcement beneath the slope, the weight of fill overlying the reinforcement for a distance L from the toe and a side slope of s(h):1(v) is $0.5\gamma_{emb}L^2/s$ as shown in Fig. 7.2. The available shear resistance between the fill and reinforcement is $(0.5\gamma_{emb}L^2/s)\tan\phi_{sf}$ where ϕ_{sf} is the friction angle between the soil and reinforcement. Assuming a cohesive foundation with an interface shear strength of c_{sf}, the available resistance is Lc_{sf} (Fig. 7.2). Therefore, beneath the slope F_R is limited by

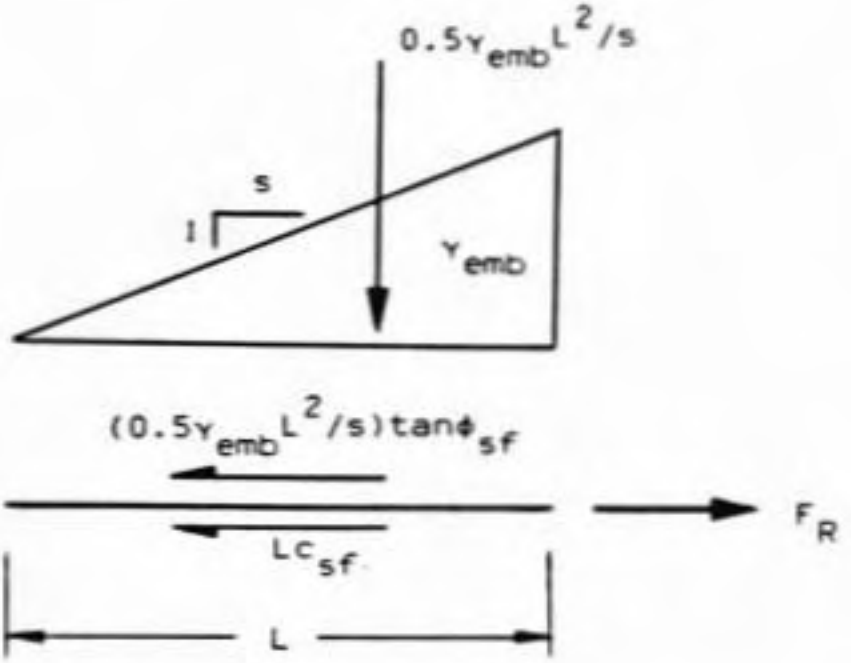

Figure 7.2 Shear between reinforcement and surrounding soil.

$$F_R = Lc_{sf} + (0.5\gamma_{emb}L^2/s)\tan\phi_{sf} \qquad (7.3)$$

This factor generally controls the allowable F_R only near the toe of the embankment.

The third factor is the reinforcing force that can develop due to deformations prior to failure of the foundation soils. The FE analyses in Chapter 5 showed that this occurs before the tensile strength of typical reinforcement is reached. Similar results were found by Rowe and Soderman (1985). Estimating the force at this point is difficult and can only be done by comparison with reported results from case histories (Table 2.2) or by FE analysis (Chapter 5). Rowe and Soderman (1985) have summarized the results of a large number of FE analyses in a format that allows the force to be estimated as discussed in Chapter 5. For strong reinforcement this factor generally controls the allowable force.

Analyses with simplified Bishop's method using the distribution of force in the reinforcement at failure determined with FE analyses showed that the critical circle roughly coincides with the location of the maximum force in the reinforcement and was well away from the toe where the force is limited by Eq. 7.3. Furthermore, the location of the critical circle and the safety factor were nearly identical to those obtained with a uniform distribution of force

equal to the maximum value. Therefore, it is acceptable to use a uniform distribution of force in the reinforcement equal to the estimated maximum value.

7.4 SOIL PROPERTIES AND EMBANKMENT GEOMETRIES ANALYZED

Limiting equilibrium methods were applied to the same embankment geometries and soil properties as used for the FE analyses in Chapter 5. The embankment fill was granular with a unit weight of γ_{emb} = 125 pcf and friction angle of $\phi' = 32^{o}$. The foundation had a 7.5-ft thick crust with a shear strength of 250 psf (strong crust case) or 125 psf (weak crust case). In addition a case with no crust was considered. Underlying the crust was normally consolidated soil with s_u/σ'_{vo} = 0.32. For analyses with simplified Bishop's method the increase in strength with depth was approximated by dividing the foundation soil into layers with the average undrained strengths shown in Table 7.1. In the FE analyses foundation thicknesses of 15, 30, and 60 ft were used but in the limiting equilibrium analyses the critical circles were all less than 15 ft deep so the thickness was not a factor. Also, embankment width was not a factor in the limiting equilibrium analyses.

Table 7.1
Undrained shear strength in foundation
for analyses with simplified Bishop's method.

Depth (ft)	---- s_u (psf) ---- Strong Crust	Weak Crust	No Crust
0.00- 3.75	250	125	26.6
3.75- 7.50	250	125	99.6
7.50-10.00	147	147	147
10.00-12.50	189	189	189
12.50-15.00	231	231	231
15.00-17.50	274	274	274
17.50-20.00	316	316	316

The embankment side slope was 2h:1v except for 2 cases which had a slope of 3h:1v. The reinforcing layer was located at the base of the embankment and was assumed to have a uniform distribution of force equal to the maximum value from the FE analyses. For each case the height at failure (SF = 1.0) was determined. The cases analyzed are summarized in Table 7.2 and are discussed in Sections 7.5 and 7.7. It is recalled from Section 5.2.7 that failure heights calculated by the FE method are approximate.

7.5 CIRCULAR FAILURE MODE

The effect of the magnitude and direction of the reinforcing force on the failure height for embankments with 2h:1v slopes was investigated with simplified Bishop's method. The percent increase in height due to reinforcement

Table 7.2
Comparison of results from FE and limiting equilibrium analyses.

			FE Analysis				Limiting Equilibrium		
Base Width	Side Slope	Foundation Depth	-Ht. at Failure- Unreinf.	Reinf.	Max. F_R at Failure	Relative Increase	-Ht. at Failure- Unreinf.	Reinf.	% Increase
(a.) Strong crust cases (s_u = 250 psf)									
180	2:1	15	9.4	10.3	1.3	5%	9.7	10.3	6%
180	2:1	30	8.4	11.3	1.5	7%	9.7	10.3	6%
180	2:1	60	11.3	11.3	1.1	9%	9.7	10.1	4%
180*	2:1	30	8.4	8.4	1.4	22%	9.7	10.3	6%
180	3:1	30	9.4	10.3	0.8	7%	10.1	10.6	5%
120	2:1	30	7.5	10.3	1.2	6%	9.7	10.2	5%
(b.) Weak crust cases (s_u = 125 psf)									
180	2:1	15	6.6	8.4	1.6	15%	5.8	7.2	24%
180	2:1	30	7.5	8.4	1.3	22%	5.8	7.0	21%
180*	2:1	30	6.6	7.5	1.8	29%	5.8	7.4	28%
90	2:1	30	7.5	9.4	2.2	11%	5.8	7.7	33%
(c.) No crust cases									
180	2:1	15	2.8	4.7	1.0	60%	1.3	2.9	123%
180	2:1	30	3.8	6.6	1.7	70%	1.3	4.5	246%
180*	2:1	30	2.8	2.8	0.6	50%	1.3	2.2	69%
180	3:1	30	3.8	6.6	1.1	53%	1.3	3.5	169%

* Compressible foundation

Notes:
1. See Chapter 5 for details of parameters used in FE analysis.
2. Relative increase for the FE analysis is defined in Section 5.2.7.
3. The limiting equilibrium analyses were made using simplified Bishop's method with a horizontal reinforcing force equal to the maximum F_R from the FE analyses.

versus force in the reinforcement for the strong and weak crust cases are shown in Fig. 7.3. It is seen that the reinforcement is much more beneficial for the weak crust case. Also, Bishop's method with F_R tangent to the slip circle gives an increase in failure height that is significantly greater than with F_R horizontal. Failure heights calculated with the maximum force in the reinforcement from the FE analyses are summarized in Table 7.3. Also shown are failure heights determined with Eq. 2.5 (Milligan and La Rochelle, 1984) which assumes a horizontal reinforcing force and replaces the failure surface in the embankment by the active force.

Table 7.3
Comparison of failure heights
for the circular failure mode.

Crust Strength	Failure Height (ft) - Simplified Bishop- Horizontal	Simplified Bishop- Tangent	Milligan & La Rochelle
Strong	10.1-10.3	10.5-10.8	9.8-10.0
Weak	7.0- 7.4	7.5- 8.5	6.6- 7.3
None	2.2- 4.5	---	---

The failure heights were lowest for Milligan and La Rochelle's equation and were slightly higher for simplified Bishop's method with a horizontal reinforcing force. Simplified Bishop's method with a tangent reinforcing force gives the highest failure heights.

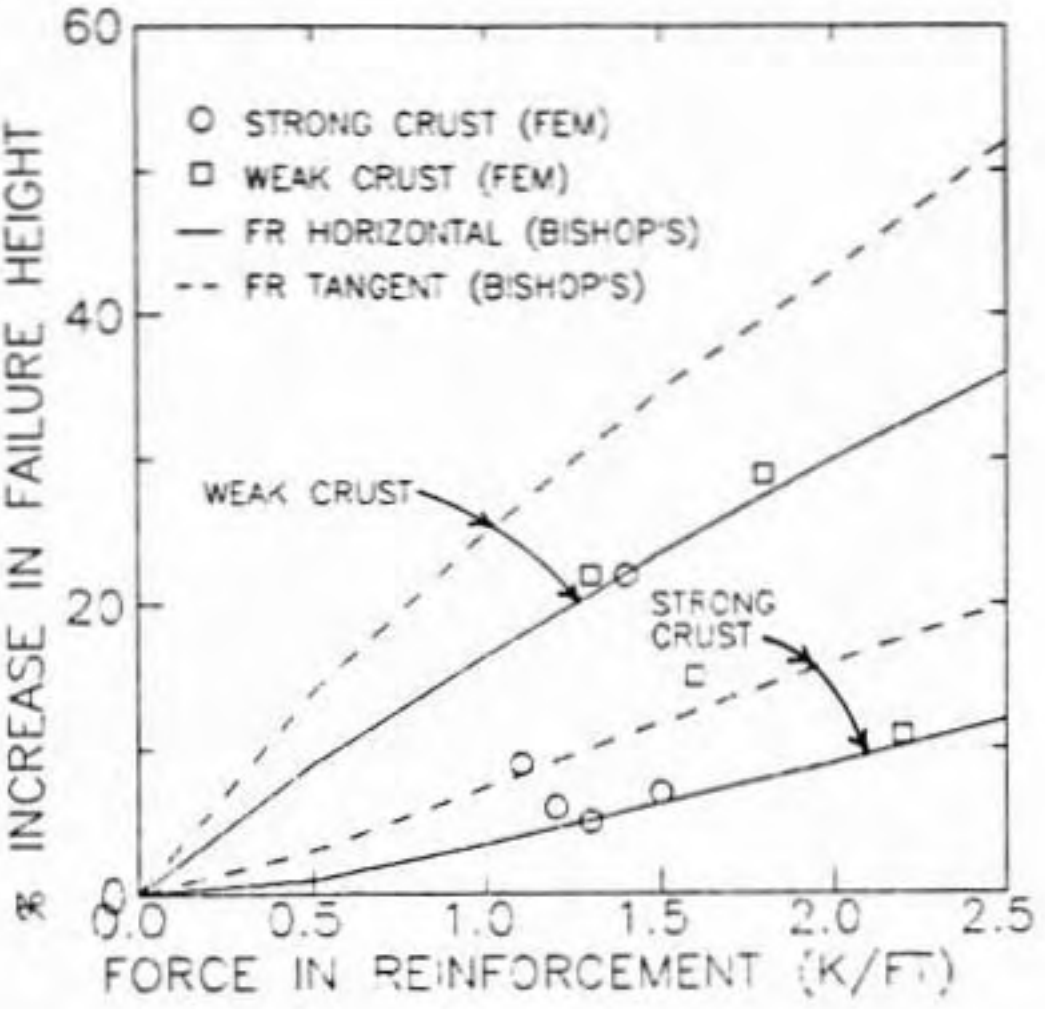

Figure 7.3 Percent increase in height at failure due to reinforcement vs. force in reinforcement.

7.6 SLIDING BLOCK FAILURE MODE

A sliding block failure mode may be more critical especially if there is a weak layer in the foundation. This occurs for the strong crust case where the soil immediately beneath the crust has a shear strength of 126 psf. Eq. 2.10 is applicable to this case. It gave failure heights of 8.4 to 8.7 ft for the range of maximum reinforcing forces obtained from the FE analyses. These heights are lower than obtained with circular failure surfaces so the sliding block failure mode is more critical for this case.

7.7 COMPARISON OF LIMITING EQUILIBRIUM WITH FEM RESULTS

The results of stability analyses with circular failure surfaces are compared to FE analyses with PS-NFAP which were presented in Chapter 5. The failure heights for the FE analysis and simplified Bishop's method with a horizontal reinforcing force are shown in Table 7.2. It is seen that the failure heights are similar for most strong crust cases but are higher for the FE analysis for the weak and no crust cases. The difference may be due partially to the approximations used to represent the linear increase in strength with depth in the normally consolidated soils, namely: (1) in PS-NFAP the strength is calculated only at the four integration points in each element; and (2) in the simplified Bishop analyses the strength was represented with 2.5 to

3.75-ft thick layers (Table 7.1). The influence of these factors could be reduced with thinner elements in the FE analysis and thinner layers in the simplified Bishop analysis. Furthermore, the FE method uses as Drucker-Prager failure criterion but the simplified Bishop method uses a Mohr-Coulomb failure criterion. This leads to slightly different ultimate strengths and failure heights. In general it should be noted that failure heights obtained with PS-NFAP are only approximate as discussed in Chapter 5.

Horizontal displacement at the toe versus embankment height obtained from the FE analyses for for the three crust strength and an embankment with 2h:1v side slopes on a 30-ft thick foundation is shown in Fig. 7.4. Also shown are the failure heights calculated with simplified Bishop's method. For the strong crust case the simplified Bishop failure height was greater than the FE failure height. This may be partly because a sliding block failure mode is more critical. For the weak crust case the FE failure height was greater than the simplified Bishop failure height but note that the latter coincides with a rapid increase in rate of displacement. This was also observed for the other weak crust cases. It is seen for the no crust case that the FE failure height was much greater than the simplified Bishop failure height. Similar behavior occurred for the other weak crust cases (Table 7.2).

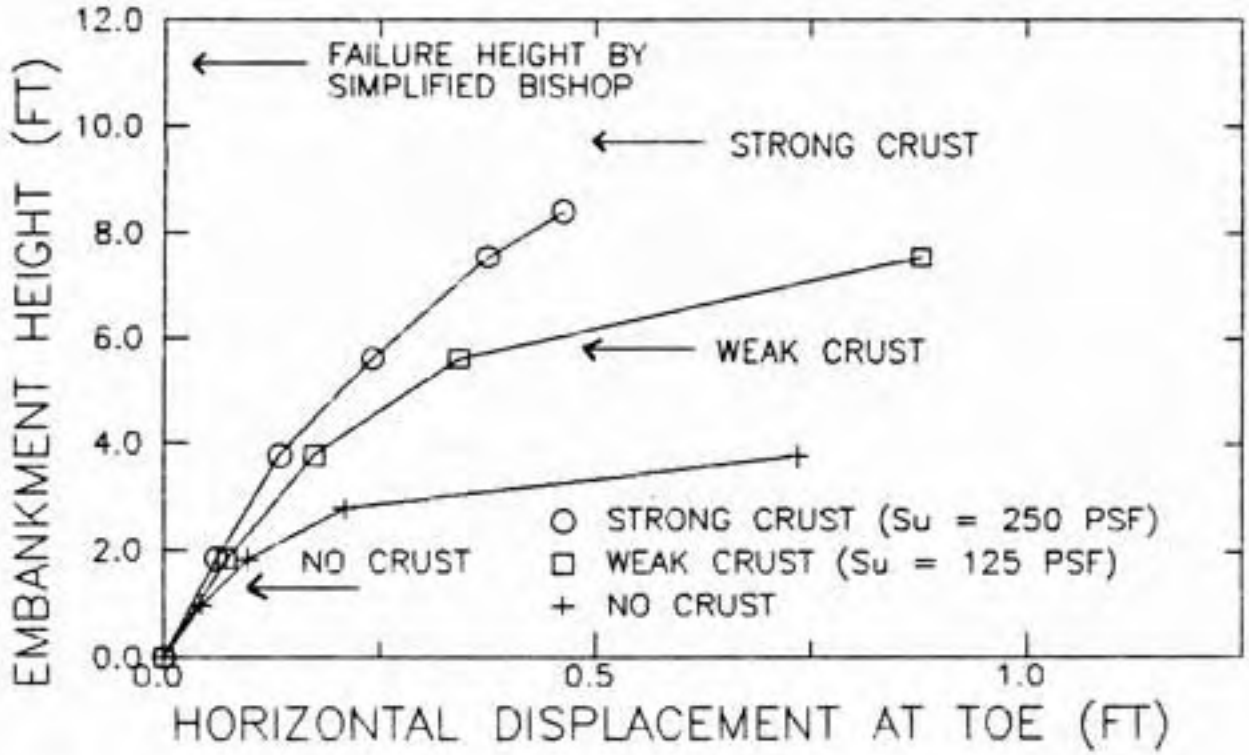

Figure 7.4 Failure height for unreinforced embankment by simplified Bishop's method compared to horizontal displacement at toe vs. embankment height from FE analysis.

The failure height calculated with classical bearing capacity theory using the strong crust strength was 10.3 ft. This is about the same as obtained with simplified Bishop's and FE methods. Using the weak crust strength, a height of 5.1 ft was obtained which is slightly less than for simplified Bishop's and FE methods.

The relative increase in height at failure made possible by reinforcement (defined in Section 5.2.7) from FE and simplified Bishop analyses are shown in Table 7.2 and on Fig. 7.3. On the whole, for the strong and weak crust cases the values from the FE analyses agree better with simplified Bishop's method using a horizontal reinforcing force although for some cases there is a substantial difference. Also the FE analyses indicated that deformations prior to failure were too small to develop the reinforcements full tensile strength so the deformation are probably insufficient to to orient the reinforcement tangent to the slip circle. Both suggest that the reinforcing force should be taken as horizontal in simplified Bishop's method. For the no crust case, the percent increase for simplified Bishop's method with a horizontal force was much greater than for the FE method indicating the caution that must be used when analyzing extremely weak foundations with s_u less than 125 psf.

Comparison with the summary of case histories of reinforced embankment failures (Table 2.2 and Fig. 2.15) shows that greater benefit is possible with reinforcement than calculated by any of the methods in this study. The reason for this is not known.

7.8 EFFECT OF REINFORCEMENT ON STRESSES ON FAILURE SURFACE

The effect of reinforcement on normal and shear stresses on the simplified Bishop critical failure surfaces was studied using stresses calculated with PS-NFAP for the weak and strong crust cases with 2h:1v side slopes and a 30-ft thick foundation. The normal and shear stresses for the weak crust case are shown in Figs. 7.5 and 7.6, respectively. It is seen that reinforcement increases the normal stress in the fill only slightly so the shear resistance in the fill is almost unchanged. The normal stress on the failure surface in the fill from limiting equilibrium (simplified Bishop method) was slightly less than that from the FE method as shown in Fig 7.5. The FE method showed that the normal stress is reduced substantially near the toe of the surface but this would have no effect on the shear resistance since the shear strength in the foundation is based on total stresses. The shear stress is reduced slightly in the fill and is reduced substantially near the toe of the surface. This would significantly increase the safety factor. The safety factor based on the stresses

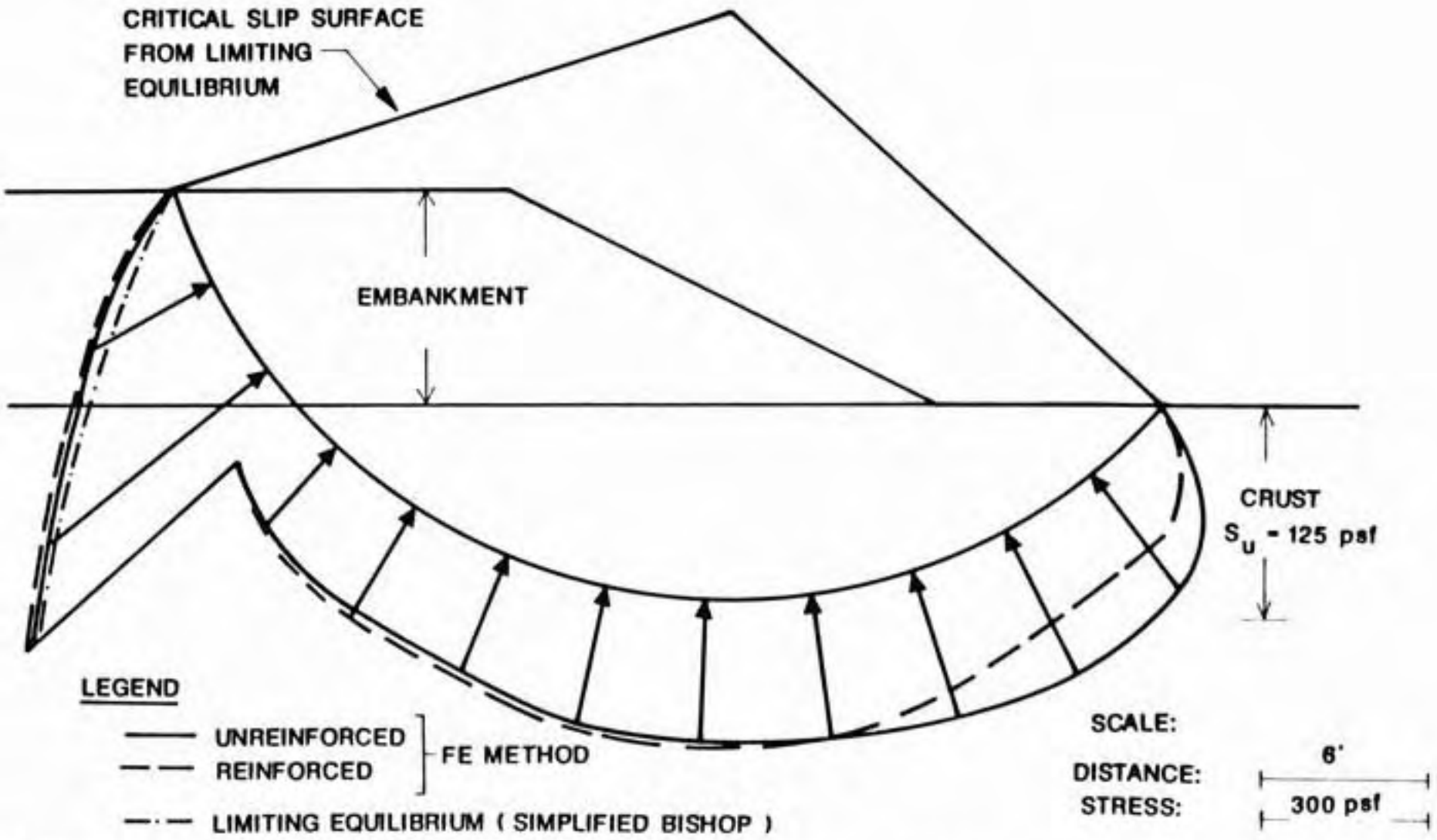

Figure 7.5 Effect of reinforcement on normal stress acting on critical failure surface, 30-ft thick foundation, weak crust.

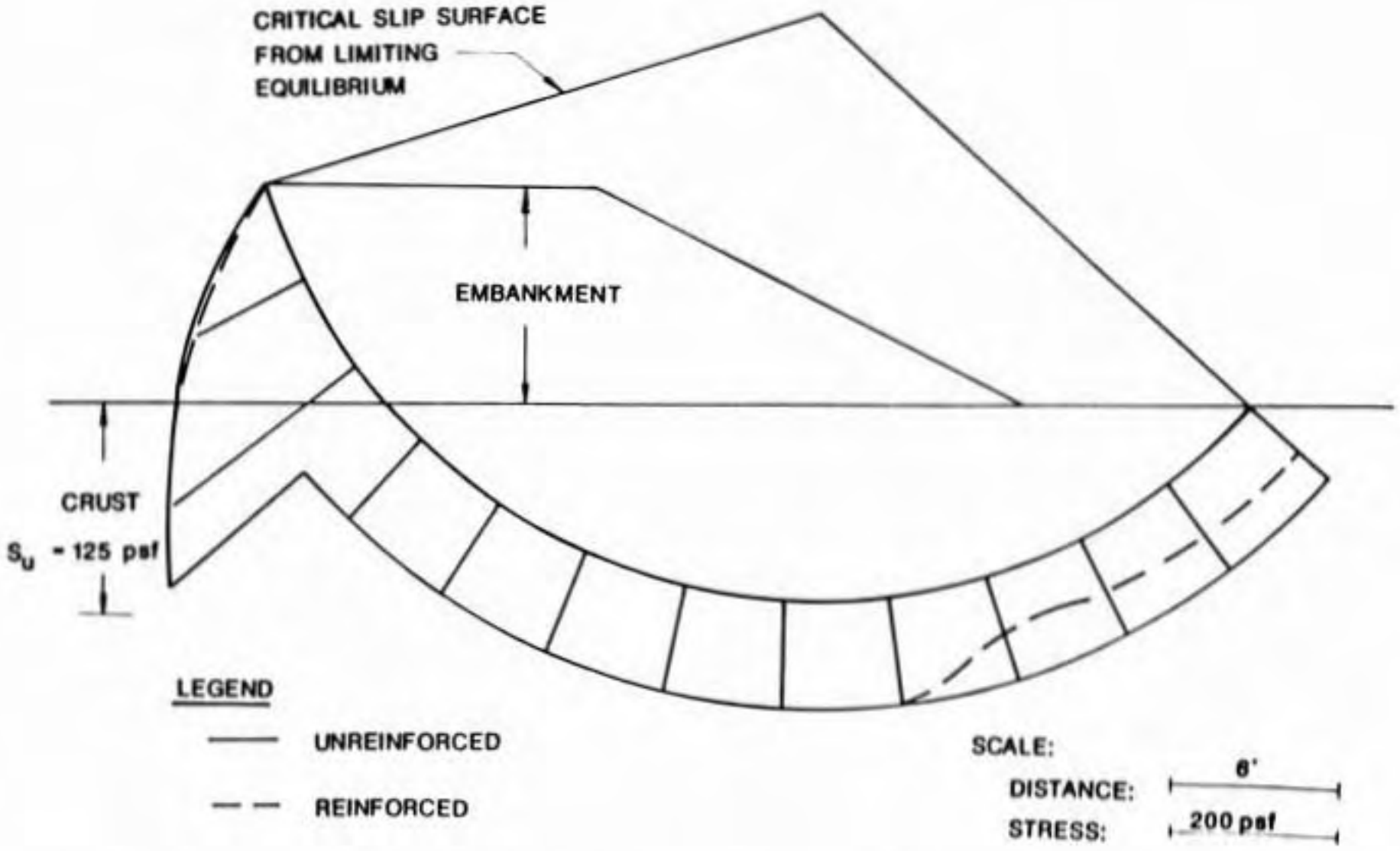

Figure 7.6 Effect of reinforcement on shear stress acting on critical failure surface, 30-ft thick foundation, weak crust.

calculated by PS-NFAP is 1.03 for the unreinforced embankment and 1.17 for the reinforced embankment. Neglecting the increase in normal stress in the fill reduces the reinforced safety factor by less than 1%.

Reinforcement had a smaller effect on the normal and shear stresses for the strong crust case as shown in Figs. 7.7 and 7.8. The normal stress on the failure surface in the fill from limiting equilibrium (simplified Bishop's method) was nearly identical to that from the FE analysis. Also shown on Fig. 7.8 is the available shear strength. The safety factors based on stresses calculated with the FE method were 1.17 and 1.19 for the unreinforced and reinforced embankments, respectively. Again, neglecting the increase in normal stress in the fill reduced the reinforced safety factor by less than 1%.

It is concluded that the main effect of the reinforcement is to reduce the applied shear stress in the overconsolidated crust near the toe of the critical slip surface. This conclusion is considered to be valid even though the cap model only approximately represents the behavior of overconsolidated soil (see Sections 4.2.4.3 and 5.2.8). There is a negligible increase in normal stress in the fill and correspondingly there is an insignificant effect on the available shear resistance. Therefore, the assumption made

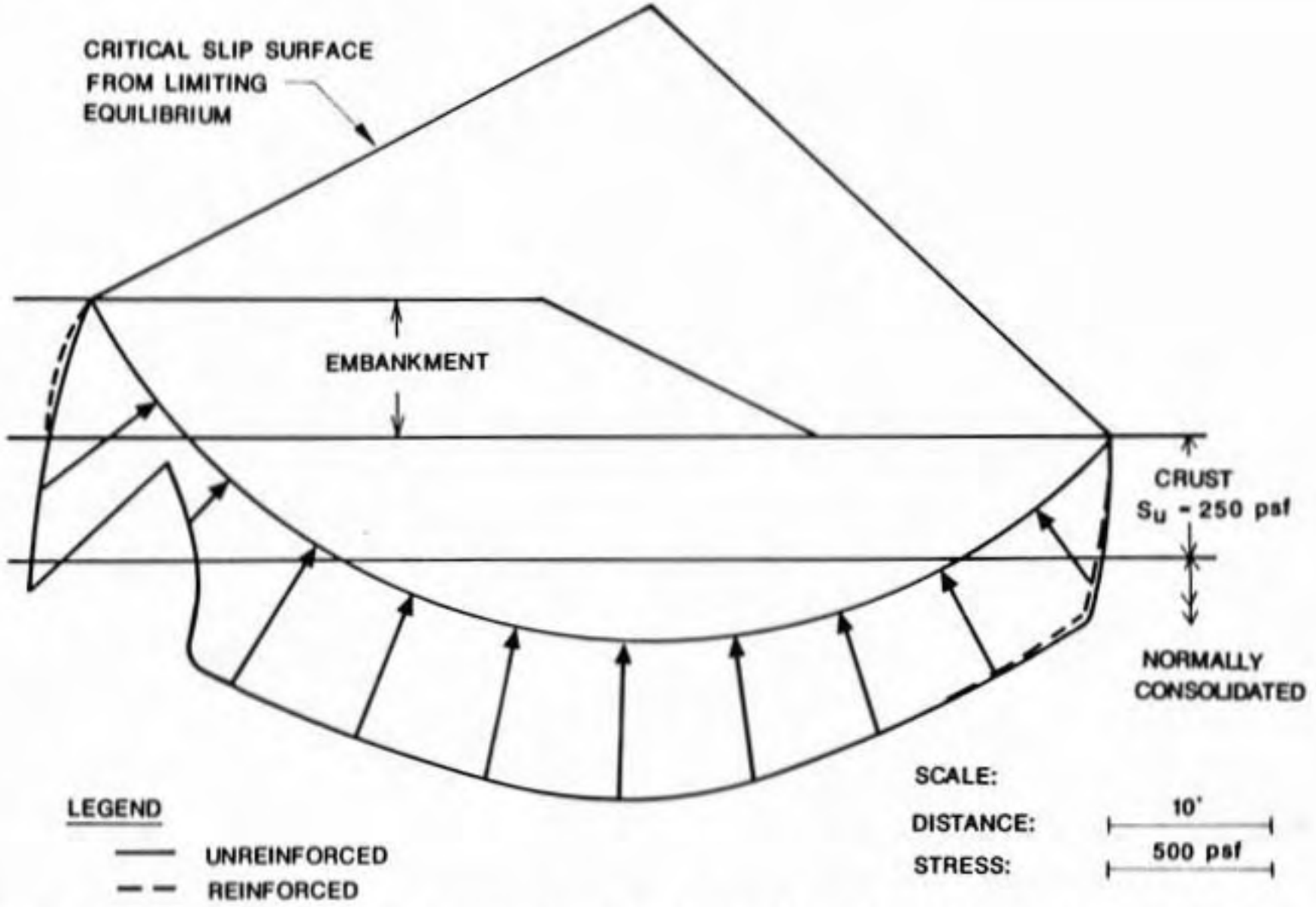

Figure 7.7 Effect of reinforcement on normal stress acting on critical failure surface, 30-ft thick foundation, strong crust.

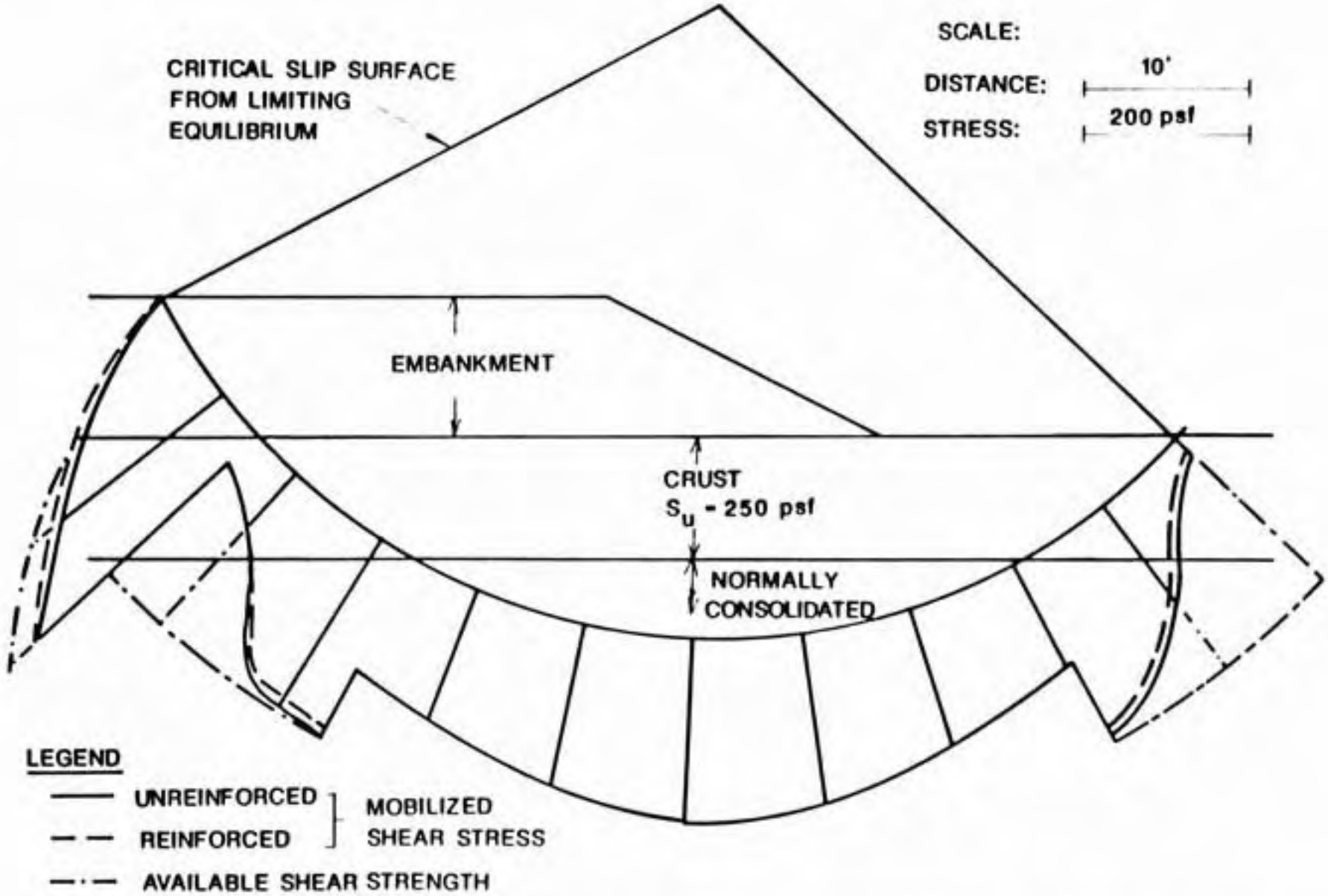

Figure 7.8 Effect of reinforcement on shear stress acting on critical failure surface, 30-ft thick foundation, strong crust.

in simplified Bishop's method that the shear resistance in unchanged by presence of the reinforcement is justified.

7.9 SUMMARY

The failure heights and percent increase in failure height calculated with limiting equilibrium and FE methods are similar but greater increases have been observed for several case histories. Comparison of stresses on critical slip surfaces for reinforced and unreinforced embankments showed there is little effect on normal stresses in the fill; therefore, the assumption made by simplified Bishop's method that the normal stress and resulting shear strength in the fill remains unchanged is valid. The comparison also showed that the main effect of the reinforcement was to reduce the shear stresses in the foundation near the toe of the circle. It is suggested that the reinforcing force be taken to act in the original direction of the reinforcement. Caution should be used when designing embankments on extremely weak foundations with s_u less than 125 psf.

The finite element method is best used to estimate the force in the reinforcement when the foundation soils fail and for comparative studies of reinforced and unreinforced embankment behavior. This is primarily because of the cap model's inability to represent reversal of principal stress which leads to overestimation of height at failure (see

Sections 4.2.4.4 and 5.2.8). Limiting equilibrium methods have been calibrated to field experience (at least for unreinforced embankments) and should be used to estimate the safety factor for design purposes.

CHAPTER 8

SUMMARY, CONCLUSIONS, AND RECOMMENDATIONS

A finite element analysis based on the cap soil behavior model was applied to analysis of reinforced embankments constructed on soft ground. A procedure was developed to determine the cap model parameters from standard soil test results. The analysis technique was applied to several embankment and foundation geometries with different soil properties to identify the situations where reinforcement is likely to be the most beneficial. Critical assumptions of limiting equilibrium analysis methods that are modified to include the effect of reinforcement were examined.

8.1 SUMMARY

A literature review was made of previous finite element (FE) studies of reinforced embankments constructed on soft ground (Section 2.1). Models for the foundation soils ranged from linear elastic for the earlier studies to elastic-plastic for the more recent studies. The properties of the foundation soils were generally taken to be uniform with depth. There were no systematic studies for embankments on

foundations with an overconsolidated crust or foundation strength and modulus increasing with depth. The studies showed the importance of modeling incremental construction of the embankment and the large deformations which occur. Reinforcement was found to reduce shear stresses and lateral deformations in the foundation soils and increase embankment stability. The benefit from reinforcement increases as the strength of the foundation soil decreases and the reinforcement modulus increases.

Limiting equilibrium methods which are modified to account for the stabilizing effect of reinforcement are the most common procedures used to design reinforced embankments (Section 2.2). The methods assume that the reinforcement provides a stabilizing force or moment but does not alter the normal stress or frictional resistance on the slip surface. For circular sliding surfaces there is considerable controversy as to whether the reinforcing force acts in the original plane of the reinforcement (generally horizontal) or tangent to the slip circle. The latter assumption yields a much higher safety factor. A sliding block failure mode may be more critical for foundations with a weak layer.

A summary was made of 37 case histories of reinforced embankments constructed on soft ground (Section 2.3). Foundation materials were generally weak organic soils with

shear strengths of less than 15 kPa (300 psf) and the embankment fill was typically granular. In many cases it was necessary to combine reinforcement with other special construction techniques to achieve an acceptable safety factor. The failure heights were compared to available bearing capacity theories. Reinforcement has been applied to a few cases where existing embankments were widened and had their grade raised but there have been no systematic studies of the effectiveness of reinforcement in this application.

Soil behavior in the present FE study was represented with the cap soil behavior model. It is an elastic-plastic isotropic work-hardening plasticity model with a Drucker-Prager ultimate failure surface and an elliptical shaped cap. Its main features and governing equations are summarized in Chapter 3.

A straight forward procedure was developed to obtain the cap model parameters from standard soil test results (Chapter 4). In the past the parameters were determined with a trial and error procedure and it was difficult to determine a set of cap parameters that were consistent with the corresponding soil properties. The input soil properties for the new procedure are C_c, C_r, ϕ', c', and s_u/σ'_{vo}. The procedure includes an approximate method to match the Drucker-Prager and Mohr-Coulomb failure criteria. The cap

parameters were calculated for Boston Blue Clay and used as input into the model. Computed behavior agreed well with laboratory test results except for tests that underwent 90 degree rotation of principal stress. Cap parameters were calculated from isotropically consolidated triaxial test results for 52 clayey soils. The cap aspect ratio is independent of the initial vertical stress but varies with K_o. For at least some soils it is important to calibrate the model with shear strengths from tests that properly represent the initial state of stress. A procedure to determine the initial position of the cap for overconsolidated soil was presented.

A comparative finite element study of reinforced and unreinforced embankment behavior was made with the plane strain finite element analysis program PS-NFAP (Chapter 5). The program accounts for large strains and uses an incremental procedure to simulate embankment construction. Soil behavior was represented with the cap model. The foundation soils were taken to be undrained and had an overconsolidated crust underlain by normally consolidated soil whose strength and modulus increased with depth. Crust strength was found to have the largest effect on the benefits possible with reinforcement. In contrast to other studies, the effect of foundation depth and embankment width were small, at least for the wide embankments considered herein, possibly because

the strength and modulus of the foundation soils increased with depth. The effect of side slope was small and reinforcement is very beneficial for compressible foundation soils. Reinforcement increased the height at failure and reduced the displacements and shear stresses in the foundation near the embankment toe. The force in the reinforcement when the foundation soils failed were less than typical reinforcement ultimate strengths.

Special procedures were developed to use PS-NFAP for analysis of existing embankments that are widened and have their grade raised (Chapter 6). Construction of the existing embankment under drained conditions was simulated followed by placement of the widened section under undrained conditions. It was found that reinforcement placed beneath the widened section and on the slope and crest of the existing embankment was very beneficial for some combinations of existing embankment height, width of the widened section, and crust strength. For narrow widened sections the benefit was small and for wide widened sections behavior approached that of a normal embankment constructed under completely undrained conditions.

Limiting equilibrium methods that are modified to include the stabilizing effect of the reinforcement were also studied (Chapter 7). The main difficulty in applying

these methods is estimating the available force in the reinforcement. It is limited by: (1) the ultimate strength of the reinforcement; (2) the shear strength between the reinforcement and the surrounding soil; and (3) deformation in the reinforcement prior to failure of the foundation soil.

Simplified Bishop's (1955) slope stability method was modified to include the stabilizing moment provided by the reinforcement. The method assumes that the normal stress and shear resistance on the portion of the failure surface that passes through the granular fill are unchanged by the presence of the reinforcement. Comparison with stresses for reinforced and unreinforced embankments calculated with PS-NFAP showed that this is indeed the case. In addition the comparison showed that reinforcement reduces the shear and normal stresses near the toe of the slip surface. Simplified Bishop's method with a horizontal reinforcing force equal to the maximum value at failure obtained with PS-NFAP yielded benefits from reinforcement that were similar to the FE studies. The benefit was greater than the FE studies when the reinforcing force was assumed to act tangent to the slip circle which suggests that a horizontal force is more appropriate. Comparison with available case histories of reinforced embankment failures showed that for many cases observed increases in failure height were greater than calculated by the analysis methods used in this study.

8.2 CONCLUSIONS

The following conclusions are drawn from the work presented in this thesis:

1. Based on a review of case histories, there is a relation between the undrained shear strength of the foundation and the height of reinforced embankments at failure. The height is greater than predicted by classical bearing capacity theory.

2. A straightforward procedure was developed to determine the cap parameters from standard soil test results. It is important to calculate the model parameters using soil strengths from tests which correctly represent the initial state of stress for at least some soil types.

3. The cap aspect ratio R was found to be independent of the initial vertical stress σ'_{vo} but dependent on the coefficient of lateral earth pressure at rest K_o.

4. The cap model poorly predicts soil behavior when there is a 90 degree rotation of principal stresses. For overconsolidated soils the hardening rule does not correctly predict contraction of the cap.

5. Crust strength and foundation compressibility have the greatest influence on the possible benefit with reinforcement. Other variables including embankment width, embankment side slope, and foundation depth have only a secondary influence.

6. Failure of the foundation soil occurs before there are sufficient deformations to develop the full tensile strength of typical reinforcement.

7. Reinforcement is beneficial for existing embankments that are widened and have their grade raised except for narrow widened sections where the benefit is small.

8. Reinforcement reduces the shear stresses in the foundation near the embankment toe.

9. Modified limiting equilibrium methods of analysis assume that the reinforcement does not alter the normal stress or shear strength on the portion of the failure surface that passes through the granular embankment fill. This assumption is valid based on comparison of stresses in reinforced and unreinforced embankments calculated with the FE method.

10. The benefit due to reinforcement predicted by the FE method and simplified Bishop's method agree better when the reinforcing force in the latter is taken to be in the direction of the reinforcement rather than tangent to the slip circle.

11. At present finite element analysis with PS-NFAP is best suited to comparative studies of reinforced and unreinforced embankment behavior and for predicting the force in the reinforcement at the point where the foundation soils fail. Assessments of the safety of reinforced embankments for design purposes should be made with limiting equilibrium methods.

8.3 RECOMMENDATIONS FOR FURTHER RESEARCH

The work presented herein is an advance in application of the cap soil behavior model to practical problems and in design of reinforced embankments. Nonetheless there are some aspects of reinforced embankment design that would benefit by further study and the ability of the cap model to accurately predict soil behavior could be extended to a wider range of stress paths and drainage conditions. The following are recommended as additional research topics:

1. A parametric study of the effect of reinforcement should be made using PS-NFAP for a wider range of

embankment geometries and soil properties. It should include narrow embankments, different crust thicknesses, and different reinforcement moduli. Special attention should be given to the allowable force in the reinforcement. The results should be summarized in a form that would permit the allowable reinforcing force to be estimated for preliminary embankment designs.

2. The effect of inaccuracies in the input soil properties on embankment response predicted with the cap soil behavior model should be studied to identify the properties which have the greatest influence and the range of possible errors in calculated response.

3. The Mohr-Coulomb failure criteria which has an irregular hexagonal cross-section in stress space is known to predict the ultimate failure strength of many soils. The model presently uses the cone shaped Drucker-Prager criteria. This should be modified to a surface which approximates the Mohr-Coulomb criteria. This would eliminate the need to make an approximate match between the two.

4. The cap model should be extended to improve its ability to model soil behavior during rotation of principal stress and the behavior of overconsolidated soils.

5. Compacted cohesive soils are sometimes used as the fill material for reinforced embankments but the present study and all other analytical studies assume the fill is granular. The behavior of reinforced embankments with cohesive fill should be studied with the cap model or some other soil model.

6. Reinforced embankments are often constructed on peaty foundation soils which experience significant drainage during construction. First, the ability of the cap model to predict the drained and undrained behavior of peat should be confirmed; then, the model should be extended to partially drained conditions.

8. Bakker, J. G. (1977), "Mechanical behavior of membranes in road foundations," Proceedings of the International Conference on the Use of Fabrics in Geotechnics, Ecole Nationale des Ponts et Chaussees, Paris, France, Vol. I, PP. 139-142.

9. Barsvary, A. K., MacLean, M. D., and Cragg, C. B. H. (1982), "Instrumented case histories of fabric reinforced embankments over peat deposits," Proceedings of the Second International Conference on Geotextiles, Las Vegas, Nevada, August, Vol. III, pp. 647-652.

10. Bell, J. R., Greenway, D. R., and Vischer, W. (1977), "Construction and analysis of a fabric reinforced low embankment," Proceedings of the International Conference on the Use of Fabrics in Geotechnics, Ecole Nationale des Ponts et Chaussees, Paris, France, Vol. I, pp. 71-75.

11. Belloni, L., and Sembenelli, P. (1977), "Road embankments on compressible soils constructed with the aid of synthetic fabrics," (In French), Proceedings of the International Conference on the Use of Fabrics in Geotechnics, Ecole Nationale des Ponts et Chaussees, Paris, France, Vol. I, pp. 49-54.

12. Bishop, A. W. (1955), "The use of the slip circle in the stability analysis of slopes," Geotechnique, Vol. 5, No. 1, pp. 7-17.

13. Bjerin, L. (1977), "Results of deformation measurements on woven polyester fabric used as reinforcement in a road embankment," Proceedings of the International Conference on the Use of Fabrics in Geotechnics, Ecole Nationale des Ponts et Chaussees, Paris, France, Vol. III, PP. 28-29.

14. Bjerrum, L. (1972), "Embankments on soft ground," Proceedings of the Specialty Conference on Performance of Earth and Earth-Supported Structures, ASCE, Vol. II, pp. 1-54.

15. Bjerrum, L., and Simons, N. (1960), "Comparison of shear strength characteristics of normally-consolidated clays," Shear Strength of Cohesive Soils, ASCE, pp. 711-726.

16. Bonaparte, R., Holtz, R. D., and Giroud, J. P. (1985), "Soil reinforcement design using geotextiles and geogrids," Preprint, Geotextile Testing and the Design Engineer, ASTM Committee D-35, June, 80 pp.

LIST OF REFERENCES

25. Carpenter, J. R. (1985), "STABL5...The Spencer method of slices: Final report," Report No. JHRP-85-17, Joint Highway Research Project, School of Civil Engineering, Purdue University, West Lafayette, Indiana, August, 26 pp.

26. Chang, T. Y. (1980), A Nonlinear Finite Element Analysis Program - NFAP, User's Manual, Vol. 2, Department of Civil Engineering, The University of Akron, Akron, Ohio.

27. Chen, W. F. (1984), "Constitutive modeling in soil mechanics," Chapter 5 in Mechanics of Engineering Materials, Desai, C. S., and Gallagher, R. H., Ed., John Wiley and Sons, Ltd., pp. 91-119.

28. Chen, W. F., and Baladi, G. Y. (1985), Soil Plasticity-Theory and Implementation, Elsevier Science Publishing Company, Inc., New York, 231 pp.

29. Chen, W. F., and McCarron, W. O. (1983), "Modeling of soils and rocks based on concepts of plasticity," Proceedings of the Symposium on Recent Developments in Laboratory and Field Tests and Analysis of Geotechnical Problems, Asian Institute of Technology, Bangkok, Thailand, December 6-9, 96pp.

30. Chen, W. F., and Saleeb, A. F. (1982), Constitutive Equations for Engineering Materials, Vol. I, Elasticity and Modeling, John Wiley & Sons, New York, 580 pp.

31. Cheung, K. F. H. (1985), "A stress-strain model for the undrained response of oil sand," Masters Thesis, Department of Civil Engineering, The University of British Columbia, Vancouver, British Columbia, 137 pp.

32. Christie, I. F. (1982), "Economic and technical aspects of embankments reinforced with fabrics," Proceedings of the Second International Conference on Geotextiles, Las Vegas, Nevada, August, Vol. III, pp. 659-664.

33. Christie, I. F., and El Hadi, K. M. (1977), "Some aspects of the design of earth dams reinforced with fabric," Proceedings of the International Conference on the Use of Fabrics in Geotechnics, Ecole Nationale des Ponts et Chaussees, Paris, France, Vol. I, pp. 99-103.

34. Christopher, B. R. (1983), "Evaluation of two geotextile installations in excess of a decade old," Transportation Research Record 916, TRB, National Academy of Science, Washington, D. C., pp. 79-88.

LIST OF REFERENCES

1. Almeida, M. S. S., Britto, A. M., and Parry, R. H. G. (1986), "Numerical modeling of centrifuged embankment on soft clay," Canadian Geotechnical Journal, Vol. 23, No. 2, May, pp. 103-114.

2. Amerasinghe, S. F., and Parry, R. H. (1975), "Anisotropy in heavily overconsolidated kaolin," Journal of the Geotechnical Engineering Division, ASCE, Vol. 101, No. GT12, Dec., pp. 1277-1293.

3. Andersen, K. H., Pool, J. H., Brown, S. F., and Rosenbrand, W. F. (1980), "Cyclic and static laboratory tests on Drammen Clay," Journal of the Geotechnical Engineering Division, ASCE, Vol. 106, No. GT5, May, pp. 499-530.

4. Andrawes, K. Z., McGown, A., Mashhour, M. M., and Wilson-Fahmy, R. F. (1980), "Tension resistant inclusions in soils," Journal of the Geotechnical Engineering Division, ASCE, Vol. 106, No. GT12, December, pp. 1313-1326.

5. Andrawes, K. Z., McGown, A., Wilson-Fahmy, R. F., and Mashhour, M. M. (1982), "The finite element method of analysis applied to soil-geotextile systems," Proceedings of the Second International Conference on Geotextiles, Las Vegas, Nevada, August, Vol. III, pp. 695-700.

6. Atkinson, J. H., and Bransby, P. L. (1978), The Mechanics of Soils- A Introduction to Critical State Soil Mechanics, McGraw-Hill Book Company (UK) Limited, Maidenhead, England, 375 pp.

7. Azzouz, A. S., Krizek, R. J., and Corotis, R. B. (1976), "Regression analysis of soil compressibility," Soils and Foundations, JSSMFE, Vol. 16, No. 2, pp. 19-29.

45. Davis, E. H. (1968), "Theories of plasticity and failure of soil masses," Chapter 6, In Soil Mechanics--Selected Topics, I. K. Lee, Ed., Butterworth & Co., Ltd., London.

46. Davis, E. H., and Booker, J. R. (1973), "The effect of increasing strength with depth on the bearing capacity of clays," Geotechnique, Vol. 23, No. 4, pp. 551-563.

47. deGraft-Johnson, J. W. S., Bhatia, H. S., and Gidigasu, D. M. (1969), "The strength characteristics of residual micaceous soils," Proceedings of the Seventh International Conference on Soil Mechanics and Foundation Engineering, Mexico City, Vol. 1, pp. 165-172.

48. Desai, C. S., and Christian, J. T. (1977), "Introduction, numerical methods, and special topics," Chapter 1 in Numerical Methods in Geotechnical Engineering, C. S. Desai and J. T. Christian, Eds., McGraw-Hill Book Company, New York, pp. 1-64.

49. Desai, C. S., and Siriwardane, H. J. (1984), Constitutive Laws for Engineering Materials with Emphasis on Geologic Materials, Prentice-Hall, Inc., Englewood Cliffs, NJ, 468pp.

50. Dhowian, A. W., and Edil, T. B. (1980), "Consolidation behavior of peats," Geotechnical Testing Journal, ASTM, Vol. 3, No. 3, Sept., pp. 105-114.

51. DiMaggio, F. L., and Sandler, I. S. (1971), "Material model for granular soils," Journal of the Engineering Mechanics Division, ASCE, Vol. 97, No. EM3, June, pp. 935-950.

52. Donaghe, R. T., and Townsend, F. C. (1978), "Effects of anisotropic versus isotropic consolidation in consolidated-undrained compression tests of cohesive soils," Geotechnical Testing Journal, ASTM, Vol. 1, No. 4, Dec., pp. 173-189.

53. Drucker, D. C., and Prager, W. (1952), "Soil mechanics and plastic analysis or limit design," Quarterly of Applied Mathematics, Vol. 10, No. 2, pp. 157-165.

54. Drucker, D. C., Gibson, R. E., and Henkel, D. J. (1957), "Soil mechanics and work-hardening theories of plasticity," Transactions, ASCE, Vol. 122, pp. 338-346.

17. Boutrup, E., and Holtz, R. D. (1982), "Fabric reinforced embankments constructed on weak foundations," Report No. FHWA/IN/JHRP-82/21, Joint Highway Research Project, School of Civil Engineering, Purdue University, West Lafayette, Indiana, December, 468 pp.

18. Boutrup, E., and Holtz, R. D. (1983), "Analysis of embankments on soft ground reinforced with geotextiles," VIII European Conference on Soil Mechanics and Foundation Engineering, Helsinki, May, pp. 469-472.

19. Brakel, J., Coppens, M., Maagdenberg, A. C., and Risseeuw, P. (1982), "Stability of slopes constructed with polyester reinforcing fabric, test section at Almere - Holland, '79," Proceedings of the Second International Conference on Geotextiles, Las Vegas, Nevada, August, Vol. III, pp. 727-732.

20. Broms, B. B. (1977), "Polyester fabric as reinforcement in soil," Proceedings of the International Conference on the Use of Fabrics in Geotechnics, Ecole Nationale des Ponts et Chaussees, Paris, France, Vol. I, pp. 129-135.

21. Broms, B., and Ratnam, M. (1963), "Shear strength of an anisotropically-consolidated clay," Journal of the Soil Mechanics and Foundations Division, ASCE, Vol. 89, No. SM6, Nov., pp. 1-26.

22. Brown, S. F., Lashine, A., and Hyde, A. (1975), "Repeated load triaxial testing of a silty clay," Geotechnique, Vol. 25, No. 1, Mar., pp. 95-114.

23. Burwash, W. J. (1980), "A case history involving the use of a geotextile for a highway embankment on muskeg," Proceedings of the First Canadian Symposium on Geotextiles, The Canadian Geotechnical Society, Calgary, Alberta, September 23, pp. 225-235.

24. Busbridge, J. R., Chan, P., Milligan, V., La Rochelle, P. R., and Lefebvre, L. D. (1985), "The effect of geogrid reinforcement on the stability of embankments on a soft sensitive Champlain Clay deposit," Transport Canada Report No. TP 6308E, Transportation Development Center, National Research Council, Quebec, Canada, 277 pp.

65. Giroud, J. P., Nhiem, T. V., and Obin, J. P. (1973), Tables pour le calcul des fondations, Dunod, Paris, 445pp.

66. Greenway, D. R., and Bell, J. R. (1976), "Analysis of a low fabric reinforced embankment on muskeg," Report to Crown Zellerbach Corp., Department of Civil Engineering, Oregon State University, Corvallis, 79 pp.

67. Haliburton, T. A. (1981), "Use of engineering fabric in road and embankment construction," Seminar on the Use of Synthetic Fabrics in Civil Engineering, Consulting Engineers of Ontario, Toronto, Ontario, November, pp. 66-94.

68. Haliburton, T. A., Anglin, C. C., and Lawmaster, J. D. (1978), "Testing of geotechnical fabric for use as reinforcement, Geotechnical Testing Journal, ASTM, Vol. 1, December, pp. 203-212.

69. Haliburton, T. A., Fowler, J., and Langan, J. P. (1980), "Design and construction of fabric reinforced embankment test section at Pinto Pass, Mobile, Alabama," Transportation Research Record No. 749, pp. 27-33.

70. Hannon, J. (1982), "Fabrics support embankment construction over Bay Mud," Proceedings of the Second International Conference on Geotextiles, Las Vegas, Nevada, August, Vol. III, pp. 653-658.

71. Hannon, J. B., and Walsh, T. J. (1982), "Wick drains, membrane reinforcement and lightweight fill for embankment construction at Dumbarton," Paper prepared for presentation at 61st annual meeting of Transportation Research Board, Washington, D. C., January.

72. Henkel, D. J. (1960), "The shear strength of saturated remoulded clays," Shear Strength of Cohesive Soils, ASCE, University of Colorado, pp. 533-554.

73. Henkel, D. J., and Sowa, V. A. (1964), "The influence of stress history on stress paths in undrained triaxial tests on clay," Laboratory Testing of Soils, ASTM STP 361, pp. 280-291.

74. Henkel, D. J., and Wade, N. H. (1966), "Plane strain tests on a saturated remolded clay," Journal of the Soil Mechanics and Foundations Division, ASCE, Vol. 92, No. SM6, pp. 67-80.

35. Christopher, B. R., and Holtz, R. D. (1984), "Geotextile engineering manual," Federal Highway Administration, Washington, D. C., 850 pp.

36. Clough, R. W., and Woodward, R. J. (1967), "Analysis of embankment stresses and deformations," Journal of the Soil Mechanics and Foundations Division, ASCE, Vol. 93, No. SM4, pp. 529-549.

37. Cook, R. D. (1974), Concepts and Applications of Finite Element Analysis, John Wiley and Sons, Inc., New York, 402 pp.

38. Coumoulos, D. G. (1979), "Determination of settlement design parameters from conventional oedometer tests," Design Parameters in Geotechnical Engineering, Proceedings of the Seventh European Conference on Soil Mechanics and Foundation Engineering, Brighton, England, Vol. I, pp. 111-118.

39. Cragg, C. B. H. (1980), "Geotextile applications within Ontario Hydro," Proceedings of the First Canadian Symposium on Geotextiles, The Canadian Geotechnical Society, Calgary, Alberta, September 23, pp. 125-136.

40. Crawford, C. (1964), "Some characteristics of Winnepeg Clay," Canadian Geotechnical Journal, Vol. 1, No. 4, Nov., pp. 227-235.

41. Croce, A., Japelli, R., Pellegrino, A., and Viggiani, C. (1969), "Compressibility and strength of intact clays," Proceedings of the Seventh International Conference on Soil Mechanics and Foundation Engineering, Mexico City, Vol. I, pp. 81-89.

42. daCruz, P. T. (1963), "Shear strength characteristics of some residual compacted clays," Proceedings of the Second Panamerican Conference on Soil Mechanics and Foundation Engineering, Mexico, Vol. I, pp. 73-102.

43. D'Appolonia Associates, Inc. (1964a), "Shear stress analysis, Northwest Fill Area, Youngstown Sheet and Tube Co., Indiana Harbor Works," D'Appolonia Associates, Inc., Consulting Engineers, Pittsburg, PA.

44. D'Appolonia Associates, Inc. (1964b), "Consolidation characteristics, Northwest Fill Area, Youngstown Sheet and Tube Co., Indiana Harbor Works," D'Appolonia Associates, Inc., Consulting Engineers, Pittsburg, PA.

85. Humphrey, D. N., and Holtz, R. D. (1986a), "Finite element analysis of plane strain problems with PS-NFAP and the cap model," Report No. JHRP-86, Joint Highway Research Project, School of Civil Engineering, Purdue University, West Lafayette, Indiana, August, 175 pp.

86. Humphrey, D. N., and Holtz, R. D. (1986b), "STABL6 with reinforcing layer option - User's manual," Report No. JHRP-86, Joint Highway Research Project, School of Civil Engineering, Purdue University, West Lafayette, Indiana, August, 33 pp.

87. Hvorslev, M. J. (1960), "Physical components of the shear strength of saturated clays," Shear Strength of Cohesive Soils, ASCE, University of Colorado, pp. 169-273.

88. IDOH (1985a), Private communications with G. Crosby.

89. IDOH (1985b), Soils Report for I-164, Project No. I-164-1(2)9, Vanderburg County, IN., Sta. 840+00 to 1000+95, Prepared by Atlas Soils, Inc., Hillsboro, IL.

90. Ingold, T. S. (1982), "An analytical study of geotextile reinforced embankments," Proceedings of the Second International Conference on Geotextiles, Las Vegas, Nevada, August, Vol. III, pp. 683-688.

91. Janbu, N. (1963), "Soil compressibility as determined by oedometer and triaxial tests," Proceedings of the Third European Conference on Soil Mechanics and Foundation Engineering, Wiesbaden, pp. 19-24.

92. Janbu, N. (1985), "Soil models in offshore engineering," Geotechnique, Vol. 35, No. 3, pp. 241-281.

93. Jewell, R. A. (1981), "A computer design method for reinforced soil structures using limit equilibrium analysis," unpublished report, Netlon, Ltd., 6 pp.

94. Jewell, R. A. (1982), "A limit equilibrium design method for reinforced embankments on soft foundations," Proceedings of the Second International Conference on Geotextiles, Las Vegas, Nevada, August, Vol. III, pp. 671-676.

95. Johnson, W., and Mellor, P. B. (1983), Engineering Plasticity, Ellis Horwood, Ltd., Chichester, England, 646 pp.

55. Duncan, J. M., and Chang, C. Y. (1970), "Non-linear analysis of stress and strain in soils," Journal of the Soil Mechanics and Foundations Division, ASCE, Vol. 96, No. SM5, pp. 1629-1653.

56. Edgar, S. (1984), "The use of high tensile polymer grid mattress on the Musselburgh and Portobello bypass," Paper No. 3.5, Symposium on Polymer Grid Reinforcement in Civil Engineering, Science and Engineering Research Council, London, March 22-23, 9 pp.

57. Egan, J. A. (1977), "A critical state model for the cyclic loading pore pressure response of soils," Thesis submitted in partial fulfillment of the requirements for the degree of Master of Science, Cornell University, Ithaca, N. Y., June.

58. El-Fermaoui, A., and Nowatzki, E. (1982), "Effect of confining pressure on performance of geotextiles in soils," Proceedings of the Second International Conference on Geotextiles, Las Vegas, Nevada, August, Vol. III, pp. 799-804.

59. Fowler, J. (1981), "Design, construction, and analysis of fabric-reinforced embankment test section at Pinto Pass, Mobile, Alabama," Technical Report EL-81-7, U. S. Army Engineer Waterways Experiment Station, Vicksburg, Mississippi, October, 238 pp.

60. Fowler, J. (1982), "Theoretical design considerations for fabric-reinforced embankments," Proceedings of the Second International Conference on Geotextiles, Las Vegas, Nevada, August, Vol. III, pp. 665-670.

61. Fowler, J. (1985), "Building on muck," Civil Engineering, ASCE, Vol. 55, No. 5, May, pp. 67-69.

62. Fowler, J., and Haliburton, T. A. (1980), "Design and construction of fabric reinforced embankments," The Use of Geotextiles for Soil Improvements, Preprint 80-177, ASCE National Convention, Portland, Oregon, pp. 89-118.

63. France, J., and Sangrey, D. A. (1977), "Effects of drainage in repeated loading of clays,' Journal of the Geotechnical Engineering Division, ASCE, Vol. 103, No. GT7, July, pp. 769-785.

64. Gale, S. M., and Henderson, J. S. (1984), "Design and construction of a geotextile reinforced taxiway embankment over peat," Geotechnical Fabrics Report, Vol. 2, No. 1, Summer, pp. 7-11.

106. Ladd, C. C. (1972), "Test embankment on sensitive clay," Proceedings of the Specialty Conference on Performance of Earth and Earth-Supported Structures, ASCE, Purdue University, Vol. I, Part 1, pp. 101-128.

107. Ladd, C. C. (1975), "Foundation design of embankments constructed on Connecticut Valley varved clays," Research Report R75-7, Geotechnical Publication 343, Department of Civil Engineering, Massachusetts Institute of Technology, 438 pp.

108. Ladd, C. C., Bovee, R. B., Edgers, L., and Rixner, J. J. (1971), "Consolidated-undrained plane strain shear tests on Boston Blue Clay," Research Report R71-13, Soils Publication 273, Department of Civil Engineering, Massachusetts Institute of Technology, 243 pp.

109. Ladd, C. C., and Edgers, L. (1972), "Consolidated-undrained direct-simple shear tests on saturated clays," Research Report R72-92, Soils Publication 284, Department of Civil Engineering, Massachusetts Institute of Technology, 245 pp.

110. Ladd, C. C., and Foott, R. (1974), "New design procedure for stability of soft clays," Journal of the Geotechnical Engineering Division, ASCE, Vol. 100, No. GT7, July, pp. 793-786.

111. Ladd, C. C., Foott, R., Ishihara, K., Schlosser, F., and Poulos, H. G. (1977), "Stress-deformation and strength characteristics," Proceedings of the Ninth International Conference on Soil Mechanics and Foundation Engineering, Tokyo, Vol. II, pp. 421-494.

112. Ladd, C. C., and Lambe, T. W. (1963), "The strength of an undisturbed clay determined from undrained tests," Laboratory Shear Testing of Soils, ASTM STP 361, Philadelphia, Pa., pp. 342-371.

113. Ladd, C. C., and Varallyay, J. (1965), "The influence of stress system on the behavior of saturated clays during undrained shear," Phase Report No. 1, Part II, Research Report R65-11, Department of Civil Engineering, Massachusetts Institute of Technology.

114. Lahtinen, P. (1983), "Building a floating shore embankment with reinforced fabrics in the bay of the 'Old Town' of Helsinki," VIII European Conference on Soil Mechanics and Foundation Engineering, Helsinki, May, Vol. III, pp. 1186.

75. Hoffman, G. L., and Turgeon, R. (1983), "Long-term in situ properties of geotextiles," Transportation Research Record 916, TRB, National Academy of Science, Washington, D. C., pp. 89-94.

76. Hollingshead, G. W., and Raymond, G. P. (1972), "Field loading tests on muskeg," Proceedings of the 14th Muskeg Research Conference, Technical Memorandum No. 102, National Research Council of Canada, Ottawa, January, pp. 69-87.

77. Holtz, R. D. (1975), "Recent developments in reinforced earth," Proceedings of the VII Scandinavian Geotechnical Meeting, published by Polyteknisk Forlag, Copenhagen, Denmark, pp. 281-291.

78. Holtz, R. D. (1982), "Closing report: Sessions 2C, 3C, 4C, and 5C- Walls and foundations, slopes and embankments," Proceedings of the Second International Conference on Geotextiles, Las Vegas, Nevada, August, Vol. IV, pp. 140-141.

79. Holtz, R. D., and Kovacs, W. D. (1981), An Introduction to Geotechnical Engineering, Prentice-Hall, Inc., Englewood Cliffs, New Jersey, 733 pp.

80. Holtz, R. D., and Massarsch, K. R. (1976), "Improvement of the stability of an embankment by piling and reinforced earth," Proceedings of the VI European Conference on Soil Mechanics and Foundation Engineering, Vienna, Vol. 1.2, pp. 473-478.

81. Houlsby, G. T. (1985), "The use of a variable shear modulus in elastic-plastic models for clays," Computers and Geotechnics, Elsevier Applied Science Publishers, Ltd., England, Vol. 1, No. 1, pp. 3-13.

82. Humphrey, D. N. (1985a), "Application of the CAP model to a silty sand," Unpublished report for CE 597W with Professor D. Znidarcic, School of Civil Engineering, Purdue University, West Lafayette, Indiana, January, 71 pp.

83. Humphrey, D. N. (1985b), "Task 4 - Development of a simplified FEM program - Progress report," Unpublished report, School of Civil Engineering, Purdue University, West Lafayette, Indiana, 10 pp.

84. Humphrey, D. N. (1985c), "Geotextile testing and properties," Unpublished report, School of Civil Engineering, Purdue University, West Lafayette, Indiana, 25 pp.

125. Lupien, C., Lefebvre, G., Rosenberg, P., Pare, J. J., and Lavallee, J. G. (1983), "Use of fabrics for improving the placement of till on peat foundation," Transportation Research Record 916, TRB, National Research Council, Washington, D. C., pp. 54-59.

126. Maagdenberg, A. C. (1977), "Fabrics below sand embankments over weak soils, their technical specifications and their application in a test area," Proceedings of the International Conference on the Use of Fabrics in Geotechnics, Ecole Nationale des Ponts et Chaussees, Paris, France, Vol. I, pp. 77-82.

127. MacDonald, A. B., and Sauer, E. K. (1970), "The engineering significance of Pleistocene stratigraphy in the Saskatoon area, Saskatchewan, Canada," Canadian Geotechnical Journal, Vol. 7, No. 2, pp. 116-126.

128. Mandel, J., and Selencon, J. (1969), "Force portante d'un sol sur une assise rigide," Proceedings of the Seventh International Conference on Soil Mechanics and Foundation Engineering, Mexico City, Vol. II, pp. 157-164.

129. Mayne, P. W. (1980), "Cam-clay predictions of undrained strength," Journal of the Geotechnical Engineering Division, ASCE, Vol. 106, No. GT11, Nov., pp. 1219-1242.

130. Mayne, P. W., and Swanson, P. G. (1980), "The critical-state pore pressure parameter from consolidated undrained shear tests," Proceedings of the Symposium on Shear Strength of Soil, ASTM STP 740, pp. 410-430.

131. McCarron, W. O. (1985), "Soil plasticity and finite element applications," PhD. Thesis, School of Civil Engineering, Purdue University, West Lafayette, Indiana, 265 pp.

132. McCarron, W. O., and Chen, W. F. (1985), "An input guide to AUTOGEN- A preprocessor for 2-D F.E. with NFAP," Structural Engineering Report No. CE-STR-85-41, School of Civil Engineering, Purdue University, West Lafayette, Indiana, 48 pp.

133. McCarron, W. O., and Chen, W. F. (1986a), "Documentation for a cap model subroutine," Structural Engineering Report No. CE-STR-86-5, School of Civil Engineering, Purdue University, West Lafayette, Indiana, 76 pp.

96. Kaufman, R. I., and Sherman, W. C., Jr. (1964), "Engineering measurements for Port Allen Lock," Journal of the Soil Mechanics and Foundations Division, ASCE, Vol. 90, No. SM5, pp. 221-247; also in Design of Foundations for Control of Settlement, ASCE, pp. 281-307.

97. Kerisel, J. (1973), "Le barrage d'Arzal un barrage sur sol tress compressible construit au travers d'un estuaire a maree," Geotechnique, Vol. 23, No. 1, pp. 49-65.

98. Koerner, R. M. (1986), Designing with Geosynthetics, Prentice-Hall, Englewood Cliffs, NJ, 424 pp.

99. Koerner, R. M., and Welsh, J. P. (1980), Construction and Geotechnical Engineering Using Synthetic Fabrics, John Wiley and Sons, pp. 267.

100. Korhonen, K. H. (1977), "Stresses and strains in undrained tests," Proceedings of the Ninth International Conference on Soil Mechanics and Foundation Engineering, Tokyo, Vol. 1, pp. 165-168.

101. Koutsoftas, D., and Fischer, J. (1976), "In-situ undrained shear strength of two marine clays," Journal of the Geotechnical Engineering Division, ASCE, Vol. 103, No. GT9, Sept., pp. 989-1005.

102. Kulhawy, F. H., and Duncan, J. M. (1972), "Stresses and movements in Oroville Dam," Journal of the Soil Mechanics and Foundations Division, ASCE, Vol. 98, No. SM7, pp. 653-655.

103. Ladanyi, B., et al. (1965), "Some factors controlling the predictability of stress-strain behavior of clay," Canadian Geotechnical Journal, Vol. 2, No. 2, May, pp. 60-89.

104. Ladd, C. C. (1964), "Stress-strain behavior of saturated clay and basic strength principles," Report No. R64-17 to the U. S. Army Waterways Experiment Station, Vicksburg, Miss., Apr.

105. Ladd, C. C. (1965), "Stress-strain behaviour of anisotropically consolidated clays during undrained shear," Proceedings of the Sixth International Conference on Soil Mechanics and Foundation Engineering, Montreal, Vol. 1, pp. 282-286.

144. Mizuno, E., and Chen, W. F. (1982), "CAP models in soil mechanics," Preprint 82-005, ASCE Convention, Las Vegas, Nevada, April 26-30, 14pp.

145. Montgomery, M. W. (1978), "Geotechnical investigation-Gas centrifuge enrichment plant, Portsmouth, Ohio," Report No. MK 7502, Law Engineering Testing Company, Apr.

146. Morgat, C. P. (1976), "Finite element analysis of embankments on weak clay foundations," Engineer Degree Thesis, Stanford University, 144 pp.

147. Murray, R. T. (1982), "Fabric reinforcement of embankments and cuttings," Proceedings of the Second International Conference on Geotextiles, Las Vegas, Nevada, August, Vol. III, pp. 707-713.

148. Murray, R. T., Wrightman, J., and Burt, A. (1982), "Use of fabric reinforcement for reinstating unstable slopes," Supplementary Report No. 751, Transport and Road Research Laboratory, 32 pp.

149. Naylor, D. J. (1973), Discussion of: "Numerical analysis of plasticity in soils," by I. M. Smith, Proceedings of the Symposium on the Role of Plasticity in Soil Mechanics, Cambridge, U.K., Sept., pp. 291-293.

150. Naylor, D. J., Pande, G. N., Simpson, B., and Tabb, R. (1981), Finite Elements in Geotechnical Engineering, Pineridge Press, Swansea, U.K., 245 pp.

151. Ohta, H., Mochinaga, R., and Kurihara, N. (1980), "Investigation of soft foundations with surface reinforcement," Proceedings of the Third Australia-New Zealand Conference on Geomechanics, Wellington, May 12-16, Vol. I, pp. 1-123 to 1-128.

152. Olivera, A. (1982), "Use of non-woven geotextiles to construct a deep highway embankment over swamp soil," Proceedings of the Second International Conference on Geotextiles, Las Vegas, Nevada, August, Vol. III, pp. 625-630.

153. Olson, R. (1962), "The shear strength properties of calcium illite," Geotechnique, Vol. 12, No. 1, March, pp. 23-43.

154. Olson, R., and Hardin, J. (1963), "Shearing properties of remolded sodium illite," Proceedings of the Second Panamerican Conference on Soil Mechanics and Foundation Engineering, Mexico, Vol. 1, pp. 204-218.

115. Lambe , T. W., and Whitman, R. V. (1969), Soil Mechanics, John Wiley & Sons, Inc., New York, 553 pp.

116. Lambe, T. W. (1963), "An earth dam for the storage of fuel oil," Proceedings of the Second Panamerican Conference on Soil Mechanics and Foundation Engineering, Mexico, Vol. II, pp. 257-308.

117. Landva, A. O. (1980), "Vane testing in peat," Canadian Geotechnical Journal, Vol. 17, No. 1, February, pp. 1-19.

118. Lefebvre, G., Langlois, P., Lupien, C., and Lavallee, J.-G. (1984), "Laboratory testing and in situ behaviour of peat as embankment foundation," Canadian Geotechnical Journal, Vol. 21, No. 2, May, pp. 322-337.

119. Leroueil, S., Tavenas, F., Mieussens, C., and Peignaud, M. (1978), "Construction pore pressures in clay foundations under embankments; Part II: Generalized behaviour," Canadian Geotechnical Journal, Vol. 15, No. 1, pp. 66-82.

120. Lo, K. Y. (1962), "Shear strength properties of a sample of volcanic material of the Valley of Mexico," Geotechnique, Vol. 12, No. 4, Dec., pp. 303-318.

121. Lovell, C. W., Sharma, S. S., and Carpenter, J. R. (1984), "Slope stability analysis with STABLE4," Report No. JHRP-84-19, Joint Highway Research Project, School of Civil Engineering, Purdue University, West Lafayette, Indiana, August, 109 pp.

122. Lowe, J., III, Zaccheo, P. F., and Feldman, H. S. (1964), "Consolidation testing with back pressure," Journal of the Soil Mechanics and Foundations Division, ASCE, Vol. 90, No. SM5, pp. 69-86; also in Design of Foundations for Control of Settlement, ASCE, pp. 73-90.

123. Lukanen, E. O., and Teig, G. (1976), "Design and evaluation of roadway widening sections through swamps," Investigation No. 199 Initial Report, Research and Standards Section, Office of Materials, Research and Standards, Minnesota Department of Transportation, 40 pp.

124. Lupien, C., Lefebvre, G., Rosenberg, P., and Lavallee, J. G. (1981), "Observation during construction of till embankments on peat foundation," 34th Canadian Geotechnical Conference, Fredricton, New Brunswick, September.

166. Roscoe, K. H., Schofield, A. N., and Thurairajah, A. (1963), "Yielding of clays in states wetter than critical," Geotechnique, Vol. 13, pp. 211-240.

167. Rowe, R. K. (1982), "The analysis of an embankment constructed on a geotextile," Proceedings of the Second International Conference on Geotextiles, Las Vegas, Nevada, August, Vol. III, pp. 677-682.

168. Rowe, R. K. (1984), "Reinforced embankments: analysis and design," Journal of the Geotechnical Engineering Division, ASCE, Vol. 110, No. 2, February, pp. 231-246.

169. Rowe, R. K., Fisher, D. G., and Ko, T. (1982), "An examination of the role of geotextiles as reinforcement for embankments on soft foundations," Geotechnical Research Report GEOT-9-82, Faculty of Engineering Science, The University of Western Ontario, May, 135 pp.

170. Rowe, R. K., MacLean, M. D., and Barsvary, A. K. (1984a), "The observed behaviour of a geotextile-reinforced embankment constructed on peat," Canadian Geotechnical Journal, Vol. 21, No. 2, pp. 289-304.

171. Rowe, R. K., MacLean, M. D., and Soderman, K. L. (1984b), "Analysis of a geotextile-reinforced embankment constructed on peat," Canadian Geotechnical Journal, Vol. 21, No. 3, August, pp. 563-576.

172. Rowe, R. K., and Soderman, K. L. (1984), "Comparison of predicted and observed behavior of two test embankments," International Journal of Geotextiles and Geomembranes, Vol. 1, No. 1, pp. 157-174.

173. Rowe, R. K., and Soderman, K. L. (1985a), "An approximate method for estimating the stability of geotextile-reinforced embankments," Canadian Geotechnical Journal, Vol. 22, No. 3, pp. 392-398.

174. Rowe, R. K., and Soderman, K. L. (1985b), "Geotextile reinforcement of embankments on peat," International Journal of Geotextiles and Geomembranes, Vol. 2, No. 4, pp. 277-298.

175. Saarelainen, S. M. I. (1981), "On the compressibility of clays in Helsinki Region," Proceedings of the Tenth International Conference on Soil Mechanics and Foundation Engineering, Stockholm, Vol. II, pp. 557-562.

134. McCarron, W. O., and Chen, W. F. (1986b), "NFAP - User's manual (1986 Purdue version)," Structural Engineering Report No. CE-STR-86-4, School of Civil Engineering, Purdue University, West Lafayette, Indiana, 210 pp.

135. McGown, A., Andrawes, K. Z., Mashhour, M. M. and Myles B. (1981), "Strain behaviour of soil-fabric model embankments," Proceedings of the Tenth International Conference on Soil Mechanics and Foundation Engineering, Stockholm, Vol. III, pp. 739-744.

136. McGown, A., Paine, N., and DuBois, D. D. (1984), "Use of geogrid properties in limit equilibrium analysis," Paper No. 1.4, Symposium on Polymer Grid Reinforcement in Civil Engineering, Science and Engineering Research Council, London, March 22-23, 5 pp.

137. Mesri, G. (1975), Discussion of "New design procedures for stability of soft clays," by C. C. Ladd and R. Foott, Journal of the Geotechnical Engineering Division, ASCE, Vol. 103, No. GT5, pp. 417-430.

138. Mesri, G., and Olson, R. (1970), "Shear strength of montmorillonite," Geotechnique, Vol. 20, No. 3, Sept., pp. 261-270.

139. Milligan, V. (1985), "Design and construction of reinforced embankments on weak soils," Preprint, Kersten Lecture, University of Minnesota, January 22, 24 pp.

140. Milligan, V., and La Rochelle, P. (1984), "Design methods for embankments over weak soils," Paper no. 3.4, Symposium on Polymer Grid Reinforcement in Civil Engineering, Science and Engineering Research Council, London, March 22-23, 8 pp.

141. Mitachi, T., and Kitago, S. (1976), "Change in undrained strength characteristics of a saturated remolded clay due to swelling," Soils and Foundations, JSSMFE, Vol. 16, No. 1, Mar., pp. 45-58.

142. Mitchell, J. K. (1976), Fundamentals of Soil Behavior, John Wiley and Sons, Inc., New York, N.Y., pp. 283-339.

143. Mizuno, E., and Chen, W. F. (1980), "Analysis of soil response with different plasticity models," Application of Plasticity and Generalized Stress-Strain in Geotechnical Engineering, ASCE, pp. 115-138.

187. Simon, R. M., Christian, J. T., and Ladd, C. C. (1974), "Analysis of undrained behavior of loads on clays," Analysis and Design in Geotechnical Engineering, ASCE, Vol. 1, pp. 51-84.

188. Simons, N. E. (1960a), "Comprehensive investigations of the shear strength of an undisturbed Drammen Clay," Shear Strength of Cohesive Soils, ASCE, University of Colorado, pp. 727-745.

189. Simons, N. E. (1960b), "The effect of overconsolidation on the strength characteristics of an undisturbed Oslo clay," Shear Strength of Cohesive Soils, ASCE, University of Colorado, pp. 747-763.

190. Skempton, A. W. (1961), "Horizontal stresses in an overconsolidated Eocene clay," Proceedings of the Fifth International Conference on Soil Mechanics and Foundation Engineering, Paris, Vol. 1, pp. 351-357.

191. Skempton, A. W., and Henkel, D. J. (1953), "Post glacial clays of the Thames Estuary at Tilbury and Shellhaven," Proceedings of the Third International Conference on Soil Mechanics and Foundation Engineering, Zurich, Vol. 1, pp. 302-312.

192. Skempton, A. W., and Sowa, V. A. (1963), "The behavior of saturated clays during sampling and testing," Geotechnique, Vol. 13, No. 4, pp. 269-290.

193. Soderman, L. G., and Kim, Y. D. (1970), "Effect of groundwater levels on stress history of the St. Clair clay till deposit," Canadian Geotechnical Journal, Vol. 7, No. 2, pp. 173-187.

194. Sparrow, R. W., Swanson, P. G., and Brown, R. E. (1979), "Report of laboratory testing of Gulf of Alaska Cores," Open File Report to the United States Geological Survey, Law Engineering Testing Company, Mar.

195. Sridharan, A., Rao, S. and Rao, G. (1971), "Shear strength characteristics of saturated montmorillonite and kaolin clays," Soils and Foundations, JSSMFE, Vol. 11, No. 3, Sept., pp. 1-22.

196. Steward, J., Williamson, R., and Mohney, J. (1977), "Guidelines for use of fabrics in construction and maintenance of low-volume roads," Forest Service, U. S. Dept. of Agriculture, Washington, D. C. 20013.

155. Parry, R. H., and Nadarajah, V. (1973), "Observations on laboratory prepared, lightly overconsolidated specimens of kaolin," Geotechnique, Vol. 24, No. 3, Mar., pp. 345-358.

156. Paul, J. (1983), "Geotextile mattress," VIII European Conference on Soil Mechanics and Foundation Engineering, Helsinki, Vol. III, May, pp. 1182-1184.

157. Perloff, W. H., and Osterberg, J. O. (1963), "The effect of strain rate on the undrained shear strength of cohesive soils," Proceedings of the Second Panamerican Conference on Soil Mechanics and Foundation Engineering, Brazil, Vol. I, pp. 103-128.

158. Petrik, P. M., Baslik, R., and Leitner, F. (1982), "The behavior of reinforced embankments," Proceedings of the Second International Conference on Geotextiles, Las Vegas, Nevada, August, Vol. III, pp. 631-634.

159. Pilot, G. (1972), "Study of five embankment failures on soft soils," Proceedings of the Specialty Conference on Performance of Earth and Earth-Supported Structures, ASCE, Vol. I, Part 1, pp. 81-100.

160. Quast, P. (1983), "Polyester reinforcing fabric mats for the improvement of embankment stability," VIII European Conference on Soil Mechanics and Foundation Engineering, Helsinki, May, Vol. II, pp. 531-534.

161. Rankilor, G. (1981), Membranes in Ground Engineering, John Wiley and Sons, 377 pp.

162. Raymond, G. P. (1972), "Kars Leda Clay," Proceedings of the Specialty Conference on Performance of Earth and Earth-Supported Structures, ASCE, Purdue University, Vol. I, Part 1, pp. 319-340.

163. Raymond, G. P. (1973), "Foundation failure of New Liskeard Embankment," Highway Research Board Bulletin, No. 463, pp. 1-17.

164. Risseeuw, P. (1977), "STABILENKA woven reinforcement fabric in raising mounds on soft soils," Report No. CTI IN 77/22, Akzo Research Laboratories, Arnhem, April 14, 16 pp.

165. Roscoe, K. H., and Burland, J. B. (1968), "On the generalised stress-strain behavior of 'wet' clay," Engineering Plasticity, J. Heyman and F. A. Leckie, eds., Cambridge University Press, pp. 535-609.

207. Williams, D. (1984), "Reinforced embankments at Great Yarmouth bypass," Paper No. 3.3, Symposium on Polymer Grid Reinforcement in Civil Engineering, Science and Engineering Research Council, London, March 22-23, 7 pp.

208. Wong, K. S., and Duncan, J. M. (1974), "Hyperbolic stress-strain parameters for non-linear finite element analysis of stresses and movements in soil masses," Report No. TE 74.3, Department of Civil Engineering, University of California, Berkeley, 90 pp.

209. Wroth, C. P., and Houlsby, G. T. (1985), "Soil mechanics- Property characterization and analysis procedures," Proceedings of the Eleventh International Conference on Soil Mechanics and Foundation Engineering, San Francisco, Vol. I, pp. 1-55.

210. Wu, T. H. (1958), "Geotechnical properties of glacial clays," Journal of the Soil Mechanics and Foundation Division, ASCE, Vol. 84, No. SM3, Paper no. 1732, 34 pp.

211. Wu, T. H., Chang, N., and Ali, E. M. (1978), "Consolidation and strength properties of a clay," Journal of the Geotechnical Engineering Division, ASCE, Vol. 104, No. GT7, July, pp. 889-905.

212. Wu, T. H., Douglas, A., and Goughnour, R. (1962), "Friction and cohesion of saturated clays," Journal of the Soil Mechanics and Foundations Division, ASCE, Vol. 90, No. SM3, June, pp. 1-32.

213. Yamada, Y. (1969), "Recent Japanese developments in matrix displacement method for elastic-plastic problems," Japan-U.S. Seminar on Matrix Methods of Structural Analysis and Design, Tokyo, Japan, August 25-30, 31 pp.

214. Yudhbir, and Varadarajan, A. (1974), "Undrained behavior of overconsolidated saturated clays during shear," Soils and Foundations, JSSMFE, Vol. 14, No. 4, Dec., pp. 1-12.

176. Saleeb, A. F., and Chen, W. F. (1982), "Constitutive modeling of soils- An overview," Preprint 82-006, ASCE Convention, Las Vegas, Nevada, April 26-30, 14pp.

177. Sandler, I. S., DiMaggio, F. L., and Baladi, G. Y. (1976), "Generalized CAP model for geological materials," Journal of the Geotechnical Engineering Division, ASCE, Vol. 102, No. GT7, July, pp. 683-699.

178. Sangrey, D. A., Henkel, D. J., and Esrig, M. I. (1969), "Effective stress response of saturated clay soil to repeated loading," Canadian Geotechnical Journal, Vol. 6, No. 3, Aug., pp. 241-252.

179. Saxena, S., Hedberg, J., and Ladd, C. C. (1978), "Geotechnical properties of Hackensack Valley varved clays of New Jersey," Geotechnical Testing Journal, ASTM, Vol. 1, No. 3, Sept., pp. 148-161.

180. Schneider, H. R., and Holtz, R. D. (1985), "Design of slopes reinforced with geotextiles and geogrids," unpublished report, 37 pp.

181. Schofield, A. N., and Wroth, C. P. (1968), Critical State Soil Mechanics, McGraw-Hill Book Company, London.

182. Sherif, M. A., Wu, M. J., and Bostrum, R. C., "Reduction in soil strength due to dynamic loading," Microzonation Conference, National Science Foundation and ASCE, Vol. II, Nov., pp. 439-454.

183. Shibata, T., and Karube, D. (1969), "Creep rate and creep strength of clays," Proceedings of the Seventh International Conference on Soil Mechanics and Foundation Engineering, Mexico City, Vol. I, pp. 361-368.

184. Shrestha, S. C., and Bell, J. R. (1982), "Creep behavior of geotextiles under sustained loads," Proceedings of the Second International Conference on Geotextiles, Las Vegas, Nevada, August, Vol. III, pp. 769-774 and discussion Vol. IV, pp. 120-122.

185. Siegel, R. A. (1975), "STABL user manual," Report No. IN/JHRP-75/9, Joint Highway Research Project, School of Civil Engineering, Purdue University, W. Lafayette, Indiana, 104 pp.

186. Silvestri, V. (1983), "The bearing capacity of dykes and fills on soft soils of limited thickness," Canadian Geotechnical Journal, Vol. 20, No. 3, August, pp. 428-436.

197. Swanson, P. G., and Brown, R. E. (1977), "Triaxial and consolidation testing of cores from the 1976 Atlantic margin coring project," Open File Report No. 78-124 to the United States Geological Survey, Law Engineering Testing Company, Washington, D.C., Nov.

198. Tavenas, F., Trak, B., and Leroueil, S. (1980), "Remarks of the validity of stability analyses," Canadian Geotechnical Journal, Vol. 17, No. 1, February, pp. 61-73.

199. Taylor, P., and Bacchus, D. (1969), "Dynamic cyclic strain tests on a clay," Proceedings of the Seventh International Conference on Soil Mechanics and Foundation Engineering, Mexico City, Vol. 1, pp. 401-409.

200. Terzaghi, K., and Peck, R. B. (1967), Soil Mechanics in Engineering Practice, Second edition, John Wiley & Sons, New York, 429pp.

201. Van Eekelen, H., and Potts, D. M. (1978), "The behavior of Drammen Clay under cyclic loading," Geotechnique, Vol. 28, No. 2, Feb., pp. 173-196.

202. Van Leeuwen, J. H., and Volman, W. (1976), "An exploration of the constructive function of STABILENKA in an embankment," Industrial Fibres of Enka Glanzstoff, 30 pp.

203. Vaziri, H. (1985), PhD. Thesis, Department of Civil Engineering, The University of British Columbia, Vancouver, British Columbia.

204. Volman, W., Krekt, L., and Risseeuw, P. (1977), "Reinforcement with fabrics, a new technique to improve the stability of embankments on weak subsoils," (Originally in French, translated by D. N. Humphrey), Proceedings of the International Conference on the Use of Fabrics in Geotechnics, Ecole Nationale des Ponts et Chaussees, Paris, France, Vol. I, pp. 55-60.

205. Wager, O. (1981), "Building of a site road over a bog at Kilanda, Alvsborg County, Sweden, in preparation for erection of three 400kV power lines," Report to the Swedish State Power Board, AB Fodervavnader, Boras, Sweden, 16 pp.

206. Whitman, R. V. (1960), "Some considerations and data regarding the shear strength of clays," Shear Strength of Cohesive Soils, ASCE, University of Colorado, pp. 581-614.

VITA

Dana Norman Humphrey was born on June 30, 1956 in Marblehead, Massachusetts. He was active in Boy Scouts and was awarded the rank of Eagle Scout in 1973. In 1974 he graduated with honors from Marblehead High School. From 1974 through 1978 he studied civil engineering at the University of New Hampshire. While at UNH he was elected to Tau Beta Pi, Mortar Board, Pi Mu Epsilon, and Phi Kappa Phi honor societies. In 1978 he was awarded a Bachelor of Science in Civil Engineering, summa cum laude. He then pursued graduate studies at Purdue University specializing in geotechnical engineering. He received a Master of Science in Civil Engineering in 1979. From 1980 through 1983 he worked for a private geotechnical consulting firm in Denver, Colorado and was involved in a wide range of earth and tailing dam projects. In 1984 he returned to Purdue University to pursue the Degree of Doctor of Philosophy. He was granted his Professional Engineer's license in 1986. In addition, he was inducted into Sigma Xi, the scientific research society.